

1-1-2011

Oscillator strength measurements in singly-ionized, doubly-ionized and neutral lanthanides and transition elements (sm, nd, pr, gd, cu, and fe) using laser-induced breakdown spectroscopy.

Caleb Ryder
Wayne State University,

Follow this and additional works at: http://digitalcommons.wayne.edu/oa_dissertations

 Part of the [Astrophysics and Astronomy Commons](#), [Atomic, Molecular and Optical Physics Commons](#), and the [Plasma and Beam Physics Commons](#)

Recommended Citation

Ryder, Caleb, "Oscillator strength measurements in singly-ionized, doubly-ionized and neutral lanthanides and transition elements (sm, nd, pr, gd, cu, and fe) using laser-induced breakdown spectroscopy." (2011). *Wayne State University Dissertations*. Paper 474.

This Open Access Dissertation is brought to you for free and open access by DigitalCommons@WayneState. It has been accepted for inclusion in Wayne State University Dissertations by an authorized administrator of DigitalCommons@WayneState.

**OSCILLATOR STRENGTH MEASUREMENTS IN SINGLY-IONIZED,
DOUBLY-IONIZED AND NEUTRAL LANTHANIDES AND TRANSITION
ELEMENTS (SM, ND, PR, GD, CU, AND FE) USING LASER-INDUCED
BREAKDOWN.**

by

CALEB A. RYDER

DISSERTATION

Submitted to the Graduate School

of Wayne State University,

Detroit, Michigan

in partial fulfillment of the requirements

for the degree of

DOCTOR OF PHILOSOPHY

2012

MAJOR: PHYSICS

Approved by:

Advisor

Date

DEDICATION

I would like to dedicate my dissertation to my wife Michelle, my Mother, and all of my family; without whose support, patience, and understanding none of this would have been possible.

For all the times I literally felt like going insane would be a reasonable option, when I was so stressed out I gave myself stomach ulcers, and during the times when quitting seemed like a viable option I would like to thank my Father and dedicate this work to Him.

ACKNOWLEDGMENTS

First and foremost I would like to thank my advisor Dr. Steven Rehse for his direction, patience and understanding. When discussing topics and answering questions he was always patient with me and helped me to want to rise to a higher level of understanding and performance. His guidance helped me through many tough obstacles throughout this work. I would also like to thank my committee members Dr. Ashis Mukhopadhyay, Dr. Arthur Suits, and Dr. Zhixian Zhou. I would also like to thank Dr. Ratna Naik for her support and motivation throughout my graduate studies at Wayne State University.

Graduate school would not have been as memorable and academically stimulating without the continued support and collaboration of my friends and associates in the physics department. I'd like to especially thank Dr. Qassem Mohaidat and Dr. Khozima Hamasha, Aditya Yechan Gunja, Mackenzie Smith, Nicholas Davis, Dr. Alan Sebastian, Kristopher Healey, Ming-Wei Lin, and Justin Deherder.

I would also like to acknowledge Jim Barlow from the machine shop who tossed ideas around with me about how to actually make this experiment happen. Last, but definitely not least I would like to show my appreciation to the ladies in the front office for all their help: Delores Cowen, Doris King, Lashara Montgomery and Wynnell Pitts.

TABLE OF CONTENTS

Dedication	ii
Acknowledgement	iii
List of Tables	xi
List of Figures	xiv
Chapter 1. Introduction	1
1.1 Need for Atomic Data.....	1
1.2 Theory.....	5
1.2.1 Nucleosynthesis.....	5
1.2.2 Stellar Opacities.....	8
1.2.3 Stellar abundances.....	9
1.3 Atomic Data.....	11
1.3.1 Branching Ratios.....	11
1.3.2 Transition Probabilities.....	14
1.3.3 Atomic Lifetimes.....	15
1.3.4 Oscillator Strength.....	16
1.4 LIBS ability to determine atomic data.....	19
1.4.1 Atomic Data from LIBS.....	19
1.5 Other Methods.....	21
1.5.1 Branching Ratios measurements.....	21
1.5.2 Lifetime measurements.....	23
1.5.3 Copper.....	25
1.5.4 Iron.....	26

1.5.5 Gadolinium.....	27
1.5.6 Neodymium.....	28
1.5.7 Praseodymium.....	29
1.5.8 Samarium.....	30
1.6 Summary and Scope of Dissertation.....	31
References.....	32
Chapter 2. Laser-Induced Breakdown Theory.....	42
2.1.1 Laser Parameters.....	42
2.1.2 Laser-Matter Interactions.....	44
2.1.2.1 Nanosecond Regime.....	45
2.1.2.2 Femtosecond Pulse Regime.....	58
2.1.2.3 Picosecond Pulse Regime.....	59
2.2 Equilibrium and Plasma Modeling.....	60
2.2.1 Equilibrium Distributions in Plasma.....	60
2.2.2 Corona Model.....	66
2.2.3 Local Thermodynamic Equilibrium Model.....	69
2.2.4 Collisional-Radiative Model.....	73
2.2.5 Partial Local Thermodynamic Equilibrium.....	74
2.3 Uniqueness of Laser-Induced Plasmas.....	77
2.3.1 Spectral Emission.....	77
2.4 Experimental Data and Parameter Determinations.....	92
2.4.1 Pressure Effects on Plasma.....	92
2.4.2 Temporal Evolution.....	96

2.4.3 Spatial Distribution of the Plasma.....	99
2.4.4 Buffer Gas Effects.....	102
2.4.5 Clean Pulses.....	103
2.4.6 Sample Concentration.....	104
References.....	106
Chapter 3. Experimental.....	111
3.1 Incident Laser and Focusing Optics.....	111
3.2 Vacuum Chamber and Target.....	115
3.3 Light Collection.....	121
3.4 Light Dispersion in an Echelle Spectrometer.....	126
3.5 Detection and Analysis.....	128
3.6 Experimental Parameters.....	133
References.....	134
Chapter 4. Determination of Uncertainties.....	137
4.1 Spectral Calibration.....	137
4.1.1 Condenser Lens.....	138
4.1.2 Emission Lamp Calibration via Fiber Optic Cable.....	141
4.2 Uncertainty in Spectral-Correction Factor.....	143
4.2.1 Error from the Spectral Correction Factor's Graphical Approximation.....	144
4.2.2 Uncertainty from Multiple-Day Scatter in Spectral Correction Factor.....	145
4.2.3 Uncertainty from Scatter between Data and Fitted Value.....	146
4.3 Uncertainty in Emission Lines.....	147
4.3.1 Spectral Resolution: Blended, Broadened, Shouldered, and Weak Lines.....	147

4.3.2 Uncertainty in 1000 Branching.....	149
4.3.3 Multiple Day Scatter in Branching Ratios.....	149
4.4 Categorizing Uncertainties According to Branching Ratio Strength.....	150
4.5 Total Uncertainty Attributed to Data.....	151
References.....	153
Chapter 5. Radiative Parameters for Nd and Pr.....	155
5.1 Introduction.....	155
5.2 Previous Works.....	157
5.2.1 Previous Work in Praseodymium.....	157
5.2.2 Previous Works in Neodymium.....	158
5.3 Experimental Setup.....	161
5.4 Data Analysis.....	162
5.4.1 Summary of Uncertainties.....	165
5.5 Results.....	167
5.6 Conclusions.....	214
5.6.1 Neutral Neodymium.....	214
5.6.2 Singly-Ionized Neodymium.....	221
5.6.3 Doubly Ionized Neodymium.....	228
5.6.4 Neutral Praseodymium.....	230
5.6.5 Singly-Ionized Praseodymium.....	232
5.6.6 Doubly Ionized Praseodymium.....	239
5.7 Summary.....	245
References.....	249

Chapter 6. Radiative Parameters for Gd and Sm	254
6.1 Introduction.....	254
6.2 Previous Works.....	254
6.2.1 Previous Works in Gadolinium.....	254
6.2.2 Previous Works in Samarium.....	255
6.3 Experimental Setup.....	258
6.4 Data Analysis.....	258
6.5 Conclusions.....	332
6.5.1 Neutral Samarium.....	332
6.5.2 Singly-Ionized Samarium.....	339
6.5.3 Doubly-Ionized Samarium.....	346
6.5.4 Neutral Gadolinium.....	353
6.5.5 Singly-Ionized Gadolinium.....	360
6.5.6 Doubly-Ionized Gadolinium.....	367
6.7 Summary.....	372
References.....	377
Chapter 7. Radiative Parameters for Cu and Fe	382
7.1 Introduction.....	382
7.2 Previous Works.....	384
7.2.1 Previous Works in Copper.....	384
7.2.2 Previous Works in Iron.....	386
7.3 Experimental Setup/ Data Analysis / Uncertainties.....	389
7.4 Results.....	390

7.5 Conclusions.....	450
7.5.1 Neutral Copper.....	450
7.5.2 Singly-Ionized Copper.....	457
7.5.3 Neutral Iron.....	468
7.5.4 Singly Ionized Iron.....	474
7.6 Summary.....	480
References.....	483
Chapter 8. Conclusions and Future Work.....	492
8.1 Improvements to the Branching Ratio Apparatus.....	493
8.2 Lifetime Experiment.....	495
8.3 LIBS-LIF.....	498
References.....	482
Appendix 1. Tabulated Relative Intensities.....	501
Appendix 2. Programming Codes.....	502
Appendix 2.1 Roi Maker.....	502
Appendix 2.2 CreateFoldersForEachRoiInEUpList.....	509
Appendix 2.3 AutomaticFinalDataCreatorV1.....	512
Appendix 2.4 AutomaticImportantHeaders2ExcelAndValueCorrectV.....	516
Appendix 2.5 AutomaticAllPressureOutput2ExcelAllEUpWithRelIntV5.....	523
Abstract.....	532
Autobiographical Statement.....	535

LIST OF TABLES

Table 2.1: Nd:YAG laser parameters and harmonics.....	43
Table 2.2: Typical lasers used in LIBS and their parameters.....	43
Table 2.3: Experimental conditions used in this research.....	106
Table 3.1: Experimental conditions used in this research.....	134
Table 4.1: Summary of uncertainties.....	153
Table 5.1: Summary of uncertainties.....	167
Table5.2: Neutral neodymium radiative parameters.....	171
Table 5.3: Singly ionized neodymium radiative parameters.....	176
Table5.4: Doubly ionized neodymium radiative parameters.....	189
Table 5.5: Neutral praseodymium radiative parameters.....	190
Table 5.6: Singly ionized praseodymium radiative parameters.....	191
Table 5.7: Doubly ionized praseodymium radiative parameters.....	204
Table 6.1: Neutral samarium radiative parameters.....	259
Table 6.2: Singly ionized samarium radiative parameters.....	264
Table 6.3: Doubly ionized samarium radiative parameters.....	288
Table 6.4: Neutral gadolinium radiative parameters.....	291
Table 6.5: Singly ionized gadolinium radiative parameters.....	313
Table 6.6: Doubly ionized gadolinium radiative parameters.....	330
Table 7.1: Neutral copper branching ratios.....	391
Table 7.2: Singly ionized copper branching ratios.....	395
Table 7.3: Neutral iron branching ratios.....	397
Table 7.4: Singly ionized iron branching ratios.....	419

Table Appendix 2.1: Chart Format for Roi Maker505

LIST OF FIGURES

1.1 Abundances of chemical elements.....	6
1.2 Curve of growth plot.....	11
1.3 Decay channels in Nd II.....	13
2.1 Electron avalanche process.....	50
2.2 Multi-photon absorption process.....	51
2.3 Plasma types according to temperature and electron density.....	53
2.4 Chronological schematic of laser-induced plasma formation.....	54
2.5 Examples of continuum and discrete line emissions with energy level transitions.....	57
2.6 Types of radiative transitions.....	64
2.7 Departure of plasma models from LTE.....	76
2.8 Neodymium LIBS spectrum.....	80
2.9 FWHM of the 430 nm line in Nd II	82
2.10 Temperature determination from a Boltzmann plot.....	89
2.11 Integrated Emission intensity vs pressure in Nd I and Nd II lines.....	95
2.12 plasma plume expansion at various vacuum pressures.....	96
2.13 Integrated emission intensity vs delay time for Nd I and Nd II lines.....	97

2.14 Cascading graph.....	98
2.15 Schematic of optical fiber viewing regions in plasma plume.....	100
2.16 Plasma regions integrated intensity vs delay time.....	101
2.17 S/N vs delay time in Argon and Air environments.....	103
3.1 Schematic representation of the experimental setup.....	113
3.2 Nd:YAG Quanta Ray laser	114
3.3 Schematic representation of the incident laser's optical path.....	115
3.4 Vacuum Chamber.....	116
3.5 Schematic representation of the ablation chamber with feed through.....	118
3.6 Feed through and mount schematic.....	119
3.7 Buffer gas calibration curve.....	120
3.8 Experimental apparatus.....	123
3.9 Comparison of Spectra with and without optical train.....	125
3.10 Blazed échelle grating	127
3.11 operating principles used in the échelle spectrometer.....	128
3.12 Single CCD chip's operating principles.....	130
3.13 CCD arrays operating principles.....	131

3.14 Exponential fit to image intensifier output.....	133
4.1 Spectral calibration comparison.....	139
4.2 Spectral efficiency factor plot.....	143
4.3 Limit of spectral efficiency factor below 225 nm.....	146
4.4 Rayleigh's criterion.....	148
4.5 Branching ratio uncertainty.....	151
5.1 Schematic of LIBS apparatus for branching ratio measurements.....	162
5.2 Overlying spectrum of Nd and Pr.....	164
5.3 Example of resolving capability with weak lines.....	169
5.4 Example of resolving capability with strong lines.....	170
5.5 Nd I Log(gf) comparison.....	215
5.6 Nd I gA comparison.....	216
5.7 Nd I strong branches gA percent difference histogram	218
5.8 Nd I medium branches gA percent difference histogram.	219
5.9 Nd I weak branches gA percent difference histogram.....	220
5.10 Nd II Log(gf) comparison	222
5.11 Nd II gA comparison.....	223

5.12 Nd II strong branches gA percent difference histogram	225
5.13 Nd II medium branches gA percent difference histogram	226
5.14 Nd II weak branches gA percent difference histogram.....	228
5.15 Nd III Log(gf) comparison.....	229
5.16 Pr I Log(gf) comparison.....	230
5.17 Pr I strong branches gA percent difference histogram	232
5.18 Pr II Log(gf) comparison.....	233
5.19 Pr II gA comparison.....	234
5.20 Pr II strong branches gA percent difference histogram	236
5.21 Pr II medium branches gA percent difference histogram	237
5.22 Pr II weak branches gA percent difference histogram.....	238
5.23 Pr III Log(gf) comparison.....	240
5.24 Pr III gA comparison.....	241
5.25 Pr III medium branches gA percent difference histogram.....	243
5.26 Pr III weak branches gA percent difference histogram.....	244
6.1 Sm I gA comparison.....	334
6.2 Sm I strong branches gA percent difference histogram	336

6.3 Sm I medium branches gA percent difference histogram	337
6.4 Sm II weak branches gA percent difference histogram.....	338
6.5 Sm II gA comparison.....	340
6.6 Sm II Log(gf) comparison	341
6.7 Sm II strong branches gA percent difference histogram	343
6.8 Sm II medium branches gA percent difference histogram	344
6.9 Sm II weak branches gA percent difference histogram.....	345
6.10 Sm III Log(gf) comparison.....	347
6.11 Sm III gA comparison.....	348
6.12 Sm III strong branches gA percent difference histogram	350
6.13 Sm III medium branches gA percent difference histogram	351
6.14 Sm III weak branches gA percent difference histogram.....	352
6.15 Gd I Log(gf) comparison.....	354
6.16 Gd I gA comparison.....	355
6.17 Gd I strong branches gA percent difference histogram	357
6.18 Gd I medium branches gA percent difference histogram	358
6.19 Gd I weak branches gA percent difference histogram.....	360

6.20 Gd II Log(gf) comparison.....	361
6.21 Gd II gA comparison.....	362
6.22 Gd II strong branches gA percent difference histogram	364
6.23 Gd II medium branches gA percent difference histogram	365
6.24 Gd II weak branches gA percent difference histogram.....	366
6.25 Gd III Log(gf) comparison.....	367
6.26 Gd III gA comparison.....	368
6.27 Gd III strong branches percent difference histogram	369
6.28 Gd III medium branches percent difference histogram.....	371
6.29 Gd III weak branches percent difference histogram.....	372
7.1 Overlying spectrum of Fe and Cu.....	390
7.2 Cu I branching ratio comparison.....	452
7.3 Cu I strong branches percent difference histogram.....	454
7.4 Cu I medium branches percent difference histogram.....	455
7.5 Cu I weak branches percent difference histogram	457
7.6 Cu II branching ratio comparison.....	459
7.7 Cu II strong branches percent difference histogram	460

7.8 Cu II medium branches percent difference histogram	461
7.9 Cu II weak branches percent difference histogram.....	462
7.10 Cu II LIBS branching ratio comparison.....	464
7.11 Cu II LIBS strong branches percent difference histogram	465
7.12 Cu II LIBS medium branches percent difference histogram	467
7.13 Cu II LIBS weak branches percent difference histogram.....	468
7.14 Fe I branching ratio comparison.....	470
7.15 Fe I strong branches percent difference histogram	472
7.16 Fe I medium branches percent difference histogram	473
7.17 Fe I weak branches percent difference histogram.....	474
7.18 Fe II branching ratio comparison.....	476
7.19 Fe II strong branches percent difference histogram	478
7.20 Fe II medium branches percent difference histogram	479
7.21 Fe II weak branches percent difference histogram.....	480
8.1 Singly-ionized gallium Grotian diagram.....	496
8.2 Lifetime measurement apparatus schematic.....	497
8.3 Gallium spectrum.....	498

Appendix 2.1 Typical Nd II roi for 23229.991cm^{-1}	503
Appendix 2.2 Picture of the <i>RoiMaker</i> user interface.....	504

Chapter 1 – Introduction

1.1 - Need for Atomic Data

Lanthanides (elements with atomic mass numbers between 57 and 71) are becoming more common place in commercial products. Lanthanide metals, commonly called rare earth metals, include all the lanthanide elements as well as yttrium ($Z=39$) and scandium ($Z=21$). Some common uses of lanthanides are seen in magnetic devices such as strong household magnets, magnetic resonance imaging (MRI) where they are used as a contrast reagent, cell phones, rechargeable batteries, cd players, phosphor televisions, and even night vision goggles. With the current interest in alternate forms of energy, the hybrid car has become very popular due to rising gas prices. The battery in the Toyota Prius is comprised of lanthanum-hydride, utilizing on average about 10 lbs of lanthanum, and the lanthanum battery works about twice as well as the common lead-acid car battery. The many uses of lanthanides in magnetic materials are due to the unpaired f -shell electrons which create strong spin-orbit coupling to an external magnetic field.

Lanthanides are also used in lasers because of their slow cascading processes to the ground state which provide convenient population inversions. For example, the Nd:YAG laser used in this work operates with neodymium doped into a yttrium aluminum garnet crystal. For this same reason lanthanides are commonly doped into glass materials as absorbers for certain wavelengths of light. Numerous decay channels make lanthanide elements valuable additives - via doping - to metal halide-high intensity discharge (MH-HID) lamps. These lamps are becoming increasingly important commercially due to their high efficiency (about 5 to 6 times better than incandescent light sources). Den Hartog et al.¹ note that, "...transition probabilities of

both the first and second spectra of the rare earths are needed by lighting scientists for diagnostics and modeling of these lamps.”

In astrophysics, *lanthanides* and *transition metals* (the 38 elements in groups 3 through 12 of the d-block on the periodic table) play an important role in our understanding of the universe and its evolution. In the simple model, elements from hydrogen up to iron were created through simple neutron capture. Beyond this, the formation of elements via nucleosynthesis processes becomes unclear and numerous theories exist to explain the processes involved. Spectroscopically observed stellar abundances of certain elements within a star are compared to the nucleosynthesis models in order to contrast observations with the predictions of current theories.

The focus of the laboratory astrophysics work described in this dissertation is on determining atomic data in several lanthanide elements (neodymium, samarium, gadolinium, and praseodymium) and two transition metals (copper and iron) through spectroscopic measurements of laser-ablated metal samples using laser-induced breakdown spectroscopy. Laser-induced breakdown spectroscopy is the application of optical emission spectroscopy (OES) to a laboratory-generated laser-induced micro-plasma. The focus of laboratory astrophysics in general is to make precision laboratory measurements of atomic properties of both atoms and ions that are of interest to observational astronomers.

The application of laboratory astrophysics is imperative in order to get a more accurate understanding of the processes involved in astronomical phenomenon through the comparison of theoretically calculated atomic properties and experimentally measured atomic properties.

Accurate laboratory-acquired atomic data is necessary in order to correct elemental abundance discrepancies in stars, to help resolve anomalies in nucleosynthesis models such as the even-odd effect (where *even* atomic numbered elements appear to have higher abundances in stars than the *odd* numbered elements), to compute stellar matter opacities, and to predict abundances for element-specific emitting species within a star. There are even some unexplained phenomena observed by astrophysicists where stellar abundances are much larger than the theoretical solar models can account for, called *chemically peculiar* (CP) stars. It is within these CP stars that lanthanides are often observed in large over-abundances. Furthermore, some of the oldest stars in our galaxy found in the galactic halo of the Milky Way, the metal deficient halo stars, show increased lanthanide abundances.^{2,3,4}

The current techniques used to determine astrophysically relevant data depend strongly on laboratory astrophysics' ability to provide accurate atomic data. Lawler et al.⁵ in their 2011 paper noted that, "Interest in the spectroscopy of rare earth elements has been rekindled due to applied science needs in lighting research and development and basic science needs in astrophysical studies of stellar spectra." Den Hartog et al.⁶ stated, "Singly ionized gadolinium is one of the remaining Rare Earth species in need of modern measurements." Wahlgren's 2006 paper⁷ states, "...still, various aspects of current research in CP stars underscore the need for both additional and improved data for the lanthanides both for individual lines and large groups of lines." Furthermore, in 2006 Sneden et al.⁸ stated that:

"Greater understanding of the production of the whole range of n-capture elements is essential, and this task cannot be accomplished without the best possible astronomical spectra of n-capture-rich halo stars and continuing progress on laboratory data. Nucleosynthesis theory can be confronted only at the level of accuracy that can be established by abundance analyses. Improving atomic data and stellar spectra go jointly forward in this endeavor."

It is obvious then that without accurate atomic data, the furthering of knowledge concerning certain astrophysical phenomenon like nucleosynthesis processes and abundance determinations is at a standstill.

Of significance to this work are four *lanthanide metals*, neodymium (Nd), samarium (Sm), gadolinium (Gd), praseodymium (Pr), as well as two *transition metals*, iron (Fe) and copper (Cu), which have astrophysical relevance. The four lanthanide elements are found in over-abundance (relative to solar abundances) in certain chemically peculiar (CP) stars and old galactic halo stars.⁷ These and other lanthanides are of large enough importance that the D.R.E.A.M. database (Database on Rare-Earths At Mons University) was created to provide atomic information concerning the wavelengths, oscillator strengths, transition probabilities and radiative lifetimes of lanthanides to observational astronomers.

Copper is found in Ap and Bp stars (the “p” denoting that it is a peculiar case of the common ‘A’ and ‘B’ type main sequence stars), as well as in H I interstellar clouds and galactic halo stars. Copper emission lines have been used as abundance determinations in interstellar H I clouds by Morton and Smith.⁹ The use of copper atomic data from emission lines also helps in the field of plasma physics since copper is used in electrode materials.¹⁰ Copper’s atomic properties are also of interest to atomic theorists because of copper’s single unpaired electron outside of the core.

Determination of iron transition probabilities and other atomic data is so significant to astrophysicists that numerous groups have been dedicated to determining multiple aspects of iron atomic properties through experimental and theoretical methods. The Iron Project (IP), fathered

by M. J. Seaton, is a collaboration of many international scientists in order to compute collisional data for the iron-peak elements in various ionization stages. The Iron Project is a daughter collaboration from the Opacity Project (OP) which involved research groups from the United States, France, the United Kingdom, Germany, and Venezuela focusing on calculating opacities for astrophysically significant stars and formations. The Ferrum Project (FP), organized by S. Johansson, is an international collaboration and its focus is to produce reliable oscillator strengths (f-values) or transition probabilities (A-values) of singly ionized iron lines.

As stated earlier, the most significant hindrance to astrophysicists in this area of research is poor accuracy in atomic data leading to inaccurate calculations in age determinations and over-abundances in CP stars;¹ thus, the need for accurate atomic data is evident.¹¹ In particular, accurate branching fractions (or branching ratios), relative intensities, transition probabilities, atomic lifetimes, oscillator strengths, hyperfine constants, and isotope shifts of both neutral atoms and multiply-ionized atomic species need to be studied. My research aims are to improve existing atomic data and contribute completely new measurements by incorporating the use of laser-induced plasmas to obtain branching ratios (B.R.) from measured relative emission intensities (R.I.).

1.2 – Theory

1.2.1 - Nucleosynthesis

Galactic nucleosynthesis is the process in which nuclides heavier than that of hydrogen are generated in celestial bodies. The history of nucleosynthesis in the galaxy can be revealed by studying the abundances in metal-poor galactic halo stars. Two processes in nucleosynthesis

responsible for the synthesis of nuclides heavier than ^{56}Fe , typically found in supernovae, are the r(apid)-process and the s(low)-process. Figure 1.1 is a diagram from Jorissen et al.¹² exhibiting the abundance levels of elements within our solar system. It is worthwhile to note that the r-process and s-process are believed to be the mechanisms mostly responsible for the creation of heavy elements in the universe.

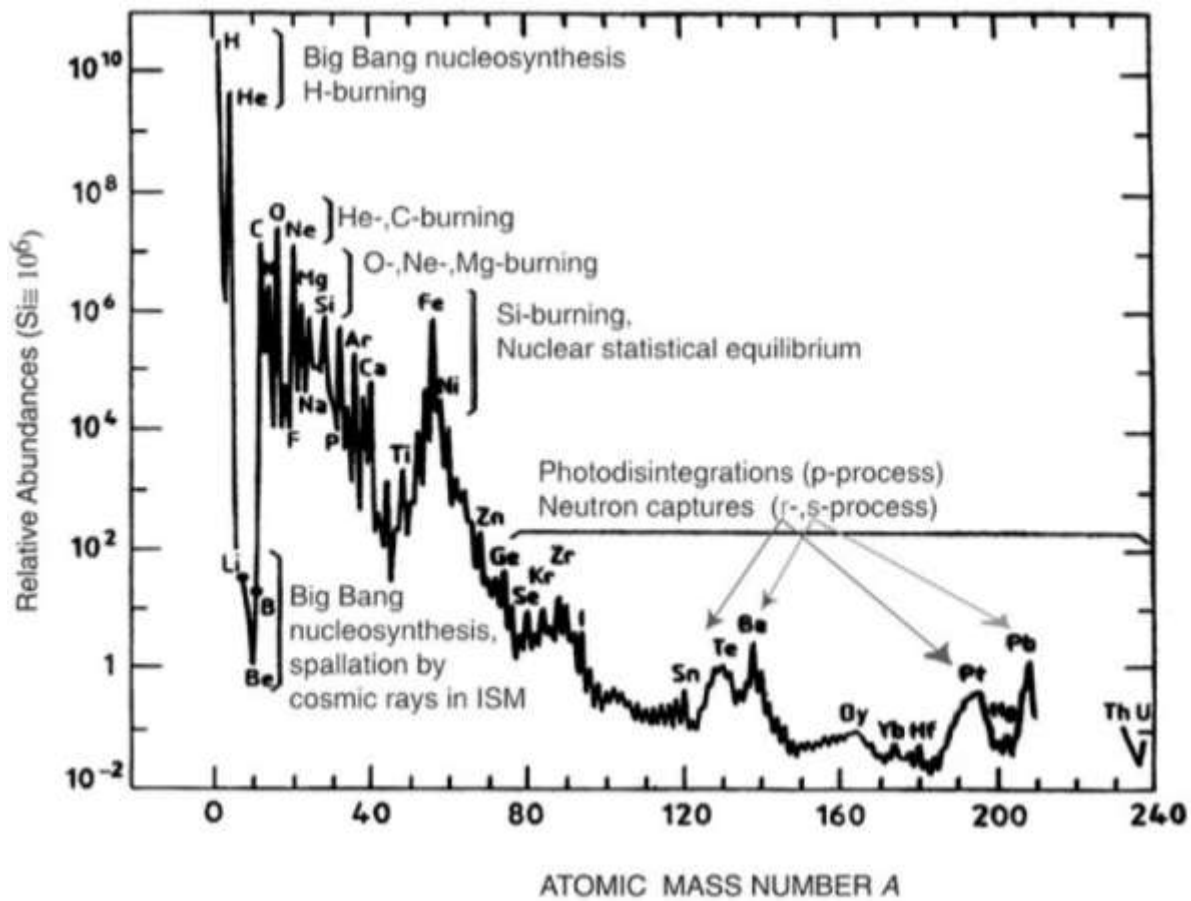
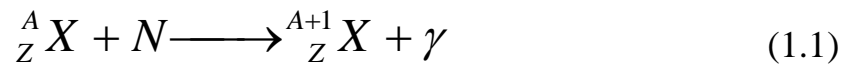


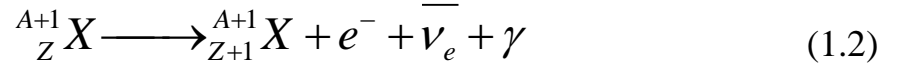
Fig 1.1. A diagram from Jorissen et al.¹² showing abundances of the chemical elements in the solar system and the major nucleosynthesis processes responsible for their production.

Study of the nucleosynthesis r-process allows for an age determination of some of the earliest galactic halo stars. The Milky Way's galactic halo is located on the outer edges, surrounding the disk, and is spherical in shape. This halo region is devoid of the necessary star forming ingredients and is therefore composed of only cooler, dimmer, older stars. This is why the study of such stars is significant, because they contain information from earlier times in our galaxy's star-formation period. The abundances within these halo stars can be helpful in further understanding the nucleosynthesis processes. Halo age determinations are possible by comparing the abundances of heavy elements within the halo stars to other more stable, lighter elements created through neutron capture within the galaxy. One of the difficulties with this comparison is that the transition probabilities for the necessary ionic species – especially the singly ionized species – are poor in accuracy.⁸

Neutron capture occurs when neutrons approach the powerful Coulomb barrier created by large nuclei ($A > 60$). They bypass the barrier, having no electrical charge themselves, and bombard the nucleons within the atom. Capture of these neutrons creates more massive nuclei (increasing the mass number A), the process is shown below in equation 1.1.



These “more massive nuclei” are either stable or unstable against beta-decay (electron emission). In the *s-process*, beta-decay occurs more rapidly than the capture of another incident neutron, resulting in the creation of a new stable element (shown in equation 1.2). When a second neutron capture takes place more rapidly than the onset of beta-decay, the process is called *r-process*.



Heavy elements ($Z > 30$) are of significant importance to astrophysicists studying galactic elemental abundances, stellar age predictions, as well as stellar opacities.¹³ Atomic and molecular data, determined by experimental and theoretical methods, are used in astrophysics in order to compute the opacity of stellar objects as well as determine abundances for elements from the equivalent widths of spectral lines or from spectral synthesis. Accurate atomic data is essential for testing models of *s-process* and *r-process* nucleosynthesis¹⁴ as we have already seen, and to further develop our understanding of the radiative, convective, and gravitational processes that determine the dynamics of migration of these elements from a star's core to its surface.^{15,16,17}

1.2.2 – Stellar Opacities

The full explanation of stellar opacities is beyond the scope of this dissertation and quite complex, but I will mention how opacity can be related to atomic data here. The opacity of a star or gaseous atmosphere can be thought of as the ability of the medium to absorb passing radiation. The absorption of radiation therefore plays an important role as will be shown in chapter two. There are three general types of atomic transitions within molecular, atomic, and ionic species which result in absorption: free-free transitions, bound-free transitions, and bound-bound transitions. Each transition type has its own absorption cross-section and therefore its own opacity coefficient $\kappa(\nu)$. The opacity for bound-bound transitions is dependent upon the density of particles in the absorbing medium, the populations of energized states, and the absorption cross-sections for the various transitions and scattering processes. Note that bound-bound

transitions have the weakest cross-section due to the high temperature within the plasma or star ($T \geq 10^5$ K), therefore bound-bound opacities (contributing approximately 10%) are typically disregarded and ionizational processes therefore dominate. Without derivation, the cross-section, σ_{12} , for an allowed electric-dipole transition between energy levels 1 and 2 is given in equation 1.3 below.¹⁸

$$\sigma_{12} = \frac{m^2 e^2}{16\pi^3 \epsilon_0^2 h^2} \frac{1}{v^2} S_{12} \ln \left(\frac{2mv^2}{E_2 - E_1} \right) \quad (1.3)$$

Here m , e , ϵ_0 , h , v , E_2 , E_1 are the electron mass, electronic charge, permittivity of free space, Planck's constant, electron velocity, energy of level 2 and energy of level 1 respectively. Note that it is related to the electric dipole transition strength S_{12} , which is in turn directly expressed as a function of the Einstein absorption coefficient B_{12} shown in equation 1.4 where all terms are previously expressed above.

$$S_{12} = S_{21} \equiv \sum_{m_j} \sum_{m_i} \left| \left\langle jm_j \mid e\vec{r} \mid im_i \right\rangle \right|^2 = \frac{4\epsilon_0 m h v}{e^2} \cdot B_{12} \quad (1.4)$$

The opacity of free-free and free-bound transitions also depends on typical atomic parameters like the electron density and temperature, but will not be shown here. For more information on stellar opacity see Griem,¹⁹ Mihalas,²⁰ and Carroll.²¹

1.2.3 – Stellar abundances

In order to determine stellar abundances, astronomers concern themselves with a concept called the *curve of growth*. The curve of growth is typically shown as a log-log plot of the

equivalent width versus the number of absorbers in the line of sight. For a given emission line the equivalent width is $W(\lambda)$ and the number of absorbers in the line of sight is given by $N_1 f_{12} d$, where N_1 is the number of atoms in energy state 1 (a.k.a the abundance), f_{12} is the oscillator strength for the transition from level 1 to 2, and d is the optical depth of the observed line of sight. The equivalent width W is a function of the emission line and is expressed in equation 1.5 with I_c and $I_\lambda(d)$ being the line intensity at the central wavelength and the line intensity over the profile from optical depth d .

$$W(\lambda) = \int_{line} \left[\frac{I_c - I_\lambda(d)}{I_c} \right] d\lambda = \frac{e^3}{4\pi\epsilon_0 mc} N_1 f_{12} d \quad (1.5)$$

The form of the curve depends on the width and shape of the particular line. Normalizing the width by the Doppler FWHM allows one to eliminate the width dependence and obtain a dimensionless quantity. Through the use of the Boltzmann and Saha equations, conversion of the number of atoms in energy state i can be made and the total number of atoms (abundance) can be calculated.

A typical curve of growth reveals the optical thickness of the medium. As the number density increases from optically thin (an emitted photon is not typically absorbed before escaping the plasma) towards the optically thick limit (an emitted photon is typically absorbed before escaping the plasma), the log-log plot deviates from linear and begins to flatten out as the number density increases. As the flattening of the curve begins, the slope is no longer linear and the expression for the relationship between the equivalent width and the number of absorbers

changes (no longer being in LTE). This flattening of the curve of growth occurs because of the saturation of the line profile which in turn affects the equivalent width value.²² An example for the Ca II line from a typical star is shown below in figure 1.2

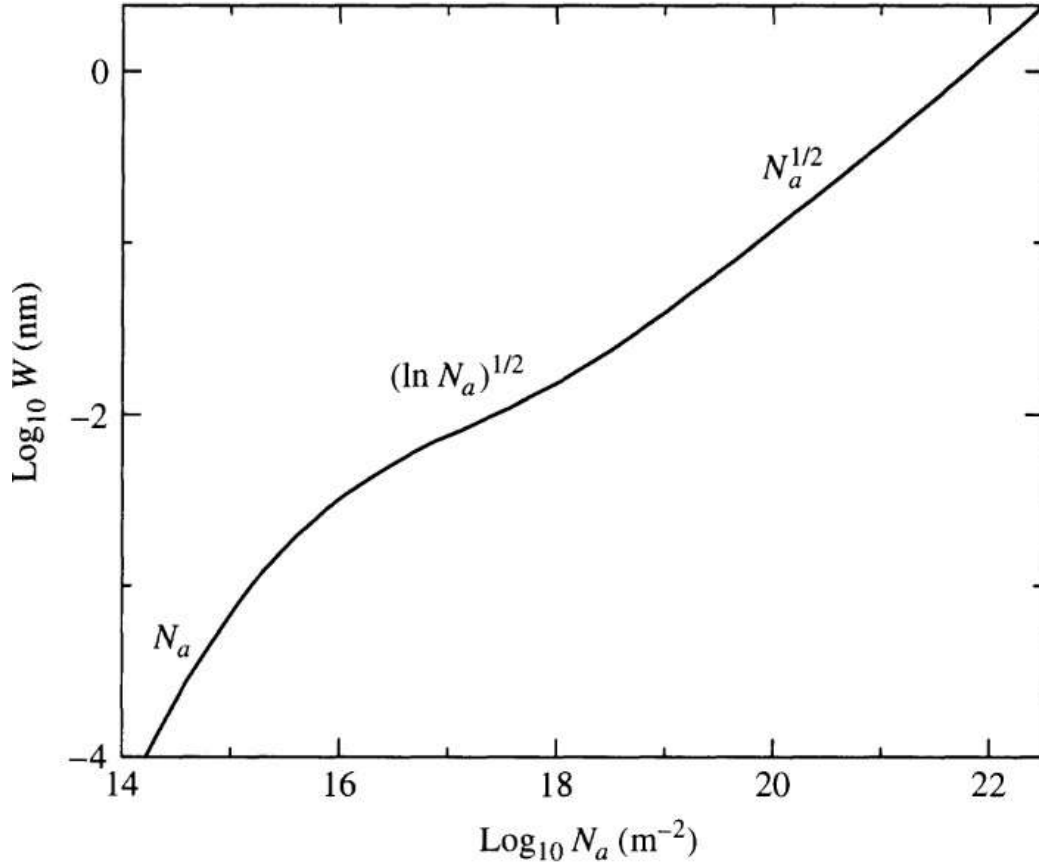


Figure 1.2 (adapted from Carroll's *Introduction to Modern Astrophysics*, 2007).²¹ The curve of growth reveals the approximate trends of the equivalent width's dependence on absorber concentration (N_a). Note that the curve's slope changes non-linearly as the medium becomes optically thick due to larger absorber concentrations.

1.3 - Atomic Data

1.3.1 - Branching Ratios

In an environment free from external interactions such as collisional depopulations, excited atomic energy states must decay to a lower state via an allowed transition. The probability of a transition decaying through a specific single transition, or branch, of the many allowed transitions is defined as a branching ratio. The sum of all branching ratios from a given energy level must equal one by definition. The branching ratio of an emission line can be calculated using equation 1.6

$$\beta_{ji} = \frac{A_{ji}}{\sum A_{ji}} = \frac{I_{ji}}{\sum I_{ji}} = A_{ji} \tau_j \quad (1.6)$$

where β_{ji} is the branching ratio of a given transition from an excited state j to a lower level i , A_{ji} is the Einstein A coefficient for spontaneous emission from j to i which is the rate of that transition, I_{ji} is the observed emission intensity from that transition, and τ_j is the lifetime of the excited state j . Thus, as long as the detection system is not sensitive to photon energy, a careful measurement of the emission intensities of all the transitions out of a given energy level allows the accurate calculation of the branching ratios for all of the observed transitions. However, in some cases accurate measurement of a given emission line is made more difficult or is impossible (e.g. due to line blending or poor S/N). How I deal with such cases will be discussed in more detail in subsequent chapters.

A graphical representation can help to better explain the concept. In singly-ionized neodymium (Nd II) the excited energy level at $23,229.991 \text{ cm}^{-1}$ ($E_j = 2.8805 \text{ eV}$) has 8 possible allowed-transitions (8 branches). Note that in this dissertation I will use the common astrophysics/spectroscopy notation for ionized species. Specifically, singly-ionized Nd (Nd^+) is

referred to as Nd II, doubly-ionized Nd (Nd^{2+}) is referred to as Nd III, etc. The branching ratio is the probability of any single branch's decay relative to the sum of all the allowed branches. In words, it is a measure of the likelihood that a transition will occur along any particular branch. The strength of these branches can be measured by the relative emission line intensity (which is proportional to photon counts or transition rates as long as the detector is not photon energy dependent) as described above or using the theoretical Einstein A-coefficient for spontaneous decay (transition probability). It is important to note that if one branch of the decay tree is missing from the spectrum or immeasurable (particularly a strong branch), then none of the BR can be calculated.

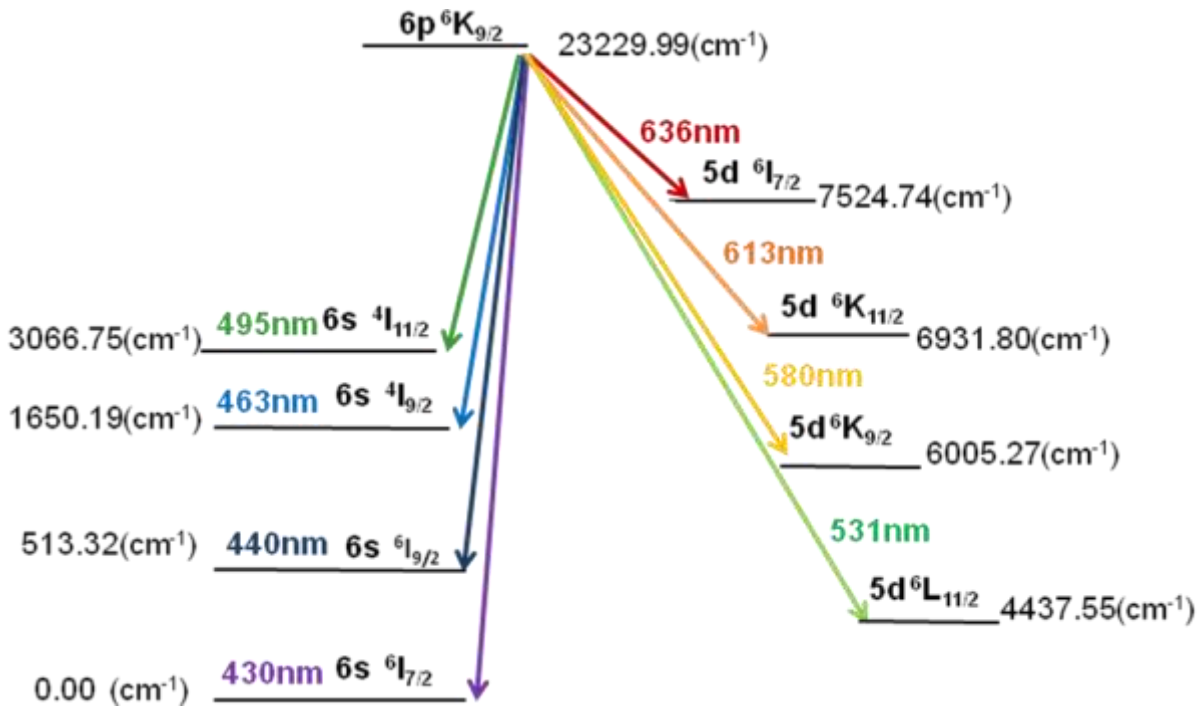


Figure 1.3 shows the eight allowed decay channels from the $6p\ ^6K_{9/2}$ state at $23,229.991\text{ cm}^{-1}$ in singly-ionized neodymium.

1.3.2 – Transition Probabilities

The transition probability A_{ki} is defined as the probability per unit time that an excited atom in energetic state k makes an allowed (electric dipole) transition to a lower level i . Generally the transition probability is considered from the quantum mechanical point of view where one uses time-dependent perturbation theory to determine the electric dipole strength $S_{ji} = S_{ij} = \sum_{m_j} \sum_{m_i} \left| \langle jm_j | e\vec{r} | im_i \rangle \right|^2$, and then relates this to the transition probability by equation 1.7.

$$A_{21} = \frac{1}{g_2} \cdot \frac{16\pi^3 \nu^3}{3\varepsilon_0 hc^3} \cdot S_{21} \quad (1.7)$$

The transition probability for spontaneous emission (A_{21}) is generally related to the coefficient for stimulated emission (B_{21}) using Planck's radiation equation and the principle of detailed balance which are able to derive the expression for spontaneous decay in terms of stimulated emission $A_{21} = \frac{8\pi h \nu^5}{c^4} \cdot B_{21}$. It is common practice for theorists to calculate the transition probability of a given atomic/ionic transition, however this is no easy task for lanthanides, and approximations and specific models must be assumed. In addition, often times the accuracy of a transition is limited due to inaccurate lifetimes, which are also required, as can be seen in equation 1.6.

1.3.3 – Atomic Lifetimes

An atomic lifetime can be loosely defined as the amount of time an atom spends in a given atomic level before spontaneously decaying to another level, but is more correctly defined as the inverse of the sum of the rates of all spontaneous transitions out of the level of interest, shown in equation 1.8.

$$\tau_k^{-1} = \sum_i A_{ki} \quad (1.8)$$

Expressed another way, if at time $t=0$ a system contains $N_j(0)$ atoms in an upper state j characterized by a lifetime τ_j , the rate of change of the population in state j is given by equation 1.9.

$$N_j(t) = N_j(0) \cdot \exp(-t / \tau_j) \quad (1.9)$$

Experimentalists often determine lifetimes with techniques which use time-resolved spectroscopy of the emitted transitions. Some difficulties that arise in this area of research are long waiting periods in order to obtain sufficient quantities of photons from the transition of interest and of course the necessity of measuring phenomena on nanosecond timescales (characteristic of many atomic energy level lifetimes). Lifetimes are commonly measured using three different experimental methods: delay-time measurements, Hanle effect experiments, and beam measurements.

In practice, branching ratios defined by equation 1.6 and lifetimes defined by equation 1.8, whether obtained experimentally or theoretically, are combined to determine transition probabilities, alternately called absolute oscillator strengths, using equation 1.10.

$$A_{ki} = \frac{2\pi e^2}{m_e c \epsilon_o \lambda^2} \cdot \frac{g_i}{g_k} \cdot f_{ik} = \frac{6.67 \times 10^{-5}}{\lambda^2} \cdot \frac{g_i}{g_k} \cdot f_{ik} \quad (1.10)$$

In equation 1.10, g_i is the multiplicity of level i , f_{ik} is the absorption oscillator strength for a transition from a lower level i to an upper level k , A_{ki} is the Einstein A coefficient for spontaneous emission from k to i , and λ is the wavelength (in Angstroms) of the transition. Although the absorption oscillator strength f_{ik} is determined, the value desired by observational astronomers is the “ $\log(gf)$ ” value of the transition, which is just $\log_{10}(gf_{ik})$.

Note that it is not uncommon to encounter the term “transition probability” in experimental or theoretical literature where what is being referred to as a transition probability is not solely the Einstein coefficient for spontaneous emission, A_{ki} , but rather the Einstein coefficient for spontaneous emission multiplied by the upper state degeneracy $A_{ki}g_k$. Although confusing, this convention of reporting Ag is common.

1.3.4 - Oscillator Strength

The oscillator strength of a transition is defined as the number of classical oscillators equivalent to one real atom for a given transition. It can be thought of as the effective number of electrons per atom for a particular transition. In introductory atomic physics texts^{23,24,25} the oscillator strength is commonly derived by considering the energy loss $\frac{dW}{dt}$ of a classical two-level damped-oscillatory atomic system and comparing it to its quantum mechanical equivalent. The classical rate of energy loss (equation 1.11),

$$\frac{dW_{CLASSIC}}{dt} = -\gamma W \approx -\frac{1}{4\pi\epsilon_0} \cdot \frac{2}{3} \cdot \frac{e^2}{c^3} \left(\frac{1}{2} x_0^2 \omega_0^4 \right) \quad (1.11)$$

where x_0 , ω_0 , γ are the equilibrium position of the oscillator, the singular oscillatory frequency of the atom, and damping constant, respectively, is then compared to the quantum mechanical equivalent for transitions induced by electric dipole radiation (equation 1.12).

$$\frac{dW_{QM}}{dt} = -\frac{1}{4\pi\epsilon_0} \cdot \frac{4}{3} \cdot \frac{\omega_{ji}^4}{c^3} \left| \langle j | e\vec{r} | i \rangle \right|^2 = A_{ji} \cdot \frac{h}{2\pi} \omega_{ji} \quad (1.12)$$

To account for the fact that the 1-dimensional classical oscillator is able to only emit radiation at one single frequency ω_0 while the quantum oscillator can emit at many frequencies ω_{ji} , each 1-D classical oscillator must be endowed with an oscillator strength $-f_{ji}$ (negative for emission) to make the two comparable. To account for the fact that the quantum radiator can polarize in three-dimensions while the classical is capable of only one, one should multiply the classical energy loss rate by $-3 \cdot \frac{h}{2\pi} \omega_{ji} \cdot f_{ji}$. Upon comparing the two rate equations presented in 1.11 and 1.12, it can be seen that $A_{ji} = -3\gamma f_{ji}$, and therefore the oscillator strength can be defined as equation 1.13.

$$f_{ji} = -\frac{2}{3} \cdot \frac{m}{e^2} \frac{4\pi^2}{h^2} \cdot \left| \langle j | e\vec{r} | i \rangle \right|^2 \cdot \frac{h\omega_{ji}}{2\pi} = -\frac{4\pi}{3} \frac{m}{he^2} \cdot S_{ji} \cdot \omega_{ji} \quad (1.13)$$

Direct determination of oscillator strengths in emission experiments incorporates using absolute intensities of a spectral emission line per unit cross-sectional area I_{ji} (equation 1.14).

$$I_{ji} = N_j A_{ji} \cdot h\nu_{ji} \cdot d \quad (1.14)$$

The spontaneous emission coefficient A_{ji} is then related to the oscillator strength through equation 1.10. In 1.14, N_j is the upper level population, $h\nu_{ji}$ the difference in energy of the transition and d is the optical depth in the line of sight.

In practice, the method of obtaining calculated oscillator strengths f of an atomic/ionic transition from experimentally determined lifetimes τ and branching ratios β is to use equation 1.15,¹⁸

$$f_{ki} = -1.499 \times 10^{-7} \cdot \lambda^2 \cdot \left(\frac{g_i}{g_k} \right) \left(\frac{\beta_{ki}}{\tau_k} \right) \quad (1.15)$$

where the wavelength λ is in units of Angstroms, the upper state lifetime τ_k is in nanoseconds, and g_k and g_i are the statistical weights (multiplicities) of the energy levels in consideration which depend on the total angular momentum for the level i as $g_i = 2J_i + 1$. Given that atomic data is often too inaccurate for the accuracy needed in astrophysics, refined experimental branching ratios and lifetimes are needed.

When applying absorption or dispersion techniques to determine f -values, the equivalent width method is sometimes employed (see section 1.2.3 for abundances). Also the integrated line intensity can be used to determine oscillator strengths which require high resolution spectrometry in cases when the line width is small. For dispersion methods, one incorporates the Hook method making use of the index of refraction and its proportion to the oscillator strength.

The most important atomic property in astrophysics is the oscillator strength for a transition of known wavelength. The difficulty with calculating transition probabilities in lanthanides is the huge number of levels arising from the atomic configuration involving an open 4f shell, and the situation is complicated even more by relativistic effects, configuration interactions, and the lack of accurate experimentally determined energy levels for many low-lying levels.²⁶

1.4 – LIBS Ability to Determine Atomic Data

The experimental method which I have used to determine the necessary atomic data for my research goals is called laser-induced breakdown spectroscopy (LIBS) (further discussed in chapter 2). The process involves focusing an intense pulsed laser beam onto a target. Heating of the surface leads to evaporation and ionization of the material in the focal region of the pulsed laser. Observation of the emitted radiation from the resulting plasma by time-resolved spectroscopy allows a wavelength-dependent measurement of the intensity of light, from which atomic data may be calculated as described above in section 1.3. The high temperature of the laser-induced plasma is able to excite not only atomic transitions but more importantly transitions from excited energy levels in multiply-ionized species.

1.4.1 – Atomic Data from LIBS

In practice, LIBS is a relatively new technique for use in the laboratory astrophysics field. As such, few studies have actually employed the sole use of LIBS for atomic data measurements.

Some advantages LIBS has over other emission techniques is that LIBS is able to easily populate highly-excited states in ions which other techniques cannot, and this occurs almost instantaneously and without multi-step laser-excitation. Very limited sample preparation is required for spectral acquisition and all the target elements can be easily ablated. The entire process from absorption of pulsed laser energy on the target to detected spectrum takes only seconds. The spectral range of observation from the plasma is limited only by the detection system.

LIBS is not perfect, and in some cases not the optimum technique to measure certain atomic properties (i.e. atomic lifetimes or absolute line intensities). Some problems with using plasmas for spectroscopy (LIBS and also high energy discharge tubes) is that determination of accurate atomic level populations and ionization populations using the Boltzmann and Saha equations respectively, depends on the plasma conditions. The plasma must be in local thermodynamic equilibrium (LTE) or some partial form of it (PLTE) in order to use these distributions. In practice, this just means that one must have knowledge about the plasma dynamics and parameters such as the number density of electrons using McWhirter's criterion (see chapter 2). Also, optical thickness can affect strong lines such as resonance lines (transitions into the ground state) and a few low-lying metastable states. Lastly, the largest difficulties arise from the inability to resolve blended emission lines in the spectrum and measure weak emissions due to relatively strong noise.

Nonetheless, previous work has shown that LIBS is a technique capable of measuring atomic data. In 2007, Ortiz et al.²⁷ calculated transition probabilities (TP) for 41 lines in singly ionized copper (Cu II). Incorporating previously determined lifetimes, they converted the relative

TP to an absolute scale and reported uncertainties ranging from 6 – 13%. In 2009, I was able to show that transition probabilities are measureable in Nd II emission lines using our LIBS apparatus.²⁸ In that study, branching ratios from a level at 23,229.991 cm^{-1} in Nd II were determined and compared to previously determined values as a method for optimizing laser-induced plasma parameters in my apparatus. Absolute emission intensities for the transitions were measured to determine branching ratios for comparison with previous studies using alternate methods and ion sources.^{27,32,34,64} Our work was in agreement with previously reported data.

1.5 - Other Methods

1.5.1 - Branching Ratios Measurements

Experimentally, lifetimes and branching ratios can be determined via multiple methods which can excite the necessary atomic transitions. Branching ratios (sometimes called branching fractions) are most frequently measured by laser-induced plasmas, fast ion beam-laser beam measurements,²⁹ and Fourier Transform Spectroscopy (FTS) methods used with hollow cathode discharge tubes.³⁰

Laser-induced breakdown spectroscopy (LIBS) is a time-resolved optical emission of neutral and multiply-ionized atoms within a weakly-ionized (~10% ionized) micro-plasma generated from absorption of electromagnetic radiation via a pulsed laser source. The resulting atomic emission from the micro-plasma reveals characteristic information pertinent to identification and quantification of the emitting species derived from the ablated sample. The specimen used as the ablation target can be in gas, liquid, or solid form; or even a combination of

these. This sample-versatility is one of the advantages LIBS has over other techniques in atomic emission spectroscopy (AES). When applying this technique, the plasma radiation must be focused and directed into the detector and the use of such optics requires careful spectral calibration (since absorption is wavelength dependent). This usually accrues a few percent error to the measurements. Typical accuracies for relative emission lines and branching ratios are on the order of ~10%.²⁷ One of the greatest advantages in LIBS is that it is able to excite and ionize many levels of the given species simultaneously. However, this also gives rise to its greatest weaknesses: the inability to resolve strong oversaturated lines, the simultaneous presence of hundreds to thousands of emission lines lead to irresolvable-blended neighboring lines, as well as the inability to measure some weak emission lines because of strong background emission and noise. Another advantage is that at early times in the plasma evolution, temperatures can exceed 50,000 Kelvin, leading to the production of highly-ionized atoms in some lanthanides metals, which is something that almost no other emission technique can duplicate.

Fast-ion-beam laser induced fluorescence (FIBLIF) methods incorporate an ion vapor source, typically derived from a thermo-oven source or hot-cathode tube, which is accelerated and directed into overlap with an incident tunable-laser beam. The laser beam is tuned to resonance with a single atomic transition. This method produces a spectrum containing only a few well-resolved lines making measurements easier in terms of broadening and blending (except for lines from the same multiplet state) compared to LIBS or FTS. Another advantage in FIBLIF, due to the single upper energy level excitation, is that every visible emission line in the spectrum can be accurately noted as having originated from that given upper state – removing any potential ambiguity which is sometimes seen in theoretical determinations. However, it

requires a very stable laser source and ion beam source. This technique is capable of accuracies comparable to FTS methods.

Hollow cathode discharge tubes used with Fourier Transform Spectroscopy (FTS) incorporate interference effects derived from varying path lengths of a given radiation source (the hollow cathode discharge) by an interferometer. The spatial modulation frequency distinguishes between different wavelengths and the signal is compared with a laser of known frequency. A spectrum is obtained from the resulting interferogram by means of a fast Fourier transform. With this method a large spectral range is acquired. One of the limits is the detector calibration required, which yields an accuracy of a few percent. As with LIBS, in the discharge tube all energy levels are simultaneously excited, so the problems of saturation and line blending are equally prevalent.

1.5.2 - Lifetime Measurements

A large variety of techniques have been developed and utilized for lifetime measurements in the nanosecond region. Among these, fast ion beam laser technique (FIBLAS) and time-resolved beam-foil spectroscopy (BFS) are common. Other methods for determination of ns lifetimes are based on different kinds of techniques, some using laser-induced plasmas and laser-induced fluorescence techniques (LIF). In such measurements, the laser-induced plasma serves as an ion source characterized by a high temperature ($\sim 10,000$ K), electron density, and ionization degree.

In the fast ion beam-laser technique, an ion vapor source, typically derived from a thermo-oven source or hot-cathode tube, is accelerated and directed into overlap with an incident

tunable-laser beam. Typically these beams are perpendicular to each other. The short-lived upper level lifetimes (on the order of nanoseconds) are determined from time-resolved fluorescence signals recorded by a fast detection system. This method, although able to produce accurate lifetimes, is limited by the ionization ability of the ion source. Usually only singly ionized species are produced.

In time-resolved beam-foil spectroscopy a beam of ions is accelerated through a thin foil (50-200 nm) and emerges in a range of low-lying ionization states. The valence electrons are distributed over many different energy states, most of which result in decay via photon emission. This method too is limited by its ability to excite only certain low-level ionization states.

Pulsed laser excitation followed by time-resolved fluorescence measurements is limited to levels which can be reached from the ground state (typically the only statistically populated state in an ion beam). However step-wise or multi-photon excitation can allow higher excitation energies. This technique usually provides good accuracies (~5%), but the ionization population is limited to the step-wise ability of the lasers.

Laser-induced fluorescence is the optical emission from atomic and molecular excitation via absorption of electromagnetic radiation (laser beam). In order to measure the atomic lifetime of a given energy level, a laser-induced excitation is used to excite a transition above the level of interest and a resulting spontaneous decay into this level allows for photon detection. The lifetime can then be measured by single-photon detection from the decay out of the level of interest to a lower-lying state. Utilizing the cascade-photon-coincidence (CPC) technique the lifetime of the level can be measured. The CPC technique uses observation of “start-photons”

signifying a transition into the level of interest (λ_{start}) from some higher-lying state, detected by a photo-multiplier tube (PMT) or an avalanche photodiode (APD) and “stop-photons” signaling a transition out of the level of interest (λ_{stop}) detected by a second APD. A careful measurement of the time delay between these two observed photons is then made. A histogram plot of the measured delay times between the start and stop photons reveals the lifetime of the given level.

In this dissertation, I will present a scheme for utilizing the cascading-photon coincidence method in order to determine the atomic lifetime of the $4s5d\ ^3P_2$ state in singly ionized gallium, which is required in order to check against abundance calculations in HgMn stars. However, no direct measurements of atomic lifetimes were performed. Therefore, it will be essential to use the experimental lifetimes obtained by other researchers to calculate oscillator strengths using the experimental branching ratios reported in this dissertation

I will now briefly summarize some of the most relevant work performed by others on the elements studied in this dissertation.

1.5.3 – Copper

In 1986, semi-empirical calculations for Cu II lifetimes were determined by Theodosiou.³¹ To make the calculations he used the Hartree-Slater approximation and experimentally determined energies which gave rise to lifetimes having uncertainties of 10%; however there were large discrepancies with previously reported experimental results. To date, theirs is the largest contribution to Cu II lifetimes, having hundreds of level’s lifetimes presented. In 1999, Donnelly et al.³² calculated oscillator strengths using an LS-coupling approximation and a relativistic approach.

Experimental lifetimes in Cu I and Cu II, determined using beam-foil spectroscopy, were measured by Cederquist et al.³³ in 1984, and Curtis et al.³⁴ in 1976. Maleki et al.³⁵ used beam-gas spectroscopy in 1976 to measure lifetimes. Kono and Hattori,³⁶ in 1982, as well as Osherovich et al.,³⁷ in 1981, used the delay-coincidence technique for lifetimes determinations. In 1994, Crespo Lopez-Urrutia et al.³⁸ determined branching ratios from an intensity-calibrated spectrometer and previously determined lifetimes. Pinnington et al.³⁹ in 1997 used laser excitation of a fast beam for lifetimes and also calculated some lifetimes with the relativistic Hartree-Fock method (HFR). Biemont et al.⁴⁰ in 2005 measured transition probabilities using laser-induced plasma and also experimentally calculated lifetimes using HFR method. Federman et al.⁴¹, in 2008, used beam-foil technique to determine lifetimes in Cu II and P II. In 2009 lifetimes and oscillator strengths were determined by Brown et al.⁴² using beam-foil experiments.

1.5.4 – Iron

In 1993, Nahar and Pradhan⁴³ contributed large scale calculated oscillator strengths (OS) and cross sections in Fe II using LS coupling schemes to the Opacity Project. In 1994, Nahar⁴⁴ calculated OS for allowed transitions in Fe II for the Opacity Project. His reported data show better agreement than the current experimental results from NIST and Kurucz databases. In 2005, Correge and Hibbert⁴⁵ calculated OS for two strong lines arising in the B and D Wigt blobs of η Carinae which were compatible with prior estimations. Calculations of OS in the near-infrared emissions of Fe II were compiled by Correge and Hibbert⁴⁶ in 2006 with arguably more accurate OS listed. The full list of theoretical calculations in Fe is too long to list here, but I've shown some works that are relevant to my research interests above.

For experimental considerations in Fe, I will not exhaust the list because the list is far too extensive; I will however point out a few key reports significant to my research. Absorption oscillator strengths for six transitions in the vacuum-ultra-violet region in Fe II were reported by Mullman et al.⁴⁷ in 1996 having accuracies to within 10%. Bergeson et al.⁴⁸ showed new experimental BR and TP from 56 transitions in Fe II spectrum, in 1996 using FTS and a hollow cathode discharge tube (HCD) with agreements between 1.6% – 14.8% compared to other theoretical work. In 2000, Schnabel and Kock⁴⁹ determined radiative lifetimes and BR in Fe II using LIF. Schnabel et al.⁵⁰ used LIF to measure radiative lifetimes in 21 levels of Fe II and calculated the corresponding transition probabilities for the given lines in 2004 with 6% error for strong lines. Absolute transition probabilities are derived from experimentally determined BR and lifetimes in some forbidden transition in Fe II by Hartman et al.⁵¹ in 2003. Melendez and Barbury⁵², in 2009, presented oscillator strengths in Fe II for 142 lines between 400-800 nm, with which they made abundance comparisons which were found to be in excellent agreement with known solar abundances.

1.5.5 – Gadolinium

Theoretical lifetimes were calculated using core-polarization effects for Gd III in 2002 by Biemont et al.⁵³ and transition probabilities were calculated as a result.

Transition probabilities in Gd II were determined in 1998 by Bergstrom et al.⁵⁴ and an improved solar abundance was given using LIF. In 1997, Miyabe et al.⁵⁵ measured lifetimes and BR in Gd I via the delayed photoionization method. 74 lifetimes were determined and their corresponding BR tabulated from their work. Zhang et al.⁵⁶ measured 20 experimental lifetimes

in Gd II and 5 in Gd III using LIF-LIBS, the results showing good agreement with prior published data. In 2003, lifetimes of Gd I and Gd II were determined by Xu et al.⁵⁷ using LIF for 38 levels. The resulting uncertainties were within 5%. Den Hartog et al.⁵⁸ in 2006 measured lifetimes with accuracies to 5% in Gd II for 63 lifetimes using LIF and 611 transition probabilities were constructed from BR using FTS. Branching ratios with better accuracy than prior investigations were determined for 1290 lines in Gd I using Fourier Transform Spectroscopy (FTS) and converted to absolute transition probabilities using lifetimes from LIF by Lawler et al.⁵⁹ in 2011.

1.5.6 – Neodymium

Bord⁶⁰ calculated oscillator strengths in Nd III in 2000 using an HFR method, the accuracy of his results are mostly better than 5%. In 2003, Xu et al.⁶¹ calculated radiative lifetimes and determined the same lifetimes experimentally for 24 levels of Nd II yielding 107 transition probabilities, they were found to be in good agreement with one another having uncertainties less than 10%.

In 1985, Ward et al.⁶² measured lifetimes for 24 levels in Nd II using a laser-ion beam technique which at the time were of greater accuracy than prior developments. In 2002, Zhang et al.⁶³ measured lifetimes using LIF in Nd III which was used as a confirmation of HFR calculations of the lifetimes and shown to be in good agreement. Nd II was studied by Den Hartog et al. in 2003, in which atomic data determined with accuracies better than 5% were reported.⁶⁴ In their research, over 700 lines were resolved and a collection of transition probabilities were presented from experimentally determined branching ratios and atomic

lifetimes using laser-induced fluorescence. Lifetimes of 15 levels Nd I and 18 levels in Pr I were determined by Biemont et al.⁶⁵ in 2004 using LIF for abundance calculations. In 2007, Rehse, along with Li et al., measured branching ratios of 46 levels in Nd II using laser-induced fluorescence (LIF) at the University of Western Ontario in Canada.¹⁵ Along with previously determined lifetimes, transition probabilities and oscillator strengths were presented for 430 transitions. Laser-induced fluorescence was employed by Xu et al.¹⁴ in order to determine atomic data for 24 levels of Nd II, 17 of which were previously undetermined. Hartree-Fock methods were employed for calculating theoretical branching ratios. The resulting data were found to be in agreement with previous works and data previously unmeasured had discrepancies less than or equal to 10%. In particular, 6 levels had large discrepancies around 30% attributed to inaccurate eigenvalue compositions.⁶⁶

1.5.7 – Praseodymium

Theoretical OS were determined in Pr II by Palmeri et al.⁶⁷ for comparison to Chemically Peculiar stars (CP). The relativistic Hartree-Fock method was employed.

Radiative lifetimes were found in 1974 by Andersen and Sorensen⁶⁸ for Pr II, Tm II, Lu II, and Ce III using beam-foil method and compared to OS from Corliss for abundance determinations. Biemont et al.⁶⁹ in 2001 determined radiative lifetimes in Pr III using LIP-LIF in order to excite the highly ionized species. Also theoretical lifetimes were calculated using HFR method and compared with previous known experimental results which were in good agreement. Fourier Transform Spectroscopy (FTS) was employed by Dolk et al.⁷⁰ in 2001, lifetimes were determined in Pr and Nd and resulting in transition probabilities for many emission lines. Again

in 2003, Biemont et al.⁷¹ combined experimentally determined lifetimes with theoretically determined OS for transition probabilities of 150 lines in Pr II. Lifetimes of 15 levels Nd I and 18 levels in Pr I were determined by Biemont et al.⁶⁵ in 2004 using LIF for abundance calculations. In 2005, Furmann et al.⁷² reported 42 experimentally determined energy levels in Pr II using LIF. Li et al.⁷³ in 2007 found 32 energy levels and transition probabilities for 260 lines incorporating previously determined lifetimes of Pr II by fast-ion-beam laser-induced-fluorescence. The data were found to have uncertainties within 10%.

1.5.8 – Samarium

In 1988, Vogel et al.⁷⁴ determined 18 levels of Sm II for solar abundance comparisons using beam-laser techniques. Lifetimes of six levels of samarium III were determined using LIF by Biemont et al.⁷⁵ in 2002 and showed excellent agreement with empirical data. In 2002, Scholl et al.⁷⁶ measured radiative lifetimes in Sm II for 82 levels via the beam-laser technique. The data had uncertainties less than 7% and transition probabilities for 35 lines were reported. Xu et al.⁷⁷ reported LIF-determined lifetimes for 47 levels in Sm II and HFR transition probabilities for 162 transitions with good agreement to previous reports. Rehse et al.⁷⁸ in 2005 studied branching ratios and oscillator strengths for 69 levels in Sm II using a 10 keV fast-ion-beam laser-induced-fluorescence spectroscopy (FIBLAS). The branches detected between 250 and 850 nm were determined with accuracies on the order of 10%. Experimentally determined branching ratios were combined with previously determined atomic lifetimes to calculate the transition probabilities and oscillator strengths for 608 transitions. In 2006, Lawler et al.⁷⁹ showed Sm II lifetimes with accuracy to 5% for 212 levels using LIF methods. These were combined with BR from FTS and a total of 900 transition probabilities for lines in Sm II were determined. In 2010,

Zhang et al.⁸⁰ provided lifetimes for 79 odd-parity levels in Sm I using LIF with an atomic beam by laser ablation. Good agreement was shown.

1.6 - Summary and Scope of Dissertation

The fact that LIBS applied to laboratory astrophysics for atomic data is a relatively new technique means that little work has been done in this field using this technique (as seen by the references above). The value of what LIBS brings to the “atomic data table” is substantial – the ability to excite hundreds to thousands of transitions within an ionic state of an atom in a single experiment and the ability to do this almost instantaneously. There is currently a good framework of atomic databases from other techniques for comparison between data. The need for astrophysically relevant atomic data is presently in “full bloom”. The lanthanides neodymium, samarium, gadolinium, praseodymium, as well as two main transition metals - copper and iron - were studied in this work and the resulting branching ratios presented in an effort to help satiate the need for accurate atomic data in stellar models.

In this chapter I have overviewed my work and provided much of the necessary background information. Chapter 2 discusses the theory behind laser-induced plasma and its formation, various models that are used in order to apply certain equilibrium distributions, and certain plasma parameters which allow for optimum data acquisition. Chapter 3 will describe the experimental side of the research: detailing the apparatus, various experimental parameters, and explanation of some of the equipment. Chapter 4 focuses on the various sources of uncertainty encountered in this work: calibrating the optical system, resolving emission lines, and other sources of uncertainty. Chapter 5 reports on the results of our gadolinium and neodymium

radiative parameters; presenting my newly measured values and comparing the reported values with previous works. In Chapter 6 I will list measured radiative parameters from neodymium and praseodymium. I again compare my results with prior works. Chapter 7 shows the results of the copper and iron investigations by tabulating the data and comparing them to previous works. In Chapter 8 I conclude by surveying some possible ideas for future work in this area of research including a system for lifetime measurements using LIBS only, incorporating laser-induced fluorescence with laser-induced breakdown spectroscopy for lifetime measurements and single-level excitations, and incorporating parabolic mirrors into the ablation chamber for greater light-collection efficiency. Appendix 1 tabulates large lists of relative intensities from my research which had no published lifetimes to my knowledge. Appendix 2 is a listing of the programs and codes which I wrote in order to help quickly analyze the data and sort it.

¹ E.A. Den Hartog, K.A. Bilty, J.E. Lawler, “Radiative lifetimes of neutral gadolinium,” J. Phys. B **44**, 292-314 (2011).

² C. Sneden, “Evidence of multiple *r*-process sites in the early galaxy: new observations of CS 22892-052,” Astrophys. J. **533**, L139-L142 (2000).

³ J. Westin, C. Sneden, B. Gustafsson, J.J. Cowan, “The *r*-process-enriched low-metallicity giant HD 115444,” Astrophys. J. **530**, 783-799 (2000).

⁴ J.J. Cowan, “The chemical composition and age of the metal-poor halo star BD +17°3248,” Astrophys. J. **572**, 861-879 (2002).

⁵ J.E. Lawler, K.A. Bilty, E.A. Den Hartog, “Atomic transition probabilities of Gd I,” J. Phys. B **44**, (2011).

-
- ⁶ E.A. Den Hartog, J.E. Lawler, C. Sneden, J.J. Cowan, “Improved laboratory transition probabilities for Gd II and application to the gadolinium abundances of the sun and three 4-process rich, metal-poor stars,” *Astrophys. J. Suppl. Ser.* **167**, 292-314 (2006).
- ⁷ G.W. Wahlgren, “The lanthanide elements in stellar and laboratory spectra,” *Phys. Scr.* **T100**, 22-36 (2002).
- ⁸ C. Sneden, J.E. Lawler, J.J. Cowan, “Galactic cosmochronometry from radioactive elements in the spectra of very old metal-poor stars,” *Phys. Scr.* **T100**, 15-21 (2002).
- ⁹ D.C. Morton and W.H. Smith, “A summary of transition probabilities for atomic absorption lines formed in low-density clouds,” *Astrophys. J. Suppl. Ser.* **26**, 333–363 (1973).
- ¹⁰ J.R. Crespo López-Urrutia, B. Kenner, T. Neger, H. Jäger, “Absolute transition probabilities of Cu II lines,” *J. Quant. Spectrosc. Radiat. Transfer* **52**, 111 (1994).
- ¹¹ E. Biemont and P. Quinet, “Recent advances in the study of lanthanide atoms and ions,” *Phys. Scr.* **T105**, 38-54 (2003).
- ¹² A. Jorissen, “Atomic and molecular data for stellar physics: former successes and future challenges,” *Phys Scr.* **T112**, 73-86 (2004).
- ¹³ E. Biemont, “Recent advances and difficulties in oscillator strength determination for rare-earth elements and ions,” *Phys. Scr.* **T119**, 55-60 (2005).
- ¹⁴ G. Wallerstein, J.I. Iben, P. Parker, A.M. Boesgaard, G.M. Hale, A.E. Champagne, C.A. Barnes, F. Kappeler, V.V. Smith, R.D. Hoffman, F.X. Timmes, C. Sneden, R.N. Boyd, B.S. Meyer, D.L. Lambert, “Synthesis of the elements in stars: forty years of progress,” *Rev. Mod. Phys.* **69**, 995-1084 (1997).

-
- ¹⁵ R. Li, S.J. Rehse, T.J. Scholl, A. Sharikova, R. Chatelain, R.A. Holt, S.D. Rosner, “Fast-ion-beam laser-induced-fluorescence measurements of branching fractions and oscillator strengths in Nd II,” *Can. J. Phys.* **85**, 1343-1378 (2007).
- ¹⁶ G. Michaud, “Diffusion processes in peculiar A stars,” *Astrophys. J.* **160**, 641-658 (1970).
- ¹⁷ K.C. Smith, “Chemically peculiar hot stars,” *Astrophys. Space Sci.* **237**, 77-105 (1996).
- ¹⁸ A.P. Thorne, *Spectrophysics*, Chapman and Hall, London, (1974).
- ¹⁹ H.R. Griem, *Principles of Plasma Spectroscopy*, Cambridge University Press, Cambridge, (1997).
- ²⁰ D. Mihalas, *Stellar Atmospheres*, W.H. Freeman and Company, San Francisco, (1970).
- ²¹ B.W. Carroll and D.A. Ostlie, *An Introduction to Modern Astrophysics*, 2nd ed., Pearson Education Inc, San Francisco, (2007).
- ²² F. LeBlanc, *An Introduction to Stellar Astrophysics*, John Wiley and Sons, Ltd. West Sussex, (2010).
- ²³ B.W. Shore and D.H. Menzel, *Principles of Atomic Spectra*, John Wiley & Sons, Inc. New York, (1968).
- ²⁴ E.U. Condon and G.H. Shortley, *The Theory of Atomic Spectra*, Cambridge University Press, New York, (1977).
- ²⁵ S. Svanberg, *Atomic and Molecular Spectroscopy Basic Aspects and Practical Applications*, 4th ed., Springer-Verlag Berlin, Berlin, (2004).
- ²⁶ E. Biémont, “Recent advances and difficulties in oscillator strength determination for rare-earth elements and ions,” *Phys. Scr.* **T119**, 55–60 (2005).

-
- ²⁷ M. Ortiz, R. Mayo, E. Biemont, P. Quinet, G. Malcheva, K. Blagoev, "Radiative parameters for some transitions arising from $3d^9 4d$ and $3d^8 4s_2$ electronic configurations in the Cu II spectrum," J. Phys. B **40**, 167-176 (2007).
- ²⁸ S.J. Rehse and C.A. Ryder, "Laser-induced breakdown spectroscopy for branching ratio and atomic lifetime measurements in singly-ionized neodymium and gallium," Spectrochim. Acta B **64**, 974-980 (2009).
- ²⁹ H.L. Xu, S. Svanberg, R.D. Cowan, P.H. Lefebvre, P. Quinet, E. Biemont, "Theoretical and experimental lifetime and oscillator strength determination in singly ionized neodymium," Mon. Not. R. Astron. Soc. **346**, 433-440 (2003).
- ³⁰ R.S. Maier and W. Whaling, "Transition probabilities in NdII and the solar neodymium abundance," J. Quant. Spectrosc. Radiat. Trans. **18**, 501-505 (1977).
- ³¹ C.E. Theodosiou, "Lifetimes of singly excited states in Cu^+ and Ag^+ ," J. Opt. Soc. Am. B **3**, 1107 (1986).
- ³² D. Donnelly, A. Hibbert, K.L. Bell, "Oscillator strengths for transitions in singly-ionized copper," Phys. Scr. **59**, 32-48 (1999).
- ³³ H. Cederquist, S. Mannervik, M. Kisielinski, P. Forsberg, I. Martinson, L.J. Curtis, P.S. Ramanujam, "Lifetimes of some excited levels in Cu I and Cu II," Phys. Scr. **T8**, 104-107 (1984).
- ³⁴ L.J. Curtis, B. Engman, I. Martinson, "Lifetime Measurements in Cu I and Cu II," Phys. Scr. **13**, 109-113 (1976).
- ³⁵ L. Maleki, D.G. King, C.E. Head, T.N. Lawrence, *Beam-foil spectroscopy*. Edited by I.A. Sellin and D.J. Pegg. Plenum Publ. Corp., New York, (1976).

-
- ³⁶ A. Kono and S. Hattori, “Lifetimes and transition probabilities in Cu II,” *J. Opt. Soc. Am.* **72**, 601-605 (1982).
- ³⁷ A.L. Osherovich, G.L. Plekhotkina, V.R. Obidin, “Excited state radiation lifetimes of copper atoms and ions,” *Opt. Spectrosc. (USSR)* **50**, 576 (1981).
- ³⁸ J.R. Crespo López-Urrutia, B. Kenner, T. Neger, H. Jäger, “Absolute transition probabilities of Cu II lines,” *J. Quant. Spectrosc. Radiat. Trans.* **52**, 111-114 (1994).
- ³⁹ E.H. Pinnington, G. Rieger, J.A. Kernahan, E. Biemont, “Beam-laser measurements and relativistic Hartree-Fock calculations of the lifetimes of $3d^9 4p$ levels in Cu II,” *Can. J. Phys.* **75**, 1-9 (1997).
- ⁴⁰ E. Biemont, K. Blagoev, J. Campos, R. Mayo, G. Malcheva, M. Ortiz, P. Quinet, “Radiative parameters for some transitions in Cu II and Ag II spectrum,” *J. Elect. Spectr. Rel. Phen.* **144–147**, 27–28 (2005).
- ⁴¹ S.R. Federman, L.J. Curtis, M. Brown, S. Cheng, R.E. Irving, S. Torok, R.M. Schectman, “Oscillator strengths for ultraviolet transitions in P II and Cu II,” *J. of Phys: Conference Series* **130**, (2008).
- ⁴² M.S. Brown, S.R. Federman, R.E. Irving, S. Cheng, L.J. Curtis, “Lifetime and oscillator strengths for ultraviolet transitions in singly-ionized copper,” *Astrophys. J.* **702**, 880-883 (2009).
- ⁴³ S.N. Nahar and A.K. Pradhan, “Atomic data for opacity calculations: XX. Photoionization cross sections and oscillator strengths for Fe II,” *J. Phys. B* **27**, 429-446 (1994).
- ⁴⁴ S.N. Nahar, “Atomic data from the Iron Project VII. Radiative dipole transition probabilities for Fe II,” *Astron. Astrophys.* **293**, 967-977 (1995).

-
- ⁴⁵ G. Corregge and A. Hibbert, “The oscillator strengths of Fe II,” *Astrophys. J.* **627**, L157–L159 (2005).
- ⁴⁶ G. Corregge and A. Hibbert, “Oscillator strengths of near-infrared lines of Fe II,” *Astrophys. J.* **636**, 1166–1171 (2006).
- ⁴⁷ K.L. Mullman, M. Sakai, J.E. Lawler, “Absolute transition probabilities for the a^6D to y^6P multiplet of Fe II,” *Astron. Astrophys. Suppl. Ser.* **122**, 157-161 (1997).
- ⁴⁸ S.D. Bergeson, K.L. Mullman, M.E. Wickliffe, J.E. Lawler, U. Litzen, S. Johansson, “Branching fractions and oscillator strengths for Fe II transitions from the $3d^6(^5D) 4p$ subconfiguration,” *Astrophys. J.* **464**, 1044-1049 (1996).
- ⁴⁹ R. Schnabel and M. Kock, “Time-resolved nonlinear laser-induced fluorescence technique for a combined lifetime and branching-fraction measurement,” *Phys. Rev. A* **63**, 12519 (2000).
- ⁵⁰ R. Schnabel, M. Schultz-Johanning, M. Kock, “Fe II lifetimes and transition probabilities,” *A&A* **414**, 1169–1176 (2004).
- ⁵¹ H. Hartman, A. Derkatch, M.P. Donnelly, T. Gull, A. Hibbert, S. Johansson, H. Lundberg, S. Mannervik, L.-O. Norlin, D. Rostohar, P. Royen, P. Schel, “The FERRUM Project: Experimental transition probabilities of [Fe II] and astrophysical applications,” *A&A* **397**, 1143–1149 (2003).
- ⁵² J. Melendez and B. Barbury, “Both accurate and precise gf-values for Fe II lines,” *A&A* **497**, 611-617 (2009).
- ⁵³ E. Biemont, G. Kohnen, P. Quinet, “Transition probabilities in Gd III,” *A&A* **393**, 717-720 (2002).

-
- ⁵⁴ H. Bergstrom, E. Biemont, H. Lundberg, A. Persson, “Transition probabilities for Gd II and a new determination of the solar abundance of gadolinium,” *A&A* **192**, 335-337 (1998).
- ⁵⁵ M. Miyabe, I. Wakaida, T. Arisawa, “Measurement of radiative lifetime and branching ratio of Gd I using three-step resonance ionization spectroscopy,” *Z. Phys. D* **39**, 181-187 (1997).
- ⁵⁶ Z.G. Zhang, A. Persson, Z.S. LI, S. Svanberg, J. Zhankui, “Lifetime measurements in Gd II and Gd III using time-resolved laser spectroscopy,” *Eur. Phys. J. D* **13**, 301-304 (2001).
- ⁵⁷ H. Xu, Z. Jiang, S. Svanberg, “Radiative lifetimes of Gd I and Gd II,” *J. Phys. B* **36**, 411–417 (2003).
- ⁵⁸ E.A. Den Hartog, J.E. Lawler, C. Sneden, J.J. Cowan, “Improved laboratory transition probabilities for Gd II and application to the gadolinium abundances of the sun and three r-process rich metal-poor stars,” *Astro. J. Suppl.* **167**, 292-314 (2006).
- ⁵⁹ J.E. Lawler, K.A. Bility, E.A. Den Hartog, “Atomic transition probabilities of Gd I,” *J. Phys. B* **44**, 095001 (2011).
- ⁶⁰ D.J. Bord, “Ab initio calculations of oscillator strengths and Lande factors for Nd III,” *Astron. Astrophys. Suppl. Ser.* **144**, 517-522 (2000).
- ⁶¹ H.L. Xu, S. Svanberg, R.D. Cowan, P.H. Lefebvre, P. Quinet, E. Biemont, “Theoretical and experimental lifetime and oscillator strength determination in singly ionized neodymium,” *Mon. Not. R. Astron. Soc.* **346**, 433-440 (2003).
- ⁶² L. Ward, O. Vogel, A. Arnesen, R. Hallin, A. Wannstrom, “Accurate experimental lifetimes of excited levels in Nd II,” *Phys. Scr.* **31**, 161-165 (1985).

-
- ⁶³ Z.G. Zhang, S. Svanberg, P. Palmeri, P. Quinet, E. Biemont, “Measurement of lifetimes by laser-induced fluorescence and determination of transition probabilities of astrophysical interest in Nd III,” *A&A* **385**, 724-732 (2002).
- ⁶⁴ E.A. Den Hartog, J.E. Lawler, C. Sneden, J.J. Cowen, “Improved laboratory transition probabilities for Nd II and application to the neodymium abundances of the Sun and three metal-poor stars,” *Astrophys. J. Suppl. Ser.* **148**, 543-566 (2003).
- ⁶⁵ E. Biemont, P. Quinet, S. Svanberg, H.L. Xu, “Experimental lifetime determination in neutral praseodymium and neodymium,” *J. Phys. B* **37**, 1381–1389 (2004).
- ⁶⁶ H.L. Xu, S. Svanberg, R.D. Cowan, P.H. Lefebvre, P. Quinet, E. Biemont, “Theoretical and experimental lifetime and oscillator strength determination in singly ionized neodymium,” *Mon. Not. R. Astron. Soc.* **346**, 433-440 (2003)
- ⁶⁷ P. Palmeri, P. Quinet, Y. Fremat, J.-F. Wyart, E. Biemont, “Theoretical oscillator strengths in Pr III and application to some CP stars,” *Astrophys. J. Suppl. Ser.* **129**, 367-376 (2000).
- ⁶⁸ T. Andersen and G. Sorensen, “Determinations of atomic lifetimes for the rare earth ions Pr II, Tm II, Lu II Ce III,” *Solar Physics* **38**, 343-350 (1974).
- ⁶⁹ E. Biemont, H.P. Garnir, P. Palmeri, P. Quinet, Z.S. Li, Z.G. Zhang, S. Svanberg, “Core-polarization effects and radiative lifetime measurements in Pr III,” *Phys. Rev. A* **64**, 02250 (2001).
- ⁷⁰ L. Dolk, G.M. Wahlgren, H. Lundberg, Z.S. Li, U. Litzen, S. Ivarsson, I. Ilyin, S. Hubrig, “The presence of Nd and Pr in HgMn stars,” *A&A* **385**, 111-130 (2002).

-
- ⁷¹ E. Biemont, P.-H. Lefebvre, P. Quinet, S. Svanberg, H.L. Xu, “Radiative lifetime measurements and oscillator strength determination for transitions in singly ionized praseodymium (Pr II),” *Eur. Phys. J. D* **27**, 33–41 (2003).
- ⁷² B. Furmann, D. Stefanska, J. Dembczynski, E. Stachowska, “New levels and hyperfine structure evaluation in singly ionized praseodymium,” *Phys. Scr.* **72**, 300–308 (2005).
- ⁷³ R. Li, R. Chatelain, R.A. Holt, S.J. Rehse, S.D. Rosner, T.J. Scholl, “Oscillator strength measurements in Pr II with the fast-ion-beam laser-induced-fluorescence technique,” *Phys. Scr.* **76**, 577–592 (2007).
- ⁷⁴ O. Vogell, B. Edvardsson, A. Wannstroml, A. Arnesen, R. Hallin, “Radiative lifetimes in Sm II and the solar samarium abundance,” *Phys. Scr.* **38**, 567-572 (1988).
- ⁷⁵ E. Biemont, H.P. Garnir, U. Litzen, K. Nielsen, P. Quinet, S. Svanberg, G.M. Wahlgren, Z.G. Zhang, “Radiative lifetime and oscillator strength determinations in Sm III,” *A&A* **399**, 343–349 (2003).
- ⁷⁶ T.J. Scholl, R.A. Holt, D. Masterman, R.C. Rivest, S.D. Rosner, A. Sharikova, “Measurement of radiative lifetimes in Sm II,” *Can. J. Phys.* **80**, 1621 (2002).
- ⁷⁷ H.L. Xu, S. Svanberg, P. Quinet, H.P. Garnir, E. Biemont, “Time-resolved laser-induced fluorescence lifetime measurements and relativistic Hartree-Fock calculations of transition probabilities in Sm II,” *J. Phys. B* **36**, 4773–4787 (2003).
- ⁷⁸ S.J. Rehse, R. Li, T.J. Scholl, A. Sharikova, R. Chatelain, R.A. Holt, S.D. Rosner, “Fast-ion-beam laser-induced-fluorescence measurements of spontaneous-emission branching ratios and oscillator strengths in Sm II,” *Can. J. Phys.* **84**, 723-769 (2006).

-
- ⁷⁹ J.E. Lawler, E.A. Den Hartog, C. Sneden, J.J. Cowan, “Improved laboratory transition probabilities for Sm II and application to the samarium abundances of the sun and three r-process-rich metal-poor stars,” *Astrophys. J. Suppl. Ser.* **162**, 227–260 (2006).
- ⁸⁰ W. Zhang, Y. Feng, Z. Dai, “Radiative lifetime measurements of odd-parity moderately excited levels belonging to J=0,1,2,3 series in Sm I,” *J. Opt. Soc. Am. B* **27**, 2255 (2010).

Chapter 2 – Laser-Induced Breakdown Theory

2.1 - Introduction

Laser-induced breakdown spectroscopy (LIBS) is the time-resolved spectroscopy of optical emission from neutral and multiply-ionized atoms within a weakly-ionized (~10% ionized) micro-plasma generated from absorption of electromagnetic radiation via a pulsed laser source. The term “laser-induced breakdown” was coined by E. Damon and R. Thomlimson in 1963¹. The resulting atomic emission from the micro-plasma reveals characteristic information pertinent to identification and quantification of the emitting species derived from the ablated sample. The specimen used as the ablation target can be in gas, liquid, or solid form or even a combination of these. This sample-versatility is one of advantages LIBS has over other techniques in atomic emission spectroscopy (AES).

The basic processes involved in the creation of an ionized-plasma plume generated via laser-induced breakdown can be characterized in three steps:

- (i) An incident pulsed-laser beam focused optically on the target sample, achieving an irradiance (power per unit area) sufficient to heat the sample to vaporization and to subsequently ionize (“breakdown”) the vapor forming a micro-plasma ($\sim 10^5\text{K}$)
- (ii) Excitation and ionization of the atoms/ions within the plasma plume.
- (iii) Detection and analysis of the characteristic photons emitted from the atoms/ions within the plasma after a suitable delay time.

2.1.1 - Laser Parameters

The laser parameters which are significant for plasma formation in LIBS experiments typically include: pulse energy, pulse duration, pulse repetition rate, beam mode quality (ability to focus), and laser wavelength. Given these parameters, it is common for LIBS researchers to use solid-state lasers like the neodymium:yttrium-aluminum garnet (Nd:YAG) laser because of their high peak power density, good mode quality, fundamental infrared wavelength, and the ability to easily switch between wavelengths by using the second, third, or fourth harmonics. In my research we have employed a Nd:YAG laser (Spectra Physics, LAB-150-10) operating at its fundamental wavelength of 1064 nm with peak output energy of 650 mJ/pulse. Table 1 below reveals the typical range of attributes for Nd:YAG lasers.

Nd:YAG harmonics	Wavelength (nm)	Pulse duration (ns)	Energy/pulse (J)
1 st harmonic	1064	5 -10	1 - 3
2 nd harmonic	532	4 - 8	0.5 - 2
3 rd harmonic	354.7	4 - 8	0.2 – 0.7

Table 2.1 above shows the harmonics of the Nd:YAG laser and their corresponding parameters.

Other solid-state lasers commonly used in LIBS² besides the Nd:YAG are ArF excimer, CO₂, KrF excimer, N₂, ruby, and XeCl excimer. The range of attributes for the typical LIBS lasers (excluding the femtosecond lasers) are listed in table 2 below.

	Minimum	Maximum
Wavelength (nm)	193 (ArF excimer)	10,600 (CO ₂ repetitive)
Pulse Duration (ns)	3 (N ₂ laser)	10 ⁶ (Ruby laser)
Energy / pulse (mJ/pulse)	0.1 (N ₂ laser)	5x10 ⁵ (Ruby Normal Pulse)

Table 2.2 above shows the range of important parameters for typical lasers used in LIBS studies.

When a high peak-power nanosecond laser pulse is focused onto a solid sample, the irradiance can lead to rapid local heating, intense evaporation, and ablation of material. Laser pulse energies required to ignite a plasma are dependent upon mode quality, wavelength, and pulse duration. Laser irradiances (power/unit area) are usually on the order of 10^9 to 10^{11} W/cm² given laser pulse energies of 10-100 mJ. Of course, the degree of irradiance necessary to ablate the sample is dependent upon what type of sample is targeted and the phase (solid, liquid, gas, plasma) that the sample is in. The breakdown threshold of the ablating material depends strongly upon reflectivity at the laser wavelength (in solids) and sample density. In general, nanosecond laser pulse irradiances required to ablate solids³ are $\sim 10^6$ W/cm², liquids are $\sim 10^8$ W/cm², and gases/aerosols are on the order of $\sim 10^8$ W/cm².

Beam mode quality is important for its effect on the ability to focus the beam to smaller waists (producing higher beam irradiances) as well as producing uniform (for low TEM modes) or non-uniform heating (for more complex modes). This is particularly useful when increasing the beam fluence (absorbed energy per area). By focusing the laser beam to a smaller waist at the target's surface, the fluence is increased; this is limited only by the quality of the laser's mode. The ablation site can be as small or as large as one can make the beam's waist, while still providing enough energy to heat the sample sufficiently. However, on average the mass of material ablated is on the order of nanograms to picograms, with crater diameters ~ 100 μ m.

2.1.2 – Laser-Matter Interactions

There are three scenarios in which laser-induced plasmas are generated, each depending on the laser's pulse duration and the absorbed irradiance. First, the nanosecond regime

incorporates irradiances below 10^8 W/cm^2 which involves a three-step phase transition from solid to liquid to vapor to plasma. The second situation involves picosecond laser pulses with higher irradiances typically around 10^{12} W/cm^2 . This picosecond regime involves both thermal heating of the material as well as non-thermal heating of the target. Non-thermal heating occurs in Coulomb explosions. Thirdly, femtosecond pulses, having typical irradiances in excess of 10^{13} W/cm^2 , induce plasmas by processes dominated by non-thermal heating methods. Because my experiment utilizes a nanosecond pulse laser, I will now explain the theory of plasma production in the nanosecond regime in more detail.

2.1.2.1 – Nanosecond Regime

When an incident nanosecond laser pulse is optically focused to a small area ($\sim 10^{-3} \text{ cm}^2$) via a simple lens and subsequently absorbed by a solid target, thermal heating ensues around the targeted area. Provided that the initial edge of the absorbed laser pulse has an irradiance sufficient to raise the temperature of the target material to its boiling point and overcome the latent heat of fusion, melting of the surface layer begins. Melting can be defined as the loosening of crystalline bonds due to lattice vibrations to a less structured organization. Laser light is absorbed by the electrons within the atoms of the metal and are excited to a higher energy level into the conduction band. These electrons eventually collide with lattice vibrations (phonons) and thermally excite the vibrations, thus heating the area. When the amplitude of these vibrations is larger than some certain fraction of the lattice spacing, generally accepted to be near 10% of the lattice spacing,⁴ bond breaking and melting then follows. In nanosecond laser ablation, the target's inability to dissipate the absorbed radiation from the point of contact faster than it absorbs further radiation is what causes local increased temperatures leading to melting. Typical

absorption depths are on the order of 10's of nanometers, whereas the diameter of the laser is approximately 100 micrometers, therefore a 1 dimensional model of the temperature below the surface of the sample can be considered for thermal propagation.⁵ The heat conduction equation written below (equation 2.1) shows how the temperature just under the surface varies in time.

$$\frac{\partial T(x,t)}{\partial t} = \frac{\partial}{\partial x} \left(\left(\frac{\kappa}{\rho \cdot c_p} \right) \frac{\partial T(x,t)}{\partial x} \right) + \frac{\alpha}{\rho \cdot c_p} \left[I_0(t) \cdot (1 - R) \cdot \exp(-\alpha x) \right] \quad (2.1)$$

I is the laser irradiance, T is the temperature within the target, x , t , κ , c_p , ρ , α denote the distance below the surface of the sample, the time, thermal conductivity, heat capacity at constant pressure, mass density, and absorption coefficient respectively. The last term in brackets is the laser irradiance having R as the reflectivity of the surface, $I_0(t)$ the incident irradiance at the surface, and α , t , x are described above. The reflectivity is generally 1 for metals but during the melting process can deviate to 0.1 during laser ablation processes. The process of radiation absorption leading to melting of the lattice structure takes place on the order of 10^{-13} s (or picoseconds) for most metals.⁶

Melting occurs near the surface of the target after sufficient energy to overcome the latent heat of fusion is absorbed. Typical melting temperatures for common Earth metals are around one to two thousand Kelvin at standard temperature and pressure (STP), with common latent heat of fusions around 10^2 J/g. The onslaught of pressure from the incident pulsed laser creates a large pressure gradient on the surface of the target. This pressure raises the melting temperature and allows the material to absorb more energy before melting compared to regular STP

conditions. As a result of the incident pressure some particulates are ejected from the surface and are reheated above the sample surface. The focal spot size is on the order of 10^{-1} mm^2 (or $10^5 \mu\text{m}^2$) and therefore the region which was melted is localized to a spot size approximately $\sim 100 \mu\text{m}$ in diameter.

The transition from liquid to vapor follows directly due to the continued absorption of the laser pulse, which has an approximate duration of 10 nanoseconds. Some common metals at STP have boiling points and latent heats of vaporization near 2000 – 3000 K and 2000 - 5000 J/g respectively. When the temperature in the sample is large enough, the phase transition into vapor becomes significant and the resulting vapor pressure can be expressed by equation 2.2 below⁷.

$$p_{vap}(T_S) = p_0 \cdot \exp\left(\frac{L_V \cdot (T_S - T_B)}{R \cdot T_S \cdot T_B}\right) \quad (2.2)$$

P_{vap} is the vapor pressure at the surface, T_S is the surface temperature, T_B denotes the boiling point at original pressure p_0 , L_V is the latent heat of vaporization, and R is the ideal gas constant.

Particle Ejection and Evaporation

Simultaneous to the melting and evaporation processes, some of the target matter is blown off of the sample's surface due to the large radiation pressure. When the ablated mass and vaporized material is ejected into a gas atmosphere, shockwaves are produced by the compression of the surrounding gas. This ablated material will later mix with the vaporized matter above the surface of the target forming a plume. The plume consists of neutrals and multiply-ionized atoms and molecules, as well as excited particulates of various sizes. Within the

plume, laser absorption continues to further excite and ionize the atomic species. Continued heating and ionization is exponentially increased by inverse bremsstrahlung (IB) leading to a cascade effect (or avalanche effect) of liberated electrons. Heating of the plume leads to further dissociation, excitation, and ionization of even the cooler ejected matter. Eventually the threshold for electron density leading to a plasma is realized. Laser absorption is maximized when the frequency of the plasma is equal to the frequency of the laser radiation. The expansion of the plume in nanosecond laser pulses is fueled by the absorption of the radiation and the rate of expansion is increased until the laser pulse ceases.

Plasma Production

Continued absorption of the laser energy by free electrons and ionized species through the inverse bremsstrahlung process leads to the creation of more free electrons. The increase of free electrons raises the electron number density as well as the temperature within the plasma; both of which are important quantities for theoretical quantification of emission line intensities. The elapsed time between the absorption of the incident laser beam to the vaporization and ionization of the sample material is on the order of 10's of ns, which is also the duration of the incident laser beam used in this research.

Electron cascading within a laser-induced ionized gas/plasma results from a two-step process. The two steps are cascade ionization (equation 2.3) and multiphoton absorption (equation 2.4). If at least one free electron is present in the focal volume of the incident laser beam, the breakdown can initiate. Causes for the production of the initial free electron can be due to cosmic ray ionization or the liberation of an electron from an atom via the absorption of

simultaneous-multiple photons from the laser source itself (multiphoton ionization). Inverse bremsstrahlung then increases the energy of the electron, i.e. photon absorption causes the free electron(s) to accelerate and gain energy. The energetic electron(s) then collide with other atoms causing further ionization. The remaining bound electrons continue to absorb energy from the laser, repeating the above collision process and thus causing an exponential increase in the number of free electrons. Typically, irradiances on the order of $10^6 - 10^{10} \text{ W/cm}^2$ are required to initiate breakdown within the target. The collision process, responsible for cascade breakdown is represented in equation 2.3 below.



Above, M is the neutral species, M^{+} is the ionized species, e^{-} represents an electron, and e^{-*} is an electron with higher initial velocity.

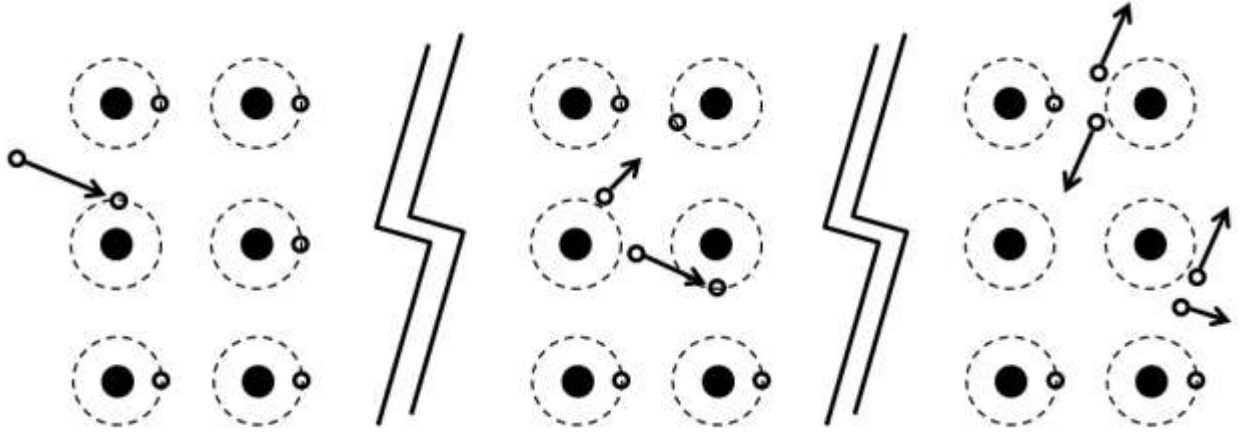
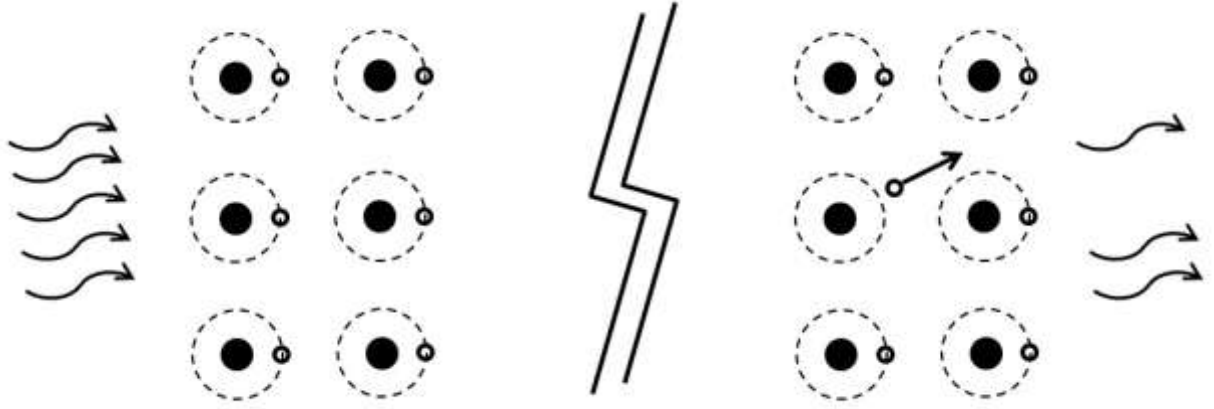


Figure 2.1 above shows a single highly-energetic free electron (seed electron) incident from the left colliding with a second bound electron. The result is that both are liberated with less energy due to momentum conservation. After some time of accelerating in the intense electric field of the laser pulse, the electrons have sufficient energy to again liberate two more electrons, thus creating four liberated electrons from the initial one. This process is called impact ionization and is one of the main mechanisms which leads to avalanche ionization in the laser-induced plasma.

In the multiphoton absorption process an atom simultaneously absorbs multiple photons whose collective energies are sufficient to ionize the atom, thus freeing an electron. This process is represented in equation 2.4 below, where M is the neutral species with bound electrons, n is the number of simultaneously absorbed photons, h is Planck's constant and ν the frequency of the absorbed photons. It is worth noting that of the two electron generation processes, inverse bremsstrahlung is by far the principle process in contributing to the exponential growth of liberated electrons within the plasma plume





In figure 2.2 above, multi-photon absorption is shown with an incident number of photons from the left approaching a lattice structure of atoms and bound electrons. After the absorption of multiple photons by an atom the electron is liberated leaving behind an ion.

Breakdown via the increase of electron density occurs for longer laser wavelengths ($\lambda > 1000 \text{ nm}$) because of a few initial electrons within the focal volume which initiate the avalanche of further liberated electrons. For shorter wavelengths ($\lambda < 1000 \text{ nm}$) multiphoton ionization is the responsible process for the creation of the seed electrons and again electron avalanche follow. In both cases the avalanche is driven by the inverse bremsstrahlung process which scales according to the equation 2.5 below.

$$\sigma_{IB} \sim \lambda^3 \left(1 - \exp \left[-hc / \lambda k_B T \right] \right) \quad (2.5)$$

Above σ_{IB} denotes the inverse bremsstrahlung cross section, λ , h , c , k_B , T are the laser wavelength, Planck's constant, speed of light, Boltzmann's constant, and temperature respectively.

Plasma Expansion and Cooling

A plasma is a many-particle ionized gas consisting of free electrons, ions, and atoms or molecules characterized by its long-range collective behavior. The charged particles comprising the plasma are coupled by self-generated and self-consistent electric and magnetic fields.⁸ The accepted percentage of ionization within a collection of species which constitutes it as a weakly-ionized plasma is 10%, often seen in LIBS. In local thermodynamic equilibrium (LTE) there are two main parameters which describe the plasma and most of its characteristics: the electron density (N_e) and the electron temperature (T_e). These plasma parameters are of significant interest to atomic physicists and plasma physicists since they play such a significant role in determining other properties like velocity distribution of the species, ionization populations, and radiational distributions within the plasma. The graph below depicts the various types of plasma often encountered in science and contrasts them according to the two main parameters.

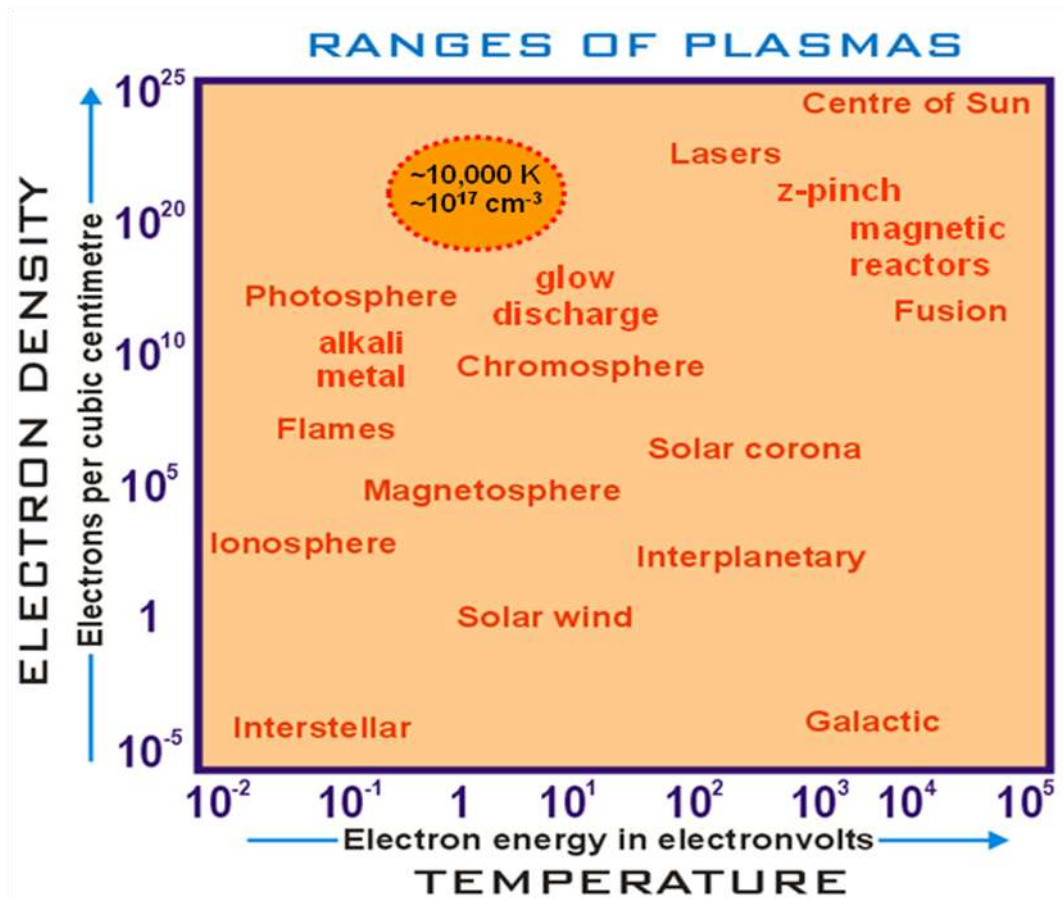


Figure 2.3 above shows some various forms of plasma and their electron densities and electron temperatures. Note that laser-induced plasmas fall within the region encompassed by the dashed-oval near the top.

The initial creation of the plasma plume and expansion occurs on the order of $< 25 \text{ ns}$ for nanosecond laser pulses following the peak of the nanosecond laser pulse and can last up to a few milliseconds depending on the laser pulse used. The evolution of the plasma occurs as follows. The ablated material expands at speeds near supersonic, establishing a shock wave which propagates away from the ablation site. Then, after the extinguishment of the laser pulse and the consequent constituent excitations, the plume begins to reduce its expansion velocity resulting from interactions with the surrounding atmospheric or buffer gas, and slows down to

speeds less than that of sound. The plasma then cools down by self-absorption (quenching) and recombination between electrons and ions, which generates neutral species after the extinction of the plasma. In nanosecond laser pulses, the plasma is reheated by absorbing the laser radiation, thus elongating the plasma lifetime. The entire process, from absorption of the laser pulse until plasma exhaustion, has a duration on the order of microseconds to milliseconds depending on the laser duration. A graphical representation of the entire process is shown below in figure 2.4

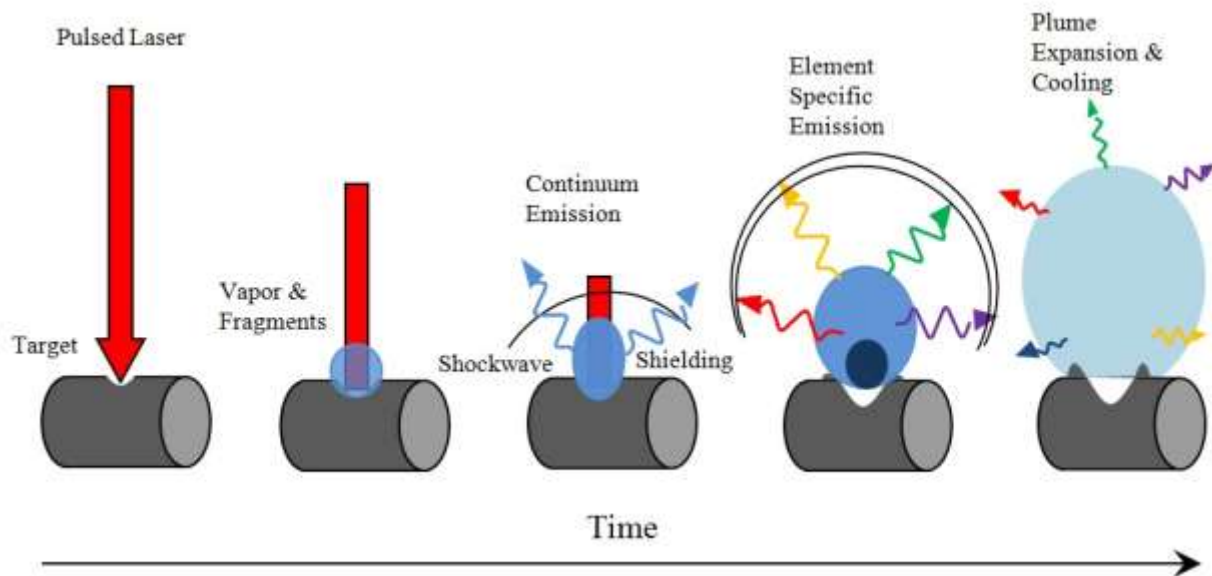


Fig 2.4. A chronological schematic of the plasma formation and target ablation process in LIBS. The thick red arrow represents the laser pulse and its length is representative of the pulse duration.

Plasma shielding of nanosecond laser pulses causes the target's surface temperature and the crater depth to vary in time nonlinearly. At first the target is heated in a linear fashion until plasma formation initiates. When the plasma frequency (equation 2.6) matches or exceeds the frequency of the laser radiation the plasma begins to absorb radiation and blocks (or shields) the target from further absorption of radiation since it becomes opaque to the laser light. The strong

absorption of the laser beam causes an elongation of the plasma plume in the direction of the incident beam. Because of the shielding, there is a decrease in the rate of surface heating and an eventually halting altogether.

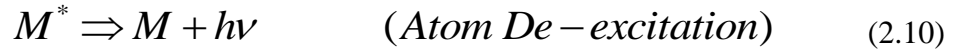
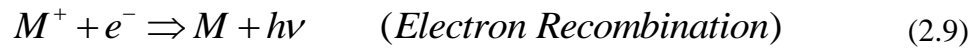
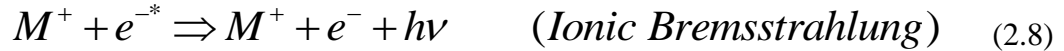
$$\omega_{plasma} = \sqrt{e^2 N_e / \epsilon_0 m_e} = 56.4 \cdot \sqrt{N_e} \quad (2.6)$$

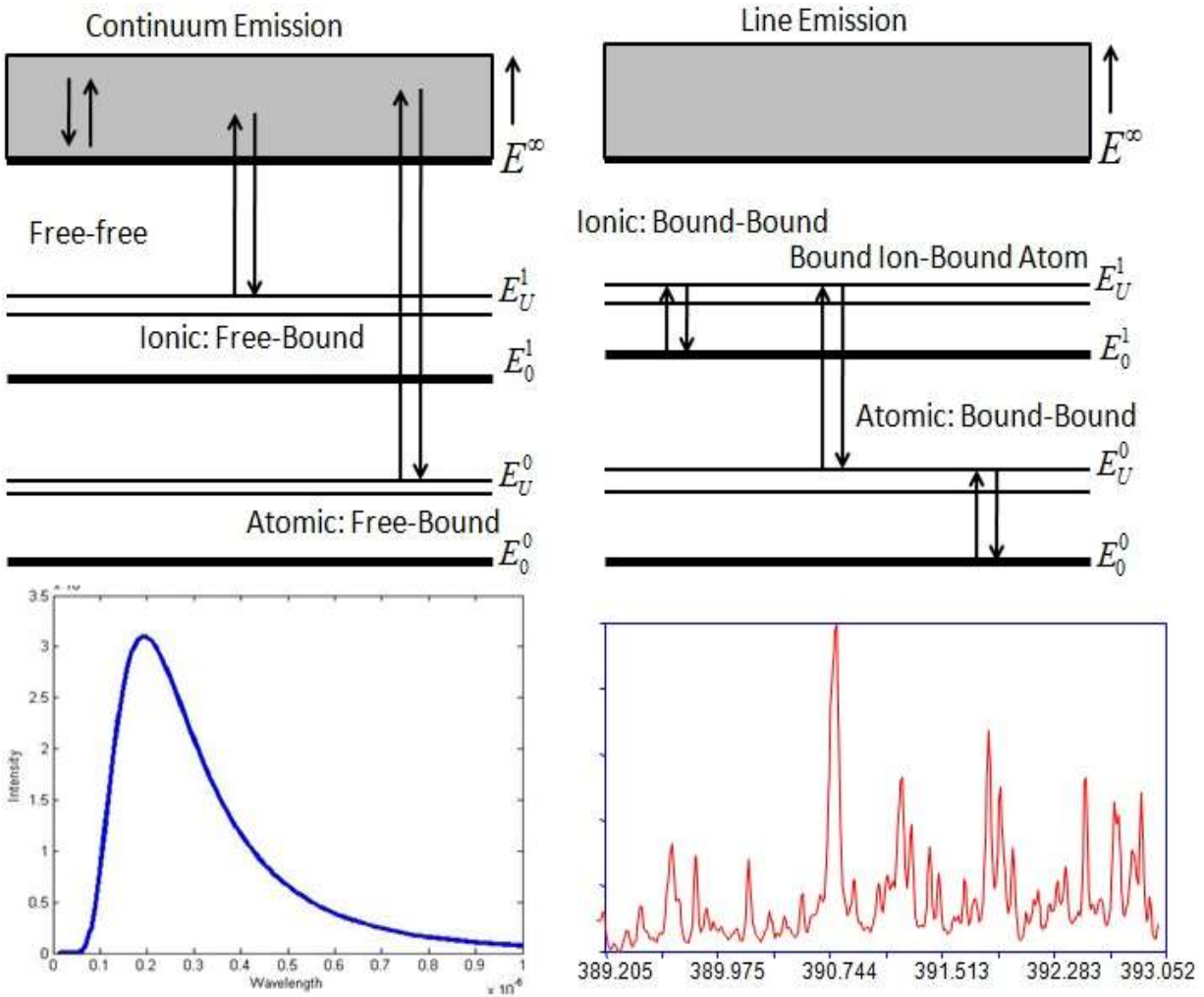
N_e is the number of free electrons per unit volume in meters, ω_{plasma} is the plasma frequency in rad/s, e , ϵ_0 , m_e are the electron charge, permittivity of free space, and mass of the electron respectively.

Radiative Transitions and Plasma Cooling

At the exhaustion of the laser pulse the luminous plasma plume continues its spatial expansion and begins to exhaust its fuelling resources. The plasma advances towards the incident laser beam, because the absorption of photons is asymmetric in that direction which yields a slight conical shape (upside down raindrop). At early times after the laser pulse, ionization density is near its peak, and electron-ion recombination rapidly begins. Following the recombination is the formation of neutral atoms and molecules. Throughout these formations there exists a continuum background radiation from the plasma. This continuum emission is mainly derived from bremsstrahlung (free-free) and recombination (free-bound) processes. Temporal resolution of the emitted light from these two processes allows for discrimination of the emitted species.

As the constituents within the plasma emit radiation the plasma as a whole begins to cool down. The emitted spectral radiation originates from three processes. The first emission is from *free-bound transitions* called electron recombination, from which continuum radiation is derived. This occurs because of electron transitions from free (unbound) states to a bound states (or orbital), and the resulting photons can have any broadband wavelength. Second, *free-free emissions* are also responsible for some of the continuum emission. These occur when an unbound electron loses some of its energy and “transitions” to a lower kinetic energy with a slower velocity. These types of free-free transitions occur within the bremsstrahlung process where the electric field of a charged particle (ion or atom) causes the electron to bend its trajectory and slow down, thus emitting a quantum of energy (photon). Third, we have *bound-bound transitions*, know as de-excitation of an atom or ion, in which a bound and energetic electron relaxes to a less excited bound state. From bound-bound transitions we get the spectral emission known as the atomic emission spectrum of the species. The basic processes are expressed below in equations 2.7 - 2.11





In figure 2.5 above, continuum radiation is displayed on the left and discrete line emissions on the right. States are represented with ionization levels denoted by the superscript and energy (or excitation) levels expressed as the subscript of the energy level E . In this way, the first ionization level and its corresponding bound upper energy state is designated E_U^1 . Similarly, E^∞ represents complete ionization of the species, and E_0^0 is the ground state of the neutral atom. Note that the Planck's blackbody representation for continuum emission is only valid for free-free transitions. In free-bound transitions there is a series of steps (like descending stairs) which signify that the energy ($\Delta E = h\nu$) has reached another lower bound level.

The effect of various surrounding gaseous environments can play a large role in the production of the plasma and its growth. The ambient (or buffer gas) can be used with LIBS systems in order to modify the emission signal. For example, argon has been proven to result in a longer lifetime and a hotter plasma than air.⁹

Given an ambient pressure greater than 0.75 torr (or 1 mbar), there is less energy loss due to expansion and interactions with the surrounding environment, as well as a more uniform distribution of temperature within the plasma.² The results of higher pressure are that the plasma is denser and more uniform which is good for signal detection, leading to better reproducibility; and furthermore at higher pressures the plasma expands less rapidly, meaning the lifetime of the plasma is longer which allows for more opportunities for signal emission. Extreme vacuum is not good for LIBS due to the decrease in collisions in a diffuse plasma environment, thus making thermal equilibration difficult. In the extreme case there would be no plasma generation.

2.1.2.2 - Femtosecond Pulse Regime

Unlike the nanosecond (10^{-9} s) ablation described above where thermal heating of the target leads to the formation of a vapor plume which in turn generates the plasma through laser absorption and heating, the femtosecond (10^{-15} s) ablation and plasma formation process is dominated by a process called Coulomb heating. In non-thermal heating, electron-hole plasmas are directly generated within the target, where the electrons are ejected from the material while leaving the lattice modes basically undisturbed from their normal vibrations. After approximately 10% of the valence electrons are ejected, the lattice weakens and melts. Femtosecond laser

pulses with irradiances near or above 10^{13} W/cm² produce ablation through this Coulomb explosion.

In conductors, the electron-hole plasma is directly created by the free electrons, whereas in semi-conductors, processes like multi-photon absorption, electron avalanche, and ionization tunneling are responsible for the electron-hole plasma formation. Either way, the electron-hole plasma is the mechanism responsible for laser radiation absorption thus generating the plasma through breakdown via exponentially increasing the free electron density.²

In femtosecond laser-induced breakdown there is no reheating of the plasma. Therefore the temperature of the plasma decreases faster and the lifetime of the plasma is shorter. Lastly, the ablation process in femtosecond lasers tends to be more reproducible owing to the lack of thermal heating which can vaporize material in a stochastic process, whereas the Coulomb explosion process generally is more consistent in its ablation.

2.1.2.3 - Picosecond Pulse Regime

In picosecond (10^{-12} s) laser ablation, either Coulomb explosion (non-thermal heating), thermal heating (lattice vibrations leading to phase transitions and eventually vapor plume), or a mixture of both processes can be responsible for the plasma formation depending on the irradiance of the laser beam. For irradiances greater than $10^{10} - 10^{13}$ W/cm², Coulomb explosion is the main source for the plasma generation. The electrons are ejected from the target surface and absorb radiation from the laser. It is these free electrons in the air which are the source of the plasma formation as opposed to nanosecond lasers where the vaporized material and particulates are the plasma source. Due to the short duration of the picosecond laser, there is no reheating of

the plasma as well as no shielding of the target surface. There is some thermal heating of the target's surface and an eventual plume is formed, but this is after the laser pulse has ceased and the plasma is exhausted.²

2.2 – Equilibrium and Plasma Modeling

2.2.1 – Equilibrium Distributions in Plasma

As the plasma expands and cools, there can be significant energy loss via radiation. It is this emitted spectrum of radiation which is identical (in theory) to the emitted spectra from stars which makes atomic emission spectroscopy possible and significant to astrophysicists and other scientific studies. Depending on the density of the plasma, some of that radiation may be absorbed by other atoms or ions before escaping the plume. This is known as “self-absorption” and is directly related to the absorption coefficient of the plasma. This self-absorption also defines whether a plasma is “optically thin” (an emitted photon is not absorbed before escaping the plasma) or “optically thick” (an emitted photon will be re-absorbed somewhere in the plasma before it can escape).

An interesting feature of laser-induced plasmas is that x-ray emission is the dominant form of radiation from the plasma; with nearly 70% of all laser energy absorbed by the plasma re-emitted as x-rays with typical energies varying from 50 eV to 1 keV depending on the laser irradiation. As a result of the cooling and expansion of the plasma, photon emission changes from x-ray to visible wavelengths. Generally the emission starts with continuum radiation from free-free and free-bound transition. This continuum radiation is much like black body radiation and this stage lasts for 100's of nanoseconds. Directly following the broad band continuum

emission is the emission from ionized species. These result from bound-bound transitions in ions and are generally observed near 500 ns. Lastly, line emission from neutral species is emitted and can last up to a few milliseconds depending on the lifetime of the plasma.

Within any plasma there are certain characteristics (e.g. the distribution of the emitted radiation, population of excited levels, distribution of velocities, relative populations of ionizations) which will determine how the species within the plasma behave. The full interpretation is immensely complex and requires systems of rate equations which involve population (depopulation) of excited states through ionization (recombination) and collisional excitation (de-excitation), as well as spontaneous emission, stimulated absorption, and stimulated emission. The basic idea involved in solving the complex system of equations is the principle of detailed balance or some portion of it. The principle of detailed balance simply states that for every emitted photon a second photon must be absorbed elsewhere in order to keep the balance, or for each excitation within an atom, another state must relax and so on. Consider a hot plasma contained in some closed volume with radiation and particles enclosed and maintained at a constant temperature T , so that radiation and particles cannot escape the enclosure. This would be the ideal model for the principle of detailed balance.

The distribution functions involved in the balancing equation are the Planck (radiation), Maxwell (kinetic), Boltzmann (excitation), and Saha (ionization) relations, these are listed below.

$$L(\lambda, T) = \frac{2hc}{\lambda^5} \frac{1}{\left(\exp\left(\frac{hc}{k_B T} \right) - 1 \right)} \quad (2.12)$$

Planck's blackbody distribution (equation 2.12 above) is expressed as irradiance L ($\text{W/m}^2 \text{ sr nm}$) rather than the typical energy per unit wavelength per unit volume ($\text{J m}^{-3} \text{ nm}^{-1}$). In 2.12, h , c , λ , k_B , T are Planck's constant, the speed of light, the wavelength of the emitted radiation, Boltzmann's constant, and temperature respectively.

$$\frac{dN(v)}{N} \equiv \left(\frac{m}{2\pi k_B T} \right)^{3/2} \exp\left(\frac{mv^2}{2k_B T} \right) 4\pi v^2 dv \quad (2.13)$$

Maxwell's velocity distribution (equation 2.13) relates the fraction of particles within some volume which have velocity between v and $v + dv$. The equation is expressed in terms of total speed v and not the three-dimensional velocity component. dN is the number of particles with velocity in the specified velocity region, N is the total number of particles, and m is the mass of the particle.

$$\frac{N_j}{N_i} = \frac{g_j}{g_i} \exp\left(-\frac{(E_j - E_i)}{k_B T} \right) \quad (2.14)$$

Boltzmann's relation (equation 2.14) expressed in terms of relative populations of the energy levels E_i (lower) and E_j (upper) reveals the relation between the population of energy states within the same species (atom or ion) as a function of plasma temperature.

$$\frac{N_{z+1}}{N_z} = \frac{1}{N_e} \frac{2(2\pi m_e k_B T)^{3/2}}{h^3} \frac{Q_{z+1}(T)}{Q_z(T)} \exp\left(\frac{-\chi_z}{k_B T} \right) \quad (2.15.a)$$

$$\frac{N_{I,k}}{N_{A,j}} = \frac{1}{N_e} \frac{2(2\pi m_e k_B T)^{3/2}}{h^3} \frac{g_{I,k}}{g_{A,j}} \exp\left(\frac{-(\chi_z + E_k - E_j)}{k_B T}\right) \quad (2.15.b)$$

Saha's expression (the Saha-Boltzmann equation) for relative ion populations is shown in equations 2.15.a and 2.15.b. Equation 2.15.a shows the relative population density of the higher ionic state $z+1$ (N_{z+1}) to the lower ionized state z (N_z), and N_e is the electron number density. Each number density incorporates the total number of ions per unit volume, regardless of what particular energy levels they may occupy. Q_{z+1} and Q_z are the partition functions of the higher and lower ionized species. The ionization potential is denoted by χ_z . Equation 2.15.b expresses Saha's equation in terms of excited-atomic to excited-ionic states. The number density $N_{I,k}$ refers to the number of ions per unit volume in the k th energy state. $N_{A,j}$ denotes the number density in the j th energy level E_j (not necessarily the ground state) of the atomic species A . E_k refers to the k th energy level (again not necessarily the ground state) of the higher ionization state I . $g_{I,k}$ is the degeneracy of the k th level of the ion I , while $g_{A,j}$ is the degeneracy belonging to the atom's j th level.

There are many possible modes of excitation and ionization within an atom and the simplest way to describe them is in a graphical representation. Below in figure 2.6 all of the possible modes of excitation or de-excitation, ionization, or recombination are shown.

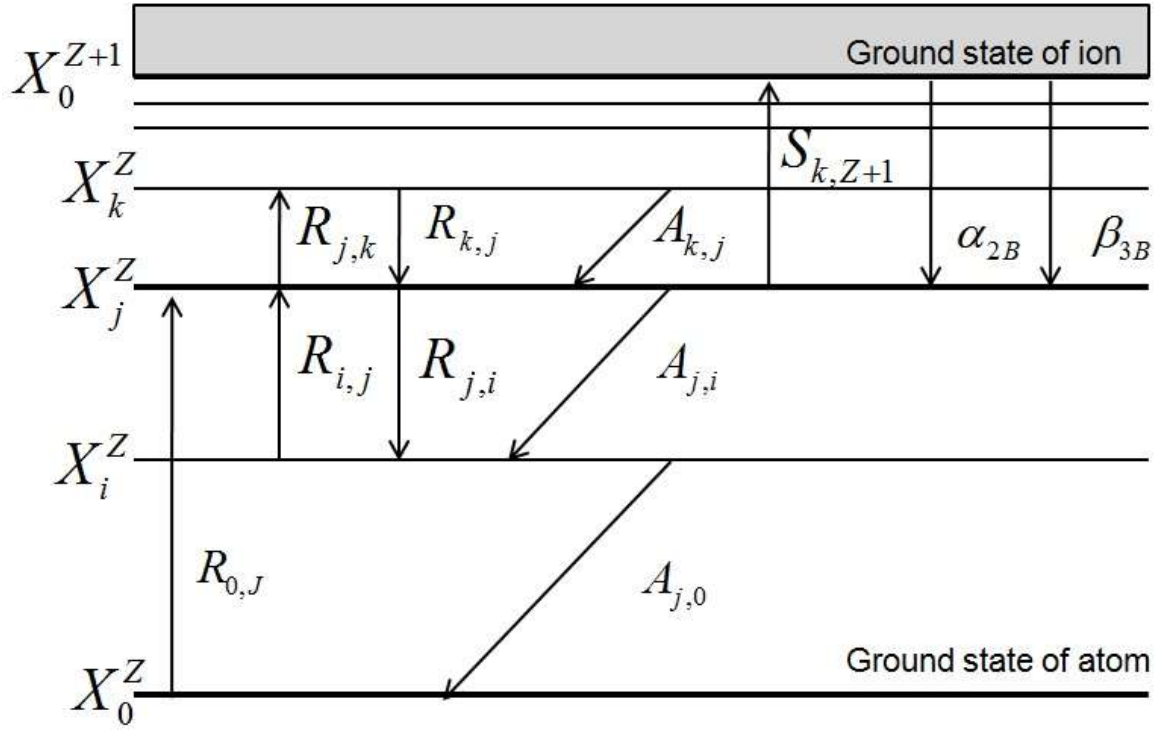


Figure 2.6 (above) shows the various forms of energetic transitions and ionic transitions from within the atom (ion) to the state of interest. Here the state of interest is X_j^Z where j is the energy state and Z the ionization level. $R_{n,m}$ is the generic form for the rate of impact ionization or de-excitation depending on the transition. $A_{n,m}$ is Einstein's spontaneous emission coefficient, $S_{k,Z+1}$ is the electron impact ionization rate. α_{2B} , β_{3B} are the two- and three-body radiative recombination coefficients.

In plasmas it is impossible to have equilibrium between all four processes so that a single temperature can be attributed to the entire medium (plasma). Because of the complexities in achieving a plasma which is in complete thermal equilibrium, four plasma models are typically used to approximate the behavior within the plasma each distinguished primarily by the plasma's electron density (N_e). The models use two or more of the energy distributions said to be in equilibrium for their defining feature. The models are the Corona model (CM), Collisional-

Radiative model (CRM), Local Thermodynamic Equilibrium (LTE), and lastly, Partial Local Thermodynamic Equilibrium (PLTE).

Because the plasma is dynamically expanding in time and because there are spatial inhomogeneities, restrictions must be placed on the validity of any of these models. One must require that on time scales which are on the order of the de-excitation rates there is (i) no significant change in the local electron temperature, also (ii) insufficient time elapsed for the atoms or ions to diffuse into regions of different electron density.

A two-level atomic model can serve to show some of the qualitative properties of these various plasma models. The balanced rate equation for a neutral atom having energetic transitions only (excluding ionizational transitions), is shown below in equation 2.16. N_1 , N_2 , N_e , are the population densities of levels one, two, and the electron population density respectively. C_{12} and C_{21} are the collisional coefficients for upward and downward transitions respectively. B_{12} , B_{21} , and A_{21} are the Einstein coefficients for stimulated absorption, emission, and spontaneous emission respectively. Lastly, $\rho(\nu)$ is the spectral density (radiation density).

$$N_1 N_e C_{12} + N_1 \rho(\nu_{12}) B_{12} = N_2 N_e C_{21} + N_2 \rho(\nu_{12}) B_{21} + N_2 A_{21} \quad (2.16)$$

C_{12} , or inversely C_{21} , are defined as the average value of the velocity times the cross-section ($\nu \cdot \sigma(\nu)$), which is velocity dependant, weighted with Maxwell's velocity distribution (described earlier) for electrons. This is expressed in equation 2.17 below and Maxwell's distribution function $f(\nu)$ is shown again below.

$$C_{12} = \langle v\sigma(v) \rangle = \int_0^{\infty} v\sigma(v)f(v)dv \quad (2.17)$$

$$f(v) = \left(\frac{m_e}{2\pi k_B T_e} \right)^{3/2} \cdot \exp\left(\frac{mv^2}{k_B T_e} \right) \cdot 4\pi v^2$$

2.2.2 - Corona Model

The first class of equilibrium relations is applicable to situations where excitation and ionization from the lower states are caused by electron collisions but de-excitations leading into these states are caused both by radiative and collisional processes. In this model the radiation density is small and it is assumed that transitions within the same ionization state to higher energy states are due to electron collisions ($C_{12} \gg B_{12}$) while transitions within the same ionization state to lower energy levels occur by spontaneous emission only ($A_{21} \gg C_{21}, B_{21}$). The coronal equilibrium model is important because it is applicable to the Sun's corona having high temperature ($\sim 10^6$ K) and low electron density ($\sim 10^8$ cm⁻³).

In CM equilibrium, the excited level populations are determined from a balance between collisional excitation and radiative decay to the ground level. Ground level populations of ions are determined from a balance between collisional ionization, radiative, and electronic recombination rates. When estimating relative fractions of ions, excited level populations are assumed to be negligible compared to ground state populations because of low collisional

excitation rates compared with spontaneous decay rates. Meanwhile, free electrons in CM are usually assumed to have a Maxwellian velocity distribution.

Consider the two-level atomic system for qualitative analysis using the simplifications above in the balanced rate equation (equation 2.16). Therefore with these simplifications we can write the equation as:

$$N_1 N_e C_{12} = N_2 A_{21} \quad (2.18)$$

This can be rewritten to express the relative populations of the states as:

$$\frac{N_2}{N_1} = N_e \frac{C_{12}}{A_{21}} \quad (2.19)$$

We can see that the relative population depends on knowing the electron density and the rate coefficients. When in thermal equilibrium the relative population of N_2 to N_1 is described by Boltzmann's equation. But according to the principle of detailed balance the collisional and radiative rates must balance separately and therefore this is the same as writing the ratio of the collisional excitation to the collisional de-excitation coefficients.

$$C_{12}/C_{21} = N_2/N_1 = g_2/g_1 \cdot e^{-(E_2-E_1)/k_B T}$$

Since the spontaneous transition probability A_{21} is much larger than the collisional coefficient of absorption C_{21} in the coronal model, we know that the relative population of N_2 to N_1 is a small

number when N_e is small. As N_e increases to very large number, we leave the coronal model and transition into the local thermodynamic equilibrium model.

Similarly the ionization relations for the CM require only a small fraction of the population be ionized and is independent of the electron density (to a first order approximation), as will be shown below in the balanced two level ionization expression (equation 2.20.a). For optically thin plasmas, the CM ionization processes requires two conditions: (i) that two-body radiative recombination (α_{Z+1}) exceeds three-body collisional recombination (β_{Z+1}), ($\alpha_{Z+1} \gg \beta_{Z+1}$) and (ii) collisional excitation from levels other than the ground state are negligible due to low densities (optically thin). Below, N_Z , N_{Z+1} , and N_e are the population densities for the lower ionized level, the higher ionized level, and the electrons respectively. S_Z , α_{Z+1} , and β_{Z+1} are the electron impact ionization, two-body radiative recombination, and three-body radiative recombination rate coefficients respectively.

$$N_Z N_e S_Z(T_e) = N_{Z+1} \cdot N_e \cdot \alpha_{Z+1}(T_e, N_e) + N_{Z+1} \cdot N_e^2 \cdot \beta_{Z+1}(T_e, N_e) \quad (2.20.a)$$

This equation can be manipulated to show the relative ionization population expressed below.

$$\frac{N_{Z+1}}{N_Z} = \frac{S_Z(T_e)}{\alpha_{Z+1}(T_e, N_e)} \quad (2.20.b)$$

The above first order approximation is independent of N_e and is smaller than the value given by Saha's equation for the relative population of neighboring ionization levels. According to Griem¹⁰ the above two-level approximation can be used to estimate the degree of ionization if it results in smaller fractional ionization than the Saha equation, if the plasma is optically thin

and if equilibrium (steady-state) criteria corresponding to those for inhomogeneous and transient LTE plasmas are fulfilled ($t_{\text{atomic transition}} \ll t_{\text{plasma expansion}}$). The general relation is not independent of N_e and therefore is only valid for small values of N_e . Even when this criterion is satisfied the full expression for CM falls apart for highly excited states because of the rapid decrease of A_{21} with v^3 .

2.2.3 - Local Thermodynamic Equilibrium Model

In local thermodynamic equilibrium (LTE), particle collisions are assumed to dominate over radiative transitions so that collisional processes determine the distribution of population densities. Therefore the electrons, being ~ 1000 times lighter than the nuclei, are the only particles considered to collide with sufficient rapidity and the distribution responds instantaneously to any change in plasma conditions. The forms of energy transfer which balance out separately in the LTE Model are the excitation (Boltzmann), ionization (Saha), and kinetic (Maxwell). These distributions are considered to be in equilibrium in various locations and segments of time, but not uniformly in equilibrium throughout the entire medium; meaning specifically that a single temperature can be used to describe their distributions. In LTE collisional process within the plasma must dominate so that the minor loss of energy through escaping radiation is miniscule in comparison. Or in terms of atomic properties, a given excited state must have a higher probability of de-excitation through collision than spontaneous emission of a photon. The physical requisite for this situation to occur is to have a high electron density

within the plasma. The plasma's electron density which fulfills this criteria as is typically seen in LIBS research^{2,10,11,12} is $N_e > 10^{24} \text{ cm}^{-3}$.

We can again gain a qualitative understanding using the crude two-level atomic model. If we consider again equation 2.16, and use the criteria for LTE models (small ρ , so that collisions dominate over photon-absorption processes, $C_{21} \gg A_{21}$ so collisional depopulation dominates spontaneous emission, and lastly large electron densities, $N_e > 10^{24} \gg 1$) we can reduce the said equation to

$$N_1 N_e C_{12} = N_2 N_e C_{21} + N_2 A_{21} \quad (2.21)$$

Since N_e is extremely large and $C_{21} \gg A_{21}$, we can eliminate the last term on the right. After solving for the ratio of upper state population to lower state population (N_2 / N_1) we are left with

$$\frac{N_2}{N_1} = \frac{C_{12}}{C_{21}} = \frac{g_2}{g_1} \exp(-[E_2 - E_1] / k_B T) \quad (2.22)$$

From here we know that since the model is in thermal equilibrium we can implement the Boltzmann distribution, so that the ratio becomes the expression in equation 2.22. Recalling that

the criterion for this relation to hold was based upon $N_e \gg A_{21} / C_{21}$, as it turns out this relation

in fact holds for LTE. This relation can be estimated to give an expression in terms of

wavelength and temperature by substituting $A_{21} = \frac{2.026 \cdot 10^{18}}{g_2 \cdot \lambda^3} \cdot S_{21}$ where S_{21} is the electric

dipole line strength and $C_{21} \equiv \int_0^{\infty} \nu \cdot \sigma(\nu) \cdot f_{Maxwell}(\nu) d\nu \propto S / \nu$. So then the expression

can be approximated in units of m^{-3} as

$$N_e \gg \text{const} \cdot \nu \cdot \lambda^{-3} = 1.6 \cdot 10^{18} \sqrt{T} \cdot (\Delta E)^3 \quad (2.23)$$

Some examples of the electron densities required for LTE in optically thin plasmas reveal that N_e is very large. For hydrogen at $k_B T = 1 \text{ eV}$ ($\sim 11,600 \text{ K}$), N_e is on the order of $1.2 \times 10^{17} \text{ cm}^{-3}$, for helium at $k_B T = 4 \text{ eV}$ ($\sim 45,000 \text{ K}$), N_e is on the order of $1.5 \times 10^{19} \text{ cm}^{-3}$. Typical electron densities that I calculated for a pressure of 8.3 torr and delay time 1000 ns with a temperature of 16,000K were on the order of $\sim 3.3 \times 10^{17} \text{ cm}^{-3}$. Note that this expression (equation 2.23) is called “McWhirter’s criterion”² for LTE, but it does not consider the spatial gradient and time-variation of a laser-induced plasma and is therefore only approximately true. For a more thorough treatment of radiative rates in the various plasma models see Griem’s “*Plasma Spectroscopy*” 1964,¹⁰ Mihalas’ “*Stellar Atmospheres*” 1970,¹¹ and Salzman’s “*Atomic Physics in Hot plasmas*” 1998.¹³

G. Cristoforetti et al.¹⁴ gives a more complete condition for LTE by adding that McWhirter’s criterion for LIBS plasmas,

“...cannot be sufficient for assessing the validity of LTE, even in the approximation of a stationary and homogenous plasma, because of the extremely high ionization degree of the plasma after the breakdown, which causes an unbalance between the ionization and recombination processes, the latter

prevailing. Therefore, in this case, within the dominance of electron collision excitation and de-excitation mechanisms over radiative decay, it is important to check the equilibrium within different inelastic processes leading to the Boltzmann and Saha balances.”

Cristoforetti¹⁴ therefore proposes the use of a relation where the Boltzmann and Saha equations can be used separately to determine the level population for a particular ionized (or neutral) state N_i .

$$b_i = \frac{N_i^{Boltz}}{N_i^{Saha}} \quad (2.24)$$

So that if $b_i = 1$ then the two distributions are in agreement and the plasma is said to be in LTE. An even more thorough check would be to compare the ratio of two different ionizations and energy states of the same atomic species by use of Boltzmann and Saha equations respectively, as shown below in equation 2.25. This agreement (disagreement) which is representative of not only a lower lying state i but also a upper level j , would suffice to compare some of the varying thermal distributions and complications which occur in lower lying states with a higher ionized level in LTE.

$$\frac{N_i^{Boltz}}{N_j^{+,Boltz}} = \frac{N_i^{Saha}}{N_j^{+,Saha}} \quad (2.25)$$

Using the LTE criteria proposed by McWhirter, which checks that radiative transitions are less than collisional transitions by determination of N_e , and using the condition proposed by

Cristoforetti,¹⁴ which accounts for ionizational thermal contrasts often seen in lower lying states of an ionic species, LTE can be more confidently assumed in laser-induced plasmas. It has been noted that McWhirter's criteria should be relaxed by about an order of magnitude due to strong resonance line absorption leading to low populations of N_e .^{15,16,17,18}

2.2.4 - Collisional-Radiative model

In the collisional-radiative plasma model (CRM), collision and radiation rates are comparable. This is the most general case of energy behavior, where collisional excitation and de-excitation compete with radiative transitions. In the CM model, the population distribution at any location within the plasma does not depend only upon the specific plasma parameters at the point, unlike in the LTE model. The local population distribution is determined by balancing collisional processes of a local nature and radiative processes of a non-local nature. This state of plasma is different from a CM plasma since collisional depopulation processes and collisional processes affect the population distributions. Laboratory plasmas frequently satisfy the above situation in various regimes of electron density and temperature.

In general the CRM contains all collisional and radiative processes in its detailed balanced equations, thus it is generally the most difficult to solve analytically - usually requiring detailed modeling of rate coefficients and advanced level computational methods. In the CRM, atomic level populations are calculated by solving multi-level atomic rate equations self-consistently with a radiation field. If collisional processes prevail in the plasma, the population distribution converges to the LTE population distribution. In the limiting case that N_e increases

sufficiently, the CRM tends to LTE model, and in the limiting case that N_e is low, CRM tends to the CM.

The most extensive use of the CRM modeling can be found in x-ray spectroscopy used to diagnose laser-produced plasmas in relation to inertial confinement fusion or other x-ray sources. Plasmas produced by high-power lasers can have electron temperatures as high as a few keV and electron densities as high as $10^{21} - 10^{25} \text{ cm}^{-3}$. For more detailed information see Griem's *Principles of Plasma Spectroscopy* (1997),¹⁹ Mihalas's *Stellar Astrophysics*,¹¹ and Salzman's *Atomic Physics in Hot Plasmas*.¹³

2.2.5 - Partial Local Thermodynamic Equilibrium

Partial Local Thermodynamic Equilibrium (PLTE) is a model which bridges the gap for circumstances when none of the above models fit the equilibrium condition of the plasma precisely. PLTE focuses on the significance of transfer processes and external effects compared to collisional effects, which is the case when plasma density is decreased from LTE. In this case, it is assumed that the temperatures derived from the Saha, Boltzmann, and Maxwell distributions can differ, and that some of these distributions might not hold for all the constituents within a given species (for example the higher energy levels of a given ion could have higher temperatures according to the Maxwell's equation, compared to the low-lying neutral energy states due to an external electric field). However, in PLTE at least one of the equilibrium relations above should hold for some species of particles. In short, it could be the case that a single equilibrium model describes only part of the ensemble of ions and atoms within the

plasma so that there would exist a set of different *partial* temperatures for different energies of ions or atoms.

It is not uncommon for PLTE to be assigned when Boltzmann's equation holds for the excited levels of a given atom (or ion) but the lower lying ground state fails to adhere to the distribution having a different temperature. This can be due to the fact that the energy gap from ground to first excited state is in itself larger than all of the rest of the populated states' energy differences combined. In this case, it is common to solve the steady state equations for the excited states, while treating the ground state population as a time-dependent parameter.

Furthermore, referencing the temperature of a species in PLTE by noting which distribution is found in partial equilibrium is often found to be the case. For example, if Saha's equation is found to provide a temperature which describes a majority of its ionized species sufficiently, the system's temperature is said to be an 'ionization temperature'. For Boltzmann's energy spectrum distribution, one would label the temperature best describing the ensemble as a 'distribution temperature', and so on.

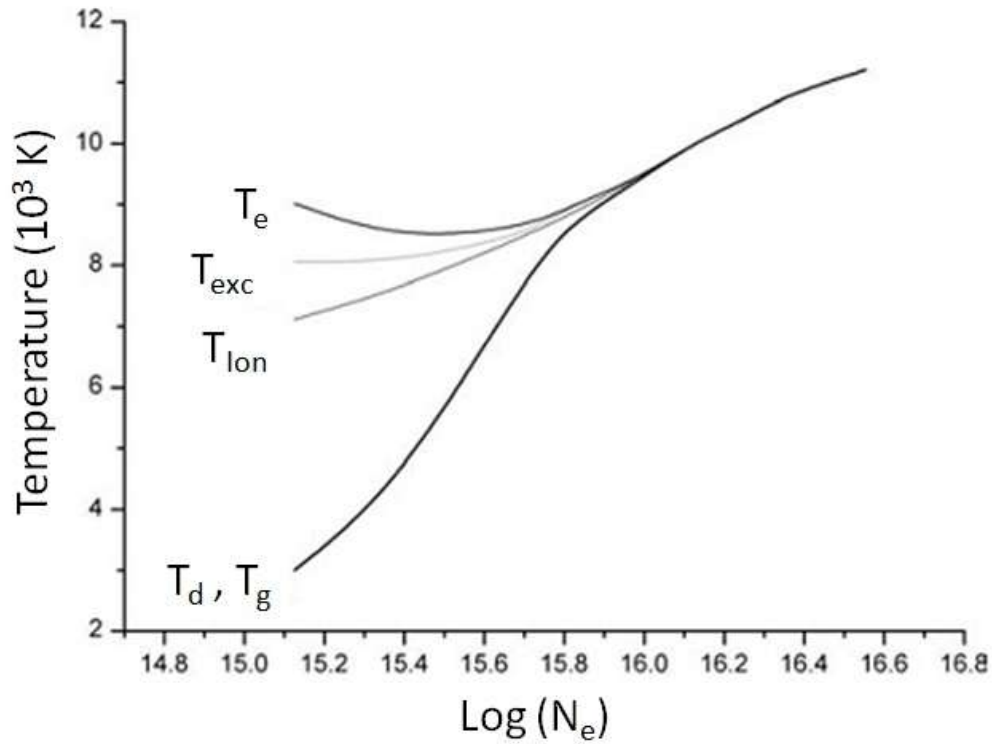


Figure 2.7 presents the results of measurements reported in Ochkin's "Spectroscopy of low temperature plasmas,"²⁰ in which he makes use of data from McWhirter et al. (1963)²¹ of various temperatures in the plasma of an arc discharge in argon with an admixture of hydrogen. The temperatures from various distributions were plotted: excitation (T_{exc}), distribution (T_d), ionization (T_{ion}), neutral gas (T_g), and electron (T_e) temperatures were measured by separate independent methods.

It is clear from the graph in figure 2.7 that at low electron densities ($N_e < 10^{15} \text{ cm}^{-3}$) obvious discrepancies are seen between the temperatures determined from various independent methods (e.g. excitation temperature, ionization temperature, neutral species temperature, electron temperature, velocity distribution temperature). It is the conditions of the plasma that give rise to the observed distribution's temperature discrepancies which correspond to the PLTE

model. For high electron densities ($N_e > 5 \times 10^{15} \text{ cm}^{-3}$) virtually all the temperatures coincide, which indicates the transition to LTE.

2.3 - Uniqueness of Laser-Induced Plasmas

Astrophysics relies heavily on spectroscopic examination of stars and their plasmas. Astrophysics has benefited greatly from laboratory plasma spectroscopy by significantly improved accuracy on astronomically relevant atomic data - like oscillator strengths and atomic lifetimes.^{22,23,11} Plasma spectroscopy was originally developed as a method of determining plasma temperature T and electron number density N_e . However, with improvements in detection methods, three basic uses have developed. (i) Laser-induced plasmas can be used as a light source for determining oscillator strengths and atomic cross sections for the ionized species. (ii) In plasmas of known composition and temperature particle interactions can be studied. These interactions include collisions with each other, interactions with plasma fields, and with radiation. These three interactions can be investigated via emission line broadening or shifting, appearance of forbidden lines, or the relaxation rates of the plasma^{10,12,24,13,25,3} (iii) In the case of very dense plasmas, spectroscopic techniques are used to study plasma dynamics and radiation transportation methods.^{26,27}

2.3.1 - Spectral Emission

In LIBS, plasma radiation is ideal for spectral emission and detection when the plasma is optically thin and in local thermodynamic equilibrium (LTE). Fundamentally, optical thinness is achieved when the emitted radiation traverses and escapes from the plasma without significant absorption or scattering effects, as mentioned earlier. The second plasma characteristic which is

often cited in LIBS literature as fundamentally necessary for spectral line identification is local thermodynamic equilibrium (LTE). In general, thermodynamic equilibrium means that all processes in the entire expanse of the plasma are separately balanced thus creating a plasma which is collisionally-dominated, and therefore the entire plasma could be described using a single temperature, also described in detail earlier. For an adiabatically expanding plasma this is not possible on the whole and can only be locally true at specific segments in time and certain spatial regions. LTE can be approximately quantifiably verified using McWhirter's criterion²¹ (equation 2.21) and the two other criteria stated above (equations 2.24 and 2.25).

In an optically thin plasma the measured intensity of a given transition which decays from energy level j to i is given by equation 2.26, where C_i contains geometric factors and also the spectrometer and detector responses at the wavelength λ_{ji} . A_{ji} , h , c , and N_j are the Einstein coefficient for spontaneous decay, Planck's constant, speed of light, and population density of the upper level j . Lastly, s is the plasma thickness along the line of sight.

$$I(\lambda_{ji}) = \frac{1}{4\pi} \int C_i \cdot A_{ji} \cdot \frac{hc}{\lambda_{ji}} \cdot N_j \cdot ds \quad (2.26)$$

It is of spectroscopic interest to investigate the *relative* line emissions from two transitions rather than to investigate the absolute line emission intensity due to large erroneous factors in the absolute case such as inaccurate transition probabilities or spectral calibration effects (usually contained in C_i). When the two conditions, LTE and optical thinness, are achieved within the plasma the Boltzmann equation can be incorporated into the integral

emission-line intensity and a ratio between two line-emissions can be used as in by equation 2.27 for levels arising within the same species and ionization degree.³

$$\frac{I_2}{I_1} = \frac{\lambda_1}{\lambda_2} \frac{A_2 g_2}{A_1 g_1} e^{-\frac{(E_2 - E_1)}{k_B T}} \quad (2.27)$$

I_2 and I_1 are the integrated intensities, λ_1 and λ_2 are the central wavelengths of the emission lines, A_2 and A_1 are the transmission probabilities for the decays, g_2 and g_1 are the degeneracies of the energy levels, E_2 and E_1 are the energies of the given levels with respect to the ground state, k_B is Boltzmann's constant, and T is the plasma temperature.

Time-resolved detection of the photons emitted from the plasma plume creates a characteristic spectrum of the emitting species involving both continuum and line emissions. In the nanosecond laser regime, atomic and molecular emission occurs microseconds after the laser pulse, whereas ionic species are generally seen at approximately 100's of ns to a few microseconds after the laser pulse. Prior to this, the spectrum is dominated by continuum emission arising from Bremsstrahlung radiation. Pictured below in figure 2.8 is such a spectrum for neodymium revealing superimposed line emission on top of continuum emission.

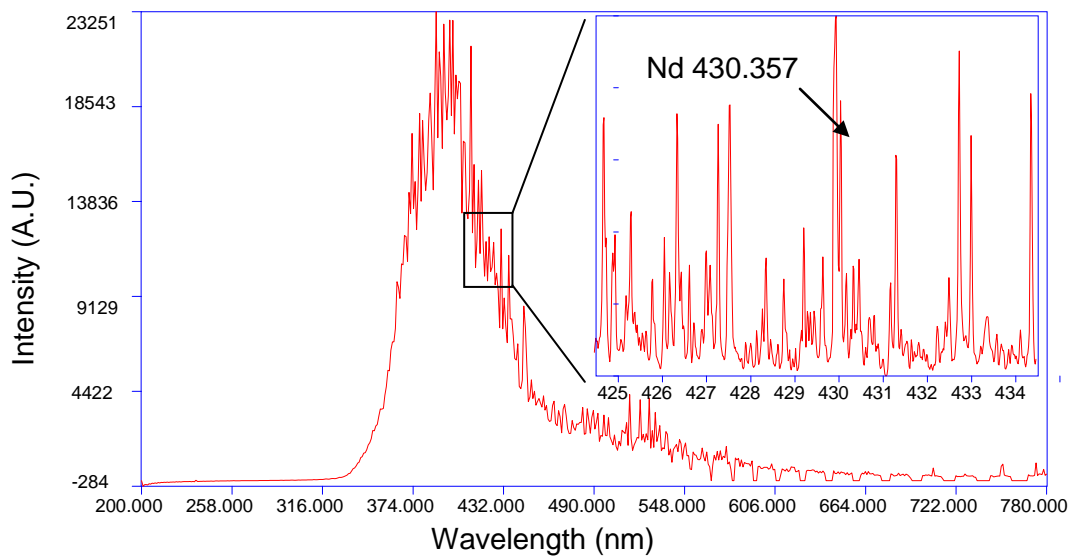


Fig 2.8. LIBS neodymium spectrum obtained at a pressure of 7.7 mbar, gate delay of 600 ns. The full spectrum ranging from 200-800 nm is shown. (*Inset*) A zoomed-in detail of the Nd spectrum with focus on the 430.357 nm emission line which is the strongest branch from the $23,229.991 \text{ cm}^{-1}$ level studied in this work.

Spectral profiles and line broadening

Observed spectral line profiles are a convolution of the actual source profile, instrumentation limitations, and other phenomenological factors such as the collisional broadening effect. Even without any environmental or outside broadening mechanisms the atomic properties of emitted photons will be broadened through a natural line broadening effect which is the result of a finite lifetime of the upper state before a transition occurs. There are three main broadening mechanisms commonly responsible for broadening LIBS spectral lines: natural line width, collisional broadening, and Doppler broadening.

Line shapes are determined by experimental data and used against broadening models as comparisons. The *natural broadening* of a spectral line is inherent to the probabilistic behavior

of the atom itself and the classical damping of its oscillatory motion; it is therefore independent of the environment and is seen in any spectroscopic measurement. The broadening of *natural line width* results in a profile width (FWHM) on the order of ~0.001 nm, which for most LIBS detectors is beyond the resolution of the detector. Natural line widths arise because of two mechanisms: (i) the probabilistic behavior of the atom due to Heisenberg's uncertainty principle, $\Delta E \Delta t \approx h / 2\pi$, and (ii) the damping harmonic motion of the electron in the field of the atom. The length of time that an atom can spend in a certain state – defined as the *lifetime* of the given state - is related by the inverse of the uncertainty of energy belonging to that state. The exponentially decreasing amplitude of oscillatory motion of the electron can be Fourier transformed and the resulting frequency spectrum has a FWHM equal to $\delta\nu_{Natural} = 1 / 2\pi\tau_{Classic}$. This is characterized by a Lorentzian line profile, the expression of which is shown below (equation 2.28) where λ is the wavelength λ_0 is the central profile wavelength and γ is the Lorentzian FWHM.

$$I(\lambda) = I_0 \frac{\gamma / 2\pi}{(\lambda - \lambda_0)^2 + \gamma^2 / 4} \quad (2.28)$$

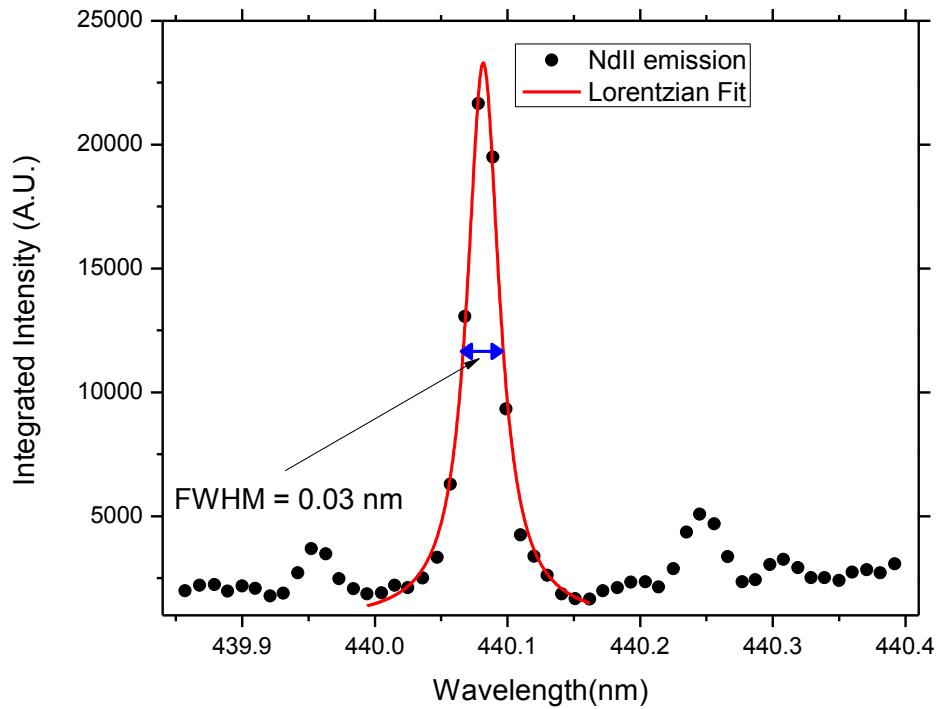


Figure 2.9 shows the FWHM from the 430.357 nm line in Nd II emission from our LIBS spectrum. It was fit using a Lorentzian profile which determined the FWHM to be 0.03 nm. Clearly, a Lorentzian fit is a fairly good approximation of the actual measured line-shape.

The second significant broadening contribution seen in LIBS spectra are *Doppler broadened* spectral lines.^{28,13} In this case the atoms and ions within the plasma are constantly in random motion on a microscopic scale since the plasma is usually only 10% ionized at times and spatial distances where neutral and ionic observations are concerned. When light is emitted from a moving object there is a Doppler effect which distorts the observed wavelength shifting it to shorter or longer wavelengths according to the directional motion – toward or away from the observer respectively. It is this effect, seen on a smaller scale but multiplied many times by the

large number of randomly moving emitters, which makes up the detected *Doppler broadening*. This broadening is significantly greater than natural broadening effects for typical LIBS spectra.

The profiles of spectral lines resulting from Doppler broadening are Gaussian in shape and can be derived from the Maxwell velocity distribution of atoms in LTE. The Gaussian line profile is expressed in equation 2.29 below.

$$I(\lambda) = \frac{1}{\sqrt{2\pi} \cdot \delta\lambda_{Dop}} \exp\left(\frac{-(\lambda - \lambda_0)^2}{2 \cdot \delta\lambda_{Dop}^2}\right) \quad (2.29)$$

The corresponding Doppler FWHM value for the wavelength is given by equation 2.30 below, where λ_{Dop} , λ_0 , T , and M are the FWHM Doppler width, the central wavelength of the profile, the temperature, and mass of the kinetic species, respectively. Shaikh et al.²⁹ determined the Doppler width in a LIBS Cd line at 226.50 nm with an approximate temperature of 12,000 Kelvin to be 0.002 ± 1 nm, which is beyond the resolution limit of most spectrometers used in LIBS.

$$\delta\lambda_{Dop} = 2\lambda_0 \sqrt{\frac{2RT \ln(2)}{M}} = 7.16 \cdot 10^{-7} \cdot \lambda_0 \cdot \sqrt{\left(\frac{T}{M}\right)} \quad (2.30)$$

The third broadening mechanism which affects LIBS spectra is called *Stark broadening*, sometimes referred to as *Pressure broadening*. This mechanism arises due to collisions or near collisions of charged particles like ions, electrons, and neutral species colliding within the plasma. The interaction of atomic or ionic species with electric fields causes a Stark effect which

opens degenerate energy levels. These degenerate levels act to broaden the emission lines of the spectra. In the case of neutral and electron collisions which are the only significant factors in LIBS spectra³⁰ the Lorentzian fit of the FWHM wavelength for stark broadening can be calculated by equation 2.31 (under the assumption that the species is heavy compared to hydrogen thus making Doppler broadening negligible). Here w is the electron impact half-width which is temperature-dependent and has values which can be found in literature.¹⁰ The other parameters are described above. In practice, Stark broadening is typically only ever observed for hydrogen, or hydrogen-like atoms in LIBS plasmas. For a fuller treatment on the Stark broadening of charged particles in plasma see Griem's "*Spectral Line broadening by plasmas*" (1974)³¹ and Salzmann's "*Atomic Physics in Hot Plasmas*."¹³

$$\delta\lambda_{Stark} \approx 2w \left(\frac{N_e}{10^{16}} \right) \quad (2.31)$$

Opacity and Self-Absorption

Sometimes atomic radiators in a plasma emit photons and the photons are absorbed by other species within the plasma. This phenomenon of absorption from within the same conglomeration of species is related to the opacity of the plasma. Opacity can loosely be defined as the opaqueness of an object; therefore the more opaque the object is the more it absorbs light. The amount of radiation that is emitted from an optically thick or optically thin plasma will be related to the coefficient of absorption α , and coefficient of emission ϵ as shown in equation 2.32.

$$I(\lambda) = \left[\frac{\varepsilon(\lambda)}{\alpha(\lambda)} \right] \cdot (1 - \exp[-\alpha(\lambda) \cdot L]) \quad (2.32)$$

If the plasma is optically thin then the exponential can be approximated to first order as $\exp[-\alpha(\lambda) \cdot L] \approx 1 + [-\alpha(\lambda) \cdot L]$ and the line intensity is simply related to the thickness of the plasma and the emission coefficient $I(\lambda) = \varepsilon(\lambda) \cdot L$.

One way to determine if the plasma is optically thick is to check the calculated relative intensities of two strong lines emitted from the same species and ionization against one another. Then, using calculated relative intensities from atomic physics coupling theory (L - J or j - j , etc.), the same emission lines can be compared. If the absorption is nominal then the experimentally determined ratio of the intensity of the stronger line to the weaker line will be smaller than the theoretical calculated fraction. If absorption is substantially large then the stronger resonance lines will be self-reversed due to atoms absorbing part of their own profile at the central wavelength and again the fraction would be smaller compared to the theoretical fraction.

A second method used by Shaikh et al.²⁹ to determine optical thinness suggests that the absorption coefficient α for any given line multiplied by the plasma thickness L should be much less than 1, $\alpha[cm^{-1}] \cdot L[cm] \ll 1$. The absorption coefficient α can be estimated for laser-induced plasmas (LIPs) as³² $\alpha_{ji} = 8.85 \cdot 10^{-13} \cdot f_{ji} \cdot \lambda_0^2 \cdot N_i \cdot P_{ji}(\lambda_0)$, where $P_{ji}(\lambda_0)$ is the profile of the line, N_i is the population density of the lower level i which is assumed to be equal to the number density for electrons, and f_{ji} is the oscillator strength. Shaikh et al.²⁹

calculated the self absorption factor (αL) of their strong line to be $\sim 1\%$ using a plasma thickness of $\sim 1\text{mm}$ and an absorption coefficient equal to 0.1 cm^{-1} . For my own work, I was able to calculate the expression for optical thinness (αL) to be $\alpha L = 0.01 \pm 0.04$ using the experimentally determined absorption coefficient α which was found using Lorentz-fitted Stark-broadening to be $\alpha = 0.10 \pm 0.04\text{ cm}^{-1}$ and the plasma thickness L was approximated as $L \sim 0.1\text{ cm}$, which does indeed satisfy the condition for optical thinness of the plasma, being 100 times smaller.

Temperature Calculations

It is common practice to determine temperature and electron density within the plasma by calculation of parameters using experimentally determined features of the emitting species. Because of the dynamics of the plasma morphology, certain experimental conditions are better suited for various methods of determining temperatures. For example, when comparing ionized species to neutral species, spectroscopic delay times on the order of microseconds should be used.

One method of determining temperature incorporates the use of the expression for relative line intensities from two emission lines of the same species and ionization shown in equation 2.27 (above). Solving this equation for temperature we get

$$T = \frac{E_2 - E_1}{k_B \cdot \ln \left(\frac{I_1 g_2 A_2 \lambda_1}{I_2 g_1 A_1 \lambda_2} \right)} \quad (2.33)$$

Typical difficulties encountered with this method of temperature calculation include poor accuracy for theoretical transition probabilities. Note that increased accuracy in the temperature is achievable when there is a large difference in the energy between the energy levels.

A second common practice in spectroscopic plasma-temperature determination is to use multiple temperature calculations from a species within the plasma. This assumes LTE and optical thinness are observed. Then by plotting observed emission intensities against upper state energies and fitting these in what is known as a “Boltzmann plot” a weighted temperature can be calculated. Using the Boltzmann distribution substituted into the integrated line intensity (equation 2.34) for a single emission line we find that

$$I(\lambda_0) = \frac{hc}{\lambda_0} \frac{sA_{ji}g_jN_i}{Q} \exp\left(-E_j/k_B T\right) \quad (2.34)$$

where I is the integrated observed intensity from the transition, λ_0 is the central wavelength of the emission line profile, s is plasma depth, A_{ji} is the Einstein coefficient for spontaneous transition, g_j is the degeneracy of the level upper level j , N_i is the number density of the species, E_j is the energy of the j th level with respect to ground state, and Q the electronic degrees of freedom (partition function) given by equation 2.35.

$$Q = \sum_j g_j e^{-E_j/k_B T} \quad (2.35)$$

In 2.35, Q is the partition function, the sum is over all allowed electronic levels; g_j is the degeneracy of the level j , and E_j the energy of the j th level. Note that at low temperatures, if the

first excited state is large with respect to $k_B T$, it is convenient to use only the ground state degeneracy since it is much larger than the other contributions.

By taking the natural logarithm of both sides of the integrated intensity expression the equation for temperature can be simplified using equation 2.34 above and it can be used multiple times for emissions from within the same species, in order to create a best-fit line.

$$\ln\left(\frac{I}{A_{ji} g_j}\right) = \text{const.} + \ln\left(\frac{N_i}{Q}\right) - \left(\frac{E_j}{k_B T}\right) \quad (2.36)$$

The above equation has a linear ' $y = mx + b$ ' form and can be graphed on a plot of $\log(y)$ versus x , where y is $(I / A_{ji} g_j)$ and x is E . The advantage of this is that numerous constants do not need to be determined. With the assumption that the emitted spectral lines all approximately stem from the same location within the plume, we can make a plot of the multiple temperature determinations and the slope of the best fit line through the data points " m " (equal to $-1/k_B T$) will give the weighted temperature. Such a plot is shown below in figure 2.10

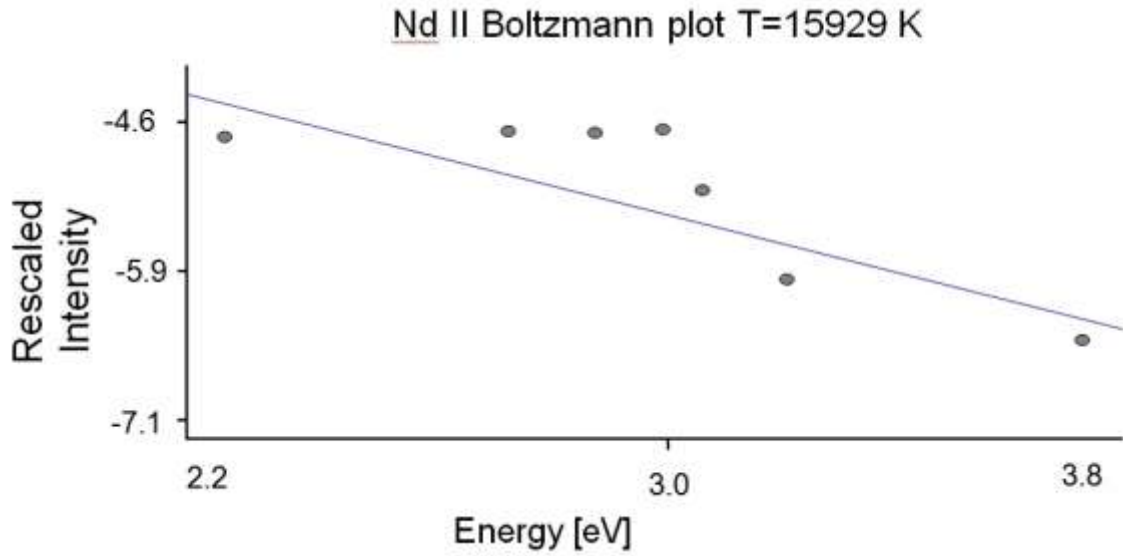


Figure 2.10 is a Boltzmann plot used to calculate temperature for Nd II. The integrated intensities from singly-ionized lines of neodymium were used to create this temperature plot. The resulting temperature is calculated to be 1.59×10^4 Kelvin.

Another method incorporates Saha's ionization distribution for identical species of neighboring ionization states. This method is often used in two ways, (i) first it is used to assess the temperature's variation in spatial and temporal distribution within the plasma plume. This is done by using the calculated intensity of strong lines from each ionization stage of interest at certain locations in the plasma and delay times and plotting the profiles' intensities versus temperature; then comparing the relative intensities of the calculated intensities with the experimentally determined values. (ii) Secondly, the Saha distribution can be used directly as a single calculation of the temperature.

One can make use of the Saha and Boltzmann expressions together to get temperatures from neighboring ionic species at certain energy separations, as shown in equation 2.37. Here

χ_{ion} is the ionization potential and $\Delta\chi_{\text{ion}}$ is the lowering correction parameter from the ionization decrease caused by the Debye shielding of atomic nuclei in plasmas.³³

$$\frac{I_{ji}^{Z+1}}{I_{nm}^Z} = \left(\frac{A_{ji}^{Z+1} g_i^{Z+1} \lambda_{mn}^Z}{A_{nm}^Z g_m^Z \lambda_{ji}^{Z+1}} \right) \left(\frac{2(2\pi m_e k_B T)^{3/2}}{N_e h^3} \right) \cdot \exp \left[\frac{(\Sigma)}{k_B T} \right] \quad (2.37)$$

A log-log plot can be made from this expression with the x-axis describing the energy difference and the y-axis incorporating the natural log of the relative intensities, transition probabilities, and degeneracies belonging to the two emission lines as shown below in equation 2.38. The inverse slope will again yield the temperature if the plasma is in LTE.

$$\ln \left(\frac{I_{ji}^{Z+1} A_{nm}^Z g_m^Z}{I_{nm}^Z A_{ji}^{Z+1} g_i^{Z+1}} \right) = \text{const.} + \ln \left(\frac{2(2\pi m_e k_B T)^{3/2}}{N_e h^3} \right) - \frac{(\Sigma)}{k_B T} \quad (2.38)$$

In both 2.37 and 2.38 $\Sigma \equiv \chi_{\text{ion}} - \Delta\chi_{\text{ion}} + E_i^{Z+1} - E_m^Z$.

Other methods of determining temperature include calculating the temperature from the FWHM of a Doppler broadened line which relates to the species' velocity distribution.^{33,3} Also using the absolute intensity of an emission line from an optically thick plasma the temperature can be determined since the optical depth scales as $T^{-1/2}$.

Electron Density Calculations

Another attribute of plasmas which is often of interest in plasma spectroscopy is the electron number density, N_e . The electron number density can be used in numerous ways to

model plasma expansion and temperature, and to help understand important line broadening techniques. There are multiple ways to calculate this value; I will only highlight the two methods often used in LIBS below.

The first method of determining the electron density is to use line broadening and shifting techniques.^{33,2,31,3} For most LIPs the line broadening and shifting can be attributed almost entirely to the *Stark effect* - due to collision between ions, electrons and neutrals, and to *Doppler broadening* – resulting from moving emitting species. These two broadening mechanisms were discussed in detail earlier. For larger mass species within the plume, the Doppler effect becomes less significant due to its dependence on the inverse of the species' mass. The FWHM of a Stark broadened line scales linearly with N_e for those ions which are hydrogen-like. For heavier elements the quadratic Stark effect plays an important factor. For typical LIBS conditions, ion broadening contributions to the Stark effect are negligible and to a good approximation the Stark broadening can be determined by equation 2.39 below. Here $\Delta\lambda_{Stark}$ is the FWHM value of the line, w is the electron impact halfwidth - which can be found in Griem's "*Spectral line broadening by plasma*,"³¹ – and N_e is the electron density.

$$\Delta\lambda_{Stark} = 2 \cdot w \cdot \left(\frac{N_e}{10^{16}} \right) \quad (2.39)$$

The second method of determining the electron density is to use Saha's ionization equation. The Saha relation (equation 2.15) relates relative ionization populations of two neighboring species, $Z+I$ and Z , having energies n and j respectively, and it depends linearly on the electron density. If the conditions for LTE hold true within the emitting environment then

substituting for the relative populations $\left(\frac{N_j^{Z+1}}{N_n^Z} \right)$ the relative intensity along with the corresponding transition probabilities and other factors $\left(\frac{I_{nm}^Z A_{ji}}{I_{ji}^{Z+1} A_{nm}} \right)$, the Saha equation can be solved for the electron density and expressed below in equation 2.40 where the terms are defined above.

$$N_e = \frac{2(2\pi m_e k_B T)}{h^3} \frac{I_{nm}^Z A_{ji} g_j^{Z+1}}{I_{ji}^{Z+1} A_{nm} g_n^Z} \exp \left(- \frac{\chi_{ion} - \Delta \chi_{ion} + E_j^{Z+1} - E_n^Z}{k_B T} \right) \quad (2.40)$$

2.4 – Experimental Data and Parameter Determinations

The plasma is dynamically changing and in constant motion during its expansion and lifetime. The various conditions in which the plasma is formed and at which the spectral observation is made will affect the resulting spectrum. Therefore care must be taken when endeavoring to calculate desired conditions from within the plasma such as ionization populations, continuum or spectral emission, temperature, electron density, etc. The experimental parameters which affect the plasma have been carefully studied and the results are shown below.

2.4.1 - Pressure Effects on Plasma

The ambient pressure plays a significant role in plasma plume expansion and even in the initial stages of electron-avalanche leading to plasma generation. If the pressure is too small the

plume expands too rapidly and thermal heating due to collisions may never sufficiently diffuse to the surrounding plume therefore insufficiently heating the plasma and not generating the necessary fraction of ionized species required for plasma initiation. In the other extreme when the pressure is too large the plume is short lived and confined, causing significant re-absorption of the radiated light thus making accurate and useful spectral measurements very difficult.

Numerous research groups have reported various ambient pressures for use in LIBS in the literature. Ortiz et al.³⁴ determined transition probabilities for Cu II using LIPs at a pressure of ~8 torr (~6 mbar) in an argon buffer gas. Rojas et al.³⁵ used a 4 mbar (3 torr) argon atmosphere to observe the plasma plume. Kuzuya et al.³⁶ showed that the most intense emissions were obtained in argon gas environment at a pressure of 200 torr and Sdorra et al.³⁷ found that at a pressure of 105 torr the 285.21 nm line of Mg produced its largest intensity. However Kuzuya³⁶ also found that the best signal to noise was found at a pressure of 40 torr when using a 20 mJ laser pulse. Since my research is often strongly based on the ability to measure small emission lines from weak transition our goal was to use a pressure and other parameters which yield good signal to noise (S/N) instead of focusing solely on maximum line intensity.

In my preliminary research, LIBS spectra were collected from 0.41 mbar to 1040 mbar. At low pressures it was evident that the plasma plume was able to expand more readily, thereby creating a plasma which was less electronically dense and a corresponding decrease in plasma lifetime was revealed. This less-dense plasma is typically problematic for spectroscopy, in that the number of atomic excitations per unit volume becomes significantly reduced because of insufficiency of collisions to excite the necessary transitions. A reduction in excitation decreases the ability to detect sufficient amounts of spontaneously decaying photons for branching ratio

measurements. At larger pressures, however, the plasma is confined to smaller volumes, thus creating an optically dense plasma. This dense plasma plume is capable of causing plasma shielding, thus blocking the incident laser and hindering further target ablation as well as the corresponding increase of electronic number density. Any significant changes within the plasma's composition can directly affect branching ratio and atomic lifetime measurements, when determining absolute intensities from the plasma.

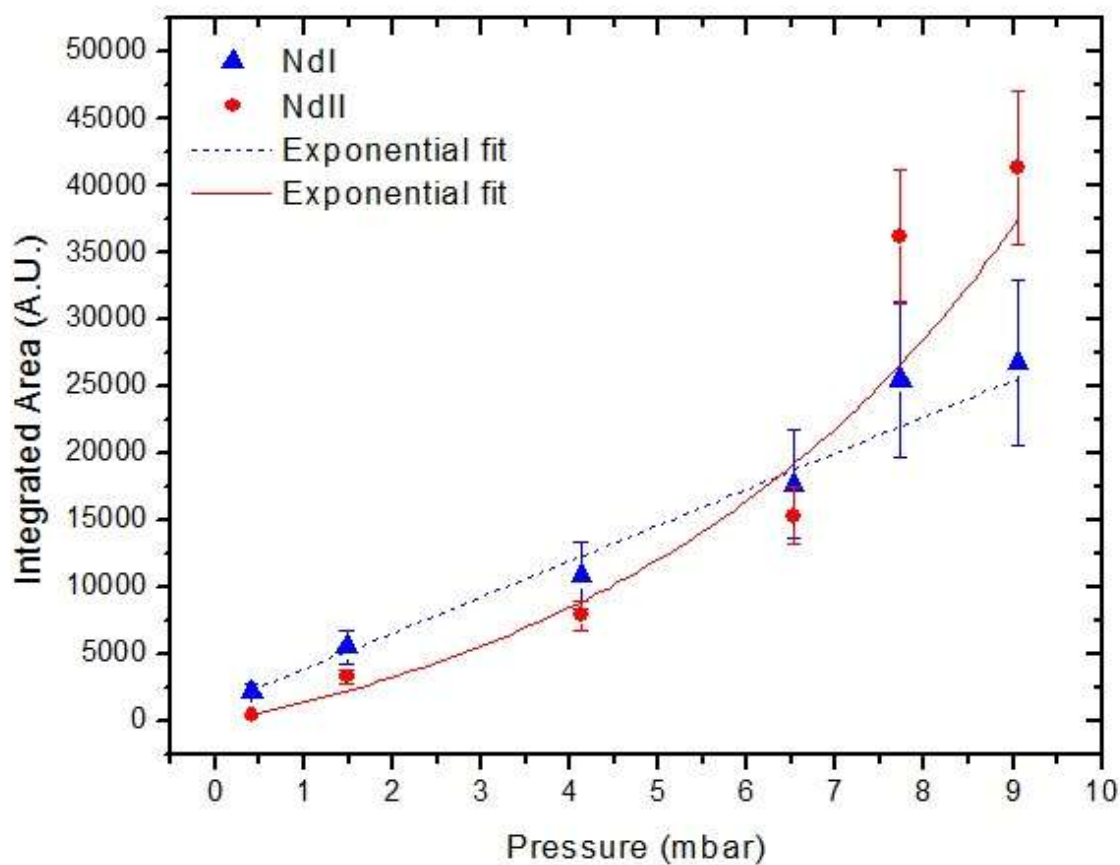


Figure 2.11 Absolute emission intensity vs. vacuum chamber pressure (in mbar) at a constant observation delay time for a line of Nd I at 492 nm (triangles) and Nd II at 532 nm (solid circles). Data have been fit exponentially.

A pressure between extrema which optimized key parameters was determined to be 7.7 mbar in an argon buffer gas environment. A graph of the resulting integrated emission intensity versus vacuum chamber pressure for a line of Nd I at 436.357 nm and Nd II at 536.147 nm is shown in Figure 2.11 above. The data have both been fit by an exponential growth curve. Although the Nd I data look fairly linear at this delay time, my other studies of intensity vs. pressure at later delay times showed a more clear exponential growth behavior. Therefore an exponential growth function was used for all delay times. The error bars were obtained by

calculating the standard deviation of 20 identical spectra. To give the reader an idea of the various plasma densities, pictures of the plume are shown in figure 2.12 at pressures ranging from 2.3 mbar to 0.08 mbar. The pictures were the result of a common point-and-click Kodak camera with typical exposure time of tenths of a second. It is clear that at 0.08 mbar the plume is very spread out and diffuse, whereas at 2.3 mbar the plume looks much brighter and the emission from the central region is very strong.

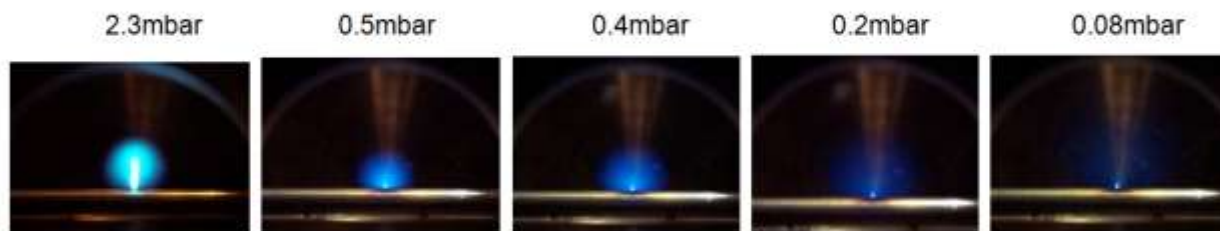


Figure 2.12 above shows the plume at various pressures in an argon environment. It is evident that as pressure is decreased in the chamber, the plume becomes more diffuse and less dense.

2.4.2 - Temporal Evolution

The effect that delay time had on measurements of plasma was also investigated. Delay time is the amount of time between the initial laser pulse and spectroscopic observation of the plasma. Using a time-resolved spectrometer allows me to vary this time from 10's of ns after the laser pulse to 10's of microseconds. A graph of the observed emission intensity as a function of delay time for a line of Nd I at 492.453 nm and Nd II at 536.147 nm is shown in Figure 2.13.

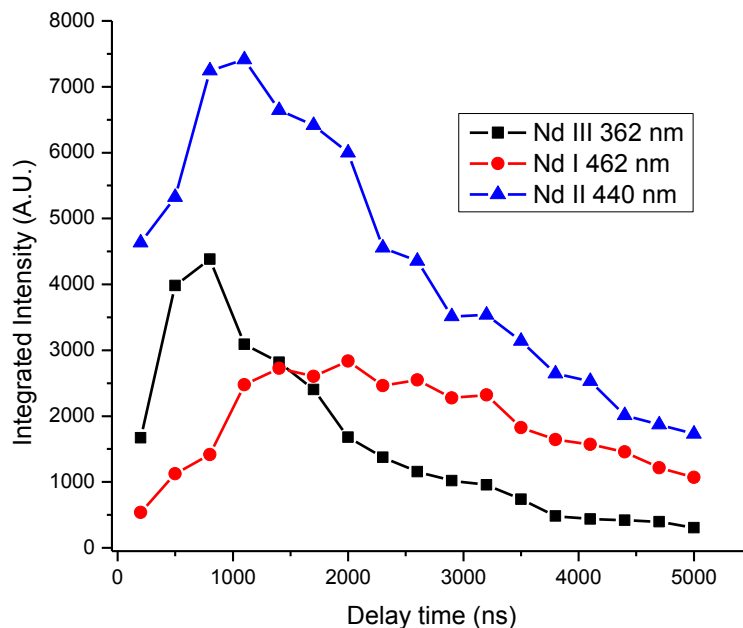


Figure 2.13 Absolute emission intensity vs. delay time for a line of Nd I at 462 nm (red circles), Nd II at 440 nm (blue triangles), and Nd III at 362nm (black squares). The neighboring data points were connected by straight lines as a guide to the eye to show the trends in time.

The effects of delay time on the measured signal-to-noise ratio and signal-to-background of the observed emission lines were also studied. Lastly, Einstein A -coefficients for the eight branches of interest in Nd II were calculated at various delay times and compared to known values. It was decided that a delay time of 1000 ns would be used in all subsequent measurements to maximize emission from the strongest, most obvious emission lines while minimizing the contribution from the broadband background emission and to provide reproducible data most in agreement with previous experiments.

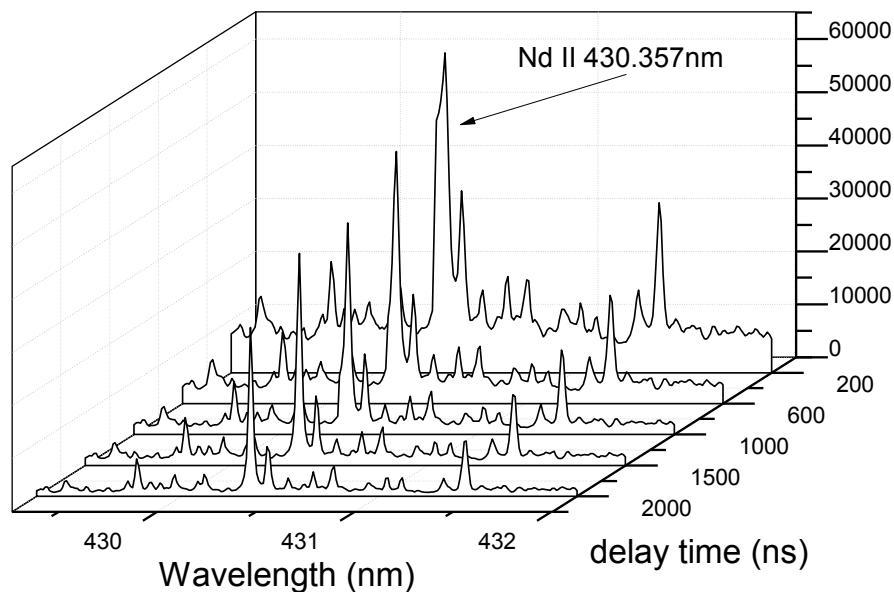


Figure 2.14 depicts a waterfall figure showing absolute emission intensity vs. wavelength for five delay times for a line of Nd II at 430.357 nm. Line intensity decreases with time. It is worth noting that as the time elapses the background and noise also tend to decrease.

Previous LIBS studies have shown that the measured emission intensity is definitely time dependent and that other parameters like ambient pressure, gas environment, and laser irradiance also play an important role in emission intensities. Rojas et al.³⁵ used a 4 mbar (3 torr) argon atmosphere to observe the plasma plume at a delay time of 300 ns. Ortiz et al.³⁴ searched for the best S/N ratio at various delay times and found 200 ns to be best for their parameters. Leis et al.³⁸ showed that the ratio of singly-ionized to neutral iron intensities was maximized around 3 μ s and after about 10 μ s the neutral line dominates. Castle et al.³⁹ concluded that the best S/N was found near 6 μ s. Clearly, as with the ambient pressures noted above, every experimental condition

tends to yield its own unique optimum delay time and pressure, depending on what criteria are used to define “optimum” for that experiment.

2.4.3 - Spatial Distribution of the Plasma

At a pressure of ~8 mbar (~ 6 torr) the plasma plume took on an ovular shape with height and width dimensions of approximately 1.4 cm and 1.0 cm respectively. Because of the large plume size, it was not possible to image the entire plasma onto the core of the multimode fiber which carried emission to the spectrometer. After demagnification through the light collection optics and given an optical fiber diameter of 600 μm , the plasma image in the image plane of the fiber was approximately four fiber-core diameters in height. This corresponded to the ability to view four sections of the plasma independently, but not simultaneously. This is shown below in Figure 2.15. Previous work shows that Kim et al.⁴⁰ found that at a height above the target's surface of 3mm at delay time of 30 μs produced the highest intensity when observing the plasma perpendicularly to the incident laser beam.

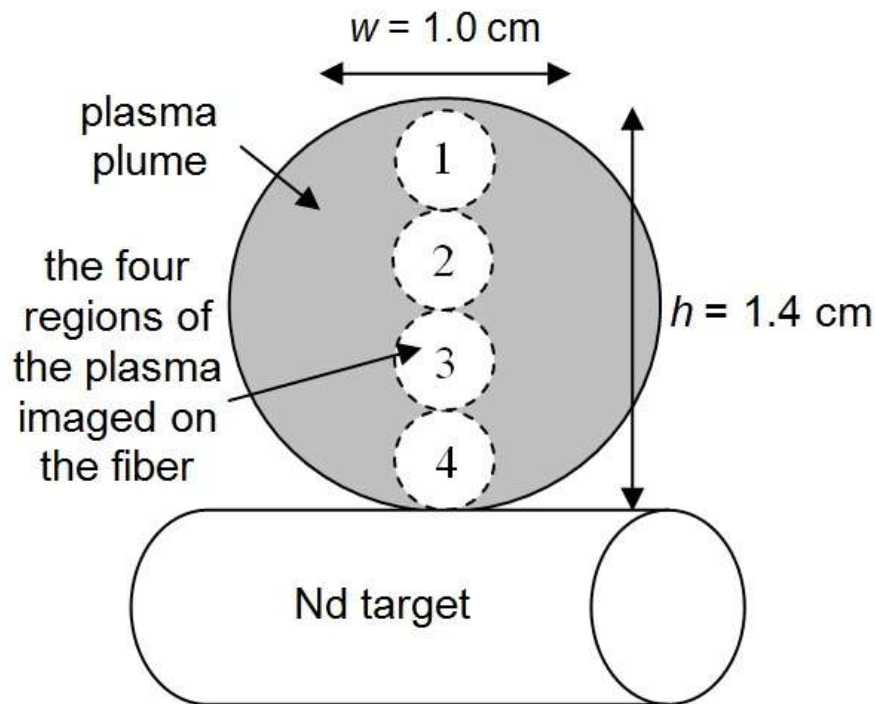


Figure 2.15 A schematic of the Nd plasma at low pressures. The spatial extent of the expanding plasma precluded observation of the entire plasma with the light collection optics. The image of the plasma in the image plane spanned four optical fiber diameters, so four distinct regions of the plasma could be observed independently, but not simultaneously.

The section of the plasma plume which was observed had a direct effect upon atomic data. The major parameters which were investigated were emission intensity, signal-to-noise ratio, and the measured Einstein A coefficients and their discrepancy with previously reported A -coefficients.⁴¹ The bottom most region (region 4) of the plasma plume had signal intensities which were of the smallest magnitude (~ 500 A.U.) and largest percent discrepancy ($\sim 33\%$); this is not surprising given the density of the plasma in this region. Region 3, the next section above the bottom, revealed signal intensities on the average of ~ 5000 A.U., which were still small with respect to the continuum background. Region 3 also had a poor A -coefficient percent discrepancy

compared to those previously reported in other works, approximately 19.7%. Region 2 showed the lowest consistent percent discrepancy (10%) and the highest emission intensity (~9000 A.U.), with the best signal-to-noise. Region 1, the top most portion of the plasma, revealed a decrease in signal intensity compared with region 3 (~4000 A.U. at delay times ranging from 400 ns to 1000 ns), with rapidly increasing percent discrepancies as a function of delay time (>10%). It was decided that the region of the plasma plume which yielded data best fit for comparison to previous works was the mid-upper region (region 2).

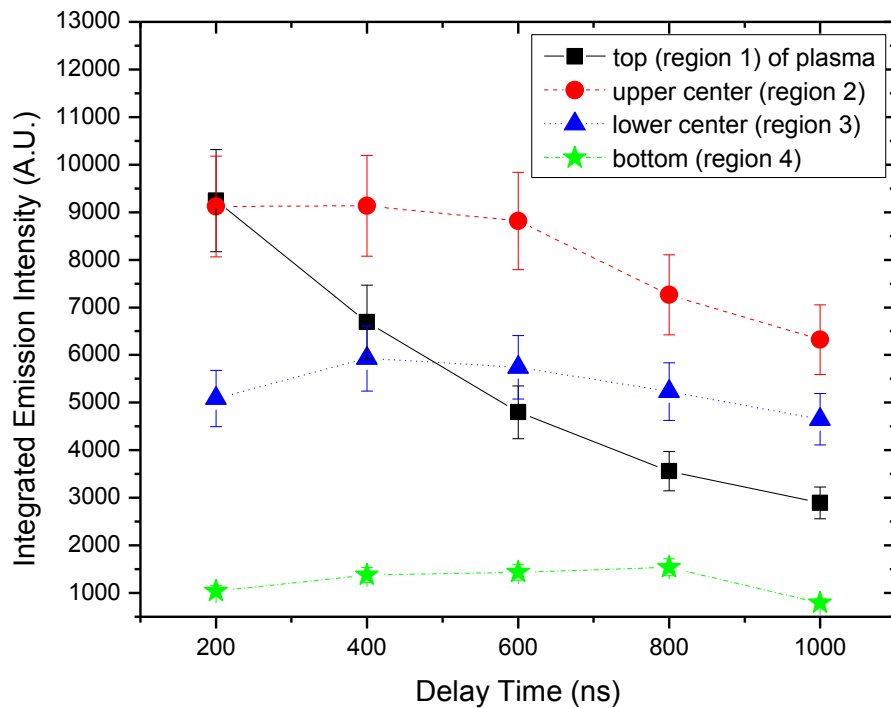


Figure 2.16. The four regions which were resolvable using the optical fiber's aperture were researched. The effect of delay time on the emission from within each region's collection volume is shown in the figure above.

2.4.4 - Buffer gas effects

As already stated above, the ambient gas environment also plays an important role in plasma production and evolution. Multiple LIBS experiments have shown that an argon buffer gas produces the best S/N ratio out of all the buffer gases commonly used (helium, air, nitrogen, neon) in LIBS measurements. Kuzuya et al.³⁶ showed that the most intense emissions were obtained in an argon gas environment at a pressure of 200 torr. Sdorra et al.³⁷ showed that of the 5 gases, argon demonstrated higher plasma temperatures and higher electron densities. Furthermore, they showed that by using argon the plasma lifetime was elongated. Kim et al. also showed that argon produces longer plasma lifetimes and larger signal intensity. Wisburn et al.⁴² showed that argon was preferred in terms of emission intensity and better reproducibility than air.

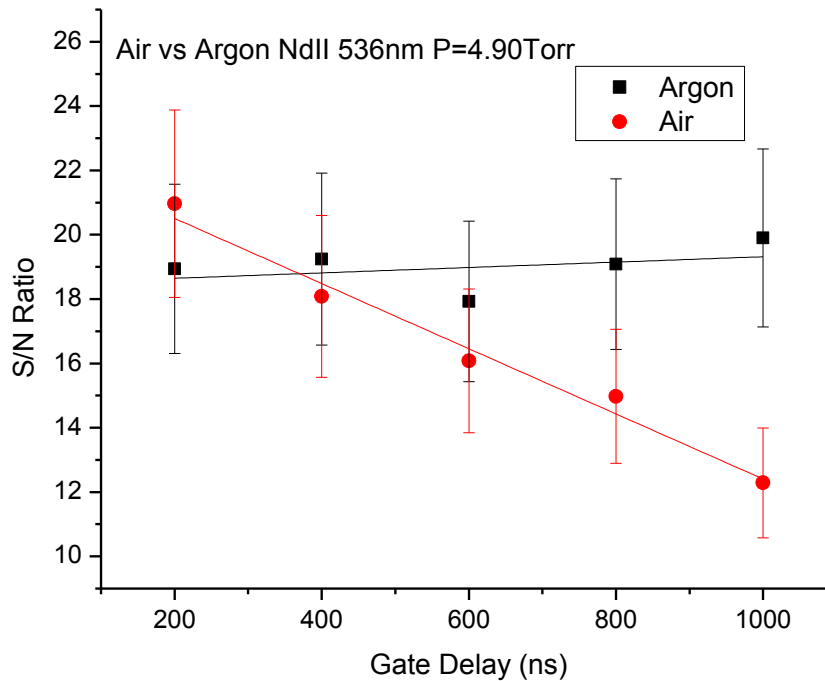


Figure 2.17 Shows the signal to noise comparison between two buffer gases as a function of delay time for LIBS environments in my vacuum chamber.

By performing experiments in both air and argon, it was found that the signal to noise was larger and more consistent in argon than in air at the delay times used to conduct the experiment. Thus argon was the buffer gas of choice. The graph above (Figure 2.16) shows the comparison.

2.4.5 – Clean Pulses

Clean pulses can be defined as the initial laser shots which strike the target causing ablation and plasma sparking in order to provide a fresh “clean” target surface for the subsequent analysis pulses from which emission was collected. This pulse may remove surface impurities or any native oxide layer. In my apparatus I found that a single clean pulse was best for producing

emission signals with the largest line intensities and minimal background. It was also noted that an increase of clean pulses beyond one shot did not improve spectroscopic data. Castle et al.³⁹ and Wisburn et al.⁴² also found that their S/N obtained a greater reproducibility when each laser shot was focused on a fresh surface on a solid sample.

2.4.6 - Sample Concentration

The final parameter which affects the plasma concentration and temperature depends strongly upon the matrix conditions of the sample target. In this study I compared sample concentrations in a neodymium / wax mixture with neodymium concentrations of 1% to 10% to 100% (pure metal). My results for the 1% and 10% Nd concentrations showed that weaker transitions in the spectrum were not resolvable because of a poor SNR (signal-to-noise ratio). Remember that line emission intensity depends on species concentration, as shown in equation 2.34. The poor SNR for these weaker transitions made branching ratio measurements almost impossible. Since one needs to observe all of the transitions from a given upper state to make a completely accurate branching ratio measurement, the lower concentrations were considered insufficient for our needs. It also seems that the extra wax content in the lower-concentration samples caused the plasma temperature to be insufficient for populating the necessary upper energy levels in Nd. The studies from Wisburn et al.⁴² support our theory that the more humid a sample is the lower the emission intensity will be due to the waste of energy in evaporating the substance. This in turn affects the amount of ablated mass which becomes incorporated into the plasma plume which produces the desired spectral emissions. As stated earlier, larger concentrations of ablated material in the emitting plasma should result in larger emission lines given that absorption is negligible in LTE.

In summary, in this chapter I have described all the key plasma and experimental parameters and optimized them (delay time, open shutter gate width, buffer gas, chamber pressure, plume morphology, sample concentration) for singly ionized species in order to obtain the best emission measurement using the LIBS apparatus. The target used in my experiments were all >99.99% pure solid cylindrical rods which showed the best reproducible spectra with optimum signal to noise, while allowing observation of most of the weak transitions, as opposed to the targets of weaker concentrations which did not. The delay time was chosen to be 1000 ns after the laser pulse in order to observe mainly the singly-ionized species emitted from the plasma while still being able to observe neutral and doubly-ionized species and reducing the continuum emission from the plasma. We found that an open shutter time of 1000 ns was sufficient to collect the necessary emission intensities to perform our research while minimizing the noise. Argon was chosen as the buffer gas due to its ability to provide large S/N. The chamber pressure was set to 8.3 torr in argon in order to optimize signal to noise while maintaining a plasma which was not too diffuse for LTE. One clean shot from the laser was used because we found more than this did not increase the signal to noise ratio. Rotation and translation of the sample was found to increase reproducibility thus I have used an apparatus where a screw threaded into a fixture is coupled to the sample in order to translate and simultaneously rotate the cylindrical target. Observation of the plasma emission is primarily focused at the second region shown in figure 2.15 because of its high emission intensity and best signal to noise. The experimental parameters which we have optimized for measurements on singly ionized species used in this experiment are listed in table 2.3.

Parameter	Setting
Gate delay (τ_d)	1000 ns
Gate width (τ_w)	1000 ns
Buffer gas	argon
Pressure	8.3 Torr
ICCD gain	2800
On-chip accumulations	10
Averaged spectra	10

Table 2.3 shows the optimized parameters used in this experiment

¹ E. Damon and R. Thomlimson, "Observation of ionization of gases by a ruby laser," Appl. Opt. **2**, 546-550 (1963).

² J.P. Singh and S.N. Thakur, *Laser-Induced Breakdown Spectroscopy*, Elsevier, Amsterdam, (2007).

³ L.J. Radziemski and D.A. Cremers, *Laser-Induced Plasmas and Applications*, Marcel Dekker Inc, New York, (1989).

⁴ P. Hofmann, *Solid State Physics an Introduction*, Wiley-VCH Verlag GmbH & Co. Weinheim, (2006).

⁵ W. Svendsen, O. Ellegnard, J. Schou. "Laser ablation deposition measurements from silver and nickel," Appl. Phys. A **63**, 247-255 (1996).

⁶ M. Von Allmen, *Laser Beam Interactions with Materials*, Springer-Verlag, New York, (1998).

⁷ P. Atkins, *Atkins Physical Chemistry*, 8th ed., Oxford Press, Oxford, (2006).

⁸ F.F. Chen, *Introduction to Plasma Physics and Controlled Fusion*, Springer Science+Business Media, New York, (2006).

-
- ⁹ D.E. Kim, K.J. Yoo, H.K. Park, K.J. Oh, D.W. Kim, “Quantitative analysis of aluminum impurities in zinc alloy by laser-induced breakdown spectroscopy,” *Appl. Spectrosc.* **51**, 22-27 (1997).
- ¹⁰ H.R. Griem, *Principles of Plasma Spectroscopy*, Cambridge University Press, Cambridge, (1997).
- ¹¹ D. Mihalas, *Stellar Atmospheres*, W. H. Freeman and Company, San Francisco, (1970).
- ¹² R.H. Huddleston and S.L. Leonard, *Plasma Diagnostic Techniques*, Academic Press, New York, (1965).
- ¹³ D. Salzman, *Atomic Physics in Hot Plasmas*, Oxford University Press, New York, (1998).
- ¹⁴ G. Cristoforetti, A. De Giacomo, M. Dell'Aglio, S. Legnaioli, E. Tognoni, V. Palleschi, N. Omenetto, “Local thermodynamic equilibrium in laser-induced breakdown spectroscopy: beyond the McWhirter criterion,” *Spectrochim. Acta Part B* **65**, 86-95 (2010).
- ¹⁵ H.W. Drawin, “Validity conditions for local thermodynamic equilibrium,” *Z. Phys.* **228**, 99–119 (1969).
- ¹⁶ H.R. Griem, “Validity of local thermal equilibrium in plasma spectroscopy,” *Phys. Rev.* **131**, 1170–1176 (1963).
- ¹⁷ M.C. Quintero, A. Roderio, M.C. Garcia, A. Sola, “Determination of the excitation temperature in a non-equilibrium high pressure helium microwave plasma torch,” *Appl. Spectrosc.* **51**, 778–784 (1997).
- ¹⁸ T. Fujimoto and R.W.P. McWhirter, “Validity criteria for local thermodynamic equilibrium in plasma spectroscopy,” *Phys. Rev. A* **42**, 11 (1990).

-
- ¹⁹ H.R. Griem, *Principles of Plasma Spectroscopy*, Cambridge University Press, Cambridge, (1997).
- ²⁰ V.N. Ochkin, *Spectroscopy of Low Temperature Plasma*, Wiley-VCH Verlag GmbH & Co. KGaA, Weinheim, (2009).
- ²¹ R.W.P. McWhirter and A.G. Hearn, "Calculation of the instantaneous population densities of excited levels of hydrogen-like ions in plasma," *Proc. Phys. Soc.* **82**, 641-645 (1986).
- ²² L.H. Aller, *Atmospheres of the Sun and Stars*, Ronald Press, New York, (1963).
- ²³ C.R. Cowley, *The Theory of Stellar Spectra*, Gordon and Breach, New York, (1970).
- ²⁴ W. Lochte-Holtgreven, *Plasma Diagnostics*, North-Holland, Amsterdam, (1968).
- ²⁵ G. Marr, *Plasma Spectroscopy*, Elsevier, New York, (1968).
- ²⁶ R. More, "Atomic processes in high density plasmas," in *Atomic and Molecular Physics of Controlled Thermonuclear Fusion*, (ed. C.J. Joachain and D.E. Post), Plenum Press, New York, (1983).
- ²⁷ D.D. Burgess, "Spectroscopy of dense laser-generated plasmas," in *Laser-Plasma Interactions* 2 ed., Scottish Universities summer school in Physics, Edinburgh, (1990).
- ²⁸ In *Atomic, Molecular, & Optical Physics Handbook*, Chaps. 19 and 57, ed. by G.W.F. Drake, AIP, Woodbury, (1996).
- ²⁹ N.M. Shaikh, B. Rashid, S. Hafeez, S. Mahmood, M. Saleem, M.A. Baig, "Diagnostics of cadmium plasma produced by laser ablation," *J. Appl. Phys.* **100**, 073102 (2006).
- ³⁰ E. Togononi, V. Palleschi, M. Corsi, G. Cristoforetti, "From sample to signal in laser-induced breakdown spectroscopy: a complex route to quantitative analysis," in A.W. Miziolek, *Laser-*

Induced Breakdown Spectroscopy Fundamentals and Applications, Cambridge University Press, New York, (2006).

³¹ H.R. Griem, *Spectral Line Broadening by Plasmas*, Academic Press, New York, (1974).

³² B. Le Drogoff, J. Margot, M. Chaker, M. Sabsabi, O. Barthélemy, T.W. Johnston, S. Laville, F. Vidal, Y. von Kaenel, "Temporal characterization of femtosecond laser pulses induced plasma for spectrochemical analysis of aluminum alloys," *Spectrochim. Acta B* **56**, 987 (2001).

³³ A.P. Thorne, *Spectrophysics*, William Clowes & Sons Ltd, London, (1988).

³⁴ M. Ortiz, R. Mayo, E. Biemont, P. Quinet, G. Malcheva, K. Blageov, "Radiative parameters for some transitions arising from the $3d^94d$ and $3d^84s_2$ electronic configurations in Cu II spectrum," *J. Phys. B* **40**, 167-175 (2007).

³⁵ J.A.M. Rojas, M. Ortiz, J. Campos, "Determination of transition probabilities of some Sb III lines by time resolved spectrometry of laser produced plasmas," *Phys. Scr.* **62**, 364-367 (2000).

³⁶ M. Kuzuya, H. Matsumoto, H. Takechi, O. Mikami, "Effects of laser energy and atmosphere on the emission characteristics of laser-induced plasmas," *Appl. Spectrosc.* **47**, 1659-1664 (1993).

³⁷ W. Sdorra and K. Niemax, "Basic investigations for laser microanalysis: III. Application of different buffer gases for laser-produced sample plumes," *Mikrochim. Acta* **10**, 319-327 (1992).

³⁸ F. Leis, W. Sdorra, J.B. Ko, K. Niemax, "Basic investigations for laser microanalysis: I. Optical emission spectrometry of laser-produced sample plumes," *Mikrochim. Acta* **2**, 185-199 (1989).

-
- ³⁹ B.C. Castle, K. Talabardon, B.W. Smith, J.D. Windfordner, "Variables influencing the precision of laser-induced breakdown spectroscopy measurements," *Appl. Spectrosc.* **52**, 649-657 (1998).
- ⁴⁰ D.E. Kim, K.J. Yoo, H.K. Park, K.J. Oh, D.W. Kim, "Quantitative analysis of aluminum impurities in zinc alloy by laser-induced breakdown spectroscopy," *Appl. Spectrosc.* **51**, 22-29 (1997).
- ⁴¹ A.M. Gonzalez, M. Ortiz, J. Campos, "Experimental transition probabilities for lines arising from $5p^2\ 6s$ configuration of neutral Sb," *J. Quant. Spectrosc. Radiat. Transfer* **57**, 825-829 (1997).
- ⁴² R. Wisburn, I. Schechter, R. Niessner, H. Schroder, K. Kompa, "Detector for trace elemental analysis of solid environmental samples by laser plasma spectroscopy," *Anal. Chem.* **66**, 2964-2972 (1994).

Chapter 3 – Experimental

In general, the apparatus used in typical LIBS experiments are composed of six elements, with some variations depending on the composition of the target, the choice of focusing and collecting optics, and whether or not a vacuum system is used. Those six elements are:

1. A high intensity pulsed-laser to create the microplasma.
2. An optics system which directs and focuses the laser beam onto the target sample.
3. A target housing to allow ablation in a controlled environment (which may be a vacuum) and regulate the buffer gas environment.
4. A light collection system (including optics, mirrors, and/or fiber-optic cables) which collects the emitted light and conveys it to the spectrometer.
5. A detection system (spectrometer, camera/detector, computer) to disperse, analyze, record, and display the emitted light spectrum.
6. A computer and monitor to control the timing between the firing of the laser, collection of emitted light, and display of the emission spectrum.

3.1 – Incident Laser and Focusing Optics

The LIBS experimental setup used to make branching ratio measurements in my research is shown schematically in figure 3.1. The laser source (shown in figure 3.2) is a Nd:YAG laser (Spectra Physics, LAB-150-10) firing 10 ns laser pulses at a repetition rate of 10 Hz and operating at its fundamental frequency of 1064 nm to ablate the target. The laser pulse energy used in this work is 20 mJ/pulse on the target. The initial output of the laser is 650 mJ/pulse. A pulse-energy of this magnitude is much larger than necessary for LIBS on solid metals therefore attenuation of the beam is necessary to decrease it to 20 mJ/pulse. To attenuate the laser beam, we pass the vertically polarized output beam through a half-wave plate, which retards polarization parallel to the fast axis by half of a wavelength. This causes a rotation in the

polarization of the beam to double the difference in angle between the half-wave plate's fast axis and the plane of polarization. The beam then passes through a polarized beam splitter which directs the horizontally polarized component into a beam dump and passes the vertically polarized portion of the beam toward the target. By rotating the half-wave plate one can arbitrarily control the amount of laser light directed toward the target. This energy is monitored by a Coherent Field-Max energy meter to insure it is set reproducibly at 200 mW/pulse.

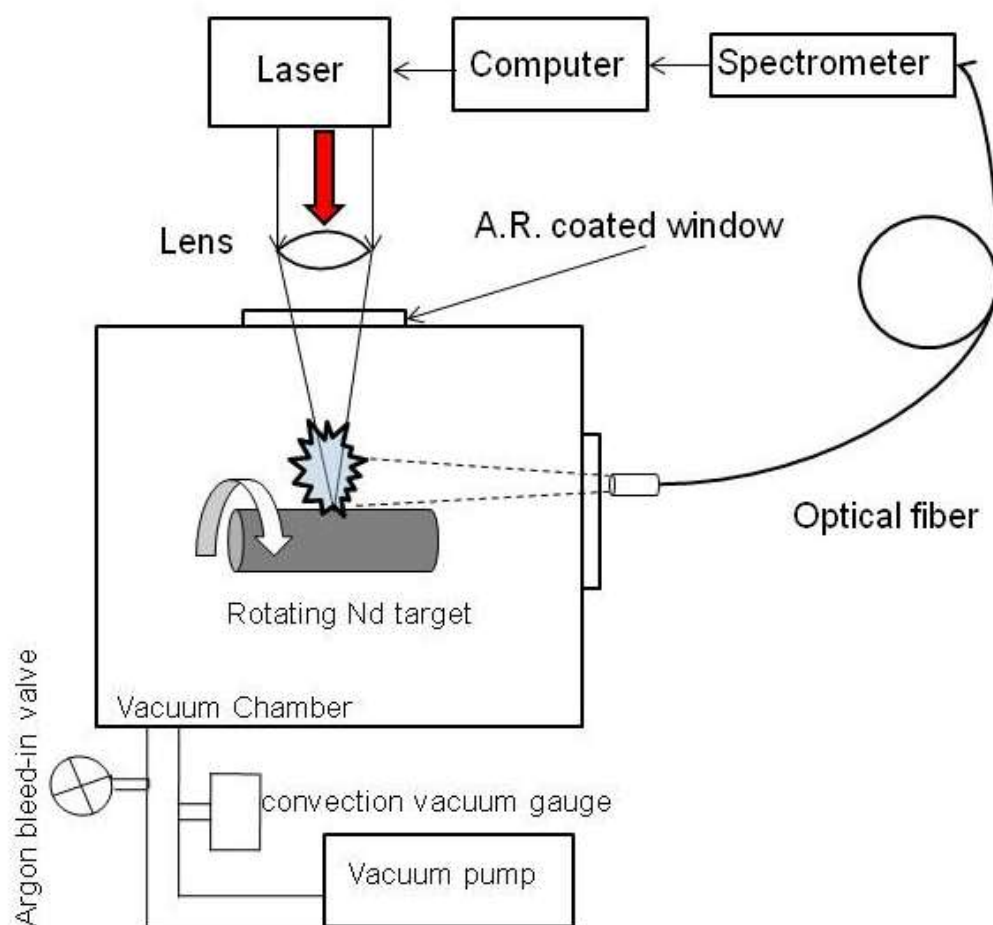


Figure 3.1 The LIBS experimental setup used to make branching ratio measurements. A side-view of the apparatus is shown. The path of the infrared Nd:YAG laser coming through the top of the vacuum cube is depicted with an arrow and solid lines. Visible wavelength plasma emission is collected through a quartz side window and is depicted with dotted lines. The chamber is typically held at a pressure of from 1-15 mbar in argon.



Figure 3.2 The high-energy Lab 150-10 nanosecond laser system used in this research from Spectra-Physics.

In order to direct the laser downward into the vacuum chamber through an anti-reflection coated window on the top flange of the cube vacuum system, 5 mirrors (with 99.9% reflection at 1064 nm) were used in succession. These mirrors were coated for high reflectivity at 1064 nm, so the energy loss per reflection was negligible. The configuration of the mirrors and the lens directing the laser into the chamber is shown schematically in figure 3.3 below

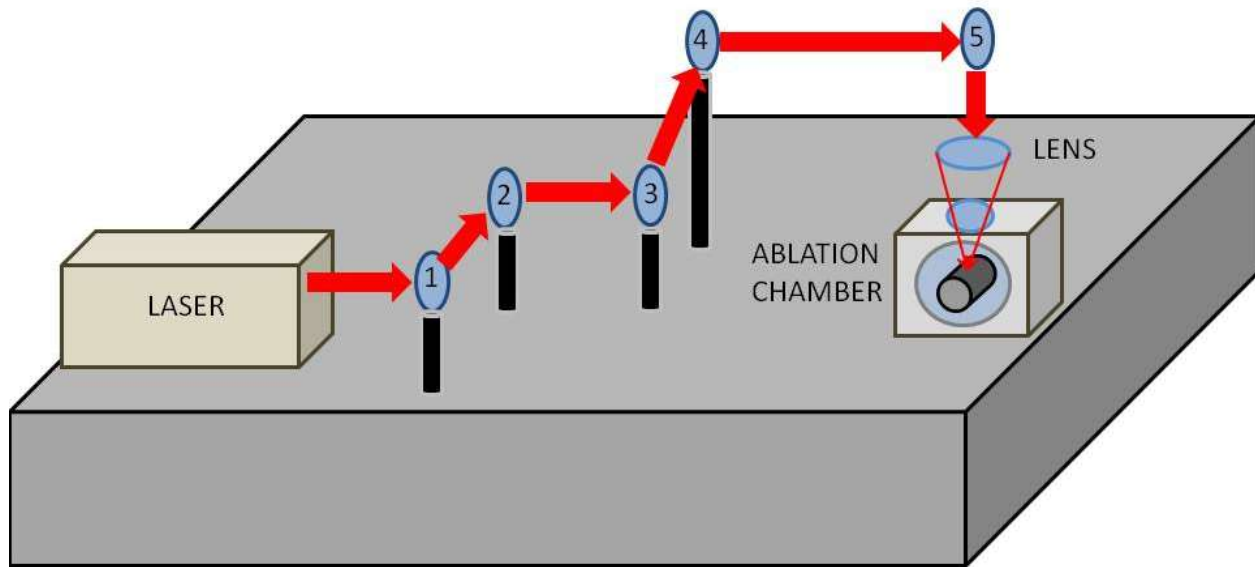


Figure 3.3 shows a schematic representation of the laser's optical path leading to the target. The red arrows signify the pulsed laser beam.

A 75 mm diameter plano-convex lens with effective focal length of 18.5 cm located outside of the ablation chamber was used to focus the laser beam downward into the ablation chamber and incident upon the top side of a rotating and translating cylindrical sample (see figure 3.1). Rotation/translation of the stage was achieved by a motorized rotational vacuum feed-through and a DC-voltage electric motor outside the chamber.

3.2 – Vacuum Chamber and Target

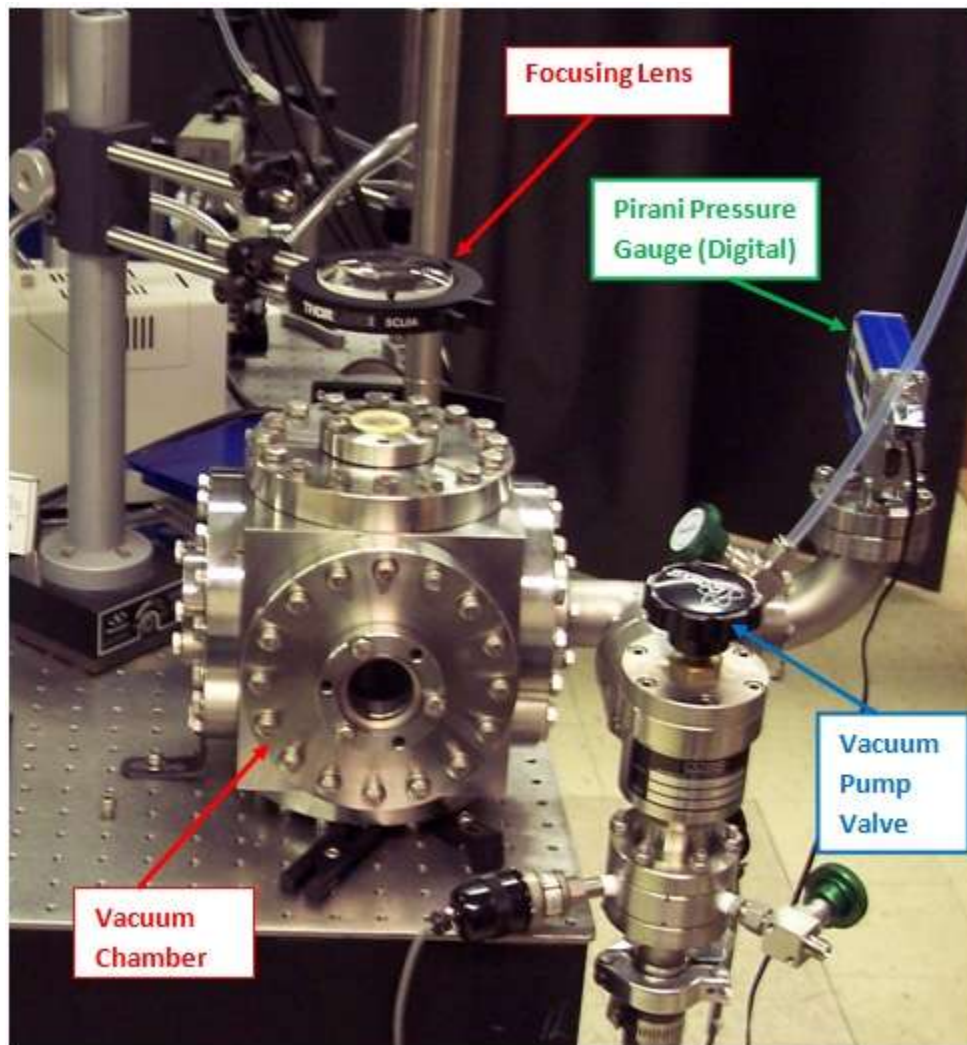


Figure 3.4 The vacuum (ablation) chamber, focusing lens, pressure gauge, and vacuum pump valve are shown.

The ablation chamber, shown above in figure 3.4, is a cubical stainless-steel container with volume of 3500 cm^3 which has a 15.24 cm circular flange on each of the 6 sides for accessibility. The chamber is evacuated by a mechanical vacuum pump (Varian DS-302) to achieve an ambient gas pressure of 11.0 mbar (true pressure of 94mbar) in an argon buffer gas to help create optimal plasma parameters for atomic emission.^{1,2,3} The use of a vacuum chamber in order to decrease pressure has been shown to improve signal to noise in emission spectra.⁴ When

using pressures lower than atmosphere, argon buffer gas produces the highest plasma temperature, highest electron density, and highest emission intensity as compared to such gases as air, helium, or nitrogen.⁵ The argon buffer gas is introduced via short bursts from a needle-valve and the pressure is monitored by a convection module pressure gauge (Kurt J. Lesker 300-series) capable of measuring pressure ranges from 10^{-4} to 1,333 mbar. A wide range of pressures (0.41 - 1040 mbar) were investigated and it was concluded that the best signal to noise, while maintaining optical thinness in the plasma and still exciting most of the weak emissions lines necessary for branching ratio measurements, occurred at 11.0 mbar in an argon atmosphere (or ~94 mbar absolute pressure reading on the convection pressure gauge).

The 0.25 inch cylindrical metal target was mounted onto a 0.25 inch diameter steel feedthrough from an MDC manufactured 115 VAC inline mechanical rotary motor (figure 3.5). The purpose of the rotary motor was to rotate the sample via a 1.70 inch long threaded screw, with $1/40^{\text{th}}$ of an inch thread spacing, which was mounted onto the feedthrough rod. The screw serves to rotate and simultaneously translate the sample in order to give a fresh location for each subsequent laser pulse. The translation and rotation of the sample was achieved by mounting a 0.5 inch rectangular aluminum support onto four stainless steel 0.25 inch diameter posts which were tapped and screwed into one of the vacuum chamber's 1.75 inch stainless steel flanges. The four highly polished steel posts held the aluminum support in place so that the threaded screw, mounted inside of the aluminum support via a reversed-thread sleeve, could be spun by a $1/8^{\text{th}}$ inch Alan key (hexagonal key). On the back side of the aluminum support, the $1/8^{\text{th}}$ inch Alan key's cross-section was machine tapped inside of the screw so that the Alan key slid freely inside; allowing the screw to translate over top of it while the Alan key spun the screw from

within. On the front side of the aluminum support – where the target is attached to the screw – an aluminum cup-like holder was fabricated with inner diameter just larger than 0.25 inches in order to hold the 0.25 inch cylindrical target in place. The holder was screwed onto the 1/40th inch screw and the target was held inside of it. Figure 3.6 shows a schematic of the sample holder apparatus

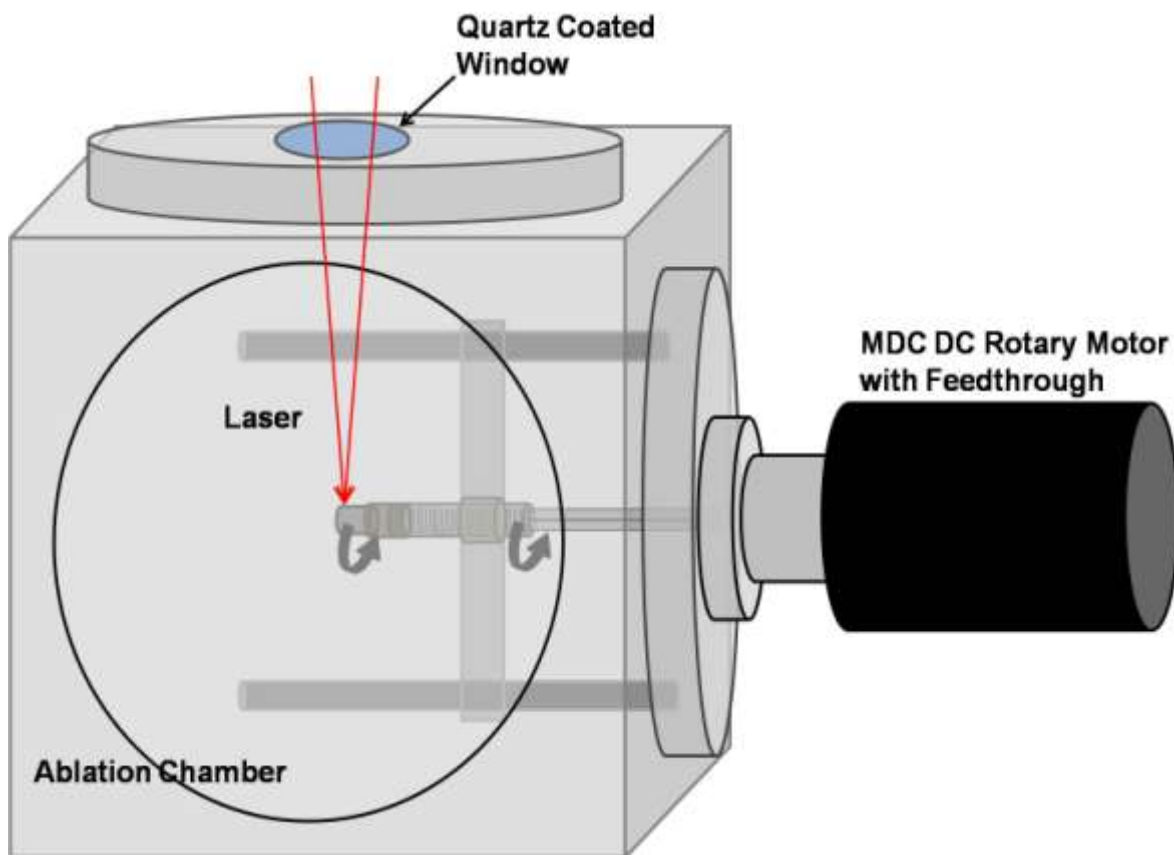


Figure 3.5 shows the ablation chamber with the attached MDC rotary motor and feedthrough which rotates and translates the target.

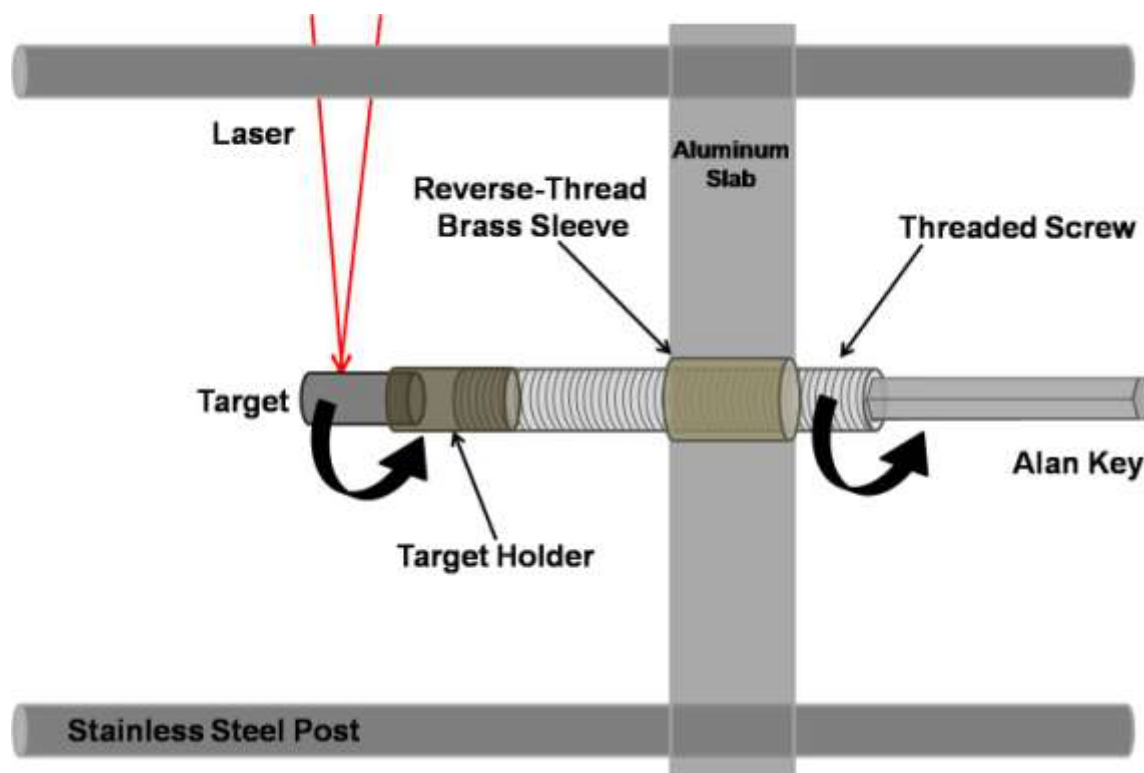


Figure 3.6 is a side view of the target mounting apparatus inside of the ablation chamber. The apparatus was designed to allow for simultaneous translation and rotation of the sample, providing fresh locations for laser ablation.

The Pirani convection gauge used in this research operates by maintaining the temperature of a hot filament within the module. The electrical current (or voltage) required to maintain a constant temperature on the gold-plated tungsten filament against thermal cooling via conduction with the surrounding gas environment yields an indirect measure of the pressure. For higher pressures of the gas environment there are more collisions with the filament, and thus a greater transfer of heat via conduction which registers as a larger current. Normally Pirani gauges are calibrated with nitrogen; however since different gases have different thermal conductivities, the displayed pressure readings and outputs can be different (e.g. an argon atmosphere). Therefore a piece-wise calibration curve for the use of argon in the chamber was

created. Figure 3.7 shows the calibration curve between argon and air (the Pirani gauge always displays pressure as if it is measuring air) for the pressure range used in this work.

However, unlike the Pirani conduction gauge, our gauge also incorporates the use of convection measurements for low pressures (below 1 Torr) expanding the gauge's range of measureable pressures. At high pressure, the gauge's response depends on the thermal conductivity of the gas, while at lower vacuums it depends on convective cooling by the gas molecules. Depending upon the vacuum, the Pirani convectron device will automatically switch between the two sensors.

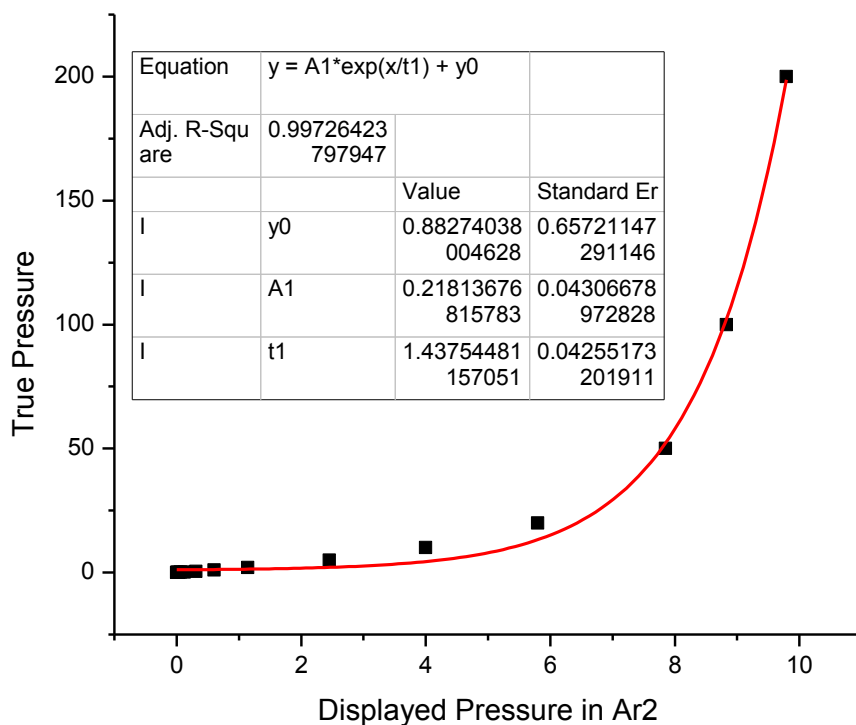


Figure 3.7 shows the calibration curve for converting between the use of argon and air in the Pirani convectron pressure gauge.

Two different types of metallic target samples were used: a solid cylinder (0.25 inch diameter) composed of >99% target material and a thin foil (~0.004 inches or 0.01cm thick) composed of >99% of the target material wrapped around a 0.25 inch diameter solid steel cylinder used to mount the foil. The target was seated into its fixture mounted onto one side flange of the cubical chamber. Given that some samples were thin foils, sample rotation is significant because it provides a fresh location for laser ablation, thus not allowing the formation of deep craters leading to disintegration of the sample. Also, rotation of the sample provides the laser a fresh ablation spot, which has been shown^{6,7} to yield better reproducibility. Two sides of the chamber each have 3.8 cm quartz window: one for transmitting the emitted light from the plasma to the spectrometer and the other for the researcher's benefit.

All vacuum systems having flanges and feedthroughs will constantly "leak", allowing air to seep into the chamber through imperfect seals in the flanges and windows. In order to control the leaks, we monitored the leakage rate after the chamber was evacuated and the pump valve was closed and determined that the rate of pressure increase in the chamber was 0.576 Torr/hour which is 9.61 mTorr/minute in absolute pressure (or in terms of an argon atmosphere reading, 3.5 mTorr/minute). This was an acceptable leakage rate because of the fact that the typical data acquisition time was approximately 20 seconds and the chamber itself was maintained at a pressure of 94 mbar (71 Torr). Furthermore after every 10 spectra acquired the chamber was pumped down to vacuum and refilled with argon to the set pressure. In this way, we could insure that the pressure of argon inside the chamber was constant for every experiment.

3.3 - Light Collection

The plasma emission was collected by a 1 m long steel encased multimode fiber optical cable (FOC) with an acceptance cone, or numerical aperture (N.A.), of 0.22 and core diameter of 600 μm , located just outside the chamber's window, approximately 3 inches from the ablation site. The light collecting FOC was oriented at 90° to the axis of the incident laser beam and positioned so that it was held directly against the quartz window at the desired height and lateral displacement so as to catch the plasma's radiation. Figure 3.1 shows a schematic of the fiber placed near the chamber.

This FOC transmits plasma emission to an Échelle spectrometer with an intensified CCD-array (LLA Instruments, Inc., ESA 3000) of 1024×1024 pixels (24 $\mu\text{m} \times 24 \mu\text{m}$ pixel area). The spectrometer has a useful spectral range of 200 to 800 nm and a resolution of 0.005 nm in the UV region. A computer equipped with software for controlling a fast-pulse generator which controlled the firing of the pulsed-laser and the gating of the spectrometer ICCD was used.

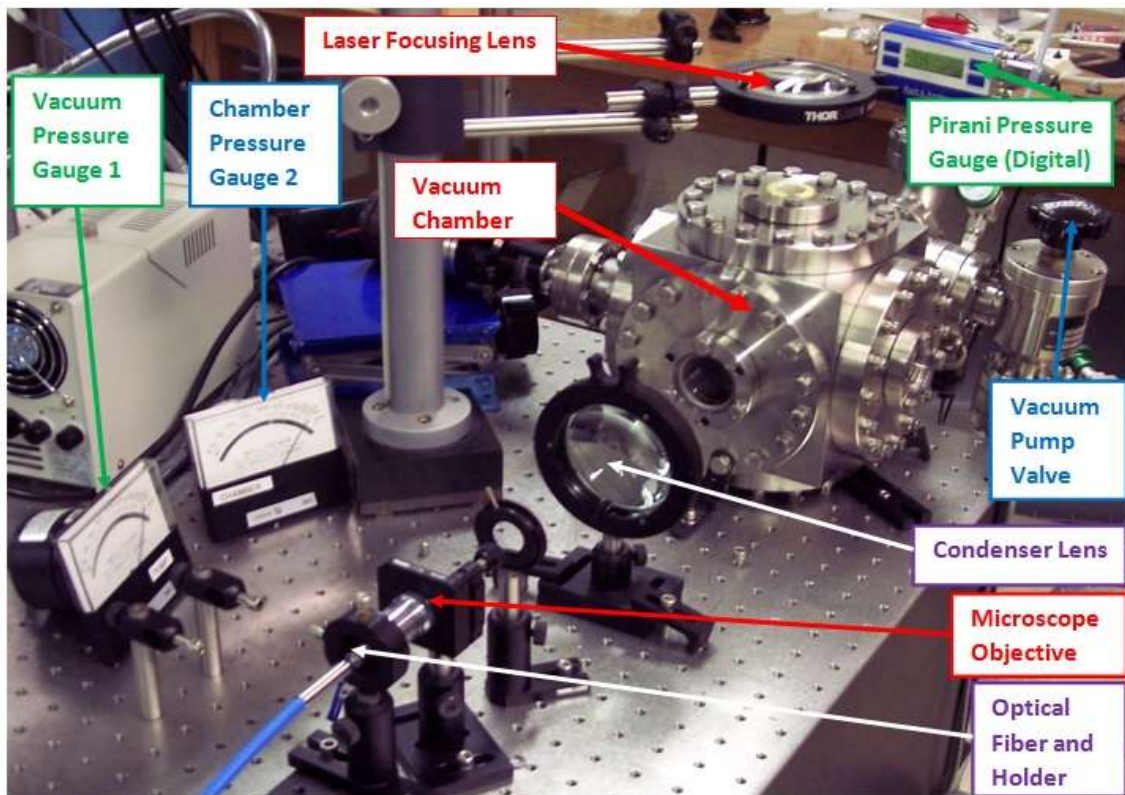


Figure 3.8 shows the ablation apparatus used initially for branching ratio determinations. It includes the spectrally-sensitive optical train: condenser lens, microscope objective, and fiber.

Prior to utilizing just the input optical fiber from the spectrometer, a more complex light collection scheme was used (see figure 3.8). This scheme utilized a large glass aspheric "condenser" lens and a glass microscope objective to collect light and focus it into the core of the multimode fiber. The objective was an uncoated 20x microscope objective at a distance of 14.5 cm from the lens. This microscope objective had an aperture of 8 mm, an effective focal length of 10 mm, a numerical aperture of 0.4 and a working distance of 6 mm. The microscope objective was used to focus the emitted light into the same 1-m steel encased multimode optical fiber (diameter = 600 μm , N.A. = 0.22) described earlier. The advantage of this system was that the large numerical aperture of the aspheric lens placed in close proximity to the plasma allowed the collection of a large amount of emitted light. The disadvantage of this system, which far

outweighed the initial advantages, was the dramatic achromatic behavior of the entire system, which resulted in drastic changes in observed emission intensity across the entire optical spectrum when even the slightest misalignments or any changes to alignment were introduced.

In theory, this achromatic behavior can be compensated for by careful spectral calibration and an alignment procedure guaranteed to always realign the optical train in exactly the same way, but in practice it was found to be impossible to always realign the system to the desired tolerance.

The biggest difference between these two optical systems was the transmission spectrum. Because the optical fiber core and the window were both high quality quartz, a large amount of UV light was transmitted. Since the lanthanides have strong emission in this spectral region, this was important. The aspheric condenser and the microscope objective were not made of quartz however, which led to a large loss of light at wavelengths below a UV cut-off of about 350 nm. This can be seen in Figure 3.9 where nominally identical light spectra were input to the system, but vastly different spectra were recorded. Note that the strong spikes in the green emission spectrum below 328 nm are noise spikes, and not evidence of real light collection.

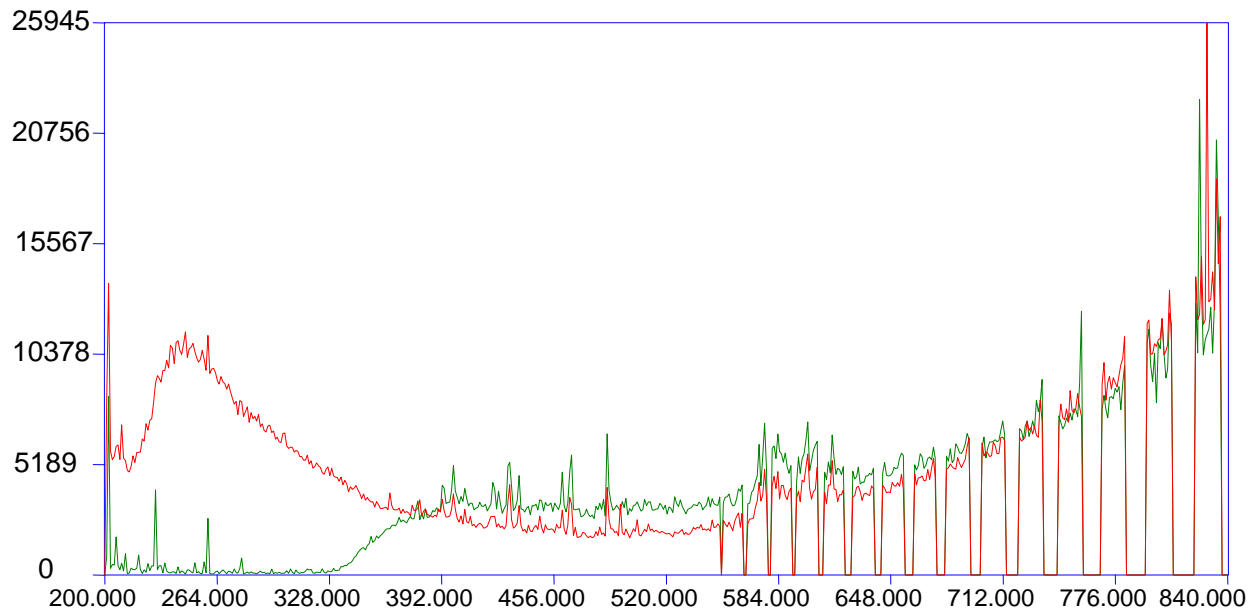


Figure 3.9 compares emission from a deuterium-tungsten calibration lamp with the optical train (green) and without (red). Notice the loss of light between 200-330 nm mostly due to the glass in the condenser lens and microscope objective.

Much time was spent in determining the spectral response and calibration of the optical train in order to correct for the lost light, but because of the extreme sensitivity of the system we ultimately decided to use a simpler but less efficient light collection method, as described earlier. The collection lens and microscope objective were replaced by an optical fiber put in close proximity to the quartz window (see figure 3.1). The fiber itself has a spectral response which was easily reproducible and calibrated; it was also much less sensitive to slight variations in location. The major downfall to using the optical fiber was that the fiber's 600 μm core was only able to collect less than 1% of the $\sim 4\pi$ steradians of emitted light from the plasma, but this was sufficient for my research. Another reason for using the fiber optical cable in place of the optical train is that a large number of UV emission lines were regained, as figure 3.7 clearly shows.

Due to the need for relative emission intensities, spectral calibration of the instrumentation across the observed optical spectrum was necessary. Each optical component of the LIBS detection system (i.e. window, fiber) had a certain spectral response associated with it. Spectral calibration of the system was performed using two external light sources. A calibrated deuterium-tungsten lamp with a known spectral output over the entire 200 nm to 840 nm spectral range was used to correct the spectra to account specifically for any loss in the glass of the window or fiber. In this way, a spectral efficiency factor $\varepsilon(\lambda)$ used to correct the observed branching ratio intensity of every line was created. Measured spectral efficiency factors were confirmed by observing the attenuation and subsequent renormalization of several known emission lines from a well-characterized fiber-coupled mercury argon discharge lamp.

3.4 - Light Dispersion in an Echelle Spectrometer

The échelle spectrometer consists of an échelle diffraction grating and a dispersing prism. The diffraction grating within the spectrometer is composed of many equally spaced ‘grooves’ on a plane surface which reflects the incident light, thus generating a large number of coherent light sources. Depending upon the angle, the wavelets interfere constructively or destructively. The expression for constructive interference is given in equation 3.1 where m is the order number which is an integral value, λ , d , θ , ϕ , are the wavelength, groove (or step) spacing, incident angle, and diffracted angle, respectively.

$$m\lambda = d(\sin \theta + \sin \phi) \quad (3.1)$$

The grooves of the *échelle* grating are step-like and oriented at an angle α with respect to the grating's normal. In practice the angle α is typically around 50° - 70° for *échelle* spectrometers.⁸ This tilted axis configuration is referred to as a *blazed grating* and serves to direct a majority of the reflected light in a particular direction. In the *échelle* spectrometer the steps are oriented perpendicular to the axis of the spectrometer (called the Littrow configuration)⁹ so that the incident light falls on the smaller side of the step. The *échelle* grating makes use of relatively larger distances between steps so as to create order blending of the diffracted light which is subsequently filtered according to order via a dispersing prism. Figure 3.10 shows incident light on the *échelle* grating and the resulting diffracted light.

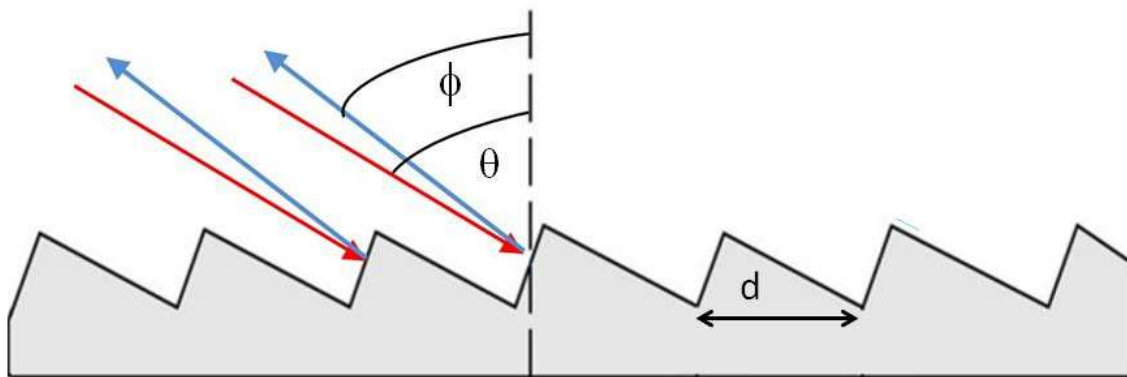


Figure 3.10 shows the blazed *échelle* grating used in this work. The red arrow signifies incident light and the blue is diffracted light. The separation between grooves is d .

The *échelle* spectrometer makes use of an *échelle* grating which separates the light via diffraction and a prism which further resolves the light orthogonally according to the order number (m). This cross-dispersion is used in order to create a two-dimensional array of light separated according to order (vertical spread) and according to the spread in wavelength from diffraction (horizontal spread). This two-dimensional spread of light is then directed via a mirror

onto the intensified charge-coupled device (ICCD) in order to detect the localized irradiance on each individual pixel and thus measure the strength of an emission line.¹⁰ Because the échelle spectrometer contains no moving parts, a unique map exists between incident wavelength and its diffracted location on the two-dimensional ICCD.

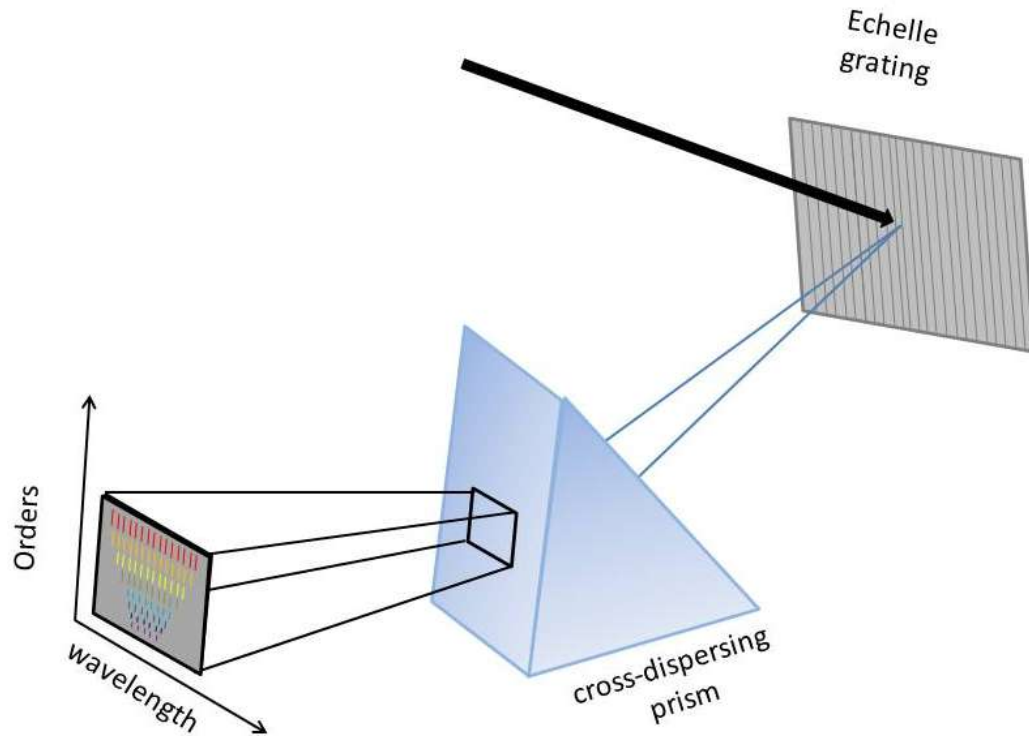


Figure 3.11 shows the operating principles within the échelle spectrometer and the resulting two-dimensional array of light from the échelle grating and prism.

3.5 – Detection and Analysis

The emission spectra were obtained with an ICCD open-gate duration of 1000 ns, and a gate delay time of 1000 ns. These times were chosen for optimum plasma characteristics including signal-to-noise ratio and integrated signal intensity, as described earlier, yielding atomic data comparable with previous studies.³ The spectra from 10 laser pulses were integrated

together on the charge-coupled device (CCD) chip by allowing 10 exposures of the camera prior to read-out to achieve an integrated emission to improve the signal-to-noise ratio. We call these separate spectra “on-chip accumulations” or OCA’s and they are a simple way to increase signal intensity without too great an increase in dark count. The number of OCA’s is a user-determined parameter of the experiment. Each integrated CCD image (composed of 10 OCA’s) was then averaged with another 9 separate spectra to reduce background noise by averaging (increasing the signal-to-background ratio). We call these separate spectra “accumulations,” or just “accums” for short, and this also is a user-determined experimental parameter. Therefore the resulting final emission spectrum was comprised of a total of 100 spectra.

The CCD camera in the ESA 3000 spectrometer is composed of 1024×1024 pixels.¹¹ Each pixel is a conducting plate electrode (gate) which is separated from a p-type silicon substrate by an insulating oxide layer. When a photon strikes the semitransparent conductor it absorbs into the silicon substrate. If the absorbed photon has energy greater than the band gap of the semiconductor it creates an electron-hole pair which is subsequently pulled apart by the electric field from the gate voltage. The positive voltage applied to the gate attracts the electrons near the surface while the base electrode beneath the silicon layer attracts the holes, eventually leading to ground. Each absorbed photon contributes another electron stored near the positively charged gate, and in this manner the intensity of light can be quantifiably represented by the number of stored electrons. Figure 3.12 depicts the situation inside of a CCD chip.

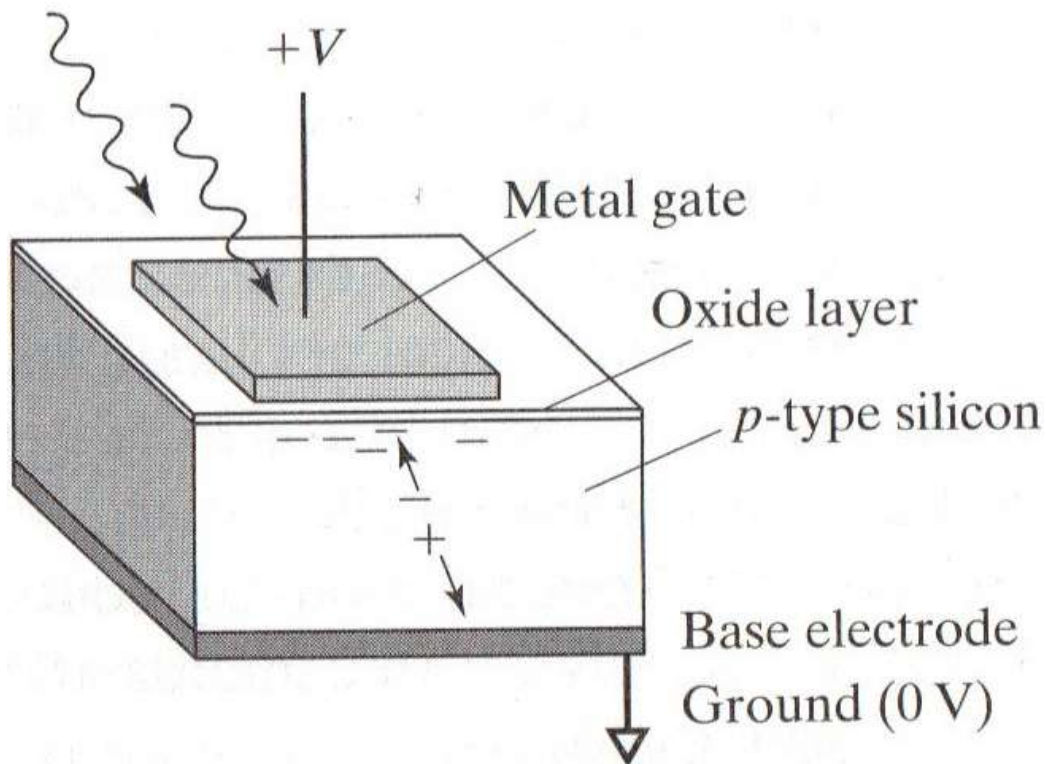


Figure 3.12 adapted from Serway's *Modern Physics*, shows the operation of a CCD absorbing a photon in the p-type semiconductor, creating an electron-hole pair, splitting the electron-hole pair by a strong potential. The hole is repelled from the gate and attracted to the base electrode and eventually ground, while the electron is attracted to the positively charged gate.

When a two-dimensional grid of CCD chips are arrayed next to each other they can act as individual picture elements or pixels which work together to record an image. Following the exposure from a focused image onto the array, the electric charge which accrues on each CCD chip is stored temporarily until it is transferred sequentially to its neighbor and the process repeated until all the charge from each separate row of CCD's is stored in the furthest chip at the end of the row. Then the gate voltage is adjusted so that the last row containing all the charge information is transferred down its column to an amplifier circuit and converted into a digital

signal so that the image can be reconstructed.¹² Figure 3.13 shows the situation of transference of charge along rows and columns of the CCD array

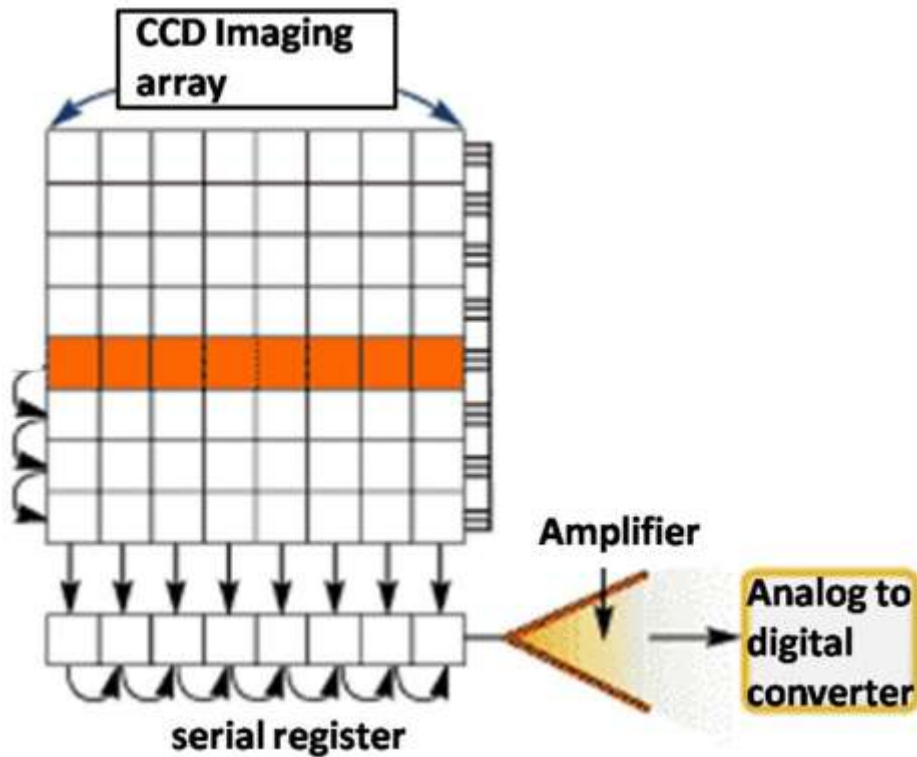


Figure 3.13, adapted from <http://www.clamart.org/Video/capteur.htm>, shows a schematic of a CCD array transferring along the stored charge, which becomes amplified and eventually converted into a digital signal.

The ESA 3000 spectrometer used in this research incorporates a cylindrically shaped intensified charge-coupled device (ICCD) for detecting the incident photons. The image intensifier is a vacuum device which is 25 mm in diameter consisting of a photocathode, microchannel plate, and a phosphor screen in this sequence. The photocathode is a photosensitive material with a relatively low work function which when struck by a photon ejects an electron via the photoelectric effect. A potential difference applied along the photocathode

increases the kinetic energy of the ejected electrons and steers them into the micro-channel plate (MCP) where the electrons are multiplied. The phosphor screen converts the multiplied electrons back into photons, but photons of a single wavelength (approximately), reducing systematic errors due to the wavelength-dependent quantum efficiency of the CCD detector. The whole process results in a larger gain of incident photons onto the CCD. Importantly, by reversing the voltage on the MCP the image intensifier can act as a nanosecond-response shutter or gate, so that the user has temporal control of the CCD array exposure.

The fact that the image intensifier is cylindrical in shape and the CCD array is square necessarily creates portions of the CCD which are unused. These un-illuminated portions result in unavoidable gaps in the spectrum (see the “drop-outs” above 550 nm in figure 3.9 above). In our spectrometer, this shape mismatch was designed to only yield spectral gaps above 550 nm. Unfortunately, any emission peak that occurs in a spectral gap is completely unobserved, and nothing can be done about this. The lanthanides, however, have almost all of their spectral emission at much lower wavelengths, so this was not a serious concern for this dissertation.

The gain of the image intensifier is yet another user-controlled parameter which is referred to as the amplification of the ICCD. By adjusting the high-voltage applied to the MCP, more or less photo-electrons can be generated per photon, providing amplification or “gain.” In an effort to sort out any non-linearity of the spectral response as a function of amplification setting, I conducted an experiment by adjusting the gain of the ICCD (leaving all other parameters identical) and observed its effect on signal intensity. A plot of the integrated intensity for the 430.357 nm emission line in singly-ionized neodymium versus increasing amplification is shown in figure 3.14. It can be seen from the graph that the response of the system to the

increasing amplification is well characterized by an increasing exponential function. While this behavior is interesting, the actual amplification setting, or changes to that setting should not impact the measured branching ratios in any way. This is because the amplification was never changed during any experimental run and also because I was only interested in measuring relative emission intensities between lines in a given spectrum.

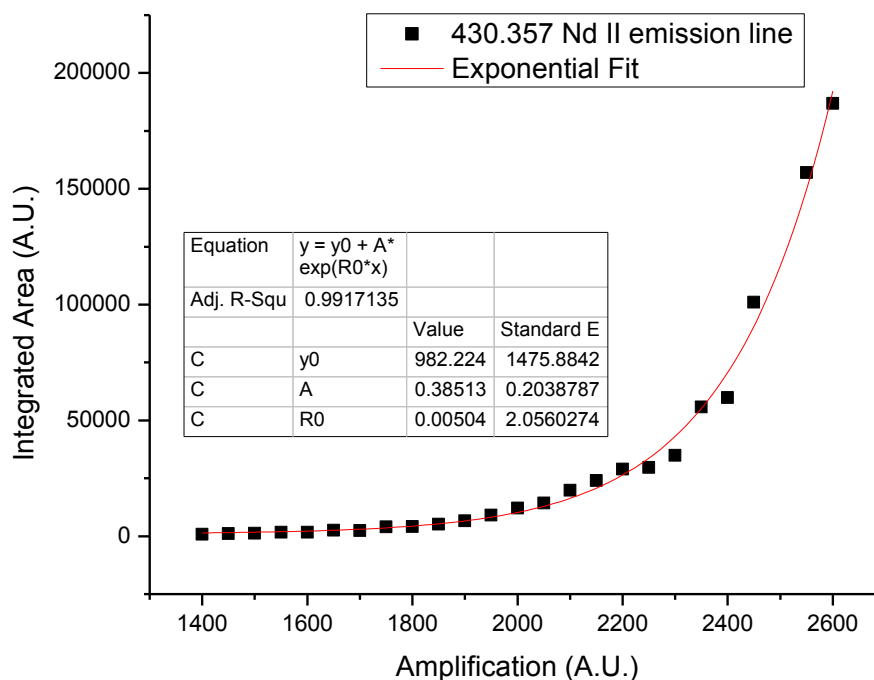


Figure 3.14 shows the effects on integrated intensity of a single emission line as the image intensifier gain is increased.

3.6 – Experimental Parameters

As explained in this chapter and chapter 2, observed LIBS emission spectra were subject to change depending upon many user-controlled parameters, including: the observation time (a.k.a delay time, τ_d), ICCD gate width (τ_w), chamber pressure (P), buffer gas, ICCD gain

(amplification), number of on-chip accumulations (OCA), and number of averaged spectra (“accums”). The settings ultimately used in this research are summarized in table 3.1.

Parameter	Setting
Gate delay (τ_d)	1000 ns
Gate width (τ_w)	1000 ns
Buffer gas	argon
Displayed Pressure	8.3 Torr
True Pressure	71 Torr
ICCD gain	2800
On-chip accumulations	10
Averaged spectra	10

Table 3.1 shows the settings used in this research

In conclusion, using the apparatus described above with the optimized experimental parameters listed in table 3.1 I have performed branching ratio measurements in four lanthanide elements (Nd, Sm, Gd, Pr) and two transition metals (Cu, Fe) and their corresponding neutral, singly-, and doubly-ionized states (neutral and singly ionized for the transition metals). The results of these measurements will be presented in the following chapters.

¹ E. Biemont and P. Quinet, “Recent advances in the study of lanthanide atoms and ions,” Phys. Scr. **T105**, 38-54 (2003).

² J.A.M. Rojas, M. Ortiz, J. Campos, “Determination of transition probabilities of some Sb III lines by time resolved spectrometry of laser produced plasmas,” Phys. Scr. **62**, 364-367 (2000).

-
- ³ S.J. Rehse and C.A. Ryder “Laser-induced breakdown spectroscopy for branching ratio and atomic lifetime measurements in singly-ionized neodymium and gallium,” *Spectrochim. Acta B* **64**, 974-980 (2009).
- ⁴ T.L. Thiem, R.H. Salter, J.A. Gardner, Y.I. Lee, J. Sneddon, “Quantitative simultaneous elemental determinations in alloys using laser-induced breakdown spectroscopy (LIBS) in an ultra-high vacuum,” *Appl. Spectrosc.* **48**, 58-64 (1994).
- ⁵ A.M. Gonzalez, M. Ortiz, J. Campos, “Experimental transition probabilities for lines arising from $5p^2\ 6s$ configuration of neutral Sb,” *J. Quant. Spectrosc. Radiat. Transfer* **57**, 825-829 (1997).
- ⁶ B.C. Castle, K. Talabardon, B.W. Smith, J.D. Winefordner, “Variables influencing the precision of laser-induced breakdown spectroscopy measurements,” *Appl. Spectrosc.* **52**, 649-657 (1998).
- ⁷ M. Ortiz, R. Mayo, E. Biemont, P. Quinet, G. Malcheva, K. Blagoev, “Radiative parameters for some transitions arising from the $3d^9\ 4d$ and $3d^8\ 4s^2$ electronic configurations in Cu II spectrum,” *J. Phys. B* **40**, 167-176 (2007).
- ⁸ A.P. Thorne, *Spectrophysics*, Chapman Hall, London, (1974).
- ⁹ D.J. Schroeder, “An Echelle spectrometer-spectrograph for astronomical use,” *Appl. Opt.* **6**, 1976-1980 (1967).
- ¹⁰ D.A. Cremers and L.J. Radziemski, *Handbook of Laser-Induced Breakdown Spectroscopy*, John Wiley & Sons, Ltd., West Sussex, (2006).

¹¹ M. Sabsabi and V. Detalle, “New spectral detectors for LIBS.” in A.W. Miziolek, *Laser-Induced Breakdown Spectroscopy Fundamentals and Applications*. Cambridge University Press, New York, 556-584, (2006).

¹² R.A. Serway, C.J. Moses, C.A. Moyer, *Modern Physics*, 3rd ed. Thomson Learning Inc., New York, (2005).

Chapter 4 - Determination of Uncertainties

The measurement of branching ratios belonging to a given excited energy level essentially consists of simultaneously measuring the atomic emission intensity from multiple transitions which occur at many different wavelengths. The branching ratios are given by the relative intensity of these transitions. Therefore, all the measurements I made were only relative intensity ratios. Because no absolute measurements of emission intensity were made, no absolute calibration of the experimental apparatus was required. However, I was critically aware of sources of uncertainty which could alter the measurement of the actual emission intensity ratios. A careful accounting of all sources of uncertainty is therefore critical. The experimental uncertainties in this project stemmed from multiple sources: calibration of the spectrum due to optical losses, day-to-day variations in emission signals from the dynamic plasma, and blending or broadening of spectral lines. Care was taken in order to account for each source of error. These will be described in further detail in the following sections.

4.1 – Spectral Calibration

The transmission of light through an optical component isn't perfect, and as such there is a wavelength-dependent absorption coefficient for light transmission. Lenses, mirrors, and windows all contribute some form of loss to the spectrum. Anti-reflective coatings can help to diminish some of these losses, but still, calibration of the optical system via a full spectrum broadband emission lamp is needed.

One of the methods we used to determine uncertainties in our optics was to compare spectra obtained using the optics to spectra obtained without the optical pieces by forming a ratio

of the spectra from both situations as a function of wavelength. This comparison then gives us a quantitative measurement of the loss of relative light intensity due to optical absorption. I define this factor as the spectral efficiency factor and it is further explained in the subsequent sections.

4.1.1 - Condenser lens

As noted in chapter 3, our first attempt at light collection was using an optical train composed of a condenser lens, microscope objective, and optical fiber (see figure 3.8). However this system proved immensely sensitive to even the smallest deviations in lens height or rotational orientation with respect to the incident plasma radiation. For example, one investigation performed involved assembling and disassembling the optics system and acquiring spectra from a broadband calibrated standard deuterium-tungsten lamp. Three attempts following identical procedures for alignment showed drastically different results (see figure 4.1). Figure 4.1 (below) shows the ratio of the emission spectrum from the deuterium-tungsten calibration lamp passed through the optical train to the spectrum of the deuterium-tungsten lamp collected without the optical train. This ratio is defined as the spectral efficiency factor. It gives a quantitative value for the optical losses within our spectral range due to the optics used in collecting the light.

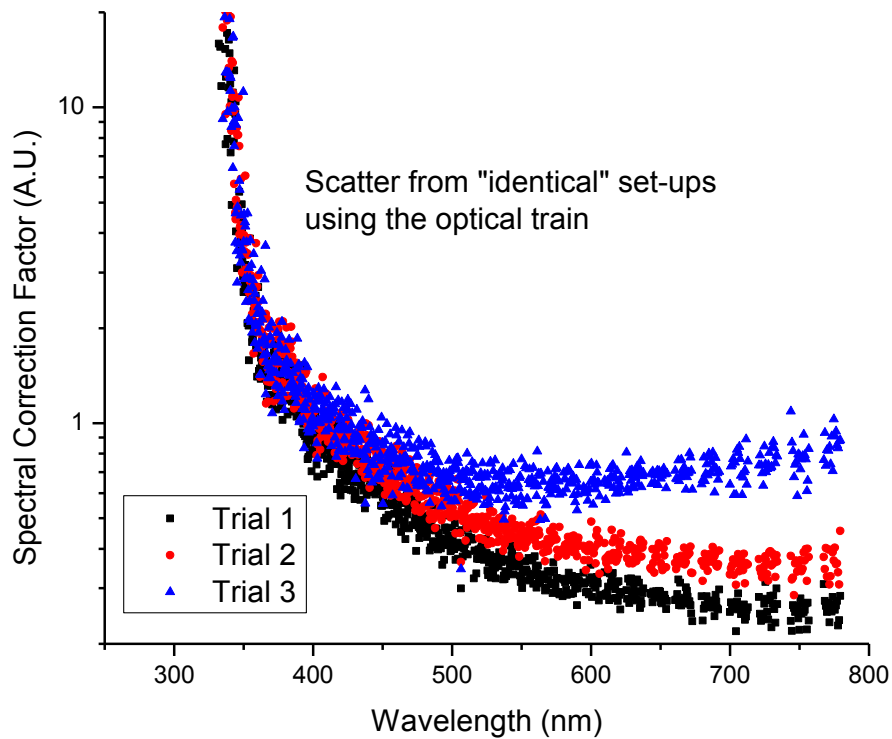


Figure 4.1 shows how the results differ for seemingly “identical” spectral correction factors from three experimental setups using the aforementioned calibration process with the optical train mentioned above.

The procedure for alignment of the collection optics involved 6 main steps:

- 1) A helium-neon laser (He-Ne) coupled to the output end of the fiber-optic cable normally used to collect plasma emission was used to align and focus the optics (microscope, iris, lens, chamber window) to the desired spot just above the sample. Due to the optical principle of reversibility, the location where the He-Ne laser light was focused corresponded to the location where light from the plasma would be collected. A second fiber-optic cable was placed at this point in such a way as to

- represent emission from the plasma at the specified height and lateral location of the plasma.
- 2) A deuterium-tungsten calibration lamp was connected to this second fiber-optic cable within the ablation chamber in order to represent plasma emission at the location where the plasma would be, but with a known calibrated spectrum.
 - 3) Both the emission from the He-Ne laser (via the fiber optic cable) and the deuterium-tungsten emission (via the second fiber optic cable) were coupled by centering them best by “eye”.
 - 4) The He-Ne laser was then removed from the output end of the collection fiber and replaced with a power meter. In this way the emission from the deuterium-tungsten lamp coupled into the collection fiber could be measured and optimized with the power meter.
 - 5) Using the power meter, miniscule vertical and horizontal adjustments were made with the fiber holder in order to maximize the power from the deuterium-tungsten lamp coupled into the collection fiber. In principle this should signify optimum coupling between the optics and the light collecting fiber.
 - 6) When the power meter showed values comparable to prior optimum calibration of the broadband calibration source, the collection fiber was reconnected to the échelle spectrometer and a calibration lamp spectrum was recorded. The resulting spectrum was then compared to a similar spectrum which did not incorporate the use of the optical train (the calibrated standard emission lamp was connected directly to the

spectrometer via the collection fiber) in order to determine the wavelength dependent losses in the entire system.

Despite these time-consuming fairly intricate and supposedly reproducible manipulations of the optical train, the spectra were not identical within an acceptable tolerance (see figure 4.1). Because of this, we deemed the system to be too sensitive to perturbations and we adopted the use of a single fiber-optic cable to collect the light. The fiber gave suitably reproducible results in exchange for a smaller numerical aperture leading to less collected light per spectrum as noted in chapter 3. However, despite the decrease of collected light due to the fiber's smaller numerical aperture, the spectra suffered no apparent degradation of signal to noise because of the ability to increase the amplification on the ICCD and accumulate (on-chip accumulations) more integrated spectra.

4.1.2 - Emission Lamp Calibration via Fiber Optic Cable

Despite replacing the optical train with the fiber optical cable, spectral calibration of the optics in use (now reduced to only a quartz window and a quartz optical fiber) was still necessary. In order to do this we used a broad-band deuterium-tungsten lamp which covered the entire spectral range (200-800 nm) of the échelle spectrometer. The resulting emission measured through the window and fiber was compared to emission through the same fiber without the window and a wavelength-dependent spectral correction function, $\varepsilon(\lambda)$, was created for the whole spectral range. The use of broadband emission lamps for the calibration of optics and detectors is common.¹

At wavelengths less than 225 nm there were large discrepancies due to losses from the quartz window and the fiber. Because of these large discrepancies, no measurements smaller than 225 nm are included in this work with confidence and any data reported from this region are annotated. At each face of the optics, there was a 4% loss of intensity for transmitted light, therefore the window diminished the collected light intensity by ~8% and the fiber-optic cable also diminished the light by ~8%. Figure 4.2 shows the typical spectral calibration function for the range of interest to this work. Note that a spectral correction value of one would signify that the relative optical loss at that wavelength was zero, meaning that the optic had perfect transmission at that wavelength; a factor greater than one means that the optic system has some loss of transmission and therefore needs to be scaled up accordingly. In general the scaled intensity I' is equal to the measured integrated intensity I times the spectral correction factor ε as shown in equation 4.1.

$$I'(\lambda) = I(\lambda) \cdot \varepsilon(\lambda) \quad (4.1)$$

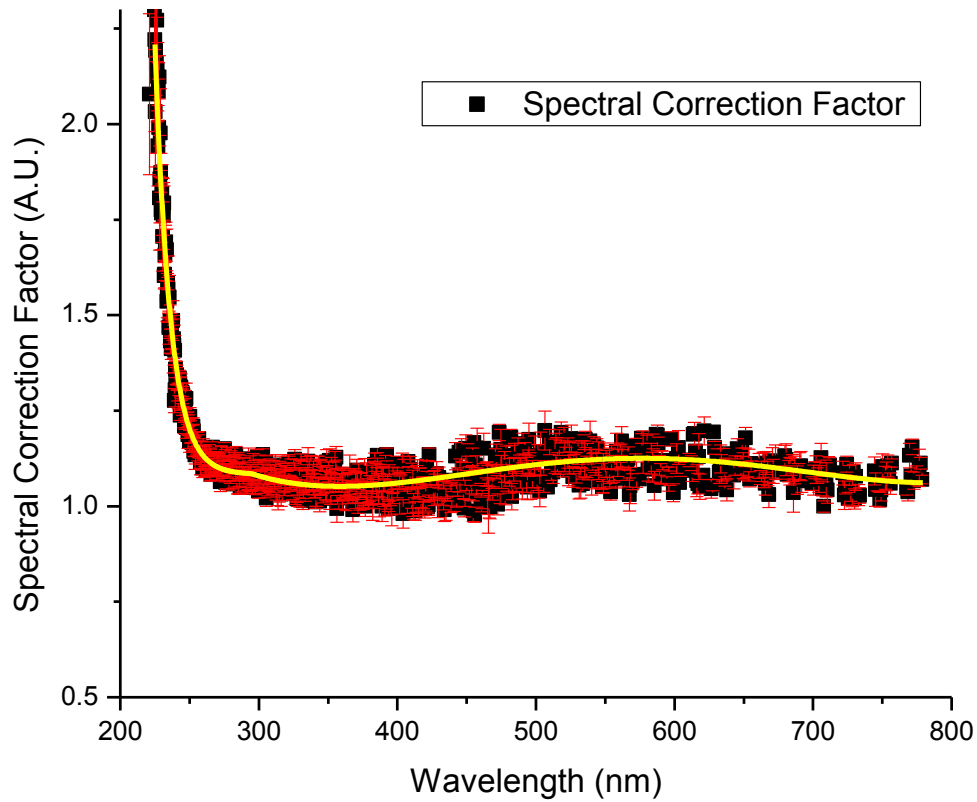


Figure 4.2 shows the spectral-correction factor (data points in black) and its statistical uncertainty (red error bars) against wavelength for the chamber's quartz window, using only the fiber-optic cable for light collection. The yellow line is the 3 piece-wise fits of the graphically-determined spectral-correction factor overlaid on top of the experimentally-determined spectral-correction factor to show the agreement between the two.

4.2 - Uncertainty in Spectral-Correction Factor

The uncertainty from spectral calibration of the optics is derived from three methods, all of which will be described in detail below. Firstly, a graphically-fit spectral correction function was used to approximate the spread shown in figure 4.2. This approximation gave a small contribution to the uncertainty. Secondly, the spectral correction function was measured

numerous times over the course of a month and the scatter in the measurements was incorporated into the total uncertainty. Thirdly, the scatter between the graphically-fit spectral correction function (yellow line in figure 4.2) and the measured data (black data points in figure 4.2) was incorporated into the total uncertainty.

4.2.1 – Error from the Spectral Correction Factor’s Graphical Approximation

The first method in which we attributed error to the spectral correction function used a least-squares fitting regime where we approximated the trends in the spectral correction factor by 3 piecewise non-linear functions (see figure 4.2). At first we investigated the determination of a spectral calibration factor measured at each wavelength. However the scatter observed in the data (shown in Figure 4.2) does not denote any real physical transmission variation. The spectral behavior of the transmission of the system should be “smooth” as a function of wavelength (although it definitely does change with wavelength). To approximate this smooth behavior, it was decided to numerically fit the data with a function that could then be used for the spectral correction factor. As this is obviously not an analytic function, piece-wise fitting was performed with the requirement that the endpoints match. In all cases multiple functions were investigated to determine what type of fit gave the lowest chi-squared and therefore best described the data. In the range from 200-225 nm a decaying exponential function was used having a chi-squared (χ^2) value of 3.0. In the range from 225-280 nm a decaying exponential function was used with a χ^2 value of 0.006. In the range from 280-800 nm a fourth-order polynomial was used which yielded a χ^2 value of 0.002. Altogether the error from this method was derived from uncertainties in the parameters which were given from the two piecewise fits (the < 225 nm section was not

included). The small uncertainties on these fit parameters turned out to be insignificant in comparison to the error from the other methods and were therefore not included in the total uncertainty.

4.2.2 – Uncertainty from Multiple-Day Scatter in Spectral Correction Factor

The spectral calibration function was tested many times on many different days in order to verify its reproducibility and to determine any day to day scatter in its measurement. The scatter below 225 nm is substantial and is the result of absorption; it is inherent to the chamber window and fiber and not a by-product of any statistical uncertainty from day to day scatter. The average uncertainty from the spread in data for the spectral calibration function from wavelengths 225-800 nm was found to be 3.0% for the entire range; with a fractional standard deviation of 0.6. On the whole, the scatter between days was fairly consistent with wavelength; there were not any obvious systematic trends in the scatter between days. This suggests that using a single average uncertainty determined over the whole range is appropriate. The spectral-correction value and its corresponding uncertainty are presented in figure 4.3 for wavelengths less than 255 nm. The graph shows that the scatter below 225 nm is quite large and the scatter above 225 nm rapidly improves and becomes more consistent. The error bars shown in the graph are the standard deviation from multiple calibrations.

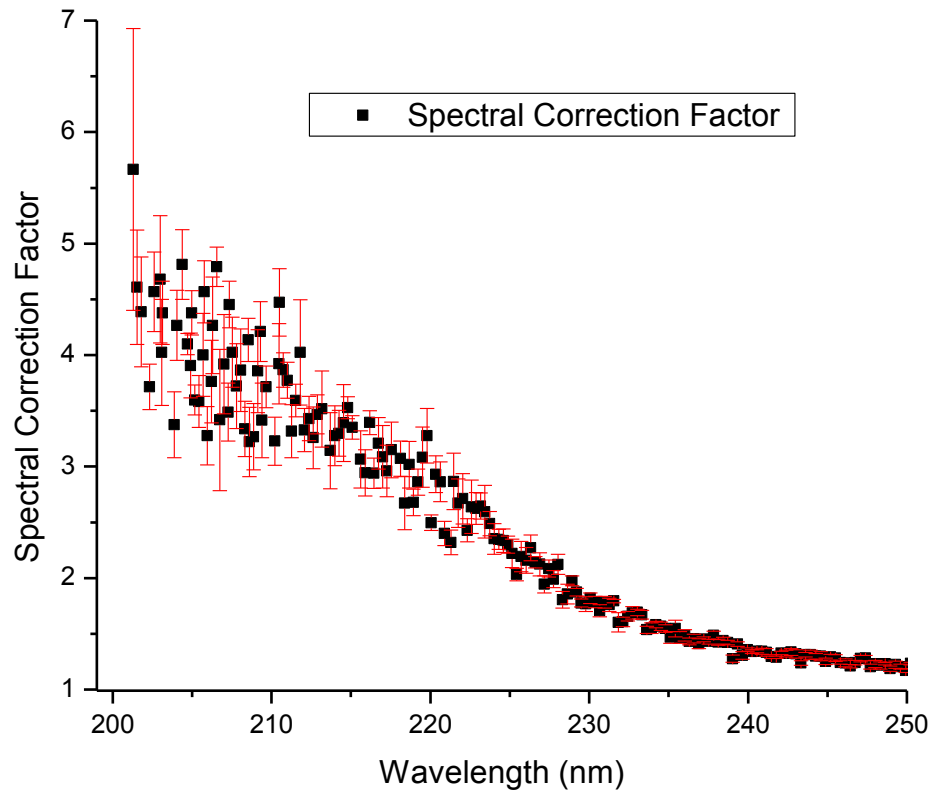


Figure 4.3 shows the large scatter in the spectral correction factor at wavelengths smaller than 225 nm, and the more precise scatter above 225 nm

4.2.3 – Uncertainty from Scatter between Data and Fitted Value

The third contribution to the error in the spectral calibration function comes from the scatter between the actual value of the spectral calibration function averaged over the month long study and the graphical fit value of the spectral calibration function. Within the range of 225-800 nm the averaged absolute-value of the scatter between the actual spectral correction factor $\varepsilon(\lambda)$ (spectral intensity without optics / spectral intensity with optics from data) and the graphically-fit value was 4.0%. The 225-800 nm range had a standard deviation of 5.5% from the averaged

absolute-value. Within the range of 200–225 nm the averaged absolute-value of scatter was 52.8%. When including the scatter from the 200–225 nm range with the 225–800 nm scatter the average absolute-value was 8.4%.

4.3 – Uncertainty in Emission Lines

Another source of uncertainty stemmed from the measurement of the intensity of the emission peaks themselves. The uncertainty from emission lines was derived from 3 contributions: the fitting of emission peaks to determine the area under the curve, statistical uncertainty from repeated measurements taken sequentially on a single day, and random scatter systematic uncertainties in excess of the statistical uncertainty from repeated identical experiments on different days.

4.3.1 – Spectral Resolution: Blended, Broadened, Shouldered, and Weak Lines.

The blending, broadening, shouldering, and weakness of emission lines create difficulties for spectroscopists, especially in LIBS spectra where there can be thousands of lines to consider in a single spectrum. To overcome these difficulties many of today's current spectroscopic software codes, such as the ESAWIN program used in this work, incorporate analytical methods of handling these effects. One of the principles used in determining if a blended line can be resolved is the Rayleigh criterion. The Rayleigh criterion is concerned with the overlap between the blended peaks. The criterion states that the minimum of one of the profiles should lie directly beneath the maximum of the other in order for the two peaks to be resolved.² This criterion gives the limiting case for spectrally resolving two lines. If the separation between peaks is smaller than the separation between the minima then the lines are irresolvable.

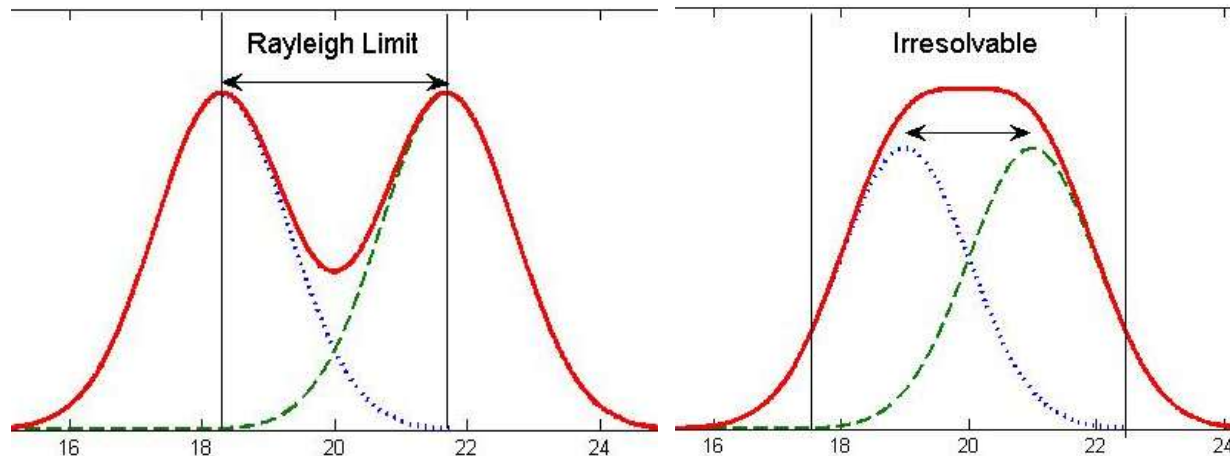


Figure 4.4 depicts two scenarios of resolving blended lines using the Rayleigh criterion. (Left) the Rayleigh limit is achieved when the minimum of one line is collinear with the maximum of the other and therefore the blend is resolvable. (Right) the minimum of one line exceeds the other's maximum and therefore the blend is irresolvable. The vertical lines denote minima.

However, despite the ESAWIN software's resolving capability, the techniques are not perfect - sometimes two blended lines can be counted as a single large peak. Therefore every emission line used in branching ratio calculations was checked by eye (~60,000 lines) and annotated accordingly (strong, blended, shouldered, or weak). To recalculate integrated areas using fitting software by hand for the thousands of problematic lines would be unreasonable, therefore when presenting data from emission lines which were unresolved or problematic an annotation is made for the measurement. The annotation of problematic emission lines is common practice for experimentalists in LIBS and other similar atomic emission spectroscopic techniques.¹⁶³ No quantitative measurement of uncertainty was attributed to the fitting of emission lines. The ESAWIN program is capable of measuring full-widths at half-max as well as integrated emission intensity and other parameters but no value of uncertainty is presented.

Nonetheless, it is known from previous studies³ that the fitting of such lines is a negligible source of uncertainty, due to the fact that it is only a relative determination of emission intensity.⁴

4.3.2 –Uncertainty in 1000 Identical Measurements

Spectral reproducibility is a key factor in LIBS research given that the plasma is dynamically changing and the amount of ablated material which generates the characteristic spectral emission is never exactly the same from plasma to plasma. Therefore we conducted an investigation to determine the uncertainty of 1000 identically acquired spectra for emissions from the neodymium target within a single experiment. In this investigation we found the average fractional standard deviation of relative intensities from all elements and ionizations to be 4.1% over the entire spectral range with maximum uncertainty of 40% for only a few very weak lines which were undetected in some of the averaged spectra. The uncertainty determined from this investigation or reproducibility is incorporated into the total error for the measurements.

4.3.3 – Multiple Day Scatter in Measurements

Another method which was used to investigate the reproducibility of the plasma emission and the corresponding uncertainty was to investigate the reproducibility of branching ratios and relative intensities measured over multiple days with nominally identical experimental conditions. The experiment spanned 10 straight days (1000 total spectra acquired per data point, 100 spectra per day) without deliberately changing the experimental configuration and the results showed good agreement, yielding typical (average) fractional uncertainties of 5.2%, and the fractional uncertainty ranged from ~0.2% for large branches to ~35% for very small branches

which were not detected in some of the averaged spectra. The error from this investigation is also incorporated into the final uncertainty determination.

4.4 – Categorizing Uncertainties According to Branching Ratio Strength

It is well known that under LTE plasma conditions and optimum calibration of the equipment and experimental conditions weaker emission lines yield larger fractional uncertainties (standard deviation divided by branching ratio strength) due to the inability to resolve such small profiles from the background and noise.^{4,5,6,7} Because of this fact, and due to the large number of branches reported in typical studies of lanthanides, it is not uncommon practice to incorporate the use of a categorically-assigned value of uncertainty to various branching ratios based solely on the relative strength of the branch.^{4,7,8} The only other way to report uncertainty would be to measure it for each of the thousands of observed lines. Not only is this tedious, more importantly it is non-physical, as there is no physical reason why several emission lines of comparable strength very close in wavelength should possess different uncertainties.

In order to assign uncertainty to a branch based on its the strength, the uncertainty from the 1000 spectra accumulation (section 4.3.2) and the uncertainty from multiple day scatter (section 4.3.3) were added in quadrature. This uncertainty does not include any uncertainty in the spectral calibration factor – it only accounts for variations in relative emission intensity. Figure 4.5 displays the combined fractional uncertainty in the branching ratios from Gd II, Nd II, Pr II, and Sm II from this work. I have attributed uncertainties on the basis of branching ratio strengths: 4.0% uncertainty for branches stronger than 0.30, 5.0% for braches between 0.3 and

0.10, and 18% uncertainty for branches weaker than 0.10. This is consistent with previously published work.^{4,1}

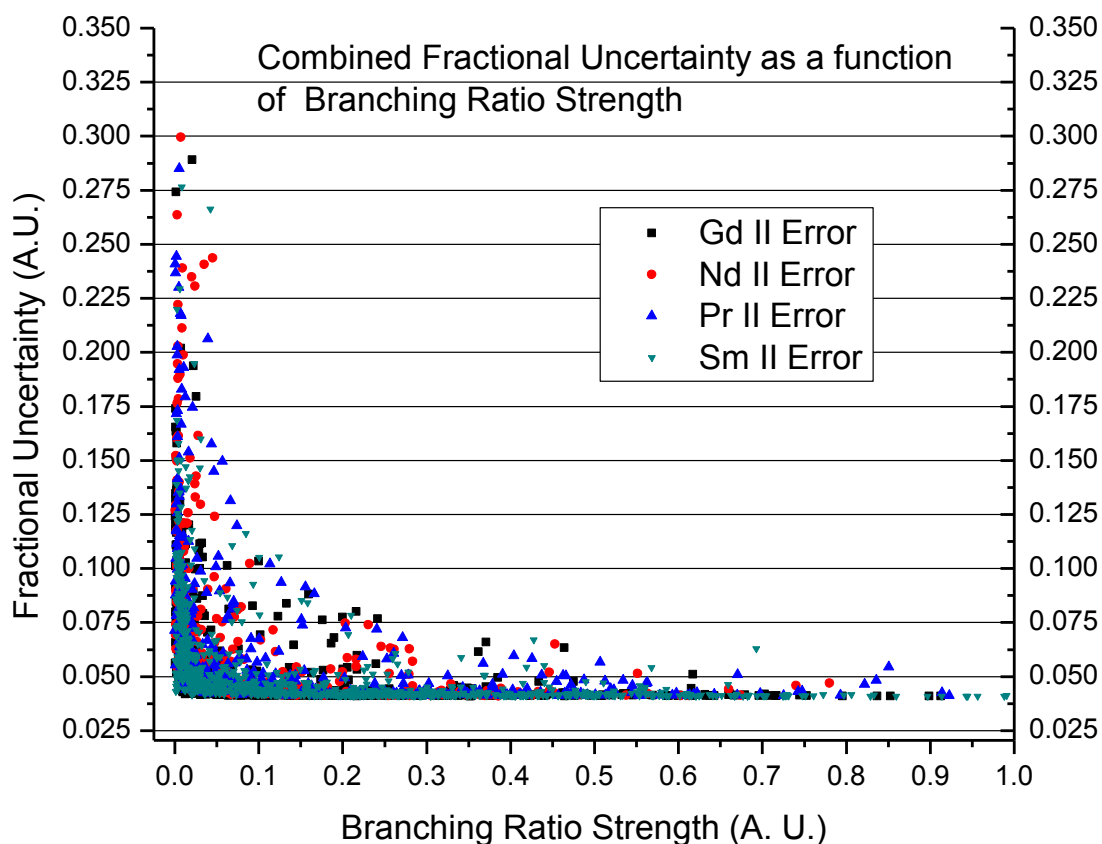


Figure 4.5 shows the combined (1000 spectra and multiple day scatter) fractional uncertainty for the singly ionized lanthanide metals Gd II, Nd II, Pr II, Sm II according to the strength of the branching ratio. Note that weaker branches tend to have larger uncertainties.

4.5 - Total Uncertainty Attributed to Data

Given the multiple sources which contribute to the uncertainty of this experiment we have been cautious to consider all of them. The chart below (Table 4.1) summarizes the sources

of uncertainty and their corresponding contribution to the total uncertainty. The contribution to the spectral correction factor (SCF) uncertainty from the *deviation between fit and data* is the uncertainty discussed in section 4.2.3 and shown in figure 4.2 which pertains to the scatter in the graphical fit of the SCF, and the *Multiple Day Scatter* uncertainty is the result of error bars in figure 4.2 discussed in section 4.2.2. *Branch Uncertainty (combined)* is the uncertainty reported from figure 4.5, which graphically combines the uncertainty from 1000 identical spectra and the multiple-day scatter in branching ratios. The *total error* combines the *spectral correction factor's* combined uncertainty with that from the *branching ratio*

From the given contributions listed in the above sections, the total uncertainties (after adding in quadrature the spectral calibration's uncertainty $\sim 5.3\%$) are $\sim 6.6\%$ for branches larger than 0.30, $\sim 7.3\%$ for branches weaker than 0.30 but larger than 0.10, and 19% error for branches weaker than 0.10. While these uncertainties are large, they are also not far from those of previously reported measurements. As well, observational astrophysicists do not require atomic data with high-precision to greatly improve their calculations. Often order-of-magnitude data is sufficient to accomplish their tasks.

Source of Uncertainty	Uncertainty (%)		
	Branch Strength		
	Strong (>30%)	Moderate (10-30%)	Weak (<10%)
Systematic Uncertainty			
SCF – Deviation Between Fit and Data	3	3	3
SCF – Multiple Day Scatter	4.4	4.4	4.4
Systematic Total (added in quadrature)	5.3	5.3	5.3
Statistical Uncertainty			
Branch Uncertainty (combined)	4	5	18
Total Uncertainty (added in quadrature)	6.6	7.3	19

Table 4.1 Estimated uncertainties in the determination of branching ratios listed according to branching ratio strength, where SCF stands for spectral correction factor.

¹ M. Ortiz, R. Mayo, E. Biemont, P. Quinet, G. Malcheva, K. Blagoev, “Radiative parameters for some transitions arising from $3d^94d$ and $3d^84s^2$ electronic configurations in Cu II spectrum,” J. Phys. B **40**, 167-176 (2007).

² W. Demtroder, *Laser Spectroscopy Basic Concepts and Instrumentation*, Springer-Verlag, Berlin Heidelberg, New York, (1996).

³ R. Li, S.J. Rehse, T.J. Scholl, A. Sharikova, R. Chatelain, R.A. Holt, S.D. Rosner, “Fast-ion-beam laser-induced-fluorescence measurements of branching fractions and oscillator strengths in Nd II,” Can. J. Phys. **85**, 1343-1378 (2007).

⁴ S.J. Rehse, R. Li, T.J. Scholl, A. Sharikova, R. Chatelain, R.A. Holt, S.D. Rosner, “Fast-ion-beam laser-induced fluorescence measurements of spontaneous-emission branching ratios and oscillator strengths in Sm II,” Can. J. Phys. **84**, 723-771 (2006).

⁵ X.L. Xu, S. Svanberg, R.D. Cowan, P.H. Lefebvre, P. Quinet, E. Biemont, “Theoretical and experimental lifetime and oscillator strength determination in singly ionized neodymium (Nd II),” *Mon. Not. R. Astron. Soc.* **346**, 443-440 (2003).

⁶ J.A.M. Rojas, M. Ortiz, J. Campos, “Determination of transition probabilities of some Sb III lines by time resolved spectrometry of laser produced plasmas,” *Phys. Script.* **62**, 364-367 (2000).

⁷ H.L. Xu, S. Svanberg, P. Quinet, H. P. Garnir, E. Biemont, “Time-resolved laser-induced fluorescence lifetime measurements and relativistic Hartree-Fock calculations of transition probabilities in Sm II,” *J. Phys. B* **36**, 4773–4787 (2003).

⁸ R.A. Holt, R. Li, R. Chatelain, S.J. Rehse, S.D. Rosner, T.J. Scholl, “Fast-ion-beam laser-fluorescence measurements of oscillator strengths in the lanthanides,” *Phys. Scr.* **T134**, 014012 (2009).

Chapter 5 – Praseodymium & Neodymium

5.1 - Introduction

Astrophysically relevant radiative parameters from lanthanide elements are required for comparison of astrophysical calculations of stellar abundances in chemically peculiar (CP) stars. These CP stars show anomalies in surface layer abundance determinations through abnormally strong and/or weak absorption lines in the optical range. Abundance calculations are derived mainly from oscillator strengths f which are commonly reported as the $\log(gf)$ value, where g is the degeneracy of the level. Comparison between astrophysically determined $\log(gf)$ values and their experimental/theoretical counterparts can help to refine abundance models.

Extending our knowledge of lanthanide spectra and radiative properties in neutral and singly ionized atoms helps us to better understand the opacity of the solar atmosphere which is used as a standard for all other opacities including the CP stars. The opacity of the sun's atmosphere is dominated mainly by the hydrogen ion H^+ . Within the sun's atmosphere most of the elements are singly ionized; but in the case of lanthanide elements two valence electrons can be liberated.

The recent ability to increase the accuracy of radiative parameters like the oscillator strength and transition probability through laboratory astrophysics allows astronomers to revisit unresolved problems with new insight. For example, questions regarding the observed deviations in oscillator strengths from solar spectra might point to a diffusive process of heavy elements towards the sun's core, thus altering the observed abundance.¹

The galactic halo region of our galaxy includes some of the oldest stars in our galaxy. In general, the abundances determined within galactic halo stars are much lower than solar abundances. However, a few of these metal deficient stars have observed lanthanide overabundances compared to their iron abundance.¹ These measured overabundances are derived from singly-ionized spectral lines. Study of the atomic properties of singly ionized lanthanides like Nd and Pr can help to improve stellar nucleosynthesis models.

The observation of spectral lines from strongly magnetized CP stars show relatively large Zeeman splittings for degenerate levels especially within the lanthanide elements. The observation of near infrared emission lines from neutral lanthanides allow improvements to be made in models of magnetic field topology. The spectral range of near infrared to near ultraviolet allows a “spectral probing” of various depth within the stellar medium since the range of emitted species are derived from various depths of the star. Transition probabilities of Nd I and Pr I are currently meager and this work aims at furthering these radiative parameters in an effort to support these interests.

The chemically peculiar type A metallic-line stars (or Am star) and mercury-manganese stars (HgMn) have observed overabundances in praseodymium and neodymium.² These overabundances are thought to be the consequence of a diffusive process within the atmosphere of the star. In cooler CP stars, strong spectral lines from singly ionized lanthanides are apparent, while in hotter cases above 7,000 K the CP stars show line depth dominance in the doubly ionized lanthanides.¹ The lack of atomic data in the doubly ionized states of Nd and Pr creates difficulties for astronomers in this area of research. One of the goals of this research is to provide astronomers with radiative parameters in Nd I, II, III and Pr I, II, III relating to these interests.

5.2 - Previous Works

5.2.1 - Previous Work in Praseodymium

The first reported radiative parameters in neutral praseodymium were from Gorshkov and Komarovskii in 1985.³ They determined lifetimes for 14 levels between 19,123 and 24,195 cm^{-1} in neutral praseodymium (Pr I) using a delayed-coincidence method. In 1998 Song et al.⁴ measured 14 levels between 16,887 and 28,501 cm^{-1} using pulsed laser excitation on an atomic beam. In 2004, Biémont et al.⁵ used time-resolved LIF to determine 18 even-parity levels of Pr I and 15 odd-parity levels in Nd I. In 2006, Furmann et al.⁶ presented 57 new levels of odd parity in neutral Pr using LIF.

The early work of determining radiative parameters in singly ionized praseodymium (Pr II) was accomplished by Meggers et al.⁷ who used intensities to determine oscillator strengths. These values however were found to be poor in accuracy stemming from assumptions of local thermodynamic equilibrium which involved self-absorption. Lifetime calculations were first presented by Andersen and Sorensen⁸ in 1974 using beam-foil spectroscopy, but these values were erroneous due to non-selective excitation and Doppler limited spectral resolution. A more accurate approach to determine oscillator strengths combines branching ratios (BR) from a given energy level with its corresponding spontaneous emission lifetime. In this way, Lage and Whaling⁹ used BR's from Andersen and Sorensen to determine oscillator strengths in Pr II. Goly et al.¹⁰ in 1991 obtained BRs for 62 transition in Pr II. Kurucz and Bell¹¹ in 1995, using data from Lage and Whaling, and Meggers et al. presented a list of radiative parameters including $\log(gf)$ values and transition probabilities (TP's) in Pr II which can be obtained online

(<http://www.cfa.harvard.edu/amp/ampdata/kurucz23/sekur.html>). In 2001, oscillator strengths for 31 lines in Pr II were determined by Ivarsson et al.¹² Lifetimes from 10 levels between 22,675 and 28,201 cm^{-1} in Pr II were presented by Dolk et al.² in 2002 using laser-induced fluorescence (LIF) in a laser-induced plasma. In 2003, Biémont et al.¹³ determined 20 new lifetimes in Pr II using time-resolved LIF; these lifetimes in combination with theoretical branching ratios produced transition probabilities for nearly 150 lines. In 2005 Furmann et al.¹⁴ measured 42 new levels having energies between 9,164 and 38,434 cm^{-1} in Pr II via LIF. Li et al.¹⁵ in 2007 used LIF on a fast-ion-beam in order to measure branching fractions (another name for branching ratios) of 32 levels in singly-ionized praseodymium.

The first set of transition probabilities in Pr III was presented by Palmeri et al.¹⁶ in 2000 using the theoretical relativistic Hartree-Fock method and some 191 newly determined energy levels in Pr III. Prior to that study, only wavelength and energy level information was available for the second spectrum in praseodymium. However it was soon after shown that the oscillator strengths presented by Palmeri et al. were affected by large uncertainties due to theoretical core-polarization assumptions of the dipole operator which have recently been shown to be invalid. In 2001 Biémont et al.¹⁷ provided eight radiative lifetimes in Pr III using a laser-produced plasma source combined with time-resolved LIF. These values were checked against updated theoretically determined values. 16 oscillator strengths were listed as a result.

5.2.2 – Previous Works in Neodymium

Transition probabilities were determined in 1962 by Corliss and Bozman¹⁸ using arc discharge measurements. Penkin and Komarovskii¹⁹ measured relative intensities in 1973. 18

lifetimes were determined by Marek and Stahnke²⁰ in Nd I using the delayed coincidence method and laser-induced fluorescence in 1980. Gorshkov et al.²¹, in 1982, measured 38 lifetimes of levels between 17,787 and 25,662 cm^{-1} in Nd I using a pulsed-electron delayed coincidence method. Biémont et al.⁵ measured lifetimes in Nd I using time-resolved LIF to determine 15 levels in 2004. For most of these levels there were no previous data for comparison. Radiative lifetimes of 100 levels in neutral neodymium were measured by Den Hartog et al.²² in 2011 using LIF on a beam-laser ion source.

Prior to the combination of branching ratios and atomic lifetimes to determine oscillator strengths, absolute line intensities and atomic densities were used by Meggers et al.²³ and Corliss et al.²⁴ The uncertainties in this method were problematic and more accurate methods of determining oscillator strengths began with Maier and Whaling.²⁵ Maier and Whaling determined TP's for nine levels by combining lifetimes presented by Andersen et al.²⁶ In 1984 eight radiative lifetimes in singly ionized neodymium with improved accuracies were listed by Ward et al.²⁷ In 2001, Pinciuc et al.²⁸ measured 35 radiative lifetimes in Nd II levels having energies between 22,696 and 29,434 cm^{-1} using a collinear beam-laser method with LIF. In 2002, Scholl et al.²⁹ determined radiative lifetimes for 13 levels in Nd II between 23,171 and 29,955 cm^{-1} using a beam-laser LIF apparatus. Xu et al.³⁰ in 2003 determined 107 oscillator strengths (OS) derived from radiative lifetimes in 24 levels of Nd II which were measured using an LIF setup. Den Hartog et al.³¹ in 2003 determined TP and OS for more than 700 transitions using lifetimes for 168 levels which were derived by time-resolved LIF measurements. From their work, branching ratios were also measured via Fourier-transform spectroscopy (FTS) from an Ar-Nd hollow-cathode discharge lamp. In 2007 Biémont et al.³² studied 29 metastable states in

Nd II and presented a comparison of transition probabilities and calculated lifetimes from various theoretical models. In 2009 I presented our first reported measurements of transition probabilities using laser-induced breakdown spectroscopy (LIBS),³³ a relatively new technique in the field of astrophysically relevant atomic data. The results were in agreement with other experimental techniques within the proposed uncertainty.

With the recent discovery of doubly ionized lanthanides within abundance determinations of CP stars³⁴ there is increasing importance in measuring radiative parameters in doubly ionized species. For Nd III however there is currently very little work in terms of measured lifetimes, transition probabilities, and oscillator strengths. In 1998 Cowley and Bord³⁵ presented theoretical $\log(gf)$ values for a few strong resonance lines in Nd III using the limited energy level identifications at that time and compared their findings to abundances in HR 6870. $\log(gf)$ values and abundances were determined for 10 levels of Nd III by Bord³⁶ in 2000 using relativistic Hartree-Fock (HFR) calculations. In 2002, $\log(gf)$ values from Dolk et al.² were determined for 20 spectral lines. Lifetimes for 5 energy levels in Nd III between 27,788 and 32,832 cm^{-1} were measured by Zhang et al.³⁷ in 2002 using LIF.

This work is aimed at furthering the measurements of radiative parameters relevant to astrophysics by using laser-induced breakdown spectroscopy on neodymium and praseodymium samples. By obtaining relative values of emission line intensities in a laser-produced plasma, radiative parameters were determined. Radiative parameters (e.g. relative intensities, branching ratios, $\log(gf)$ values, and gA values) in Pr I, II, III and Nd I, II, III are presented in the tables

below and compared to previous works by converting the relative transition probabilities to an absolute scale using lifetimes from previous works.

5.3 - Experimental Setup

A diagram of the experimental apparatus is shown in figure 5.1 and described in much greater detail in chapter 3. The laser source is an Nd:YAG laser (Spectra Physics, LAB-150-10) firing 10 ns laser pulses at a repetition rate of 10 Hz and operating at its fundamental wavelength of 1064 nm to ablate the target. The energy of the laser pulse used in this work was 20 mJ/pulse which was incident on a >99.99% pure target in both neodymium and praseodymium.

Within the chamber a pressure of 11 mbar (8.3 Torr) is maintained and an argon buffer gas is introduced through an inlet valve. After every accumulation of 10 shots the chamber was evacuated to the desired pressure and filled with argon to ensure a clean and reproducible environment.

The plasma emission was observed at right angles to the incident laser via a 600 μm optical fiber cable coupled to an Échelle spectrometer. 10 on-chip accumulations were acquired and averaged with another 10 spectra. A delay time of 1000 ns was used after the ablation pulse in conjunction with an ICCD open shutter time of 1000 ns to observe the emitted radiation.

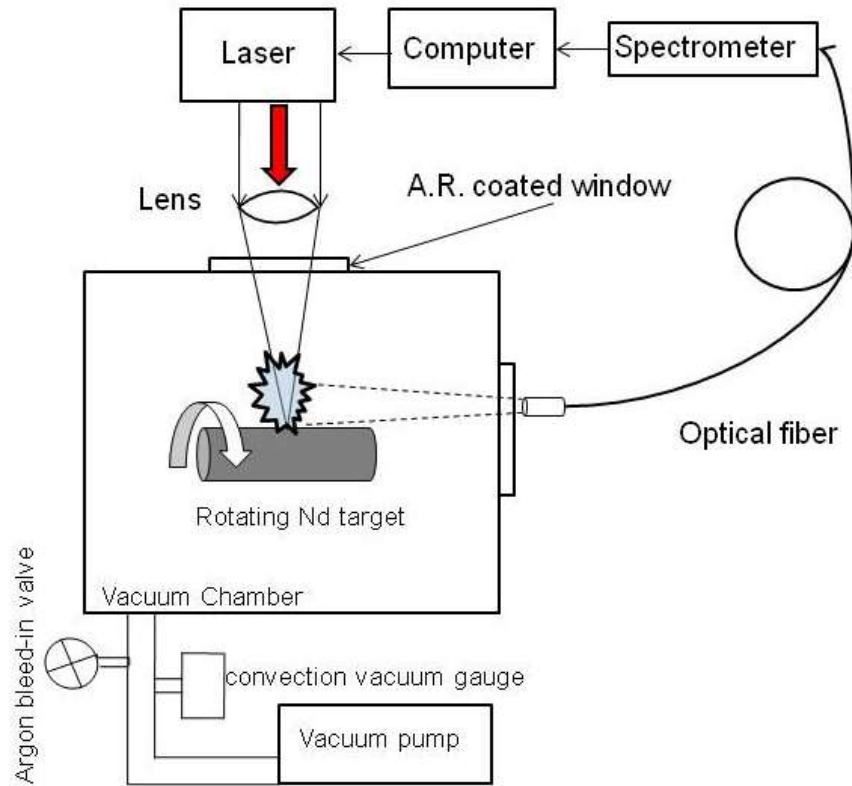


Figure 5.1 The LIBS experimental setup used to make branching ratio measurements. A side-view of the apparatus is shown. The path of the infrared Nd:YAG laser coming through the top of the vacuum cube is depicted with an arrow and solid lines. Visible wavelength plasma emission is collected through a quartz side window and is depicted with dotted lines. The chamber is typically held at a pressure of from 1-15 mbar in argon.

5.4 - Data Analysis

Relative intensities used in this work were derived from integrated emission intensities I_{ul} measured by the ESA 3000's fitting software. The integrated emission intensities were scaled by a wavelength dependent spectral efficiency factor $\varepsilon(\lambda)$ which accounts for optical losses (from the optical fiber and quartz window) in order to create the spectrally corrected integrated emission intensity I'_{ul} as shown in equation 5.1.

$$I'_{ul} = I_{ul} \cdot \varepsilon(\lambda) \quad (5.1)$$

Branching ratios were obtained from spectral emission lines like the ones shown in figure 5.2. Branching ratios (or branching fractions) are the relative probabilities of spontaneous emission de-excitation transitions that originate from the same excited-state energy level but terminate in different lower energy levels. The branching ratios are calculated using all allowed transitions out of an excited state and thus they must sum to one (there is a probability of one that an atom in a given energy level will make a transition to a lower state). If a detection system is not sensitive to photon energy, then the observed emission intensities of the transitions from an excited energy level can be used to calculate the branching ratios.

To calculate a branching ratio, β_{ul} , expressed in equation 5.2, from observed emission intensities, the integrated emission intensity from a single transition, I'_{ul} , from a given upper energy state E_u to a lower energy state E_l is normalized by the sum of all integrated emission intensities $\sum_u I'_{ul}$ stemming from spontaneous transitions of the upper state E_u . This is expressed in equation 5.2

$$\beta_{ul} = \frac{I'_{ul}}{\sum_u I'_{ul}} \quad (5.2)$$

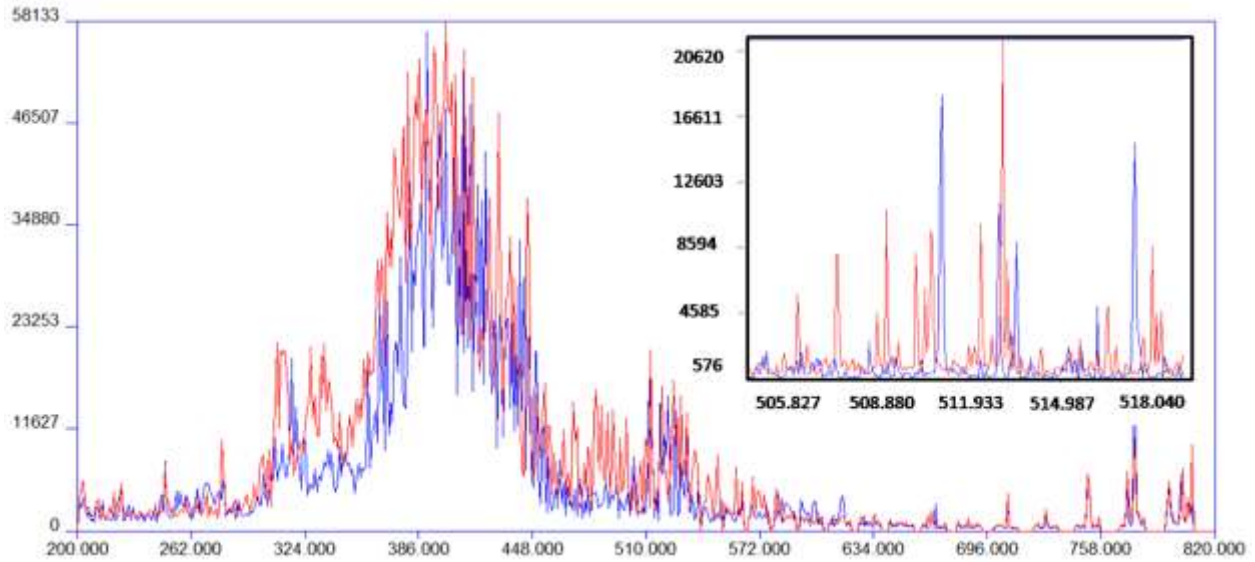


Figure 5.2 Shown above is an overlay of a neodymium spectrum (red) and a praseodymium spectrum (blue). Both are lanthanide elements and their resulting spectra are similar in the spectral region shown. The inset shows a few emission lines from both elements' spectra near 511 nm.

Because the branching ratios are related to the normalized intensities of transitions out of a given energy level, it is not necessary to know absolute emission intensities, only relative intensities. Relative intensities, R_{ul} , were derived for each branch from an upper state by dividing the observed integrated emission intensity I'_{ul} by the strongest observed integrated emission intensity $I'_{uk,max}$ from that upper energy state as shown in equation 5.3, where the subscript u denotes identical upper states.

$$R_{ul} = \frac{I'_{ul}}{I'_{uk,max}} \quad (5.3)$$

In this way, the strongest observed branch has a relative intensity of 1.0, and all weaker transitions will have a relative intensity between 0.0 and 1.0.

Incorporating the (usually known) lifetime of an energy level (τ_u) allows for the calculation of the transition probability A_{ul} for a given branch as shown in equation 5.4.

$$A_{ul} = \beta_{ul} / \tau_u \quad (5.4)$$

The oscillator strength f_{lu} can be determined once the transition probability is calculated by using equation 5.5, where g_l and g_u are the degeneracies of the lower and upper states respectively, defined as $g_{u,k} = 2J_{u,l} + 1$ and λ is the wavelength in nanometers for the given transition.

$$A_{ul} = \frac{2\pi e^2}{m_e c \epsilon_o \lambda^2} \cdot \frac{g_l}{g_u} \cdot f_{lu} = \frac{6.67 \times 10^{-5}}{\lambda^2} \cdot \frac{g_l}{g_u} \cdot f_{lu} \quad (5.5)$$

In the present work relative intensities and branching ratios are tabulated for all recognized emission lines from established upper energy states. For those energy states which have documented lifetimes, $\log(g_l f_{lu})$ values and transition probabilities $g_u A_{ul}$ were calculated and listed.

5.4.1 - Summary of Uncertainties

Within the range of 225-800 nm the averaged absolute-value of the scatter between the actual spectral correction factor $\epsilon(\lambda)$ (spectral intensity without optics / spectral intensity with optics from data) and the graphically-fit value was 4.0%, the 225-800nm range had a standard deviation of 5.5% from the averaged absolute-value.

Uncertainties in the relative intensities (RI) from radiative transitions are derived from repeated measurements of the RIs from many branches over many months as well as the uncertainty in 1000 spectra acquired with identical parameters measured in a single experiment. The uncertainty attributed to emission lines was assigned according to the strength of the branching ratio. Branches having branching ratio strength greater than 0.30 have 4%, branches between 0.30 and 0.10 have 5% error and less than 0.10 have 18%.

Table 5.1 (same as Table 4.1) shows the sources of uncertainties and their estimates for this study. The total uncertainty for the spectral calibration was obtained by adding in quadrature the uncertainty from the spectral efficiency from statistical variations (4.4%) and the uncertainty from the scatter between the fit and reported values (3%). Therefore the total uncertainty given to branches stronger than 0.30 is ~6.6%, for branches between 0.30 and 0.10 an error of ~7.3% and for those branches weaker than 0.10 we estimate ~19% error.

Source of Uncertainty	Uncertainty (%)		
	Branch Strength		
	Strong (>30%)	Moderate (10-30%)	Weak (<10%)
Systematic Uncertainty			
SCF – Deviation Between Fit and Data	3	3	3
SCF – Multiple Day Scatter	4.4	4.4	4.4
Systematic Total (added in quadrature)	5.3	5.3	5.3
Statistical Uncertainty			
Branch Uncertainty (combined)	4	5	18
Total Uncertainty (added in quadrature)	6.6	7.3	19

Table 5.1 Estimated uncertainties in the determination of branching ratios listed according to branching ratio strength, where SCF stands for spectral correction factor.

5.5 - Results

In LIBS spectra it sometimes occurs that line profiles are unresolved due to blending of emission lines with neighboring lines or weak signal to noise. Because of this fact some of the branching ratios are inaccurate, and therefore we list the branching ratios of all of our measured lines with annotations for the strong, blended, shouldered, or weak lines.

As an example of the ESA 3000's resolving capability figure 5.3 shows several typical emission lines from the $23103.660 \text{ cm}^{-1}$ level of Gd II where a blended emission line at 597.723 nm is visible and a very weak and hard to resolve emission line at 647.082 nm is present. The experimental conditions are identical for all the spectra shown (5.3 A through E). Figure 5.3A shows the two problematic lines being resolved and fit; the vertical line denoting the center of the peak and the horizontal green line denoting the full-width at half max (FWHM). Figure 5.3

shows that sometimes there are good reproducible spectra, particularly take notice of the integrated areas (black values above the windows) from the profile's fit which ESAWIN automatically generates. When the green vertical and horizontal lines are not present, the fitting software was unable to measure the peak (figure 5.3 C, D, and E), and refers to the measurement either as noise or no peak "np". Notice in figure 5.3E that the line at 597.723 nm shows a much larger integrated area (3741) and unless detected by the user would go unnoticed and register as a larger peak. I would also like to draw attention to the line at 784.482 nm which is an example of emission lines falling within the spectral gaps of our Echelle spectrometer. As mentioned earlier there is nothing we can do about the gaps and a small minority of lines tends to reside within these gaps which are beyond 600 nm where we do not anticipate the majority of strong lines to lie in the elements used in this research. The point of these figures is to show that with so many lines neighboring one another and so many weak emission lines from the spectrum, issues can arise when making relative branching ratio determinations. These problematic emission lines shown in Gd II are sometimes typical for the weak and blended emission lines.

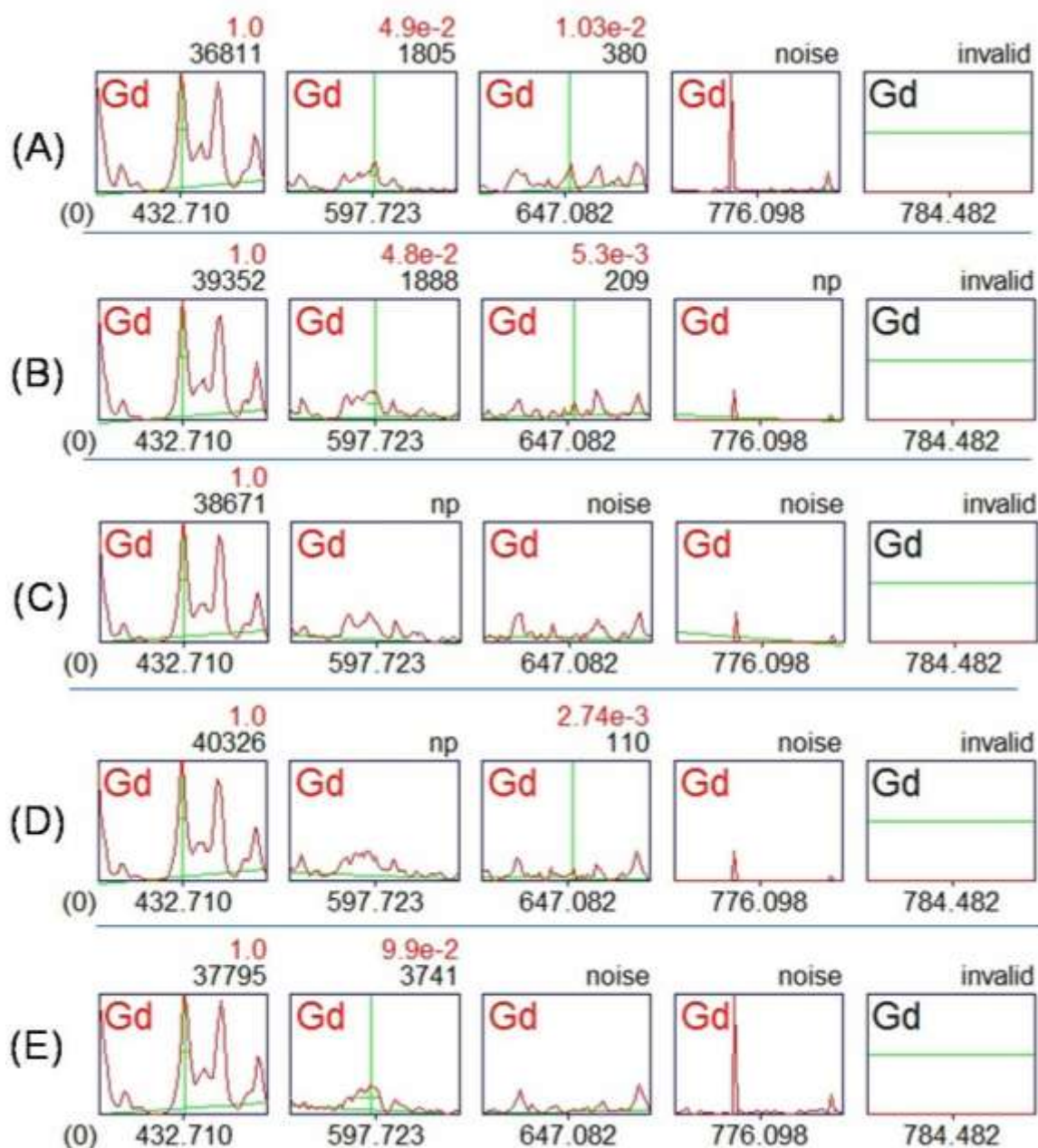


Figure 5.3 shows the inability of the ESAWIN software's resolving capability when weak emission lines (647.082nm) and weak-and-blended lines (597.723nm) are present. The invalid line at 784 lies within one of our spectral gaps and is not detected.

On the other side of the coin, a typical strong branch is shown in figure 5.4, where the emission line at 437.384nm shows how the software is capable of resolving otherwise blended emission lines when the peaks are large and fit a Voigt-profile rather well.

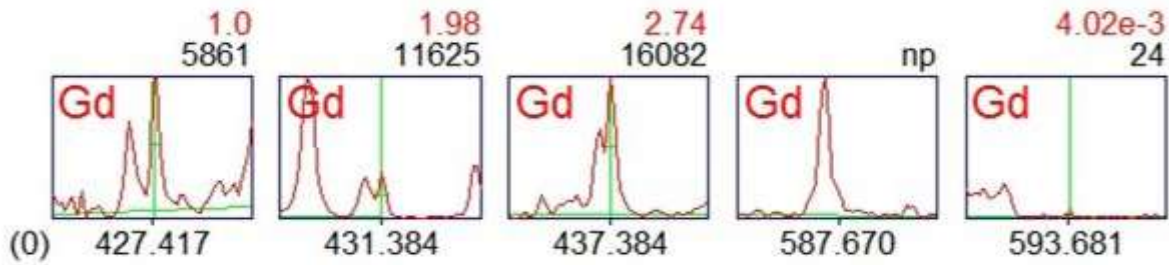


Figure 5.4 shows the ESAWIN software's resolving capability with two large profiles which are seemingly blended at 437.384nm.

Branching ratios (BR), transition probabilities, and $\log(gf)$ values for neodymium are listed in tables 5.2, 5.3 and 5.4 according to ionization state and energy level and are compared to previous results. Branching ratios (BR), transition probabilities $g_u A_{ul}$, and $\log(gf)$ values for praseodymium are listed in tables 5.5, 5.6, and 5.7 according to ionization state and energy level and are compared to previous results. In this work only transitions in the spectral range of 200 - 800nm were observed and the corresponding radiative parameters presented.

Nd I Data

Upper												
Energy	Lifetime	Wavelength	Branch	BR		$g_i \cdot A_{ki} (10^6 \text{ s}^{-1})$				Log gf		
(cm ⁻¹)	T (ns)	(nm)	Ratio	Error		This Work	error	Kurucz	Gorshkov	This Work	Kurucz	Gorshkov
16979.352	615a	588.7875	1.00	0.09	w	11.38	1.47	28.92	75.74	-1.23	-0.93	-0.93
17786.992	76.3	562.0526	1.00	0.09		91.74	9.69	102.69	138.31	-0.36	-0.42	-0.42
18741.337	81	533.4315	0.12	0.00	w	14.47	1.66	15.80	155.13	-1.21	-1.17	-0.41
18741.337		567.5959	0.88	0.05		102.43	10.82	119.68	70.02	-0.31	-0.33	-1.08
19209.262	229	520.4373	0.28	0.01	w	6.30	0.72	42.08	76.34	-1.59	-0.77	-1.17
19209.262		552.9069	0.72	0.03	s	24.27	2.56	22.01	110.49	-0.95	-1.08	-0.68
19700.856	300b	507.4507	0.00	0.00		0.00	0.00	26.67	105.29	0.00	-0.90	-0.90
19700.856		576.7323	1.00	0.09	w	36.67	4.58	32.70		-0.74	-0.86	
19769.507	123	505.6885	1.00	0.09	w	73.17	7.73	68.09	145.47	-0.55	-0.58	-0.58
19815.981	91.3	534.9561	0.69	0.06	w	83.48	8.81	25.54	181.23	-0.45	-0.96	-0.25
19815.981		572.9272	0.75	0.07	b	90.71	9.58	160.03	83.73	-0.35	-0.18	-0.89
20176.912	32.6	495.4777	1.00	0.09		337.42	35.63	259.83	290.71	0.09	0.07	0.07
20300.875	10.6	492.4521	1.00	0.09		1037.74	109.57	809.10	479.48	0.58	0.56	0.56
20360.673	81.3	491.0058	0.61	0.06	s	68.01	7.18	84.66	128.42	-0.61	-0.51	-0.77
20360.673		519.8053	0.39	0.04	w	42.70	4.51	63.00	160.96	-0.76	-0.68	-0.43
20541.833	77.8	486.6755	0.93	0.09		131.35	13.87	80.78	159.39	-0.33	-0.46	-0.57
20541.833		514.9547	0.07	0.02	w	10.04	2.39	83.05	174.08	-1.40	-0.48	-0.37
20839.206	127	507.1857	0.29	0.01	w	41.17	4.35	72.45	160.12	-0.80	-0.48	-0.48
20839.206		541.1916	0.33	0.01	w	47.42	5.01	25.53		-0.68	-0.95	
20839.206		582.6736	0.38	0.01	s	55.03	5.81	67.95	116.40	-0.55	-0.52	-0.52

20963.071	178	504.0184	1.00	0.09	w	61.80	6.53	69.34	147.17	-0.63	-0.58	-0.58
21005.439	103	475.9341	0.51	0.05		54.07	5.71	18.23	95.88	-0.74	-1.12	-1.12
21005.439		502.9441	0.49	0.05		52.72	5.57	101.59	174.11	-0.70	-0.41	-0.41
21184.881	28.7	471.9027	1.00	0.09		313.59	33.11	299.34	298.05	0.02	0.00	0.00
21314.254	101	495.2498	0.58	0.05	w	74.08	7.82	75.98	167.93	-0.56	-0.48	-0.48
21314.254		566.9753	0.85	0.08	s	109.27	11.54	179.40	183.02	-0.28	-0.13	-0.12
21314.439	69.9	469.0343	0.80	0.07		102.49	10.82	114.66	198.61	-0.47	-0.42	-0.42
21314.439		495.2452	0.20	0.02	w	26.27	3.01	109.75		-1.01	-0.48	
21345.572	21.8	494.4826	1.00	0.09		596.33	62.97	506.99	383.98	0.34	0.34	0.34
21345.837	20.5	468.3443	1.00	0.09		439.02	46.36	465.30	365.57	0.16	0.19	0.18
21488.39	111	465.2373	1.00	0.09	w	81.08	8.56	47.16	136.29	-0.58	-0.82	-0.82
21543.326	16.0	489.6927	0.65	0.06		528.98	55.85	646.36	431.37	0.28	0.44	0.44
21543.326		521.3202	0.35	0.03		283.52	29.94	245.31		0.06	0.00	
21558.796	74.6	463.7179	0.76	0.07		34.84	3.99	31.93	126.09	-0.44	-0.90	-0.90
21558.796		489.3219	0.24	0.02	w	112.61	11.89	119.35	192.79	-0.90	-0.37	-0.37
21572.61	11.3	463.421	1.00	0.09		619.47	65.41	753.48	409.27	0.30	0.28	0.28
21718.328	133	485.5306	1.00	0.09	w	97.74	10.32	73.78	169.57	-0.46	-0.51	-0.51
21726.771	121	485.3316	1.00	0.09		90.91	9.60	87.26	169.71	-0.49	-0.51	-0.51
21797.9	75.3	483.6614	1.00	0.09	s	172.64	18.23	79.66	176.08	-0.22	-0.48	-0.48
21926.903	86.1	480.6615	1.00	0.09		104.53	11.04	112.53	175.68	-0.44	-0.50	-0.50
22010.34	95.2	454.2046	0.00	0.00	w	0.00	0.00	69.72	166.09	0.00	-0.67	-0.67
22010.34		478.741	1.00	0.09		94.54	9.98	39.16	111.53	-0.49	-0.96	-0.96

22049.736	173	477.8395	0.73	0.07	w	54.58	5.76	35.30	125.46	-0.73	-0.85	-0.84
22049.736		507.9075	0.27	0.03	w	20.56	2.35	115.43		-1.10	-0.35	
22076.64	193	477.2258	1.00	0.09	w	46.63	4.92	78.63	151.66	-0.80	-0.66	-0.66
22128.6	184	476.045	1.00	0.09	w	59.78	6.31	61.46	149.05	-0.69	-0.68	-0.68
22229	180b	449.7366	1.00	0.09		38.89	5.63	49.55	129.81	-0.93	-0.93	-0.93
22241.911	219	473.4902	1.00	0.09		50.23	5.30	85.76		-0.77	-0.54	
22255.855	35.7	473.1777	1.00	0.09		308.12	32.53	281.71	290.65	0.01	-0.02	-0.02
22303.048	234	501.4539	1.00	0.09		55.56	5.87	137.80	199.57	-0.68	-0.28	-0.28
22471.21	42.3	468.4032	1.00	0.09	w	212.77	22.47	204.05		-0.15	-0.26	
22482.764	154	496.9739	1.00	0.09	w	97.40	10.28	155.22	225.79	-0.44	-0.18	-0.18
22490.97	84	444.4981	1.00	0.09	w	83.33	10.41	93.60	173.43	-0.61	-0.67	-0.67
22605.665	44.8	465.4709	1.00	0.09		245.54	25.93	236.61	274.67	-0.10	-0.11	-0.11
22677.81	64c	463.9125	1.00	0.09		140.63	17.08	133.43	196.83	-0.34	-0.45	-0.45
22736.693	82c	462.6483	0.14	0.01	w	18.48	2.62	82.29	174.66	-1.23	-0.58	-0.58
22736.693		490.7787	0.86	0.08		115.66	15.59	101.08		-0.38	-0.51	
22738.85	185	490.7267	1.00	0.09	w	70.27	7.42	85.55		-0.60	-0.51	
22761.44	14.0	490.1832	1.00	0.09		1071.43	113.13	538.33		0.59	0.35	
22814.888	72.2	460.9802	1.00	0.09		152.35	16.09	119.24		-0.31	-0.42	
22870.686	240	487.5714	1.00	0.09		54.17	5.72	4.21	137.88	-0.71		-0.71
23016.512	85.0	434.3486	0.57	0.02		52.78	5.57	57.30	164.10	-0.83	-0.79	-0.77
23016.512		456.7338	0.43	0.01	w	53.11	5.61	79.75	158.17	-0.78	-0.69	-0.70

23049.76	87.5	456.0411	1.00	0.09	w	125.71	13.27	84.70	179.76	-0.41	-0.58	-0.58
23283.635	32.1	477.9455	1.00	0.09		404.98	42.76	333.58	309.40	0.14	0.06	0.06
23324.278	69.7	477.0187	1.00	0.09		186.51	19.69	198.12	247.16	-0.20	-0.17	-0.17
23433.84	73c	448.1885	1.00	0.09	s	150.68	18.70	102.32	199.00	-0.34	-0.51	-0.51
23438.44	45c	448.096	1.00	0.09		200.00	25.73	201.08	244.64	-0.22	-0.31	-0.31
23474.023	156	505.1055	1.00	0.09	w	108.97	11.51	225.30	236.52	-0.38	-0.01	-0.10
23487.08	93.8	425.6462	1.00	0.09		74.63	7.88	76.73	166.91	-0.69	-0.79	-0.79
23517.752	98.9	472.6552	0.50	0.05	w	75.59	7.98	97.42	195.35	-0.60	-0.42	-0.42
23517.752		503.9919	0.50	0.05	w	76.08	8.03	84.93		-0.54	-0.49	
23744.797	158	498.2884	1.00	0.09	w	94.94	10.02	181.05	226.36	-0.45	-0.17	-0.17
23755.75	174	467.3959	1.00	0.09		74.71	7.89	111.05	196.75	-0.61	-0.44	-0.44
23876.922	157	495.0284	1.00	0.09	w	95.54	10.09	142.77		-0.45	-0.28	
23968.31	61.0	462.7966	1.00	0.09		180.33	19.04	267.67	168.34	-0.24	-0.14	-0.14
23985.826	194	462.4217	1.00	0.09		67.01	7.08	77.05	271.17	-0.67	-0.61	-0.61
23991.098	145	492.2454	1.00	0.09	w	103.45	10.92	147.75	169.85	-0.42	-0.27	
23996.513	20.1	462.1932	1.00	0.09		646.77	68.29	729.82	451.44	0.32	0.37	0.37
23996.513		492.1142	0.00	0.00				170.55			-0.27	
24121.478	13.1	489.1054	1.00	0.09	b	1297.71	137.02	1068.30	527.70	0.67	0.64	0.64
24168.695	88.5	487.9782	1.00	0.09		192.09	20.28	370.50	333.87	-0.16	0.18	0.18
24212.928	123	486.9268	1.00	0.09		121.95	12.88	164.40	222.76	-0.36	-0.23	-0.23
24291.93	45c	455.9656	1.00	0.09		244.44	31.45	445.25		-0.12	0.07	

24688.275	152	475.9083	1.00	0.09		111.84	11.81	103.40		-0.42	-0.40	
24702.585	54.3	447.5824	0.84	0.08		201.20	21.24	73.48	313.40	-0.22	-0.66	-0.06
24702.585		475.5843	0.16	0.02	w	38.21	4.38	341.70	162.82	-0.89	0.00	-0.59
24729.558	39.6	474.9748	1.00	0.09		378.79	40.00	398.55	336.63	0.11	0.13	0.13
24935.096	77.9	502.7136	1.00	0.09		243.90	25.75	380.97		-0.03	0.21	
24968.49	41.9	469.6434	1.00	0.09	w	358.00	37.80	317.25	308.72	0.07	0.02	0.02
24984.183	261	442.0097	1.00	0.09		49.81	5.26	107.90		-0.84	-0.50	
25063.72	133	467.5517	1.00	0.09		112.78	11.91	137.16	215.59	-0.43	-0.35	-0.35
25141.541	54.1	497.5484	1.00	0.09		351.20	37.08	531.93	380.01	0.12	0.34	0.34
25190.77	45.7	496.3324	1.00	0.09		371.99	39.28	459.51	340.75	0.14	0.23	0.23
25197.765	26.4	464.6388	1.00	0.09	w	568.18	59.99	71.90	325.00	0.26	0.05	0.05
25478.135	24b	458.662	1.00	0.09		541.67	84.39	602.55	393.88	0.23	0.22	0.22
25513.721	48.2	488.4999	1.00	0.09		352.70	37.24	474.47	351.76	0.10	0.23	0.23
25518.7	9.3	488.3811	1.00	0.09		2043.01	215.72	1486.14	606.38	0.86	0.77	0.77
25555.233	65.6	431.1245	1.00	0.09		167.68	17.71	187.59	251.59	-0.33	-0.35	-0.35
25596.531	50.4	456.184	1.00	0.09	w	297.62	31.43	226.80		-0.03	-0.15	
25609.372	68.1	430.1202	1.00	0.09		190.90	20.16	106.34		-0.28	-0.53	
25662.081	50.4	454.8236	1.00	0.09		257.94	27.24	278.85	284.41	-0.10	-0.13	-0.12
25746.414	29.2	526.6627	0.12	0.01	w	52.36	5.99	126.13		-0.66	-0.28	
25746.414		529.1656	0.31	0.03	w	136.82	14.45	506.00		-0.24	0.40	
25746.414		589.9455	0.58	0.05	s	256.02	27.03	123.67		0.13	-0.19	

25750.895	41.5	452.9932	1.00	0.09		313.25	33.08	376.50	325.58	-0.02		
25864.308	28.4	574.9183	1.00	0.09		387.32	40.90	384.34		0.28	0.28	
26333.118	28.6	557.55	0.51	0.02	w	313.25	33.08	222.30		0.82	0.07	
26333.118		600.7648	0.45	0.01		273.51	28.88	289.80		0.64	0.25	
26333.118		642.984	0.04	0.00	w	25.47	6.07	47.58		-0.48	-0.53	
26634.857	37.9	463.1281	1.00	0.09	w	395.78	41.79	232.73		0.10	-0.18	
26763.662	49.1	460.3809	1.00	0.09		346.23	36.56	361.08		0.04	0.06	
26835.359	26.5	498.0886	0.79	0.07	w	449.44	47.46	232.83		0.22	0.00	
26835.359		554.3245	0.21	0.02		116.60	13.35	375.18		-0.27	0.30	
26842.129	17.1	563.9535	1.00	0.09	s	760.23	80.27	355.94		0.56	0.23	
26842.129		607.1702	0.00	0.00		0.00	0.00	197.12		0.00	0.11	
27130.927	47.3	452.7239	1.00	0.09	w	359.41	37.95	497.93	391.24	0.04	0.19	0.18
27691.315	55.0	394.7594	1.00	0.09		200.00	21.12	373.10		-0.33	-0.13	
27785.804	17.2	560.191	0.68	0.06	s	589.89	62.29	464.70		0.44	0.34	
27785.804		599.4752	0.26	0.03	s	226.46	25.93	320.71		0.09	0.30	
27785.804		635.5934	0.06	0.01	w	55.74	13.28	106.55		-0.47	-0.19	

Table 5.2 Nd I radiative properties

Lifetimes from Den Hartog et al.²² unless noted.

a lifetime from Blageov et al.³⁸

b lifetime from Gorshkov et al.³⁹

c lifetime from Biémont et al.¹⁷

s emission line has shoulder

w weak emission line

b blended emission line

Gorshkov refers to work by Gorshkov et al.³⁹

Kurucz refers to work by Kurucz et al.¹¹

Nd II Data:

Upper Energy (cm ⁻¹)	Lifetime T (ns)	Wavelength (nm)	Branch Ratio	BR Error	Log (g _i *f _{ik})			
					this work	DREAM	UWO	D.H.
22696.885	80.6	450.659	0.24	0.02	-0.96		-1.08	-1.04
		470.971	0.22	0.02	-0.96		-1.02	-0.97
		497.092	0.06	0.01	-1.46		-1.47	-1.39
		509.28	0.31	0.02	-0.74		-0.67	-0.61
		547.514	0.09	0.02	-1.19		-2.37	
		580.923	0.03	0.01	b -1.62		-1.58	-1.71
		634.139	0.05	0.01	-1.38		-1.68	-1.72
		700.257	0.00	0.00	w -2.53		-1.78	
		749.478	-	-	-		-1.89	
		779.835	-	-	-		-1.23	
22850.552	85.6	437.503	0.56	0.04	-0.82		-1.12	-1.05
		447.558	0.10	0.02	-1.56		-1.74	
		471.559	0.28	0.02	-1.06		-1.00	-0.90
		593.474	-	-	-		-1.61	
		652.314	0.01	0.00	-2.24		-1.37	
		692.799	-	-	-		-1.62	
		711.336	0.00	0.00	w -2.86		-2.53	
		732.284	0.00	0.00	w -2.84		-2.03	
		758.764	-	-	-		-1.49	
		772.472	0.06	0.01	b -1.31		-1.79	
23159.979	79.6	441.443	0.10	0.02	-1.28		-1.49	-1.59
		460.916	0.19	0.01	b -0.96		-2.10	-2.30
		464.775	0.06	0.01	-1.43		-1.58	-1.69
		485.903	0.64	0.04	-0.38		-0.45	-0.44
		536.117	-	-	-		-1.41	-1.48
		724.33	0.01	0.00	w -2.10			
		752.646	0.00	0.00	w -2.46		-1.59	
		779.642	-	-	-		-1.50	
23229.991	13.3	430.357	0.60	0.06	0.10	0.06	0.10	0.08
		440.082	0.11	0.01	-0.63	-1.03	-0.69	-0.60
		463.267	0.01	0.00	-1.53	-1.17	-1.46	-1.52
		495.814	0.02	0.00	-1.25	-1.24	-1.27	-1.24
		531.982	0.18	0.02	-0.24	-0.17	-0.21	-0.14

		580.4	0.05	0.01	-0.71	-0.65	-0.67	-0.53
		613.396	0.02	0.01	b -1.01		-1.66	
		636.554	0.00	0.00	w -1.66	-1.45	-1.18	-1.20
23397.385	66.6	427.278	0.28	0.02	-1.03		-1.22	-1.14
		436.863	0.41	0.03	-0.85		-0.88	-0.81
		459.701	0.20	0.01	-1.11		-1.22	-1.15
		574.814	0.03	0.01	-1.73		-1.40	
		629.841	0.02	0.00	-1.75		-1.25	-1.43
		684.696	0.04	0.01	-1.52		-1.40	
		704.083	0.00	0.00	w -2.61		-1.92	
		728.528	0.00	0.00	w -2.65		-1.32	
		741.156	-	-	-		-1.95	
		798.878	-	-	-		-1.88	
		799.133	-	-	-			
23409.537	70.5	427.057	0.20	0.01	-1.11		-1.30	-1.27
		436.632	0.25	0.02	-0.98		-1.35	-1.35
		455.673	0.08	0.02	-1.43		-1.32	-1.35
		459.445	0.11	0.01	-1.30		-1.35	-1.36
		491.438	0.22	0.02	-0.94		-0.73	-0.70
		526.947	0.10	0.02	-1.24		-1.37	
		574.413	0.02	0.00	w -1.86		-1.63	
		606.713	-	-	-		-1.93	
		629.36	0.01	0.00	b -2.12		-2.18	
		666.963	0.01	0.00	w -2.10		-1.77	
		703.481	0.00	0.00	w -2.68		-2.12	
		711.467	-	-	-			
		738.767	-	-	-		-1.97	
		740.489	-	-	-			
		784.545	-	-	-		-1.53	
		787.854	-	-	-			
		798.103	0.00	0.00	w -2.83		-1.93	
23537.387	26.6	424.737	0.35	0.03	-0.45		-0.29	-0.21
		434.206	0.15	0.02	-0.79		-1.23	-1.18
		453.033	0.05	0.01	-1.22		-1.66	
		456.761	0.09	0.02	-1.00		-1.33	-1.31
		488.369	0.11	0.01	-0.84		-1.67	
		523.419	0.18	0.02	-0.56		-0.58	-0.51
		570.244	0.08	0.02	-0.85		-0.87	-0.88

		624.334	-	-	-	-1.25	-1.69
		697.207	-	-	-	-1.69	
		731.852	-	-	-	-1.72	
		733.542	-	-	-		
		790.039	-	-	-		
23857.278	66.1	428.257	0.38	0.04	-0.72	-1.20	-1.21
		446.56	0.15	0.02	-1.08	-1.09	-1.10
		450.181	0.28	0.03	-0.81	-0.74	-0.69
		516.792	0.03	0.01	-1.67	-1.10	-1.18
		544.226	0.11	0.01	-1.05	-0.91	
		590.662	0.04	0.01	-1.46	-1.08	
		647.618	0.01	0.00	w -2.20	-1.52	
		715.106	-	-	-	-1.62	
24053.354	74.3	415.626	0.61	0.04	-0.63	-1.11	-1.06
		424.689	-	-	-	-1.77	-1.79
		442.682	0.02	0.00	-2.08	-1.72	-1.75
		446.241	0.21	0.02	-1.03	-0.89	-0.91
		476.362	0.11	0.01	-1.25	-1.28	-1.27
		509.652	0.03	0.01	-1.77	-1.27	
		553.922	0.01	0.00	w -1.99	-1.69	
		583.898	0.01	0.00	w -2.36	-2.20	
		604.845	0.00	0.00	w -2.62	-2.30	
		639.495	-	-	-	-1.90	
		705.214	0.00	0.00	w -2.70	-1.72	
		746.813	0.00	0.00	w -2.73	-1.94	
		749.81	-	-	-		
		762.489	-	-	-	-1.94	
24134.095	24.6	423.237	0.22	0.02	-0.54	-0.53	-0.47
		441.105	0.19	0.01	-0.58	-0.65	-0.60
		444.638	0.36	0.02	-0.28	-0.37	-0.35
		463.937	0.05	0.01	-1.13	-1.38	-1.43
		507.562	0.01	0.00	w -1.80	-1.68	
		536.147	0.12	0.01	-0.59	-0.45	
		551.455	-	-	-	-1.90	
		581.157	0.04	0.01	-1.02	-0.85	-0.86
		636.209	0.01	0.00	-1.37	-1.13	
		724.597	-	-	-	-0.86	

24321.262	51.7	411.047	0.21	0.02		-0.98	-0.82	-0.71
		419.91	0.08	0.02		-1.37	-1.50	-1.52
		437.492	0.38	0.02		-0.68	-1.08	-1.08
		470.357	0.22	0.02		-0.85	-0.99	-1.00
		502.785	0.05	0.01		-1.39	-1.22	-1.19
		545.82	-	-		-	-1.70	
		574.82	0.02	0.00		-1.65	-1.34	-1.14
		628.721	0.03	0.01	w	-1.50	-1.38	-1.57
		693.646	-	-		-	-1.16	-1.51
		732.16	0.00	0.00	w	-2.47	-1.68	
		735.041	-	-		-		
24445.389	15.62	417.732	0.25	0.02			-0.13	-0.10
		435.128	0.28	0.02			-0.59	-0.61
		438.566	0.28	0.02			-0.28	-0.30
		499.665	0.01	0.00			-1.36	
		501.544		-			-0.26	-0.18
		527.343	0.09	0.02			-1.51	
		542.146	0.03	0.01			-0.61	
		570.827	0.06	0.01			-1.03	
		623.85	-	-				
24468.033	166	408.581	0.33	0.02		-1.40	-1.24	-1.16
		417.337	0.21	0.02		-1.57	-1.56	-1.50
		438.131	0.39	0.03		-1.27	-2.68	
		541.48	0.03	0.01		-2.17	-1.62	-1.62
		590.041	0.03	0.01		-2.16	-1.60	
		637.919	0.02	0.00	w	-2.34	-2.05	
		675.801	-	-		-	-1.84	
24842.878	31.6	410.907	0.52	0.03	s	-0.15	-0.25	-0.16
		427.728	0.12	0.01		-0.75	-1.45	-1.49
		431.05	0.10	0.02		-0.83	-1.40	-1.42
		449.163	0.02	0.00	w	-1.56	-1.64	-1.68
		459.091	0.10	0.02	b	-0.78	-1.87	
		491.738	0.02	0.00		-1.31	-1.36	-1.44
		516.513	0.07	0.01		-0.80	-0.81	-0.74
		558.159	0.03	0.01		-1.10	-1.17	-1.19
		593.905	-	-		-	-1.77	
		608.751	-	-		-	-1.71	
		668.01	0.01	0.00		-1.29	-1.58	

		719.182	-	-	-	-1.28	
		753.827	0.00	0.00	w -1.89	-0.87	
		780.157	-	-	-	-1.11	
		795.538	-	-	-	-0.97	
24913.863	61	401.27	-	-	-	-0.78	-0.60
		409.712	0.07	0.01	s -1.61	-2.26	
		429.734	0.21	0.02	s -1.08	-1.53	-1.52
		528.713	0.40	0.03	-0.61	-1.29	
		574.913	0.13	0.01	-1.03	-1.40	
		606.131	0.08	0.01	w -1.20	-1.91	
		620.273	0.01	0.00	w -2.16	-1.76	
		636.141	0.08	0.02	s -1.15	-1.34	
		656.03	-	-	-	-1.55	
		666.252	0.02	0.00	w -1.79	-1.38	
		712.532	0.00	0.00	w -2.33	-1.37	
		712.735	0.01	0.00	w -2.02		
25080.88	39.5	406.927	0.24	0.03	-0.74	-0.56	-0.57
		423.417	0.21	0.02	-0.76	-1.94	
		426.671	0.19	0.02	-0.81	-0.90	-0.97
		444.411	0.05	0.01	-1.31	-1.91	-2.03
		454.127	0.17	0.02	-0.80	-0.65	-0.74
		484.284	0.00	0.00	w -2.50	-1.91	
		486.048	-	-	-		
		510.239	0.11	0.01	-0.88	-0.74	
		550.84	0.02	0.01	-1.52	-1.18	
25138.556	34.2	397.683	0.41	0.04	-0.65	-0.39	-0.40
		405.973	0.32	0.03	-0.73	-1.82	-1.89
		425.623	0.14	0.01	-1.04	-1.38	-1.41
		522.504	0.08	0.02	-1.13	-0.96	
		567.579	0.05	0.01	-1.21	-1.13	
25200.913	98.3	404.948	0.19	0.01	s -1.13	-1.88	
		421.275	-	-	-	-1.54	
		424.496	0.11	0.01	s -1.34	-1.65	
		442.052	0.10	0.01	s -1.31	-1.52	
		451.664	0.35	0.02	b -0.77	-1.48	
		483.227	0.20	0.01	-0.94	-0.71	
		507.132	0.01	0.00	w -2.47	-2.11	

		581.536	0.01	0.00	w	-2.07	-1.64	
		631.02	0.04	0.01		-1.46	-1.44	
		693.935	-	-		-	-1.21	
25295.288	30.64	395.219	0.40	0.03	b	-0.51	-1.14	-1.16
		403.406	0.21	0.02		-0.78	-0.91	-0.91
		422.802	0.29	0.02		-0.59	-0.96	-1.12
		518.259	0.06	0.01	w	-1.08	-1.38	-1.54
		562.573	0.03	0.01		-1.31	-1.45	
		621.066	0.00	0.00	w	-2.04	-1.33	
		640.01	-	-	w	-		
		648.736	0.00	0.00		-2.56	-0.87	-1.32
		649.736	0.00	0.00		-2.15		
		693.866	-	-		-		
25352.384	59.9	402.478	0.11	0.01		-1.24	-0.87	-0.85
		418.603	0.26	0.02		-0.83	-1.31	-1.31
		439.111	0.24	0.02	s	-0.83	-1.24	-1.25
		448.594	0.05	0.01		-1.46	-1.43	-1.44
		479.715	0.24	0.02		-0.74	-0.75	-0.69
		503.265	0.03	0.01	s	-1.63	-1.59	
		542.721	0.01	0.00	w	-1.93	-2.03	
		574.478	0.06	0.01		-1.22	-1.26	
		625.044	-	-		-	-1.23	-1.36
		700.843	-	-		-	-1.08	
25389.217	35.1	393.757	0.01	0.00	s	-2.15	-1.57	-1.54
		401.882	0.15	0.01		-0.99	-0.86	-0.85
		417.958	0.24	0.02		-0.75	-0.60	-0.64
		421.129	0.40	0.03		-0.51	-0.82	-0.86
		447.854	0.02	0.00	w	-1.73	-1.80	-1.85
		541.637	0.08	0.02		-0.97	-1.01	
		559.615	0.03	0.01		-1.39	-2.23	
		589.151	0.04	0.01		-1.18	-1.01	
		617.464	0.00	0.00	w	-2.44	-1.93	
		644.483	0.00	0.00	w	-2.29	-1.55	
		645.793	0.01	0.00	w	-1.75		
		651.923	0.01	0.00	w	-1.86		
		679.049	-	-		-	-1.23	
		681.526	-	-		-		

25481.274	50.6	400.401	0.54	0.04		-0.43	-0.63	-0.57
		416.356	0.05	0.01		-1.47	-0.79	-0.78
		419.502	0.14	0.01		-0.98	-1.16	
		436.639	0.15	0.01		-0.92	-1.71	-1.68
		446.015	0.06	0.01		-1.29	-1.58	
		475.069	0.00	0.00	w	-2.44		-1.62
		476.767	0.01	0.00		-1.86	-1.65	
		500.021	0.05	0.01		-1.26		
		687.603		-		-	-0.85	-0.93
		719.206	-	-		-	-0.87	
		742.742	-	-		-		
25524.485	8.79	415.608	0.26	0.02		0.05	0.17	0.16
		435.816	0.19	0.01		-0.03	-0.18	-0.16
		445.156	0.30	0.02		0.18	0.04	0.07
		460.222	0.01	0.00		-1.42		
		498.942	0.08	0.01	s	-0.31	-1.02	-1.19
		529.316	0.10	0.01		-0.13	0.07	0.10
		568.852	0.05	0.01		-0.37	-0.23	-0.31
		618.39	0.01	0.00		-1.11		-0.92
25877.176	14.4	386.332	0.39	0.03		-0.22	-0.66	-0.58
		394.151	0.35	0.02		-0.25	-0.04	-0.02
		409.602	0.06	0.01		-0.96	-1.69	-2.09
		412.647	0.08	0.02		-0.85	-1.43	-1.55
		438.273	0.09	0.02		-0.77	-1.00	-1.04
		466.296	0.01	0.00	w	-1.84	-1.45	-1.67
		527.687	-	-		-	-0.59	
		572.683	0.03	0.00		-1.06	-0.77	-0.81
		605.187	0.01	0.00	w	-1.64	-1.06	
		624.827	-	-		-	-0.86	-1.05
		657.264	-	-		-		
26031.487	90.9	426.392	0.37	0.02		-0.75	-1.44	-1.59
		449.726	0.09	0.02		-1.30	-1.25	-1.38
		464.576	0.26	0.02		-0.82	-0.71	-0.76
		477.288	0.08	0.02		-1.30	-1.05	-1.05
		498.716	0.17	0.01		-0.96	-0.71	-0.79
		631.272	0.02	0.00	w	-1.71	-1.50	
		729.873	0.00	0.00	w	-2.33		

26274.095	19.7	388.077	-	-	-	-0.39	-0.31
		403.047	0.65	0.06	-0.01	-0.76	-0.70
		405.995	0.15	0.02	-0.65	-0.53	-0.52
		422.025	0.12	0.01	-0.70	-0.79	-0.80
		430.777	0.04	0.01	-1.17	-0.92	-0.92
		545.58	0.01	0.00	-1.64	-0.76	-0.75
		590.986	0.02	0.01	w -1.12	-0.86	
		649.558	-	-	-	-1.17	
		680.398	-	-	-	-0.58	
		701.426	0.00	0.00	w -2.18	-1.32	
		701.776	-	-	-		
		714.197	-	-	-	-1.00	
		788.661	-	-	-		
26328.01	42.7	402.173	0.67	0.06	-0.27	-0.30	-0.31
		429.778	0.16	0.02	-0.84	-0.81	-0.82
		479.704	0.13	0.01	-0.82	-1.84	
		507.715	-	-	-	-1.01	
		543.98	0.01	0.00	-1.88	-1.50	
		545.754	0.03	0.01	b -1.43		
		578.368	-	-	-	-1.19	
		625.182	-	-	-	-1.37	
		744.871	0.00	0.00	w -2.38	-1.33	
		767.3	-	-	-	-1.94	
		785.32	-	-	-	-1.61	
		786.483	-	-	-		
26761.11	35.4	380.877	0.26	0.03	-0.72	-0.74	-0.65
		395.386	-	-	-	-0.73	-0.67
		398.121	0.18	0.02	-0.84	-0.99	-0.91
		413.523	0.45	0.04	-0.40	-1.60	
		421.923	0.03	0.01	-1.52	-1.92	-2.29
		449.34	0.06	0.01	-1.23	-1.10	-1.03
		531.455	0.02	0.00	-1.59	-1.35	-1.33
		658.57	-	-	-	-0.85	
		742.616	-	-	-	-0.30	
26772.093	11.1	380.717	0.17	0.01	-0.40	-1.34	-1.51
		395.114	0.31	0.02	-0.11	0.02	0.04
		397.947	0.16	0.01	-0.38	-0.31	-0.33
		413.335	0.15	0.01	-0.39	-0.40	-0.49

		421.727	0.05	0.01	-0.81	-1.04	-1.27
		531.145	0.06	0.01	-0.56	-0.27	-0.42
		544.756	0.03	0.01	-0.79		
		574.086	0.06	0.01	-0.52	-0.34	-0.53
		608.29	-	-	-		
		658.093	-	-	-		0.85
		663.719	0.01	0.00	s -1.01		-0.84
26912.765	7.31	410.945	0.37	0.03	0.31	0.35	0.35
		432.576	0.14	0.01	-0.06	-0.07	-0.02
		446.298	0.25	0.03	0.22	0.04	0.04
		493.073	0.02	0.00	-0.91	-1.04	
		524.958	0.14	0.01	0.09	0.18	0.20
		527.205	0.00	0.00	w -1.66		
		559.442	0.07	0.02	-0.16	-0.10	-0.16
		603.127	0.01	0.00	-0.82	-0.42	-0.74
26991.889	90.8	377.557	0.45	0.03	-0.89	-1.64	-1.55
		391.712	0.13	0.01	w -1.39	-1.65	-1.62
		394.495	0.05	0.01	w -1.78	-2.09	-2.30
		409.612	0.10	0.01	-1.47	-0.77	-0.74
		417.853	0.24	0.02	-1.07	-1.30	-1.33
		444.727	-	-	-		
		526.666	0.00	0.00	w -2.64	-1.45	
		566.93	-	-	-	-1.49	
		620.613	0.01	0.00	w -2.09	-1.48	
		622.885	-	-	-		
27445.854	36.1	402.133	0.48	0.03	-0.28	-0.34	-0.10
		422.823	0.28	0.02	-0.47	-1.59	-1.44
		435.924	0.04	0.01	-1.26	-1.23	-1.20
		447.098	0.11	0.01	-0.82	-1.21	-1.25
		512.789	0.01	0.00	w -2.05	-0.84	
		543.236	0.03	0.01	-1.28	-1.15	-1.13
		579.515	0.02	0.00	-1.27	-1.09	-1.13
		584.335	0.02	0.00	-1.38	-0.94	
		622.014	-	-	-	-0.79	
		667.112	0.00	0.00	w -1.96	-0.58	
		760.592	-	-	-	-0.42	
27448.715	16.6	384.823	0.38	0.02	-0.13	-0.30	-0.25

		402.086	0.26	0.02		-0.26	-0.25	-0.19
		410.024	0.05	0.01		-0.97	-0.89	-0.87
		422.772	0.20	0.01		-0.34	-0.55	-0.50
		435.869	-	-		-	-0.95	-0.94
		480.375	0.01	0.00		-1.45	-1.51	-1.54
		543.152	0.07	0.01		-0.58	-0.49	-0.47
		584.237	0.04	0.01		-0.78	-0.56	
		687.467	0.00	0.00	w	-1.65	-0.45	
27611.719	20.5	399.467	0.47	0.03		0.01	0.05	0.04
		419.877	0.17	0.01	w	-0.37	-1.52	-1.68
		432.793	0.22	0.02		-0.25	-0.44	-0.40
		476.641	0.00	0.00	w	-1.88	-1.64	
		506.372	0.06	0.01		-0.70	-0.56	-0.62
		538.383	0.02	0.00	w	-1.03	-1.22	-1.26
		573.995	0.03	0.01		-0.85	-0.85	-0.93
		615.66	0.02	0.00	w	-1.07	-1.27	
		654.069	0.00	0.00	w	-1.56	-1.54	
		654.377	0.00	0.00	w	-1.85		
		751.113	0.00	0.00	w	-1.85	-0.66	-0.70
		790.039	-	-		-	-0.91	
27816.793	55.8	396.221	0.32	0.03		-0.66	-0.55	-0.57
		439.801	0.15	0.02		-0.89	-1.61	
		457.931	0.36	0.03		-0.49	-0.48	-0.48
		501.167	0.10	0.02		-0.99	-0.89	-0.99
		532.503	0.02	0.00	w	-1.69	-1.40	-1.58
		571.934	0.05	0.01		-1.17	-1.31	
27993.254	60.6	413.255	0.28	0.02		-0.67	-1.22	-1.09
		436.414	0.22	0.02		-0.74	-0.84	-0.79
		454.26	0.44	0.03		-0.40	-0.30	-0.28
		531.004	0.04	0.01		-1.27	-0.97	-0.98
		561.692	0.01	0.00	w	-1.94	-1.31	
		602.205	0.01	0.00	w	-1.62	-1.25	
		643.603	0.00	0.00	w	-2.19	-1.05	
28196.156	77.6	390.351	0.03	0.01	w	-1.90	-1.41	-1.33
		397.828	-	-		-	-1.39	-1.36
		409.817	0.34	0.03		-0.81	-0.65	-0.63
		422.113	0.45	0.04		-0.67	-1.00	-1.01

		582.336	0.02	0.00	-1.23		-0.76	-0.96
		655.898	-	-	-		-0.72	
		702.096	0.00	0.00	-1.79		-0.37	
28748.524	62.4	400.743	0.47	0.04			-0.48	-0.40
		422.484	0.13	0.01			-0.88	-0.90
		439.187	0.15	0.02			-1.76	-2.27
		478.803	0.06	0.01			-1.53	
		510.523	0.16	0.02			-0.59	-0.61
		538.826	0.01	0.00	w		-1.16	-1.29
		575.999	0.02	0.01			-1.44	
28856.898	12.4	380.534	0.36	0.03	0.01		-0.17	-0.27
		399.01	0.29	0.03	-0.05		0.10	0.13
		410.656	0.07	0.02	-0.62		-0.97	-1.05
		420.558	0.14	0.01	-0.31		-0.43	-0.55
		437.106	0.01	0.00	-1.34		-1.31	
		476.33	-	-	-		-1.35	-1.46
		478.18	0.00	0.00	w	-2.55		
		479.55	0.00	0.00	w	-1.84		
		535.697	0.06	0.01	-0.47		-0.18	-0.28
		571.812	0.05	0.01	-0.51		-0.38	-0.40
		642.578	0.01	0.00	-1.16			-0.71
29027.543	12.3	396.311	0.38	0.04	0.12		0.14	0.23
		417.56	0.13	0.01	-0.31		-0.31	-0.24
		433.869	0.32	0.03	0.12		-0.18	-0.09
		472.489	-	-	-		-1.32	
		503.351	0.07	0.02	-0.42		-0.45	-0.47
		530.843	0.02	0.00	-0.88		-0.87	
		566.886	0.05	0.01	-0.45		-0.30	-0.31
		603.423	0.02	0.01	-0.72		-0.36	
		678.896	-	-	-		-1.45	
		687.305	0.00	0.00	w	-1.31	-0.96	
		752.9	0.00	0.00	w	-1.50	-0.54	-0.41
29434.27	13.1	372.35	0.13	0.01	-0.54	-0.91	-0.35	-0.40
		379.147	0.18	0.02	-0.38		-1.49	-1.62
		390.022	0.37	0.03	-0.04	0.11	0.14	0.10
		426.343	0.20	0.02	-0.23	-0.58	-0.55	-0.79

		540.617	0.03	0.01	-0.93		-0.74	-0.84
		553.532	0.02	0.01	-0.97	-0.87	-0.73	-0.83
		574.127	0.09	0.02	b -0.32	-0.87	-0.97	-0.83
		584.632	0.01	0.00	w -1.20	-1.11	-1.21	
		658.802	-	-	-	-1.07	-0.89	-0.90
29955.418	49.1	382.25	0.22	0.02	-0.81		-1.12	
		392.926	0.22	0.02	-0.79		-0.66	
		401.981	0.28	0.03	-0.66		-0.77	
		417.074	0.27	0.03	s -0.64		-1.21	
		454.308	-	-	-		-1.33	
		455.545	-	-	-		-1.93	
		505.917	0.02	0.00	-1.64		-1.28	
		538.008	0.02	0.01	w -1.46		-1.34	
		571.42	0.01	0.00	w -1.86		-1.46	
		600.199	0.01	0.00	w -1.82		-1.21	
		636.928	0.00	0.00	w -2.35		-1.14	
		642.166	-	-	-		-1.01	
		666.58	0.00	0.00	w -2.50		-1.00	

Table 5.3 Nd II radiative parameters

Lifetimes adopted from Pincuic et al.²⁸

Transition probabilities and relative intensities may be found in appendix #3

w denotes weak emission line*b* denotes blended emission line*s* denotes emission line has shoulder*DREAM* refers to work by Xu et al.^{28,30}*UWO* refers to work by Scholl et al.²⁹*D.H.* refers to work by Den Hartog et al.³¹**Nd III Data:**

Energy Up (cm ⁻¹)	T (ns)	Wavelength (nm)	Branch Ratio	BR error		g _k *A _{ki} (10 ⁶ s ⁻¹)			Log (g _i *f _{ik})		
						this work	error	DRM	this work	DRM	Bord
28745.3	170	347.7834	0.07	0.02	w	3.50	0.859	6.00	-2.17	-1.97	-1.87
28745.3		362.1171	0.93	0.09		49.44	5.97	76.80	-0.98	-0.82	-0.74

Table 5.4 Nd III radiative parameters
 Lifetimes adopted from Zhang et al.³⁷
w denotes weak emission line.
DRM denotes work by Zhang et al.³⁷
Bord denotes work done by Bord et al.³⁶

Pr I Data:

Energy Up (cm ⁻¹)	Lifetime T (ns)	Wavelength (nm)	Branching Ratio	BR Error		g _k *A _{ki} (10 ⁶ Hz)			Log (g _i * f _{ik})		Doidge
						This Work	Error	Kurucz	This Work	Kurucz	
19122.57	89B	522.7967	1.00	0.09	w	134.83	12.74	134.04	-0.257	-0.260	
19474.75	26	513.3424	1.00	0.09		461.54	55.70	449.88	0.261	0.250	
19820.69	58	504.3827	1.00	0.09		206.90	23.95	213.00	-0.103	-0.090	
19861.89	83	503.3364	1.00	0.09		144.58	18.15	147.96	-0.260	-0.250	
20089.26	76	497.6396	1.00	0.09		157.89	20.67	130.32	-0.232	-0.315	
20154.6	104	496.0262	1.00	0.09		96.15	12.21	90.96	-0.450	-0.474	
20190.85	12.2	495.1357	1.00	0.09		819.67	89.57	840.30	0.479	0.490	0.31
20344.28	34	491.4015	1.00	0.09		294.12	32.37	278.60	0.027	0.004	
20827.15	69	513.9811	1.00	0.09		202.90	23.92	207.06	-0.095	-0.086	
21072.64	62B	474.4163	1.00	0.09		129.03	17.32	129.28	-0.361	-0.360	
21105.88	19B	473.6691	1.00	0.09		421.05	40.70	419.68	0.151	0.150	
21159.76	34B	505.3395	1.00	0.09		411.76	45.31	413.70	0.198	0.200	
21263.71	25B	502.6981	1.00	0.09		560.00	68.70	551.18	0.327	0.320	
21677.15	17B	492.46	1.00	0.09		705.88	105.86	690.48	0.410	0.400	

22498.81	23B	508.7107	1.00	0.09	695.65	67.19	647.04	0.431	0.400
22509.4	30	473.0657	1.00	0.09	333.33	38.14	358.10	0.049	0.080
22921.34	71	464.0205	1.00	0.09	140.85	17.70	270.30		-0.059
22924.39	29	463.9548	1.00	0.09	344.83	39.92	676.00	0.047	0.339
24195.13	14B	504.5522	1.00	0.09	1285.71	150.77	1282.50	0.691	0.690

Table 5.5 Pr I Radiative Parameters

Lifetimes adopted from Biemont et al.⁵, unless noted as *B*

B denotes lifetimes from Blaegov et al.⁴⁰

b denotes blended lines

w denotes weak emission line

Doidge denotes work by Doidge et al.⁴¹

Kurucz denotes work by Kurucz et al.¹¹

Pr II data:

Upper Energy (cm ⁻¹)	T(ns)	Wavelength (nm)	Branch Ratio	BR Error	g _k * A _{ki} (10 ⁶ Hz)				log (g _i * f _{ik})		
					This Work	Error	DRM	UWO	This Work	DRM	UWO
22040.1	67.5	453.592	0.348	0.023	56.9	5.9		62	-0.76		-0.72
		462.874	0.352	0.023	57.5	5.9		44	-0.73		-0.85
		490.275	-	-	-	-		11	0		-1.38
		492.563	0.072	0.014	11.8	2.1			-1.37		
		536.423	0.008	0.001	w	1.2	0.2	0.8	-2.27		-2.47
		550.915	0.161	0.012		26.3	2.7	27	-0.92		-0.9
		557.183	0.048	0.009		7.9	1.4	12	-1.43		-1.26
		684.659	0.005	0.001	w	0.8	0.1	5	-2.24		-1.47
22571.5	51.8	685.046	0.005	0.001	w	0.9	0.2		-2.21		
		442.913	0.725	0.073		154	23.6	109	-0.34		-0.5
		451.758	0.118	0.021		25.1	5.4	30	-1.11		-1.03
		477.822	0.025	0.005		5.3	1.1	8.5	-1.74		-1.53
		479.994	0.008	0.001	w	1.8	0.4		-2.22		

		521.551	0.034	0.006		7.2	1.5		4.4	-1.53	-1.75
		535.24	0.057	0.010		12.2	2.6		42	-1.28	-0.74
		541.154	0.031	0.006		6.7	1.4		18	-1.53	-1.1
22675.4	13.5	440.882	0.457	0.046		372.2	66.5		394	0.04	0.05
		449.646	0.305	0.031		248.8	44.5		144	-0.12	-0.37
		532.276	0.176	0.018		143.1	25.6		170	-0.22	-0.12
		538.126	0.062	0.011		50.7	11.8		78	-0.66	-0.46
		656.107	-	-	-	-	-		29	0	-0.72
		656.462	-	-	-	-	-			0	
22885.6	35	436.833	0.670	0.044		210.6	47.1		158	-0.22	-0.35
		445.436	-	-	-	-	-		21	0	-1.2
		470.754	0.090	0.017		28.2	7.6		18	-1.03	-1.23
		472.863	0.047	0.009		14.7	4		19	-1.31	-1.21
		513.142	0.008	0.001	s	2.4	0.7		5.8	-2.02	-1.64
		526.388	0.103	0.008		32.5	8.7		62	-0.87	-0.59
		532.107	0.072	0.014		22.7	6.1		24	-1.02	-0.99
		647.181	0.002	0.000	w	0.6	0.2		7	-2.43	-1.33
		647.526	0.009	0.002	w	2.8	0.8			-1.75	
23261.4	48.8	429.777	0.611	0.061		137.7	14.5	96.4	134	-0.42	-0.58
		438.101	-	-	-	-	-	41.7	5	0	-0.93
		464.605	0.061	0.011		13.8	2.5	15.2	22	-1.35	-1.31
		503.432	0.221	0.022		49.7	5.2	7.2	3.6	-0.72	-1.55
		516.174	0.079	0.014		17.7	3.2	25.2	48	-1.15	-1
		521.673	0.022	0.004	w	4.9	0.9	5.5	13	-1.7	-1.59
		631.813	0.007	0.001		1.6	0.3	7.9		-2.03	-1.3
		659.374	-	-	-	-	-	3.6		0	-1.6
23660.2	7.57	422.535	0.416	0.027		602.6	1195.5		786	0.21	0.32
		430.576	0.302	0.020		437.1	867.2		269	0.08	-0.13
		511.038	0.222	0.016	b	321.8	638.4		134	0.1	-0.28
		616.278	0.001	0.000	w	0.9	1.7			-2.31	-0.28
		616.594	0.037	0.007		53.9	107.3			-0.51	

		628.128	0.021	0.004		30.7	61.2			-0.74		
23977.8	36	424.763	0.265	0.019		97.6	9.8		103	-0.58	-0.56	
		447.726	0.107	0.008		39.5	7.1		49	-0.92	-0.83	
		449.634	0.411	0.027		151.6	15.2		57	-0.34	-0.76	
		476.523	0.030	0.006		10.9	2		23	-1.43	-1.11	
		485.9	0.071	0.013	w	26.1	4.7		15	-1.03	-1.28	
		529.809	0.080	0.015		29.5	5.3		85	-0.91	-0.45	
		533.148	0.034	0.006		12.4	2.2		30	-1.28	-0.9	
		645.484	0.003	0.001	w	1.2	0.2			-2.12		
		716.777	-	-		-	-			0		
24115.5	7.92	422.293	0.345	0.034		565.6	1072.8	735	642	0.18	0.29	0.24
		444.983	0.264	0.026		433.3	821.7	181	185	0.11	-0.27	-0.26
		446.866	0.173	0.017		283.2	537.1	299	321	-0.07	-0.04	-0.02
		473.42	0.017	0.003		28.6	54.4	2.2	80	-1.02	-2.12	-0.57
		482.67	0.025	0.005	s	41.3	78.6	12		-0.84	-1.36	
		494.372	0.007	0.001		11.5	21.8	5.9		-1.38	-1.65	
		525.171	0.012	0.002		19.7	37.6	365	286	-1.09	0.19	0.07
		525.973	0.086	0.015		141.1	268.4	122		-0.23	-0.28	
		529.262	0.071	0.013		117.1	222.8	2.4	128	-0.31	-1.85	-0.27
		564.765	-	-		-	-	17.3		0	-0.94	
		639.796	-	-		-	-			0		
24393.7	80.9	441.377	0.588	0.039		95.3	9.6		94	-0.56		-0.56
		476.272	0.114	0.008		18.5	3.3		27	-1.2		-1.03
		492.567	0.115	0.008		18.6	3.4			-1.17		
		518.385	0.067	0.013		10.8	1.9		22	-1.36		-1.06
		521.58	0.102	0.007		16.5	3		5.3	-1.17		-1.66
		627.625	-	-		-	-		1.1	0		-2.18
		628.605	0.006	0.001		1	0.2			-2.21		
		702.534	0.008	0.002		1.3	0.2		4.2	-2.01		-1.51
		770.489	-	-		-	-		8	0		-1.16
24716	6.4	404.481	0.168	0.012		289	497.6		207	-0.15		-0.29

		411.846	0.292	0.021		501.7	863.7		588	0.11	0.18
		433.397	0.167	0.012		287.5	494.9		251	-0.09	-0.15
		435.184	0.217	0.016		373.2	642.5		374	0.03	0.03
		480.114	0.034	0.006		57.7	99.7			-0.7	
		512.952	0.080	0.015		137.3	237.3		186	-0.27	-0.13
		578.617	-	-		-	-			0	
		578.892	0.000	0.000	w	0.3	0.5			-2.8	
		601.648	0.013	0.003		22.7	39.3			-0.91	
		616.118	0.029	0.005		49.6	85.7		112	-0.55	-0.2
		641.368	-	-		-	-			0	
24754	37B	403.846	0.419	0.028		101.9	13.1	66.2		-0.6	-0.81
		411.187	0.042	0.008		10.3	2	116		-1.58	-0.54
		434.448	0.475	0.031		115.6	14.9	22.4		-0.49	-1.21
		483.954	0.026	0.005		6.3	1.2	3.7		-1.66	-1.9
		577.317	0.019	0.004		4.7	0.9	7.1		-1.63	-1.44
		577.59	0.001	0.000	w	0.3	0.1	11.1		-2.86	-1.21
		600.246	0.012	0.002		2.8	0.6	9		-1.77	-1.25
		636.363	0.007	0.001		1.6	0.3	1.6		-2	-2
		639.771	-	-							
24835	92.7	409.84	0.470	0.031		66.1	6.7		8.2	-0.78	-1.69
		432.941	0.243	0.018		34.2	3.4		49	-1.02	-0.86
		457.817	0.089	0.017		12.6	2.3		17	-1.4	-1.28
		466.465	0.108	0.008		15.2	2.7		40	-1.3	-0.88
		506.043	0.020	0.004	w	2.8	0.5		7	-1.97	-1.57
		506.788	0.005	0.001	w	0.7	0.1			-2.56	
		542.705	0.057	0.011	w	8	1.4		3.2	-1.45	-1.85
		658.218	-	-		-	-		2.6	0	-1.78
		681.404	0.003	0.001	w	0.5	0.1		7.7	-2.48	-1.27
		699.147	-	-		-	-		2.5	0	-1.74
		745.145	0.005	0.001	w	0.7	0.1		3.4	-2.25	-1.54
		746.771	-	-		-	-			0	
25248.7	96.6	423.615	0.452	0.045		70.2	7.2		54	-0.72	-0.84

		449.306	0.091	0.016	s	14.1	2.6	10.7	-1.37	-1.49		
		457.632	0.177	0.018		27.5	2.8	20	-1.06	-1.2		
		480.369	0.049	0.009	w	7.6	1.4	3.4	-1.58	-1.93		
		495.664	0.209	0.021		32.5	3.3	40	-0.92	-0.84		
		530.896	0.021	0.004	w	3.2	0.6	11	-1.86	-1.32		
		740.581	-	-		-	-	4	0	-1.48		
		743.052	-	-		-	-	5	0	-1.4		
		768.712	-	-		-	-	2	0	-1.66		
		818.134	-	-		-	-	5	0	-1.34		
25467.5	11.6	392.547	0.305	0.031		236.7	185.2	206	-0.26	-0.32		
		399.479	0.556	0.056		431.3	337.4	392	0.01	-0.03		
		421.4	-	-		-	-	9	0	-1.62		
		467.818	0.028	0.005		21.4	17	14	-1.15	-1.33		
		554.501	0.050	0.009		39.1	31.1	40	-0.74	-0.73		
		554.753	0.002	0.000	w	1.5	1.2		-2.17			
		575.617	0.059	0.011		45.9	36.6	61	-0.64	-0.52		
		608.752	-	-		-	-	54	0	-0.52		
25499.5	16.2	392.053	0.085	0.016		58.7	17.9	54	-0.87	-0.91		
		398.968	0.291	0.021		200.9	53.5	0.33	-0.32	-0.28		
		419.16	0.256	0.019		176.8	47.1	158	-0.33	-0.38		
		420.832	0.185	0.014		127.9	34.1	110	-0.47	-0.54		
		452.438	0.037	0.007	w	25.7	7.9	6.2	-1.1	-1.72		
		462.704	0.011	0.002		7.8	2.4	8.7	-1.6	-1.55		
		493.13	0.023	0.004	s	15.6	4.8	4.6	-1.24	-1.78		
		553.517	0.037	0.007		25.7	7.8	39	-0.93	-0.75		
		553.768	0.005	0.001	w	3.6	1.1		-1.79			
		574.56	0.009	0.002	w	5.9	1.8	7	-1.53	-1.46		
		586.883	0.041	0.008		28.6	8.8	34	-0.83	-0.76		
		610.672	0.011	0.002	w	7.4	2.3	12	-1.38	-1.18		
		649.893	0.004	0.001	w	2.7	0.8	10	-1.77	-1.2		
		651.879	0.005	0.001	w	3.2	1	15	-1.69	-1.01		
25569.2	6.32	417.939	0.273	0.020		651.4	4020.5	1240	1099	0.23	0.51	0.46

		442.925	0.305	0.020		726.4	4483.4	162	305	0.33	-0.32	-0.05
		451.015	0.168	0.012		401.7	2478.9	302	323	0.09	-0.03	-0.01
		487.91	0.006	0.001		13.3	82	2.9		-1.32	-2.01	
		488.6	0.012	0.002		27.9	172	7.1	26	-1	-1.58	-1.03
		491.44	-	-		-	-	18.3		0	-1.18	
		521.905	0.079	0.015		189.3	1168.4	9.4		-0.11	-1.46	
		522.011	0.140	0.010		332.8	2054.8	170	621	0.13	-0.15	0.41
		558.21	0.009	0.002		22.2	137.3	508		-0.98	0.32	
		627.868	0.008	0.002	b	19.5	120.5	4.8		-0.94	-1.58	
25610.2	21.1	397.214	0.256	0.019		157.7	33.8	24.5	179	-0.43	-1.22	-0.37
		417.225	0.348	0.023		214.4	46		237	-0.25		-0.21
		418.88	-	-		-	-	350		0	-0.01	
		442.122	0.189	0.014		116.7	25	8.4	58	-0.47	-1.58	-0.77
		450.182	0.032	0.006		19.5	5.1	117	12	-1.23	-0.41	-1.44
		486.936	0.006	0.001	w	3.6	0.9		15	-1.89		-1.26
		487.626	0.032	0.006		19.8	5.2	23.1		-1.15	-1.06	
		520.79	0.078	0.015		48.2	12.6		55	-0.71		-0.65
		583.094	0.021	0.004		13.2	3.5		21	-1.17		-0.96
		583.939	0.003	0.001	w	2.1	0.6			-1.96		
		615.91	0.014	0.003		8.5	2.2		11	-1.32		-1.22
		626.255	0.016	0.003		9.9	2.6		16	-1.24		-1.02
		663.195	0.003	0.001	w	2.1	0.6	4.4	4	-1.86	-1.54	-1.58
25656.7	9.05	704.445	0.002	0.000	w	1.1	0.3	13	8	-2.1	-0.94	-1.2
		396.481	0.237	0.017		349.9	812.6		498	-0.08		0.07
		416.416	0.269	0.020		397.3	922.9		569	0.01		0.17
		418.065	0.052	0.010	s	76.8	178.7			-0.7		
		441.215	0.065	0.012		95.8	222.9		47	-0.55		-0.86
		449.242	0.018	0.003		26.7	62.1		15	-1.09		-1.34
		485.836	0.037	0.007	b	54.4	126.7		29	-0.72		-0.99
		486.523	0.032	0.006		46.7	108.7			-0.78		
		519.531	0.164	0.012		242.2	562.6		132	-0.01		-0.27
		548.742	0.017	0.003		25.3	59		8	-0.94		-1.45

		581.517	0.065	0.012		96.3	224		59	-0.31	-0.52
		582.358	0.026	0.005		38.3	89.1			-0.71	
		614.151	0.012	0.002	w	17.6	41.1		15	-1	-1.08
		624.435	-	-		-	-		30	0	-0.76
		702.151	0.005	0.001		7.3	16.9		34	-1.27	-0.6
25814.4	125B	387.27	-	-		-	-	13.8		0	-1.5
		394.016	0.914	0.091		65.8	10.3	44.5		-0.81	-0.98
		544.031	0.047	0.008	w	3.4	0.7	2.9		-1.83	-1.85
		564.346	-	-		-	-	2.8		0	-1.83
		596.158	0.039	0.007	w	2.8	0.6	2.6		-1.82	-1.82
25842.4	45B	386.851	0.085	0.016	s	20.8	4	7.5		-1.33	-1.79
		387.27	-	-		-	-	56.9		0	-0.89
		393.582	0.219	0.016		53.5	6.4	103		-0.86	-0.59
		413.219	0.167	0.012		40.9	4.9	32.2		-0.98	-1.09
		414.843	0.359	0.024		87.8	10.6	9.3		-0.41	-1.37
		543.204	0.062	0.012	s	15.1	2.9	10.5		-1.12	-1.27
		575.302	0.019	0.004	w	4.7	0.9	3.5		-1.63	-1.75
		576.125	0.005	0.001	w	1.3	0.3	7.4		-2.15	-1.38
		598.144	0.073	0.014		17.8	3.4	3.1		-0.97	-1.7
		635.723	0.007	0.001	w	1.7	0.3	2.6		-1.98	-1.79
26146	18.8	637.622	0.003	0.001	w						
		382.359	-	-		-	-		16	0	-1.45
		388.934	0.146	0.011		89.1	11.1		102	-0.69	-0.63
		408.098	0.261	0.019		158.8	19.8		144	-0.4	-0.45
		409.682	0.145	0.011		88.2	11		221	-0.65	-0.26
		439.576	0.373	0.025	b	226.6	28.3		15	-0.18	-1.36
		449.261	0.021	0.004		13.1	2.5		5	-1.4	-1.84
		534.388	0.023	0.004		13.8	2.7		23	-1.23	-1.01
		534.623	0.001	0.000	w	0.5	0.1			-2.64	
		565.423	-	-		-	-		21	0	-0.99
		566.219	0.005	0.001	w	2.8	0.5		7	-1.87	-1.46
		587.474	0.011	0.002		6.9	1.3		12	-1.45	-1.22

		625.51	0.012	0.002		7.4	1.4		15	-1.36	-1.05
		648.487	0.002	0.000	w	1.1	0.2		4	-2.16	-1.62
26226.6	12.4B	381.185	0.107	0.008		77.5	40	84.7		-0.77	-0.73
		387.718	0.613	0.040		445.2	220	516		0	0.07
		408.334	0.169	0.012		122.7	60.6	16.1		-0.51	-1.38
		532.097	0.052	0.010		37.7	19.5	19.1		-0.8	-1.05
		540.908	0.004	0.001	w	3	1.5	5.5		-1.88	-1.58
		551.515	-	-		-	-	33		0	-0.78
		563.647	0.016	0.003	w	11.7	6	8.6		-1.25	-1.35
		581.858	0.028	0.005		20.6	10.6	31.6		-0.98	-0.75
		593.38	-	-		-	-	2.1		0	-1.91
		620.564	0.011	0.002	w	7.8	4	2.7		-1.35	-1.75
26398.5	8.19	385.155	0.128	0.009		202.4	201.1		151	-0.35	-0.48
		403.934	0.151	0.011		239.3	234.9		188	-0.23	-0.34
		405.488	0.222	0.016		352.4	346		657	-0.06	0.21
		427.227	0.226	0.017		358.9	352.5		244	-0.01	-0.18
		434.749	0.136	0.010		216	214.5		167	-0.21	-0.33
		500.246	0.035	0.007		55	54.6		36	-0.69	-0.87
		527.271	0.008	0.001	w	12.4	12.3			-1.29	
		557.461	0.005	0.001	w	8.2	8.2		4	-1.42	-1.7
		558.235	0.011	0.002		17.8	17.7			-1.08	
		587.383	0.005	0.001	w	7.4	7.3		8	-1.42	-1.37
		596.782	0.026	0.005		40.8	40.6		45	-0.66	-0.62
		615.782	0.002	0.000	w	3.4	3.3		8	-1.72	-1.34
		630.236	0.011	0.002		17.7	17.6		14	-0.98	-1.08
		667.378	0.034	0.006		53.8	53.5		65	-0.44	-0.36
		684.547	0.001	0.000	w	2	2			-1.85	
26445.1	26.4	403.175	0.162	0.012		92.5	10.5		217	-0.65	-0.28
		426.378	0.249	0.018		142.5	16.1		75	-0.41	-0.69
		433.87	0.213	0.016		121.8	13.8		103	-0.46	-0.54
		454.254	0.117	0.009		67	12.6		12	-0.68	-1.44
		467.908	0.052	0.010		29.9	5.6		32	-1.01	-0.98

		468.545	0.002	0.000	w	1	0.2		-2.5	
		499.083	0.016	0.003	w	9.1	1.7	20	-1.47	-1.13
		499.18	0.021	0.004		11.9	2.2		-1.35	
		532.182	0.090	0.017	w	51.6	9.7	38	-0.66	-787
		595.127	0.060	0.011		34.1	6.4	3.4	-0.74	-1.75
		609.038	-	-		-	-	24	0	-0.88
		647.509	0.010	0.002	w	5.5	1	5	-1.46	-1.52
		680.287	0.003	0.000	w	1.5	0.3	9	-1.99	-1.2
		682.372	0.003	0.001	w	1.8	0.3		-1.91	
		745.174	0.004	0.001	w	2.2	0.4	31	-1.73	-0.59
26524	77	383.296	0.232	0.017		40.2	5.4	26	-1.05	-1.24
		403.433	0.451	0.030		78.1	10.6	34	66	-0.72
		424.948	0.121	0.009		20.9	4.2	28.7	27	-1.25
		432.39	-	-		-	-	24.8	16	0
		497.125	0.103	0.007		17.8	3.6		3.1	-1.18
		553.588	-	-		-	-		2.4	0
		554.35	0.064	0.012	w	11.1	2.2		-1.29	
		592.346	-	-		-	-		6.4	0
		625.289	-	-		-	-		3.1	0
		661.834	0.030	0.006	w	5.2	1		18	-1.47
26640.9	26.2	400.017	0.577	0.038		242.6	30.5		127	-0.23
		401.539	0.268	0.020		112.7	14.2		180	-0.56
		430.215	0.128	0.009		53.9	10.5		23	-0.83
		579.136	-	-		-	-		34	0
		588.274	0.010	0.002	w	4.4	0.9		11	-1.65
		605.004	0.017	0.003	s	7.3	1.4		27	-1.4
		606.727	-	-		-	-		18	0
26707.3	30	374.323	0.004	0.001	w	1.6	0.3		4.4	-2.48
		380.622	0.202	0.020		74.1	8.2		6.2	-0.79
		400.47	0.475	0.048		174.2	19.2		234	-0.38
		428.988	0.120	0.022		44	8.2		36	-0.92
		465.402	0.043	0.008	w	15.9	3		7.7	-1.29

		518.822	0.016	0.003		5.7	1.1		15	-1.64	-1.23	
		519.043	0.074	0.013	w	27.2	5			-0.96		
		537.266	0.008	0.002	w	3.1	0.6		1.6	-1.88	-2.16	
		548.026	0.052	0.009	w	19.1	3.5		10	-1.07	-1.33	
		548.772	0.047	0.009		17.3	3.2			-1.11		
		568.717	0.024	0.004		8.8	1.6		3.7	-1.33	-1.75	
		576.916	0.016	0.003	s	6	1.1		17	-1.52	-1.07	
		604.287	0.022	0.004	w	8	1.5		31	-1.36	-0.77	
26861	6.69	396.525	0.238	0.017		623.5	4847	307	643	0.17	-0.14	0.18
		418.948	0.324	0.021		848.4	6595	1410	1025	0.35	0.57	0.43
		426.179	0.160	0.012	b	418.3	3251.3		39	0.06		-0.98
		445.83	0.044	0.008		115.8	900.6	34.9	51	-0.46	-0.97	-0.82
		459.588	0.020	0.004		52.7	409.5			-0.78		
		488.933	-	-	-	-	-		51	0		-0.74
		489.026	0.046	0.009		120	932.8	23.6		-0.37	-1.07	-0.74
		520.655	0.089	0.017		231.9	1802.7	227	220	-0.03	-0.02	-0.05
		534.032	0.011	0.002		28.1	218.8			-0.92		
		580.752	0.010	0.002		27.1	211	8.1	12	-0.86	-1.36	-1.21
		593.99	0.031	0.006		81.9	636.5	93.8	120	-0.36	-0.28	-0.2
		598.729	0.010	0.002		26.3	204.5	15.9		-0.85	-1.05	-0.2
		619.745	0.008	0.001	w	20.3	157.6	34.5	29	-0.93	-0.67	-0.78
		630.523	0.008	0.001	s	20.6	160.4	15.8	29	-0.91	-1	-0.89
		722.77	0.001	0.000	w	3.7	28.7	3.3	722.77	-1.54	-1.57	6
26962	11.7	376.967	0.067	0.012		74.4	34.5			-0.8		
		394.943	0.291	0.029		323	141.8		293	-0.12		-0.16
		396.426	0.120	0.022		133.6	62		250	-0.5		-0.23
		417.182	0.291	0.029		323.9	142.1		288	-0.07		-0.12
		424.351	0.081	0.015		90.3	41.9		104	-0.61		
		456.856	0.011	0.002	w	12.4	5.8			-1.41		-0.55
		486.529	0.044	0.008		48.7	22.6			-0.76		
		540.48	0.012	0.002		13.1	6.1		10	-1.24		-1.34
		568.56	0.007	0.001	s	8.3	3.9		10	-1.39		-1.32
		590.445	0.023	0.004		25	11.6		38	-0.88		-0.7

		595.127	0.033	0.006		37.1	17.2		46	-0.71		-0.61
		643.184	0.014	0.003		15.8	7.3		52	-1.01		-0.49
		644.391	0.005	0.001	w	5.6	2.6			-1.46		
26973.5	18B	394.763	0.548	0.036		337.6	43.9	106		-0.1		-0.59
		396.245	0.234	0.017		144.2	18.8	333		-0.47		-0.09
		424.144	-	-		-	-	60.1		0		-0.77
		459.705	0.097	0.018		59.7	11.8	8.2		-0.72		-1.57
		511.752	0.021	0.004	w	12.9	2.6	6.1		-1.29		-1.58
		540.869	0.006	0.001	w	3.6	0.7	4.9		-1.81		-1.63
		568.19	0.057	0.011		35.4	7	23.6		-0.77		-0.89
		576.98	0.015	0.003	s	9.1	1.8	9.9		-1.34		-1.26
		593.066	-	-		-	-	16		0		-1.02
		594.719	0.019	0.004	w	12	2.4	21.6		-1.2		-0.9
		643.913	0.002	0.000	w	1.5	0.3	3.6		-2.04		-1.65
27128	5.79	414.311	0.463	0.031		1364.1	719.8	1910	1561	0.55	0.7	0.6
		440.583	0.124	0.009		366	200.8	124	297	0.03	-0.43	-0.06
		453.415	0.158	0.012		465.3	245.5	103	175	0.16	-0.48	-0.27
		454.014	0.003	0.001	w	9	4.9			-1.55		
		482.629	0.018	0.003	b	53.8	29.5	10.4		-0.73		-1.43
		482.72	0.013	0.002		38.5	21.1	18.7		-0.87		-1.18
		513.514	0.072	0.014		211.9	116.2	214	222	-0.08		-0.06
		517.39	0.125	0.009		367.8	201.7	616	569	0.17	0.41	0.36
		550.22	0.005	0.001	w	13.5	7.4			-1.21		
		584.713	0.012	0.002		35.7	19.6	16.8	112	-0.74	-1.03	-0.24
		620.081	0.006	0.001	w	16.4	9	9.6		-1.02		-1.22
		644.278	0.002	0.000	w	5.4	3			-1.47		
27198.2	15.3B	391.29	0.501	0.050		360.1	43			-0.08		
		392.746	0.412	0.041		296	35.4			-0.16		
		561.024	0.038	0.007		27.6	5.3			-0.88		
		569.592	0.024	0.004		16.9	3.2			-1.08		
		585.263	0.026	0.005		18.3	3.5			-1.03		

27781.7	18.4	403.383	0.188	0.019		173.4	59.1	366	-0.37	-0.05
		428.242	0.491	0.049		453.2	154.6	278	0.1	-0.12
		440.36	0.174	0.017		161.1	54.9	122	-0.33	-0.45
		500.459	0.064	0.011		58.7	21.9	35	-0.66	-0.88
		531.112	0.059	0.011		54.9	20.5	70	-0.63	-0.53
		618.234	0.024	0.004		22.6	8.4	44	-0.89	-0.6
		764.566	-	-		-	-		0	-1.1
28009.8	6.97	379.244	0.040	0.008		87.3	263.6	91	-0.72	-0.71
		399.704	0.094	0.018		205.9	621.4	256	-0.31	-0.21
		406.281	0.480	0.032		1046.8	3155.5	871	0.41	-0.33
		424.101	0.179	0.013		389.7	1174.7	408	0.02	-0.04
		435.979	0.106	0.008		231.1	697.4	157	-0.18	-0.35
		436.532	0.000	0.000	w	0.5	1.5		-2.84	
		491.26	0.031	0.006		67.9	205	65	-0.61	0.63
		587.925	0.025	0.005		54.8	165.4	111	-0.55	-0.24
		614.824	0.009	0.002		20.3	61.3	63	-0.94	-0.44
		616.527	-	-		-	-		0	
		658.456	-	-		-	-		0	
		667.341	0.032	0.006	b	68.7	207.3	131	-0.34	0.06
		683.05	0.003	0.001	w	6.8	20.6		-1.32	
28034.1	48.4	399.316	0.065	0.012	b	17.8	3.4	28	-1.37	-1.17
		405.88	0.191	0.014		51.9	6.1	158	-0.89	-0.41
		435.518	0.375	0.025		102.1	12	50	-0.54	-0.85
		436.07	0.092	0.017	s	25	4.8	8	-1.15	-1.64
		438.328	0.277	0.020	s	75.4	8.9		-0.66	
		577.729	-	-		-	-	25	0	-0.91
28173	70.6	397.116	0.272	0.020		57.8	6	29	-0.86	-1.17
		403.605	-	-		-	-	16	0	-1.4
		421.186	0.166	0.012		35.3	3.7	86	-1.03	-0.64
		432.899	0.555	0.037		117.9	12.2	59	-0.48	-0.78
		608.717	-	-		-	-	22	0	-0.91
		610.385	0.007	0.001	w	1.5	0.3		-2.07	

28202	10.7	396.657	0.092	0.016		145.5	85.7	314	-0.46	-0.13
		420.672	0.393	0.039		625.1	356	779	0.22	-0.32
		432.355	0.063	0.011		99.9	58.9	87	-0.55	-0.61
		432.9	0.241	0.024		382.5	217.9		0.03	
		458.84	0.011	0.002		17.8	10.5	33	-1.25	-0.98
		458.922	0.005	0.001		7.5	4.4		-1.63	
		490.147	0.019	0.003		29.4	17.3	43	-0.97	-0.81
		519.511	0.133	0.024		211.7	124.7	163	-0.07	-0.18
		581.355	0.003	0.001	w	5.5	3.2	25	-1.56	-0.89
		602.572	0.030	0.005		47.3	27.9	117	-0.59	-0.2
		609.306	0.005	0.001		8.7	5.1		-1.32	
		626.454	0.005	0.001	w	7.9	4.7	26	-1.33	-0.81
		740.757	-	-		-	-		0	
28508.8	5.6	391.886	0.372	0.037		863.6	622.9		0.3	
		398.205	0.464	0.046		1077.2	776.9		0.41	
		562.304	0.062	0.011		144.1	106.1		-0.17	
		571.165	0.019	0.003		43.1	31.7		-0.68	
		585.968	0.044	0.008		103	75.9		-0.28	
		598.121	0.039	0.007		90.4	66.6		-0.31	
28577.8	7.03	390.829	0.404	0.027		874.7	3484.8	361	0.3	-0.08
		397.116	0.104	0.008		225.4	898.5	285	-0.27	-0.17
		414.122	0.283	0.021		613	2442.2	935	0.2	-0.38
		425.44	0.091	0.017		197.5	787.4	151	-0.27	-0.39
		425.967	0.017	0.003	s	36.3	144.9		-1	
		477.923	0.011	0.002		24.6	97.9		-1.07	
		560.13	0.003	0.001	w	7.2	28.8	51	-1.47	-0.62
		568.921	0.008	0.002	s	18.1	72.3		-1.06	
		589.225	0.015	0.003		32	127.7		-0.78	
		594.072	0.022	0.004		48.4	193.1	219	-0.59	0.06
		595.66	0.025	0.005		54.4	217		-0.54	
		634.711	0.008	0.002	w	18.2	72.7	131	-0.96	-0.1
		642.963	0.008	0.001		16.5	65.9		-0.99	

29724	6	374.067	0.075	0.014	w	228.7	121.5	18.4	-0.32	-1.41
		395.351	0.283	0.021		864.7	440.9	739	0.31	0.25
		405.654	0.405	0.027		1233.9	629.2	1550	0.48	0.59
		406.132	0.083	0.016		252.8	134.3	5.3	-0.1	-1.78
		456.111	0.002	0.000	w	6.5	3.5	55.6	-1.65	-0.7
		481.434	0.046	0.009		139.5	74.1	3.2	-0.27	-1.89
		507.636	0.009	0.002	s	27.4	14.6	15.2	-0.9	-1.13
		551.939	-	-		-	-	45.7	0	-0.61
		571.908	0.032	0.006		96.8	51.5	16.1	-0.28	-1.05
		598.82	0.012	0.002	s	35.3	18.7	88.4	-0.7	-0.28
		611.438	0.025	0.005		76	40.4	288	-0.3	0.31
30018.1	5.3	369.995	0.033	0.006	s	93.2	55.3	9.9	-0.72	-1.69
		390.805	-	-		-	-	1010	0	0.37
		400.869	0.543	0.036		1541.4	886	1330	0.57	0.51
		401.337	0.121	0.009		343.9	204.3	7.3	0.01	-1.66
		403.249	0.093	0.018		265	157.4	3.4	0	-1.88
		447.135	0.013	0.003	w	38.1	22.6	2.2	-0.81	-2.02
		500.166	0.005	0.001	s	14.3	8.5	2.6	-1.21	-1.94
		518.303	0.009	0.002	w	26.9	16	3.8	-0.92	-1.75
		537.497	0.001	0.000	w	2.2	1.3	9.7	-2	-1.35
		543.119	0.003	0.001	s	9	5.4	160	-1.37	-0.09
		547.235	0.004	0.001	w	10.4	6.2	6.5	-1.28	-1.5
		562.444	0.052	0.010		148.1	88	26.7	-0.11	-0.85
		581.533	0.077	0.015		218	129.5	118	0.07	-0.18

Table 5.6 Pr II Radiative Parameters

Lifetimes adopted from Li et al.¹⁵ unless noted as *B*

B denotes lifetime from Biémont et al.¹³

w denotes weak emission line

s denotes shouldering emission line

b denotes blended

DRM refers to Biémont et al.¹³

UWO refers to the work by Li et al.¹⁵

Pr III Data:

Upper Energy (cm ⁻¹)	T (ns)	Wavelength (nm)	Branching Ratio	BR Error		g _k * A _{ki} (10 ⁶ s ⁻¹)			Log(gf)	
						This Work	error	Dream	This Work	Dream
58158	2.12	220.6261	1.14E-02	2.23E-03	r	44.24	11.12	509	-1.49	-0.43
58158		229.291	2.98E-03	5.85E-04	w	11.61	2.92	180	-2.04	-0.85
58158		231.8812	5.68E-03	1.12E-03	w	22.15	5.57	538	-1.75	-0.36
58158		237.8974	9.95E-03	1.95E-03		38.77	9.75	829	-1.48	-0.16
58158		240.0695	3.81E-03	7.48E-04	w	14.86	3.73	25.4	-1.89	-1.66
58158		246.6497	1.05E-03	2.06E-04	w	4.09	1.03	8.27	-2.43	-2.12
58158		249.3342	2.27E-03	4.45E-04	w	8.84	2.22	0.21	-2.08	-3.72
58158		250.2605	4.75E-03	9.32E-04	w	18.51	4.65	41	-1.76	-1.41
58158		255.2339	4.53E-03	8.89E-04	w	17.65	4.44	16.7	-1.76	-1.79
58158		261.1165	-	-	-	-	-	33.8	-	-1.46
58158		264.1749	1.52E-03	2.99E-04	w	5.93	1.49	3.11	-2.21	-2.49
58158		267.9473	2.60E-03	5.10E-04	w	10.13	2.55	147	-1.96	-0.8
58158		271.1929	1.75E-03	3.43E-04	w	6.82	1.71	37.8	-2.12	-1.38
58158		272.1079	-	-	-	-	-	23.4	-	-1.59
58158		272.9723	1.24E-02	2.43E-03	w	48.27	12.13	4.53	-1.27	-2.3
58158		273.5401	2.49E-03	4.88E-04	w	9.7	2.44	6.76	-1.96	-2.12
58158		277.102	-	-	-	-	-	1.61	-	-2.73
58158		280.5767	5.85E-03	1.15E-03	w	22.81	5.73	1.54	-1.57	-2.74
58158		288.7222	6.49E-03	1.27E-03	w	25.29	6.36	15.7	-1.5	-1.71
58158		289.7181	3.41E-03	6.70E-04	w	13.3	3.34	4.46	-1.78	-2.25
58158		290.5575	4.99E-03	9.78E-04	w	19.43	4.88	0.86	-1.61	-2.96
58158		296.6771	1.34E-02	2.63E-03	s	52.19	13.12	0.72	-1.16	-3.03
58158		296.7622	1.98E-02	3.88E-03		77.07	19.37	0.5	-0.99	-3.18
58158		299.5825	6.18E-03	1.21E-03	w	24.1	6.06	0.8	-1.49	-2.97
58158		305.2702	6.11E-03	1.20E-03	b	23.81	5.99	0.74	-1.48	-2.98
58158		310.2463	2.08E-02	4.08E-03		80.98	20.36	1.73	-0.93	-2.6
58158		315.2556	3.22E-02	6.33E-03	b	125.65	31.59	0.74	-0.73	-2.96
58158		322.2845	1.06E-02	2.07E-03		41.13	10.34	10.9	-1.19	-1.77
58158		327.197	2.34E-02	4.58E-03	w	91.04	22.89	0.19	-0.84	-3.52
58158		335.9402	3.51E-02	6.89E-03		136.84	34.4	704	-0.64	0.08
58158		339.6068	1.16E-02	2.28E-03	w	45.29	11.39	263	-1.11	-0.33
58158		341.5145	5.84E-03	1.14E-03	w	22.74	5.72	443	-1.4	-0.12
58158		346.0388	-	-	-	-	-	4.62	-	-2.08
58158		352.9692	6.14E-02	1.21E-02		239.35	60.17	3.62	-0.35	-2.17
58158		368.0359	-	-	-	-	-	7.45	-	-1.82
58158		371.5949	-	-	-	-	-	0.26	-	-3.26
58158		408.0799	5.15E-01	3.51E-02		2008.04	266.01	2.6	0.7	-2.19

58158		422.9319	9.03E-02	1.77E-02		351.81	88.44	3.17	-0.03	-2.06
58158		432.1503	2.75E-02	5.40E-03		107.34	26.98	0.23	-0.52	-3.19
58158		438.9756	-	-		-	-	2.44	-	-2.16
58158		447.1625	2.93E-02	5.75E-03		114.14	28.69	0.27	-0.47	-3.1
58158		472.7668	1.57E-03	3.08E-04	w	6.12	1.54	0.78	-1.69	-2.59
58158		513.6372	1.68E-03	3.30E-04	b	6.55	1.65	0.11	-1.59	-3.37
58158		754.2439	-	-		-	-	0.16	-	-2.89
58158		878.9228	-	-		-	-	0.04	-	-3.29
58174	1.81	220.5479	1.01E-02	3.70E-03	r	107.57	27.74	1180	-1.11	-0.07
58174		223.0351	1.65E-02	6.05E-03	r	175.91	45.36	2120	-0.88	0.2
58174		229.2065	2.09E-03	7.66E-04	w	22.28	5.75	93.5	-1.76	-1.14
58174		230.8002	7.88E-03	2.89E-03	w	83.94	21.65	15.2	-1.17	-1.92
58174		234.4022	9.69E-04	3.55E-04	w	10.31	2.66	13.7	-2.07	-1.95
58174		237.8064	2.91E-03	1.07E-03	w	31	7.99	215	-1.58	-0.74
58174		239.9769	1.81E-03	6.61E-04	w	19.23	4.96	3.64	-1.78	-2.5
58174		246.5519	2.09E-03	7.65E-04	w	22.25	5.74	18	-1.69	-1.79
58174		249.2343	2.01E-03	7.35E-04	w	21.39	5.52	11.5	-1.7	-1.97
58174		250.3465	-	-		-	-	20.4	-	-1.72
58174		255.1292	-	-		-	-	19.1	-	-1.73
58174		257.2224	1.36E-03	4.98E-04	w	14.48	3.73	0.66	-1.84	-3.18
58174		259.8432	3.63E-03	1.33E-03	b	38.66	9.97	1.04	-1.41	-2.98
58174		261.0069	1.30E-03	4.75E-04	w	13.8	3.56	33.8	-1.85	-1.46
58174		264.0628	-	-		-	-	1.69	-	-2.76
58174		271.0747	5.20E-03	1.91E-03	w	55.41	14.29	33.5	-1.21	-1.43
58174		272.8526	4.19E-03	1.54E-03	w	44.66	11.52	17.5	-1.3	-1.71
58174		274.506	-	-		-	-	3.77	-	-2.37
58174		276.9786	-	-		-	-	8.31	-	-2.02
58174		280.4502	4.35E-03	1.59E-03	w	46.29	11.94	6.84	-1.26	-2.09
58174		282.1918	1.36E-03	4.96E-04	w	14.44	3.72	1.79	-1.76	-2.67
58174		287.8353	1.06E-03	3.89E-04	w	11.3	2.91	0.91	-1.85	-2.95
58174		289.5832	2.59E-03	9.48E-04	w	27.57	7.11	0.24	-1.46	-3.52
58174		291.2088	1.16E-03	4.27E-04	w	12.41	3.2	0.2	-1.8	-3.61
58174		296.6207	-	-		-	-	0.15	-	-3.71
58174		299.4383	1.05E-02	3.83E-03		111.4	28.73	1.83	-0.82	-2.61
58174		301.6601	9.05E-03	3.31E-03		96.35	24.85	0.98	-0.88	-2.87
58174		305.1205	2.31E-03	8.46E-04	w	24.6	6.34	1.34	-1.46	-2.73
58174		311.6408	1.75E-03	6.40E-04	b	18.62	4.8	1.4	-1.57	-2.69
58174		315.0959	1.71E-02	6.27E-03		182.34	47.02	0.37	-0.57	-3.27
58174		322.1176	6.50E-04	2.38E-04	w	6.93	1.79	0.16	-1.97	-3.59
58174		324.6466	1.68E-02	6.16E-03		179.07	46.18	13.1	-0.55	-1.69

58174		327.025	1.51E-04	5.54E-05	w	1.61	0.42	2.25	-2.59	-2.44
58174		335.7589	3.29E-03	1.20E-03	w	35.03	9.03	1000	-1.23	0.23
58174		339.4215	5.09E-02	1.86E-02		542.23	139.83	331	-0.03	-0.24
58174		341.3271	1.05E-02	3.84E-03	w	111.74	28.81	636	-0.71	0.04
58174		364.3194	6.10E-02	8.59E-03		649.74	98.15	2.82	0.11	-2.25
58174		367.8183	1.75E-01	2.23E-02	w	1864.19	269.24	33.4	0.58	-1.17
58174		371.3731	-	-		-	-	0.29	-	-3.21
58174		428.1696	1.49E-01	2.09E-02	b	1584.03	239.28	0.06	0.64	-3.81
58174		431.8503	7.86E-02	1.11E-02	b	836.96	126.43	0.51	0.37	-2.85
58174		446.8413	-	-		-	-	0.56	-	-2.78
58174		447.388	4.80E-02	1.76E-02		511.1	131.8	0.1	0.19	-3.52
58174		464.9087	2.07E-03	7.56E-04	w	22	5.67	1.19	-1.15	-2.42
58174		493.578	2.94E-02	1.08E-02	w	313.38	80.81	0.03	0.06	-3.9
58174		514.0577	8.97E-03	3.28E-03	w	95.48	24.62	0.07	-0.42	-3.57
58174		522.0511	2.51E-01	3.20E-02	b	2676.22	386.51	0.11	1.04	-3.35
58174		546.1775	1.30E-03	4.76E-04	w	13.84	3.57	0.9	-1.21	-2.39
58174		877.6828	-	-		-	-	0.03	-	-3.45
61606	1.51	205.0246	-	-	r	-	-	23.5	-	-1.83
61606		212.487	1.01E-02	2.65E-03	r	60.19	16.13	610	-1.39	-0.39
61606		214.7097	-	-	r	-	-	7.5	-	-2.28
61606		219.8581	-	-	r	-	-	49.8	-	-1.44
61606		221.712	6.05E-03	1.59E-03	r	36.22	9.71	693	-1.57	-0.29
61606		227.3128	4.44E-03	1.17E-03	w	26.6	7.13	62.6	-1.69	-1.32
61606		229.591	-	-		-	-	53.2	-	-1.38
61606		230.3762	5.08E-03	1.34E-03	w	30.44	8.16	509	-1.62	-0.39
61606		234.5841	2.82E-03	7.43E-04	w	16.91	4.53	7.61	-1.86	-2.2
61606		239.5442	5.05E-03	1.33E-03	w	30.22	8.1	220	-1.58	-0.72
61606		242.1158	8.90E-03	2.34E-03		53.32	14.29	57	-1.33	-1.3
61606		245.2807	6.86E-03	1.81E-03	w	41.1	11.01	103	-1.43	-1.03
61606		247.9978	2.66E-03	7.01E-04	w	15.93	4.27	133	-1.83	-0.91
61606		248.7627	-	-		-	-	48.4	-	-1.35
61606		249.485	4.68E-03	1.23E-03	w	28.04	7.51	7.7	-1.58	-2.14
61606		249.9592	1.95E-03	5.13E-04	w	11.67	3.13	18.4	-1.96	-1.76
61606		252.9302	9.26E-03	2.44E-03	w	55.43	14.86	40	-1.27	-1.42
61606		257.2704	3.42E-03	9.00E-04	w	20.47	5.49	0.14	-1.69	-3.84
61606		262.5764	2.35E-03	6.20E-04	w	14.09	3.78	30.4	-1.84	-1.5
61606		263.3998	3.61E-03	9.50E-04	w	21.59	5.79	0.41	-1.65	-3.37
61606		264.0936	-	-		-	-	1.37	-	-2.84
61606		264.7441	5.70E-03	1.50E-03	w	34.16	9.15	2.37	-1.44	-2.6
61606		269.1395	1.00E-02	2.63E-03	b	59.87	16.05	8.83	-1.19	-2.02

61606		269.2096	6.95E-03	1.83E-03	w	41.63	11.16	0.14	-1.34	-3.82
61606		271.5285	3.11E-03	8.19E-04	s	18.63	4.99	0.87	-1.69	-3.02
61606		276.1926	3.11E-03	8.19E-04	w	18.62	4.99	0.14	-1.67	-3.78
61606		280.2597	3.12E-02	8.22E-03	b	187.01	50.12	0.34	-0.66	-3.4
61606		284.3411	8.76E-03	2.31E-03	w	52.43	14.05	2.45	-1.2	-2.53
61606		290.0467	7.57E-03	1.99E-03	w	45.32	12.15	0.13	-1.24	-3.77
61606		292.7126	5.64E-03	1.49E-03	w	33.79	9.06	0.35	-1.36	-3.35
61606		301.0606	2.86E-02	7.52E-03		171.02	45.84	1090	-0.63	0.17
61606		304.002	5.04E-03	1.33E-03	w	30.16	8.08	260	-1.38	-0.44
61606		305.5298	2.01E-03	5.28E-04	w	12.02	3.22	442	-1.77	-0.21
61606		309.1459	7.78E-02	2.05E-02	b	465.64	124.8	5.44	-0.18	-2.1
61606		314.6656	8.23E-02	2.17E-02		492.64	132.04	2.72	-0.14	-2.39
61606		326.5846	-	-	-	-	26.4	-	-	-1.37
61606		329.3841	6.12E-03	1.61E-03	w	36.62	9.82	0.5	-1.22	-3.09
61606		357.7351	8.08E-02	2.13E-02		484.14	129.76	27.4	-0.03	-1.28
61606		369.0977	-	-	-	-	5.93	-	-	-1.91
61606		373.3045	2.13E-01	2.48E-02		1275.23	213.96	2.14	0.43	-2.35
61606		376.0993	-	-	-	-	0.42	-	-	-3.05
61606		379.9084	-	-	-	-	1.33	-	-	-2.54
61606		381.2584	-	-	-	-	4.09	-	-	-2.06
61606		387.8298	1.38E-01	1.61E-02		825.78	138.55	0.49	0.27	-2.95
61606		406.4927	3.49E-02	9.18E-03	w	208.73	55.94	1.06	-0.29	-2.58
61606		431.7082	9.79E-02	1.14E-02		586.32	98.38	0.11	0.21	-3.51
61606		436.3461	-	-	-	-	0.22	-	-	-3.21
61606		590.6545	3.09E-03	8.13E-04	n	18.49	4.96	0.02	-1.01	-3.94
61606		598.5563	6.14E-02	1.62E-02	b	367.42	98.47	0.37	0.3	-2.72
61606		632.7941	1.01E-02	2.67E-03	w	60.62	16.25	0.03	-0.44	-3.74
61606		674.4857	-	-	-	-	0.03	-	-	-3.64
					-	-		-		
63576	1.72	205.9902	2.28E-03	6.66E-04	r	9.97	2.6	15.3	-2.2	-2.01
63576		210.7244	8.57E-03	2.50E-03	r	37.41	9.74	371	-1.6	-0.61
63576		212.427	-	-	r	-	-	60.5	-	-1.39
63576		220.3679	1.04E-02	3.04E-03	r	45.58	11.87	103	-1.48	-1.12
63576		224.2151	1.55E-02	4.53E-03	r	67.83	17.66	782	-1.29	-0.23
63576		228.7423	1.44E-02	4.19E-03	w	62.78	16.35	30	-1.31	-1.62
63576		230.2594	-	-	-	-	64.9	-	-	-1.29
63576		233.9675	5.95E-03	1.74E-03	w	25.98	6.76	168	-1.67	-0.86
63576		235.6222	5.59E-03	1.63E-03	w	24.42	6.36	58.5	-1.69	-1.31
63576		236.4385	1.12E-02	3.27E-03	w	48.93	12.74	3.56	-1.39	-2.52
63576		237.1337	7.55E-03	2.20E-03	w	32.98	8.59	222	-1.56	-0.73
63576		238.2207	1.52E-02	4.42E-03	w	66.15	17.23	81.1	-1.25	-1.16

63576	240.9177	2.71E-03	7.90E-04	w	11.82	3.08	13.4	-1.99	-1.93
63576	242.0654	1.27E-03	3.69E-04	w	5.52	1.44	31.6	-2.31	-1.55
63576	243.54	8.62E-03	2.51E-03	s	37.61	9.79	13.7	-1.48	-1.91
63576	246.6826	7.92E-03	2.31E-03	w	34.58	9	62.8	-1.5	-1.24
63576	249.6537	4.23E-03	1.23E-03	w	18.45	4.8	0.17	-1.76	-3.81
63576	250.398	-	-	-	-	-	2.92	-	-2.56
63576	251.0248	3.82E-03	1.11E-03	w	16.68	4.34	15.6	-1.8	-1.83
63576	254.2106	4.98E-03	1.45E-03	w	21.75	5.66	51	-1.68	-1.31
63576	254.5899	2.67E-02	7.77E-03		116.39	30.31	10.9	-0.95	-1.97
63576	255.5795	2.97E-03	8.65E-04	w	12.96	3.37	7.77	-1.9	-2.12
63576	255.6427	5.46E-03	1.59E-03	w	23.82	6.2	13.6	-1.63	-1.87
63576	261.9315	7.37E-03	2.15E-03	w	32.19	8.38	0.11	-1.48	-3.95
63576	265.5867	7.48E-03	2.18E-03	w	32.63	8.5	4.49	-1.46	-2.32
63576	274.3597	1.88E-02	5.48E-03	w	82.04	21.36	40.1	-1.03	-1.34
63576	276.7439	1.48E-02	4.32E-03		64.74	16.86	0.89	-1.13	-2.99
63576	284.1944	4.57E-03	1.33E-03	w	19.97	5.2	373	-1.62	-0.34
63576	288.6005	5.86E-03	1.71E-03	w	25.57	6.66	0.96	-1.5	-2.92
63576	291.3884	5.76E-03	1.68E-03	w	25.13	6.54	12	-1.49	-1.81
63576	319.5256	2.02E-02	5.90E-03		88.36	23.01	0.34	-0.87	-3.29
63576	330.6156	5.76E-02	1.68E-02	w	251.26	65.43	546	-0.39	-0.05
63576	334.1701	-	-	-	-	-	367	-	-0.21
63576	344.0644	-	-	-	-	-	7.37	-	-1.87
63576	347.7171	1.02E-01	1.32E-02		445.44	69.19	2.03	-0.09	-2.44
63576	350.1407	1.15E-01	1.48E-02	w	500.76	77.79	1.1	-0.04	-2.69
63576	351.5361	1.32E-02	3.84E-03	w	57.42	14.95	0.76	-0.97	-2.85
63576	354.608	9.01E-02	1.16E-02		393.46	61.12	23.1	-0.13	-1.37
63576	359.9314	1.29E-01	1.66E-02	w	563.38	87.51	0.81	0.04	-2.8
63576	360.7447	6.51E-02	1.90E-02	w	284.04	73.97	3.33	-0.26	-2.19
63576	371.1463	-	-	-	-	-	0.5	-	-2.98
63576	371.3105	9.57E-02	1.23E-02		417.61	64.87	0.16	-0.06	-3.47
63576	376.3374	-	-	-	-	-	0.65	-	-2.86
63576	378.9871	2.46E-02	7.16E-03	w	107.19	27.91	0.19	-0.64	-3.4
63576	389.6515	-	-	-	-	-	0.07	-	-3.79
63576	401.7873	-	-	-	-	-	0.1	-	-3.63
63576	402.3045	-	-	-	-	-	0.11	-	-3.57
63576	529.0572	4.65E-02	1.36E-02	w	203.06	52.88	0.09	-0.07	-3.45
63576	535.388	9.76E-03	2.85E-03	w	42.63	11.1	0.84	-0.74	-2.46
63576	595.3344	1.61E-03	4.70E-04	w	7.03	1.83	0.12	-1.43	-3.2
63576	658.8127	-	-	-	-	-	0.08	-	-3.31
63576	748.9427	-	-	-	-	-	0.02	-	-3.76
				-	-	-	-	-	

64236	3.88	201.2362	-	-	r	-	-	83.6	-	-1.3
64236		202.4637	-	-	r	-	-	49.3	-	-1.52
64236		205.2304	2.82E-03	6.90E-04	r	7.63	1.87	577	-2.32	-0.44
64236		207.8355	5.35E-04	1.31E-04	r	1.45	0.36	3.84	-3.03	-2.61
64236		209.4915	-	-	r	-	-	5.59	-	-2.43
64236		214.4851	1.65E-03	4.02E-04	r	4.45	1.09	33.8	-2.51	-1.63
64236		216.5123	3.66E-03	8.95E-04	r	9.89	2.43	349	-2.16	-0.61
64236		217.3512	1.45E-03	3.54E-04	r	3.92	0.96	206	-2.56	-0.84
64236		220.9474	-	-	r	-	-	8.79	-	-2.19
64236		222.5157	1.23E-03	3.00E-04	r	3.32	0.81	126	-2.61	-1.03
64236		224.4743	9.25E-04	2.26E-04	r	2.5	0.61	4.86	-2.72	-2.43
64236		225.3423	7.14E-04	1.74E-04	w	1.93	0.47	26.2	-2.83	-1.7
64236		227.6166	-	-	-	-	-	83.4	-	-1.19
64236		232.8077	1.78E-03	4.36E-04	s	4.82	1.18	45.8	-2.41	-1.43
64236		234.1179	1.36E-03	3.32E-04	w	3.67	0.9	19.6	-2.52	-1.79
64236		235.3342	1.37E-03	3.35E-04	w	3.7	0.91	120	-2.51	-1
64236		237.1492	2.28E-03	5.57E-04	w	6.16	1.51	29.6	-2.28	-1.6
64236		239.6897	1.88E-03	4.59E-04	w	5.08	1.25	142	-2.36	-0.91
64236		240.9607	1.37E-03	3.35E-04	w	3.7	0.91	0.85	-2.49	-3.13
64236		245.0637	2.26E-03	5.52E-04	w	6.1	1.5	4.11	-2.26	-2.43
64236		246.3296	-	-	-	-	-	72.9	-	-1.18
64236		247.5049	4.09E-03	1.00E-03	w	11.07	2.72	42.5	-1.99	-1.41
64236		251.4036	3.58E-04	8.74E-05	w	0.97	0.24	2.84	-3.04	-2.57
64236		253.4247	7.44E-04	1.82E-04	w	2.01	0.49	7.02	-2.71	-2.17
64236		255.0144	2.47E-03	6.04E-04	w	6.68	1.64	54.7	-2.19	-1.27
64236		257.4831	-	-	-	-	-	7.72	-	-2.12
64236		262.1111	2.25E-03	5.49E-04	s	6.07	1.49	2.14	-2.2	-2.66
64236		264.551	4.51E-04	1.10E-04	w	1.22	0.3	2.32	-2.89	-2.61
64236		269.4832	2.07E-03	5.07E-04	w	5.61	1.38	1.26	-2.21	-2.86
64236		271.251	1.94E-03	4.75E-04	w	5.26	1.29	4.77	-2.24	-2.28
64236		278.9653	8.34E-04	2.04E-04	w	2.25	0.55	8.17	-2.58	-2.02
64236		281.4891	8.33E-04	2.04E-04	w	2.25	0.55	73.2	-2.57	-1.05
64236		282.7985	3.59E-03	8.77E-04	w	9.7	2.38	31	-1.93	-1.43
64236		290.6081	5.53E-03	1.35E-03		14.94	3.67	21.6	-1.72	-1.56
64236		296.3864	3.08E-02	7.53E-03	w	83.33	20.46	4.77	-0.96	-2.2
64236		298.4019	-	-	-	-	-	206	-	-0.56
64236		300.7451	9.86E-03	2.41E-03	w	26.66	6.55	435	-1.44	-0.23
64236		303.1175	6.68E-05	1.63E-05	w	0.18	0.04	2.35	-3.6	-2.49
64236		324.9066	2.17E-02	5.32E-03	w	58.8	14.43	9.65	-1.03	-1.82
64236		339.9215	1.95E-03	4.76E-04	w	5.26	1.29	18.2	-2.04	-1.51
64236		342.2372	1.84E-02	4.50E-03	b	49.76	12.22	0.4	-1.06	-3.16

64236		351.585	1.21E-03	2.96E-04	w	3.27	0.8	22.5	-2.22	-1.38
64236		351.9234	1.10E-02	2.69E-03	w	29.8	7.32	5.78	-1.26	-1.97
64236		362.2782	3.55E-02	8.67E-03		95.93	23.55	0.31	-0.72	-3.22
64236		362.675	1.46E-02	3.57E-03	w	39.53	9.7	0.47	-1.11	-3.03
64236		387.6789	-	-	-	-	-	5.47	-	-1.91
64236		391.9058	4.00E-01	3.90E-02		1080.09	130.63	2.33	0.4	-2.27
64236		396.5347	3.99E-01	3.89E-02		1078.86	130.48	0.23	0.41	-3.26
64236		410.3016	5.81E-03	1.42E-03	w	15.71	3.86	0.72	-1.4	-2.73
						-	-		-	
64401	2.5	202.5475	5.58E-03	1.87E-03	r	19.3	4.75	3.16	-1.93	-2.71
64401		207.1231	-	-	r	-	-	45.8	-	-1.53
64401		208.7678	-	-	r	-	-	163	-	-0.97
64401		216.4325	-	-	r	-	-	6.1	-	-2.36
64401		220.1425	9.33E-04	3.13E-04	r	3.22	0.79	7.81	-2.63	-2.25
64401		224.5051	1.55E-03	5.19E-04	r	5.34	1.32	27.1	-2.39	-1.68
64401		229.5365	2.38E-03	7.99E-04	w	8.23	2.03	24.7	-2.19	-1.71
64401		231.1289	1.68E-03	5.65E-04	w	5.82	1.43	275	-2.33	-0.66
64401		231.9143	-	-	-	-	-	8.17	-	-2.18
64401		232.5831	3.85E-03	1.29E-03	w	13.3	3.28	274	-1.97	-0.65
64401		233.6287	4.96E-03	1.66E-03	w	17.14	4.22	11.4	-1.85	-2.03
64401		236.2222	2.76E-03	9.25E-04	w	9.53	2.35	39.9	-2.1	-1.48
64401		237.3254	3.91E-03	1.31E-03	w	13.52	3.33	172	-1.94	-0.84
64401		238.7427	2.68E-03	8.99E-04	w	9.26	2.28	27.3	-2.1	-1.63
64401		241.762	1.19E-03	4.00E-04	w	4.12	1.02	1.31	-2.44	-2.94
64401		244.6151	1.19E-03	4.00E-04	w	4.12	1.01	10	-2.43	-2.05
64401		245.3296	5.83E-03	1.95E-03	w	20.13	4.96	8.52	-1.74	-2.11
64401		245.9313	2.54E-03	8.51E-04	w	8.77	2.16	50.8	-2.1	-1.34
64401		248.9883	3.44E-03	1.16E-03	w	11.9	2.93	56.1	-1.96	-1.28
64401		249.3522	2.64E-03	8.87E-04	w	9.14	2.25	13.2	-2.07	-1.91
64401		250.3014	5.48E-03	1.84E-03	w	18.94	4.67	57.2	-1.75	-1.27
64401		250.362	1.59E-03	5.35E-04	w	5.51	1.36	19.3	-2.29	-1.74
64401		256.3907	1.80E-03	6.04E-04	w	6.22	1.53	14.9	-2.21	-1.83
64401		259.8918	-	-	-	-	-	3.36	-	-2.47
64401		263.3979	3.42E-03	1.15E-03	w	11.81	2.91	0.1	-1.91	-4
64401		268.2868	9.92E-04	3.33E-04	w	3.43	0.84	20.5	-2.43	-1.65
64401		270.5662	3.65E-03	1.23E-03	w	12.63	3.11	6.31	-1.86	-2.16
64401		277.6835	9.59E-03	3.22E-03	s	33.15	8.17	34.8	-1.42	-1.39
64401		284.5477	7.36E-03	2.47E-03	w	25.45	6.27	0.43	-1.51	-3.28
64401		311.3187	2.82E-02	9.46E-03		97.42	24	0.25	-0.85	-3.44
64401		321.837	2.60E-03	8.74E-04	w	9	2.22	1.79	-1.85	-2.56
64401		334.5673	5.08E-03	1.71E-03	w	17.57	4.33	1.28	-1.53	-2.66

64401		338.0202	-	-	-	-	450	-	-0.12	
64401		340.31	3.07E-02	1.03E-02		106.15	26.15	104	-0.73	-0.74
64401		341.628	-	-		-	-	0.12	-	-3.69
64401		344.5285	2.28E-02	7.64E-03	w	78.74	19.4	127	-0.85	-0.65
64401		349.5514	9.29E-04	3.12E-04	w	3.21	0.79	23.4	-2.23	-1.37
64401		350.3185	4.24E-02	1.42E-02		146.46	36.08	0.78	-0.57	-2.84
64401		360.1194	3.50E-02	1.17E-02	w	120.93	29.79	6.72	-0.63	-1.88
64401		360.2739	-	-		-	-	0.2	-	-3.41
64401		365.0046	4.62E-02	1.55E-02		159.54	39.3	1.95	-0.5	-2.41
64401		367.4966	7.10E-02	1.05E-02		245.42	32.01	0.44	-0.3	-3.06
64401		377.5156	-	-		-	-	2.65	-	-2.24
64401		388.8962	-	-		-	-	0.19	-	-3.36
64401		389.3807	-	-		-	-	0.79	-	-2.75
64401		411.3664	3.31E-01	4.43E-02	b	1142.94	140.21	0.23	0.46	-3.22
64401		413.187	-	-		-	-	1.29	-	-2.49
64401		427.6496	1.86E-01	2.76E-02		644.14	84.01	0.09	0.25	-3.59
64401		506.9311	9.81E-02	1.46E-02	w	339.16	44.23	0.49	0.12	-2.74
64401		512.7405	9.41E-04	3.16E-04	w	3.25	0.8	0.64	-1.89	-2.61
64401		537.6604	1.71E-02	5.75E-03		59.22	14.59	0.05	-0.59	-3.64
64401		538.7484	-	-		-	-	0.05	-	-3.66
64401		567.4635	-	-		-	-	0.05	-	-3.58
64401		638.5746	7.92E-04	2.66E-04	w	2.74	0.67	0.26	-1.78	-2.8
64401		705.3605	-	-		-	-	0.39	-	-2.53
64401		763.835	-	-		-	-	0.08	-	-3.17
64401		807.9154	-	-		-	-	0.1	-	-3.01
						-	-		-	
64818	4.42	200.8523	-	-	r	-	-	7.62	-	-2.33
64818		205.3508	9.04E-03	2.39E-03	r	13.91	3.38	216	-2.06	-0.86
64818		206.9673	2.17E-03	5.74E-04	r	3.34	0.81	52.3	-2.67	-1.47
64818		214.4981	4.89E-03	1.29E-03	r	7.52	1.83	30.9	-2.28	-1.67
64818		218.1415	3.48E-03	9.19E-04	r	5.35	1.3	234	-2.42	-0.78
64818		222.4245	3.24E-03	8.55E-04	r	4.98	1.21	49.9	-2.43	-1.43
64818		223.8587	-	-	r	-	-	6.14	-	-2.34
64818		227.362	9.20E-03	2.43E-03	w	14.16	3.44	19.4	-1.96	-1.82
64818		228.9243	8.62E-03	2.28E-03	w	13.28	3.22	36.5	-1.98	-1.54
64818		229.6947	3.11E-03	8.21E-04	w	4.78	1.16	1.11	-2.42	-3.05
64818		230.3508	-	-		-	-	44.8	-	-1.45
64818		231.3764	5.18E-03	1.37E-03	w	7.98	1.94	0.83	-2.19	-3.18
64818		233.9198	7.53E-03	1.99E-03	w	11.6	2.81	67.3	-2.02	-1.26
64818		235.0016	1.49E-02	3.93E-03		22.89	5.55	237	-1.72	-0.7
64818		236.3912	6.17E-03	1.63E-03	w	9.49	2.3	53.4	-2.1	-1.35

64818	239.351	-	-	-	-	-	19.6	-	-1.77
64818	242.1471	7.39E-03	1.95E-03	w	11.38	2.76	14.6	-2	-1.89
64818	243.4368	6.89E-03	1.82E-03	w	10.6	2.57	52.2	-2.03	-1.33
64818	246.4318	-	-	-	-	-	2.4	-	-2.66
64818	246.7882	2.72E-03	7.19E-04	w	4.19	1.02	0.49	-2.42	-3.35
64818	247.718	1.76E-03	4.66E-04	w	2.71	0.66	64.1	-2.6	-1.23
64818	247.7773	-	-	-	-	-	15.2	-	-1.85
64818	253.6807	3.66E-03	9.67E-04	w	5.63	1.37	1.5	-2.26	-2.84
64818	257.1077	2.67E-03	7.05E-04	w	4.11	1	14.4	-2.39	-1.84
64818	260.5386	6.26E-03	1.65E-03	w	9.63	2.34	0.38	-2.01	-3.41
64818	267.55	1.42E-02	3.75E-03		21.84	5.3	6.83	-1.63	-2.13
64818	274.5075	-	-	-	-	-	17.9	-	-1.69
64818	278.6163	3.39E-03	8.95E-04	w	5.21	1.27	0.71	-2.22	-3.08
64818	281.2137	5.09E-03	1.35E-03	w	7.84	1.9	1.33	-2.03	-2.8
64818	297.8618	1.94E-02	5.13E-03	w	29.87	7.25	1.94	-1.4	-2.58
64818	307.3324	5.63E-03	1.49E-03	w	8.66	2.1	1.1	-1.91	-2.8
64818	317.5786	4.34E-02	1.15E-02	w	66.88	16.23	3.88	-0.99	-2.23
64818	320.8569	6.51E-03	1.72E-03	w	10.03	2.43	47.3	-1.81	-1.14
64818	329.9678	-	-	-	-	-	15	-	-1.6
64818	333.3259	5.91E-02	1.56E-02	w	90.99	22.08	242	-0.82	-0.4
64818	335.5524	1.34E-01	1.56E-02		205.69	25.37	60.5	-0.46	-0.99
64818	336.8337	7.83E-03	2.07E-03	w	12.05	2.93	11.6	-1.69	-1.7
64818	339.6531	3.85E-02	1.02E-02		59.28	14.39	28.7	-0.99	-1.31
64818	344.5338	4.19E-02	1.11E-02	b	64.48	15.65	50.8	-0.94	-1.04
64818	345.279	5.26E-02	1.39E-02	b	81	19.66	0.3	-0.84	-3.27
64818	354.7961	3.82E-02	1.01E-02		58.82	14.27	4.94	-0.95	-2.02
64818	354.9462	8.68E-02	2.29E-02		133.67	32.44	0.07	-0.6	-3.88
64818	359.5371	4.29E-02	1.13E-02	b	66.07	16.03	0.45	-0.89	-3.06
64818	361.9547	2.08E-01	2.43E-02		320.23	39.5	0.2	-0.2	-3.41
64818	404.435	-	-	-	-	-	0.08	-	-3.68
64818	406.1946	-	-	-	-	-	0.37	-	-3.04
64818	420.1636	-	-	-	-	-	0.09	-	-3.61
64818	496.4462	4.50E-02	1.19E-02	w	69.36	16.83	0.2	-0.59	-3.14
64818	502.0165	-	-	-	-	-	0.06	-	-3.63
64818	525.8806	-	-	-	-	-	0.07	-	-3.51
64818	526.9215	3.64E-02	9.63E-03		56.1	13.61	0.61	-0.63	-2.59
64818	608.9973	-	-	-	-	-	0.05	-	-3.6
64818	622.0261	-	-	-	-	-	0.18	-	-2.99
64818	685.2241	2.60E-03	6.88E-04	w	4.01	0.97	0.13	-1.55	-3.04
64818	740.2774	-	-	-	-	-	0.02	-	-3.77
64818	781.6072	-	-	-	-	-	0.09	-	-3.09

Table 5.7 Pr III Radiative Parameters

Lifetimes adopted from Biémont et al.¹⁷*r* denotes emission line outside of spectral efficiency range*w* denotes weak emission line*s* denotes shouldering emission line*b* denotes blended*DREAM* see reference^{16,17}

5.6 - Analysis

Transition probabilities for neutral, singly ionized, and doubly-ionized neodymium and praseodymium are presented in the tables above and compared to other previous works. For each of these elements and their respective ionizations we show a graphical representation of the data above in order to see how our measurements agree with previous works. For each element and ionization I present a transition probability (TP) comparison where the TP's of others and this work are plotted against the other's TP's in order to show any systematic trends. However this type of plot gives a biased perspective to this work's TP's, because the straight line of the other works' results gives the illusion of optimum accuracy. I could just as easily plotted their values against my measured values. Either way, the idea is to look for systematic deviations, not absolute agreement. In order to give a better representation of the level of agreement, 3 histogram plots were made showing the representative percent differences between this work's BRs and those of other works and each is discussed in further detail below. The percent difference are partitioned according to branching ratio strength (greater than 30%, between 30 and 10% and less than 10%) in order to reveal any systematic deviations which might depend upon branching ratio strength.

5.6.1 - Neutral Neodymium

Figure 5.5 and figure 5.6 show the agreement between each of the $\log(gf)$ values and gA values listed in table 5.2, respectively. The scatter between the work of Kurucz¹¹ and this work is substantial for some values of $\log(gf)$, but no systematic trends are obvious. In this work singly ionized neodymium had 93 observed energy levels with reported lifetimes for calculating oscillator strengths. Of the 121 emission lines from these 93 reported levels, 4 lines are unobserved, 2 are blended, 46 are weak transitions and 10 are shouldered. Overall there are 191 upper energy states with 245 emission lines for which we list relative intensities in appendix 1.

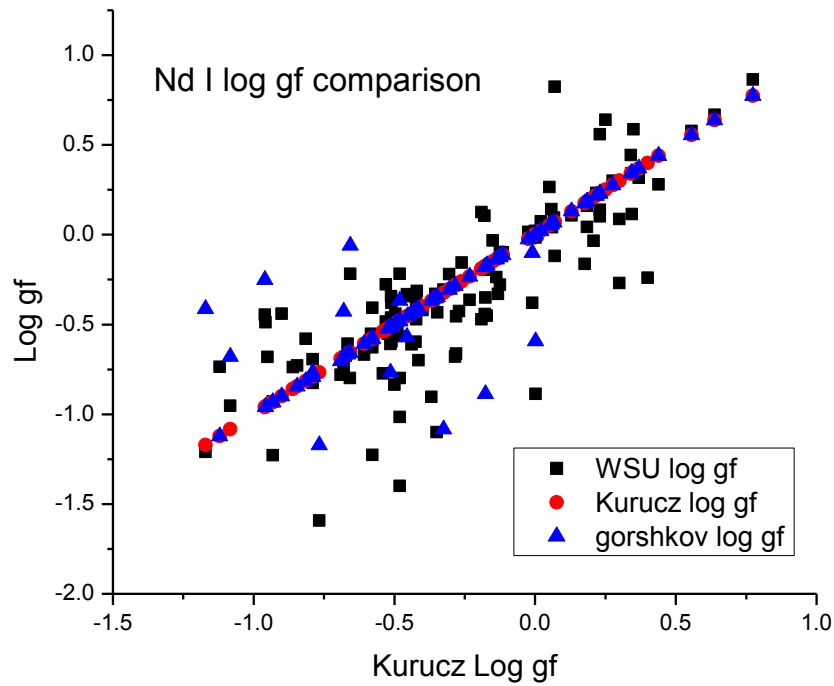


Figure 5.5 shows the $\log(gf)$ comparison between this work and other previous works. The black squares signify this work, red circles represent Kurucz' $\log(gf)$ values, and the blue triangles are the results by Gorshkov. The various works' $\log(gf)$ values are plotted against the values of Kurucz so that data which lie on a slope of one represent perfect agreement with Kurucz data.

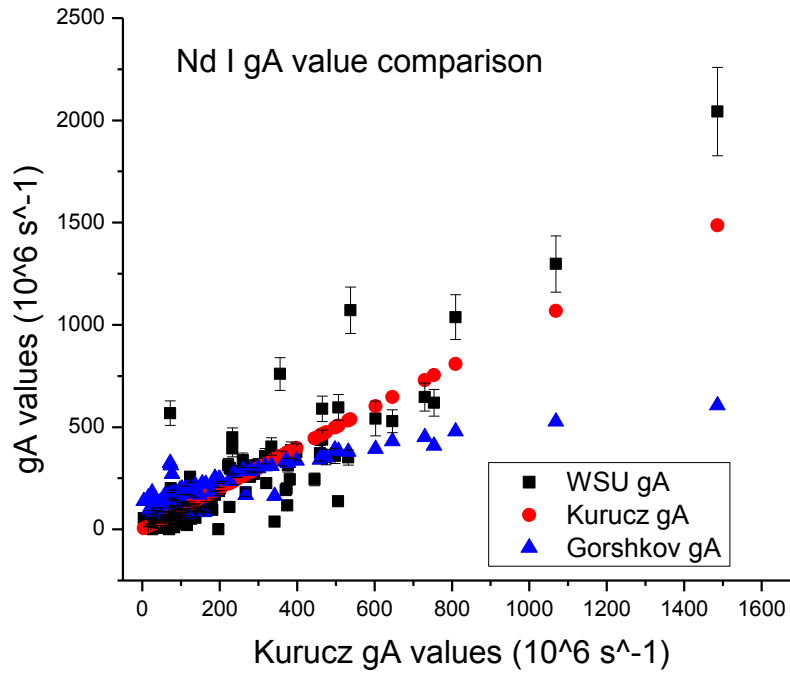


Figure 5.6 shows the transition probability (gA) comparison between this work, the work by Kurucz¹¹ and Gorshkov³. The black squares signify this work, red circles represent Kurucz' work, and the blue triangles are the results of Gorshkov. The various works' gA values are plotted against the values of Kurucz so that data which lie on a slope of one represent perfect agreement with Kurucz data. The error bars shown in this work incorporate error from lifetimes as well as uncertainties of this work.

Figures 5.7 – 5.9 are histogram representations of the percent difference ($WSU - Kurucz$)/ $Kurucz$ ($\times 100$) between this work and that of Kurucz and Bell.¹¹ The histograms show the number of times a given percent difference was reported relative to complete agreement (zero percent difference). The total percent difference was also partitioned into branching ratio strength to see if agreement between this work and others depends in any way on branching ratio strength. The idea being that weaker branches should have typically worse agreement since we

have difficulty measuring them and overly-strong lines which we saw as blended will also have large percent differences.

For those Nd I branches greater than 30%, I found that 21.7% of the values reported agree within $\pm 5\%$ with Kurucz, 45.4% agreed within $\pm 15\%$, 57.8% agreed within $\pm 25\%$, 69.1% agreed within $\pm 35\%$, 81.46% agreed within $\pm 45\%$, 85.6% agreed within $\pm 55\%$, 87.7% agreed within $\pm 65\%$ and all 100% of the reported values agreed within $\pm 195\%$. The average percent difference for branches greater than 30% was found to be 5.93%. Given that our stated uncertainty for this strength of branching ratio is 6.6% and given a 5% uncertainty in the lifetime from Kurucz and Bell for these branches in Nd I, the results show that we generally agree with those transition probabilities, since almost 50% of the values agree within our error estimates. There are outliers on the positive side of zero percent difference in Nd I, which show that our gA values were larger than Kurucz's values. I believe these larger overestimates to be caused by spectral blending of neighboring lines.

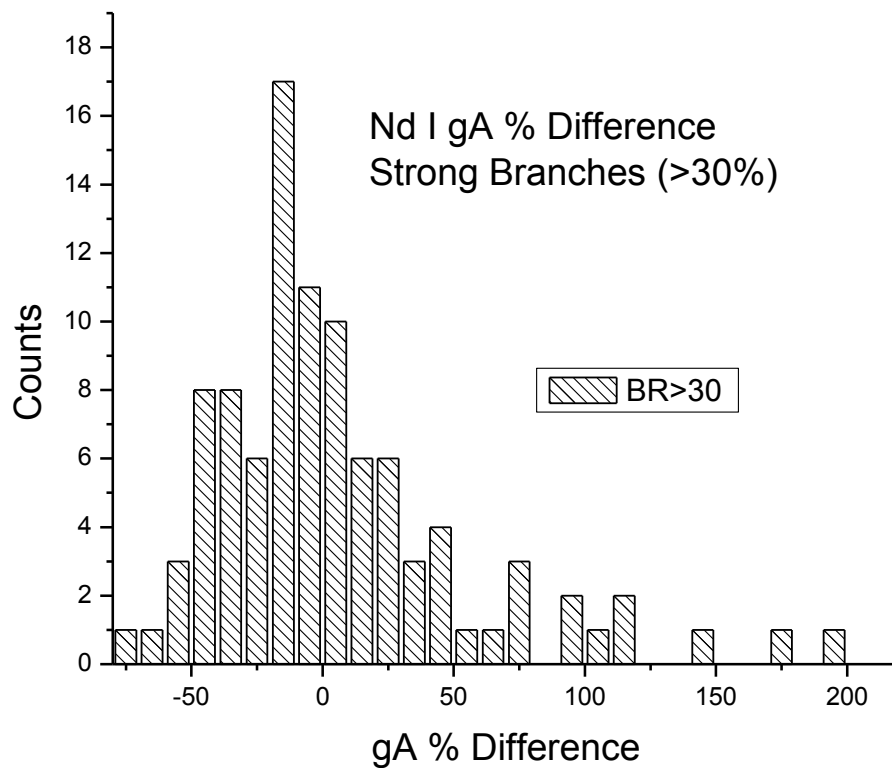


Figure 5.7 shows a histogram plot of the gA percent difference between this work and that of Kurucz and Bell for “strong” branches which are greater than 30 percent. The number of occurrences (counts) represents the number of reported branching ratio percent difference values which lie within the given bin size (10%).

For the Nd I branches which are between 30% and 10%, I found that 20% of the reported values agreed within $\pm 7.5\%$ of the Kurucz values, 30% agreed within $\pm 27.5\%$, 50% agreed within $\pm 67.5\%$, 70% agreed within $\pm 77.5\%$, and all 100% of the values agreed within a percent difference of $\pm 87.5\%$. The average percent difference for branches of medium strength was found to be -58% . Overall there is not very good agreement with the reported values from

Kurucz and Bell. The reason for the general discrepancy is not apparent although most of the values in this branching ratio bracket lie on the negative side of zero and would suggest some systematic issues within our system. It is peculiar that these discrepancies state that we are underestimating values when it seems to be the general trend that we appear to overestimate the weaker branches due to the blending of problematic emission lines in the spectrum. Note that there are only 10 measurements represented in this histogram, so it is difficult to draw any real conclusion.

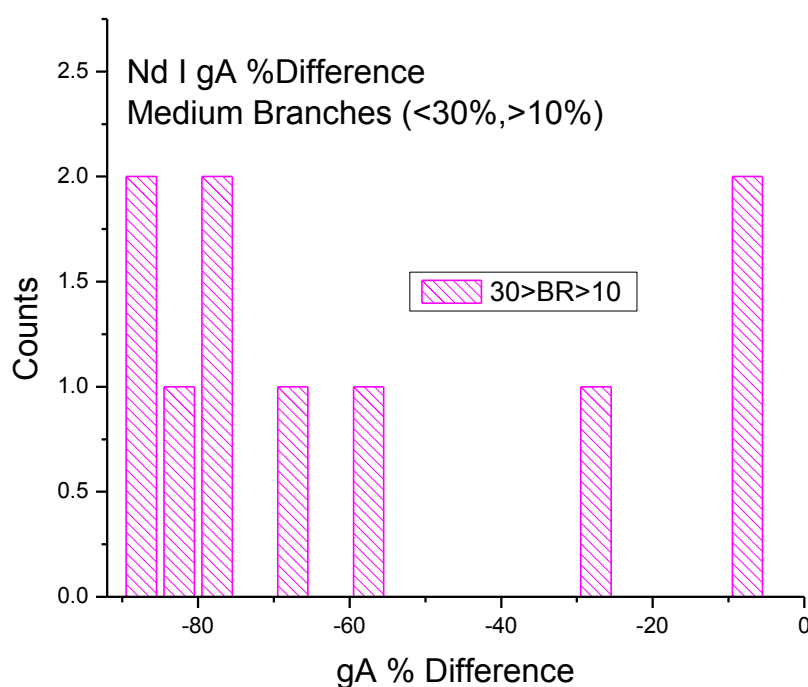


Figure 5.8 shows a histogram plot of the gA percent difference between this work and that of Kurucz and Bell for “medium” branches which are between 30 and 10 percent. The number of occurrences (counts) represents the number of reported branching ratio percent difference values which lie within the given bin size (5%).

For the three branches of Nd I which are less than 10%, I found that 66.6% of the values agreed within $\pm 47.5\%$ of the Kurucz values and all 100% agreed within $\pm 87.5\%$. The average percent difference for branches weaker than 10% was found to be -60.7% . There is a general disagreement within the stated uncertainty of our branches (19%) and the lifetimes (5%) from Den Hartog et al. which gives us an overall leeway of $\sim 24\%$. It is the case that outliers lie on the negative side of zero and could be systematically showing that our weak values are sometimes underestimated. Obviously no statistical correlation can be drawn from only three data points.

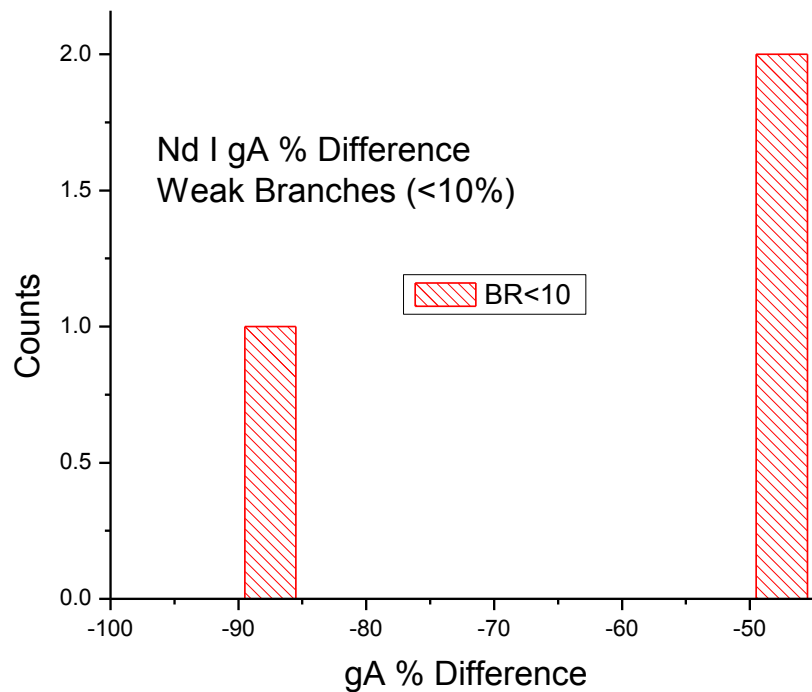


Figure 5.9 shows a histogram plot of the gA percent difference between this work and that of Kurucz and Bell for “weak” branches which are less than 10 percent. The number of occurrences (counts) represents the number of reported branching ratio percent difference values which lie within the given bin size (5%).

5.6.2 - Singly-Ionized Neodymium

In singly-ionized neodymium the results show relatively poor agreement between previous works and this work. One of the major pitfalls is from inaccurate branching ratio determinations which cause large deviations between reported radiative parameters, due to unobserved and blended lines. In the 46 Nd II levels there are 460 emission lines of which 92 lines are unobserved, 10 lines are blended, 86 lines are listed as weak, and 15 lines noted as having a shouldering peak. Most of these defects occurred for emission lines with reported $\log(gf)$ weaker than -1.64. The corresponding relative intensities and transition probabilities for all of the 460 observed transitions are reported in appendix 1.

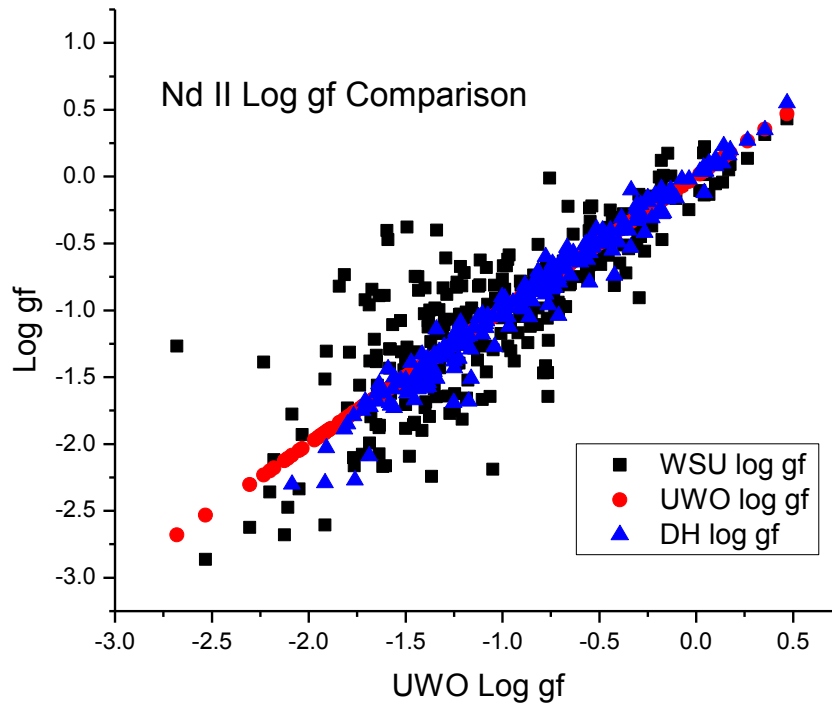


Figure 5.10 shows the comparison of $\log(gf)$ values between this work, the University of Western Ontario's (UWO) work (Li et al.⁴²) and Den Hartog's results (Den Hartog et al.³¹) plotted against the $\log(gf)$ values from UWO. Note that perfect agreement would result in a slope of one. The black squares signify this work, red circles represent UWO results, and the blue triangles are Den Hartog's results.

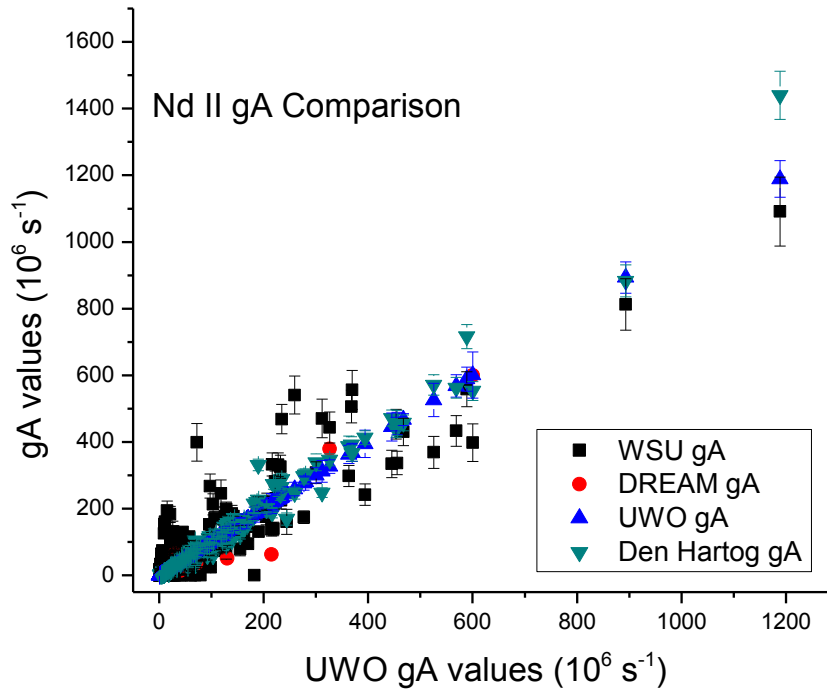


Figure 5.11 shows a comparison of transition probabilities (gA values) between this work (black squares), the results of the DREAM project from Xu et al.³⁰ (red circles), University of Western Ontario's results by Li et al.⁴² (blue upward triangles) and Den Hartog's et al.³¹ results (downward cyan triangles). The results are plotted against UWO's gA values in order to show any systematic trends so that a slope of one represents perfect agreement. The error bars shown in WSU data incorporate the error from lifetimes as well as uncertainties in this work.

Figures 5.12 – 5.14 are histogram representations of the Nd II transition probability (gA) percent differences $(WSU - UWO)/UWO (x100)$ between this work and that of Li et al.⁴² The histograms show the number of times a given percent difference was reported relative to complete agreement (zero percent difference). The entire range of percent differences was partitioned according to branching ratio strength to see if agreement between this work and others' work does vary with branching ratio strength. The idea being that weaker branches

should have typically worse agreement since we have difficulty measuring them and overly-strong lines which we saw as blended will also have large percent differences.

For those Nd II branches greater than 30%, I found that 18.2% of the values agreed with the UWO values within $\pm 5\%$, 25.0% agreed within $\pm 15\%$, 36.8% agreed within $\pm 25\%$, 52.7% agreed within $\pm 35\%$, 60.0% agreed within $\pm 55\%$, 70.1% agreed within $\pm 115\%$, and all 100% of the values agreed within $\pm 455\%$. The average percent difference was found to be 92.6%. Given that our stated uncertainty for this strength of branching ratio is 6.6%, the results show that we generally disagree with Li et al.'s transition probabilities, since less than 25% of the values agree within our error budget of 6.6% and $\sim 5\%$ for lifetimes. There are also some outliers in Nd II along the positive side of zero percent, which shows that these outlying gA values were larger than those of Li et al.'s. I believe these larger overestimates in our values to be caused by spectral blending of neighboring lines.

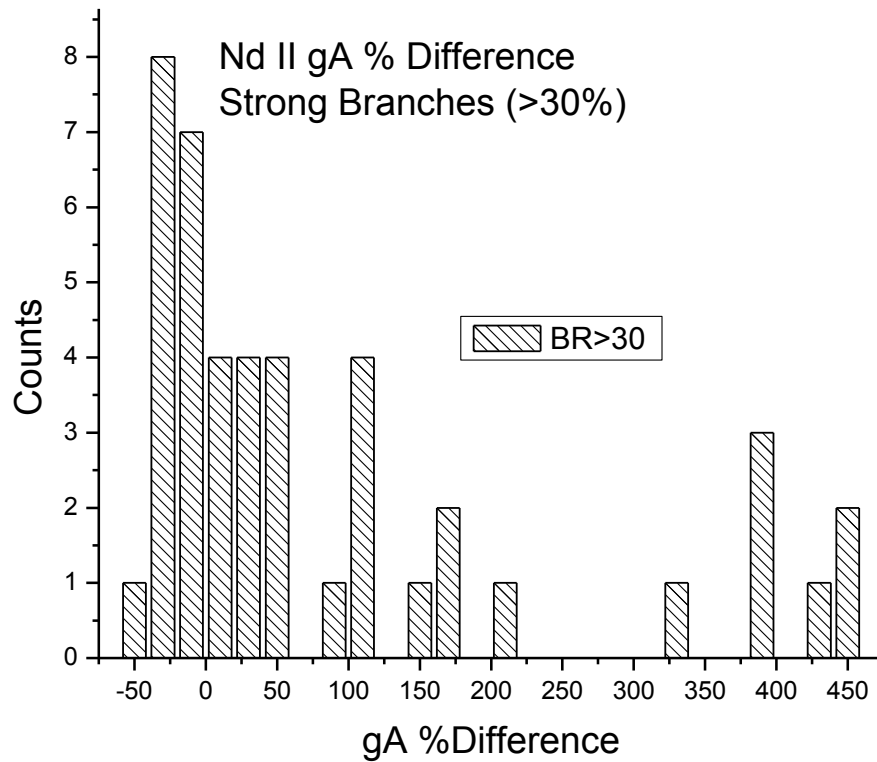


Figure 5.12 shows a histogram plot of the gA percent difference between this work and that of Li et al. (UWO) for “strong” branches which are greater than 30 percent. The number of occurrences (counts) represents the number of reported branching ratio percent difference values which lie within the given bin size (10%).

For those branches which are between 30% and 10%, I found that 14.6% of the values agreed with UWO within $\pm 5\%$, 22.3% of the values agreed within $\pm 15\%$, 37.9% of the values agreed within $\pm 25\%$, 51.4% of the values agreed within $\pm 35\%$, 55.4% of the values agreed within $\pm 45\%$, 64.1% of the values agreed within $\pm 65\%$, and by $\pm 1395\%$ all 100% of the values are accounted for. The average percent difference for branches of medium strength was found to

be 147.6%. Overall there is not very good agreement with the reported values from Li et al. in this branching ratio bracket. The reason for the general discrepancy is not apparent, although most of the values in this branching ratio bracket lie on the positive side of zero. The general trend of the data show a systematic overestimate of our gA values compared to those from Li et al. which I believe to be caused by the problematic blends and shouldering of emission lines.

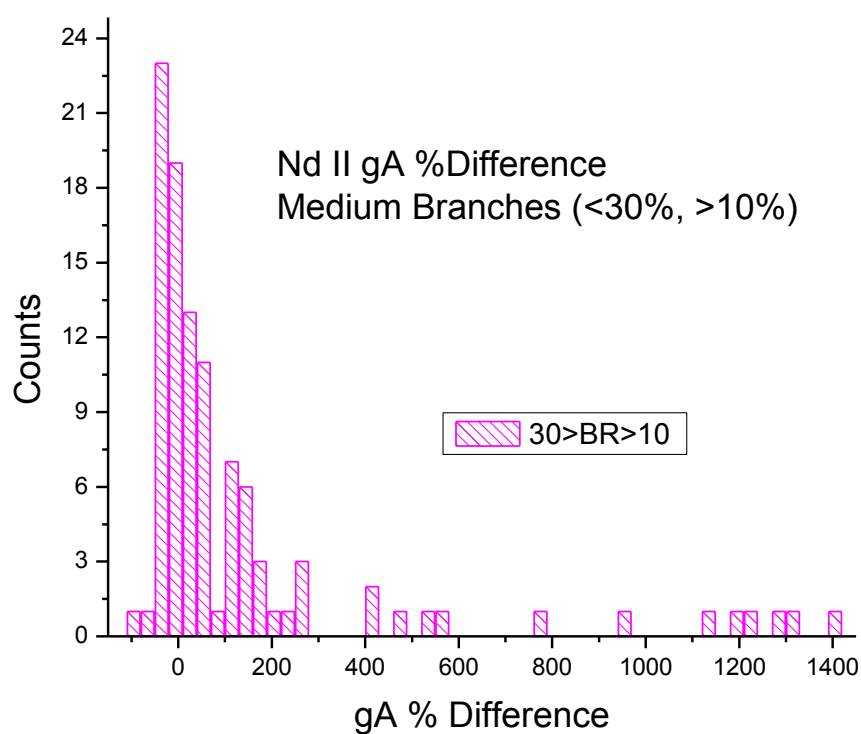


Figure 5.13 shows a histogram plot of the gA percent difference between this work and that of Li et al. for “medium” branches which are between 30 and 10 percent. The number of occurrences (counts) represents the number of reported branching ratio percent difference values which lie within the given bin size (30%).

For the branches of Nd II which are less than 10%, I found that 19.3% of the values agreed with UWO within $\pm 10\%$, 35.0% agreed within $\pm 30\%$, 56.0% agreed within $\pm 50\%$, 74.1% agreed within $\pm 70\%$, 90.5% agreed within $\pm 90\%$, and all 100% agreed within $\pm 90\%$. The average percent difference for branches weaker than 10% was found to be -6.55%. Overall for the weak branches in Nd II there is relatively poor agreement within the stated uncertainty of our weak branches (19%) and the lifetimes ($\sim 5\%$) from other works. Again it is the case that outliers lie on the positive side of zero and show that some of our weak values are largely overestimated, which I believe to be caused by the fitting procedure for weak emission lines which are blended and shoulders to neighboring lines.

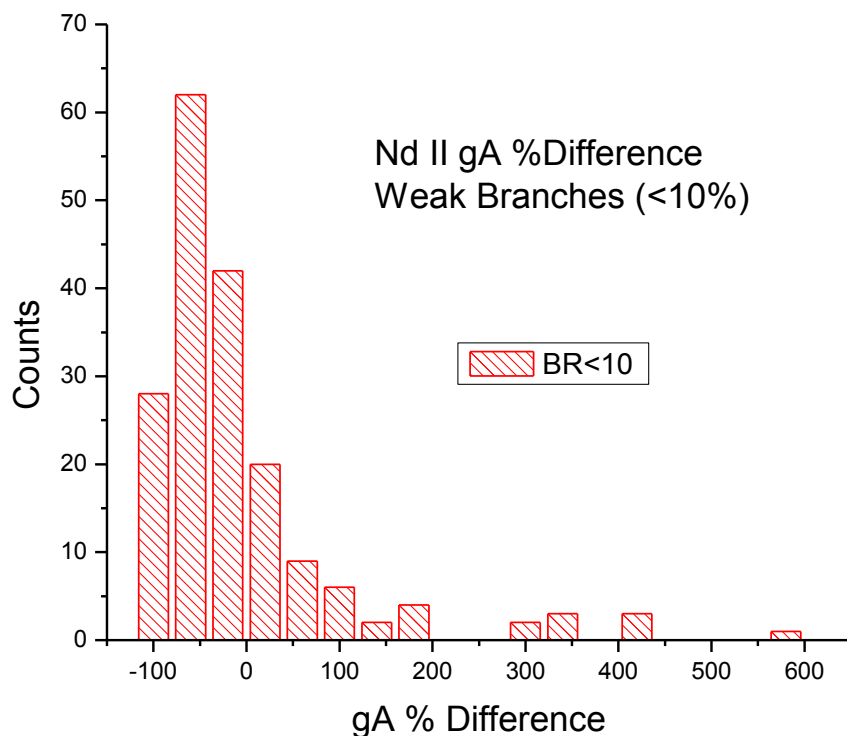


Figure 5.14 shows a histogram plot of the gA percent difference between this work and that of Li et al. for “weak” branches which are less than 10 percent. The number of occurrences (counts) represents the number of reported branching ratio percent difference values which lie within the given bin size (50%).

5.6.3 - Doubly Ionized Neodymium

In doubly-ionized neodymium (Nd III) there are currently only five reported lifetimes which could be incorporated into our branching ratio determinations in order to calculate gA values and $\log(gf)$ values. Of these 5 lifetimes, only one level was worth reporting since the radiative parameters from the other levels were significantly erroneous due to a majority of

missing branches within the level. In total we observed lines from 19 upper states in Nd III and their corresponding 48 relative intensities are reported in appendix 1.

The deviation seen in Nd III radiative parameters is again attributed to the result of weak emission lines. The average percent difference between this work's gA values presented above and those presented by Zhang et al.³⁷ and the DREAM Project is -10%. The average percent difference between this work's gA values and those of Bord et al.³⁶ is -16%.

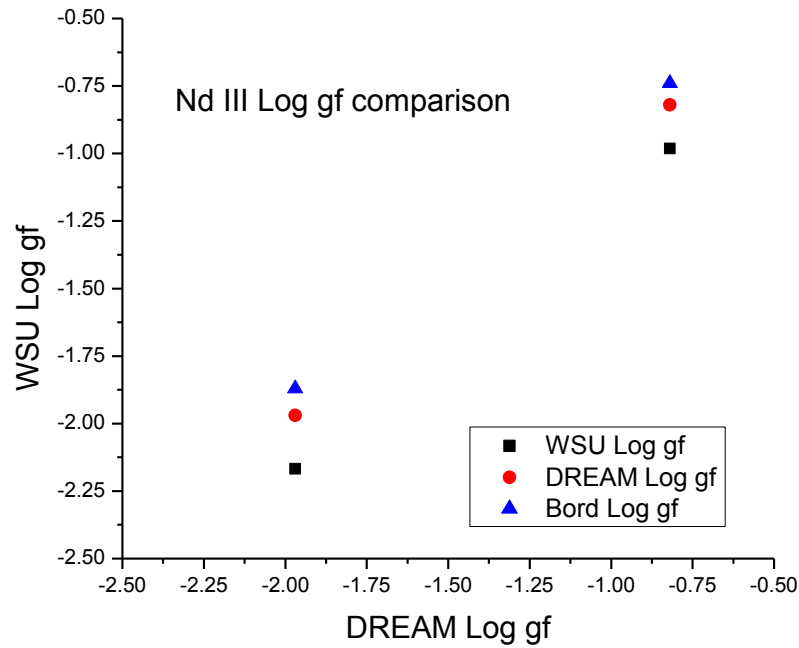


Figure 5.15 shows a $\log(gf)$ comparison for Nd III between the results of this work (black squares) the work of Zhang et al.³⁷ (red circles) associated with the DREAM project, and the results of Bord et al.³⁶ (blue triangles).

5.6.4 - Neutral Praseodymium

The results of the work on neutral praseodymium (Pr I) are in relatively good agreement with previously reported results as can be seen from the $\log(gf)$ comparison shown in figure 5.16. There are 19 emission lines originating from 19 different upper energy states which are listed in the chart above and compared in figure 5.16. A total of 80 upper energy states were observed with 93 total emission lines. Many of these levels were not included in the comparison because of a lack of reported atomic lifetimes in neutral praseodymium; the relative intensities for these emission lines are listed in appendix 1.

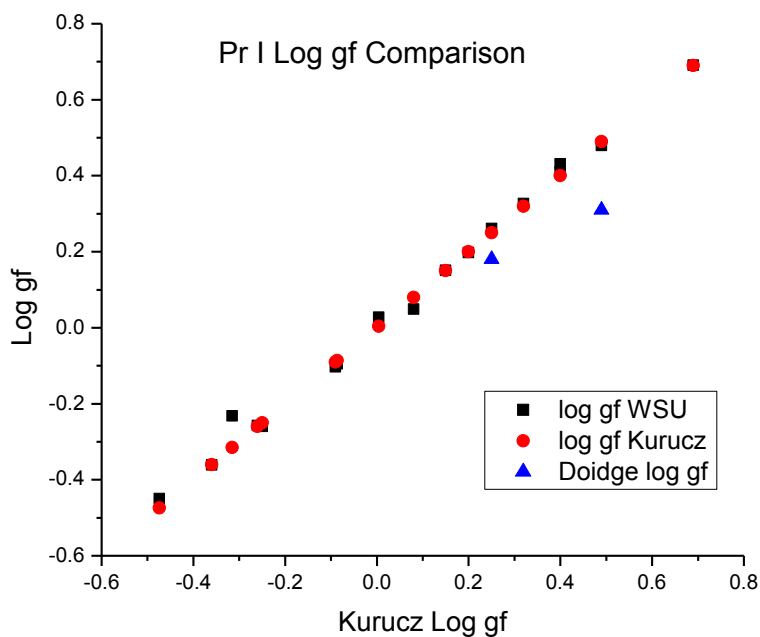


Figure 5.16 shows the agreement between the $\log(gf)$ values of this work (black squares) and those from the Kurucz database (red circles) and from Doidge et al. (blue triangles). All $\log(gf)$ values are plotted against the values of Kurucz in order to show any systematic trends.

Figure 5.17 is a histogram representation of the transition probability (gA) percent differences $(WSU - Kurucz)/Kurucz \times 100$ between this work and that of Kurucz and Bell. The histograms show the number of times a given percent difference was reported relative to complete agreement (zero percent difference). Again, the entire range of percent differences was partitioned according to branching ratio strength to see if agreement between this work and others' work varied with branching ratio strength. The idea being that weaker branches should have typically worse agreement since we have difficulty measuring them and overly-strong lines which we saw as blended will also have large percent differences. The radiative parameters presented above for Pr I are all from levels with only a single transition out of that state, therefore the branching ratios are all equal to one.

For all branches of Pr I we found that 63.2% of the reported percent differences agreed within $\pm 2.5\%$, 84.2% agreed within $\pm 7.5\%$, 89.5% agreed within $\pm 22.5\%$ and 100% agreed within $\pm 47.5\%$. The average percent difference for all branches between this work's gA values and those listed by Kurucz and Bell¹¹ is -3.5% . There is very good agreement between the gA values in our Pr I results and those of Kurucz and Bell, given that our uncertainty for these branches was 6.6% and a typical uncertainty of $\sim 5\%$ from lifetimes. In the case of Pr I all of the transition probabilities compared in the histogram stemmed from single-branch levels.

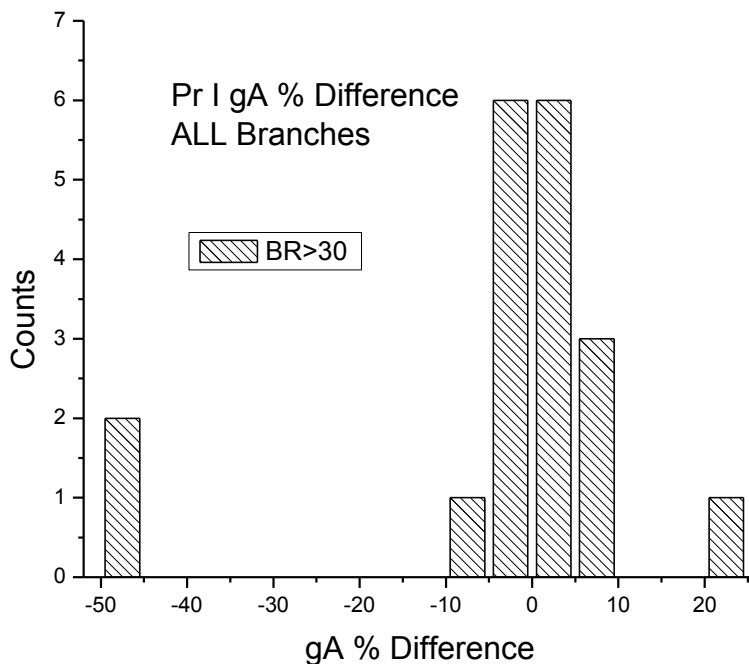


Figure 5.17 shows a histogram plot of the Pr I gA percent differences between this work and that of Kurucz and Bell. The number of occurrences are listed according to their distance away from zero percent difference.

5.6.5 - Singly-Ionized Praseodymium

In singly-ionized praseodymium (Pr II), the results show relatively poor agreement with prior works from Biemont et al.¹³ (DREAM project) and Li et al.¹⁵ (UWO). We believe that the occurrence of $\log(gf)$ values deviating from UWO's reported values is due to unobserved or problematic branches within a given upper energy state which directly affect the other "good" branches. For example in Pr II, we report 41 energy levels in table 5.6; of those 41 levels there were a total of 419 transitions, we observed 367 of these. 89 lines from these upper states were reported as weak, 8 were blended, and 21 were shouldered.

In total, we observed 551 transitions out of 87 upper energy states. These other levels were not listed due to a lack of atomic lifetimes. However the relative intensities for all lines observed are listed in appendix 1.

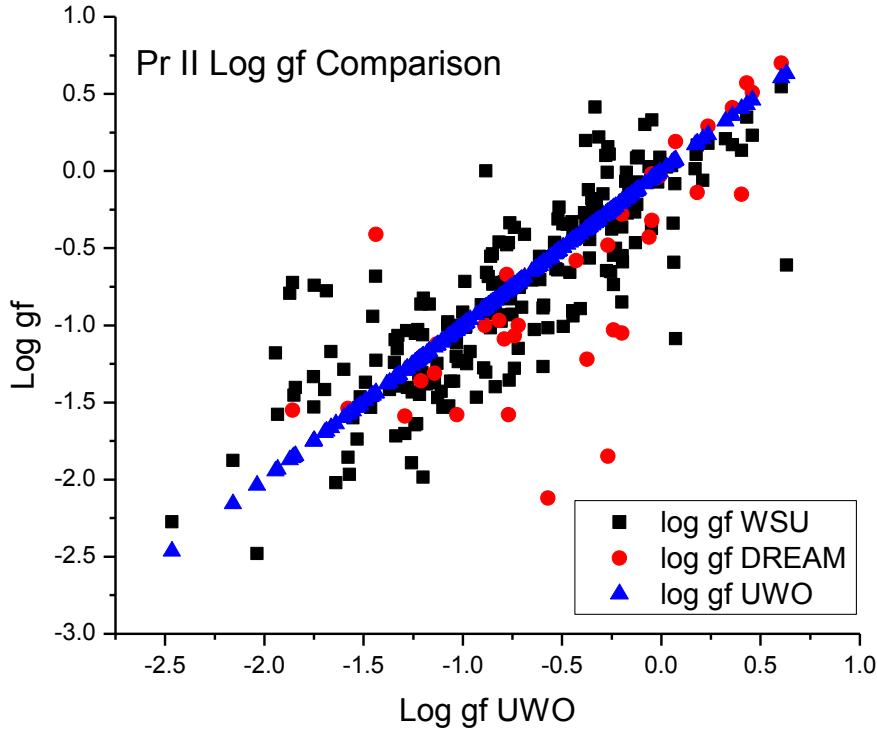


Figure 5.18 shows a comparison of $\log(gf)$ values from this work (black squares) against the work of the Biémont et al.¹³ associated with the DREAM project (red circles), and Li et al.¹⁵ associated with the group at UWO (blue triangles). All $\log(gf)$ values are plotted against the values from UWO in order to reveal any systematic trends.

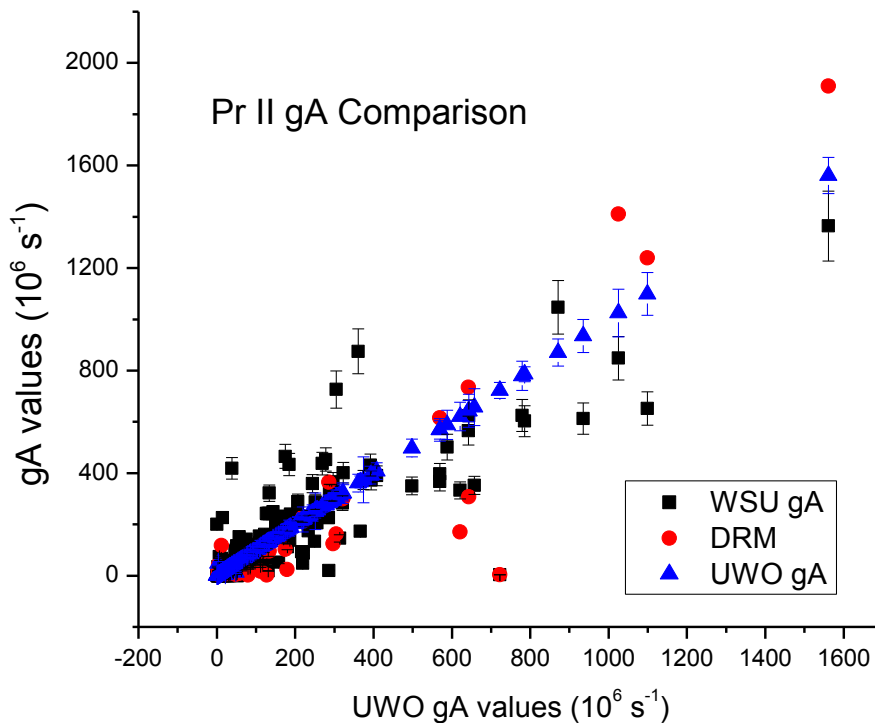


Figure 5.19 shows the comparison between gA values from this work (WSU black squares) the work of Biemont et al.¹³ associated with the DREAM project (red circles) and the results from Li et al.¹⁵ associated with the University of Western Ontario (blue triangles). The gA values are plotted against the gA values from UWO so that perfect agreement would result in a slope of 1 for all the data. The error bars shown in WSU data incorporate the error from lifetimes as well as uncertainties in this work.

Figures 5.20 – 5.22 are histogram representations of the Pr II transition probability (gA) percent differences $(WSU - UWO)/UWO \times 100$ between this work and that of Li et al.¹⁵ at (UWO). The histograms show the number of times a given percent difference was reported relative to complete agreement (zero percent difference). The entire range of percent differences

was partitioned according to branching ratio strength to see if agreement between this work and others' work does vary with branching ratio strength.

For those Pr II branches greater than 30%, I found that 19.3% of the values agreed with UWO within $\pm 7.5\%$, 34.6% agreed within $\pm 12.5\%$, 46.2% agreed within $\pm 17.5\%$, 53.9% agreed within $\pm 27.5\%$, 65.4% agreed within $\pm 32.5\%$, 77.0% agreed within $\pm 72.5\%$, 88.5% agreed within $\pm 102.5\%$ and all 100% of the values agreed within $\pm 167.5\%$. The average percent difference for branches greater than 30% was found to be 37.3%. Given that our stated uncertainty for this strength of branching ratio is 6.6% and that the uncertainty in the lifetimes from Li et al was $\sim 10\%$, the results show that we generally disagree with those transition probabilities from Li et al. There are some obvious outlying points on the positive side of zero showing that our data is overestimated compared to that of Li et al. I believe the overestimates are due to problematic lines in the spectrum. Again, the number of occurrences is not large.

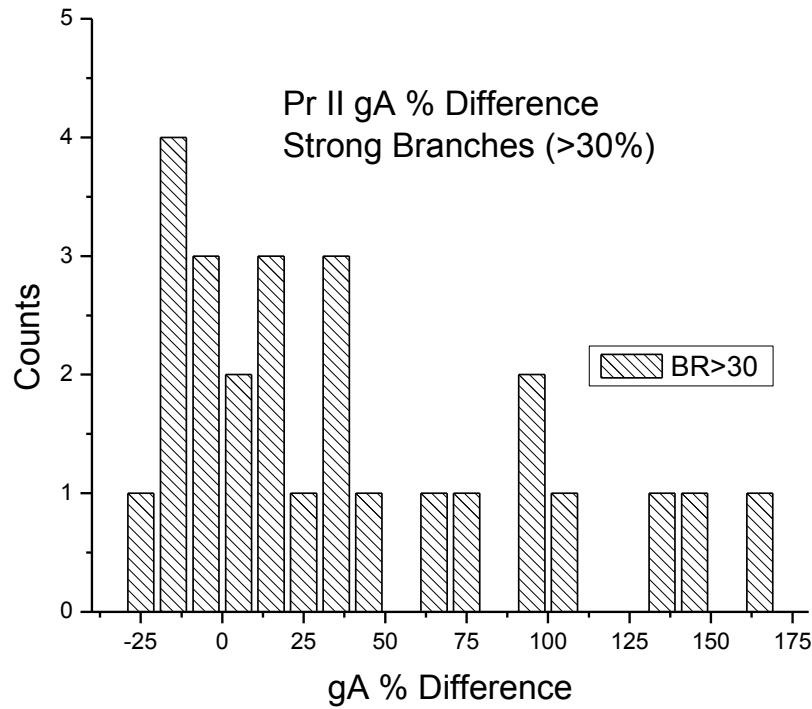


Figure 5.20 shows a histogram plot of the Pr II gA percent difference between this work and that of Li et al. for “strong” branches which are greater than 30 percent. The number of occurrences (counts) represents the number of reported branching ratio percent difference values which lie within the given bin size (10%).

For those Pr II branches which are between 30% and 10%, I found that 31.6% of the values agreed with UWO within $\pm 15\%$, 44.8% agreed within $\pm 25\%$, 55.3% agreed within $\pm 35\%$, 65.7% agreed within $\pm 45\%$, 76.2% agreed within $\pm 55\%$, and all 100% of the values agreed within a percent difference of $\pm 1285\%$. The average percent difference for branches greater than 30% was found to be 72.4%. Overall there is not very good agreement with the reported values from Li et al. for the moderate strength branches, since less than 31.6% of our values show agreement within our uncertainty. The reason for the general discrepancy is not apparent, although most of the values in this branching ratio bracket lie on the positive side of zero and

suggest some systematic issues within our system. This could be related to overestimates in the LIBS profile fitting procedures when problematic issues occur for neighboring lines.

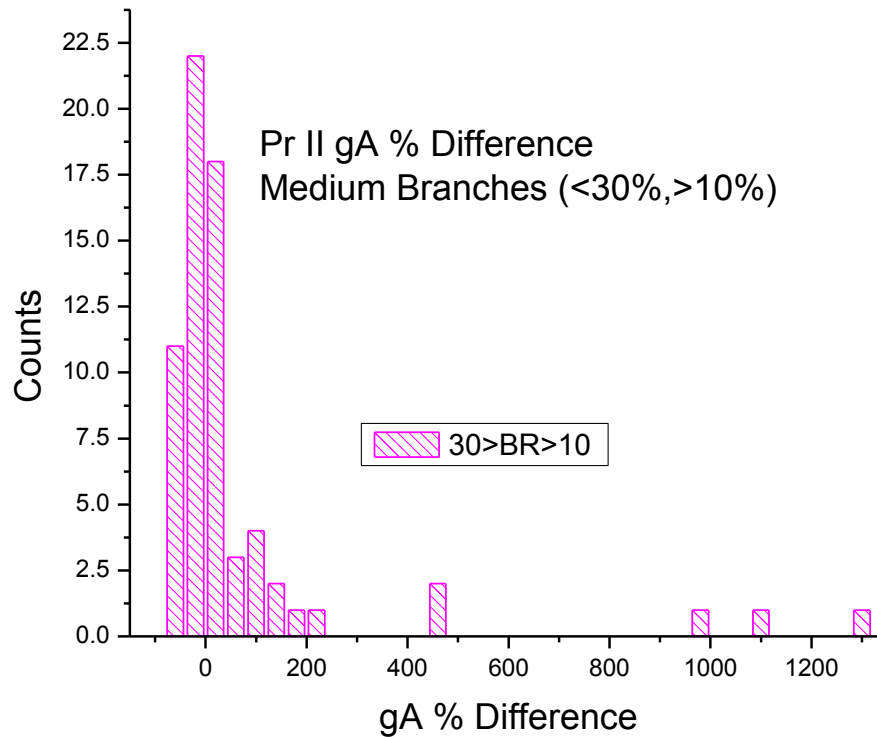


Figure 5.21 shows a histogram plot of the Pr II gA percent difference between this work and that of Li et al. for “medium” branches which are between 10 and 30 percent. The number of occurrences (counts) represents the number of reported branching ratio percent difference values which lie within the given bin size (40%).

For the branches of Pr II which are less than 10% I found that 24.6% of the values agreed with UWO within $\pm 20\%$, 41.6% agreed within $\pm 40\%$, 68.5% agreed within $\pm 60\%$, 85.0% agreed within $\pm 80\%$, and all 100% of the values agreed within $\pm 320\%$. The average percent

difference for branches weaker than 10% was found to be -10.5%. There is a general disagreement since less than half of the values lie within the stated uncertainty of our branches (19%) and the lifetimes (10%) from Li et al. which gives us an overall leeway of ~25%. The majority of the values resides on the negative side of zero and could be systematically showing that our weak values are sometimes underestimated. However this conclusion goes against the trend of overestimates in our outliers and it is difficult to generalize a reasonable conclusion as to why.

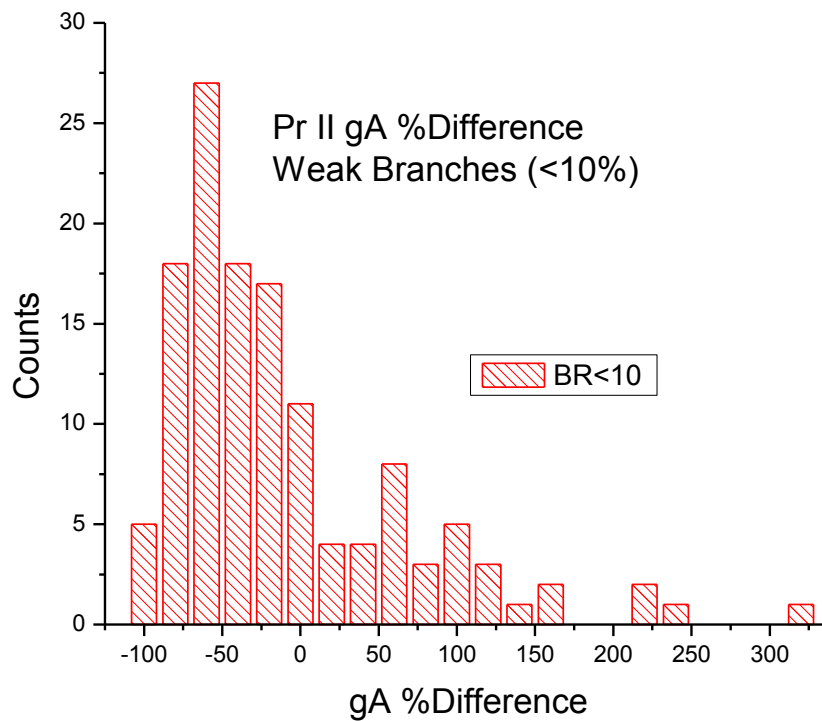


Figure 5.22 shows a histogram plot of the branching ratio percent difference between this work and that of Li et al. for “weak” Pr II branches which are less than 10 percent. The number of occurrences (counts) represents the number of reported branching ratio percent difference values which lie within the given bin size (20%).

5.6.6 - Doubly Ionized Praseodymium

The results of the radiative parameters in doubly ionized praseodymium (Pr III) show that there is strong disagreement between this work and the work of Biémont et al.¹⁷ (associated with the DREAM project) for the listed transitions in table 5.7.

In total there are 392 upper energy levels reported by Biémont et al. which we were able to detect at least most of the lines in our observed spectral range of 200 – 800 nm. Out of their total 407 upper energy levels reported by Biémont et al. there are some 17,000 reported $\log(gf)$ values, 6000 of which are outside of our spectral range. Of these other 11,000 lines we observe approximately 7,200. The relative intensities for these lines are reported in appendix 1.

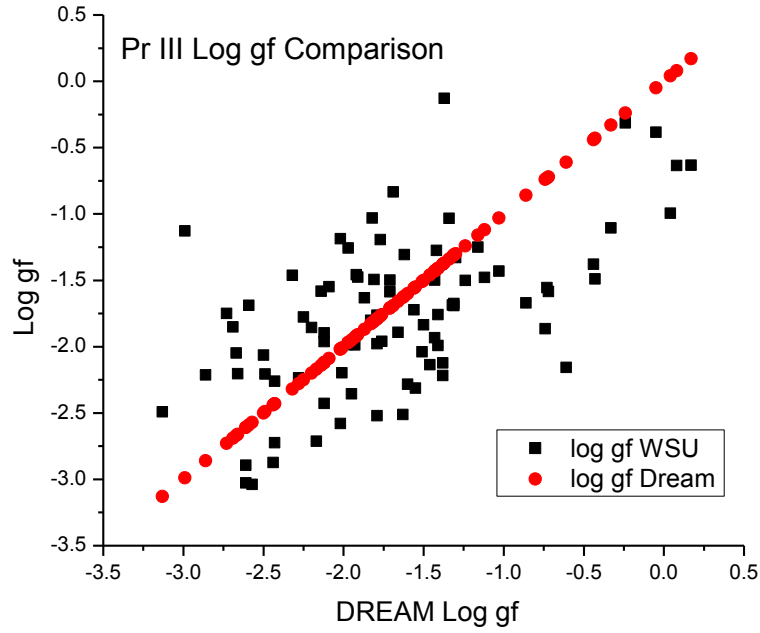


Figure 5.23 shows the $\log(gf)$ comparison between this work (black squares) and the work of Biémont et al.¹⁷ (red circles) associated with the DREAM project. All $\log(gf)$ values are plotted against the values of Biémont et al. in order to reveal any systematic trends and show the contrast between the two works.

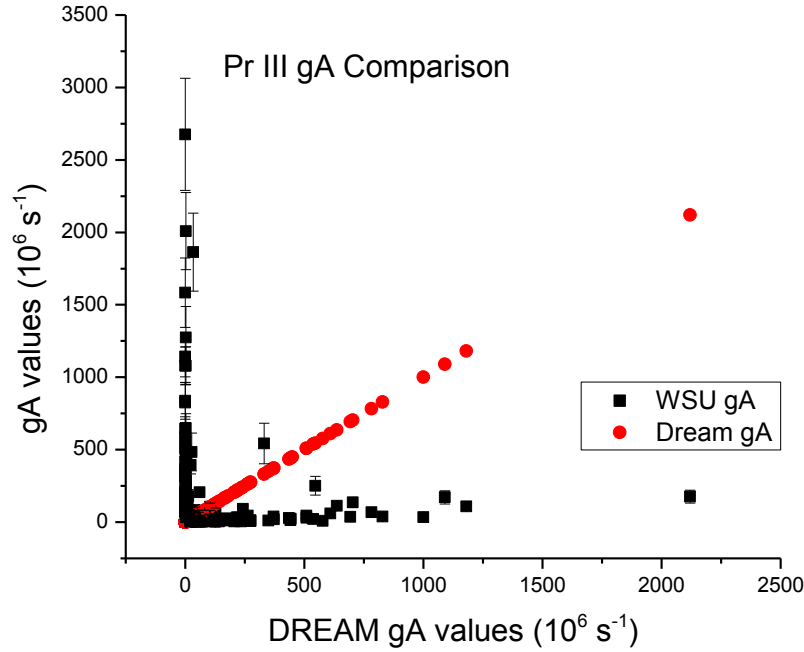


Figure 5.24 shows the gA values of this work (black squares) compared to the results of Biemont et al.¹⁷ associated with the DREAM project (red circles). Error bars shown in WSU data incorporate the error from lifetimes as well as uncertainties in this work.

Figure 5.25 and 5.26 are histogram representations of the Pr III transition probability (gA) percent differences $(WSU - DREAM)/DREAM \times 100$ between this work and that of Biemont et al. The histograms show the number of times a given percent difference was reported relative to complete agreement (zero percent difference). The entire range of percent differences was partitioned according to branching ratio strength to see if agreement between this work and others' work does vary with branching ratio strength. The idea being that weaker branches should have typically worse agreement since we have difficulty measuring them and overly-strong lines which we saw as blended will also have large percent differences.

Because of the fact that all of our reported values of Pr III had more than 20 emission lines per level the strength of the branches was very small. Because of this, there was only a single value whose branching ratio was larger than 30% of the total and it shows a percent difference of -92% with the value from Biémont et al. This doesn't agree within our uncertainty and I am confident the reason for the strong disagreement is due to shouldered and blended weak emission lines which are difficult for the ESAWIN 3000 fitting software to resolve properly.

For the Pr III branches which are between 30% and 10% I found that all values lie on the negative side of zero and 3.85% of the values agreed within 53.5%, 11.6% agreed within 80.5%, 23% agreed within 84.5%, 38.5% agreed within 90.5%, 73.1% agreed within 95.5%, and all 100% of the values agreed within 98.5%. The average percent difference for branches between 30% and 10% was found to be -90.2%. Overall there is very poor agreement with the reported value. The fact the percent difference values lie on the negative side of zero tells us that our estimates were smaller than those given by Biémont et al. The reason for these underestimates is not completely evident. It appears to be the trend that when we have many emission line lines from a given upper level and the majority of them are small branching ratios, we observe an overall negative percent difference; which suggests that the fitting software has misdiagnosed some branches to be overly large and thus diminishing the other branches from their proper values. I observed this to be the case in Pr III and found that we inaccurately measured branching ratios for 6 values to be larger than 30% while those branching ratios from Biémont et al. only list one single branch as greater than 30% from the same 6 levels. The average percent difference for these six branching ratios which we measured as larger than 30% was calculated to be 587,916%. All of these values were very much on the positive side of zero, ranging from 5481%

to 2,432,827%; indicating that we very much overestimated them. As stated throughout this thesis, the likely explanation of these discrepancies is due the poor accuracy in our ability to measure the weak and blended emission lines.

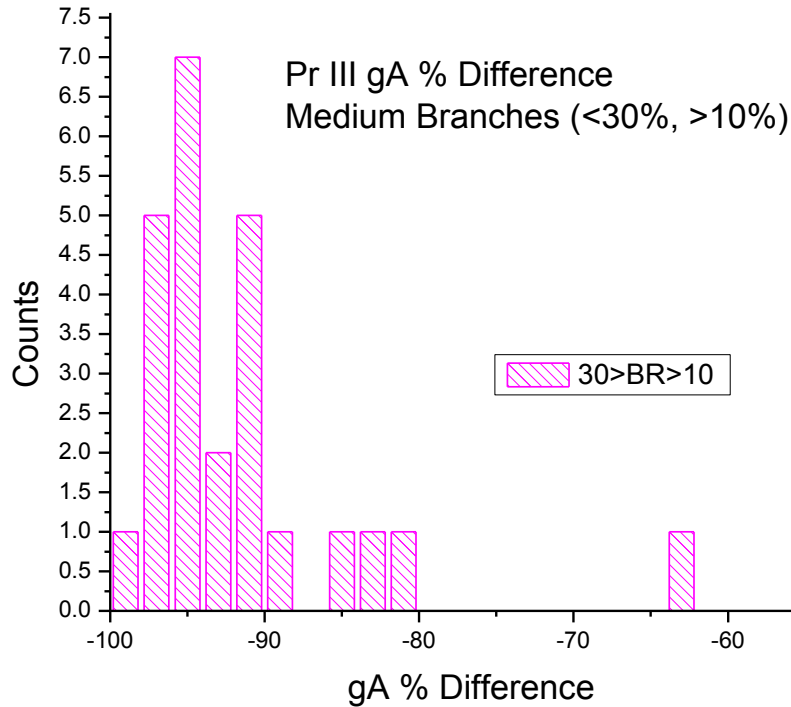


Figure 5.25 shows a histogram plot of the gA percent difference between this work and that of Biemont et al at DREAM for “medium” branches which are between 30 and 10 percent. The number of occurrences (counts) represents the number of reported gA percent difference values which lie within the given bin size (2%).

For those branches in Pr III which are less than 10% I found very poor agreement which is not worth going into detail to compare, the average percent difference was calculated to be

24,551%. When considering only those occurrences which lie within $\pm 1000\%$, which is the large bin near zero in figure 5.26, our results show that 64% of our values agree with Biemont et al values. Figure 5.26 shows the agreement, and as stated above I am fairly sure that the reason for the net overestimate is again due to inaccurate determinations of the large branches lying within one of the 7 Pr III levels thus affecting the smaller branches.

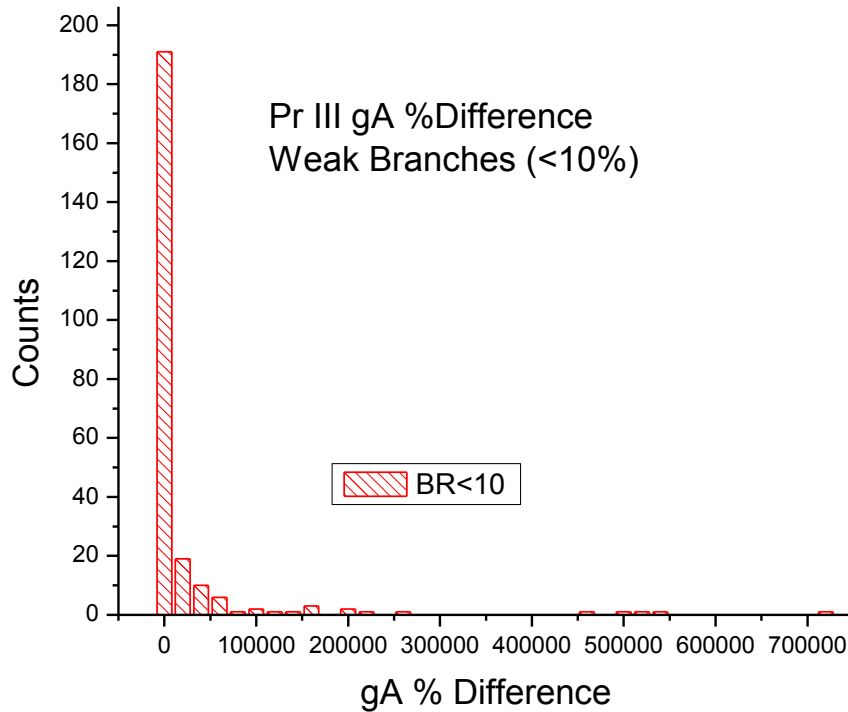


Figure 5.26 shows a histogram plot of the gA percent difference between this work and that of Biemont et al. at DREAM for “weak” branches which are less than 10 percent. The number of occurrences (counts) represents the number of branching ratio percent difference values which lie within the given bin range (20,000%).

5.7 - Summary

Overall, I am pleased with the agreement of values in Nd I despite some outliers and discrepancies among the weak branches. I found the average percent difference for Nd I branches greater than 30% was found to be 5.93% which lies within our stated uncertainty showing that we are able to measure the larger branches well when they are not affected by blending and shouldering lines. Most of the observed integrated-intensities of neutral neodymium were very small, and because of this fact it was sometimes the case that the branching ratio was inaccurate when there was more than one emission line from an upper level. This point is especially significant when considering that a fair amount (~15 levels) of the upper states in Nd I consisted of two or three allowed branches which were reported in the literature. As stated above, an accurate calculation of a branching ratio requires that all of the allowed branches from an upper level are accurately observed, if one of two emission lines are missing, depending on the strength of the unobserved line, it is likely that the branching ratio of the both line are affected and therefore the gA value and the corresponding $\log(gf)$ values will deviate from the correct value. Given that the experimental conditions for this experiment were optimized for singly ionized species, it is reasonable to expect that the unobserved lines due to poor signal to noise affected some of the Nd I values. It is possible that in the future, another measurement campaign may be conducted with parameters optimized to increase the signal-to-noise ratio of neutral emission lines. It is worth noting that for the Nd I levels with single emissions we show an absolute-value percent difference of 20% which is relatively good and since our measurements cannot be the contributing factor to these discrepancies (since the branching ratio for both groups' will be 1) it shines light on the fact that the lifetimes used in our

calculations might not be as accurate as one would like, giving a bit more leeway and room for acceptance in our determinations.

For strong branches in Nd II, the results show that we generally disagree with the Li et al. transition probabilities, since less than 25% of the values agree within our error budget of 6.6% and the incorporated ~5% uncertainty stated for most of the lifetimes. The medium branches show a general disagreement with the values from Li et al. given that only 22.3% of the values lie within $\pm 15\%$ which is close to our error budget. In the weak branches of Nd II only 35.0% of our values lie within $\pm 30\%$ which is very close to our allowed uncertainty. Overall there was a common overestimate in the outlying values of Nd II showing that our transition probabilities are larger than those of Li et al. The reason for the overall disagreement of our values is not clear; however I believe that these over estimates are related to difficulties in resolving spectral lines.

In the case of Nd III most of the emission lines from the upper levels were inaccurate due to unobserved weak transitions from parent levels, making up a majority of the branches and therefore disqualifying the use of the observed lines for branching ratio and transition probability calculations. For the single level which we did see, the two lines show underestimates in their calculated values. The weaker branch had a percent difference of -42% and the larger -36% which is not good agreement. However, the branching ratios between the two groups show that the percent difference is -8.8% for the weak transition and 0.7% for the larger transition, which lead me to again question the accuracy of the lifetimes reported. The stated uncertainty in the lifetime was reported as 7.7% but the large discrepancy between our work shows that further investigation is required in the accuracy of these lifetimes. Since Nd III has very scarce published atomic data there were no other “reliable” lifetimes to compare to.

For the transition probabilities of Pr I there were only single-transition levels to consider, thus eliminating the possibility of weak, moderate and strong discrimination. The results show that there is very good agreement between the gA values in our Pr I results and those of Kurucz and Bell, given that our uncertainty for these branches was 9.3% and a typical uncertainty of ~5% from lifetimes.

In singly-ionized praseodymium (Pr II), the results for the strong branches show relatively poor agreement with prior works from Li et al. since 34.6% lie within $\pm 12.5\%$ which is near our allotted uncertainty when including the lifetimes' uncertainty. The medium strength emission lines show that 31.6% of the values lie within $\pm 15\%$ signifying an overall disagreement between our reported values. In the weak branches only 24.6% of the values lie within $\pm 20\%$ and 41.6% lie within $\pm 40\%$ showing that there are a majority of disagreeing values between this work and that of Li et al. In Pr II some of the lifetimes had very large uncertainties. For example, the $28,009\text{ cm}^{-1}$ level had a reported lifetime of 6.97 ns with an uncertainty of ± 21 ns, and the $28,577\text{ cm}^{-1}$ level lists a lifetime of 7.03 ns with an uncertainty of ± 28 ns. These factors contribute to the minority of calculated percent differences, but one can definitely conclude that a certain amount of leeway should be given to any reported oscillator strength or transition probability which must incorporate these lifetimes with branching ratios. Overall I am fairly pleased with the results of our Pr II radiative parameters since many of the lines are publishable.

In doubly-ionized praseodymium (Pr III) we show very poor agreement with Biémont et al. I believe the discrepancy to be due to the large overestimates from blended lines which are inaccurately registered as large branches, which therefore diminish the branching ratio of the already weak emission lines and thus cause very large discrepancies within the moderate and

weak branches. We believe that the reason for the disagreement in $\log(gf)$ and gA values is due to the fact that of the 7 upper energy states which had reported lifetimes (shown in table 5.7) there is an average of 51 emission lines per upper level and most of these emission lines are very weak having an average $\log(gf)$ value of $\log(gf) = -2.17$ according to the reported data from Biémont et al.¹⁷ There is an average $\log(gf)$ value of -2.89 for all of the listed transitions weaker than -2.00 and for those listed that are greater than -2 the average is -1.21 reported by Biémont et al. As already noted one of the weaknesses of this work is measuring weaker lines and due to this fact we believe our results in Pr III deviate from the reported values. Furthermore, of the reported 7 levels and 359 emission lines in this work, which are shown in table 5.7, there were 29 emission lines which Biémont et al. reports as having $\log(gf)$ values stronger than -1.00 which were beyond our detectable spectral range below 200.000 nm.

In conclusion it is worth stating that I was never counting on 100% agreement within all brackets of branching ratio strength and within each ionization state for any of the elements in this work. Instead, I am looking for, at the very least, a few good levels without signs of strong blending in order to publish some radiative parameters in these rare earth metals. It is good to keep in mind that it is not uncommon for researchers in this area of atomic physics to only publish emissions from a single upper level. With that in mind, the fact that I see many good transitions within many levels of neutral, singly-ionized and doubly-ionized states of neodymium and praseodymium is very encouraging for the use of LIBS in further efforts to help astrophysicists in need of atomic data.

-
- ¹ G.M. Wahlgren, “The lanthanide elements in stellar and laboratory spectra,” *Phys. Scr.* **T100**, 22-36 (2002).
- ² L. Dolk, G.M. Wahlgren, H. Lundberg, Z.S. Li, U. Litzen, S. Ivarsson, I. Ilyin, S. Hubrig, “The presence of Nd and Pr in HgMn stars,” *A&A* **385**, 111-130 (2002).
- ³ V.N. Gorshkov and V.A. Komarovskii, “Lifetimes of Pr I and Pr II excited levels. Oscillator strengths of Pr I spectral lines,” *Opt. Spectrosc.* **58**, 561 (1985).
- ⁴ M. Song, Y. P. Li, W.X. Peng, Z.K. Jiang, C. Guo, Y.N. Yu, “Radiative lifetime measurements of Pr atoms by observing time-resolved laser-induced fluorescence,” *Eur. Phys. J. D* **2**, 115-116 (1998).
- ⁵ E. Biemont, P. Quinet, S. Svanberg, H.L. Xu, “Experimental lifetime determination in neutral praseodymium (Pr I) and neodymium (Nd I),” *J. Phys. B* **37**, 1381-1389 (2004).
- ⁶ B. Furmann, A. Krzykowski, D. Stefanska, J. Dembczynski, “New levels and hyperfine structure evaluation in neutral praseodymium,” *Phys. Scr.* **74**, 658–669 (2006).
- ⁷ W.F. Meggers, C.H. Corliss, B.F. Scribner, *Tables of Spectral-Line Intensities*, NBS Monograph 145, Parts I and II, US Government Printing Office, Washington, DC, (1961).
- ⁸ T. Andersen and G. Sorensen, “Determinations of atomic lifetimes for the rare earth ions: PrII, TmII, LuII, CeIII,” *Sol. Phys.* **38**, 343-350 (1974).
- ⁹ C.S. Lage and W. Whaling, “Transition probabilities in Pr(II) and the solar praseodymium abundance,” *J. Quant. Spectrosc. Radiat. Transfer* **16**, 537-542 (1976).
- ¹⁰ A. Goly, J. Kusz, B. Nguyen Quang, S. Weniger, “Transition probabilities of Pr II-lines emitted from a ferroelectric plasma source,” *J. Quant. Spectrosc. Radiat. Transfer* **45**, 157-163 (1991).

-
- ¹¹ R.L. Kurucz and B. Bell, *Atomic Line Data, Kurucz CD-ROM No. 23*, Smithsonian Astrophysical Observatory, Cambridge, MA, (1995).
- ¹² S. Ivarsson, U. Litzen, G.M. Wahlgren, “Accurate wavelengths, oscillator strengths and hyperfine structure in selected praseodymium lines of astrophysical interest,” *Phys. Scr.* **64**, 455-460 (2001).
- ¹³ E. Biemont, P.H. Lefebvre, P. Quinet, S. Svanberg, H.L. Xu, “Radiative lifetime measurements and oscillator strengths determination for transitions in singly ionized praseodymium (Pr II),” *Eur. Phys. J. D* **27**, 33-41 (2003).
- ¹⁴ B. Furmann, D. Stefanska, J. Dembczynski, E. Stachowska, “New levels and hyperfine structure evaluation in singly ionized praseodymium,” *Phys. Scr.* **72**, 300-308 (2005).
- ¹⁵ R. Li, R. Chatelain, R.A. Holt, S.J. Rehse, S.D. Rosner, T.J. Scholl, “Oscillator strength measurements in Pr II with the fast-ion-beam laser-induced-fluorescence technique,” *Phys. Scr.* **76**, 577–592 (2007).
- ¹⁶ P. Palmeri, P. Quinet, Y. Fremat, J.F. Wyart, E. Biemont, “Theoretical oscillator strengths in Pr III and application to some CP stars,” *Astrophys. J. Suppl. Series* **129**, 367-376 (2000).
- ¹⁷ E. Biemont, H.P. Garnir, P. Palmeri, P. Quinet, Z.S. Li, Z.G. Zhang, S. Svanberg, “Core-polarization effects and radiative lifetime measurements in Pr III,” *Phys. Rev. A.* **64**, 002503 (2001).
- ¹⁸ C.H. Corliss and W.R. Bozman, “Experimental transition probabilities for spectral lines of seventy elements,” *Nat. Bur. Stand. Monogr.* **53**, (1962).
- ¹⁹ N.P. Penkin and V.A. Komarovskii, “Relative values of oscillator strengths of Nd I spectral lines,” *Opt. Spectrosc.* **35**, 4-8 (1973).

-
- ²⁰ J. Marek and H.J. Stahnke, "Radiative lifetimes of optical levels of neutral erbium, gadolinium, and neodymium," *Z. Phys. A* **298**, 81-25 (1980).
- ²¹ V.N Gorshkov, V.A. Komarovskii, A.L. Osherovich, N.P. Perkin, "Lifetimes of excited levels of Nd I and Nd II. Oscillator strengths of the spectral lines of Nd II," *Astrophys. (USSR)* **17**, 437-441 (1982).
- ²² E.A. Den Hartog, A.J. Fittante, J.E. Lawler, "Radiative lifetimes of neutral neodymium," *J. Phys. B* **44**, 225011 (2011).
- ²³ W.F. Meggers, C.H. Corliss, B.F. Scribner, *Tables of Spectral-Line Intensities*, NBS Monograph 145, Parts I and II. U.S. Government Printing Office, Washington DC, (1975).
- ²⁴ C.H. Corliss and W.R. Bozman, *Experimental transition probabilities for spectral lines of seventy elements*, Monograph 53, U.S. National Bureau of Standards, Washington DC, (1962).
- ²⁵ R.S. Maier and W. Whaling, "Transition probabilities in Nd(II) and the solar neodymium abundance," *J. Quant. Spectrosc. Radiat. Transfer* **18**, 501-507 (1977).
- ²⁶ T. Andersen, O. Poulsen, T.S. Ramanujam, A.P. Petkov, "Lifetimes of some excited states in the rare earths: La II, Ce II, Pr II, Nd II, Sm II, Yb I, Yb II, and Lu II," *Sol. Phys.* **44**, 257 (1975).
- ²⁷ L. Ward, O. Vogel, A. Ahnesjo, A. Arnesen, R. Hallin, L. McIntyre, C. Nordling, "Radiative lifetimes in Nd II and the solar neodymium abundance," *Phys. Scr.* **29**, 551-556 (1984).
- ²⁸ C.M. Pinciuc, R.C. Rivest, M.R. Izawa, R.A. Holt, S.D. Rosner, T.J. Scholl, "Measurement of radiative lifetimes in Nd II," *Can. J. Phys.* **79**, 1159-1167 (2001).
- ²⁹ T.J. Scholl, R.A. Holt, D. Masterman, R.C Rivest, S.D. Rosner, A. Sharikova, "Measurement of radiative lifetimes in Pr II and Nd II," *Can. J. Phys.* **80**, 713-722 (2002).

-
- ³⁰ H.L. Xu, S. Svanberg, R.D. Cowan, P.H. Lefebvre, P. Quinet, E. Biemont, “Theoretical and experimental lifetime and oscillator strength determination in singly ionized neodymium (Nd II),” *Mon. Not. R. Astron. Soc.* **346**, 433-440 (2003).
- ³¹ E.A. Den Hartog, J.E. Lawler, C. Sneden, J.J. Cowan, “Improved laboratory transition probabilities for Nd II and application to the neodymium abundances of the sun and three metal-poor stars,” *Astrophys. J. Suppl. Ser.* **148**, 543-566 (2003).
- ³² E. Biemont, A. Ellmann, P. Lundin, S. Mannervik, L.O. Norline, P. Palmeri, P. Quinet, D. Rostohar, P. Royen, P. Schel, “Decay of metastable states in Nd II,” *Eur. Phys. J. D* **41**, 211-219 (2007).
- ³³ S.J. Rehse and C.A. Ryder, “Laser-induced breakdown spectroscopy for branching ratio and atomic lifetime measurements in singly-ionized neodymium and gallium,” *Spectrochim. Acta B* **64**, 974–980 (2009).
- ³⁴ G.M. Wahlgren, “The lanthanide elements in stellar and laboratory spectra,” *Phys. Scr.* **T100**, 22-36 (2002).
- ³⁵ C.R. Cowley and D.J. Bord, “The third spectrum of neodymium: application to HR 6870 and gamma-Equulei,” *ASP Conf. Series.* **143**, 346-349 (1998).
- ³⁶ D.J. Bord, “Ab initio calculations of oscillator strengths and Lande factors for Nd III,” *Astron. Astrophys. Suppl. Ser.* **144**, 517-522 (2000).
- ³⁷ Z.G. Zhang, S. Svanberg, P. Palmeri, P. Quinet, E. Biemont, “Measurement of lifetimes by laser-induced fluorescence and determination of transition probabilities of astrophysical interest in Nd III,” *A&A* **385**, 724-734 (2002).

-
- ³⁸ K.B. Blagoev and V.A. Komarovskii, “Lifetimes of levels of neutral and singly ionized lanthanide atoms,” *At. Data Nucl. Data Tables* **56**, 1–40 (1994).
- ³⁹ V.N. Gorshkov, V.A. Komarovskii, A.L. Osherovich, N.P. Penkin, “Lifetimes of excited levels of Nd I and Nd II. Oscillator strengths of the spectral lines of Nd I,” *Astrophysics* **17**, 437–441 (1982).
- ⁴⁰ K.B. Blagoev and V.A. Komarovskii, “Lifetimes of levels of neutral and singly ionized lanthanide atoms,” *At. Data Nucl. Data Tables* **56**, 1–40 (1994).
- ⁴¹ P.S. Doidge, “A compendium and critical review of neutral atom resonance line oscillator strengths for atomic absorption analysis,” *Spectrochim. Acta, B* **50**, 209–263 (1995); Errata: **50**, 1421–1422 (1995); **51**, 375 (1996).
- ⁴² R. Li, S.J. Rehse, T.J. Scholl, A. Sharikova, R. Chatelain, R.A. Holt, S.D. Rosner, “Fast-ion-beam laser-induced-fluorescence measurements of branching fractions and oscillator strengths in Nd II,” *Can. J. Phys.* **85**, 1343–1379 (2007).

Chapter 6 – Gadolinium & Samarium

6.1 - Introduction

As explained in Chapter 5, astrophysically relevant radiative parameters in lanthanide elements (including gadolinium and samarium) are required for better understanding the performance of lanthanide-containing metal halide-high intensity discharge (MH-HID) lamps. Transition probabilities of Gd I and Sm I are currently meager and this work aims at furthering radiative parameters in these elements in an effort to support such interests.

6.2 - Previous works

6.2.1 - Previous work in Gadolinium

Considering the more recent and more accurate work in neutral gadolinium, in 1993 Nishimura et al.¹ produced oscillator strengths for six lines in Gd I using laser-absorption in an atomic vapor. In 1995, Bisson et al.² measured Gd I branching ratios and transition probabilities using a photo-ionization method which incorporates the use of two dye lasers in order to populate the excited level of interest. Miyabe et al.³ produced lifetimes and branching ratios in neutral gadolinium in 1997 using a three step ionization process, in their paper it is noted that information on oscillator strengths in this species is limited. Xu et al.⁴ in 2003 determined lifetimes in 25 levels of Gd I level and 13 levels in Gd II using time-resolved laser-induced fluorescence (LIF). In 2011, Den Hartog et al.⁵ measured lifetimes in 136 levels of neutral gadolinium, 93 of which were measure for the first time and with good accuracies. The levels ranged from 17,750 to 36,654 cm^{-1} . A short time later in 2011, J.E. Lawler et al.⁶ used these 136

lifetimes in Gd I to generate 1290 branching fractions and many $\log(gf)$ values for lines in neutral Gd I by using Fourier transform spectroscopy (FTS) on a slow atomic beam.

Gorshkov and Komarovskii⁷ determined lanthanide content in the solar photosphere in 1986 and showed $\log(gf)$ values for two emission lines in singly ionized gadolinium Gd II. In 1988, Bergstrom et al.⁸ measured lifetimes for 3 upper energies using the fluorescence from a pulsed laser; a resulting 23 transition probabilities were reported. Zhang et al.⁹ measured 20 lifetimes in Gd II from levels having energies between 29,045 and 34,178 cm^{-1} and 5 lifetimes in Gd III from levels between 43,019 and 48,339 cm^{-1} using time-resolved LIF in a laser-induced plasma. In 2002 Xu et al.⁴ measured 13 excited levels in Gd II with time-resolved LIF in a gadolinium laser-induced plasma with uncertainties in the lifetimes near 5%. Lastly, in 2006 Den Hartog et al.¹⁰ provided 611 transition probabilities by determining 63 accurate lifetimes in singly ionized gadolinium and applied these more accuracies transition probabilities to determine the gadolinium abundance in some metal-poor stars.

The list of work determining radiative parameters in doubly ionized gadolinium is quite scarce but it begins in 1996 with transition probabilities derived from theoretical Hartree-Fock calculations by J. Sugar through private communication with Morton¹¹ who published Sugar's results in a large tabulation of atomic data in 2000. In 2001 Zhang et al.⁹ measured 5 lifetimes with good accuracies in Gd III as stated above. Lastly, Biémont et al.¹² determined theoretical lifetimes for five levels in Gd III determined using HFR with core polarization effects. The resulting transition probabilities and $\log(gf)$ values were presented for some 43 lines.

6.2.2 - Previous Works in Samarium

Hannaford and Lowe¹³ in 1984 measured radiative lifetimes in 4 levels of neutral samarium (Sm I) by time-resolved laser-induced fluorescence (LIF). Lucas et al.¹⁴, in 1997, performed oscillator strength measurements in Sm I using absorption spectroscopy and branching ratios were calculated as a result. Theoretical lifetimes were calculated by Porsev¹⁵ in 1997 using a Hartree-Fock-Dirac code to perform the calculations and the results were in good agreement with previous lifetimes. In 1999, Rochester et al.¹⁶ measured lifetimes of levels between 13,796 and 18,503 cm^{-1} using beam-laser LIF in Sm I. Shah et al.¹⁷ measured lifetimes and the resulting $\log(gf)$ and transition probabilities in 2010 by LIF on seven odd parity levels and six step-wise-excited even parity levels. Beck and O'Malley¹⁸ in 2010, determined transition probabilities and $\log(gf)$ values for some magnetic dipole transitions in the spectrum of neutral samarium. Zhang et al.¹⁹ in 2010 produced lifetimes in 79 levels of Sm I between 18,985 and 34,189 cm^{-1} using time-resolved LIF on a samarium atomic beam. Later in the same year, Zhang et al.²⁰ again measured lifetimes in neutral samarium this time for 64 odd parity levels between 21,243 and 34,723 cm^{-1} with the same apparatus.

Radiative properties from singly ionized samarium have been used in calculating abundances for 21 red giants of the galactic halo by Luck et al.²¹ and in 1981, the $\log(gf)$ values used were determined from solar radiation. In 1986 Gorshkov and Komarovskii²², determined the lanthanide content in the sun's photosphere and listed corresponding lifetimes for five levels in Sm II. In 1988, Vogel et al.²³ measured 18 lifetimes for Sm II using time a resolved beam-laser technique incorporating LIF, the lifetimes were used to calculate $\log(gf)$ values and a solar abundance of samarium was determined. Biémont et al.²⁴ in 1990 determined 35 lifetimes in levels ranging from 21,251 to 30,880 cm^{-1} in Sm II by LIF from a sputtered metal vapor source,

oscillator strengths and solar abundance calculations were derived from these new levels. Scholl et al.²⁵ in 2002 measured 82 lifetimes in Sm II using the beam-laser method with good uncertainties near 7%. A year later, Xu et al.²⁶ determined 47 lifetimes using LIF and combined these with Hartree-Fock calculations in order to determine transition probabilities for 162 lines in Sm II. In 2006, Rehse et al.²⁷ using a fast-ion-beam LIF method determined branching ratios and oscillator strengths for 69 levels in Sm II with accuracies on the order of 10%. Also in 2006, Lawler et al.²⁸ determined transition probabilities for more than 900 lines of Sm II and lifetimes for 212 odd-parity levels, which helped to determine a more accurate abundance of samarium in the sun and three metal-poor stars. Following this work in 2008, Lawler et al.²⁹ provided a comparison of transition probabilities in Sm II between his work in 2006 and the work accomplished by Rehse et al.²⁷ which showed overall good agreement between the two works.

There are very few reported radiative parameters for doubly-ionized samarium of relevant for astrophysical interests. The first comes from Dzuba et al.³⁰ in 2003, which shows energy levels and lifetimes for a few lanthanides, however no reported values were shown, only a mention that work in Sm III and other doubly-ionized species were used to confirm their accuracies. In 2003 Biémont et al.³¹ published lifetimes using LIF and oscillator strengths as determined from Fourier transform spectroscopy for Sm III.

This work is aimed at furthering the measurements of radiative parameters relevant to astrophysical studies by using laser-induced breakdown spectroscopy on gadolinium and samarium samples. By obtaining relative values of emission-line intensities in a laser-produced plasma, radiative parameters were determined. Radiative parameters (e.g. relative intensities, branching ratios, $\log(gf)$ values, and gA values) in Gd I, II, III and Sm I, II, III are presented in

the tables below and compared to previous works by converting the relative transition probabilities to an absolute scale using lifetimes from previous works.

6.3 - Experimental Setup / Data Analysis / Uncertainties

The experimental setup, analysis of data, and determination of uncertainties were all thoroughly described in Chapter 5. The measurements on gadolinium and samarium described in this chapter were all performed utilizing exactly the same apparatus, procedures and uncertainties. Therefore the information is not repeated here.

6.4 - Results

In LIBS spectra it is sometimes the case that line profiles are unresolved due to blending of emission lines with neighboring lines or weak signal to noise. Because of this fact some of the branching ratios are incalculable, and therefore we list the relative intensities of all of our measured lines with annotations for the strong, blended, shouldered, or weak lines.

Branching ratios (BR), transition probabilities $g_u A_{ul}$, and $\log(gf)$ values for samarium are listed in tables 6.1, 6.2 and 6.3 according to ionization state and energy level and are compared to previous results. Branching ratios (BR), transition probabilities $g_u A_{ul}$, and $\log(gf)$ values for gadolinium are listed in tables 6.4, 6.5 and 6.6 according to ionization state and energy level and are compared to previous results. In this work only transitions between the spectral range of 200-800nm were observed and the corresponding radiative parameters presented.

Sm I Data

Table 6.1 shows the radiative parameters for Sm I

Lifetimes are adopted from Zhang et al.^{19,20} unless otherwise noted

w denotes weak emission line

s denotes shouldered emission line

b denotes blended emission line

H denotes lifetime from Hannaford et al.¹³

S denotes lifetime from Shah et al.¹⁷

Komar refers to the work by Komarovskii et al.³⁴

Shah refers to the work by Shah et al.¹⁷

Kurucz refers to the work by Kurucz and Bell.³³

Upper Energy (cm ⁻¹)	Lifetime (ns)	wavelength (nm)	Branch Ratio	BR Error		A _{ki} (10 ⁶ s ⁻¹)				
						This work	A Error	Kurucz	Shah	Komar.
16690.76	1710H	598.968	0.495	0.050	b	0.317	0.035	0.2831		
		609.655	0.360	0.037	w	0.231	0.025	0.1246		
		629.5948	0.144	0.016	w	0.093	0.011	0.1773		
17769.71	136S	562.5992	0.353	0.040		3.140	0.387	4.23	5.6	3.9
		572.0176	0.279	0.030	w	2.409	0.297	0.578	1.1	1.21
		589.5361	0.366	0.038	w	3.007	0.371	0.5149	0.7	0.4
17810.85	342H	570.6743	1.000	0.093	s	1.754	0.193	0.9797		
17830.8	1100H	587.4199	0.781	0.084	w	0.817	0.106	0.3925		
		611.779	0.219	0.026	s	0.230	0.032	0.2386		
		642.5905	-	-	-	-	-	0.3547		
18225.13	143S	548.5405	0.162	0.017	w	1.132	0.141	4.134	4	4.4
		557.4904	0.314	0.029		2.192	0.255	1.615	2.7	2.2
		574.1174	0.525	0.049		3.669	0.427	0.6498	0.3	0.2
18475.28	63S	549.8206	0.655	0.061		10.400	1.272	5.412	0.5	
		565.9866	0.345	0.032	w	5.473	0.669	8.793	4.5	6
18788.08	121S	540.5218	0.687	0.066		5.859	1.028	5.474	4.3	5.7
		556.1379	0.313	0.030	w	2.673	0.469	0.6019	2	0.65
		577.9235	-	-	-	-	-	1.731	1.9	1.5

18948.78	308H	551.2102	0.309	0.074		2.574	0.254	2.819		
		599.5093	0.691	0.064	b	2.244	0.221	0.4048		
18985.7	343	526.5657	0.223	0.053	w	1.648	0.158	1.227		
		534.8074	0.468	0.036	w	1.144	0.110	1.575		
		550.0904	0.308	0.030	w	0.934	0.090	0.4158		
19009.52	46S	534.1268	0.253	0.026		5.493	0.614	4.939	6.3	4.9
		549.3704	0.443	0.041		9.639	0.990	11.75	8.6	11
		570.6189	0.304	0.028		6.606	0.678	4.288	6.8	
19501.27	110H	534.9153	0.278	0.029	s	0.162	0.018	0.8896		
		555.0399	0.467	0.043		0.273	0.028	5.85		
		580.2835	0.256	0.026	w	0.150	0.017	2.391		
19776.97	40H	527.139	0.355	0.033		8.864	0.936	16.98		
		546.6721	0.392	0.036		9.810	1.036	7.069		
		571.1435	0.253	0.026		6.326	0.724	0.8004		
20091.03	49.6	497.5957	0.852	0.079		17.175	1.770	18.54		
		504.9493	0.148	0.015	w	2.987	0.335	2.756		
20163	380H	535.3708	0.027	0.006	w	0.073	0.017	0.07751		
		558.8191	0.661	0.063		1.778	0.190	0.8752		
		586.7766	0.311	0.030		0.839	0.090	1.749		
20712.83	33H	520.0578	0.910	0.085		27.571	2.697	28.41		
		542.1563	0.090	0.021	s	2.732	0.642	1.894		
21062.82	150H	532.0576	0.639	0.059		4.259	0.421	4.972		
		557.3409	0.361	0.034		2.408	0.238	1.731		
21243.3	479	506.0919	1.000	0.093	w	2.088	0.199	2.149		
21458.89	74H	545.3001	0.754	0.070		10.195	0.987	10.97		
		573.2937	0.246	0.025	w	3.319	0.353	2.569		
21599.84	87H	517.2735	0.315	0.029		3.616	0.346	8.651		
		541.1397	0.196	0.020		2.250	0.237	2.593		
		568.6969	0.490	0.046		5.628	0.539	0.6364		

22160.84	83H	525.1914	0.404	0.038		4.864	0.485	12.06
		551.1093	0.596	0.055	s	7.184	0.717	1.266
22491.94	33.3	450.3371	0.373	0.035		11.212	1.086	14.72
		461.125	0.627	0.058		18.818	1.822	6.27
22632.3	8.3	458.1588	0.364	0.034		43.800	4.588	22.32
		472.8431	0.322	0.030		38.757	4.060	55.76
		491.0411	0.315	0.029		37.925	3.972	55.02
22643.12	39H	512.2138	0.709	0.066		18.188	1.755	17.38
		536.8367	0.291	0.030		7.453	0.791	8.152
22944.38	27.8H	504.4277	0.558	0.052		20.082	1.917	19.11
		528.2903	0.442	0.041		15.889	1.517	17.51
23316.63	24.8	444.2267	0.727	0.068		29.311	2.926	39.86
		458.0181	0.178	0.018		7.159	0.782	1.259
		475.0724	0.096	0.022		3.853	0.909	14.97
23337.4	55.6	517.5416	1.000	0.093		17.986	1.793	32.2
23629.98	112	423.0721	0.050	0.012	w	0.449	0.105	3.531
		438.1263	0.950	0.089		8.525	0.807	1.147
23852.43	181	433.8962	0.657	0.061		3.631	0.374	5.47
		463.2765	0.343	0.032		1.894	0.195	0.7196
23986.48	160	421.9307	0.136	0.014	w	0.851	0.088	2.954
		431.3863	0.864	0.080		5.399	0.507	1.743
24150.8	23.1	428.349	0.255	0.026		11.118	1.242	26.5
		441.158	0.690	0.065		30.031	3.081	22.21
		456.9582	0.055	0.013	w	2.379	0.564	6.793
24184.05	787	427.7398	1.000	0.093	w	1.271	0.120	0.58
24323.51	12.8	453.379	0.201	0.021		15.685	1.634	16.97
		471.6096	0.417	0.039		32.610	3.075	59.34
		492.4042	0.382	0.036		29.830	2.813	20.46

25065.37	82	424.044	0.270	0.029	w	3.382	0.380	2.804
		438.6218	0.107	0.011		1.342	0.151	10.6
		455.6627	0.623	0.060		7.810	0.807	6.567
25615.55	11.8	428.2834	0.122	0.013		10.316	1.094	49.89
		444.5155	0.255	0.026		21.569	2.288	63.2
		462.9429	0.624	0.058	b	52.861	5.096	5.157
26382.25	32.1	414.6632	1.000	0.093		31.153	2.955	1.257
26471.33	16.4	428.2208	0.118	0.012		7.166	0.750	81.21
		445.296	0.882	0.082		53.810	5.100	38.08
26507.31	339	412.5233	1.000	0.086	b	2.743	0.258	3.059
		427.5618	-	-	w	-	-	0.7879
27129.49	301	416.4793	1.000	0.093		3.322	0.332	0.8785
27338	41.5	386.7607	0.090	0.021	w	2.169	0.509	0.9886
		604.5409	0.662	0.062	b	15.944	1.553	24.16
		613.5869	0.248	0.026	w	5.983	0.640	11.97
27398.92	39.8	385.8513	1.000	0.093	b	25.126	2.378	66.23
27627.25	59.6	365.7316	0.280	0.029	b	4.709	0.494	4.361
		372.815	0.272	0.028	b	0.095	0.011	4.752
		382.4806	0.348	0.032	w	0.122	0.013	1.721
27709.4	43.3	591.2617	1.000	0.093	w	29.730	2.879	16.88
27992.35	48	589.8958	0.589	0.055		12.280	1.165	22.45
		691.8722	0.411	0.038	w	8.553	0.811	6.851
28425.3	37.7	604.1426	1.000	0.093	w	26.525	2.492	11.73
28752.34	89.4	390.1048	0.810	0.076		9.178	0.907	2.024
		613.0643	0.123	0.013	w	1.394	0.151	5.403
		684.8345	0.067	0.016	b	0.753	0.177	7.038
28853.25	73.9	573.0137	0.720	0.067		9.742	0.944	4.328

		652.9683	0.280	0.029		3.790	0.404	8.889
28855.76	65.3	572.9313	1.000	0.093	w	15.314	1.440	7.791
				-				
28913.97	36	349.2891	1.000	0.093		27.778	3.049	1.642
28942	124	364.1624	1.000	0.093		8.065	0.775	0.8515
29130.03	26.6	621.7193	1.000	0.093	w	37.594	3.567	27.45
29282.28	32	589.1407	1.000	0.093	w	31.250	3.502	16.16
29475.54	62.9	610.3395	0.694	0.065		11.041	1.042	9.893
		683.8367	0.306	0.028	w	4.858	0.458	8.562
29648.85	33	355.021	0.610	0.067	w	21.762	2.092	0.2662
		620.713	0.296	0.032		10.551	1.014	7.551
		645.2099	0.094	0.011	w	3.345	0.354	9.406
29807.75	59.4	575.7975	1.000	0.093	w	16.835	1.685	10.26
29817.84	77.9	338.5958	1.000	0.093		12.837	1.248	1.83
29855.91	36.4	362.4412	-	-	w	-	-	1.825
		609.6821	0.839	0.078	w	23.061	2.236	8.559
		638.6762	0.161	0.017	w	4.411	0.470	8.976
30312.27	65.5	580.6765	1.000	0.093	b	15.267	1.510	6.413
30330.78	51.4	580.0528	1.000	0.093		19.455	1.824	23.93
30416.8	32.2	589.517	0.629	0.059	s	19.536	2.219	12.46
		616.5822	0.371	0.034	w	11.519	1.308	10.65
30586.5	87.4	610.1957	0.719	0.069		8.462	0.804	9.376
		635.5401	0.281	0.030	w	3.311	0.347	7.041
31062.3	28.6	533.2081	1.000	0.093		34.965	3.519	24.33
31219.7	32.4	328.7685	1.000	0.093		30.864	2.996	0.5164

31493.41	54.6	333.1946	1.000	0.093	b	18.315	1.724	0.4878
31934.03	34.1	523.7603	0.371	0.034		10.874	1.019	49.28
		625.6566	0.629	0.059		18.4515492	1.72959	91.25
32086.66	128.6	543.3594	1.000	0.093	w	7.776	0.983	55.16
32149.28	21.7	534.8732	0.342	0.032	s	15.766	1.552	46.04
		552.5593	0.658	0.061	w	30.317	2.984	10.59
32289.85	43.9	324.5785	1.000	0.093		22.779	2.382	54.95
32735.62	31.1	348.1509	1.000	0.093		32.154	3.164	20.46
32868.71	24.9	535.5885	0.346	0.032	w	13.890	1.350	35.96
		546.1551	0.654	0.061	w	26.2705251	2.552342	18.87
33081.45	47.3	572.4477	1.000	0.093	w	21.142	2.016	11.84

Table 6.1 shows the radiative parameters for Sm I

Lifetimes are adopted from Zhang et al.^{19,20} unless otherwise noted

w denotes weak emission line

s denotes shouldered emission line

b denotes blended emission line

H denotes lifetime from Hannaford et al.¹³

S denotes lifetime from Shah et al.¹⁷

Komar refers to the work by Komarovskii et al.³⁴

Shah refers to the work by Shah et al.¹⁷

Kurucz refers to the work by Kurucz and Bell.³³

Sm II Data

Table 6.2 shows the radiative parameters for Sm II

Lifetimes were adopted from Scholl et al.²⁵ unless noted.

L denotes lifetime is from Lawler et al.²⁹

Lund refers to the work by Lawler et al.²⁹

UWO refers to the work by Rehse et al.²⁷

CB refers to the work by Corliss and Bozmann³²

XSQGB refers to the work by Xu et al.²⁶

w denotes weak emission line

s denotes emission line has shoulder

b denotes blended emission line

Upper Energy (cm ⁻¹)	Lifetime (ns)	Lower Energy (cm ⁻¹)	Wavelength (nm)	Branch Ratio	BR Error	log g _i *f _{ik}				
						This Work	UWO	XSQGB	CB	Lund
21507.87	92L	0	464.816	0.293	0.021	-1.390				-1.51
		326.64	471.984	0.502	0.032	-1.136				-1.24
		838.22	483.666	0.051	0.010	-2.085				-2.19
		1518.29	500.121	0.065	0.012	-2.008				-2.01
		2003.23	531.225	0.089	0.017	-1.792				-3.2
		7135.06	714.957	-	-	-				-1.67
21655.42	51.9	0	461.649	0.265	0.019	-1.486	-2.2		-2.96	-2.17
		326.64	468.719	0.579	0.036	-1.133	-1.06		-1.66	-1.15
		1518.29	496.457	0.084	0.016	-1.921	-1.83		-2.39	-1.86
		2003.23	508.707	0.041	0.008	-2.211	-2.09		-2.53	-2.1
		7135.06	688.499	0.030	0.006	-2.080	-2.36			
21702.33	40.2	0	460.651	0.552	0.035	-0.756	-1.18	-1.14	-1.96	-1.26
		326.64	467.690	0.293	0.021	-1.018	-0.82	-0.94	-1.39	-0.87
		838.22	479.158	0.079	0.015	-1.568	-1.43	-1.86	-1.83	-1.44
		1518.29	495.303	0.007	0.001	s -2.595	-2.08		-2.39	-1.9
		2688.69	525.792	0.026	0.005	-1.973	w			-2.8
		7135.06	686.281	0.043	0.008	-1.520	-1.46	-1.38	-1.96	-1.42
22039.98	181L	326.64	460.417	0.569	0.036	-1.223				-1.39
		838.22	471.527	0.356	0.022	-1.397				-1.46
		2003.23	498.944	0.070	0.013	-2.094				-2.06
		7520.0	688.747	0.005	0.001	w				
		8046	714.396	-	-	-				-1.44
22248.32	33.8	326.64	456.042	0.121	0.009	-1.171	-1.23		-2	-1.24
		838.22	466.939	0.515	0.032	-0.523	-0.6		-1.48	-0.6
		1489.16	481.581	0.281	0.020	-0.759	-0.85		-1.49	-0.82
		2003.23	493.809	0.042	0.008	-1.566	-1.42		-1.9	-1.44
		2688.69	511.115	0.010	0.002	s -2.155	-2.3			-2.33
		3499.12	533.208	0.007	0.001	-2.268	-2.47			
		7135.06	661.488	0.001	0.000	w -2.779	-2.19			
		7524.86	679.001	-	-	-	-1.24		-1.73	
		8046	703.916	0.023	0.004	-1.524	-0.85		-1.49	

22429.49	78.4L	326.64	452.304	0.577	0.036	-0.871				-0.99
		838.22	463.021	0.213	0.016	-1.284				-1.46
		1489.16	477.414	0.103	0.008	-1.555				-1.61
		2003.23	489.429	0.080	0.015	-1.671				-1.92
		2688.69	506.424	0.016	0.003	-2.327				-2.02
			670.747	0.011	0.002	w	-2.455			
		8046	695.050	-	-	-				-1.38
			767.868	-	-	-				
22788.68	195L	838.22	455.444	0.489	0.031	-1.210				-1.25
		1489.16	469.363	0.412	0.026	-1.252				-1.48
		2688.69	497.374	0.075	0.014	-1.893				-1.97
			678.116	-	-					
		8679.23	708.550	0.024	0.005	#DIV/0!				-1.33
22875.41	39.9	838.22	453.651	0.197	0.014	-0.912	-1.21	-0.7	-1.88	-1.28
		1489.16	467.459	0.470	0.030	-0.510	-0.52	-0.73	-1.05	-0.56
		2237.97	484.421	0.180	0.013	-0.896	-0.84	-1.64	-1.54	-0.89
		2688.69	495.237	0.099	0.019	-1.134	-1.23	-1.8	-1.82	-1.25
		3499.12	515.951	0.006	0.001	w	-2.346	-2.1		
		4386.03	540.701	0.009	0.002	w	-2.122	-2.66		
		7524.86	651.263	0.010	0.002	w	-1.897	-2.29		
		8046	674.150	-	-	-	-1.25	-1.05	-1.72	-1.21
		8679.23	704.221	0.030	0.006	-1.353	-0.85	-0.74	-1.42	-0.76
23177.49	48	0	431.332	-	-	-	-2.13			-2.24
		326.64	437.498	0.173	0.013	-1.384	-1.26	-1.73	-1.8	-1.37
		838.22	447.517	0.038	0.007	-2.021	-1.72		-2.42	-1.83
		1518.29	461.568	0.701	0.044	-0.729	-0.77	-0.78	-1.57	-0.84
		2003.23	472.139	0.063	0.012	-1.755	w		-2.57	-1.98
		2688.69	487.936	0.018	0.003	s	-2.268	w		-2.53
		7524.86	638.694	0.001	0.000	w	-3.345	-2.25	-1.44	
		8578.7	684.800	0.007	0.001	w	-2.409	-2.04		
23260.949	53.8	838.22	445.851	0.586	0.037	-0.586	-0.61		-1.27	-0.66
		1489.16	459.181	0.224	0.016	-0.977	-1.06			-1.12
		2237.97	475.537	0.039	0.007	-1.711	-1.84		-2.42	-1.85
		2688.69	485.956	0.108	0.008	-1.244	-1.47		-2.04	-1.51
		3499.12	505.885	0.012	0.002	s	-2.162	-2.24		-2.2
		8046	657.067	-	-	-	-1.35		-1.66	-1.38
		8679.23	685.601	0.032	0.006	-1.481	-0.92		-1.51	-0.9

23646.9	42.5	1489.16	451.183	0.278	0.020		-0.700	-0.77	-1.47	-0.82
		2237.97	466.964	0.520	0.033		-0.398	-0.5	-1.38	-0.53
		3052.65	485.437	0.073	0.014		-1.216	-1.22	-1.87	-1.25
		3499.12	496.194	0.087	0.017		-1.120	-1.07	-1.54	-1.09
		4386.03	519.043	0.003	0.001	w	-2.541	w		-2.42
		8679.23	667.922	0.016	0.003		-1.586	-1.13	-1.54	
		9406.63	702.040	0.022	0.004		-1.410	-0.63	-1.33	-0.62
23659.99	31.8	0	422.535	0.504	0.032		-1.070	-1.59		
		326.64	428.451	0.008	0.002	w	-2.861	-2.2		-2.21
		1518.29	451.510	0.468	0.030		-1.045	-0.85		-0.87
		7135.06	604.979	0.013	0.002	w	-2.352	-2.52		
		8578.7	662.890	0.006	0.001	w	-2.574	-1.81		-1.75
		10518.5	760.739	-	-		-	-1.83		
23752.7	155L	2237.97	464.668	0.581	0.037		-0.917			-1.03
		3052.65	482.956	0.302	0.019		-1.170			-1.28
		3499.12	493.602	0.117	0.009		-1.543			-1.71
		12232.34	696.863	-	-		-			-1.46
23842.199	33.6	326.64	425.131	0.057	0.011		-1.561	-2.68		-2.66
		838.22	434.585	0.206	0.015		-0.980	-1.02	-1.49	-1.05
		1489.16	447.241	0.271	0.020		-0.837	-0.94	-1.53	-0.96
		2003.23	457.769	0.282	0.021		-0.799	-0.62	-1.4	-0.65
		2688.69	472.603	0.116	0.008		-1.158	-1.25	-1.85	-1.25
		3499.12	491.430	0.024	0.005		-1.802	-2.02	-2.77	-2.13
		7135.06	598.381	0.016	0.003	s	-1.801	-2.18		
		7524.86	612.676	0.001	0.000	s	-2.822	w		
		8046	632.889	0.013	0.002	s	-1.856	-2.01		
		8578.7	654.977	0.009	0.002		-2.002	-1.61	-2.14	-1.52
		9410	692.704	-	-		-	-1.62	-2.07	
		11155.3	787.998	-	-		-			
23962.25	22.54	326.64	422.971	0.304	0.019		-0.839	-0.82	-1.39	-0.87
		838.22	432.329	0.259	0.019		-0.890	-0.88	-1.46	-0.92
		2003.23	455.266	0.292	0.021		-0.793	-0.78	-1.55	-0.82
		2688.69	469.936	0.100	0.019		-1.232	-1.42	-1.88	-1.44
		8578.7	649.866	0.045	0.009		-1.294	-1.21	-1.83	-1.15
		10743.4	756.287	-	-		-			
		10873.3	763.793	-	-		-		-1.78	-1.46

24013.561	69.1	0	416.314	0.081	0.015	-1.912	-1.52		-1.61
		326.64	422.055	0.500	0.031	-1.112	-2.13		-2.29
		838.22	431.372	0.135	0.010	-1.662	-1.62		-1.72
		2003.23	454.205	0.284	0.021	-1.293	-0.97		-1.04
24194.381	162.8	838.22	428.032	-	-	-	-1.63	-2.27	-1.74
		1489.16	440.304	0.614	0.039	-1.182	-1.6	-1.27	-1.69
		2003.23	450.504	0.288	0.021	-1.491	-1.32	-1.9	-1.42
		2688.69	464.863	-	-	-	-2.35		-2.35
		3499.12	483.068	0.026	0.005	-2.481	-2.54		-2.44
		7135.06	586.027	0.073	0.014	-1.860	-2.07	-2.34	
24221.811	15.5	326.64	418.377	0.235	0.017	-1.098	-0.99	-1.52	-1.05
		1518.29	440.337	0.328	0.021	-0.909	-1.03	-1.56	-1.06
		2003.23	449.948	0.432	0.027	-0.771	-0.8	-1.58	-0.87
		8578.7	639.082	-	-	-	-1.46	-1.98	
		10371.51	721.807	0.004	0.001	w	-2.382	w	
		11047.3	758.833	-	-	-	w		
24582.59	19.6	326.64	412.154	0.162	0.012	-0.898	-1.61	-2.15	-1.66
		838.22	421.034	0.199	0.015	-0.789	-0.94	-1.37	-0.96
		1489.16	432.902	0.283	0.021	-0.613	-0.47	-0.91	-0.51
		2003.23	442.758	0.133	0.010	-0.921	-1.25	-1.88	-1.29
		2688.69	456.620	0.193	0.014	-0.733	-0.59	-1.41	-0.59
		3499.12	474.173	0.028	0.005	-1.539	-1.65	-2.17	-1.59
		8578.7	624.675	-	-	-	-1.48	-1.73	
		9410	658.902	-	-	-	-1.81		
		10180.7	694.162	-	-	-	-1.46	-1.97	-1.37
		10518.5	710.835	-	-	-	-2.12		
		11155.3	744.547	0.003	0.000	w	-2.185	-1.39	
		11659.8	773.614	-	-	-	-1.28		
		11798.6	782.013	-	-	-		-1.82	-1.36
24588	40.7	2237.97	447.301	0.723	0.046	-0.193	-0.59	-0.62	-1.32
		3052.65	464.223	0.104	0.008	-1.003	-0.4	-0.52	-1.12
		3909.62	483.462	0.166	0.012	-0.764	-1.46	-1.65	-1.94
		4386.03	494.863	0.007	0.001	-2.131	-0.9	-1.56	-1.43
		8679.23	628.410	-	-	-			
		9406.63	658.520	-	-	-	-1.22	-1.64	-1.66
		10214.38	695.527	-	-	-	-0.62	-0.59	-1.11

24685.529	55.1	0	404.981	0.212	0.015	-1.422	-1.27	-1.46	
		326.64	410.412	0.137	0.010	-1.599	-1.46	-1.84	
		838.22	419.216	0.358	0.023	-1.165	-1.38	-1.97	
		1518.29	431.523	0.081	0.015	-1.783	-2.13		
		2003.23	440.749	0.051	0.010	-1.968	-1.78	-2.35	
		2688.69	454.483	0.098	0.019	-1.655	-1.48	-2.07	
		7135.06	569.627	0.055	0.011	-1.708	-1.99		
		9410	654.461	0.007	0.001	w	-2.493	-2.04	
24689.84	20.5	1489.16	430.901	0.196	0.014	-0.670	-0.7	-1.2	-0.74
		2237.97	445.272	0.334	0.021	-0.412	-0.37	-0.98	-0.41
		2688.69	454.394	0.267	0.020	-0.491	-0.45	-1.17	-0.49
		3499.12	471.773	0.139	0.010	-0.741	-0.88	-1.52	-0.91
		4386.03	492.381	0.047	0.009	-1.171	-1.74	-2.03	-1.62
		8679.23	624.413	-	-	-	w	-1.95	
		9410	654.276	0.011	0.002	-1.542	-1.2		
		10960.16	728.149	0.002	0.000	b	-2.130	-1.27	-1.69
		11659.8	767.246	-	-	-			
		11798.6	775.507	0.002	0.000	-2.174		-1.67	
24816.28	116L	2237.97	442.779	0.261	0.019	-1.097			-1.81
		3052.65	459.354	0.443	0.028	-0.841			-0.83
		3909.62	478.183	0.126	0.009	-1.330			-1.47
		4386.03	489.334	0.125	0.009	-1.339			-1.32
		10214.38	684.654	0.015	0.003	-1.987			-1.3
24848.471	112	326.64	407.685	0.150	0.011	-1.698	-1.77	-2.25	-1.79
		838.22	416.371	0.030	0.006	-2.373	-1.72	-2.16	-1.74
		1489.16	427.974	0.729	0.046	-0.968	-1.21		-1.24
		2003.23	437.605	0.017	0.003	-2.580	-2.42		-2.38
		3499.12	468.267	0.058	0.011	-1.987	-1.54	-1.95	-1.56
		7135.06	564.388	-	-	-	-2.36		
		7524.86	577.087	0.003	0.001	w	-3.070	-2.37	
		8046	594.986	0.002	0.000	w	-3.165	-3.19	
		8578.7	614.467	0.005	0.001	b	-2.823	-2.48	
		9410	647.554	0.002	0.000	w	-3.229	-2.43	
		10518.5	697.646	-	-	-	-2.75		
		10873.3	715.358	-	-	-	-2.57		
		11155.3	730.090	0.003	0.001	w	-2.874	-2.03	
		11395.4	743.120	-	-	-	-2.2		

		11659.8	758.018	-	-	-	-2		
24928.801	25.4	326.64	406.354	0.235	0.017	-0.862	-0.72	-1.45	-0.79
		838.22	414.983	0.180	0.013	-0.959	-0.85	-1.26	-0.91
		1489.16	426.508	0.200	0.015	-0.890	-0.99	-1.43	-1.04
		2003.23	436.072	0.294	0.021	-0.704	-0.82	-1.36	-0.87
		2688.69	449.512	0.028	0.005	-1.696	-2.06	-2.69	-2.12
		3499.12	466.512	0.049	0.009	-1.426	-1.4	-2.15	-1.42
		8578.7	611.448	0.015	0.003	-1.706	w		
		10180.7	677.866	-	-	-	w	-1.58	-1
		11798.6	761.393	-	-	-		-1.95	
25055.539	34.9	0	399.001	0.285	0.021	-1.108	-1.03	-1.04	-1.06
		326.64	404.271	0.532	0.033	-0.825	-0.97	-1.32	-0.99
		838.22	412.811	0.033	0.006	-2.013	-2.18		-2.35
		1518.29	424.739	0.020	0.004	-2.197	-1.92	-2.41	-1.96
		2003.23	433.674	0.077	0.015	-1.603	-1.83		-1.95
		2688.69	446.965	0.047	0.009	-1.792	-1.57		-1.61
		0	638.983	-	-	-	-1.47	-1.82	
		10518.5	687.708	0.003	0.001	s -2.575			
		10873.3	704.913	0.003	0.001	w -2.580	-1.48		
25175.32	81	326.64	402.322	0.293	0.021	-1.267	-0.94	-1.23	-0.93
		838.22	410.779	-	-	-	-2.06	-2.38	-2.16
		1489.16	422.069	0.540	0.034	-0.960	-2.27		-2.29
		2003.23	431.433	-	-	-	-2.23		-2.4
		2688.69	444.584	0.029	0.006	-2.180	-1.92		
		3499.12	461.207	0.060	0.011	w -1.835	-2.36		-2.57
		7135.06	554.162	0.025	0.005	w -2.053	w		
		8046	583.633	0.041	0.008	-1.800	-1.48	-1.75	-1.42
		10180.7	666.722	0.010	0.002	-2.278	-1.28	-1.95	
25178.449	23.5	0	397.053	0.212	0.015	-1.069	-1.01	-1.33	-1
		326.64	402.272	0.080	0.015	b -1.482	-1.95	-2.23	-2.02
		838.22	410.727	0.264	0.019	-0.945	-1.35	-1.24	-1.42
		1518.29	422.532	0.340	0.021	-0.810	-0.57	-1.1	-0.62
		2003.23	431.374	0.105	0.008	-1.302	-1.86	-1.84	-1.95
25304.09	22.2	838.22	419.786	0.013	0.003	-1.919	-2.17	-2.46	-1.98
		1489.16	433.414	0.334	0.021	-0.497	-0.69	-0.94	-0.5
		2237.97	442.052	0.393	0.025	-0.399	-0.62	-0.87	-0.43

		2688.69	458.483	0.237	0.017		-0.602	-0.85	-1.24	-0.65
		3499.12	477.923	0.009	0.002		-1.972	-2.31		-2.13
		4386.03	579.278	-	-		-	w		
		8046	601.343	0.003	0.001	w	-2.197	w		
		8679.23	628.991	0.009	0.002		-1.751	-1.8	-1.87	-1.46
		9410	732.706	0.001	0.000	w	-2.601	0.1		-1.45
		11659.8	764.798	-	-		-		-1.68	-1.24
25361.449	16.8	0	394.188	0.292	0.021		-0.790	-0.83	-1.08	-0.86
		326.64	399.331	0.284	0.021		-0.790	-0.88	-1.3	-0.93
		838.22	407.662	0.196	0.014		-0.934	-1.31	-1.69	-1.33
		2003.23	427.994	-	-		-	-0.97	-1.7	-1
		2688.69	440.934	-	-		-0.870	-0.85	-1.32	-0.89
		9410	626.729	0.194	0.014		-1.364	-1.12	-1.26	-1.01
		10518.5	673.535	0.031	0.006		-	w		-1.35
		10873.3	690.029	-	-	w	-2.180		-2.14	
		11047.3	698.417	0.004	0.001		-	w		
25552.801	79	326.64	396.302	0.285	0.021		-1.468			
		838.22	404.505	0.348	0.022		-1.364	-1.25	-1.38	-1.38
		1518.29	415.951	0.140	0.010		-1.736	-1.65	-2.08	-1.79
		2003.23	424.517	0.109	0.008		-1.828	-1.33	-1.99	-1.47
		2688.69	437.244	0.023	0.004	w	-2.467	-2.38		-2.47
		8578.7	588.970	0.068	0.013	b	-1.749	w		-1.92
		9410	619.300	0.021	0.004		-2.218	w		
		10743.4	675.061	-	-		-	w		
		11047.3	689.204	0.007	0.001		-2.619	w		
25565.971	31.1	838.22	404.290	0.298	0.022		-0.726	-0.69	-1.18	-0.72
		1489.16	415.220	0.242	0.018		-0.793	-0.69	-1.02	-0.72
		2237.97	428.549	0.202	0.015		-0.844	-0.83	-2.34	-0.85
		2688.69	436.992	0.098	0.019		-1.142	-1.31	-1.71	-1.27
		4386.03	472.013	0.133	0.010		-0.941	-1.58	-2.21	-1.62
		9410	618.795	0.009	0.002		-1.882	w	-1.92	
		10180.7	649.793	-	-		-	-1.5		
		10960.16	684.470	0.010	0.002		-1.742	-1.06	-1.37	
		11395.4	705.493	0.002	0.000	w	-2.395	w	-1.83	
		11798.6	726.155	-	-		-			
		12045.17	739.398	-	-		-			
		12987.86	794.813	0.006	0.001		-1.811		-1.68	

25597.699	14.2	1489.16	414.674	0.027	0.005	-1.309	-1.46	-1.88	-1.54
		2237.97	427.967	0.298	0.022	-0.239	-0.46	-0.97	-0.52
		3052.65	443.432	0.401	0.025	-0.080	-0.02	-0.75	-0.07
		3499.12	452.391	0.174	0.013	-0.424	-0.35	-1.16	-0.39
		4386.03	471.307	0.068	0.013	-0.796	-0.77	-1.3	-0.8
		5317.56	492.956	0.010	0.002	-1.588	-1.52	-2.22	-1.65
		10180.7	648.455	0.008	0.001	-1.458	-1.09	-1.64	
		10960.16	682.986	0.003	0.001	-1.801	-1.22	-1.67	-1.2
		11395.4	703.918	0.009	0.002	-1.328	w		
		11791.05	724.089	0.002	0.000	-1.984	-1.03	-1.24	-0.94
		12045.17	737.666	-	-	-		-1.57	
		12841.6	783.723	-	-	-		-1.49	-1.1
		12987.86	792.813	-	-	-		-0.93	-0.7
25664.971	44.4	3052.65	442.113	0.415	0.026	-0.416	-0.46	-1.01	-0.49
		3909.62	459.528	0.334	0.021	-0.476	-0.48		-0.5
		5317.56	491.326	0.169	0.012	-0.715	-0.89	-1.13	-0.93
		9406.63	614.899	0.023	0.004	-1.383	-2.3		
		10214.38	647.046	0.013	0.003	-1.580	-1.33	-1.93	
		11094.06	686.110	0.043	0.008	-1.014	-0.57		
		11791.05	720.578	0.002	0.000	w	-2.425	-2.09	
25790.15	57.3	838.22	400.657	0.121	0.009	-1.389	-1.48	-1.83	-1.5
		1489.16	411.390	0.226	0.016	-1.097	-1.07	-1.46	-1.07
		2237.97	424.470	0.266	0.019	-0.999	-0.8	-1.24	-0.81
		2688.69	432.751	0.085	0.016	-1.476	-1.74	-2.36	-1.76
		3499.12	448.486	0.074	0.014	w	-1.507	-2.39	
		4386.03	467.069	0.156	0.011	-1.147	-1.59		-1.59
		7524.86	547.335	0.020	0.004	w	-1.896	-2.05	
		8679.23	584.260	0.033	0.006	-1.633	-1.75	-1.97	
		9410	610.326	0.019	0.004	-1.820	-1.69		
		10180.7	640.461	-	-	-	-2.08		
		10960.16	674.124	-	-	-	-1.27		
25939.869	62.4	3052.65	436.802	0.307	0.019	-0.706	-0.9	-1.28	-0.93
		3909.62	453.794	0.531	0.033	-0.434	-0.45	-1.08	-0.48
		5317.56	484.776	0.132	0.010	-0.983	-0.85	-1.53	-0.89
		10214.38	635.735	0.023	0.004	-1.502	-1.66		
		11094.06	673.405	-	-	-	-0.81	-1.25	
25980.32	19.9	326.64	389.697	0.214	0.016	-0.831	-0.68	-0.87	-0.67

		838.22	397.627	0.313	0.020		-0.649	-0.92	-1.11	-0.9
		1489.16	408.195	0.028	0.005		-1.667	-1.74	-1.94	-1.72
		2003.23	416.947	0.139	0.010		-0.960	-0.77	-1.12	-0.76
		2688.69	429.218	0.220	0.016		-0.737	-0.94	-1.45	-0.91
		3499.12	444.691	0.032	0.006		-1.549	-1.82	-2.3	-1.79
		9410	603.322	0.008	0.001	w	-1.887	-1.79	-1.99	
		10180.7	632.752	0.033	0.006		-1.228	-1.08	-1.32	-0.88
		10873.3	661.761	0.003	0.000	w	-2.284	-1.96		
		11047.3	669.472	0.004	0.001	s	-2.050	-1.79		
		11395.4	685.451	0.004	0.001	w	-2.064	-1.6	-1.92	-1.31
		12566.8	745.311	0.002	0.000	w	-2.238	-0.92	-1.51	
										-2.3
26046.35	20.9	3052.65	434.780	0.200	0.015		-0.566	-0.4	-0.93	-0.42
		3499.12	443.389	0.516	0.032		-0.137	-0.15	-0.74	-0.19
		4386.03	461.544	0.266	0.019		-0.389	-0.67	-1.42	-0.69
		5317.56	482.286	0.006	0.001	w	-2.030	-2.23		
		8046	555.391	0.002	0.000	w	-2.360	-2.35		
		8679.23	575.641	0.002	0.000	w	-2.403	-2.24		
		9406.63	600.806	0.004	0.001	w	-2.037	-1.97		
		10180.7	630.118	0.004	0.001		-1.926	-1.56	-1.84	
		12232.34	723.703	0.001	0.000	w	-2.402	-1.29	-1.84	
		12789.81	754.137	-	-		-		-1.54	
		12841.6	757.095	-	-		-		-1.54	
		12987.86	765.575	-	-		-	-1.41	-1.86	
26086.631	70	838.22	395.953	0.083	0.016		-1.650	-1.23		-1.25
		1489.16	406.431	0.524	0.033		-0.829	-1.26		-1.28
		2237.97	419.193	0.293	0.021		-1.054	-1.02		-1.04
		3499.12	442.598	0.030	0.006		-1.990	-1.78		-1.92
		4386.03	460.688	-	-		-	-1.51		-1.49
		8679.23	574.309	0.058	0.011		-1.481	-2.3		
		10180.7	628.523	0.007	0.001	w	-2.320	-2.06		
		11659.8	692.962	-	-		-	-1.6		-1.43
		12045.17	711.980	0.003	0.001	w	-2.529	-1.15		-1.12
26159.6	93	838.22	394.811	0.645	0.041		-0.887	-0.8	-1.21	-0.84
		1489.16	405.229	0.010	0.002	w	-2.693	-2.34		-2.49
				-	-					-2.59
		2688.69	425.939	0.050	0.009		-1.933	-2.06	-2.27	-2.17
		3499.12	441.173	0.271	0.020		-1.168	-2.07		-2.05
		4386.03	459.144	-	-		-	-2.54		-2.66

		8046	551.918	-	-	-	-2.41		
		8679.23	571.912	0.025	0.005	w	-1.973	-1.92	
		11659.8	689.475	-	-	-	-	-1.38	
26190.92	39.3	326.64	386.524	0.139	0.010		-1.321	-1.42	-1.56
		838.22	394.324	0.284	0.021		-0.993	-0.99	-1.29
		1489.16	404.715	0.330	0.021		-0.906	-0.91	-1.18
		2003.23	413.317	0.095	0.018		-1.430	-1.76	-2.01
		2688.69	425.372	0.061	0.012		-1.593	-1.82	-1.74
		3499.12	440.564	0.041	0.008		-1.736	-1.83	-2.37
		9410	595.750	0.024	0.005		-1.707	-1.65	-1.9
		10180.7	624.429	-	-		-	-1.46	
		10873.3	652.663	0.012	0.002	b	-1.928	-1.52	
		11155.3	664.904	0.014	0.003		-1.858	w	
		11798.6	694.624	-	-		-	-1.15	
26214.051	66	326.64	386.179	0.327	0.021	s	-0.994	-1.55	
		838.22	393.964	0.045	0.008		-1.841	-2.09	-2.37
		1489.16	404.337	0.266	0.019	s	-1.044	-1.9	
		2003.23	412.922	0.160	0.012		-1.246	-1.13	-1.57
		2688.69	424.954	0.081	0.015		-1.515	-1.16	-1.67
		3499.12	440.116	0.121	0.009		-1.314	-1.36	
26357.9	32.2	326.64	384.045	0.164	0.012		-1.165	-1.14	-0.78
		838.22	391.744	0.167	0.012		-1.141	-1.02	-1.28
		1489.16	401.998	0.206	0.015		-1.027	-1.23	-1.4
		2003.23	410.483	0.018	0.003	w	-2.071	w	-2.89
		2688.69	422.371	0.105	0.008		-1.278	-1.23	-1.24
		3499.12	437.346	0.296	0.022		-0.797	-0.81	-1.28
		9410	589.880	0.007	0.001		-2.171	w	
		10180.7	617.983	0.014	0.003		-1.835	-1.5	-1.32
		10519	631.163	0.001	0.000	w	-2.791		-1.83
		10873.3	645.625	0.014	0.003	s	-1.776		-1.38
		11155.3	657.601	-	-		-		
		11395.4	668.153	0.009	0.002		-1.965	-1.33	-1.25
26413.29	247L	3052.65	444.247	0.479	0.030		0.566		-1.39
		3909.62	453.856	0.489	0.031		0.377		-1.23
		4386.03	563.730	0.032	0.006	w	-0.967		-1.47
26442.18	25.2L	0	378.076	0.641	0.040		-0.973		-0.99

		326.64	382.805	0.172	0.013	-1.477			-1.42
26484.66	55.8L	0	377.470	0.211	0.015	-1.484			-1.52
		326.64	-	-	-	-			-1.54
		1518.29	400.426	0.138	0.010	-1.631			-2.03
		2003.23	408.358	0.495	0.031	-1.070			-1.22
		2688.69	420.121	0.097	0.018	-1.726			-2.09
		7524.86	527.285	0.059	0.011	-1.644			-1.65
26505.529	12.7	2237.97	411.957	0.036	0.007	-1.067	-1.35	-1.82	-1.43
		3052.65	426.267	0.191	0.014	-0.308	-0.49	-0.84	-0.49
		3909.62	442.434	0.438	0.028	0.085	0.18	-0.42	0.14
		4386.03	451.963	0.227	0.017	-0.182	-0.33	-0.92	-0.35
		5317.56	471.834	0.091	0.017	-0.543	-0.81	-1.34	-0.82
		10960.16	643.101	0.004	0.001	-1.587	-1.32	-1.76	-1.15
		11791.05	679.415	0.012	0.002	-1.102	-0.61	-1.02	-0.51
		12789.81	728.890	0.001	0.000	w -1.961	w	-1.67	
		12841.6	731.653	0.001	0.000	w -2.274	-1.54		
		13466.5	766.717	-	-	-	w	-1.53	
		13604.5	774.919	-	-	-	-1.12	-1.29	-1.06
26540.119	34	3052.65	425.639	0.666	0.042	-0.127	-0.13	-0.62	-0.15
		3909.62	441.758	0.194	0.014	-0.631	-0.88	-1.31	-0.87
		5317.56	471.065	0.079	0.015	-0.965	-1.35	-1.86	
		10214.38	612.360	0.015	0.003	-1.472	-1.52	-1.82	
		11094.06	647.235	0.046	0.009	-0.924	-0.79	-1.45	-0.76
		11791.05	677.822	-	-	-	-1.22	-1.69	-1.11
		12789.81	727.056	-	-	-	-1.8		
		13604.5	772.847	-	-	-	-1.2	-1.29	
26565.609	65.6	1489.16	398.668	0.317	0.020	-0.938	-0.91	-1.15	-0.85
		2237.97	410.939	0.099	0.019	-1.416	-1.1	-1.36	-1.04
		3052.65	425.178	0.123	0.009	-1.295	-1.17	-1.54	-1.11
		3499.12	433.408	0.382	0.024	-0.785	-2.1		-2.1
		4386.03	450.739	0.028	0.005	-1.883	-2.3		-2.37
		5317.56	470.500	-	-	-	-2.18		-2.25
		8046	539.819	0.031	0.006	w -1.687	-1.9		
		8679.23	558.930	0.009	0.002	-2.206	-2.09		
		10960.16	640.625	-	-	-	-1.27	-2.03	-1.34
		11395.4	659.005	-	-	-	w		
		11791.05	676.652	-	-	-	-1.39	-1.86	

		12045.1	688.495	0.010	0.002		-1.971	-1.44	
		12232.34	697.485	-	-		-	-1.51	
		12789.81	725.711	0.002	0.000	w	-2.521	-1.12	-1.92
26599.08	17.9	0	375.846	0.100	0.019		-1.323	-1.24	-1.39
		838.22	388.076	0.196	0.014		-1.002	-0.97	-1.1
		1518.29	398.599	0.080	0.015		-1.367	-1.55	-1.85
		2003.23	406.458	0.430	0.027		-0.620	-0.98	
		2688.69	418.110	0.142	0.010		-1.075	-0.98	-1.23
		7135.06	513.626	0.012	0.002	w	-1.964	-1.82	
		10518.5	621.696	0.010	0.002	w	-1.890	-1.37	
		10743.4	630.514	0.005	0.001	w	-2.134	-1.32	
		10873.3	635.723	0.014	0.003		-1.704	-1.13	
		11047.3	642.836	0.011	0.002		-1.826	-0.97	
		11798.6	675.467	-	-		-	-1.31	-1.76
26690.3	14L	0	374.562	0.485	0.031		-0.849		-0.72
		326.64	379.202	0.122	0.009		-1.385		-1.45
		2003.23	404.956	0.271	0.020		-1.017		-1.76
26723.869	47	326.64	378.720	0.094	0.018		-1.764	-1.55	-1.52
		838.22	386.205	0.607	0.038		-0.937	-1.07	-1.17
		2003.23	404.406	0.107	0.008		-1.650	-1.35	-1.49
		2688.69	415.940	0.191	0.014		-1.374	-1.4	-1.93
26820.811	35.2	1489.16	394.651	0.144	0.010		-1.021	-0.89	-1.3
		2237.97	406.673	0.232	0.017		-0.787	-0.7	-1.05
		3052.65	420.612	0.246	0.018		-0.731	-0.68	-1.1
		3499.12	428.665	0.240	0.018		-0.725	-0.97	-1.35
		4386.03	445.611	0.074	0.014		-1.203	-1.48	-1.9
		5317.56	464.916	-	-		-	-1.99	-1.92
		9406.63	574.086	0.031	0.006		-1.363	-1.74	
		10180.7	600.792	0.008	0.001	w	-1.931	-1.65	
		10960.16	630.317	0.015	0.003		-1.606	-1.27	-1.21
		11791.05	665.163	0.008	0.002		-1.804	w	-1.68
		12789.81	712.511	0.003	0.001		-2.234	w	-1.52
26880.6	48.4	3052.65	419.557	-	-		-	-2.26	-2.19
		3909.62	435.210	0.394	0.025		-0.556	-0.61	-0.6
		4386.03	444.427	0.464	0.029		-0.466	-0.48	-0.47
		5317.56	463.627	0.106	0.008		-1.071	-1.16	-1.16

		8679.23	549.257	0.007	0.001	-2.092	-2.12		
		9406.63	572.122	0.017	0.003	-1.695	-1.89		
		10960.16	627.950	0.005	0.001	w	-2.147	-1.86	
		11791.05	662.527	0.004	0.001	b	-2.161	-1.82	
		12045.1	673.876	-	-	-	-2.41	-0.8	
		12841.6	712.105	-	-	-	-1.76		
		13466.5	745.279	0.003	0.001	w	-2.184	-1.39	
		14084.55	781.276	-	-	-			
		14115	783.140	-	-	-	-1.11		
26938.42	35.9L	838.22	383.030	0.131	0.010	-1.186		-1.12	
		1489.16	392.828	0.496	0.031	-0.593		-0.55	
		2237.97	404.737	0.298	0.022	-0.791		-1.5	
		10175.05	596.575	0.052	0.010	-1.224			
		11395.4	643.198	0.009	0.002	b	-1.846	-1.47	
		671.260	0.015	0.003	w				
26974.67	54.4	326.64	375.156	0.135	0.010	-1.501	-1.66	-1.8	-1.56
		838.22	382.499	0.052	0.010	-1.896	-1.68		-1.61
		1489.16	392.269	-	-	-	-1.68	-1.79	-2.04
		2003.23	400.344	0.401	0.025	-0.971	-1.19	-0.9	-1.52
		2688.69	411.644	0.142	0.010	-1.398	-1.24	-1.3	-1.65
		3499.12	425.855	0.251	0.018	-1.122	-1.06	-1.63	-1.57
		8046	528.152	0.013	0.002	w	-2.226	w	-1.92
		8578.7	543.447	0.006	0.001	w	-2.560	w	
		11798.6	658.750	-	-	-	w	-1.85	
27001.2	190L	1489.16	391.861	0.319	0.020	-1.417			-1.52
		2237.97	403.711	0.311	0.020	-1.400			-1.45
		3052.65	417.444	0.370	0.023	-1.287			-1.27
		5317.56	461.205	-	-	-			-2.42
27063.3	9.8L	0	369.399	0.253	0.018	-0.671			-0.64
		326.64	373.912	0.422	0.027	-0.447			-0.43
		838.22	381.206	0.123	0.009	-0.953			-1.13
		1518.29	501.661	0.049	0.009	-1.335			-1.97
		2688.69	511.669	0.144	0.010	-0.827			-2.36
		7135.06	617.494	0.009	0.002	-1.911			-1.19
		7524.86	511.842	-	-	-			-0.72
		10873.3	617.702	-	-	-			-1.37

27078.3	101L	326.64	380.988	0.607	0.038	-1.128			-1.58
		838.22	390.680	0.134	0.010	-1.744			-2.06
		1489.16	398.690	-	-	-			-1.41
		2003.23	409.895	0.177	0.013	-1.597			-1.78
		2688.69	525.276	0.082	0.016	-1.901			
27107.619	41.4	838.22	380.563	0.210	0.015	-1.055	-1.26	-1.47	-1.2
		1489.16	390.233	0.035	0.007	-1.809	-1.95	-2.11	-2.03
		2237.97	401.983	0.247	0.018	-0.936	-1.48	-1.87	-1.53
		2688.69	409.403	0.123	0.009	-1.222	-1.11	-1.45	-1.15
		3499.12	423.457	0.308	0.019	-0.795	-0.6	-1.08	-0.64
		4386.03	439.987	0.041	0.008	-1.638	-1.47	-1.88	-1.54
		8679.23	542.491	0.016	0.003	w -1.873	-1.97		
		10960.16	619.122	0.011	0.002	-1.909	-1.71		
		12045.1	663.721	0.005	0.001	w -2.162	-1.35		
		12566.8	687.529	0.003	0.001	w -2.383	w	-1.93	
27165.35	64	326.64	372.490	0.188	0.014	-1.431	-1.24	-1.45	-1.36
		838.22	379.729	0.293	0.021	-1.220	-1.38	-1.34	-1.4
		1489.16	389.356	-	-	-			
		2003.23	397.310	0.053	0.010	b -1.921	-1.96		-2.13
		2688.69	408.437	0.221	0.016	-1.279	-1.31	-1.7	-1.57
		3499.12	422.424	0.078	0.015	-1.702	-1.72	-2.16	-1.81
		7524.86	509.010	0.087	0.017	w -1.493	-1.75		
		8046	522.885	0.076	0.014	-1.532	-1.42		
		8578.7	537.871	0.003	0.001	w -2.921	-2.15		
		14667.96	799.947	-	-	-		-1.92	
27188.301	26.9	838.22	379.398	0.278	0.020	-0.749	-0.69	-0.76	-0.67
		1489.16	389.008	0.153	0.011	-0.986	-0.98	-1.14	-0.95
		2237.97	400.683	-	-	-	-1.77	-1.99	-1.77
		2688.69	408.055	0.125	0.009	-1.033	-1.2	-1.54	-1.15
		3499.12	422.015	0.204	0.015	-0.791	-1.2	-1.62	-1.17
		4386.03	438.430	0.182	0.013	-0.807	-1.06	-1.35	-1.02
		8679.23	540.126	0.010	0.002	-1.901	-1.89		
		10180.7	587.810	0.023	0.004	-1.443	-1.52	-2.01	-1.56
		10960.16	616.043	0.014	0.003	-1.624	-1.17	-1.73	-1.27
		11395.4	633.021	0.003	0.001	w -2.248	-1.37		
		12045.17	660.183	0.006	0.001	-1.931	-0.71	-1.34	-0.9
		12232.34	668.445	0.003	0.001	-2.277	-1.08		

27210.12	20L	0	367.406	0.257	0.019		-1.272				-1.62	
		326.64	389.119	0.252	0.018		-1.283				-2.12	
		1518.29	396.605	0.490	0.031		-0.958				-1.32	
		2003.23	396.741	-	-		-				-0.9	
27263.25	29.2	3909.62	428.079	0.988	0.062		0.173	0.08		-0.5	0.06	
		11094.06	618.289	0.012	0.002	w	-1.430	-1.33		-1.59	-1.14	
		12045.1	656.929	-	-		-	-0.28		-0.81	-0.18	
		14084.55	758.591	-	-		-	-1.32		-1.23		
		14503.67	783.509	-	-		-	-0.83		-1.11	-0.74	
27284.689	17.3	326.64	370.841	0.011	0.002	s	-2.082	-1.01		-1.19	-1.3	-1.01
		838.22	378.015	0.159	0.012		-0.924	-2.01				-2.11
		1489.16	387.554	0.399	0.025		-0.503	-0.98			-1.18	-0.96
		2688.69	406.455	0.369	0.023		-0.496	-0.68		-0.49	-0.76	-0.67
		3499.12	420.305	0.003	0.001	w	-2.599	-0.53		-0.61	-0.82	-0.51
		8046	519.642	0.010	0.002	w	-1.855	-2.07		-1.99		
		11047.3	615.692	0.008	0.002		-1.773	-1.5		-1.72		
		11155.3	619.815	0.024	0.005		-1.322	-1.38				
		11395.4	629.181	-	-		-	-1.2		-1.92	-1.32	
		11659.8	639.828	0.008	0.002	w	-1.763	-1.35				
		11798.6	645.562	0.006	0.001	b	-1.855	-1.22		-1.15	-1.83	
		12566.8	679.258	0.002	0.000	w	-2.344	-1.19			-1.77	
		12987.86	699.263	-	-		-			-1.8		
		14667.96	792.380	-	-		-			-1.78		
27309.73	38	1489.16	387.178	0.233	0.017		-0.860	-0.87			-1.02	-0.74
		2237.97	398.742	0.151	0.011		-1.025	-1.15			-1.36	-1.13
		3052.65	412.135	0.208	0.015		-0.855	-0.93			-1.27	-0.92
		4386.03	436.107	0.324	0.020		-0.613	-1.01			-1.47	-1.08
		5317.56	454.580	0.020	0.004		-1.798	-1.61			-2.29	-1.71
		10180.7	583.643	0.026	0.005		-1.451	-1.31				
		10960.16	611.468	0.018	0.003	w	-1.572	-1.11			-1.81	
		12232.34	663.062	0.005	0.001		-2.048	-1.12			-1.8	-1.33
		12789.81	688.519	0.010	0.002	w	-1.714				-1.45	
12841.6	690.984	0.004	0.001		-2.116				-1.74	-1.16		
27386.69	172L	1489.16	397.522	0.399	0.025		-1.262					-1.58
		2237.97	410.831	0.294	0.021		-1.391					-1.45
		3052.65	410.972		-		-					-2.42
		3499.12	434.648	0.307	0.019		-1.363					-1.77

		4386.03	434.796	-	-	-		-2.22
		5317.56	453.149	-	-	-		
27464.199	36.9	838.22	375.466	0.220	0.016	-0.978	-2.1	
		1489.16	384.876	0.182	0.013	-1.039	-1.57	-1.24
		2237.97	396.301	0.237	0.017	-0.899	-0.78	
		2688.69	403.510	0.149	0.011	-1.086	-0.79	-1.21 -1.03
		3499.12	417.156	0.108	0.008	-1.195	-0.97	-1.66 -1.24
		4386.03	433.189	0.034	0.006	w -1.671	-2.22	
		8679.23	532.193	0.020	0.004	-1.721	-2.04	
		9410	553.734	-	-	-	-2.21	
		10180.7	578.426	0.001	0.000	w -2.999		-1.49
		10873.3	602.573	0.007	0.001	w -2.082		-1.63
		10960.16	605.745	0.003	0.001	w -2.444		-1.55
		11395.4	622.152	-	-	-		-1.47
		11659.8	632.560	0.015	0.003	-1.696	-1.35	-1.58
		12045.1	648.370	0.022	0.004	b -1.506	-1.66	-1.15
		12232.34	656.337	-	-	-	-1.39	-1.69
		12566.8	671.073	0.002	0.000	w -2.470	w	
27552.45	139L	1489.16	383.573	0.398	0.025	-1.269		-1.32
		2688.69	0.000		-	-		-2.23
		3499.12	415.626	0.349	0.022	-1.283		-1.35
		4386.03	431.538	0.212	0.015	-1.517		-1.59
27631.18	9.2L	326.64	366.135	0.185	0.014	-0.615		-0.36
		838.22	373.126	0.208	0.015	-0.549		-0.33
		1489.16	382.417	0.209	0.015	-0.531		-0.94
		2003.23	390.089	0.048	0.009	-1.130		-1.34
		2688.69	400.809	0.120	0.009	-0.721		-1.64
		3499.12	414.270	0.035	0.007	-1.201		-1.7
		7524.86	497.217	0.054	0.010	-0.883		-0.94
		8046	510.448	0.131	0.010	-0.478		-0.65
27638.83	170L	2237.97	393.576	0.213	0.016	-1.457		-1.05
		3052.65	-	-	-	-		-1.79
		3909.62	421.303	0.116	0.008	-1.670		-1.81
		4386.03	429.935	0.169	0.012	-1.470		-1.51
27829.77	18.5L	326.64	363.491	0.306	0.019	-0.883		-1.27
		1518.29	379.954	0.202	0.015	-1.018		-0.92

		2688.69	397.643	0.492	0.031	-0.600			-0.58
27923.96	194L	326.64	362.251	0.227	0.017	-1.886			-1.6
		838.22	369.093	0.386	0.024	b	-1.588		-1.9
		3499.12	409.304	0.387	0.024		-1.532		-1.87
27942.33	41.2L	0	357.778	0.165	0.012	-1.495			-1.3
		326.64	362.010	0.160	0.012	-1.553			-1.54
		838.22	368.843	0.477	0.030	-1.018			-1.65
		1518.29	378.336	0.083	0.016	-1.761			-1.49
		2688.69	395.871	0.051	0.010	-1.980			-1.65
		8578.7	516.288	0.020	0.004	-2.071			-1.68
28072.33	9.96	838.22	367.082	0.286	0.021	-0.334	-0.3	-0.52	-0.24
		1489.16	376.071	0.221	0.016	-0.425	-0.46	-0.6	-0.4
		2688.69	393.843	0.018	0.003	-1.472	w	-2.38	-2.07
		3499.12	406.832	0.133	0.010	-0.576	-0.67	-0.96	-0.76
		4386.03	422.066	0.213	0.016	-0.340	-0.33	-0.89	-0.44
		8046	486.539	0.002	0.000	b	-2.167		-2.03
		8679.23	499.203	0.042	0.008	-0.876	-0.95	-1.37	-1.03
		11395.4	515.504	0.059	0.011	-0.593	-0.48	-0.63	-0.6
		12045.17	581.266	0.006	0.001	-1.520			-1.24
		12566.8	599.465	0.015	0.003	-1.134	-1.02	-1.59	
		13777.05	623.766	-	-	-		-1.48	
28151.4	29.3	2237.97	385.791	0.098	0.019	-1.047	-1.03	-1.14	-1.01
		3052.65	398.314	0.230	0.017	-0.649	-0.64	-0.96	-0.61
		3909.62	412.395	0.177	0.013	-0.732	-0.68	-0.93	-0.69
		4386.03	420.662	0.207	0.015	-0.648	-0.81	-1.33	-0.83
		5317.56	437.824	0.242	0.018	-0.546	-0.57	-0.76	-0.61
		11791.05	611.065	0.035	0.007	-1.101	-1	-1.32	
		13604.5	687.242	0.010	0.002	-1.523	-0.89	-1.35	
		14115	712.237	0.001	0.000	w	-2.389	w	-1.65
28191.961	37	1489.16	374.387	0.324	0.020	-0.734	-0.66		-0.55
		2237.97	385.188	0.128	0.009	-1.112	-1.04	-1.19	-1.03
		3499.12	404.861	0.158	0.012	-0.977	-1.51	-1.49	
		4386.03	419.945	0.165	0.012	-0.927	-0.94	-1.33	-1.06
		5317.56	437.047	0.089	0.017	-1.161	-1.33	-2.06	-1.59
		8679.23	512.344	0.023	0.004	w	-1.612	w	
		9406.63	532.183	0.021	0.004		-1.611	-1.42	

		10180.7	555.054	0.023	0.004	-1.532	-1.56		
		10960.16	580.162	0.021	0.004	-1.544	w	-2.08	
		12045.1	619.147	0.010	0.002	-1.790	w		
		12232.34	626.408	0.004	0.001	w	-2.177	w	
		12789.81	649.081	0.032	0.006	-1.259	-0.62	-1.42	-0.84
28239.54	22.4L	1518.29	374.128	0.693	0.044	-0.586			-0.59
		2003.23	381.043	0.298	0.022	-0.937			-1.09
28256.32	35.7	838.22	364.619	-	-	-	-2.57		-1.82
		1489.16	373.486	0.069	0.013	-1.489	-1.97		-1.26
		2237.97	384.235	0.111	0.008	-1.258	-1.36	-1.39	-1.63
		2688.69	391.009	0.113	0.008	-1.235	-1.71	-1.89	-1.4
		3499.12	403.809	0.081	0.015	-1.352	-1.41	-1.63	-0.44
		4386.03	418.813	0.565	0.036	-0.475	-0.42	-0.74	
		8679.23	510.659	0.029	0.005	w	-1.596	-1.73	
		11659.8	602.370	0.019	0.004	w	-1.627	-1.69	
		11798.6	607.450	-	-	-	-1.76		
		12232.34	623.892	0.001	0.000	w	-2.828	-1.59	
		12566.8	637.192	0.008	0.001	w	-1.974	-1.49	
		13777.05	690.452	0.005	0.001	w	-2.074	-1.37	
28314.18	85.2L	1489.16	372.680	0.123	0.013	-1.584			-1.46
		2237.97	383.383	0.364	0.034	-1.006			-0.95
		3052.65	395.747	0.189	0.019	-1.294			-2.01
		5317.56	417.800	0.323	0.030	-0.962			-1.79
28394.04	28.5L	838.22	362.796	0.179	0.013	-1.101			-1.38
		2003.23	378.812	0.432	0.027	-0.706			-0.54
		2688.69	388.914	0.316	0.020	-0.833			-1.36
		3499.12	401.575	0.067	0.013	-1.499			-1.71
		14667.96	728.339	0.006	0.001	w	-2.103		-0.96
28429.38	47.5L	326.64	355.736	0.264	0.019	-1.197			-1.59
		838.22	362.332	0.235	0.017	-1.194			-1.25
		1489.16	371.087	0.098	0.019	-1.601			-1.5
		2003.23	378.306	0.129	0.009	-1.437			-1.88
		2688.69	388.380	0.085	0.016	s	-1.738		-1.87
		10180.7	547.833	0.097	0.018	-1.268			-1.3
		11792.99	601.128	0.052	0.010	-1.464			
		12566.8	630.240	0.041	0.008	-1.546			-1.07

28445.43	12.5	838.22	362.121	0.217	0.016	-0.563	-0.54	-0.6	-0.51
		1489.16	370.866	0.221	0.016	-0.534	-0.63	-0.87	-0.63
		2237.97	381.463	0.082	0.016	-0.942	-1.09	-1.17	-1.18
		2688.69	388.138	0.117	0.009	-0.771	-0.88	-1.12	-0.96
		3499.12	400.748	0.095	0.018	-0.833	-0.98	-1.11	-1.07
		4386.03	415.521	0.142	0.010	-0.629	-0.56	-0.99	-0.73
		7524.86	477.865	0.035	0.007	s -1.110	w		
		8046	490.073	0.044	0.008	-0.989	-0.9	-1.75	-1.3
		8679.23	505.773	0.036	0.007	-1.053	-0.55	-1.36	-1
		11659.8	595.583	0.010	0.002	-1.485	-0.88		-1.42
28540.119	21.5	2237.97	380.089	0.227	0.017	-0.562	-0.76	-0.89	-0.65
		3052.65	392.239	0.329	0.021	-0.373	-0.33	-0.4	-0.26
		3909.62	405.886	0.143	0.010	-0.706	-0.86	-1.11	-0.86
		4386.03	413.892	0.051	0.010	-1.134	-1.48	-2.02	-1.62
		5317.56	430.495	0.147	0.011	-0.643	-0.84	-1.17	-0.87
		9406.63	522.499	0.008	0.002	w -1.736	-1.57		
		10214.38	545.529	0.005	0.001	w -1.872	-1.6		
		10960.16	568.672	0.023	0.004	-1.203	-1.07		
		11791.05	596.883	0.015	0.003	-1.363	-1.1	-1.38	-1.15
		12045.1	606.079	0.009	0.002	w -1.572	w		
		12841.6	636.827	0.010	0.002	-1.456	-0.9	-1.52	
		13466.5	663.228	0.015	0.003	-1.259	-0.54		
		13604.5	669.356	0.019	0.004	-1.151	-0.49	-0.93	
28672.08	19.2L	838.22	359.172	0.081	0.015	-1.279			-2.37
		1479.78	367.773	0.212	0.015	-0.858			
		2003.23	374.863	0.095	0.018	-1.258			-1.49
		2688.69	384.752	0.221	0.016	-0.812			-0.78
		3499.12	397.139	0.392	0.025	-0.542			-0.34
28725.529	38.1	1489.16	367.052	-	-	-	-1.75		-1.62
		2237.97	377.429	0.114	0.008	-1.193	-1.79	-1.32	
		3052.65	389.406	0.129	0.009	-1.112	-1.07	-1.14	-1
		3499.12	396.298	0.215	0.016	-0.873	-1.04		-1.05
		4386.03	410.739	0.256	0.019	-0.767	-0.54		-0.54
		5317.56	427.085	0.259	0.019	-0.728	-0.81	-1.5	-0.87
		8679.23	498.707	0.015	0.003	s -1.832	w		
		9406.63	517.484	-	-	-	w		
		10960.16	562.737	0.002	0.000	w -2.547	w		

		11395.4	576.870	0.002	0.000	w	-2.487	w		
		12789.81	627.348	-	-		-	w		
		13777.05	668.780	0.008	0.001		-1.867	w		
28730.14	66.6L	838.22	358.425	0.332	0.021		-1.096			-1.38
		1489.16	-	-	-		-			-2.07
		2688.69	383.894	0.418	0.026		-0.961			-0.9
		3499.12	396.225	0.131	0.010		-1.464			-1.56
		4386.03	410.661	0.118	0.009		-1.438			-1.58
28850.6	95.4L	2237.97	375.655	0.534	0.034		-0.752			-1.02
		3052.65	387.518	0.196	0.014	s	-			-1.07
		3909.62	400.833	0.244	0.018		-1.040			-1.62
		5317.56	-	-	-		-			-2.21
28913.99	14.9	1489.16	364.529	0.224	0.016		-0.523	-0.89	-1.2	-0.75
		2237.97	374.762	0.114	0.008		-0.792	-0.88	-1.09	-0.78
		3052.65	386.568	0.044	0.008		-1.180	-1.67	-1.83	-1.69
		3499.12	393.359	0.159	0.012		-0.607	-0.98		-0.91
		4386.03	407.583	0.198	0.014		-0.481	-0.4	-0.79	-0.43
		5317.56	423.674	0.204	0.015		-0.434	-0.15	-0.58	-0.21
		8679.23	494.062	0.012	0.002		-1.526	-1.34		
		9406.63	512.484	0.021	0.004		-1.248	-1.09		-1.07
		13777.05	660.453	0.024	0.005		-0.972	-0.68		
28929.72	84.7L	2003.23	371.276	0.302	0.019		-1.364			-1.08
		2688.69	380.975	0.614	0.039		-1.019			-1.38
		3499.12	393.116	0.084	0.016		-1.861			-1.98
28938.55	28.9L	1518.29	364.590	0.255	0.019		-1.148			-1.38
		2003.23	371.154	0.256	0.019		-1.143			-0.88
		2688.69	380.846	0.489	0.031		-0.830			-1.1
		14193.43	678.003	-	-		-			-1.18
28997.141	9.6	1489.16	363.427	0.411	0.026		-0.072	0.03	-0.23	0.02
		2237.97	373.597	0.215	0.016		-0.329	-0.25	-0.56	-0.28
		3052.65	385.329	0.108	0.008		-0.599	-1.16		
		5317.56	422.186	0.006	0.001	w	-1.754	-1.33		-1.8
		8046	477.168	0.013	0.002		-1.345	w		
		8679.23	492.039	0.053	0.010		-0.699	-0.94	-1.38	-0.9
		9406.63	510.309	0.158	0.012		-0.191	-0.36	-0.68	-0.35

		12045.17	589.739	0.018	0.003	-1.018		-1.27	-0.96
		12232.34	596.323	0.011	0.002	-1.207		-1.48	-1.18
		12789.81	616.834	0.007	0.001	-1.390	-1.18	-1.78	
		15897.54	763.177	-	-	-			
29310.16	36.5L	828.3705	351.123	0.106	0.008	-1.347			
		1489.16	-	-	-	-			-2.02
		2237.97	369.278	0.124	0.009	-1.259			-1.49
		2688.69	375.530	0.298	0.022	-0.842			-0.65
		3499.12	387.321	0.456	0.029	-0.660			-1.29
		12982.36	612.489	0.015	0.003	w			
29314.23	162L	2237.97	369.222	0.295	0.022	-1.326			-1.34
		3052.65	380.676	0.246	0.018	-1.441			-1.4
		3909.62	393.518	0.330	0.021	-1.248			-1.93
		10214.38	523.419	0.129	0.009	-1.384			-1.27
29387.869	59	1489.16	358.337	0.179	0.013	-1.127	-1.25	-1.23	-1.11
		2237.97	368.221	0.187	0.014	s -1.083	-1.67		-1.67
		3499.12	386.159	0.344	0.022	s -0.778	-1.69		-1.72
		5317.56	415.333	0.280	0.020	-0.804	-0.56	-0.9	-0.61
		8679.23	482.756	0.011	0.002	w -2.096	-1.86		
		13777.05	640.404	-	-	-	-1.18		
29591.12	16.3L	2237.97	365.485	0.074	0.014	-1.045			-1.58
		3499.12	383.151	0.281	0.021	-0.413			-0.43
		4386.03	396.633	-	-	-			-1.45
		5317.56	411.855	0.614	0.039	-0.016			-0.07
		13771.7	632.174	0.026	0.005				
		15892.9	730.068	0.005	0.001	w			
29619.89	118L	2688.69	371.211	0.670	0.042	-1.011			-1.2
		3499.12	382.860		-	-			-1.93
		4386.03	396.181	0.330	0.021	-1.313			-1.29
29640.51	17.9L	3052.65	376.005	0.178	0.013	-0.509			-0.94
		3909.62	388.528	0.588	0.037	0.017			0.06
		5317.56	411.018	0.109	0.008	-0.663			-0.98
		11791.05	560.086	0.072	0.014	-0.605			-0.8
		12784.13	593.283	-	-	-			
		13466.5	618.105	0.016	0.003	-1.232			-1.06

		14079.32	642.663	0.037	0.007	-0.750	
29801.08	28.5L	2237.97	362.700	0.344	0.022	-0.544	-0.51
		3052.65	373.748	0.255	0.019	-0.668	-0.86
		4377.31	393.356	0.356	0.022	-0.443	
		5317.56	408.323	-	-	-	-1.42
		9399.711	490.193	0.045	0.009	-1.184	
		10214.38	510.581	-	-	-	-1
29804.88	56.2L	1489.16	353.060	0.158	0.012	-1.313	-1.25
		2237.97	362.776		-	-	-1.81
		3499.12	380.037	0.234	0.017	-1.035	-1.19
		4386.03	393.298	0.188	0.014	-1.120	-1.45
		5317.56	408.259	0.420	0.026	-0.717	-0.72
29934.8	9.4L	2237.97	360.949	0.325	0.020	-0.115	0.16
		3052.65	371.888	0.199	0.015	-0.331	-0.31
		3909.62	384.266	-	-	-	-2.15
		4386.03	391.297	0.166	0.012	b -0.186	-1.45
		5317.56	406.105	0.044	0.008	-0.889	-1.34
		8672.006	470.333	-	-	-	
		9406.63	487.000	0.058	0.011	-0.597	-0.95
		10214.38	506.947	0.146	0.011	-0.167	-0.31
		12789.81	583.099	0.042	0.008	-0.589	-0.79
		12841.6	584.866	0.015	0.003	-1.055	-1.08
		13599	612.189	0.006	0.001	w -1.339	
29986.54	46.6L	326.64	337.059	0.298	0.022	s -1.110	-1.4
		838.22	342.975	0.054	0.010	-1.909	-1.71
		2688.69	366.225	0.134	0.010	-1.494	-1.28
		3499.12	377.431	0.236	0.017	-1.220	-1.17
		8046	455.650	0.278	0.020	-1.001	-1.09
30104.78	33.6L	1489.16	349.360	0.158	0.012	-1.064	-1.42
		2237.97	358.747	0.092	0.017	-1.310	-1.42
		3499.12	375.753	0.663	0.042	-0.370	-0.35
		4386.03	388.711	0.076	0.014	-1.351	-1.48
		15897.54	703.672	0.011	0.002	w -1.546	-0.93
30345.63	64L	1489.16	346.444	0.145	0.011	-1.349	-1.76
		2237.97	355.673	0.201	0.015	-1.265	-1.3

		3052.65	366.290	0.413	0.026	b	-0.863	-1.11
		3499.12		-	-		-	-2.02
		4386.03		-	-		-	-2.43
		10960.16	515.707	0.089	0.017		-1.291	-1.38
30879.74	9.3L	3052.65	359.260	0.442	0.028		0.118	0.33
		3909.62	370.675	0.398	0.025		0.069	-0.6
		5317.56	391.092	0.016	0.003		-1.268	-1.55
		10214.38	483.766	0.034	0.006		-0.706	-1.01
		11094.06	505.275	0.096	0.018		-0.232	-0.16
		13598.67	578.703	-	-		-	
		14078.89	595.244	0.004	0.001	w	-1.299	
		14498.15	610.478	0.010	0.002		-1.025	
31122.17	31.3L	2237.97	346.111	0.176	0.013		-0.894	-1.04
		3052.65	356.157	0.100	0.019		-1.136	-1.14
		4386.03	373.919	0.724	0.046		-0.241	-0.27
31309.4	32.1L	0	319.301	0.358	0.023		-1.172	-1.13
		838.22	328.084	0.343	0.022		-1.152	-1.23
		2003.23	341.127	0.142	0.010		-1.517	-1.75
		10518.5	481.009		-		-	-1.96
		10873.3	489.194	0.157	0.011		-1.153	-1.3
31521.61	80L	2237.97	341.390	0.094	0.018		0.624	-1.67
		3052.65	362.058	0.610	0.038		1.165	-1.81
		3909.62	506.687	0.074	0.014		0.017	-1.09
		4386.03	553.706	0.064	0.012		-0.107	-1.89
		14115	574.335	0.158	0.012		-0.737	-0.68
31646.49	25.2L	3909.62	360.428	0.608	0.038		-0.116	-0.03
		12045.1	510.026	0.309	0.019		-0.136	-0.49
		14503.67	583.173	0.083	0.016		-0.550	-0.89
32358.56	15.4L	1518.29	324.158	0.280	0.020		-0.944	-1.1
		2003.23	329.337	0.296	0.022		-0.912	-0.99
		2688.69	336.946	0.424	0.027		-0.719	-0.65
32945.19	40.1L	1489.16	317.812	0.296	0.022		-0.948	-1.2
		2237.97	325.562	0.116	0.008		-1.378	-1.47
		3052.65	334.436	0.404	0.025		-0.766	-0.87

		4386.03	350.050	0.184	0.013	-1.069	-1.13
		12232.34	482.821	-	-	-	-1.43
33763.45	99.2L	3909.62	334.869	0.467	0.029	-0.891	-0.76
		12045.1	460.311	0.533	0.034	-0.569	-0.74
33775.84	32.1L	2237.97	316.987	0.118	0.009	-1.189	-1
		3052.65	325.393	0.294	0.021	-0.756	-0.65
		3909.62	334.730	0.086	0.016	-1.298	-0.9
		5317.56	351.291	0.425	0.027	-0.528	-1.55
		12841.6	477.715		-	-	-1.24
		13466.5	495.615	0.076	0.015	-0.960	-1
34374.7	50.4L	3499.12	323.787	0.191	0.014	-1.207	-1.18
		4386.03	333.363	0.413	0.026	-0.859	-0.99
		5317.56	344.051	0.396	0.025	-0.870	-0.9
38505.66	43.6L	12045.1	377.814	1.000	0.093	w -0.008	-0.01

Table 6.2 shows the radiative parameters for Sm II

Lifetimes were adopted from Scholl et al.²⁵ unless noted.

L denotes lifetime is from Lawler et al.²⁹

Lund refers to the work by Lawler et al.²⁹

UWO refers to the work by Rehse et al.²⁷

CB refers to the work by Corliss and Bozmann³²

XSQGB refers to the work by Xu et al.²⁶

w denotes weak emission line

s denotes emission line has shoulder

b denotes blended emission line

Sm III Data

Table 6.3 shows the radiative parameters for doubly ionized samarium

Lifetimes are experimentally determined by Biémont et al.³¹

w denotes weak emission lines

s denotes shouldered emission lines

b denotes blended line

T denotes theoretical lifetime from Biémont et al.³¹

DREAM refers to experimental work by Biémont et al.³¹

HFR+CP denotes theoretical work using Relativistic Hartree-Fock and core polarization by Biémont et al.³¹

EXP. denotes experimental work by Biémont et al.³¹

HFR+BF refers to combined work using Relativistic Hartree-Fock calculations and experimental branching fractions by Biémont et al.³¹

Upper Energy (cm ⁻¹)	Lifetime (ns)	Wavelength (nm)	Branch Ratio	BR Error		g _k *A _{ki} (10 ⁶ s ⁻¹)			log g*f			
						This Work	Error	DREAM	WSU	HFR+ BF	EXP.	HFR+ CP
28634.34	222 T	349.130	0.07	0.02	w	0.96	0.22		-2.75			-2.96
		352.745	0.22	0.02	b	3.06	0.32		-2.24			-1.92
		359.341	0.71	0.07	w	10.07	0.94		-1.71			-1.93
29763.82	110	339.226	-	-	-	-	-	3.00	-	-2.47	-2.28	-1.99
		345.321	0.52	0.08	s	39.92	8.15	27.00	-1.15	-1.5	-1.32	-1.52
		353.617	0.48	0.08	s	37.47	7.65	15.09	-1.15	-1.73	-1.55	-1.9
30608.25	147 T	335.534	0.01	0.00	w	0.48	0.11	12.10	-3.09	-1.69		-1.51
		343.360	0.49	0.05		23.65	2.20	26.38	-1.38	-1.33		-1.36
		352.877	0.50	0.05	w	23.88	2.22	9.05	-1.35	-1.77		-2.04
31556.56	150 T	332.529	0.74	0.07	b	44.66	4.15	18.42	-1.13	-1.51		-1.26
		341.448	0.07	0.02	w	4.27	1.00	18.78	-2.13	-1.48		-1.37
		351.703	0.18	0.02	s	11.07	1.14	22.74	-1.69	-1.37		-2.32
32341.8	161 T	332.529	0.66	0.06	b	45.19	4.20		-1.13			-1.1
		342.246	-	-	w	-	-		-			-1.49
		353.071	0.34	0.03	b	23.13	2.15		-1.36			-2.81
33710	170 T	326.933	1.00	0.09	s	76.47	7.11	71.35	-0.91	-0.94		-0.96
		336.796	-	-		-	-	5.05	-	-2.06		-1.85
34846.6	45.1 T	286.888	0.52	0.05		34.53	3.21		-1.37			-1.56
		289.326	-	-		-	-		-			-2.54
		293.746	0.48	0.04	b	31.99	2.97		-1.38			-1.27
35314.66	46	285.457	0.38	0.04	w	41.12	5.88	26.52	-1.30	-1.48	-1.49	-1.3

		289.761	0.13	0.01	s	14.09	2.11	12.17	-1.75	-1.8	-1.81	-1.89
		295.579	0.51	0.05	s	54.89	7.85	69.89	-1.14	-1.03	-1.04	-1.11
35928	52	284.669	0.24	0.03	w	32.71	4.61	31.77	-1.40	-1.34	-1.41	-1.17
		290.314	0.15	0.02	b	20.42	2.88	37.02	-1.59	-1.26	-1.33	-1.45
		297.089	0.61	0.06		81.48	10.90	65.83	-0.97	-0.99	-1.06	-1.01
36347.54	75.6 T	275.040	-	-		-	-	-				-1.92
		277.279	0.56	0.06	w	24.54	2.28		-1.55			-1.65
		281.338	0.44	0.04	w	18.93	1.76		-1.65			-1.95
36826.12	52	282.935	0.30	0.03	b	51.36	7.24	30.46	-1.21	-1.36	-1.44	-1.1
		289.365	0.22	0.02	s	38.93	5.49	69.58	-1.31	-0.98	-1.06	-1.09
		296.697	0.48	0.04	b	82.79	11.07	73.04	-0.96	-0.94	-1.02	-1.01
36931.88	75	272.857	0.05	0.01	w	3.64	0.93	12.67	-2.39	-1.87	-1.85	-1.83
		276.786	0.59	0.05		39.12	5.54	33.20	-1.35	-1.44	-1.42	-1.45
		282.090	0.36	0.03	b	23.91	3.38	20.73	-1.54	-1.63	-1.61	-1.64
37715.91	72	270.905	0.07	0.02	w	6.49	1.64	21.97	-2.15	-1.76	-1.62	-1.9
		275.984	0.30	0.03	w	29.07	4.12	41.42	-1.48	-1.47	-1.32	-1.41
		282.100	0.63	0.06	b	61.66	8.30	33.44	-1.13	-1.54	-1.4	-1.52
37738.44	42.2 T	281.920	0.24	0.02	w	61.88	6.37	35.97	-1.13	-1.37		-1.1
		288.875	0.59	0.06	s	155.01	14.42	132.16	-0.71	-0.78		-0.78
		296.548	0.17	0.02	w	43.78	4.51	92.54	-1.24	-0.91		-1.1
38714.36	86.6 T	268.581	0.02	0.00	w	2.00	0.47	10.70	-2.66	-1.93		-1.89
		274.369	0.17	0.02	s	17.90	1.84	43.03	-1.69	-1.32		-1.27
		280.952	0.83	0.08		85.82	7.98	49.99	-0.99	-1.23		-1.27
38758.03	50 T	280.607	0.19	0.02	n	48.63	5.01	20.80	-1.24	-1.61		-1.41
		287.842	0.81	0.08	w	211.37	19.66	238.68	-0.58	-0.53		-0.56
39666.78	73.9 T	267.380	-	-	w	-	-	8.19	-	-2.06		-2.06
		273.627	0.27	0.03	w	40.56	4.18	49.57	-1.34	-1.25		-1.25
		280.502	0.73	0.07	w	108.29	10.07	90.95	-0.89	-0.97		-0.97

Table 6.3 shows the radiative parameters for doubly ionized samarium

Lifetimes are experimentally determined by Biémont et al.³¹

w denotes weak emission lines

s denotes shouldered emission lines

b denotes blended line

T denotes theoretical lifetime from Biémont et al.³¹

DREAM refers to experimental work by Biémont et al.³¹

HFR+CP denotes theoretical work using Relativistic Hartree-Fock and core polarization by Biémont et al.³¹

EXP denotes experimental work by Biémont et al.³¹

HFR+BF refers to combined work using Relativistic Hartree-Fock calculations and experimental branching fractions by Biémont et al.³¹

Gd I Data

Table 6.4 shows the radiative parameters for neutral gadolinium

Lifetimes are adopted from Den Hartog et al.⁵

w denotes weak emission lines

s denotes shouldered emission lines

b denotes blended line

d denotes emission line resided in a spectral gap

Kurucz refers to the tabulated data by Kurucz and Bell³²

Lawl. refers to the work by Lawler et al.⁶

Upper Energy (cm ⁻¹)	Lifetime (ns)	wavelength (nm)	Branch Ratio	BR Error	Log gf			A-values (10 ⁶ s ⁻¹)			
					This work	Kurucz	Lawl.	This work	error	Kurucz	Lawl.
18070.26	118	585.6218	0.509	0.034	-0.239	-0.973	-0.74	4.32	0.46	1.59	2.72
18070.26		611.4078	0.491	0.032	-0.217	-0.731	-0.44	4.16	0.44	2.55	4.93
18083.64	111	569.6209	0.689	0.045	-0.177	-0.863	-0.59	6.21	0.66	2.56	4.86
18083.64		585.163	0.311	0.021	-0.500	-1.077	-0.83	2.80	0.30	1.48	2.59
21857.48	141	457.3812	0.648	0.043	-0.695	-1.125	-1.17	4.60	0.49	3.41	3.1
21857.48		461.9276	-	-			-3.09				0.0363
21857.48		468.813	0.352	0.023	<i>w</i>	-0.939	-1.046	2.50	0.26	3.90	2.93
21905.35	161	478.1926	0.351	0.023	-0.776	-0.917	-0.92	2.22	0.23	3.21	3.18

21905.35		495.2481	0.625	0.041		-0.496	-1.127	-1.14	3.95	0.42	1.84	1.78
21905.35		681.4546	0.024	0.005	b	-1.637	-1.674	-1.62	0.15	0.04	0.28	0.32
22225.54	83.5	454.2031	0.627	0.041		-0.379	-0.775	-0.75	7.51	0.79	6.03	6.4
22225.54		460.8584	-	-		-	-1.569	-1.71	-	-	0.94	0.68
22225.54		470.9793	0.373	0.025		-0.572	-0.879	-0.96	4.47	0.47	4.41	3.69
22334.51	10.8	447.612	0.291	0.021		-0.090	-0.26	-0.18	27.02	3.09	36.57	43.6
22334.51		451.9654	0.705	0.047		0.303	-0.236	-0.14	65.50	6.92	37.91	46.9
22334.51		633.3733	0.004	0.001	n	-1.647	-1.565	-1.64	0.37	0.09	0.90	0.76
22452.87	110	482.17	1.000	0.066		-0.084	-0.631	-0.44	9.09	0.96	5.16	8
22563.82	13.7	443.0629	0.506	0.033		0.185	-0.222	-0.12	37.14	3.92	29.10	36.6
22563.82		447.3278	0.049	0.009	b	-0.817	-1.553	-1.38	3.63	0.86	1.33	2
22563.82		453.7818	0.436	0.029		0.141	-0.233	-0.15	31.99	3.38	27.05	32.8
22563.82		633.6331	0.008	0.002	n	-1.305	-1.536	-1.56	0.59	0.14	0.69	0.65
22718.31	45.9	450.6218	0.876	0.058		0.107	-0.365	-0.33	19.08	2.01	12.88	14.1
22718.31		460.2933	0.096	0.018		-0.834	-0.812	-0.87	2.10	0.50	4.41	3.84
22718.31		476.0749	0.028	0.005		-1.340	-0.845	-1.1	0.61	0.15	3.82	2.15
22820.9	20.8	442.2407	0.544	0.036		0.142	-0.155	-0.05	26.26	2.77	26.50	33.8
22820.9		448.5477	0.005	0.001	b	-1.854	-1.444	-1.53	0.26	0.06	1.32	1.09
22820.9		458.1295	0.450	0.030		0.091	-0.511	-0.49	21.74	2.30	10.88	11.3
23103.66	9.9	432.7102	0.941	0.062		0.210	-0.362	-0.13	96.25	10.16	51.57	89
23103.66		597.7234	0.057	0.011	b	-0.731	-0.847	-0.83	5.78	1.38	8.85	9.2
23103.66		647.0816	0.003	0.001		-1.987		-2.35	0.27	0.07		0.237
23103.66		776.0979	-	-		-		-1.55	-	-		1.05
23103.66		784.4822	-	-		-	-1.381	-1.48	-	-	1.50	1.21
23196.41	58.4	441.1155	0.926	0.061		0.018	-0.402	-0.35	16.22	1.71	12.34	14
23196.41		450.3791	0.074	0.014	s	-1.062	-1.481	-1.6	1.30	0.31	0.99	0.75
23215.03	10	430.6343	0.140	0.010		-0.409	-0.328	-0.25	14.02	1.61	33.78	40.6
23215.03		434.6622	0.830	0.055		0.373	-0.19	-0.17	83.36	8.80	45.56	47.7
23215.03		599.9071	0.019	0.004		-0.997	-0.959	-0.94	1.87	0.44	4.16	4.2
23215.03		633.2046	0.010	0.002	s	-1.199	-0.829	-2.38	1.05	0.25	5.49	0.138
23215.03		642.4505			n		-1.439				1.18	
23215.03		769.4456	0.002	0.000	w	-1.834	-1.32	-1.18	0.17	0.04	1.08	1.5

23215.03		791.0082	-	-		-	-1.62	-1.39	-	-	0.51	0.86
23215.03		1340.7			o			-2.24				0.043
23229.3	52.7	449.7128	0.917	0.061		0.138	-0.296	-0.27	17.40	1.84	12.83	13.6
23229.3		464.7654	0.083	0.016		-0.877	-0.845	-1.02	1.57	0.38	3.39	2.25
23389.78	10	427.4168	0.156	0.011		-0.220	-0.824	-0.89	15.71	1.80	7.82	6.7
23389.78		431.3845	0.373	0.025		0.165	-0.076	-0.01	37.45	3.95	42.96	50.1
23389.78		437.3836	0.453	0.030		0.262	-0.233	-0.17	45.48	4.80	29.11	33.4
23389.78		587.6701	-	-		-		-1.57	-	-		0.74
23389.78		593.6814	0.002	0.000	d	-1.809	-0.821	-0.78	0.21	0.05	4.08	4.5
23389.78		602.1124	0.011	0.002	n	-1.058	-0.992	-1.18	1.15	0.27	2.68	1.72
23389.78		618.8371	-	-		-		-2.73	-	-		0.047
23389.78		631.644	0.004	0.001		-1.487		-1.8	0.39	0.09		0.38
23389.78		767.2558	-	-		-	-1.018	-0.95	-	-	1.55	1.8
23389.78		780.22	-	-		-		-2.16	-	-		0.108
23389.78		799.3786	-	-		-	-1.585	-1.57	-	-	0.39	0.4
23389.78		1323.092			o			-2.08				0.045
23389.78		1409.423			o			-2.32				0.023
23389.78		1658.586			o			-2.01				0.034
23644.16	9.9	426.7008	0.089	0.017		-0.354	-0.812	-0.63	9.01	2.15	6.27	9.6
23644.16		432.5694	0.713	0.047		0.561	0.1	0.18	71.98	7.60	49.83	59.4
23644.16		441.4739	0.198	0.014		0.023	-0.277	-0.22	20.02	2.29	20.08	22.7
23644.16		593.0269	-	-		-	-0.791	-0.72	-	-	3.41	4
23644.16		765.0323	-	-		-	-1.067	-0.84	-	-	1.09	1.83
23644.16		783.4435	-	-		-	-1.455	-1.53	-	-	0.42	0.36
23999.91	10.2	426.0116	0.100	0.019		-0.204	-0.444	-0.41	10.43	1.19	12.01	12.9
23999.91		434.6455	0.749	0.049		0.688	0.16	0.32	78.28	8.27	46.37	68
23999.91		448.6905	0.123	0.009	w	-0.067	-0.455	-0.48	12.90	1.48	10.56	10.1
23999.91		580.7707	0.028	0.005	s	-0.489	-0.964	-1.17	2.91	0.69	1.95	1.21
23999.91		591.6749	-	-		-	-0.94		-	-		
23999.91		596.3155	-	-		-	-1.028	-1.36	-	-	0.98	0.75
23999.91		762.1941	-	-		-	-1.162	-0.84	-	-	0.67	1.51
24430.43	17.4	426.6594	0.375	0.025		0.185	-0.379	-0.37	21.55	2.28	11.77	12.1
24430.43		440.1851	0.625	0.041		0.434	0.193	0.2	35.92	3.79	41.27	42.4
24430.43		761.1754	-	-		-	-1.299	-1.28	-	-	0.44	0.46
24655.64	14.2	405.4722	0.521	0.034		-0.034	-0.28	-0.34	37.52	3.96	42.56	36.7

24655.64		409.0412	0.453	0.030		-0.088	-0.532	-0.5	32.57	3.44	23.41	25.4
24655.64		552.1728	-	-		-	-1.258	-1.42	-	-	2.41	1.66
24655.64		692.6461	-	-		-	-1.072	-1.08	-	-	2.35	2.3
24655.64		699.3165	0.021	0.004	n	-0.963	-1.06	-1.08	1.48	0.35	2.37	2.25
24655.64		710.0704	0.005	0.001	n	-1.539	-1.517	-1.44	0.38	0.09	0.80	0.95
24714.84	11.9	404.5009	0.713	0.047		0.314	-0.11	-0.15	59.92	6.33	45.18	41.1
24714.84		408.0528	0.083	0.016		-0.611	-0.979	-0.93	7.00	1.67	6.00	6.7
24714.84		413.4164	0.164	0.012		-0.305	-0.313	-0.3	13.82	1.58	27.10	28
24714.84		557.6114	0.039	0.007	w	-0.668	-1.068	-1.09	3.29	0.78		2.51
24714.84		578.2712						-2.29				0.145
24714.84		696.4324	-	-		-	-1.234		-	-	1.15	
24714.84		707.0971	-	-		-	-1.105	-1.04	-	-	1.50	1.75
24714.84		722.7968	-	-		-	-1.332	-1.16	-	-	0.85	1.25
25043.65	11	407.8704	0.877	0.058		0.642	0.21	0.31	79.93	8.44	59.08	75
25043.65		415.7778	0.011	0.002	w	-1.247	-0.985	-1.03	0.99	0.24	3.63	3.31
25043.65		428.612	0.096	0.018		-0.273	-0.495	-0.65	8.79	2.09	10.55	7.4
25043.65		547.569	0.005	0.001	n	-1.345	-1.311	-1.37	0.46	0.11	0.99	0.86
25043.65		553.3373	0.002	0.000	n	-1.751	-1.297	-1.63	0.18	0.04	1.00	0.46
25043.65		557.2517	0.005	0.001	b	-1.326	-1.199	-1.15	0.46	0.11	1.23	1.4
25043.65		569.2111	0.004	0.001	w	-1.406	-1.001	-1.06	0.37	0.09	1.87	1.61
25043.65		756.6074	-	-		-	-1.454		-	-	0.37	
25069.18	13.6	398.7834	0.597	0.039		-0.202	-0.688	-0.71	43.89	4.63	28.66	27.3
25069.18		534.8671	0.403	0.027		-0.117	-0.38	-0.23	29.64	3.13	32.38	45.5
25253.84	54.1	395.8674	0.973	0.064	b	-0.228	-1.222		17.99	1.90	3.65	
25253.84		404.4024	0.012	0.002		-2.136	-1.67		0.21	0.05	1.25	
25253.84		534.5123	0.004	0.001		-2.343	-0.73		0.08	0.02	6.21	
25253.84		541.3368	0.011	0.002		-1.893	-0.989		0.21	0.05	3.33	
25376.31	9.4	422.5848	0.899	0.059		0.887	0.43	0.61	95.86	10.12	66.98	101
25376.31		558.6301	0.072	0.014		0.034	-1.244	-1.11	7.69	1.83	0.81	1.12
25376.31		573.5966	0.018	0.003	w	-0.544	-0.899	-0.92	1.93	0.46	1.70	1.64
25376.31		738.0264	-	-		-	-1.11	-1.06	-	-	0.51	0.7
25376.31		775.5958	0.010	0.002	w	-0.527	-1.159	-0.85	1.10	0.26		1.03
25376.31		1338.398			o			-1.31				0.12
25380.89	21.2	402.3347	0.306	0.020		-0.113	-0.4	-0.29	14.44	1.53	14.90	19.2
25380.89		410.0269	0.061	0.012		-0.798	-0.315	-0.35	2.87	0.68	17.45	16.1

25380.89		422.5032	0.496	0.033		0.140	-0.74	-0.59	23.41	2.47	6.18	8.7
25380.89		709.8087	0.137	0.010		-	-1.128	-1.13	-	-	0.90	0.9
25380.89		737.7774	-	-		-	-1.445	-1.28	-	-	0.40	0.58
25380.89		1013.746	-	-	o			-1.66				0.128
25380.89		1034.895			o			-1.68				0.119
25380.89		1092.351			o			-2.1				0.04
25380.89		1754.29			o			-1.93				0.023
25380.89		1765.627			o			-1.44				0.071
25380.89		1850.623			o			-1.75				0.032
25571.67	15.9	394.2638	0.279	0.020		-0.128	-0.55	-0.53	17.73	2.03	13.43	14.1
25571.67		525.5808	0.239	0.017	s	-0.204	-0.87	-0.4	15.15	1.73	8.56	10.7
25571.67		532.1778	0.342	0.023		0.209	-0.496	-0.03	21.71	2.29	17.32	24.4
25571.67		537.6247	0.010	0.002		-1.330	-0.179	-1.85	0.61	0.15		0.36
25571.67		541.3193	0.130	0.009		-0.192		-0.57	8.24	0.94	5.36	6.7
25571.67		666.6932	-	-		-	-0.674	-2.13	-	-		0.124
25571.67		700.3221	-	-		-		-2.08	-	-		0.125
25815.33	143	414.8855	0.592	0.039		-0.499	-0.71	-0.8	4.72	0.50	5.81	4.73
25815.33		530.6711	0.408	0.027	b	-0.447	-0.859	-1	3.25	0.34	2.52	1.82
25815.33		545.254				-	-	-2.13	-	-		0.128
25815.33		750.0495				-	-	-2.17	-	-		0.062
25815.33		1077.197			o			-2.2				0.028
25815.33		1485.579			o			-1.98				0.024
25820.72	28.7	390.429	0.202	0.015		-0.536	-1.041	-0.96	7.07	0.81	4.42	5.34
25820.72		395.3366	0.385	0.025		-0.246	-0.541	-0.52	13.46	1.42	13.64	14.5
25820.72		402.7611	-	-	b	-	-0.812	-0.95	-	-	7.04	5.1
25820.72		518.7881	-	-	w	-	-0.888	-1	-	-	3.56	2.74
25820.72		525.2147	0.317	0.021		-0.082	-9.999	-0.82	11.10	1.17		4.1
25820.72		534.1165	0.032	0.006	b	-1.058	-1.113	-1.17	1.14	0.27	2.00	1.75
25820.72		537.8953	0.043	0.008		-0.934		-2.42	1.49	0.35		0.097
25820.72		543.5042	0.021	0.004		-1.236		-2.68	0.73	0.17		0.052
25820.72		655.8013	-	-	w	-		-2.35	-	-		0.077
25820.72		669.2841	-	-	w	-	-1.297	-1.4	-	-	0.83	0.66
25940.12	12.6	393.4787	0.714	0.047		0.462	-0.374	-0.28	56.77	5.99	16.54	20.7
25940.12		400.8329	0.110	0.008		-0.333	-0.754	-0.75	8.76	1.00	6.65	6.7
25940.12		521.9405	0.080	0.015		-0.242	-0.159	-0.03	6.38	1.52	15.43	20.6
25940.12		527.1789	0.008	0.002	w	-1.232	-1.25	-1.23	0.64	0.15	1.23	1.29
25940.12		530.7308	0.064	0.012		-0.325	-0.137	0.05	5.09	1.21	15.69	24

25940.12		541.5679	0.018	0.003		-0.864	-0.628	-0.57	1.41	0.34	4.87	5.6
25940.12		708.5355	0.006	0.001		-1.128		-2.49	0.45	0.11		0.039
25940.12		1004.683			o			-2.64				0.0136
26145.85	42.2	409.2715	0.964	0.064		0.242	-0.073	-0.09	23.17	2.45	22.43	21.7
26145.85		549.3415	0.036	0.007	n	-0.924	-1.172	-1.27	0.88	0.21	0.99	0.78
26145.85		698.3529	-	-		-	-1.298	-1.61	-	-	0.46	0.223
26335.66	105	387.4468	0.558	0.037	b	-0.500	-1.063	-1.1	6.38	0.67	3.49	3.2
26335.66		523.3939	0.442	0.029		-0.340	-0.44	-0.89	5.06	0.53	8.03	2.83
26337.07	12.9	394.5532	0.424	0.028		0.305	-0.07	-0.1	33.21	3.51	28.04	26
26337.07		406.0924	-	-	b	-	-	-2.14	-	-		0.23
26337.07		516.3701	0.146	0.011	b	0.074	-0.696	-0.93	11.39	1.30	3.87	2.27
26337.07		519.7773	0.207	0.015		0.232	0.05	0.1	16.20	1.85	21.30	24.1
26337.07		530.1673	0.169	0.012		0.162	-0.09	0.08	13.25	1.52	14.83	21.8
26337.07		543.6293	0.043	0.008	w	-0.408	-0.851	-0.84	3.39	0.81	2.45	2.51
26337.07		664.6833	0.010	0.002	w	-0.861	-1.242	-1.47	0.80	0.19	0.66	0.39
26337.07		689.1476	-	-	w	-		-2.04	-	-		0.099
26337.07		721.7954	-	-	w	-		-1.85	-	-		0.138
26568.27		390.9856			n			-2.65				0.076
26568.27	29	402.3141	0.893	0.059		0.294	-0.12	-0.09	31.15	3.29	24.03	26
26568.27		513.6036	0.092	0.017		-0.483	-0.675	-0.78	3.20	0.76	4.11	3.19
26568.27		536.8796	-	-	n	-	-1.015	-1.13	-	-	1.72	1.32
26568.27		678.3368	0.004	0.001	d	-1.628	-1.041	-1.16	0.13	0.03	1.01	0.77
26568.27		709.9449	0.012	0.002	n	-1.101	-1.35	-1.44	0.40	0.10	0.45	0.37
26588.34	101	375.9979	-	-	n	-1.059	-1.25	-1.42	4.12	0.21	5.30	3.59
26588.34		379.065	1.000	0.066		-0.671	-0.94	-1.33	9.90	1.05	10.65	4.35
26870.39	15	397.4812	-	-	s	-	-0.544	-0.6	-	-	8.04	7
26870.39		515.5849	0.444	0.029	s	0.621	0.427	0.36	34.96	3.69	44.69	38.2
26870.39		528.3077	0.304	0.020	s	0.478	-0.029	0.08	23.94	2.53	14.89	19.3
26870.39		544.1565	0.240	0.018	w	0.402	-1.006	-0.98	18.93	2.17	1.48	1.56
26870.39		664.7101	0.012	0.002	w	-0.719		-1.36	0.96	0.23		0.44
26870.39		695.0326	-	-	d	-		-1.76	-	-		0.161
26924.53	62.7	396.6276	0.570	0.038	s	-0.168	-0.273	-0.39	9.59	1.01	15.07	11.6
26924.53		514.1495	-	-	b	-	-0.63	-0.81	-	-	3.94	2.63
26924.53		526.8007	0.275	0.020	s	-0.238	-1.131	-1.29	4.63	0.53	1.18	0.83

26924.53		542.5579	0.097	0.018	w	-0.665		-1.63	1.63	0.19		0.35
26924.53		692.4267	0.058	0.011	w	-0.680		-1.94	0.97	0.23		0.106
27041.75	54.7	369.6933	0.440	0.029		-0.636	-1.222	-1.31	8.05	0.85	4.18	3.42
27041.75		372.658	0.164	0.012		-1.057	-1.191	-1.26	3.00	0.34	4.42	3.78
27041.75		377.1265	0.395	0.026		-0.666	-0.967	-1	7.23	0.76	7.22	6.6
27536.4	14	510.3457	0.822	0.054		0.896	0.519	0.57	59.30	6.26	49.74	56.1
27536.4		525.1201	0.166	0.012		0.226	0.103	0.01	11.96	1.37	18.03	14.6
27536.4		664.275	0.012	0.002	w	-0.717	-1.096	-1.09	0.85	0.20	0.71	0.72
27571.67		376.2213	0.059	0.011		-0.671	-0.305	-0.27	4.56	1.09	21.21	22.8
27571.67		386.6989	0.932	0.061		0.549	0.078	0.06	71.68	7.57	48.50	46.1
27571.67		491.5831	0.009	0.002	w	-1.263	-1.007	-0.95	0.68	0.16	2.47	2.83
27704.97	64.6	367.9213	1.000	0.066		-0.247	-0.703	-0.67	15.48	1.63	10.84	11.7
27731.2	12.8	367.5664	0.079	0.015		-0.504	-0.296	-1.75	7.02	1.86	21.92	0.8
27731.2		373.976	-	-	b	-		-0.33	-	-		20.3
27731.2		384.3272	0.447	0.030	s	0.286	0.114	0.08	39.60	4.18	53.34	49.9
27731.2		477.3071	0.314	0.021	b	0.321		-1.78	27.84	2.94		0.44
27731.2		484.6477	0.026	0.005	w	-0.741		-1.66	2.34	0.56		0.57
27731.2		487.7569	0.125	0.009	b	-0.060		-1.19	11.09	1.27		1.64
27731.2		608.2989	-	-	w	-		-1.92	-	-		0.197
27731.2		649.7942	0.008	0.001	w	-1.012		-1.72	0.70	0.17		0.27
27731.2		840.2885			o			-1.8				0.137
27731.2		971.4135			o			-1.17				0.43
27861.09	9	358.8211	0.130	0.009	w	-0.410	-1.301	-1.22	14.40	1.65	3.70	4.4
27861.09		365.8193	-	-	w	-	-1.321	-1.13	-	-	3.40	5.3
27861.09		465.3552	0.330	0.022		0.222	0.113	-0.07	36.68	3.87	57.04	37.3
27861.09		469.1166	0.092	0.018	w	-0.324	-0.58	-0.71	10.26	2.45	11.38	8.5
27861.09		474.3652	0.448	0.030		0.371	0.118	0.11	49.77	5.26	55.53	55.1
28111.67	11.2	358.365	0.067	0.013	n	-0.644	-1.182	-1.2	6.55	1.56	3.79	3.6
28111.67		368.7279	-	-	n	-		-1.56	-	-		1.49
28111.67		463.6646	0.407	0.027	w	0.365	0.139	0.06	39.88	4.21	47.45	39.3
28111.67		473.0129	0.030	0.006	s	-0.746	0.045	-1.11	2.97	0.71	36.28	2.56
28111.67		475.8704	0.405	0.027	s	0.384		0.08	39.62	4.18		39.3
28111.67		478.8677	0.018	0.003	w	-0.971		-1.96	1.73	0.41		0.36
28111.67		483.308	0.050	0.010		-0.508		-2.2	4.92	1.17		0.199

28111.67		580.284	0.023	0.004		-0.692		-1.41	2.23	0.53		0.85
28168.67	37.4	367.9544	0.271	0.020	n	-0.300	-0.344	-1.47	8.68	0.92	15.69	1.86
28168.67		462.4422	0.132	0.010	w	-0.668	-0.415	-0.54	3.53	0.40	12.65	10.1
28168.67		474.5828	0.081	0.015		-0.873		-0.54	2.18	0.52		9.4
28168.67		477.5639	0.647	0.043	s	0.036		-1.52	17.31	1.83		0.98
28168.67		481.9799	0.013	0.003	w	-1.920		-1.23	0.35	0.08		1.87
28414.93	31.5	358.5527	-	-	n	-	-0.917	-1.23	-	-	5.52	2.78
28414.93		364.6492	-	-	n	-	-0.101	-1.09	-	-	34.25	3.67
28414.93		374.4838	0.527	0.035	w	0.108		-0.28	18.18	1.92		22.4
28414.93		462.2183	-	-	b	-		-1.38	-	-		1.19
28414.93		466.3218	0.163	0.012	w	-0.388		-2.07	5.63	0.65		0.24
28414.93		469.0988	0.271	0.020	w	-0.162		-2.48	9.36	1.07		0.09
28414.93		472.0111	-	-	n	-		-2.4	-	-		0.109
28414.93		570.2462	0.038	0.007	n	-0.830		-2.1	1.32	0.31		0.148
28414.93		584.0028	-	-	s	-		-1.75	-	-		0.31
28414.93		824.9709			o			-1.87				0.119
28432.86	13	501.5049	1.000	0.066		1.042	0.523	0.74	76.92	8.12	46.51	77
28450.95	9.2	461.4497	0.412	0.027		0.542	0.257		49.61	5.24	51.43	
28450.95		468.3072	0.323	0.021	b	0.449	-0.627		38.87	4.10	6.52	
28450.95		476.7248	0.265	0.019		0.379	0.256		31.88	3.65	48.08	
28504.44	63.5	373.2323	1.000	0.066		-0.006	-0.585	-0.51	15.75	1.66	8.30	9.8
28841.68	9.6	457.2203	0.062	0.012	s	-0.281	-0.493	-0.72	6.42	1.53	7.88	4.66
28841.68		459.8897	0.414	0.027	s	0.552	0.198	0.25	43.18	4.56	38.25	42.7
28841.68		468.0047	0.162	0.012	s	0.158	0.023	-0.09	16.84	1.93	24.69	19.2
28841.68		478.4638	0.334	0.022	s	0.492	0.113	0.17	34.81	3.68	29.06	32.9
28841.68		569.798	0.028	0.005	s	-0.433		-0.86	2.91	0.69		2.16
28841.68		587.6823	-	-	b	-		-1.31	-	-		0.74
29119.96	43	349.7096	-	-		-	-0.784	-1.15	-	-	8.15	3.5
29119.96		364.848	0.782	0.052	s	-0.088	-0.488	-0.54	18.60	1.96	14.80	13.3
29119.96		548.2	0.218	0.016	n	-0.290	-0.81	-0.97	5.18	0.59	3.12	2.15
29125.85	17.7	349.6375	0.022	0.004	w	-1.456		-1.75	1.36	0.32		1.38
29125.85		442.8347	-	-	w	-		-1.83	-	-		0.73
29125.85		447.5088	0.085	0.016	w	-0.652		-1.75	5.30	1.26		0.84

29125.85		460.7188	-	-	w	-		-1.85	-	-		0.64
29125.85		463.6191	-	-	w	-		-1.76	-	-		0.76
29125.85	17.7	532.7321	0.383	0.025	w	0.153	-0.148	-0.17	23.85	2.52	23.87	22.5
29125.85		538.9501	0.419	0.028	s	0.202	-0.244	-0.14	26.08	2.75	18.69	23.9
29125.85		548.023	0.091	0.017	w	-0.445	-0.81	-1.09	5.69	0.65	4.91	2.6
29125.85		1028.235						-1.57				0.24
29209.22	24.2	348.6209	0.764	0.050		0.069	-0.389	-0.86	35.73	3.77	24.88	8.3
29209.22		536.5385	0.195	0.014	b	-0.150	-0.192	-0.21	9.11	1.04	16.54	15.8
29209.22		545.5297	0.042	0.008	w	-0.806	-0.671	-0.63	1.94	0.46	5.31	5.8
29293.62	9.7	458.3081	0.655	0.043	b	0.866	0.248	0.27	77.77	8.21	37.45	39.1
29293.62		468.3337	0.210	0.015		0.391	0.297	0.29	24.95	2.86	40.15	40
29293.62		480.7462	0.121	0.009	b	0.175	0.04	-	14.38	1.65	21.08	19.2
29293.62		572.4731	0.013	0.002	w	-0.640	-0.421	-0.5	1.55	0.37	5.14	4.3
29293.62		594.8229	-	-	w	-		-1.4	-	-		0.5
29358.63	27	343.0313	0.139	0.010		-0.786		-1.13	5.16	0.59		4.6
29358.63		346.8139	0.176	0.013	s	-0.674		-1.68	6.52	0.75		1.27
29358.63		352.5147	0.016	0.003	w	-1.707	-0.845	-1.01	0.59	0.14	8.52	5.8
29358.63		438.315	0.285	0.021		-0.260		-2.01	10.58	1.21		0.38
29358.63		442.8937	0.002	0.000	w	-2.438		-1.27	0.07	0.02		2.02
29358.63		446.6599	0.355	0.023	s	-0.149	0.087	-0.78	13.17	1.39	45.36	6.2
29358.63		449.207	0.009	0.002		-1.748		-1.86	0.33	0.08		0.51
29358.63		451.8769	-	-	n	-		-1.27	-	-		1.93
29358.63		532.2704	0.011	0.002	s	-1.499	-0.508	-0.55	0.41	0.10	8.12	7.4
29358.63		541.118	0.007	0.001		-1.719		-0.69	0.24	0.06		5.2
29358.63		733.0481	0.001	0.000	n	-2.392		-1.54	0.03	0.01		0.4
29358.63		964.4784			o			-1.76				0.138
29358.63		1008.493			o			-1.9				0.092
29358.63		1014.885			o			-1.78				0.119
29358.63		1065.823			o			-2.07				0.055
29358.63		1139.895			o			-1.56				0.157
29426.45	18.6	339.7328	0.042	0.008	w	-1.247	-0.396	-1.06	2.34	0.56	33.15	7.2
29426.45		342.2348	0.819	0.054	b	0.052		-1.2	45.82	4.84		5.1
29426.45		433.7495	0.071	0.013		-0.805	-0.274	-0.6	3.97	0.95	26.93	12.6
29426.45		437.0155	-	-	b	-	-0.131	-0.85	-	-	36.88	7
29426.45		441.5669	0.023	0.004		-1.282		-1.24	1.28	0.30		2.81
29426.45		450.4958	0.001	0.000	w	-2.540		-1.02	0.07	0.02		4.5
29426.45		454.4234	0.036	0.007		-1.065	-0.546	-0.8	1.99	0.47	13.12	7.2

29426.45		457.2449	0.006	0.001		-1.823		-1.19	0.34	0.08		2.94
29426.45		524.3329	0.002	0.000	w	-2.144		-1.31	0.12	0.03		1.7
29426.45		826.6135			o			-1.6				0.35
29426.45		828.6674			o			-1.87				0.19
29426.45		958.2087			o			-1.28				0.55
29426.45		960.1323			o			-2.04				0.095
29426.45		960.932			o			-1.24				0.59
29451.36	10.4	345.7018	0.275	0.020		0.021		-1.59	26.61	3.05		1.29
29451.36		351.3658	0.087	0.017		-0.465	-0.296	-0.28	8.41	2.01	24.83	26
29451.36		360.4879	0.581	0.038	b	0.383	0.105	0.06	56.27	5.94	59.39	53.7
29451.36		444.817	0.006	0.001		-1.424		-1.29	0.58	0.14		1.57
29451.36		447.3431	0.023	0.004		-0.842		-1.97	2.18	0.52		0.32
29451.36		449.9908	0.010	0.002		-1.186		-1.19	0.98	0.23		1.93
29451.36		538.4156	0.009	0.002		-1.080	-0.482	-0.47	0.87	0.21	6.89	7.1
29451.36		550.6628	0.004	0.001	w	-1.429		-1.28	0.37	0.09		1.05
29451.36		567.3484	0.006	0.001	w	-1.232		-1.8	0.55	0.13		0.3
29451.36		734.1437	-	-	n	-		-2.11	-	-		0.087
29451.36		742.633	-	-	n	-		-1.62	-	-		0.26
29451.36		756.0765	-	-	n	-		-1.77	-	-		0.18
29451.36		843.6117			o			-1.31				0.42
29451.36		865.9666			o			-0.95				0.9
29628.39		358.2012	0.876	0.058		0.312	-0.71	-0.74	48.42	5.11	9.21	8.5
29628.39		441.3405	0.069	0.013		-0.613	-0.941	-1.17	3.79	0.90	3.56	2.1
29628.39		533.3306	0.032	0.006		-0.784	0.105	0.13	1.75	0.42	27.13	29
29628.39		545.345	0.023	0.004		-0.899	-0.284	-0.29	1.28	0.31	10.60	10.5
29628.39		831.1947			o			-2.01				0.087
29628.39		852.8878			o			-1.71				0.164
29628.39		987.8329			o			-2.05				0.055
29628.39		996.1494			o			-1.8				0.098
29628.39		1005.128			o			-1.32				0.28
29631.26	9	337.3846	0.269	0.020	s	-0.101	-0.722	-1.07	33.19	3.80	15.87	7.1
29631.26		339.852	-	-	w	-		-1.5	-	-		2.6
29631.26		429.9291	0.611	0.040		0.466	0.227	-0.02	75.30	7.95	86.89	49
29631.26		433.1376	-	-	b	-	-0.016	-0.17	-	-	48.93	34.3
29631.26		437.6082	0.091	0.017	s	-0.346	-0.454	-0.66	11.22	1.28	17.48	10.8
29631.26		450.232	0.012	0.002		-1.209		-1.44	1.45	0.35		1.7
29631.26		453.0014	-	-		-		-1.66	-	-		1.01
29631.26		533.249	-	-		-		-1.78	-	-		0.55

29631.26		557.0831	0.016	0.003	w	-0.878		-1.98	2.03	0.48		0.321
29631.26		812.8486			o			-2.06				0.126
29631.26		939.7612			o			-1.86				0.15
29631.26		942.3805			o			-2.03				0.099
29754.91	89.3	458.427	0.027	0.005	b	-1.479	-0.378		0.31	0.07	7.81	
29754.91		470.3133	0.973	0.064		0.095	-0.044		11.04	1.17	16.02	
29794.75	11.4	457.591	0.237	0.017		0.351	0.11	0.07	21.03	2.41	24.13	21.9
29794.75		469.4334	0.750	0.049		0.874	0.573	0.51	66.57	7.03	66.57	57.8
29794.75		577.6005	0.014	0.003	d	-0.683	-0.127	-0.23	1.22	0.29	8.77	7
29794.75		1005.294			o			-1.19				0.25
29876.62		337.0406	0.158	0.012	b	-0.119		-1.13	24.78	2.84		4.9
29876.62	6.8	340.6916	0.102	0.007	s	-0.301	-0.378	-0.67	15.94	1.83	26.72	13.8
29876.62		428.5815	0.207	0.015	s	0.208	0.253	-0.01	32.53	3.73	72.21	39.6
29876.62		432.958	0.119	0.009		-0.024	0.201	0.14	18.68	2.14	62.77	54.4
29876.62		438.9894	0.414	0.027	s	0.529	-0.094	-0.07	65.03	6.87	30.96	32.9
30007.31		344.6315	0.024	0.004		-1.035		-1.34	1.99	0.47		1.97
30007.31		353.403	0.519	0.034		0.329		-1.24	43.78	4.62		2.4
30007.31		436.4844	0.046	0.009		-0.541		-1.9	3.87	0.92		0.34
30007.31		443.788	-	-	b	-		-0.83	-	-		3.84
30007.31		453.1818	0.042	0.008	s	-0.551		-0.74	3.51	0.84		4.52
30007.31	15.5	534.3009	0.229	0.017		0.333	0.4	0.39	19.32	2.21	45.12	44
30007.31		549.9956	0.141	0.010	b	0.146	-0.437	-0.42	11.86	1.36	6.20	6.5
30007.31		713.1799	-	-	w	-		-1.97	-	-		0.109
30007.31		959.9067			o			-1.54				0.159
30007.31		968.2409			o			-1.37				0.233
30007.31		977.6551			o			-1.37				0.231
30197.3	26.6	342.389	0.560	0.037		-0.085	0.408	-0.95	21.25	2.24	132.30	5.9
30197.3		351.0453	0.058	0.011	w	-1.049		-1.53	2.19	0.52		1.44
30197.3		427.0274	0.093	0.018	s	-0.674	-0.605	-0.84	3.52	0.84	8.25	4.84
30197.3		430.5275	-	-	w	-		-1.85	-	-		0.47
30197.3		432.8935	0.028	0.005	w	-1.186	-0.249	-0.51	1.05	0.25	18.23	10
30197.3		435.3724	-	-	b	-	-0.377	-1.57	-	-	13.14	0.87
30197.3		440.0764	0.022	0.004	s	-1.274		-0.43	0.83	0.20		11.7
30197.3		517.6206	0.240	0.017	b	-0.095		-1.47	9.09	1.04		0.76
30242.29		341.8621	0.232	0.017		0.028		-1.03	27.65	3.17		4.8

30242.29	8.4	426.2082	0.456	0.030		0.512	0.861	-0.23	54.29	5.73	242.20	19.6
30242.29		429.6948	0.264	0.019	s	0.282		-0.83	31.44	3.60		4.9
30242.29		432.0517	0.027	0.005	s	-0.700	0.243	0.12	3.24	0.77	56.81	42.8
30242.29		439.2064	0.020	0.004	s	-0.810	0.143	0.14	2.43	0.58	43.67	43
30242.29		527.6738	-	-	w	-		-1.57	-	-		0.59
30307.48		332.2147	0.115	0.008	w	-0.679		-1.49	7.03	0.80		2.19
30307.48	21.3	335.7613	0.133	0.010	w	-0.609	-0.303	-0.8	8.09	0.93	32.70	10.4
30307.48		341.1017	-	-	w	-	-0.283	-0.67	-	-	33.18	13.5
30307.48		420.8085	0.208	0.015	s	-0.217	-0.611	-1.09	12.70	1.45	10.24	3.4
30307.48		425.027	0.022	0.004	w	-1.179	-0.525	-0.88	1.36	0.32	12.24	5.4
30307.48		428.4942	-	-	b	-		-1	-	-		4
30307.48		430.8379	0.393	0.026	s	0.079		-1.31	23.95	2.53		1.96
30307.48		433.2933	0.129	0.009	w	-0.400		-1.7	7.85	0.90		0.79
30307.48		713.5352	-	-	w	-		-1.9	-	-		0.18
30307.48		725.8601	-	-		-		-2.09	-	-		0.113
30307.48		772.2697	-	-	w	-		-1.38	-	-		0.52
30307.48		776.9239	-	-	w	-		-0.92	-	-		1.48
30307.48		786.7723	-	-	d	-	-0.837	-1.05	-	-	1.74	1.07
30394.64	102	437.8552	1.000	0.066		0.147	-0.01		9.80	1.03	67.96	
30505.37	15.1	347.2882	-	-	b	-		-1.12	-	-		2.8
30505.37		434.188	0.534	0.035	s	0.724		-1.61	62.45	6.59		0.57
30505.37		443.1757	0.128	0.009	w	0.123	-0.33	-0.37	15.01	1.72	10.58	9.7
30505.37		454.2748	0.018	0.003	w	-0.717		-0.72	2.07	0.49		4.08
30505.37		535.3269	0.308	0.020		0.668	0.367	0.46	36.09	3.81	36.10	44.7
30505.37		550.5258	0.012	0.002	w	-0.714	-0.536	-1.83	1.42	0.34	4.20	0.215
30505.37		700.2561	-	-	w	-		-1.98	-	-		0.095
30505.37		923.6839			o			-1.72				0.098
30505.37		932.2478			o			-1.18				0.34
30555.83	7.3	491.6597	0.835	0.055		0.396	-0.465	-0.62	114.36	12.08	31.51	22.3
30555.83		495.0113	0.165	0.012	w	-0.302	-0.296	-0.33	22.62	2.59	45.87	43
30652.02	6.6	345.5279	-	-	w	-	-0.265	-0.6	-	-	23.33	10.7
30652.02		422.2585	-	-	w	-	-0.122	-1.33	-	-	21.48	1.33
30652.02		431.4401	0.597	0.039	s	0.596	0.439	0.24	54.32	5.74	75.70	48.4
30652.02		440.3133	0.359	0.024		-0.297	0.466	0.47	6.67	1.59	77.34	79
30652.02		531.156	0.044	0.008	w	-		-1.23	-	-		1.07
30652.02		693.1364	-	-	w			-2.05				0.095

30694.87	7.3	325.6934	0.247	0.018		-0.006		-0.75	62.00	6.55		22.5
30694.87		327.9922	-	-	b	-		-0.5	-	-		39
30694.87		429.6509	0.501	0.033	b	0.542		-1.31	125.71	13.27		3.5
30694.87		433.888	0.024	0.005	w	-0.764		-1.6	6.10	1.45		1.79
30694.87		488.3204	0.127	0.009	w	0.058	-0.181	-0.34	31.95	3.66	36.86	25.3
30694.87		496.9172	0.097	0.018	s	-0.045	-0.11	-0.17	24.34	2.79	41.91	37
30694.87		669.3117	-	-	w	-		-1.52	-	-		0.9
30694.87		669.3285	-	-	w	-		-1.39	-	-		1.22
30694.87		688.0944	0.002	0.000	w	-1.355		-1.88	0.62	0.15		0.37
30881.66	7.8	323.7234	0.009	0.002	s	-1.612		-0.99	1.11	0.26		9.3
30881.66		325.9944	0.017	0.003	s	-1.313		-0.68	2.18	0.52		18.7
30881.66		329.4087	0.022	0.004	w	-1.184	0.033	-0.42	2.87	0.68	94.69	33.4
30881.66		407.9896	0.008	0.001	w	-1.456		-2.19	1.00	0.24		0.37
30881.66		422.7721	-	-	w	-		-1.41	-	-		2.08
30881.66		426.2293	0.823	0.054		0.612		-1.42	107.26	11.33		2
30881.66		428.7105	0.007	0.001	b	-1.483		-1.48	0.85	0.20		1.73
30881.66		487.1517	0.034	0.006	b	-0.656		-0.21	4.43	1.06		24.7
30881.66		492.3461	0.075	0.014	s	-0.305	-0.011	-0.74	9.73	2.32	39.13	7.2
30881.66		499.9067	-	-	b	-	-0.182	-0.19	-	-	25.06	24.4
30881.66		660.4578	0.001	0.000	w	-1.773		-1.42	0.18	0.04		0.82
30881.66		664.3628	0.006	0.001	w	-1.151		-1.43	0.76	0.18		0.8
30881.66		737.8349	-	-	d	-		-1.29	-	-		0.9
30881.66		878.9827			o			-1.82				0.19
31135.8	6.6	323.3149	0.352	0.023	b	0.200		-0.86	56.18	5.93		9.7
31135.8		326.6731	0.046	0.009	s	-0.671	0.153	-0.3	7.40	1.76	98.72	35.1
31135.8		331.7262	0.053	0.010	s	-0.603		-0.52	8.40	2.00		20.6
31135.8		413.8028	0.028	0.005	w	-0.693	-0.619	-0.9	4.39	1.05	10.40	5.4
31135.8		418.2767	0.107	0.008	w	-0.095	-0.28	-0.64	17.00	1.95	22.22	9.7
31135.8		486.26	0.064	0.012	w	-0.188	-0.02	-0.13	10.16	2.42	29.92	23.4
31135.8		493.6335	0.300	0.020		0.498	-0.113	-0.14	47.86	5.05	23.43	22.1
31135.8		503.9088	0.034	0.007		-0.424	-0.14	-0.21	5.50	1.31	21.13	17.9
31135.8		650.1204	0.007	0.001	w	-0.904		-1.16	1.09	0.26		1.2
31135.8		653.3289	0.009	0.002	w	-0.765		-1.28	1.49	0.35		0.92
31135.8		660.0436	-	-	w	-		-1.39	-	-		0.69
31135.8		725.8267	-	-	w	-		-1.53	-	-		0.42
31135.8		866.0648			o			-1.54				0.29
31146.46	6.7	339.7222	-	-	w	-		-0.56	-	-		10.6

31146.46		422.4262	0.011	0.002	b	-0.868	-0.185	-0.75	1.69	0.40	25.15	4.45
31146.46		430.9288	0.216	0.016	s	0.430	-0.431	0.1	32.19	3.69	9.23	29.8
31146.46		441.4157	0.679	0.045	w	0.949	0.197	0.65	101.40	10.71	37.67	102
31146.46		531.7531	-	-		-	0.748	-1.75	-	-	127.70	0.28
31146.46		535.7593	0.094	0.018		0.256		-0.93	13.97	3.33		1.83
31171.62	14	440.9257	0.370	0.024	w	0.418	0.158	0.05	26.40	2.79	29.02	22.7
31171.62		535.0377	0.630	0.042	s	0.818	0.545	0.54	45.03	4.75	48.05	47.5
31457.18	6.2	323.278	0.145	0.011	b	-0.083	-0.212	-0.68	23.96	2.74	35.59	12
31457.18		328.2258	0.349	0.023	s	0.311	-0.136	-0.33	57.54	6.08	41.13	26.5
31457.18		336.1725	-	-	w	-	0.466	-0.88	-	-	106.30	7.1
31457.18		408.3702	0.154	0.011	n	0.146	-0.265	0.22	25.42	2.91	19.54	60
31457.18		410.4984	0.001	0.000	w	-1.889	-0.148	-0.59	0.23	0.06	18.25	9.3
31457.18		412.7268	-	-	w	-	0.117	-1.23	-	-	32.27	2.11
31457.18		416.9518	0.209	0.015	b	0.296		-1.33	34.44	3.94		1.65
31457.18		485.9223	0.057	0.011		-0.131		-0.36	9.49	2.26		11.1
31457.18		495.8758	0.076	0.014		0.008		-0.06	12.56	2.99		21.6
31457.18		509.3658	0.006	0.001	w	-1.104		-0.79	0.92	0.22		3.8
31457.18		627.2578	-	-		-		-1.93	-	-		0.18
31457.18		639.8894	-	-	d	-		-1.45	-	-		0.53
31457.18		646.3292	0.003	0.001	w	-1.186		-1.12	0.47	0.11		1.11
31457.18		669.9367	-	-	w	-		-1.75	-	-		0.24
31457.18		713.2008	-	-	w	-		-1.62	-	-		0.28
31457.18		849.0201			o			-1.52				0.25
31777.97	6.3	319.9588	0.289	0.021	s	0.386	-0.324	-0.86	72.07	7.61	28.07	8.1
31777.97		324.8047	0.073	0.014	s	-0.201		-0.64	18.09	2.07		13.3
31777.97		332.5847	0.037	0.007		-0.470		-1.09	9.28	2.21		4.5
31777.97		400.02	0.215	0.016	b	-	-0.424		-	-	14.27	
31777.97		403.0881	0.003	0.001		0.458	0.707	0.37	53.54	5.65	190.00	88
31777.97		405.1614	0.295	0.022	w	-1.423		-0.92	0.70	0.17		4.5
31777.97		488.109	0.075	0.014	b	0.763	-0.049	-0.15	73.61	7.77	22.72	18
31777.97		501.1742	-	-	s	0.192	-0.203	-0.33	18.77	2.15	15.12	11.3
31777.97		622.5991	-	-	w	-		-1.71	-	-		0.31
31777.97		627.0149	-	-	w	-		-1.4	-	-		0.62
31777.97		633.1969	0.013	0.002	w	-0.377		-1.18	3.17	0.76		1.01
31777.97		645.7598	-	-	w	-		-2.11	-	-		0.114
31777.97		655.838	-	-	w	-		-1.61	-	-		0.35
31777.97		677.2271	-	-	d	-		-1.89	-	-		0.17
31777.97		697.2441	-	-	d	-		-1.8	-	-		0.2

31777.97		962.3417			o			-1.87				0.088
31794.78	10.1	324.6275	0.022	0.004	w	-0.772	0.815	-1.15	2.67	0.64	206.40	3.5
31794.78		402.8152	-	-	b	0.911		0.39	87.80	9.27		78
31794.78		404.8857	0.716	0.047	s	-		-0.75	-	-		5.5
31794.78		487.7089	-	-	w	0.608		-1.32	26.91	3.08		1.03
31794.78		517.7697	0.219	0.016	w	-		-1.06	-	-		1.65
31794.78		621.9483	-	-	w	-		-0.98	-	-		1.37
31794.78		642.2502	-	-	w	-		-1.46	-	-		0.43
31794.78		664.8942	-	-	w	0.280		-0.85	5.29	1.26		1.66
31794.78		719.8457	0.043	0.008				-1.76				0.17
31794.78		960.7877			o			-1.48				0.18
31794.78		972.5127			o			-0.61				1.34
31847.48		406.1818	0.474	0.031	w	0.431		-0.66	60.58	6.40		9.9
31847.48	15.4	409.372	0.225	0.016	w	0.114	0.216	-0.13	28.73	3.03	72.68	33.1
31847.48		476.8755	0.006	0.001	w	-1.359		-0.97	0.71	0.17		3.5
31847.48		486.4581	-	-	w	-		-1.19	-	-		2.03
31847.48		495.847	0.240	0.018		0.309		-1.44	30.67	3.24		1.1
31847.48		505.1568	-	-	w	-		-1.67	-	-		0.63
31847.48		599.5758	0.040	0.008	w	-0.309		-1.38	5.05	1.20		0.86
31847.48		619.9157	-	-	w	-		-1.96	-	-		0.212
31847.48		621.363	-	-	w	-		-1.66	-	-		0.42
31847.48		624.2933	-	-	w	-		-1.27	-	-		1.03
31847.48		637.5185	0.016	0.003	w	-0.641		-1.65	2.08	0.50		0.41
31847.48		960.5578			o			-1.08				0.66
31859.28	6.2	401.7709	0.112	0.008	s	0.108	0.412	-0.03	29.45	3.37	118.50	43.1
31859.28		403.8306	0.475	0.031	w	0.741		-1.25	125.14	13.21		2.5
31859.28		405.987	0.225	0.016	s	0.421	0.605	0.27	59.19	6.25	181.00	84
31859.28		409.1742	0.019	0.004	w	-0.648	-0.545	-0.78	4.97	1.18	12.61	7.4
31859.28		476.6071	-	-	w	-		-1.59	-	-		0.84
31859.28		486.1789	0.049	0.009	w	-0.080	-0.098	-0.3	13.03	3.10	25.01	15.5
31859.28		495.5569	0.006	0.001	w	-1.015		-1.6	1.46	0.35		0.76
31859.28		504.8557	0.104	0.008		0.276		-1.78	27.42	3.14		0.48
31859.28		637.0389	0.005	0.001	w	-0.874		-1.47	1.22	0.29		0.62
31859.28		642.3859	0.006	0.001	w	-0.779		-1.35	1.49	0.36		0.81
31859.28		652.3582	-	-	w	-		-1.87	-	-		0.234
31859.28		701.1444	-	-	w	-		-1.77	-	-		0.26
31865.24	5.3	313.7307	0.280	0.020	s	-0.044	-0.264	-0.5	61.27	6.47	73.75	43

31865.24		315.8631	0.071	0.013	w	-0.636	-0.233	-0.5	15.45	3.68	78.15	42
31865.24		412.9135	0.064	0.012	w	-0.442		-1.23	14.12	3.36		4.7
31865.24		461.9136	0.092	0.017	b	-0.191	-0.226	-0.44	20.13	2.31	37.14	22.7
31865.24		464.8707	-	-	s	-	0.2	-0.3	-	-	97.78	31
31865.24		469.5984	0.116	0.009	w	-0.074		-0.4	25.50	2.92		24
31865.24		598.9377	0.216	0.016	w	0.405		-0.9	47.21	5.41		4.7
31865.24		620.1598	0.140	0.010	w	0.248		-1.16	30.67	3.51		2.4
31865.24		620.6777	0.005	0.001	w	-1.170		-1.78	1.17	0.28		0.57
31865.24		620.6921	0.016	0.003	w	-0.704		-1.07	3.42	0.82		3
31865.24		633.2496	-	-	w	-		-1.59	-	-		0.85
31865.24		636.7971	-	-	w	-		-1.8	-	-		0.52
31865.24		687.8984	-	-	w	-		-1.55	-	-		0.79
31865.24		689.3202	-	-	w	-		-1.37	-	-		1.2
31869.14	7.1	313.6923	0.077	0.015		-0.591	-0.264	-0.57	12.42	2.96	52.69	25.8
31869.14		319.0279	0.262	0.019	s	-0.044	-0.178	-0.62	42.27	4.46	62.10	22.6
31869.14		392.1844	0.065	0.012	w	-0.471		-1.83	10.47	2.49		0.92
31869.14		411.2935	0.059	0.011	w	-0.472	-0.377	-0.66	9.50	2.26	23.63	12.2
31869.14		464.7865	0.084	0.016	w	-0.212		-1.31	13.53	3.22		2.15
31869.14		469.5125	-	-	w	-		-0.53	-	-		12.8
31869.14		476.3832	0.106	0.008	b	-0.087	0.115	-0.17	17.16	1.97	54.69	28.1
31869.14		495.3149	0.199	0.015	sed	0.219	-0.135	-0.25	32.13	3.68	28.45	22
31869.14		598.7979	0.129	0.009		0.194		-0.86	20.74	2.37		3.7
31869.14		620.0099	0.005	0.001	w	-1.189		-1.51	0.80	0.19		0.77
31869.14		620.5276	0.014	0.003	w	-0.735		-1.18	2.28	0.54		1.65
31869.14		623.45	-	-	d	-		-1.63	-	-		0.57
31869.14		636.6391	-	-	w	-		-1.47	-	-		0.8
31869.14		641.9793	-	-	w	-		-1.6	-	-		0.58
31869.14		692.8388	-	-	w	-		-1.2	-	-		1.24
31869.14		1059.034						-1.19				0.55
31869.14		1078.85						-1.35				0.36
31999.81		396.4988	0.010	0.002	w	-1.353		-1.35	1.34	0.32		2.7
31999.81	7.7	403.6833	-	-	b	-	0.217	-0.11	-	-	96.32	46
31999.81		406.8342	0.196	0.014	w	-0.022	0.528	-	27.33	3.13	194.10	58
31999.81		409.0941	0.077	0.015	s	-0.422		-1.38	10.77	2.57		2.38
31999.81		466.6487	0.215	0.016		0.138		-1.12	30.07	3.44		3.3
31999.81		473.4353	0.335	0.022		0.343		-1.5	46.78	4.94		1.34
31999.81		492.1287	0.057	0.011		-0.391		-1.7	7.99	1.91		0.78
31999.81		615.0257	-	-	w	-		-1.74	-	-		0.46
31999.81		615.5351	0.039	0.007		-0.368		-1.43	5.39	1.28		0.93

31999.81		627.8975	0.011	0.002	w	-0.880		-1.28	1.59	0.38		1.27
31999.81		631.3851	0.060	0.011	w	-0.156		-1.66	8.33	1.99		0.52
31999.81		956.206			o			-1.44				0.38
32020.34		317.4959	0.388	0.026	s	0.176		-1.03	45.13	4.77		5.6
32020.34		322.2669	0.050	0.010	w	-0.696		-1.2	5.87	1.40		3.7
32020.34	9.7	403.3489	0.385	0.025		0.381	0.648	0.3	44.77	4.73	165.60	74
32020.34		472.9754	0.023	0.004	w	-0.700		-1.88	2.70	0.64		0.36
32020.34		482.4004	0.007	0.001	w	-1.194		-1.44	0.83	0.20		0.94
32020.34		495.1578	0.101	0.007	s	-0.023	-0.452	-0.6	11.71	1.34	8.73	6.3
32020.34		500.7826	0.015	0.003	w	-0.838		-1.03	1.76	0.42		2.27
32020.34		605.8503	0.011	0.002	w	-0.816		-0.93	1.26	0.30		1.93
32020.34		623.6237	-	-	d	-		-1.02	-	-		1.49
32020.34		633.0763	0.020	0.004	w	-0.515		-0.98	2.31	0.55		1.59
32020.34		685.654	-	-	w	-		-1.94	-	-		0.147
32020.34		940.4016			o			-0.95				0.76
32020.34		944.8645			o			-1.58				0.18
32091.73	7.2	321.527	0.204	0.015		0.092	-0.784	-0.1	30.63	3.51	8.16	40
32091.73		329.1489	0.100	0.019	w	-0.198	0.181	-0.23	14.99	1.72	71.80	28
32091.73		406.2014	-	-	b	-		-1.41	-	-		1.21
32091.73		414.0573	0.442	0.029	s	0.648		-0.9	66.47	7.02		3.7
32091.73		493.4131	0.083	0.016		0.073	0.522	0.4	12.47	2.97	70.07	53
32091.73		506.2966	0.081	0.015		0.085		-1.53	12.16	2.90		0.59
32091.73		509.9271	0.041	0.008	w	-0.206		-0.52	6.14	1.46		6
32091.73		610.6666	0.046	0.009	b	-0.002		-1.56	6.85	1.63		0.38
32091.73		620.8588	-	-	w	-		-1.19	-	-		0.85
32091.73		630.2271	0.004	0.001	w	-0.986		-0.58	0.67	0.16		3.41
32091.73		689.8974	-	-	w	-		-1.11	-	-		0.83
32091.73		812.1128			o			-1.33				0.37
32133.13	16.9	401.5217	0.270	0.020	w	-0.171	-0.013	-0.59	19.92	2.10	57.33	15.3
32133.13		404.6389	-	-	s	-		-1.43	-	-		2.18
32133.13		406.8744	0.289	0.021	w	-0.130	0.243	-0.38	21.32	2.25	100.70	23.9
32133.13		459.1511	0.072	0.014	w	-0.631		-1.55	5.28	1.26		1.26
32133.13		488.9201	0.369	0.024	s	0.135	-0.501	-0.51	27.20	2.87	12.57	12.4
32133.13		1030.224			o			-1.5				0.28
32149.52	7	404.3706	0.338	0.022	w	0.177	0.435	-0.01	61.30	6.47	222.00	79
32149.52		406.6032	0.219	0.016	w	-0.007	0.245	-0.33	39.64	4.54	141.80	37.6
32149.52		455.9251	0.284	0.021	w	0.206		-1.75	51.54	5.44		1.14

32149.52		458.8058	0.040	0.008	w	-0.646		-1.33	7.16	1.71		2.97
32149.52		463.4104	0.022	0.004	w	-0.900		-1.51	3.91	0.93		1.92
32149.52		609.4131	0.055	0.010	w	-0.255		-1.7	9.97	2.38		0.71
32149.52		609.9271	0.032	0.006	w	-0.485		-2.08	5.87	1.40		0.3
32149.52		619.5366	0.010	0.002	w	-0.986		-1.35	1.79	0.43		1.56
32149.52		622.0486	-	-	w	-		-1.84	-	-		0.5
32149.52		951.9765			o			-1.7				0.3
32157.09	14	397.0191	0.362	0.024	b	0.060	-0.388	-0.81	27.00	2.85	19.23	7.3
32157.09		401.1356	0.005	0.001	w	-1.753		-1.18	0.41	0.10		3.01
32157.09		404.2467	-	-		-		-1.27	-	-		2.4
32157.09		488.3477	0.226	0.016	w	0.036		-0.87	16.85	1.93		4.1
32157.09		497.3754	0.244	0.018	s	0.085		-0.89	18.21	2.08		3.88
32157.09		588.6453	0.054	0.010	w	-0.427	0.053	-0.16	4.00	0.95	24.15	14.8
32157.09		600.8705	0.048	0.009	w	-0.455	0.08	-0.2	3.60	0.86	24.66	12.9
32157.09		608.2382	-	-	w	-		-0.29	-	-		10.2
32157.09		612.4519	0.048	0.009	w	-0.444		-1.19	3.56	0.85		1.29
32157.09		618.3488	0.013	0.002	w	-1.007		-1.11	0.95	0.23		1.49
32157.09		675.7223	-	-	d	-		-1.59	-	-		0.42
32157.09		679.2829	-	-	w	-		-1.37	-	-		0.69
32157.09		686.7995	-	-	w	-		-1.4	-	-		0.63
32157.09		794.5002	-	-	w	-		-0.88	-	-		1.54
32157.09		803.7427						-0.76				1.98
32157.09		820.9059						-0.75				1.95
32206.82	13.1	312.4905	0.228	0.017	w	-0.279		-0.85	19.97	2.29		10.6
32206.82		320.3412	0.177	0.013	b	-0.367	-0.433	-1.04	15.51	1.78	26.63	6.5
32206.82		396.2365	0.138	0.010	w	-0.290		-1.75	12.09	1.38		0.84
32206.82		400.3368	-	-	w	-		-0.92	-	-		5.5
32206.82		403.4355	0.039	0.007	w	-0.819		-0.98	3.45	0.82		4.8
32206.82		462.1826	0.016	0.003	w	-1.089		-1.43	1.41	0.34		1.29
32206.82		468.839	0.077	0.015	w	-0.399		-0.87	6.72	1.60		4.5
32206.82		478.0983	0.060	0.011	w	-0.487	-0.139	-0.57	5.28	1.26	23.53	8.8
32206.82		487.1643	0.140	0.010	b	-0.105		-0.54	12.26	1.40		9
32206.82		496.1479	0.031	0.006	w	-0.750	-0.302	-0.37	2.67	0.64	15.01	12.8
32206.82		599.08	0.006	0.001	w	-1.319		-0.7	0.50	0.12		4.1
32206.82		607.7883	-	-	d	-		-1.7	-	-		0.4
32206.82		610.5917	0.088	0.017	w	-0.111		-0.86	7.69	0.88		2.74
32206.82		684.4612	-	-	w	-		-1.63	-	-		0.37
32206.82		1040.918			o			-1.3				0.34

32221.2		327.7517	0.400	0.026	w	-0.183		-0.84	15.66	1.65		6.9
32221.2	26.7	396.0108	-	-	b	-	0.059	-0.22	-	-	37.46	19.8
32221.2		398.0117	0.078	0.015	w	-0.725		-1.34	3.05	0.73		1.49
32221.2		411.8488	-	-	b	-		-1.78	-	-		0.5
32221.2		490.2801	0.176	0.013	w	-0.190		-0.7	6.88	0.79		4.3
32221.2		502.9984	0.311	0.021	w	0.079		-1.45	12.16	1.28		0.71
32221.2		605.875	0.035	0.007	w	-0.711		-1.25	1.36	0.32		0.78
32221.2		625.1249	-	-	w	-		-1.21	-	-		0.81
32221.2		646.5572	-	-	w	-		-1.44	-	-		0.44
32221.2		933.7776			o			-1.46				0.2
32356.09	6.9	404.7086	1.000	0.066		0.330	0.28	-0.03	144.93	15.30	258.50	127
32384	15	308.7048	0.151	0.011	w	-0.697	-0.523		10.04	1.15	29.97	
32384		313.8707	0.385	0.025	b	-0.275	-0.4		25.67	2.71	38.48	
32384		482.994	0.464	0.031		0.181	-0.264		30.96	3.27	22.23	
32563.6	20.4	316.7202	0.014	0.003	w	-1.603	-0.542	-1.05	0.75	0.18	17.34	5.3
32563.6		324.1133	0.443	0.029	w	-0.090		-0.48	23.46	2.48		19
32563.6		390.7114	-	-	s	-	-0.359	-0.85	-	-	17.37	5.6
32563.6		394.6975	0.035	0.007	s	-1.020		-0.78	1.86	0.44		6.5
32563.6		487.5157	0.046	0.009	b	-0.715		-1.64	2.46	0.59		0.58
32563.6		494.4798	0.205	0.015	w	-0.057		-0.99	10.88	1.25		2.5
32563.6		603.1827	0.022	0.004	w	-0.858		-1.78	1.15	0.28		0.28
32563.6		612.0215	0.008	0.002	w	-1.266		-1.32	0.44	0.10		0.78
32563.6		643.0064	-	-	w	-		-1.7	-	-		0.29
32563.6		661.0247	0.044	0.008		-0.474		-1.43	2.33	0.55		0.52
32563.6		668.1406	0.166	0.012		0.112		-0.86	8.79	1.01		1.9
32563.6		682.0861	0.017	0.003	w	-0.869	-0.215	-0.46	0.88	0.21	7.94	4.5
32585.13	8.8	311.9011	0.210	0.015	s	-0.028	-0.383	-0.94	29.21	3.34	25.79	7.2
32585.13		323.8872	0.367	0.024	b	0.247		-0.89	51.02	5.39		7.5
32585.13		394.3623	0.117	0.009	s	-0.079	0.185	-0.1	16.23	1.86	59.66	30.7
32585.13		469.6022	0.105	0.008	b	0.025		-1.21	14.56	1.67		1.68
32585.13		478.3459	0.027	0.005	s	-0.542	-0.303	-0.7	3.80	0.91	13.18	5.2
32585.13		481.6832	0.085	0.016	s	-0.042	-0.156	-0.25	11.87	1.36	18.24	14.5
32585.13		487.0044	0.048	0.009		-0.286	0.047	-0.13	6.61	1.58	28.47	18.8
32585.13		493.9538	0.021	0.004	s	-0.628		-0.43	2.92	0.70		9.1
32585.13		585.7999	0.010	0.002	w	-0.813		-0.58	1.36	0.32		4.6
32585.13		592.8005	-	-	w	-		-1.34	-	-		0.8
32585.13		602.4003	0.006	0.001	w	-1.025		-0.9	0.79	0.19		2.1

32585.13		611.2159	0.004	0.001	w	-1.147		-0.8	0.58	0.14		2.57
32585.13		613.7599	-	-	w	-		-1.48	-	-		0.53
32585.13		681.0858	-	-	w	-		-1.06	-	-		1.14
32585.13		777.0041	-	-	w	-		-1.5	-	-		0.32
32585.13		1097.887			o			-0.91				0.61
32729.5	6.9	322.3792	0.461	0.030		0.516	0.437	0.16	70.13	7.41	117.00	62
32729.5		403.4013	0.053	0.010	w	-0.230		-1.33	8.03	1.91		1.27
32729.5		412.5769	0.051	0.010	w	-0.225	-0.34	-0.63	7.78	1.85	11.93	6.1
32729.5		478.3556	0.041	0.008	w	-0.190	-0.286	-0.64	6.26	1.49	10.05	4.5
32729.5		493.8612	0.249	0.018		0.620	0.496	0.55	37.95	4.35	57.09	65
32729.5		605.8679	0.008	0.002	w	-0.685		-1.35	1.25	0.30		0.54
32729.5		625.9789	0.053	0.010	w	0.153		-0.39	8.07	1.92		4.7
32729.5		674.4518	-	-	w	-		-1.08	-	-		0.81
32729.5		776.2219	0.084	0.016	w	0.541		-1.07	12.81	3.05		0.63
32785.12	8.7	314.5129	0.771	0.051	s	0.375		-0.66	88.80	9.38		16.5
32785.12		387.3578	0.165	0.012	w	-0.113	0.242	-0.23	19.02	2.18	86.18	29.4
32785.12		389.2721	0.015	0.003	w	-1.155	-0.496	-0.96	1.71	0.41	15.60	5.4
32785.12		391.2755	0.008	0.002	w	-1.397	-0.268	-0.72	0.97	0.23	26.10	9.1
32785.12		456.4595	0.004	0.001	w	-1.536	-0.511	-0.76	0.52	0.12	10.96	6.2
32785.12		465.2317	0.012	0.002	w	-1.098		-0.45	1.37	0.33		12.2
32785.12		473.8119	0.012	0.002	w	-1.092	-0.08	-0.36	1.33	0.32	27.44	14.5
32785.12		482.3056	0.010	0.002	w	-1.122		-1.06	1.20	0.29		2.79
32785.12		567.6541	0.002	0.000	w	-1.700		-1.84	0.23	0.05		0.33
32785.12		579.0146	-	-	w	-		-1.02	-	-		2.1
32785.12		595.2273	-	-	w	-		-1.21	-	-		1.28
32785.12		981.8016			o			-1.67				0.17
32886.28	9.4	305.9915	0.051	0.010	w	-0.858	-0.451	-0.86	5.48	1.31	28.00	10.8
32886.28		313.5151	0.594	0.039		0.231		-0.94	64.19	6.78		8.6
32886.28		385.8454	0.049	0.009	w	-0.670	-0.002	-0.41	5.32	1.27	49.52	19.6
32886.28		389.7324	0.008	0.001	w	-1.456	-0.323	-0.67	0.85	0.20	23.18	10.5
32886.28		392.6685	0.087	0.017	w	-0.406	-0.084	-0.52	9.43	2.25	39.59	14.5
32886.28		454.3608	0.020	0.004	w	-0.920		-0.76	2.16	0.51		6.3
32886.28		463.0518	0.060	0.011	w	-0.425		-0.49	6.49	1.55		11.3
32886.28		471.551	0.117	0.009	w	-0.118		-0.75	12.70	1.45		6
32886.28		479.9631	-	-	b	-		-0.5	-	-		10.2
32886.28		564.412	-	-	w	-		-1.03	-	-		2.2
32886.28		586.2625	0.014	0.003	w	-0.854		-1.32	1.51	0.36		1.03
32886.28		654.0359	-	-	w	-		-1.47	-	-		0.58

32928.7	12	454.8007	1.000	0.066		0.890	0.451	0.59	83.33	8.80	60.69	83
32966.86	8.7	312.7247	0.223	0.016		0.129	-0.435	-0.9	35.28	3.72	19.26	6.6
32966.86		319.9303	0.092	0.018	w	-0.234	-0.04	-0.52	14.61	1.67	45.69	15.2
32966.86		384.649	0.045	0.009	w	-0.385	0.033	-0.3	7.15	1.70	37.39	17.4
32966.86		386.5366	0.002	0.000	w	-1.683		-1.34	0.36	0.08		1.56
32966.86		478.1133	0.071	0.014	w	0.003	-0.046	-0.44	11.29	2.69	20.18	8.1
32966.86		484.8095	0.067	0.013	w	-0.009	0.2	0.08	10.68	2.55	34.58	26.1
32966.86		488.1374	0.447	0.029	b	0.819	-0.019	-0.07	70.85	7.48	20.60	18.5
32966.86		579.6789	0.030	0.006	w	-0.206	0.205	-0.19	4.75	1.13	24.47	9.8
32966.86		597.2761	0.007	0.001	w	-0.819		-0.95	1.09	0.26		1.62
32966.86		616.8116	0.016	0.003	w	-0.433		-0.34	2.48	0.59		6.2
32966.86		626.75	-	-	w	-		-1.72	-	-		0.251
32966.86		769.7245	-	-	w	-		-1.15	-	-		0.61
32966.86		1053.713			o			-0.97				0.5
33231.1		455.7723	-	-	b	-		-1.47	-	-		0.98
33231.1	9.1	464.0041	0.058	0.011	w	-0.330	0.365	0.04	6.58	1.57	65.23	30.8
33231.1		467.1436	0.120	0.009	s	-0.012		-0.96	13.50	1.55		3.06
33231.1		472.1468	0.393	0.026		0.513	0.198	-0.17	44.26	4.67	42.89	18.3
33231.1		478.6757	0.429	0.028		0.562	0.216	0.26	48.25	5.09	43.49	47.7
33231.1		652.3756	-	-	w	-		-1.45	-	-		0.51
33348.23	7.2	304.6478	0.039	0.007	s	-0.775	-0.196	-0.75	5.48	1.31	41.58	11.7
33348.23		309.0378	-	-	s	-		-0.97	-	-		6.7
33348.23		316.0727	0.336	0.022	s	0.191		-0.64	47.12	4.98		13.8
33348.23		380.9196	0.168	0.012	s	0.052		-0.94	23.54	2.69		4.8
33348.23		382.8378	-	-	w	-		-0.87	-	-		5.6
33348.23		386.4703	0.056	0.011	w	-0.415		-1.35	7.80	1.86		1.81
33348.23		445.0175	0.242	0.018		0.346		-1.35	33.93	3.88		1.38
33348.23		453.3514	0.027	0.005	w	-0.593		-0.61	3.76	0.90		7.2
33348.23		461.4952	-	-	b	-		-0.93	-	-		3.36
33348.23		464.6007	-	-	b	-	0.381	0.02	-	-	67.50	29.5
33348.23		469.5493	0.120	0.009	s	0.088	0.394	0.18	16.82	1.93	68.10	41.5
33348.23		560.7268	0.006	0.001	w	-1.056		-1.2	0.85	0.20		1.2
33348.23		567.1377	0.008	0.001	w	-0.931		-1.61	1.10	0.26		0.47
33348.23		575.9182	-	-	w	-		-0.91	-	-		2.26
33348.23		583.9706	-	-	w	-		-0.71	-	-		3.49
33348.23		647.427	-	-	w	-		-1.51	-	-		0.45
33348.23		1012.995			o			-0.87				0.79

33704.63	8.2	377.6829	0.239	0.017		-0.060	0.246	-0.14	29.09	3.33	117.60	48.3
33704.63		380.4397	0.678	0.045	w	0.400	0.256	-0.14	82.70	8.73	118.60	47.2
33704.63		382.4152	0.083	0.016	s	-0.505	0.019	-0.39	10.17	2.42	68.03	26.4
33851.83	7.6	311.1188	0.246	0.018	w	0.092		-0.5	32.71	3.74		16.6
33851.83		385.9234	0.015	0.003	w	-0.947		-1.37	1.95	0.46		1.48
33851.83		453.9757	-	-	b	-		-0.96	-	-		2.71
33851.83		458.6994	0.230	0.017	w	0.400		0.21	30.61	3.50		39.4
33851.83		464.8593	0.205	0.015	w	0.361		-0.19	27.22	3.12		15.5
33851.83		467.9181	0.242	0.018	w	0.439		0.16	32.17	3.68		33.5
33851.83		567.2827	0.023	0.004	w	-0.413		-1.15	3.08	0.73		1.13
33851.83		584.8765	0.040	0.008	w	-0.146		-0.45	5.35	1.28		5.3
33851.83		626.9789	-	-	w	-		-1.53	-	-		0.38
33851.83		963.8125			o			-0.9				0.7
34147.34	6.4	374.1363	0.024	0.005	w	-0.870		-0.54	6.43	1.53		27.6
34147.34	6.4	376.0467	0.564	0.037	b	0.505	-0.028	-0.23	150.82	15.92	88.39	56
34147.34		377.3451	0.412	0.027	w	0.372	0.299	-0.18	110.36	11.65	186.40	62
34175.84	9.7	457.9596	1.000	0.066		0.988	0.68		103.09	10.89	101.40	
34811.79	11.7	448.4698	1.000	0.066	w	0.826	0.626	0.48	85.47	9.02	107.80	77
35603.59	8.3	433.0864	0.609	0.040		0.639		-0.69	85.96	9.08		8
35603.59		452.4123	0.228	0.017		0.251	0.568	0.46	32.22	3.69	133.80	104
35603.59		468.261	0.163	0.012		0.134		-0.67	23.01	2.64		7.3
34911.79	7.3	446.467	1.000	0.066		1.027	0.767		136.99	14.46	150.40	
35794.63	9	417.1708	0.326	0.022	w	0.319	0.389		36.27	3.74	85.28	
35794.63		493.0696	0.674	0.044	s	0.778	0.34		74.84	7.71	54.53	
36394.51	9.7	278.7681	1.000	0.066	w	0.422	-0.297		103.09	10.96	39.35	
36576.97	9.3	433.3242	0.819	0.054	w	0.541	0.33	0.11	88.07	9.30	108.40	66
36576.97		458.6082	0.181	0.013	w	-0.066		-0.11	19.46	2.23		35.3
36653.97	14.6	388.8925	0.618	0.041		0.325	0.499	0.12	42.32	4.47	126.40	53.4
36653.97		414.2368	0.382	0.025		0.171		-0.63	26.17	2.76		8.3

Table 6.4 shows the radiative parameters for neutral gadolinium

Lifetimes are adopted from Den Hartog et al.⁵

w denotes weak emission lines

s denotes shouldered emission lines

b denotes blended line

d denotes emission line resided in a spectral gap

Kurucz refers to the tabulated data by Kurucz and Bell³³

Lawl. refers to the work by Lawler et al.⁶

Gd II Data

Table 6.5 shows the radiative parameters for singly ionized gadolinium.

Lifetimes from by Den Hartog et al.¹⁰

w denotes weak emission lines

s denotes shouldered emission lines

b denotes blended line

DH denotes the work by Den Hartog et al.¹⁰

Kurucz refers to the work by Kurucz and Bell³³

Upper Energy (cm ⁻¹)	Lifetime (ns)	Wavelength (nm)	Branch Ratio	BR Error	g _k *A _{ki} (10 ⁶ s ⁻¹)				Log gf		
					This Work	error	DH	Kurucz	This Work	DH	Kurucz
25668.69	32.4	389.469	0.296	0.216	74.23	8.50	114.4	99.04	-0.77	-0.58	-0.65
25668.69		393.483	0.251	0.183	58.81	2.98	39.76	80.16	-0.86	-1.04	-0.73
25668.69		399.321	0.105	0.077	24.50	1.28	16.08	14.90	-1.23	-1.41	-1.45
25668.69		442.615	0.057	0.011	16.26	0.87	8.96	4.13	-1.32	-1.58	-1.92
25668.69		449.486	0.016	0.003	3.58	0.26	2.392	12.97	-1.96	-2.14	-1.41
25668.69		449.829	0.145	0.106	35.11	1.77	27.28		-0.97	-1.08	
25668.69		465.941	0.029	0.005	b	9.51	0.86	2.216	-1.51	-2.14	
25668.69		471.904	0.024	0.005		5.68	0.31	4	-1.72	-1.87	
25668.69		480.257	0.023	0.004		5.02	0.27	3.84	-1.76	-1.87	-2.07
25668.69		595.645	0.018	0.003		5.06	0.31	5.04	-1.57	-1.57	-1.53
25668.69		604.947	0.004	0.001	w	0.82	0.10	1.528	-2.35	-2.08	
25668.69		663.433	0.019	0.004		5.02	0.28	10	-1.48	-1.18	-1.43
25668.69		684.657	0.015	0.003		3.32	0.20	10.88	-1.63	-1.11	-1.54

25960.07	6.5	385.098	0.545	0.036		332.06	35.06	428	362.04	-0.13	-0.02	-0.09
25960.07		432.715	0.141	0.103		88.01	10.08	73.6	151.88	-0.61	-0.69	-0.37
25960.07		436.977	0.160	0.117		101.45	11.62	57.2	24.15	-0.54	-0.79	-1.16
25960.07		455.808	0.052	0.010		32.64	7.78	20.8	10.08	-0.99	-1.19	-1.50
25960.07		459.698	0.095	0.018		57.40	13.68	31.6	18.62	-0.74	-1	-1.23
25960.07		601.113	0.006	0.001		3.22	0.77	1.96		-1.76	-1.97	
25960.07		605.585	0.001	0.000	w	0.60	0.14	0.776		-2.48	-2.37	
26211.91	6.4	381.398	0.239	0.174		221.01	25.30	290.4	279.36	-0.32	-0.2	-0.22
26211.91		385.246	0.207	0.151		194.66	22.29	360	327.66	-0.36	-0.1	-0.14
26211.91		428.049	0.197	0.144		181.38	20.77	115.2	77.10	-0.30	-0.5	-0.67
26211.91		432.219	0.028	0.005		26.78	6.38	15.54	11.11	-1.12	-1.36	-1.51
26211.91		438.769	0.067	0.013		65.38	15.58	39	15.61	-0.72	-0.95	-1.35
26211.91		439.096	0.070	0.013		63.45	15.12	31.2	13.03	-0.74	-1.04	-1.42
26211.91		450.634	0.083	0.016		79.43	18.93	30.6	12.48	-0.62	-1.03	-1.42
26211.91		460.106	0.098	0.019		95.65	22.79	49.2	30.91	-0.52	-0.81	-1.01
26211.91		585.695	0.009	0.002		8.38	2.00	4.32	5.22	-1.37	-1.65	-1.57
26211.91		596.486	0.001	0.000	w	1.37	0.33	0.894		-2.14	-2.32	
26211.91		750.532	0.002	0.000	w -	-	-	1.92	0.89 -	-	-1.8	-2.12
26351.77	112	383.181	0.174	0.127		16.59	1.90	22.9	29.18	-1.44	-1.3	-1.19
26351.77		388.715	0.074	0.014		7.22	1.72	6.5	5.99	-1.79	-1.83	-1.87
26351.77		396.826	0.160	0.116	w	10.26	1.17	9.7	48.16	-1.62	-1.64	-0.94
26351.77		436.092	0.378	0.025		34.90	3.68	27.5	14.35	-1.00	-1.11	-1.39
26351.77		436.415	0.064	0.012		6.24	1.49	3.35		-1.75	-2.02	
26351.77		457.163	0.022	0.004	w	2.12	0.50	0.39		-2.18	-2.92	
26351.77		464.998	0.020	0.004		1.91	0.45	1.62		-2.21	-2.28	
26351.77		475.779	0.034	0.006		3.21	0.77	3.5		-1.96	-1.92	
26351.77		561.619	0.039	0.007		3.60	0.86	5.5	3.12	-1.77	-1.58	-1.83
26351.77		634.664	0.026	0.005		2.44	0.58	4.4	3.53	-1.83	-1.57	-1.67
26351.77		672.782	0.009	0.002		0.79	0.19	3.1	2.36	-2.27	-1.67	-1.80
26455.45	39.1	381.664	0.198	0.147		50.88	5.83	68	62.30	-0.95	-0.83	-0.87
26455.45		387.154	0.073	0.014		18.92	4.51	15.1	11.48	-1.37	-1.47	-1.59
26455.45		395.200	0.095	0.018		24.92	5.94	25.3	25.13	-1.23	-1.23	-1.23
26455.45		434.129	0.238	0.177		63.27	7.24	71	41.37	-0.75	-0.7	-0.93
26455.45		434.449	0.142	0.106		36.56	4.19	6.6		-0.99	-1.73	
26455.45		444.650	0.098	0.019		25.98	6.19	17.5	7.06	-1.11	-1.28	-1.68
26455.45		455.006	0.021	0.004	b -	-	-	0.78	-	-	-2.62	

26455.45		462.526	0.001	0.000	w	0.11	0.03	0.43		-3.44	-2.86
26455.45		462.766	0.025	0.005		6.82	1.63	3.8		-1.66	-1.92
26455.45		473.443	0.035	0.007		8.76	2.09	8.8	4.51	-1.53	-1.53
26455.45		558.367	0.035	0.007		8.57	2.04	12.3	6.50	-1.40	-1.24
26455.45		577.456	0.003	0.001	w	0.84	0.20	0.88	2.08	-2.38	-2.35
26455.45		630.514	0.027	0.005		7.05	1.68	14.4	10.01	-1.38	-1.07
26455.45		668.120	0.011	0.002		3.07	0.73	9.7	4.96	-1.69	-1.19
26455.45		764.464	-	-	-	-	-	0.74	-	-	-2.19
26595.22	6.5	375.901	0.096	0.018		117.54	28.01	61.6	67.88	-0.60	-0.89
26595.22		379.638	0.325	0.021		402.34	42.48	488	426.72	-0.06	0.02
26595.22		385.070	-	-	-	-	-	271.2	279.76	-	-0.22
26595.22		425.173	0.216	0.157		263.50	30.17	222.4	159.12	-0.15	-0.22
26595.22		441.903	0.111	0.081		136.32	15.61	68	33.13	-0.40	-0.7
26595.22		446.653	0.107	0.078		131.03	15.00	51.2	29.51	-0.41	-0.82
26595.22		452.129	0.043	0.008		51.16	12.19	10.56	5.47	-0.80	-1.49
26595.22		459.791	0.100	0.019		125.74	29.96	47.2	32.42	-0.40	-0.83
26595.22		564.483	0.000	0.000	-	-	-	5.28	3.36	-	-1.6
26595.22		572.831	0.003	0.001		3.14	0.75	1.808		-1.81	-2.05
26595.22		579.000	0.000	0.000	-	-	-	1.536	-	-	-2.11
26595.22		739.487	0.000	0.000	-	-	-	3.92	2.12	-	-1.49
27162.22	6.3	371.636	0.103	0.075		172.34	19.73	137	134.50	-0.45	-0.55
27162.22		376.840	0.318	0.021		510.57	53.91	760	848.30	0.04	0.21
27162.22		384.458	0.103	0.075		164.43	18.83	157	139.10	-0.44	-0.46
27162.22		421.502	0.165	0.121		260.23	29.80	138	141.50	-0.16	-0.44
27162.22		431.098	0.040	0.008		61.42	14.64	20.7	105.80	-0.77	-1.24
27162.22		440.825	0.089	0.017		138.13	32.92	61	9.48	-0.40	-0.75
27162.22		447.881	0.064	0.012		98.36	23.44	50	29.67	-0.53	-0.82
27162.22		448.105	0.061	0.012		96.69	23.04	60	25.50	-0.54	-0.74
27162.22		458.109	0.047	0.009		71.93	17.14	18.5	32.44	-0.65	-1.23
27162.22		537.162	0.006	0.001	s	6.90	1.64	2.47	10.07	-1.52	-1.97
27162.22		603.607	0.002	0.000	w	2.65	0.63	0.82	6.43	-1.84	-2.35
27162.22		725.266	0.002	0.000	w	3.65	0.87	6.2	2.62	-1.54	-1.31
27297.74	8.3	366.226	0.095	0.018		65.93	15.71	146.4	137.82	-0.88	-0.53
27297.74		369.773	0.187	0.137		135.39	15.50	223.8	198.60	-0.56	-0.34
27297.74		412.838	0.007	0.001		4.77	1.14	2.88		-1.91	-2.14
27297.74		418.810	0.020	0.004		14.73	3.51	12.36	9.57	-1.41	-1.49

27297.74		419.108	0.172	0.125		122.83	14.06	125.4	84.36	-0.49	-0.48	-0.65
27297.74		429.606	0.337	0.022		245.80	25.95	103.8	62.34	-0.17	-0.54	-0.76
27297.74		433.060	0.133	0.097		99.04	11.34	66.6	39.61	-0.56	-0.73	-0.95
27297.74		438.206	0.040	0.008		28.37	6.76	16.68	11.18	-1.09	-1.32	-1.49
27297.74		598.708	0.008	0.001		6.04	1.44	6.18		-1.49	-1.48	
27297.74		688.436	0.001	0.000	w -	-	-	0.57	-	-	-2.39	
27864.53	7.2	367.121	0.158	0.116		263.21	30.14	300	231.36	-0.27	-0.22	-0.33
27864.53		374.347	0.225	0.164		376.23	43.08	580.8	531.24	-0.10	0.09	0.05
27864.53		385.556	0.050	0.009		84.09	20.04	52.44	57.11	-0.73	-0.93	-0.90
27864.53		418.426	0.176	0.128		296.64	33.96	376.8	316.68	-0.11	-	-0.08
27864.53		434.218	0.182	0.133		298.71	34.20	190.8	124.56	-0.07	-0.27	-0.45
27864.53		434.429	0.057	0.011		93.62	22.31	29.88	137.16	-0.58	-1.07	-0.41
27864.53		443.825	0.087	0.016		145.24	34.61	51.6	22.42	-0.37	-0.82	-1.18
27864.53		455.095	0.024	0.005		37.88	9.03	15.84	9.33	-0.93	-1.31	-1.54
27864.53		517.629	0.032	0.006		54.56	13.00	45.6	31.03	-0.66	-0.74	-0.90
27864.53		526.731	0.002	0.000	s	3.80	0.91	2.064		-1.80	-2.07	
27864.53		595.156	0.002	0.000		4.40	1.05	3.12	10.32	-1.63	-1.78	-1.26
27864.53		610.618	0.005	0.001		8.29	1.97	6		-1.33	-1.47	
27864.53		717.224	-	-		-	-	10.68	4.75	-	-1.09	-1.44
27988.07	8.1	357.193	0.037	0.007		37.34	8.90	84	80.56	-1.15	-0.79	-0.81
27988.07		360.566	0.149	0.109		143.96	16.48	32	29.44	-0.55	-1.21	-1.24
27988.07		365.462	0.086	0.016		86.00	20.49	419.2	465.76	-0.76	-0.08	-0.03
27988.07		401.395	0.135	0.098		135.20	15.48	11.68		-0.49	-1.55	
27988.07		407.038	0.103	0.075		99.76	11.42	35.28	98.80	-0.61	-1.06	-0.61
27988.07		407.319	0.081	0.015		79.79	19.01	56	86.48	-0.70	-0.86	-0.67
27988.07		416.273	0.098	0.019		99.73	23.77	71.2	73.30	-0.59	-0.73	-0.72
27988.07		420.486	0.242	0.176		236.67	27.10	84.8	80.96	-0.20	-0.65	-0.67
27988.07		425.336	0.050	0.009		47.99	11.44	112.8	119.52	-0.89	-0.52	-0.49
27988.07		432.110	0.001	0.000		1.21	0.29	43.2	105.84	-2.47	-0.91	-0.53
27988.07		530.492	0.004	0.001		4.02	0.96	1.92		-1.77	-2.09	
27988.07		535.779	0.009	0.002		9.46	2.25	4.88	7.87	-1.39	-1.68	-1.47
27988.07		574.939	0.001	0.000		0.71	0.17	10.96	7.51	-2.45	-1.27	-1.43
27988.07		662.228	0.001	0.000	w	1.58	0.38	1.92		-1.98	-1.9	
27988.07		670.415	-	-		-	-	2.88	2.19	-	-1.71	-1.83
27988.07		558.613	0.004	0.001		4.25	1.01	1.52	2.37	-1.17	-1.62	-1.96
28502.31	14.1	358.719	0.060	0.011		48.27	11.50	26.16	20.29	-1.03	-1.3	-1.41

28502.31		365.615	0.291	0.212		245.58	28.12	476.4	427.44	-0.31	-0.02	-0.07
28502.31		376.300	0.061	0.012		48.52	11.56	20.28	21.32	-0.99	-1.37	-1.34
28502.31		407.547	0.009	0.002		9.76	2.33	5.76	25.54	-1.61	-1.84	-1.17
28502.31		422.514	0.089	0.017		72.75	17.34	40.44	35.06	-0.71	-0.97	-1.03
28502.31		422.714	0.078	0.015		69.65	16.60	44.52	84.67	-0.73	-0.92	-0.63
28502.31		431.605	0.260	0.190		228.41	26.15	127.2	12.30	-0.20	-0.45	-1.33
28502.31		501.082	0.036	0.007		30.93	7.37	19.8	12.52	-0.93	-1.13	-1.31
28502.31		509.607	0.026	0.005		21.98	5.24	14.52	25.94	-1.07	-1.25	-0.89
28502.31		573.385	0.061	0.012		52.91	12.61	43.2	14.40	-0.58	-0.67	-1.13
28502.31		587.723	0.027	0.005		21.00	5.00	21.12	2.50	-0.96	-0.96	-1.79
28629.02	13	349.196	0.187	0.137		82.89	9.49	161.4	133.86	-0.82	-0.53	-0.61
28629.02		352.419	0.156	0.114		73.15	8.37	134.4	135.12	-0.87	-0.6	-0.60
28629.02		396.686	0.006	0.001		2.69	0.64	5.88	85.92	-2.20	-1.86	-0.67
28629.02		406.359	0.496	0.033		230.35	24.32	69	41.64	-0.24	-0.77	-0.98
28629.02		409.448	0.081	0.015		38.71	9.22	55.8	19.45	-1.01	-0.85	-1.30
28629.02		414.045	0.063	0.012		28.48	6.79	23.28		-1.14	-1.22	
28629.02		521.304	0.001	0.000	w	1.02	0.24	1.08		-2.38	-2.35	
28629.02		554.500	0.009	0.002		3.87	0.92	5.22	4.78	-1.75	-1.62	-1.66
28629.02		555.527	0.001	0.000	s	0.38	0.09	0.726		-2.75	-2.47	
29045.29	4.7	347.322	0.095	0.018		198.98	47.42	237	214.00	-0.44	-0.37	-0.41
29045.29		351.863	0.009	0.002		17.11	4.08	8.5		-1.50	-1.8	
29045.29		358.496	0.271	0.198		580.62	66.48	960	851.00	0.05	0.27	0.22
29045.29		390.240	0.061	0.012		128.58	30.64	116	128.90	-0.53	-0.58	-0.53
29045.29		398.721	0.066	0.012		134.60	32.08	73	78.98	-0.49	-0.76	-0.73
29045.29		407.027	0.136	0.099		292.31	33.47	122	133.20	-0.14	-0.52	-0.48
29045.29		413.226	0.189	0.138		407.04	46.60	276	199.80	0.02	-0.15	-0.29
29045.29		421.719	0.119	0.087		256.94	29.42	154	120.50	-0.16	-0.39	-0.49
29045.29		487.806	0.004	0.001		8.56	2.04	4		-1.52	-1.85	
29045.29		495.882	0.011	0.002		22.08	5.26	11.3	28.39	-1.09	-1.38	-0.98
29045.29		502.312	0.012	0.002		25.71	6.13	14.9	12.16	-1.01	-1.25	-1.34
29045.29		541.986	0.009	0.002		15.71	3.74	8.3	6.44	-1.16	-1.43	-1.55
29045.29		556.068	0.015	0.003		31.31	7.46	17.6	7.34	-0.84	-1.09	-1.47
29045.29		626.031	0.002	0.000		3.92	0.93	4.2		-1.64	-1.6	
29045.29		638.095	0.002	0.000		4.20	1.00	11.3	11.22	-1.59	-1.16	-1.16
29197.89	11	342.392	0.097	0.018		53.10	12.65	159	171.72	-1.03	-0.55	-0.52
29197.89		345.491	0.194	0.142		105.83	12.12	127.2	139.62	-0.72	-0.64	-0.60

29197.89		379.526	0.225	0.164		122.72	14.05	12.12	13.94	-0.58	-1.58	-1.52
29197.89		388.184	0.136	0.099		74.05	8.48	13.62	19.63	-0.78	-1.51	-1.35
29197.89		397.175	0.035	0.007		19.24	4.59	78	82.02	-1.34	-0.73	-0.71
29197.89		400.125	0.083	0.016		45.23	10.78	69	86.40	-0.96	-0.78	-0.68
29197.89		404.514	0.022	0.004		12.09	2.88	32.4	24.16	-1.53	-1.1	-1.23
29197.89		498.490	0.012	0.002		6.50	1.55	5.4		-1.62	-1.7	
29197.89		503.156	-	-	-	-	-	9.24	9.23	-	-1.45	-1.46
29197.89		506.286	-	-	-	-	-	7.98	6.28	-	-1.51	-1.62
29197.89		537.539	-	-	-	-	-	7.74		-	-1.48	
29197.89		882.525	0.196	0.143		106.68	12.21	1.68		0.10	-1.71	
29242.25	7	341.873	0.136	0.129		206.49	23.64	250.4	222.40	-0.44	-0.36	-0.41
29242.25		344.962	0.042	0.010		61.16	14.57	61.6	62.57	-0.96	-0.96	-0.95
29242.25		349.441	0.154	0.146		242.13	27.72	340.8	276.16	-0.35	-0.2	-0.30
29242.25		382.151	0.016	0.004		24.85	5.92	12.08	10.65	-1.26	-1.58	-1.63
29242.25		387.262	0.042	0.010		63.25	15.07	22.08	25.22	-0.85	-1.3	-1.25
29242.25		395.613	0.007	0.002	s	10.71	2.55	3.6		-1.60	-2.08	
29242.25		399.416	0.105	0.099		156.55	17.92	78.4	120.80	-0.43	-0.73	-0.54
29242.25		403.789	0.167	0.159		261.90	29.99	155.2	131.36	-0.19	-0.42	-0.49
29242.25		409.889	0.255	0.022	-	-	-	132	99.20	-	-0.48	-0.60
29242.25		491.084	0.010	0.002		15.48	3.69	6.4		-1.25	-1.64	
29242.25		497.390	0.010	0.003		15.24	3.63	5.6		-1.25	-1.68	
29242.25		502.035	0.003	0.001		4.95	1.18	18.4	6.34	-1.69	-1.12	-1.62
29242.25		522.029	0.031	0.008		47.84	11.40	3.2	18.22	-0.70	-1.87	-1.13
29242.25		530.343	0.006	0.002		9.05	2.16	2.8		-1.41	-1.92	
29242.25		536.259	-	-	-	-	-	13.12		-	-1.23	
29242.25		550.042	0.016	0.004		23.26	5.54	0.888	10.23	-0.57	-1.99	-1.33
29353.34	5.4	354.579	0.205	0.150		544.26	62.31	812	731.92	0.01	0.19	0.14
29353.34		364.620	0.288	0.210		735.36	84.20	1050	1067.08	0.17	0.32	0.33
29353.34		407.844	0.192	0.140		507.20	58.07	236.6	254.66	0.10	-0.23	-0.20
29353.34		439.472	0.012	0.002		166.93	39.78	10.36	5.69	-0.32	-1.53	-1.78
29353.34		480.582	0.020	0.004		532.95	61.02	11.06	6.23	0.27	-1.42	-1.67
29353.34		559.719	0.005	0.001		27.05	6.45	6.3	5.10	-0.90	-1.52	-1.62
29353.34		648.010	0.003	0.001		55.90	13.32	6.58	4.66	-0.45	-1.38	-1.53
29877.94	4.7	334.599	0.102	0.074		108.65	12.44	148	109.84	-0.74	-0.6	-0.73
29877.94		369.974	0.190	0.139		199.51	22.84	248	267.64	-0.39	-0.29	-0.26
29877.94		373.085	0.182	0.133		196.51	22.50	280	311.36	-0.39	-0.23	-0.19

29877.94		386.726	0.123	0.090		139.44	15.97	34	30.14	-0.50	-1.12	-1.17
29877.94		389.523	0.293	0.214	s	89.99	10.30	37.2	36.88	-0.69	-1.07	-1.08
29877.94		486.504	0.043	0.008		45.28	10.79	38.4	46.00	-0.79	-0.87	-0.79
29877.94		489.430	0.033	0.006		35.57	8.48	20.8	23.15	-0.89	-1.12	-1.08
29877.94		580.702	0.011	0.002		11.83	2.82	12.8	8.73	-1.22	-1.19	-1.36
29877.94		582.098	0.014	0.003		14.37	3.42	17.2	14.58	-1.14	-1.06	-1.13
29877.94		584.569	0.009	0.002		9.91	2.36	10	7.15	-1.29	-1.29	-1.44
29965.75	5.4	333.618	0.135	0.099		147.77	16.92	233.4	209.10	-0.61	-0.41	-0.46
29965.75		336.559	0.022	0.004		25.05	5.97	25.8	38.44	-1.37	-1.35	-1.19
29965.75		368.775	0.259	0.189		289.31	33.12	360	652.20	-0.23	-0.13	0.12
29965.75		376.704	0.116	0.084		128.96	14.77	168.6	187.02	-0.56	-0.44	-0.40
29965.75		376.945	0.092	0.017		97.59	23.26	106.8	133.44	-0.68	-0.64	-0.55
29965.75		385.417	0.033	0.006		37.48	8.93	25.74	30.76	-1.08	-1.24	-1.16
29965.75		388.194	0.048	0.009		56.68	13.51	9.72		-0.89	-1.66	
29965.75		392.324	0.131	0.095		147.01	16.83	56.4	100.62	-0.47	-0.89	-0.63
29965.75		480.108	0.094	0.018		101.47	24.18	60	38.30	-0.45	-0.68	-0.88
29965.75		487.335	0.023	0.004		25.87	6.16	14.52	8.34	-1.04	-1.29	-1.53
29965.75		510.740	0.009	0.002		12.18	2.90	6.3		-1.32	-1.61	
29965.75		581.583	0.019	0.004		19.93	4.75	17.4	18.26	-1.00	-1.05	-1.03
29965.75		585.522	0.020	0.004		21.82	5.20	18.6	18.35	-0.95	-1.02	-1.03
30008.89	4.9	333.139	0.100	0.073		160.42	18.37	316.8	269.52	-0.57	-0.28	-0.35
30008.89		336.071	0.047	0.009		76.14	18.14	168	151.36	-0.89	-0.54	-0.59
30008.89		371.270	0.168	0.123		273.97	31.37	528	578.72	-0.25	0.04	0.08
30008.89		376.333	0.043	0.008		71.11	16.94	37.6	45.68	-0.82	-1.09	-1.01
30008.89		383.964	0.076	0.015		120.95	28.82	206.4	221.44	-0.57	-0.34	-0.31
30008.89		387.545	0.042	0.008		69.84	16.64	35.76	49.23	-0.80	-1.09	-0.96
30008.89		391.661	0.163	0.119		269.30	30.83	4.32	135.36	-0.21	-2	-0.49
30008.89		397.398	0.079	0.015		127.61	30.41	112.8	60.07	-0.52	-0.57	-0.70
30008.89		473.261	0.058	0.011		93.26	22.22	84.8	12.45	-0.50	-0.54	-1.37
30008.89		479.115	0.008	0.002		15.36	3.66	7.76	23.73	-1.28	-1.57	-1.08
30008.89		483.423	0.022	0.004		36.45	8.69	28	8.70	-0.89	-1	-1.48
30008.89		501.935	0.009	0.002		14.93	3.56	11.84	18.54	-1.25	-1.35	-1.02
30008.89		580.127	0.002	0.000		3.87	0.92	4.4	18.74	-1.71	-1.66	-1.01
30008.89		584.046	0.013	0.002		20.85	4.97	20.8		-0.97	-0.97	
30008.89		590.405	0.014	0.003		24.23	5.77	37.6		-0.90	-0.71	
30027.38	4.5	335.863	0.146	0.107		306.57	35.10	1050	838.60	-0.29	0.25	0.15

30027.38		340.107	0.008	0.002		18.39	4.38	21	21.71	-1.50	-1.44	-1.42
30027.38		346.300	0.031	0.006		68.01	16.21	47	44.26	-0.91	-1.07	-1.10
30027.38		375.832	0.104	0.076		217.23	24.87	185	305.40	-0.34	-0.41	-0.19
30027.38		376.071	0.129	0.095		274.34	31.41	122	135.30	-0.24	-0.59	-0.54
30027.38		383.692	0.062	0.012		133.69	31.86	178	215.70	-0.53	-0.4	-0.32
30027.38		391.378	0.016	0.003		32.18	7.67	10.2	14.75	-1.13	-1.63	-1.47
30027.38		396.929	0.033	0.006		69.92	16.66	58	62.15	-0.78	-0.86	-0.83
30027.38		397.106	0.023	0.004		48.67	11.60	27	32.29	-0.94	-1.19	-1.12
30027.38		404.942	0.349	0.023		841.01	88.80	335	305.60	0.32	-0.08	-0.12
30027.38		465.499	0.015	0.003		31.14	7.42	23.7	22.96	-0.99	-1.11	-1.13
30027.38		472.847	0.037	0.007		82.27	19.61	57	41.16	-0.56	-0.72	-0.86
30027.38		478.691	0.025	0.005		54.57	13.00	24	12.50	-0.73	-1.09	-1.37
30027.38		527.265	0.003	0.001	b	8.38	2.00	3.7		-1.46	-1.81	
30027.38		539.365	-	-	-	-	-	7.1	-	-	-1.51	
30027.38		600.456	0.012	0.002		26.30	6.27	31	19.18	-0.85	-0.78	-0.98
30101.37	4.6	339.253	0.076	0.014		189.67	45.20	272.4	221.28	-0.48	-0.33	-0.42
30101.37		345.415	0.033	0.006		90.27	21.51	118.8	110.46	-0.79	-0.67	-0.70
30101.37		354.936	0.187	0.136		490.91	56.21	1020	819.60	-0.03	0.29	0.19
30101.37		382.605	0.058	0.011		145.26	34.62	98.4	79.32	-0.50	-0.67	-0.76
30101.37		395.767	0.098	0.019		251.93	60.04	242.4	281.16	-0.23	-0.25	-0.18
30101.37		395.942	0.110	0.080		287.28	32.89	62.4	177.24	-0.17	-0.84	-0.38
30101.37		403.732	0.137	0.100		362.87	41.55	318	334.68	-0.05	-0.11	-0.09
30101.37		463.900	0.028	0.005		552.36	63.24	34.32	30.28	0.25	-0.96	-1.01
30101.37		471.198	0.035	0.007		77.75	18.53	17.88	15.36	-0.59	-1.23	-1.29
30101.37		618.043	0.009	0.002		96.13	22.91	21.48	20.14	-0.26	-0.91	-0.94
30366.82	4.2	336.224	0.221	0.161		621.64	71.17	1596	1160.40	0.02	0.43	0.29
30366.82		342.275	-	-	-	-	-	87.6	85.33	-	-0.81	-0.82
30366.82		378.757	0.121	0.088		335.70	38.44	228	266.16	-0.14	-0.31	-0.24
30366.82		391.651	0.198	0.144		559.59	64.07	392.4	550.92	0.11	-0.04	0.10
30366.82		391.823	0.076	0.014		216.17	51.52	22.44	30.04	-0.30	-1.29	-1.16
30366.82		408.556	0.228	0.166		655.38	75.04	396	391.20	0.22	-	-0.01
30366.82		458.256	0.133	0.097		404.83	46.35	84	38.08	0.11	-0.57	-0.92
30366.82		465.376	0.015	0.003		41.77	9.95	4.2		-0.87	-1.86	
30366.82		517.992	0.008	0.002		22.06	5.26	12.48	13.22	-1.05	-1.3	-1.27
30366.82		608.064	-	-	-	-	-	25.2	21.38	-	-0.85	-0.93
30849.65	14.7	326.833	0.026	0.006		26.82	6.39	40	33.51	-1.37	-1.19	-1.27

30849.65		330.851	0.003	0.001		3.53	0.84	5.4		-2.24	-2.05
30849.65		336.709	0.009	0.002		12.36	2.95	12.9		-1.68	-1.66
30849.65		364.562	0.215	0.200		220.61	25.26	211	231.90	-0.36	-0.38
30849.65		364.788	0.013	0.003		16.23	3.87	10.6		-1.49	-1.67
30849.65		371.953	0.207	0.194		225.51	25.82	154	493.10	-0.33	-0.5
30849.65		379.172	0.363	0.031	s	-	-	24.9	22.19	-	-1.27
30849.65		384.380	0.025	0.006		29.27	6.98	21.3	22.51	-1.19	-1.33
30849.65		448.333	0.078	0.019		84.07	20.03	127	72.22	-0.60	-0.42
30849.65		455.146	0.023	0.006		23.86	5.69	10.1		-1.13	-1.5
30849.65		460.557	0.002	0.000	w	1.69	0.40	2.32		-2.27	-2.13
30849.65		493.692	0.004	0.001		4.07	0.97	4.2		-1.83	-1.82
30849.65		562.476	0.001	0.000	w	0.95	0.23	1.55		-2.34	-2.13
30849.65		572.196	0.010	0.002		11.30	2.69	11.8	9.22	-1.26	-1.24
30996.85	3.7	335.048	0.256	0.187		1010.39	117.53	1736	1379.28	0.23	0.47
30996.85		343.999	0.295	0.216		1069.30	124.38	910	709.24	0.28	0.21
30996.85		382.217	0.027	0.005		104.72	25.05	32.9	35.01	-0.64	-1.14
30996.85		389.641	0.009	0.002		32.60	7.80	10.36	45.54	-1.13	-1.63
30996.85		398.300	0.041	0.008		161.68	38.67	39.62	813.96	-0.41	-1.03
30996.85		409.860	0.319	0.021		1204.39	129.55	938	13.60	0.48	0.37
30996.85		445.393	0.021	0.004		83.92	20.07	16.38	46.93	-0.60	-1.31
30996.85		512.556	0.031	0.006		116.79	27.93	44.8		-0.34	-0.75
30996.85		816.514	-	-		-	-	2.24	-	-	-1.64
31145.65	4.6	342.246	0.476	0.031		1649.06	174.12	2944	1880.00	0.46	0.71
31145.65		395.953	0.193	0.141		695.55	79.64	81.6	233.60	0.21	-0.71
31145.65		407.375	0.331	0.022		1133.65	119.70	444.8	97.25	0.45	0.04
31908.12	12.8	313.309	0.029	0.006		16.94	4.04	27.12	30.90	-1.60	-1.4
31908.12		319.653	0.013	0.003		7.04	1.68	10.16	51.37	-1.97	-1.81
31908.12		346.808	0.067	0.014		37.40	8.91	44.8	270.24	-1.17	-1.1
31908.12		351.013	0.019	0.004		10.93	2.60	15.36	28.16	-1.69	-1.55
31908.12		351.222	0.293	0.022	b	218.40	23.06	276	19.66	-0.39	-0.29
31908.12		357.860	0.213	0.176		123.80	14.17	40	42.92	-0.62	-1.12
31908.12		439.143	0.082	0.018		45.74	10.90	45.6	2.83	-0.88	-0.88
31908.12		442.760	0.057	0.012		31.15	7.42	30.4		-1.04	-1.04
31908.12		458.239	0.191	0.158		113.72	13.02	76.8		-0.45	-0.62
31908.12		464.633	0.031	0.007		16.73	3.99	19.6		-1.27	-1.2
31908.12		469.168	0.005	0.001		3.16	0.75	3.28		-1.98	-1.97

31908.12		723.787	-	-	-	-	1.2	-	-2.03			
31908.12		788.121	-	-	-	-	1.128	-	-1.98			
32048.84	5.4	342.460	0.281	0.206		209.06	23.94	252	291.52	-0.43	-0.35	-0.29
32048.84		345.124	0.268	0.197		199.32	22.82	312	389.88	-0.45	-0.26	-0.16
32048.84		359.144	0.070	0.013		48.88	11.65	16.4	40.28	-1.02	-1.49	-1.11
32048.84		440.018	0.034	0.007		26.20	6.24	14.4	33.22	-1.12	-1.37	-1.19
32048.84		442.410	0.072	0.014		56.57	13.48	22.8	13.55	-0.78	-1.17	-1.41
32048.84		515.675	0.046	0.009		34.95	8.33	26.4	20.43	-0.86	-0.98	-1.22
32048.84		518.722	0.122	0.089		91.96	10.53	31.6	29.12	-0.43	-0.9	-0.94
32048.84		710.171	0.002	0.000	w	-	-	3.2	29.31	-	-1.61	-0.93
32048.84		710.979	0.002	0.000	w	-	-	2.52	2.92	-	-1.72	-1.66
32048.84		711.673	0.003	0.001	s	1.80	0.43	9.6	7.30	-1.86	-1.14	-1.26
32150.14	5.2	313.504	0.049	0.009		60.53	14.42	52.8	69.54	-1.05	-1.11	-0.99
32150.14		341.275	0.044	0.008		48.49	11.55	18		-1.07	-1.51	
32150.14		343.921	0.317	0.021		371.78	39.26	672	618.00	-0.18	0.08	0.04
32150.14		348.261	0.139	0.102		156.65	17.94	186.6	180.36	-0.55	-0.47	-0.48
32150.14		355.480	0.016	0.003		18.60	4.43	20.4		-1.45	-1.41	
32150.14		357.841	0.238	0.173		271.83	31.12	27	147.42	-0.28	-1.29	-0.55
32150.14		438.064	0.111	0.081		128.29	14.69	65.4	64.86	-0.43	-0.72	-0.73
32150.14		514.083	0.037	0.007		39.23	9.35	36	46.11	-0.81	-0.84	-0.74
32150.14		516.010	0.007	0.001		9.05	2.16	7.38		-1.44	-1.53	
32150.14		519.108	0.035	0.007		42.30	10.08	28.2	30.16	-0.77	-0.94	-0.91
32150.14		700.074	0.002	0.000	s	2.81	0.67	13.8	12.58	-1.68	-1	-1.03
32150.14		705.096	0.003	0.001		4.28	1.02	3.06	10.43	-1.49	-1.64	-1.11
32150.14		706.577	0.001	0.000	b	-	-	5.16		-	-1.4	
32150.14		714.114	0.000	0.000		-	-	0.852	4.52	-	-2.14	-1.46
32260.12	5.2	309.890	0.138	0.103		160.91	18.42	52.8	64.20	-0.63	-1.12	-1.03
32260.12		312.426	-	-		-	-	37.8	40.87	-	-1.26	-1.22
32260.12		339.999	0.110	0.082		128.09	14.67	177.6	199.98	-0.65	-0.51	-0.46
32260.12		342.624	0.110	0.081	b	134.28	15.37	18		-0.63	-1.5	
32260.12		346.727	0.365	0.024		415.00	43.82	672	642.60	-0.13	0.08	0.06
32260.12		346.932	-	-		-	-	22.2	30.23	-	-1.4	-1.26
32260.12		432.456	0.026	0.005	s	34.05	8.12	18.36		-1.02	-1.29	
32260.12		435.964	0.040	0.008		48.77	11.62	15.42	14.26	-0.86	-1.36	-1.39
32260.12		438.311	0.137	0.102		159.63	18.28	81.6	66.90	-0.34	-0.63	-0.72
32260.12		462.255	0.027	0.005		29.88	7.12	1.86		-1.02	-2.22	

32260.12		465.907	0.010	0.002	s	8.38	2.00	2.94		-1.56	-2.01
32260.12		511.192	0.012	0.002		13.59	3.24	7.02		-1.27	-1.56
32260.12		516.160	0.020	0.004		15.61	3.72	5.64		-1.20	-1.65
32260.12		694.724	0.000	0.000	-	-	1.98		-	-1.85	
32260.12		705.800	0.003	0.000	w	2.68	0.64	6.78	7.68	-1.70	-1.29
32260.12		708.548	0.002	0.000	w	2.97	0.71	5.22	5.41	-1.65	-1.41
32260.12		719.703	0.000	0.000	-	-	9.36	10.20	-	-1.14	-1.10
32262.79	5.2	309.865	0.118	0.086		185.97	21.29	150.4	155.44	-0.57	-0.66
32262.79		312.400	0.189	0.138		289.58	33.16	123.2	126.00	-0.37	-0.74
32262.79		316.069	0.058	0.011		87.66	20.89	16.8	48.23	-0.88	-1.61
32262.79		342.593	0.103	0.075		154.10	17.64	140	145.68	-0.57	-0.61
32262.79		346.695	-	-	s	-	-	132	124.72	-	-0.62
32262.79		346.899	0.228	0.167		346.18	39.64	656	643.36	-0.20	0.07
32262.79		356.404	0.068	0.013		108.92	25.96	57.6	77.80	-0.68	-0.96
32262.79		432.407	0.072	0.014		116.29	27.71	72	61.25	-0.49	-0.69
32262.79		450.909	0.047	0.009		74.22	17.69	24.8	27.02	-0.65	-1.13
32262.79		457.098	0.017	0.003		25.11	5.98	13.68	14.96	-1.10	-1.37
32262.79		471.657	0.021	0.004		30.67	7.31	10.96		-0.99	-1.44
32262.79		513.027	0.032	0.006		50.25	11.98	29.6	36.36	-0.70	-0.93
32262.79		516.089	0.013	0.002		18.92	4.51	17.2	25.32	-1.12	-1.16
32262.79		521.048	0.028	0.005		41.49	9.89	26.4	31.27	-0.77	-0.97
32262.79		692.058	0.003	0.001	w	6.46	1.54	15.2	15.83	-1.33	-0.97
32262.79		694.595	0.000	0.000	-	-	-	12.4	12.86	-	-1.05
32262.79		705.667	0.001	0.000	w	-	-	2.4	-	-	-1.75
32262.79		708.414	0.001	0.000	w	2.65	0.63	3.44	3.83	-1.70	-1.58
32262.79		777.342	0.001	0.000	-	-	-	1.52	-	-	-1.87
32304.41	4.8	311.994	0.136	0.100		280.32	32.09	165	175.60	-0.39	-0.62
32304.41		315.654	0.167	0.122		332.52	38.07	367	341.50	-0.30	-0.26
32304.41		346.196	0.032	0.006		69.48	16.56	68	83.99	-0.90	-0.91
32304.41		346.399	0.241	0.176		505.60	57.89	1000	1032.00	-0.04	0.25
32304.41		352.854	0.100	0.073		212.55	24.34	130	167.40	-0.40	-0.61
32304.41		359.344	0.056	0.011		117.95	28.11	62	79.22	-0.64	-0.92
32304.41		364.019	0.072	0.014		142.82	34.04	55	100.40	-0.55	-0.96
32304.41		420.875	-	-	-	-	-	6.3	-	-	-1.78
32304.41		426.873	0.103	0.075		221.05	25.31	86	75.38	-0.22	-0.63
32304.41		450.064	0.029	0.005		62.51	14.90	8.5		-0.72	-1.59
32304.41		470.733	0.008	0.002		21.43	5.11	5.2		-1.15	-1.76

32304.41		480.353	0.020	0.004		45.54	10.85	19	21.22	-0.80	-1.18	-1.13
32304.41		514.983	0.008	0.002		20.39	4.86	10.1	17.03	-1.09	-1.4	-1.17
32304.41		519.920	0.010	0.002		20.06	4.78	12.7	25.82	-1.09	-1.29	-0.98
32304.41		528.215	0.007	0.001	s	8.48	2.02	5		-1.45	-1.68	
32304.41		685.712	0.008	0.001		16.25	3.87	33	22.68	-0.94	-0.63	-0.80
32304.41		690.070	0.003	0.001		6.39	1.52	12.3	10.67	-1.34	-1.06	-1.12
32304.41		774.835	-	-	-	-	-	4.6	2.57	-	-1.38	-1.64
32304.41		796.321	-	-	-	-	-	9.3	5.27	-	-1.05	-1.30
32490.51	5.1	307.693	0.151	0.111		239.42	27.41	228.8	228.88	-0.47	-0.49	-0.49
32490.51		310.193	0.054	0.010		90.55	21.58	48	82.88	-0.88	-1.16	-0.92
32490.51		339.940	0.024	0.005		36.34	8.66	60.8	79.08	-1.20	-0.98	-0.86
32490.51		343.979	0.295	0.217		464.27	53.16	432	331.76	-0.08	-0.12	-0.23
32490.51		350.551	0.126	0.093		40.96	9.76	480	570.64	-1.12	-0.05	0.02
32490.51		356.956	0.020	0.004		200.62	22.97	30.88	41.56	-0.42	-1.23	-1.10
32490.51		423.507	0.010	0.002		30.22	7.20	10.72	27.11	-1.09	-1.54	-1.14
32490.51		431.627	0.158	0.116		15.51	3.70	61.6	32.63	-1.36	-0.77	-1.04
32490.51		446.324	0.032	0.006		248.23	28.42	36.8	28.55	-0.13	-0.95	-1.07
32490.51		452.388	0.055	0.011	b	49.47	11.79	10.96		-0.82	-1.47	
32490.51		456.686	0.002	0.000	w	87.77	20.92	2		-0.56	-2.2	
32490.51		466.643	0.010	0.002		3.09	0.74	15.28	29.85	-2.00	-1.3	-1.01
32490.51		507.101	0.014	0.003		15.68	3.74	25.6	26.53	-1.22	-1	-0.99
32490.51		510.093	0.014	0.003		20.08	4.78	20.8	32.62	-1.11	-1.1	-0.90
32490.51		514.937	0.007	0.001	s	22.69	5.41	6.16	8.98	-1.04	-1.61	-1.45
32490.51		681.318	0.000	0.000	w	-	-	2.08		-	-1.85	
32490.51		694.504	0.000	0.000		0.54	0.13	2.72		-2.41	-1.71	
32490.51		697.164	0.000	0.000		-	-	9.76	12.17	-	-1.15	-1.05
32490.51		705.459	0.002	0.000		-	-	16	10.66	-	-0.92	-1.10
32490.51		738.597	0.000	0.000		3.21	0.76	9.92	6.87	-1.58	-1.09	-1.25
32595.35	9	406.338	0.464	0.031		723.44	76.39	864	924.96	0.25	0.33	0.36
32595.35		425.360	0.361	0.024		562.24	59.37	332.4	331.44	0.18	-0.04	-0.05
32595.35		441.347	0.018	0.003		30.22	7.20	12.96		-1.05	-1.42	
32595.35		448.249	0.150	0.110	b	8.99	1.03	3.408		-1.57	-1.99	
32595.35		703.723	0.005	0.001		8.45	2.01	27.72	17.70	-1.20	-0.69	-0.88
32595.35		718.955	-	-	-	-	-	44.4	24.12	-	-0.46	-0.73
32595.35		756.316	0.001	0.000	w	-	-	23.76	9.07	-	-0.69	-1.11
32677.54	7.8	404.985	0.705	0.023		632.67	66.80	1246	1091.44	0.19	0.49	0.43

32677.54		423.878	0.157	0.015		144.26	34.38	235.2	337.54	-0.41	-0.2	-0.04
32677.54		439.751	0.127	0.012		111.13	26.48	148.4	96.94	-0.49	-0.36	-0.55
32677.54		698.586	-	-	-	-	-	54.6	42.80	-	-0.4	-0.50
32677.54		699.675	0.011	0.001		9.39	2.24	63	51.42	-1.16	-0.33	-0.42
32677.54		714.730	-	-	-	-	-	24.36	15.76	-	-0.73	-0.92
32684.71	5.4	308.335	0.026	0.005		46.67	11.12	22	35.96	-1.18	-1.51	-1.29
32684.71		311.908	0.019	0.004		37.01	8.82	17		-1.27	-1.61	
32684.71		317.109	0.027	0.005		49.38	11.77	24	35.03	-1.13	-1.44	-1.28
32684.71		341.695	0.184	0.134		351.08	40.20	494	586.90	-0.21	-0.06	0.01
32684.71		348.180	0.321	0.021		591.33	62.44	720	726.60	0.03	0.1	0.12
32684.71		354.498	0.057	0.011		97.89	23.33	40		-0.73	-1.12	
32684.71		359.046	0.131	0.096		242.87	27.81	189	238.00	-0.33	-0.44	-0.34
32684.71		359.191	0.058	0.011		102.78	24.49	32.5	57.31	-0.70	-1.2	-0.96
32684.71		424.657	0.062	0.012		116.51	27.77	86	104.40	-0.50	-0.63	-0.55
32684.71		448.447	0.022	0.004		44.95	10.71	13		-0.87	-1.41	
32684.71		505.088	0.024	0.005		45.28	10.79	44	40.29	-0.76	-0.77	-0.81
32684.71		509.837	0.049	0.009		87.96	20.96	60	81.47	-0.46	-0.63	-0.50
32684.71		517.810	0.016	0.003		29.35	6.99	16.5	25.44	-0.93	-1.18	-0.99
32684.71		695.922	-	-	-	-	-	12	12.82	-	-1.06	-1.03
32684.71		711.884	0.004	0.001		8.79	2.09	33	18.37	-1.18	-0.6	-0.86
32684.71		742.654	-	-	-	-	-	7.1	-	-	-1.23	
32684.71		752.650	-	-	-	-	-	3.5	-	-	-1.52	
32946.20	5	314.500	0.146	0.107		349.57	40.02	468	386.88	-0.29	-0.16	-0.24
32946.20		345.038	0.161	0.117		387.89	44.41	792	638.52	-0.16	0.15	0.06
32946.20		355.706	0.172	0.126		424.79	48.64	579.6	658.68	-0.09	0.04	0.10
32946.20		355.848	0.222	0.162		513.92	58.84	144	202.44	-0.01	-0.56	-0.42
32946.20		362.127	0.009	0.002	b	22.54	5.37	8.04		-1.35	-1.8	
32946.20		409.802	-	-	-	-	-	20.64	-	-	-1.28	
32946.20		415.487	0.076	0.014		186.06	44.34	87.6	104.41	-0.32	-0.65	-0.57
32946.20		437.425	0.045	0.009		102.14	24.34	20.4		-0.53	-1.23	
32946.20		465.983	0.006	0.001		16.27	3.88	8.88		-1.28	-1.54	
32946.20		503.127	0.040	0.008		104.73	24.96	38.4	43.20	-0.40	-0.84	-0.79
32946.20		510.890	0.075	0.014		174.34	41.54	111.6	121.68	-0.17	-0.36	-0.32
32946.20		525.603	0.012	0.002		29.57	7.05	13.2		-0.91	-1.26	
32946.20		656.799	-	-	-	-	-	10.08	8.69	-	-1.18	-1.25
32946.20		683.481	0.002	0.000	w	6.37	1.52	5.28		-1.35	-1.44	
32946.20		698.871	-	-	-	-	-	11.04	9.25	-	-1.09	-1.17

32946.20		700.615	0.008	0.001		21.52	5.13	40.8	41.68	-0.80	-0.52	-0.51
32946.20		738.119	-	-		-	-	2.4		-	-1.7	
33211.48	2.5	301.013	0.229	0.175		929.28	121.20	1128	900.80	0.10	0.19	0.09
33211.48		303.405	0.197	0.150		784.70	102.34	992	691.52	0.03	0.14	-0.02
33211.48		306.865	0.136	0.104		556.55	72.58	496	437.52	-0.10	-0.16	-0.21
33211.48		335.843	0.209	0.160	b	-	-	166.4	129.28	-	-0.55	-0.66
33211.48		442.124	0.088	0.018		358.40	88.29	149.6	88.24	0.02	-0.36	-0.59
33211.48		451.450	0.137	0.105		558.38	72.82	184	90.08	0.23	-0.25	-0.56
33211.48		649.409	0.002	0.000	w	12.68	3.12	7.12		-1.10	-1.34	
33211.48		714.688	-	-		-	-	4.16		-	-1.49	
33557.95	5	316.138	0.186	0.136		506.42	57.98	506.8	486.50	-0.12	-0.12	-0.14
33557.95		348.128	0.367	0.024		1054.73	111.37	1442	1203.44	0.28	0.42	0.34
33557.95		354.277	0.157	0.114		423.43	48.48	303.8	300.72	-0.10	-0.24	-0.25
33557.95		361.421	0.054	0.010		147.93	35.25	63	153.44	-0.54	-0.9	-0.52
33557.95		370.914	0.032	0.006		90.02	21.45	40.46	34.94	-0.73	-1.08	-1.14
33557.95		399.777	0.094	0.018		265.83	63.35	123.2	201.04	-0.20	-0.53	-0.32
33557.95		453.064	0.012	0.002	w	31.52	7.51	4.76		-1.01	-1.83	
33557.95		509.225	0.087	0.017		243.42	58.01	152.6	76.05	-0.02	-0.23	-0.53
33557.95		631.422	0.004	0.001		15.33	3.65	12.32	9.47	-1.04	-1.13	-1.20
33557.95		670.209	0.002	0.000		8.44	2.01	10.64	14.77	-1.25	-1.15	-1.00
33557.95		671.813	0.004	0.001		12.95	3.09	20.3	53.07	-1.06	-0.86	-0.44
33557.95		675.265	-	-		-	-	91		-	-0.21	
33557.95		724.027	-	-		-	-	2.52		-	-1.7	
33596.03	2.3	299.905	0.166	0.121		718.52	96.85	770	571.40	-0.01	0.02	-0.11
33596.03		303.284	0.218	0.159		958.16	129.16	1440	1012.00	0.12	0.3	0.15
33596.03		308.200	0.228	0.166		989.06	133.32	1350	1029.00	0.15	0.28	0.17
33596.03		331.373	0.035	0.007		153.60	38.20	150	173.90	-0.60	-0.6	-0.54
33596.03		331.560	0.020	0.004		91.35	22.72	61	105.40	-0.82	-1	-0.76
33596.03		337.469	0.046	0.009		207.86	51.70	98	117.90	-0.45	-0.78	-0.70
33596.03		399.169	0.010	0.002		48.69	12.11	25		-0.93	-1.23	
33596.03		434.731	0.126	0.092		543.78	73.30	219	151.90	0.19	-0.21	-0.37
33596.03		443.745	0.030	0.006	b	95.58	23.77	12.1		-0.55	-1.45	
33596.03		452.284	0.106	0.078		464.45	62.61	159	215.30	0.15	-0.31	-0.18
33596.03		487.194	0.009	0.002	s	42.02	10.45	8.6		-0.83	-1.51	
33596.03		494.470	0.007	0.001		34.74	8.64	18		-0.89	-1.18	
33596.03		722.036	-	-		-	-	2.8		-	-1.67	

34108.48	10	399.631	0.302	0.020		295.96	31.25	341	513.50	-0.15	-0.09	0.09
34108.48		413.710	0.288	0.210		294.63	33.73	298	311.50	-0.12	-0.12	-0.10
34108.48		419.769	0.294	0.215		293.61	33.62	223	346.60	-0.11	-0.23	-0.04
34108.48		439.148	0.111	0.081		110.86	12.69	26.1		-0.49	-1.12	
34108.48		458.794	0.001	0.000	w	1.01	0.24	2.4		-2.49	-2.13	
34108.48		648.397	0.003	0.001		3.93	0.94	7.2		-1.61	-1.34	
34108.48		678.631	-	-	-	-	-	28	32.41	-	-0.71	-0.65
34108.48		713.313	-	-	-	-	-	14.5	10.48	-	-0.96	-1.10
34108.48		713.569	-	-	-	-	-	21.7	17.02	-	-0.78	-0.89
34108.48		784.495	-	-	-	-	-	12.4		-	-0.94	
34178.78	2.2	298.016	0.095	0.018		512.63	128.21	312	312.12	-0.17	-0.39	-0.38
34178.78		302.760	0.204	0.149		1108.49	152.29	1152	1078.20	0.18	0.2	0.17
34178.78		310.050	0.222	0.162		1193.10	163.91	2892	2032.80	0.24	0.62	0.47
34178.78		340.761	0.135	0.099		748.22	102.79	408	706.32	0.12	-0.14	0.09
34178.78		346.650	0.029	0.005		157.96	39.51	82.8	64.87	-0.55	-0.83	-0.93
34178.78		432.556	0.108	0.079		604.96	83.11	202.8	2107.20	0.23	-0.25	0.77
34178.78		440.666	0.151	0.110		824.39	113.26	300	214.56	0.38	-0.05	-0.20
34178.78		480.616	0.028	0.005		152.22	38.07	19.2		-0.28	-1.17	
34178.78		493.615	0.027	0.005		144.81	36.22	38.4		-0.28	-0.86	
34178.78		643.430	0.001	0.000	w	7.77	1.94	3.36		-1.32	-1.68	
34178.78		676.550	-	-	-	-	-	4.32		-	-1.53	
34608.12	9	391.806	0.122	0.089		160.73	18.40	68.4	99.25	-0.43	-0.8	-0.64
34608.12		405.329	0.406	0.027		551.70	58.25	673.2	693.84	0.13	0.22	0.23
34608.12		411.143	0.228	0.166		287.82	32.95	238.8	338.76	-0.14	-0.22	-0.07
34608.12		429.717	0.236	0.172		322.49	36.92	229.2	199.80	-0.05	-0.2	-0.26
34608.12		628.045	0.002	0.000	w	2.17	0.52	4.2		-1.89	-1.61	
34608.12		656.369	-	-	-	-	-	7.56		-	-1.31	
34608.12		688.758	0.006	0.001		8.43	2.01	27.36	30.53	-1.22	-0.71	-0.66
34608.12		743.255	0.001	0.000	w	-	-	12	6.27	-	-1	-1.28
34900.47	9.7	406.259	0.642	0.042		531.84	56.16	458.4	605.76	0.12	0.06	0.18
34900.47		419.765	0.191	0.139		157.14	17.99	109.6		-0.38	-0.54	
34900.47		424.384	0.045	0.009		34.95	8.33	132.8	175.12	-1.02	-0.44	-0.33
34900.47		430.346	0.091	0.017		72.39	17.25	17.68		-0.70	-1.31	
34900.47		442.703	0.003	0.001	w	2.19	0.52	25.52		-2.19	-1.12	
34900.47		644.008	-	-	-	-	-	3.04		-	-1.73	

34900.47		675.389	-	-	-	-	22.4	21.71	-	-0.81	-0.83
34900.47		697.824	0.028	0.005		26.22	6.25	10.4	16.01	-0.72	-1.12
34900.47		700.608	-	-	-	-	16.88		-	-0.91	
34900.47		778.719	-	-	-	-	14.4	12.50	-	-0.88	-0.94
35111.83	10.7	368.633	0.378	0.029		580.60	61.30	337.4	646.66	0.07	-0.16
35111.83		384.221	0.415	0.031		655.02	69.16	807.8	1123.92	0.16	0.25
35111.83		397.217	0.148	0.124	-	-	65.8	82.19	-	-0.81	-0.71
35111.83		597.029	0.032	0.007		46.88	11.17	32.2		-0.60	-0.77
35111.83		597.824	0.022	0.005	s	19.99	4.76	4.34		-0.97	-1.64
35111.83		665.658	0.004	0.001	w	5.91	1.41	5.88		-1.41	-1.41
35111.83		716.426	0.000	0.000	-	-	14.28	10.46	-	-0.96	-1.09
35272.55	6.7	366.461	0.913	0.060		2192.47	231.50	2080	2523.20	0.65	0.62
35272.55		591.353	0.087	0.017		195.59	46.61	118.4	98.00	0.01	-0.21
35272.55		592.133	-	-	-	-	24.48		-	-0.89	
35272.55		708.268	-	-	-	-	3.2		-	-1.62	
35272.55		784.636	-	-	-	-	155.2	69.90	-	0.16	-0.19
35362.63	15.5	365.255	0.276	0.204		260.44	29.82	343	592.48	-0.28	-0.16
35362.63		380.552	0.530	0.035		479.30	50.61	421.4	557.20	0.02	-0.04
35362.63		393.298	0.125	0.092		121.07	13.86	68.32	123.44	-0.55	-0.8
35362.63		588.219	0.022	0.004		19.83	4.73	22.4		-0.99	-0.94
35362.63		588.990	0.024	0.005		15.51	3.70	6.58		-1.09	-1.47
35362.63		599.623	0.007	0.001		5.32	1.27	3.22		-1.54	-1.77
35362.63		654.724	0.002	0.000	w	1.74	0.42	4.62		-1.95	-1.53
35362.63		703.777	0.013	0.003	s	-	-	7.7	-	-1.24	
35605.27	8	362.045	0.238	0.174		362.13	41.46	244.8	395.64	-0.15	-0.32
35605.27		377.070	0.444	0.029		642.23	67.81	888	1479.60	0.14	0.28
35605.27		389.579	0.279	0.203		433.98	49.69	309.6	490.56	-0.01	-0.15
35605.27		412.055	0.023	0.004	s	30.18	7.19	7.92		-1.11	-1.7
35605.27		644.483	0.009	0.002	w	17.51	4.17	11.64		-0.96	-1.14
35605.27		665.104	0.002	0.000	w	7.01	1.67	4.08		-1.33	-1.56
35605.27		691.958	0.004	0.001	w	6.96	1.66	8.52		-1.30	-1.21
35605.27		764.774	0.000	0.000	-	-	1.92		-	-1.78	
36461.16	5.1	307.707	0.169	0.125		435.27	49.84	112.8	164.64	-0.21	-0.8
36461.16		358.191	0.205	0.153		517.70	59.27	936	1251.60	0.00	0.26

36461.16		362.526	0.085	0.016	-	-	121.2	219.84	-	-0.62	-0.36	
36461.16		379.117	0.153	0.114		400.61	45.87	626.4	1040.76	-0.06	0.13	0.35
36461.16		400.384	0.032	0.006		88.18	21.01	55.2	92.66	-0.67	-0.87	-0.65
36461.16		427.502	0.014	0.003		34.83	8.30	10.68		-1.02	-1.53	
36461.16		433.094	0.150	0.111		377.39	43.21	52.8		0.03	-0.83	
36461.16		536.216	0.010	0.002		413.47	47.34	18.24		0.25	-1.1	
36461.16		551.057	0.003	0.000	w	23.08	5.50	9		-0.98	-1.38	
36461.16		562.141	0.010	0.002		7.21	1.72	26.04	34.06	-1.47	-0.91	-0.79
36461.16		598.241	0.011	0.002		24.17	5.76	32.4		-0.89	-0.75	
36461.16		605.365	0.001	0.000	w	29.12	6.94	3.12		-0.80	-1.77	
36723.70	7	347.951	0.013	0.003		24.22	5.77	22.8		-1.36	-1.39	
36723.70		361.807	0.058	0.011		98.55	23.49	44.4		-0.71	-1.07	
36723.70		373.308	0.377	0.025		634.76	67.02	529.2	730.68	0.12	0.04	0.18
36723.70		378.234	0.403	0.027		697.92	73.69	888	1449.60	0.18	0.28	0.49
36723.70		393.897	0.112	0.082		194.81	22.31	91.2	166.44	-0.34	-0.68	-0.41
36723.70		545.266	0.027	0.005		45.15	10.76	21.24		-0.70	-1.02	
36723.70		576.319	0.004	0.001	w	7.62	1.82	3.36		-1.42	-1.77	
36723.70		619.042	0.003	0.001	w	6.08	1.45	3.48		-1.46	-1.7	
36723.70		642.240	-	-	-	-	-	38.4	54.26	-	-0.62	-0.47
36723.70		704.498	0.003	0.001		5.17	1.23	19.44	18.92	-1.42	-0.84	-0.85
36723.70		783.882	-	-	-	-	-	24	21.06	-	-0.65	-0.71
36778.40	15.4	361.092	0.587	0.039		387.15	40.88	205	309.50	-0.12	-0.4	-0.22
36778.40		372.547	0.286	0.209		186.91	21.40	345	624.50	-0.41	-0.14	0.11
36778.40		389.085	0.058	0.011		34.57	8.24	45	83.33	-1.11	-0.99	-0.72
36778.40		393.050	0.069	0.013		40.71	9.70	14.3		-1.03	-1.48	
36778.40		408.713	-	-	-	-	-	10		-	-1.6	
36821.82	7.2	346.767	-	-	-	-	-	29.4		-	-1.28	
36821.82		360.526	0.251	0.183		479.20	54.87	273	383.74	-0.03	-0.27	-0.13
36821.82		371.945	0.695	0.046		1362.75	143.89	1400	2647.40	0.45	0.46	0.74
36821.82		541.709	0.017	0.003		32.92	7.84	17.92		-0.84	-1.1	
36821.82		542.364	0.022	0.004		41.05	9.78	20.3		-0.74	-1.05	
36821.82		551.367	0.009	0.002		17.21	4.10	11.48		-1.11	-1.28	
36821.82		597.614	0.006	0.001	w	11.31	2.69	9.52		-1.22	-1.29	
36821.82		638.217	-	-	-	-	-	42	42.85	-	-0.59	-0.58
36821.82		737.724	-	-	-	-	-	68.6	37.86	-	-0.25	-0.51
36821.82		777.897	-	-	-	-	-	8.54		-	-1.11	

Table 6.5 shows the radiative parameters for singly ionized gadolinium.

Lifetimes from by Den Hartog et al.¹⁰

w denotes weak emission lines

s denotes shouldered emission lines

b denotes blended line

DH denotes the work by Den Hartog et al.¹⁰

Kurucz refers to the work by Kurucz and Bell³³³³

Gd III Data

Table 6.6 shows the radiative parameters for Gd III

Lifetimes from Zhang et al.⁹ associated with the *DREAM* project

w denotes weak emission line

s denotes shouldered emission line

b denotes blended emission line

Upper Energy (cm ⁻¹)	Lifetime (ns)	T Error	wavelength (nm)	Branch Ratio	BR Error	g _k *A _{ki} (10 ⁶ s ⁻¹)			log gf	
						This work	error	DREAM	This work	DREAM
43020	1.9	0.2	232.378	0.105	0.008	386.58	56.93	827	-0.504	-0.17
43020			233.897	0.128	0.009	472.34	69.56	750	-0.412	-0.21
43020			236.191	0.067	0.013	247.69	63.33	417	-0.683	-0.46
43020			295.553	0.409	0.027	1508.97	211.95	1490	0.296	0.29
43020			300.192	-	-	-	-	32.1	-	-1.36
43020			302.894	0.274	0.020	1012.47	149.11	20.5	0.144	-1.55
43020			304.924	0.003	0.001	s 10.54	2.69	6.81	-1.833	-2.02
43020			317.666	0.014	0.003	s 52.99	13.55	190	-1.096	-0.54
43612	1.9	0.2	230.703	0.052	0.010	245.75	62.83	338	-0.707	-0.57
43612			232.935	0.107	0.008	508.14	74.84	784	-0.383	-0.2
43612			236.326	0.132	0.010	627.29	92.38	986	-0.279	-0.08
43612			290.473	0.275	0.020	1304.05	192.05	1460	0.218	0.27
43612			291.840	0.213	0.016	1012.90	149.17	235	0.112	-0.52
43612			294.951	0.007	0.001	b 32.62	8.34	52.4	-1.371	-1.17
43612			297.559	0.001	0.000	b 4.79	1.22	7.75	-2.197	-1.99
43612			311.804	0.213	0.016	1008.88	148.58	690	0.168	0
47234	1.4	0.2	214.803	0.041	0.008	o 321.32	87.82	213	-0.653	-0.83

47234			217.684	0.104	0.008	o	821.90	144.75	964	-0.233	-0.17
47234			222.394	0.442	0.029		3481.48	593.46	2760	0.412	0.31
47234			262.811	0.398	0.026		3141.61	535.52	3860	0.513	0.6
47234			263.930	0.008	0.002	w	62.69	17.13	18.5	-1.184	-1.72
47234			266.472	0.007	0.001	b	56.29	15.38	3.48	-1.222	-2.43
48339	1.5	0.2	208.008	0.022	0.004		133.49	35.84	205	-1.062	-0.88
48339			209.820	0.035	0.007		210.05	56.39	357	-0.858	-0.63
48339			212.568	0.057	0.011		343.60	92.24	272	-0.633	-0.74
48339			255.390	0.295	0.022		1770.10	298.23	1270	0.239	0.09
48339			256.447	0.160	0.012		957.90	161.39	1120	-0.025	0.04
48339			258.847	0.093	0.018	s	558.59	149.96	374	-0.251	-0.43
48339			260.853	0.110	0.008	s	660.03	111.20	73.3	-0.172	-1.13
48339			271.736	0.252	0.018		1511.59	254.68	1800	0.224	0.3
48860	1.5	0.2	204.603	0.016	0.003	w	73.64	19.77	138	-1.335	-1.06
48860			205.779	0.016	0.003	w	74.29	19.94	66.9	-1.326	-1.37
48860			207.5524	-	-		-	-	7.96	-	-2.29
48860			252.039	0.066	0.013		308.35	82.78	373	-0.532	-0.45
48860			255.405	0.322	0.021	s	1501.01	244.01	693	0.167	-0.17
48860			257.357	0.088	0.017		411.56	110.48	542	-0.388	-0.27
48860			258.822	0.198	0.014	s	924.82	155.82	208	-0.032	-0.68
48860			267.945	0.320	0.021		1495.19	243.06	1970	0.207	0.33
49195	1.7	0.2	203.2085	-	-		-	-	6.98	-	-2.36
49195			204.370	-	-		-	-	9.81	-	-2.21
49195			255.156	0.111	0.008		327.25	51.17	269	-0.495	-0.58
49195			256.596	0.217	0.016		638.11	99.78	445	-0.201	-0.36
49195			257.607	0.181	0.013		530.90	83.01	399	-0.277	-0.4
49195			265.560	0.491	0.032		1444.92	216.69	1700	0.184	0.25

Table 6.6 shows the radiative parameters for Gd III

Lifetimes from Zhang et al.⁹ associated with the *DREAM* project

w denotes weak emission line

s denotes shouldered emission line

b denotes blended emission line

6.5 - Conclusions

Transition probabilities for neutral, singly ionized, and doubly-ionized gadolinium and samarium are presented in the tables above and compared to other previous works. For each of these elements and their respective ionizations we show a graphical representation of the data in order to see how our measurements agree with previous works. For each element and ionization I present a transition probability (TP) comparison where the TP's of others and this work are plotted against the other's TP's in order to show any systematic trends. However this type of plot gives a biased perspective to the values presented in contrast to this work's TP's because the straight line of the other works' results gives the illusion of optimum accuracy. I could just as easily plotted their values against my measured values. Either way, the idea is to look for systematic deviations, not absolute agreement. In order to give a better representation of the level of agreement, 3 histogram plots were made showing the representative percent differences between this work's BRs and those of other works and each is discussed in further detail below. The percent difference are partitioned according to branching ratio strength (greater than 30%, between 30 and 10% and less than 10%) in order to reveal any systematic deviations which might depend upon branching ratio strength.

6.5.1 - Neutral Samarium

The deviation of this works' transition probabilities (A_{ki}) from prior works is rather large in neutral samarium (Sm I). The reason for the disagreement is believed to be due mainly to unobserved or "problematic" (blended, weak, or shouldered) emission lines. As was discussed earlier, when branches from an upper level are erroneous or missing the branching ratio of the other "good" lines are directly affected. The hope in this work is that the erroneous branches are

those which have small branching fractions so as not to produce a large effect on the rest of the branching ratios from that upper level. However in this case it appears that some of the problematic lines contributed rather strongly to the rest of the branches. Of those radiative parameters reported in table 6.1, there are a total of 137 emission lines from 70 upper energy levels, 4 of which were unobserved, 46 were noted as relatively weak, 11 were blended, 7 had shouldering emission lines for a total of 63 problematic lines. Figure 6.1 shows the comparison of our transition probabilities with reported works in table 6.1.

In total we observed emission lines from 79 upper energy states in Sm I yielding a total of 237 relative intensities which are reported in appendix 1.

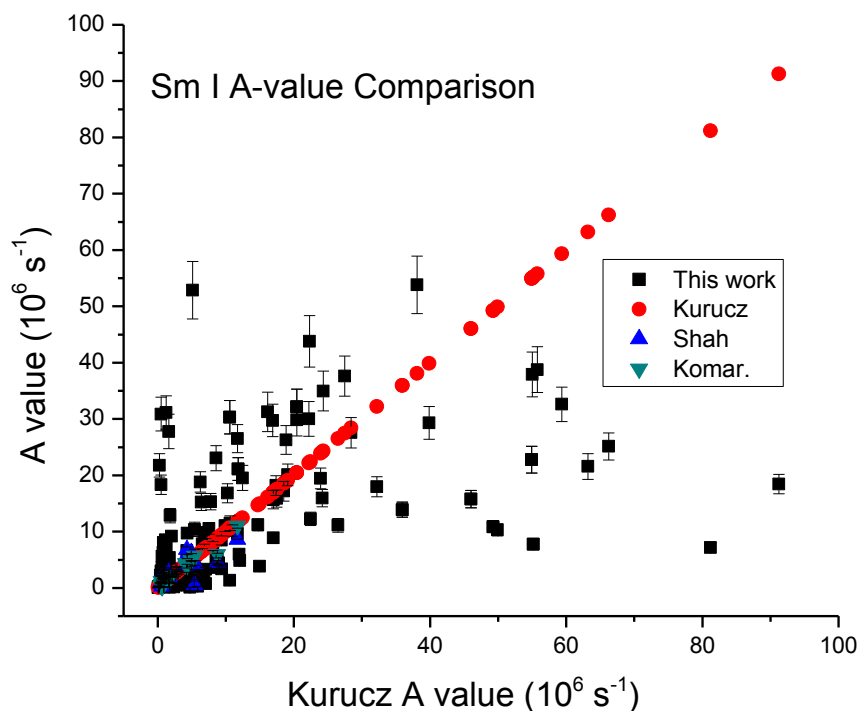


Figure 6.1 shows the comparison of Sm I transition probabilities (A_{ki}) between this work (black squares), Kurucz (red circles), Shah et al.¹⁷ (upward blue triangles), and Komarovskii et al.³⁴ (downward cyan triangles). The various gA values are plotted against the values of Kurucz, so that data which lie on a slope of one represent perfect agreement with Kurucz's data. The error bars shown in this work incorporate error from lifetimes as well as uncertainties of this work.

Figure 6.2-6.4 are histogram representations of the Sm I transition probability (gA) percent difference $(WSU - Kurucz)/Kurucz \times 100$ between this work and that of Kurucz and Bell.³³ The histograms show the number of times a given percent difference was reported relative to complete agreement (zero percent difference). The entire range of percent differences was partitioned according to branching ratio strength to see if agreement between this work and others depends in any way on branching ratio strength. The idea being that weaker branches

should have typically worse agreement since we have difficulty measuring them and overly-strong lines which we saw as blended will also have large percent differences.

For those Sm I branches greater than 30%, I found that 45.52% of the values reported agree within $\pm 25\%$ with Kurucz, 76.4% agree within $\pm 75\%$, 82.9% agree within $\pm 125\%$, 86.2% agree within $\pm 175\%$, and all 100% of the values agree within $\pm 925\%$. The average percent difference for branches greater than 30% was found to be 74.1%. Given that our stated uncertainty for this strength of branching ratio is 9.3% for all of these levels in Sm I, the results show that we generally disagree with those transition probabilities, since less than 50% of the values agree within our error estimates. It is important to keep in mind that the lifetimes used in Sm I had large uncertainties. As I noted earlier it is unexplained and peculiar that for the many levels of Sm I which have only a single branch, our A values do not agree with other works. There are also many outliers in Sm I along the positive side of zero percent, which shows that these outlier gA values were larger than Kurucz and Bell's values. I believe these larger over-estimates to be caused by spectral blending of neighboring lines.

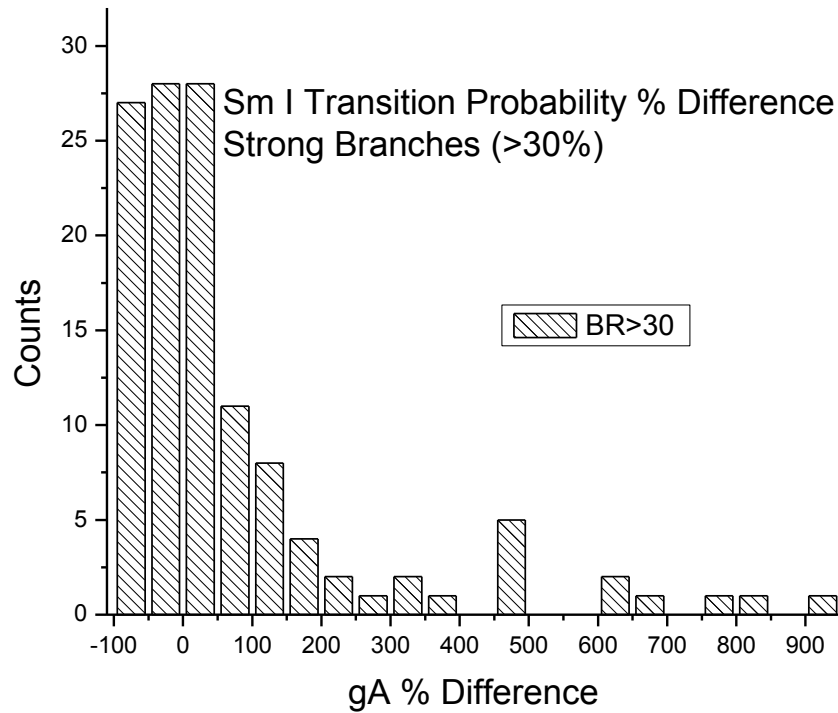


Figure 6.2 shows a histogram plot of the gA percent difference between this work and that of Kurucz and Bell for strong branches which are greater than 30 percent. The number of occurrences (counts) represents the number of percent difference values which lie within the given bin size (50%).

For the 6 Sm I branches which are between 30% and 10% I found that 16.7% of the reported values agreed within $\pm 10\%$ of the Kurucz values, and by $\pm 90\%$ all 6 values were within agreement. The average percent difference for branches of medium strength was found to be -47.0%. Overall there is not very good agreement with the reported values from Kurucz and Bell. The reason for the general discrepancy is not apparent although most of the values in this branching ratio bracket lie on the negative side. I believe there to be strong inaccuracies with the lifetimes used for these calculations since they are from very old sources (see the Sm I chart

above). The typical uncertainty of these lifetimes is reported as 10%. Despite the complications in lifetime accuracy, I know that in general the experimental conditions set for this experiment cause neutral emission lines to generally be inaccurate, so these discrepancies with prior results are not surprising. In future experiments, optimal conditions could be set for the neutral species.

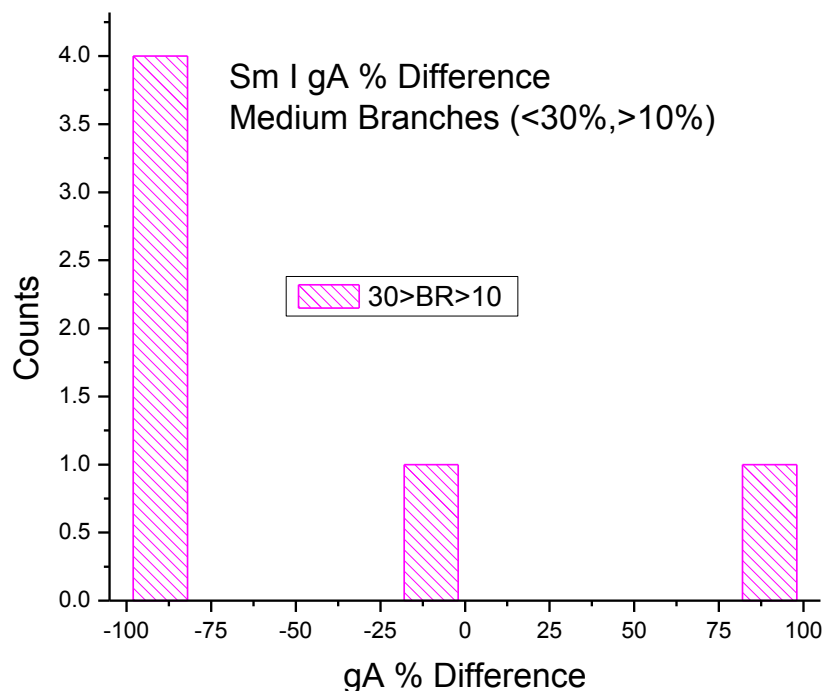


Figure 6.3 shows a histogram plot of the gA percent difference between this work and that of Kurucz and Bell for “medium” branches which are between 30 and 10 percent. The number of occurrences (counts) represents the number of reported percent difference values which lie within the given bin size (20%).

For the three branches of Sm I which are less than 10% (figure 6.4) I found that 33.3% of the reported values agreed within $\pm 20\%$ with the Kurucz values, 66.6% agreed within $\pm 40\%$, and all 100% agreed within $\pm 100\%$. The average percent difference for branches weaker than 10%

was found to be 50.0%. Overall for the weak branches in Sm I there is a relatively good agreement within the stated uncertainty of our 3 weak branches (23.3%) and the lifetimes ($\sim 10\%$) from other works. It is the case that outliers lie on the negative side of zero and could be systematically showing that one of our weak values was underestimated. In general we expect the neutral species as a whole to be less accurate than the singly-ionized.

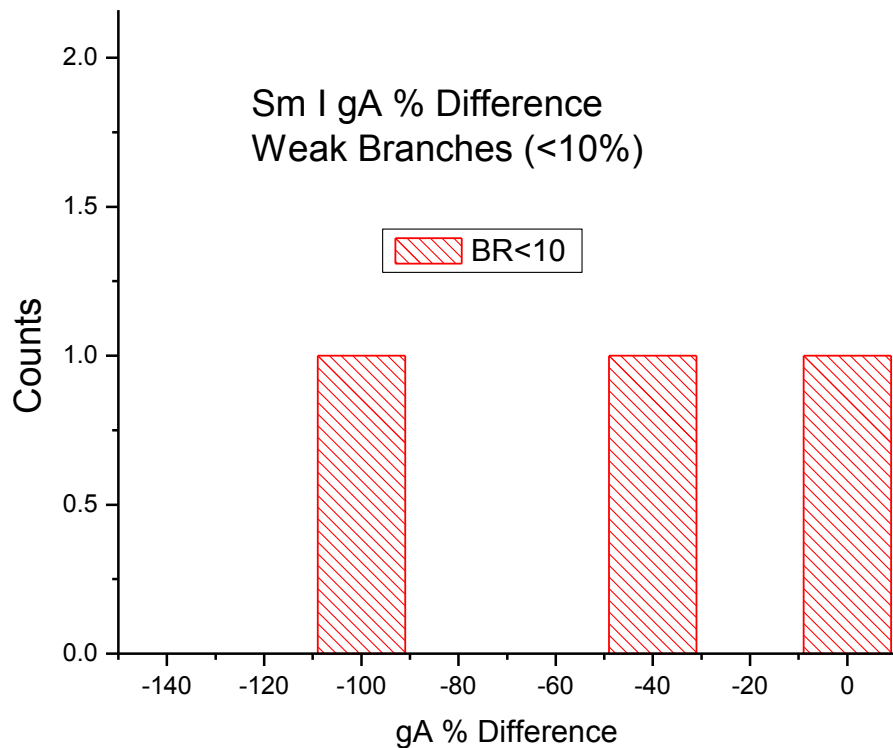


Figure 6.4 shows a histogram plot of the gA percent difference between this work and that of Kurucz and Bell for “weak” branches which are less than 10 percent. The number of occurrences (counts) represents the number of percent difference values which lie within the given bin size (20%).

6.5.2 - Singly-Ionized Samarium

Our radiative parameters in singly-ionized samarium are in relative agreement with previously reported values given our budget of uncertainty. Of the reported 115 “good” upper energy levels listed in table 6.2, we observed 713 emission lines: 100 were noted as weak, 14 were blended, 20 were shouldered. It is again believed that the deviation between this work and other agreeing works is due to problematic emission lines. Figures 6.5 and 6.6 show the Sm II gA and $\log(gf)$ comparisons between the reported works. In total there were 225 observed energy level in Sm II with a corresponding 1424 emission lines whose relative intensities are presented in appendix 1.

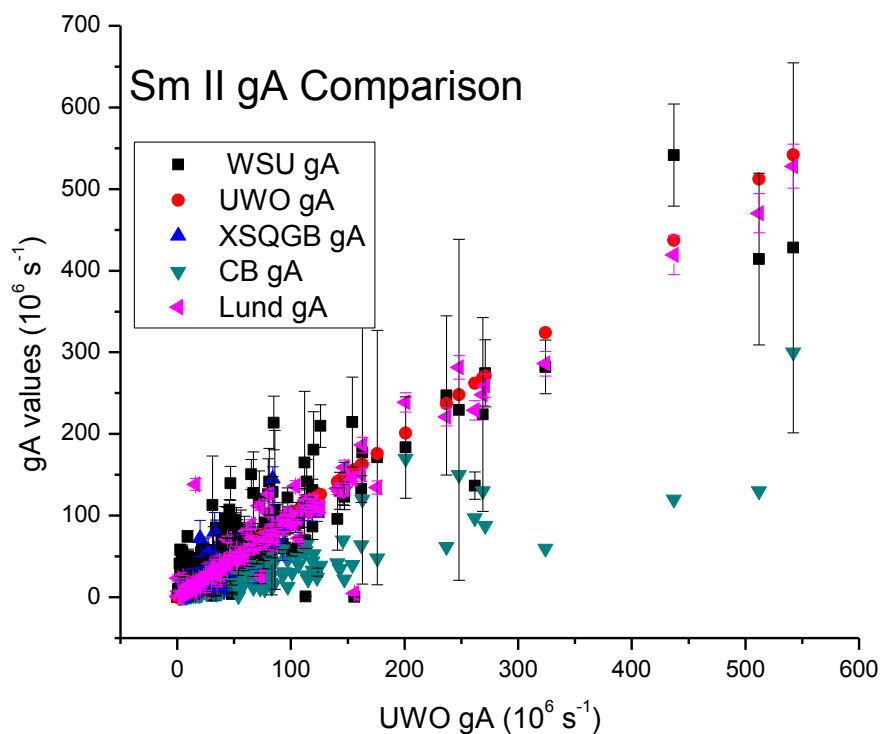


Figure 6.5 shows the transition probability (gA) comparison of Sm II between this work and other previous works. The black squares signify this work, red circles represents gA values by Rehse et al.²⁷ at the University of Western Ontario (UWO), and the upward blue triangles are the results of Xu et al.²⁶ The downward cyan colored triangles are the results of Corliss and Bozman and the sideways magenta triangles represent the results of Lawler et al.²⁸ at Lund University. The various works' gA values are plotted against the values of Rehse et al. so that data which lie on a slope of one represent perfect agreement with the UWO data. The error bars shown in this work incorporate the uncertainty from lifetimes as well as uncertainty of this work.

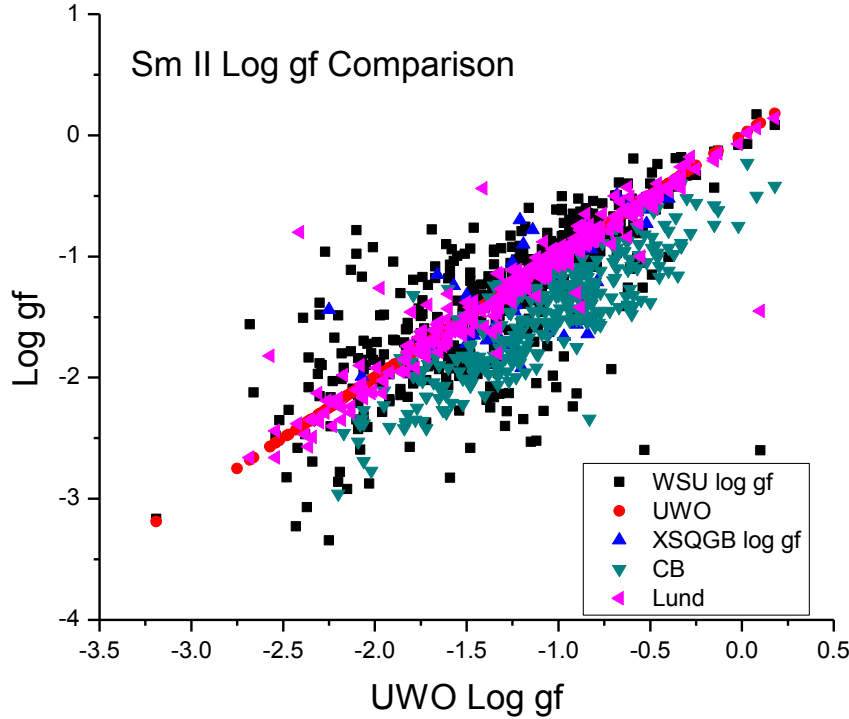


Figure 6.6 shows the $\log(gf)$ comparison of Sm II between this work and other previous works. The black squares signify this work, red circles represents $\log(gf)$ values of Rehse et al.²⁷ at the University of Western Ontario (UWO), and the upward blue triangles are the results of Xu et al.²⁶ The downward cyan colored triangles are the results of Corliss and Bozman³² and the sideways magenta triangles represent the results of Lawler et al.²⁸ at Lund University. The various works' $\log(gf)$ values are plotted against the values of Rehse et al. so that data which lie on a slope of one represent perfect agreement with the UWO data.

Figure 6.7 – 6.9 are histogram representations of the Sm II transition probability (gA) percent differences $(WSU - UWO)/UWO (x100)$ between this work and that of Rehse et al.²⁷ The histograms show the number of times a given percent difference was reported relative to complete agreement (zero percent difference). The entire range of percent differences was partitioned according to branching ratio strength to see if agreement between this work and other's work does vary with branching ratio strength. The idea being that weaker branches

should have typically worse agreement since we have difficulty measuring them and overly-strong lines which we saw as blended will also have large percent differences.

For those Sm II branches greater than 30% I found that 24.6% of our reported values agreed with the UWO values within $\pm 5\%$, 40.35% agree within $\pm 15\%$, 47.37% agree within $\pm 25\%$, 56.1% agree within $\pm 35\%$, 64.9% agree within $\pm 55\%$, 75.4% agreed within $\pm 75\%$, and all 100% of the values agreed within $\pm 1975\%$. The average percent difference for branches greater than 30% was found to be 143%. Given that our stated uncertainty for this strength of branching ratio is 9.3% the strong branches in Sm II, the results show that we generally agree with Rehse et al.'s transition probabilities, since almost 50% of the values agree within our error budgets. The agreement stands even when incorporating the typical 10% uncertainty from lifetimes. However it should be mentioned that for those lifetimes from Lawler et al. (see the Sm II chart above) there were very large uncertainties reported. There are also some outliers in Sm II along the positive side of zero percent, which shows that these outlying gA values were larger than Rehse et al.'s values. I believe these larger overestimates in our values to be caused by spectral blending of neighboring lines.

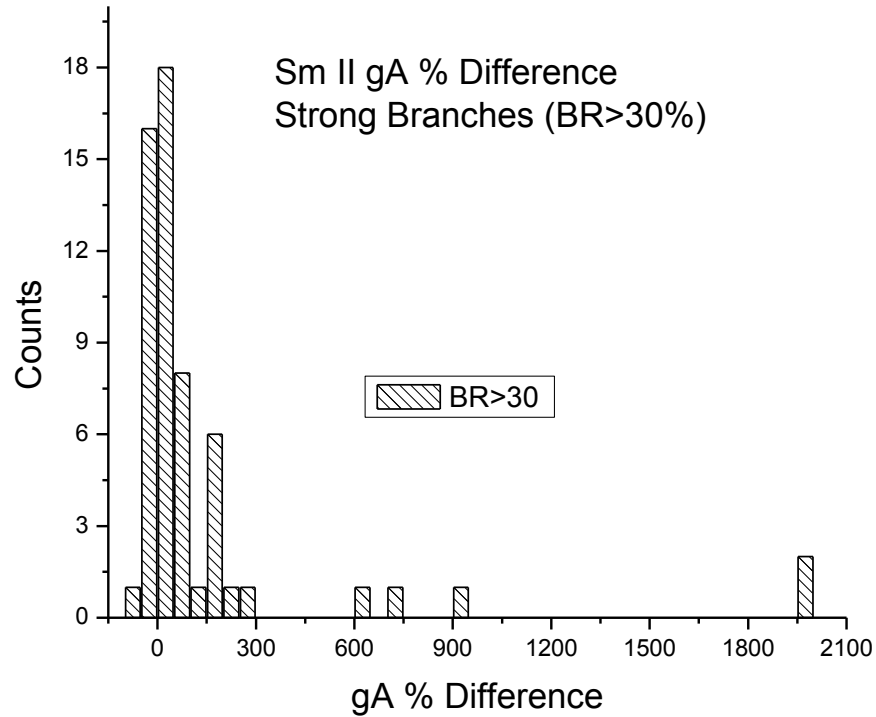


Figure 6.7 shows a histogram plot of the gA percent difference between this work and that of Rehse at UWO for strong branches greater than 30 percent. The number of occurrences (counts) represents the number of percent difference values which lie within the given bin size (50%).

For the Sm II branches which are between 30% and 10% I found that 17.45% of the values agreed within $\pm 5\%$ with the UWO values (0% difference), 34.9% of the values lie agreed $\pm 15\%$, 53.7% of the values agreed within $\pm 25\%$, 64.4% of the values agreed within $\pm 35\%$, 73.2% of the values agreed within $\pm 45\%$, 77.2% of the values agreed within $\pm 55\%$, and by $\pm 1205\%$ all 100% of the values were accounted for. The average percent difference for branches of medium strength was found to be 54.8%. Overall there is not very good agreement with the reported values from Rehse et al in this branching ratio bracket. The reason for the general

discrepancy is not apparent although most of the values in this branching ratio bracket lie on the positive side of zero. The general trend of the data show a systematic overestimate in our gA values compared to those from Rehse et al which I believe to be caused by the problematic blends and shouldering of emission lines.

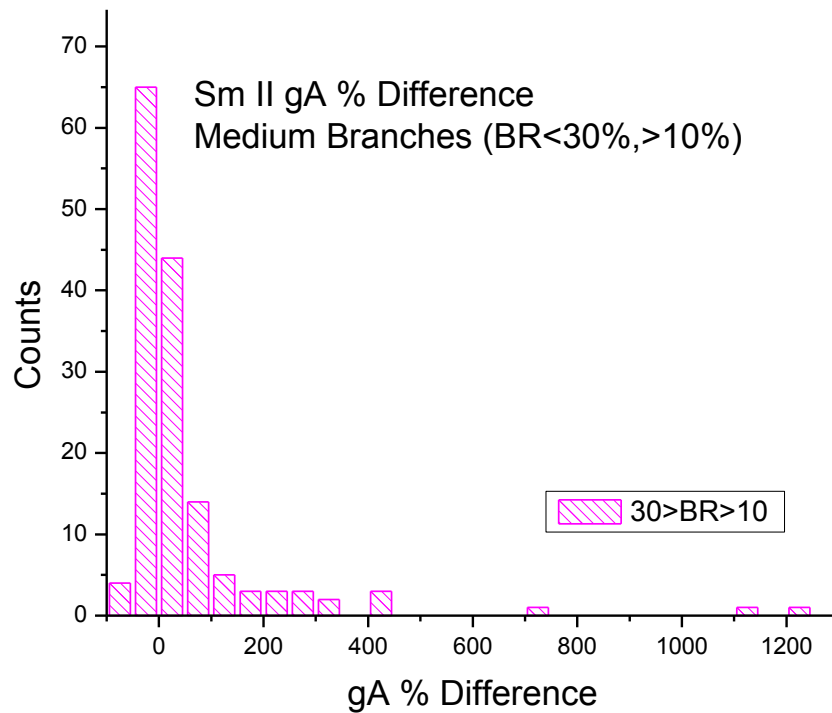


Figure 6.8 shows a histogram plot of the gA percent difference between this work and that of Rehse at UWO for “medium” branches which are between 30 and 10 percent. The number of occurrences (counts) represents the number of percent difference values which lie within the given bin size (50%).

For the branches of Sm II which are less than 10% I found that 43.8% of the values agreed within $\pm 25\%$ with the UWO values (0% difference), 90.6% agreed within $\pm 75\%$, 94.7%

agreed within $\pm 125\%$, and all 100% agreed within $\pm 725\%$. The average percent difference for branches weaker than 10% was found to be -1.4% . Overall for the weak branches in Sm II there is a relatively good agreement within the stated uncertainty of our 3 weak branches (23.3%) and the lifetimes ($\sim 10\%$) from other works. It is the case that outliers lie on the positive side of zero and show that some of our weak values are overestimated.

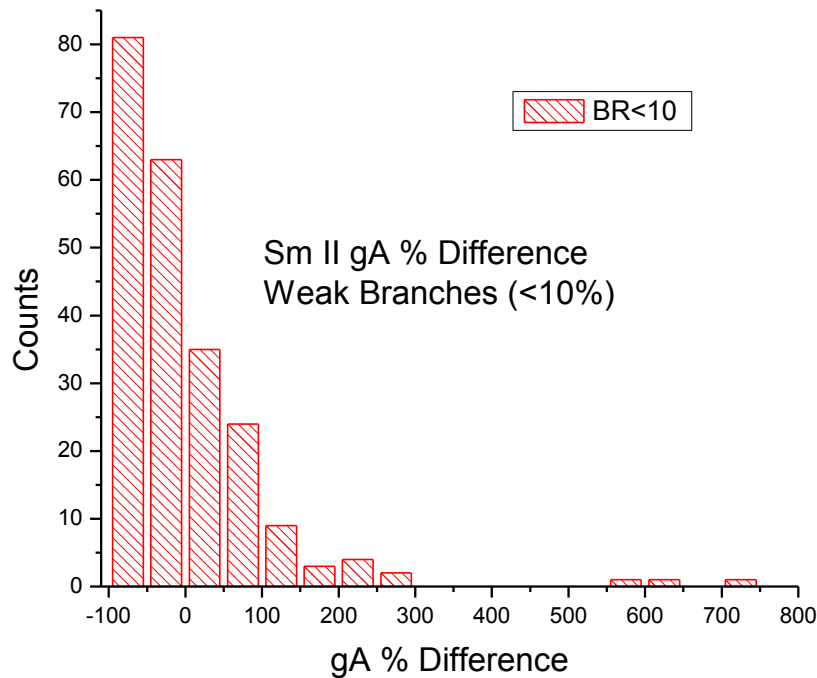


Figure 6.9 shows a histogram plot of the gA percent difference between this work and that of Rehse at UWO for “weak” branches which are less than 10 percent. The number of occurrences (counts) represents the number of percent difference values which lie within the given bin size (50%).

6.5.3 - Doubly-Ionized Samarium

In doubly-ionized samarium (Sm III) the results show a general agreement given our stated uncertainty with the work by Biémont et al.³¹ A major contributing factor to any observed disagreement is the fact that of the 49 emission lines from 17 upper energy levels shown in table 6.3, 46 of them were noted as problematic (weak, shouldered, blended, and unobserved). We believe that it is the major contributing factor as to why our data does not agree well with the only other reported radiative parameters in Sm III for some values. In total radiative parameters for 18 upper energy levels are listed in appendix 1.

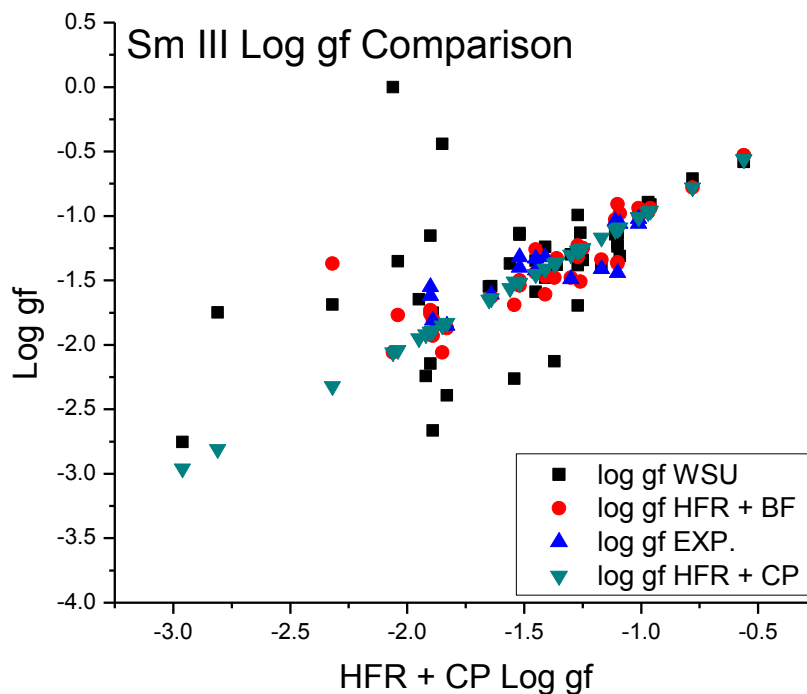


Figure 6.10 shows the $\log(gf)$ comparison between this work and the work of Biémont et al.³¹ The black squares signify this work, red circles represent Biémont's $\log(gf)$ values derived from both relativistic Hartree-Fock calculations and experimental branching fractions, the blue upward triangles are the results by Fourier transform spectroscopy by the same group, and the downward cyan triangles are the results of pure theoretical calculations using relativistic Hartree-Fock (HFR) method with core-polarization (CP) effects. The various works' $\log(gf)$ values are plotted against the values of Biémont et al. using theoretical HFR and CP, so that data which lie on a slope of one represent perfect agreement with the HFR+CP data.

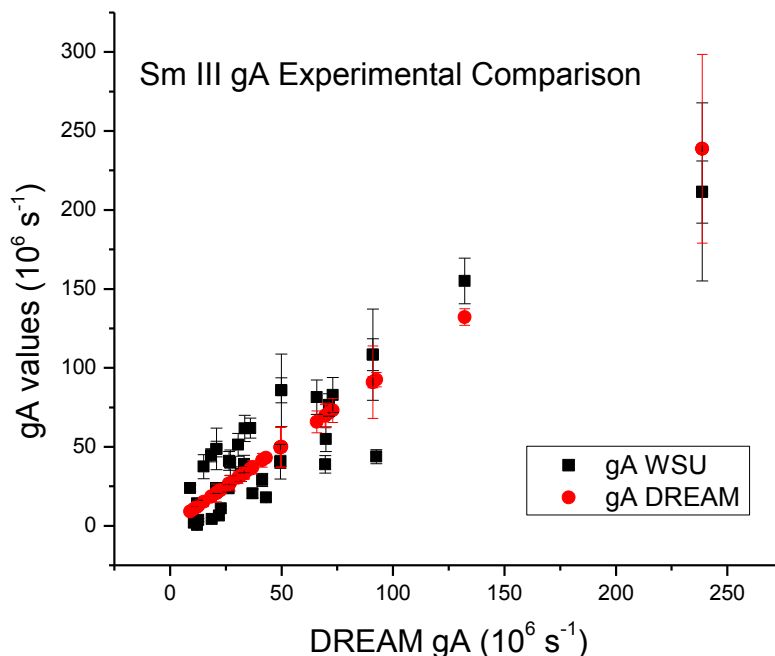


Figure 6.11 shows a comparison of transition probabilities (gA) between this work and the work by Biémont et al.³¹ The black squares signify this work and red diamonds represent Biémont et al.'s work (associated with the DREAM project.) This work's gA values are plotted against the values of Biémont et al. so that data which lie on a slope of one represent perfect agreement with the DREAM data. The error bars shown in this work incorporate error from lifetimes as well as uncertainties of this work.

Figure 6.12, 6.13 and 6.14 are histogram representations of the Sm III transition probability (gA) percent differences $(WSU - DREAM)/DREAM \times 100$ between this work and that of Biémont et al.³¹ The histograms show the number of times a given percent difference was reported relative to complete agreement (zero percent difference). Again, the entire range of percent differences was partitioned according to branching ratio strength to see if agreement between this work and other's work does vary with branching ratio strength. The idea being that

weaker branches should have typically worse agreement since we have difficulty measuring them and overly-strong lines which we saw as blended will also have large percent differences.

For those Sm III branches greater than 30%, I found that 15.8% of the reported values agreed within $\pm 5\%$ with Biémont (0% difference), 58.0% agreed within $\pm 15\%$, 68.4% agree within $\pm 25\%$, 79% agree within $\pm 55\%$, 89.5% agree within $\pm 85\%$, and all 100% of the values agreed within $\pm 165\%$. The average percent difference for branches greater than 30% was found to be 32.6%. Given that our stated uncertainty for this strength of branching ratio is 9.3% and 10% uncertainty in the lifetimes from Biémont et al., the results show that there is good agreement since more than 50% of the values agree within our error estimates. There is also a majority of outliers in Sm III along the positive side of zero percent, which shows that the outlier gA values were larger than Biémont et al.'s values. I believe these larger over-estimates to be caused by spectral blending of neighboring lines (problematic emission lines).

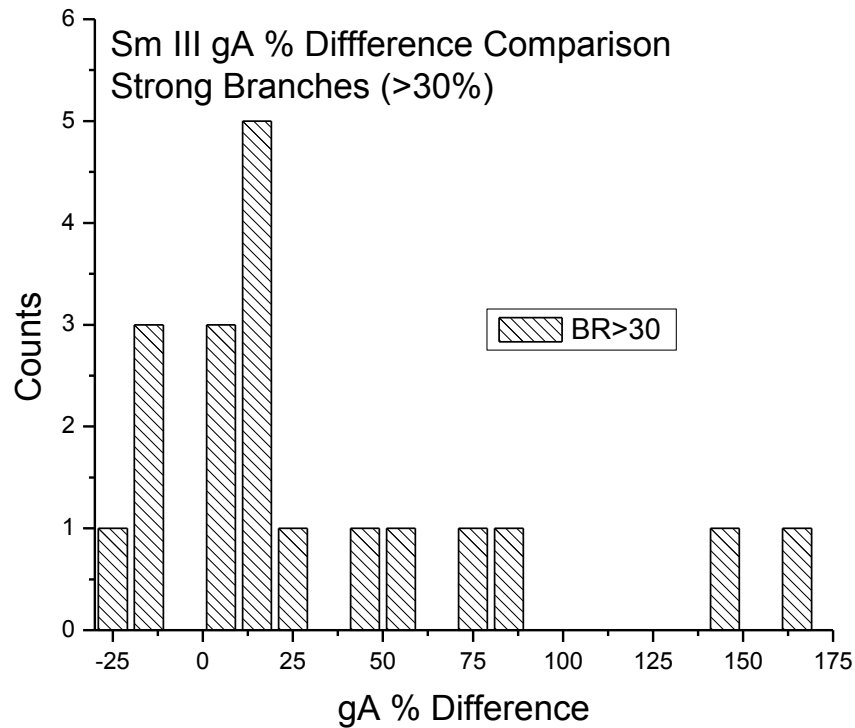


Figure 6.12 shows a histogram plot of the gA percent difference between this work and that of Biémont et al. for strong branches which are greater than 30 percent. The number of occurrences (counts) represents the number of percent difference values which lie within the given bin size (10%).

For Sm III branches which are between 30% and 10% I found that 8.3% of the values agreed within $\pm 5\%$ with Biémont (0% difference), 25.0% agreed within $\pm 15\%$, 33.3% agreed within $\pm 25\%$, 50% agreed within $\pm 45\%$, 75% agreed within $\pm 55\%$, 83.3% agreed within $\pm 65\%$, and all 100% of the values agreed within a percent difference of $\pm 135\%$. The average percent difference for branches of medium strength was found to be -0.51% . Overall there is not very good agreement with the reported values from Biémont et al. The reason for the general discrepancy is not apparent although most of the values in this branching ratio bracket lie on the

positive side of zero and could suggest some systematic issues within our system. This could be related to overestimates in the LIBS profile fitting procedures when problematic issues occur for neighboring lines, especially in the moderate strength branches.

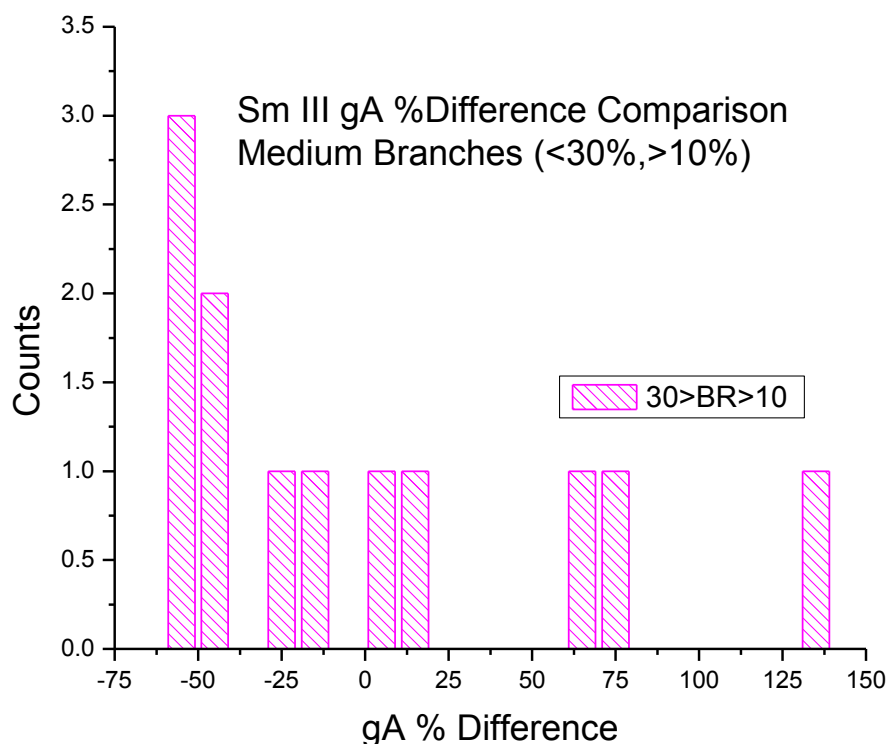


Figure 6.13 shows a histogram plot of the *gA* percent difference between this work and that of Biémont et al. for medium branches which are between 30 and 10 percent. The number of occurrences (counts) represents the number of percent difference values which lie within the given bin size (10%).

For the weak (<10%) branches in Sm III 20% of the values agreed within $\pm 70\%$ with Biémont (0% difference), 40% agreed within $\pm 72\%$, 60% agreed within $\pm 78\%$, 80% agreed within $\pm 82\%$, and all values agreed within $\pm 96\%$. The average percent difference for Sm III

branches weaker than 10% was found to be -79.3% for the 5 branches. There is a general disagreement within the stated uncertainty of our branches (23.3%) and the lifetimes (10%) from Biémont et al. which gives us an overall error budget of ~25%. All the values lie on the negative side of zero percent difference and this trend, which implies that our gA values are underestimated, is unexplained.

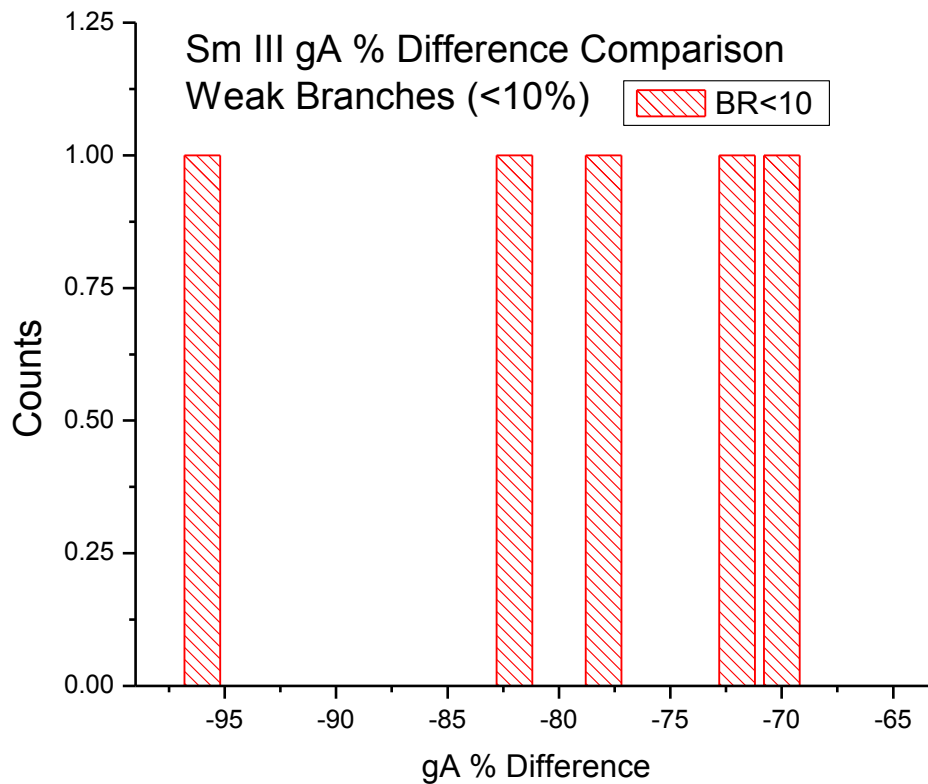


Figure 6.14 shows a histogram plot of the gA percent differences between this work and that of Biémont et al. for weak branches which are less than 10 percent. The number of occurrences (counts) represents the number of percent difference values which lie within the given bin size (2%).

6.5.4 - Neutral Gadolinium

The general disagreement of radiative parameters (transition probabilities and $\log(gf)$ values) in neutral gadolinium (Gd I) can be attributed to the numerous problematic emission lines. It was often seen to be the case that emission lines were blended causing the ESAWIN program to either not fit the peak at all, or to fit the overly-broad emission profile and attribute that integrated intensity to the emission line. As can be seen in table 6.4, we observed emission lines from 113 upper energy states and there are a total of 587 reported emission lines; 436 of which were observed to be problematic: 67 were blended, 80 were shouldered, and 289 were noted as weak. Over all we recorded relative intensities for more than 800 emission lines from 235 upper energy levels which are reported in appendix 1.

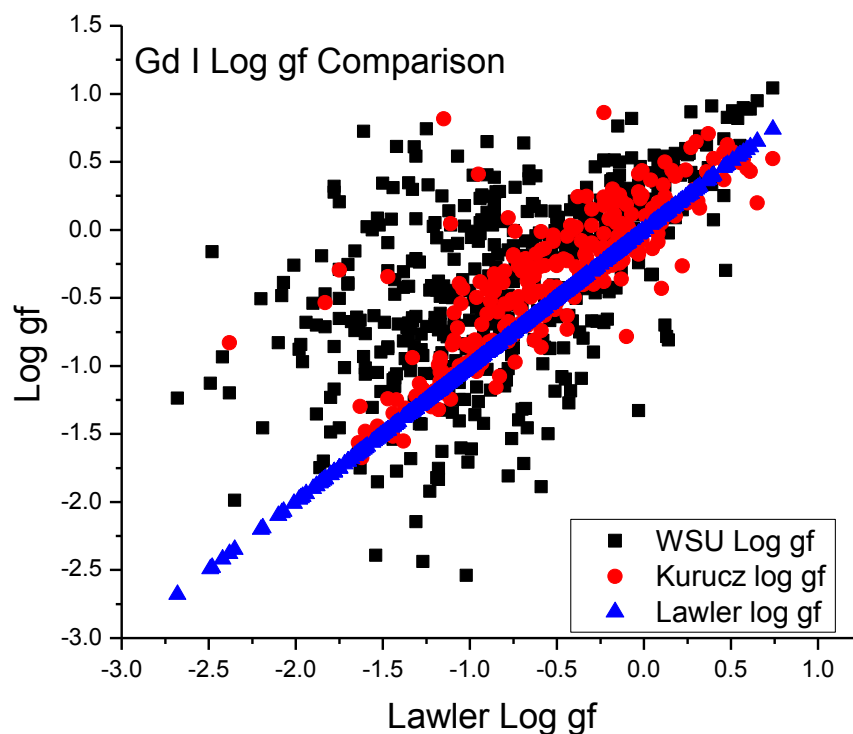


Figure 6.15 shows the $\log(gf)$ comparison of Gd I between this work and other previous works. The black squares signify this work, red circles represent $\log(gf)$ values tabulated by Kurucz and Bell³³, and the upward blue triangles are the results of Lawler et al.⁶ The various works' $\log(gf)$ values are plotted against the values of Lawler et al. so that points which lie on a slope of one represent perfect agreement with the their data.

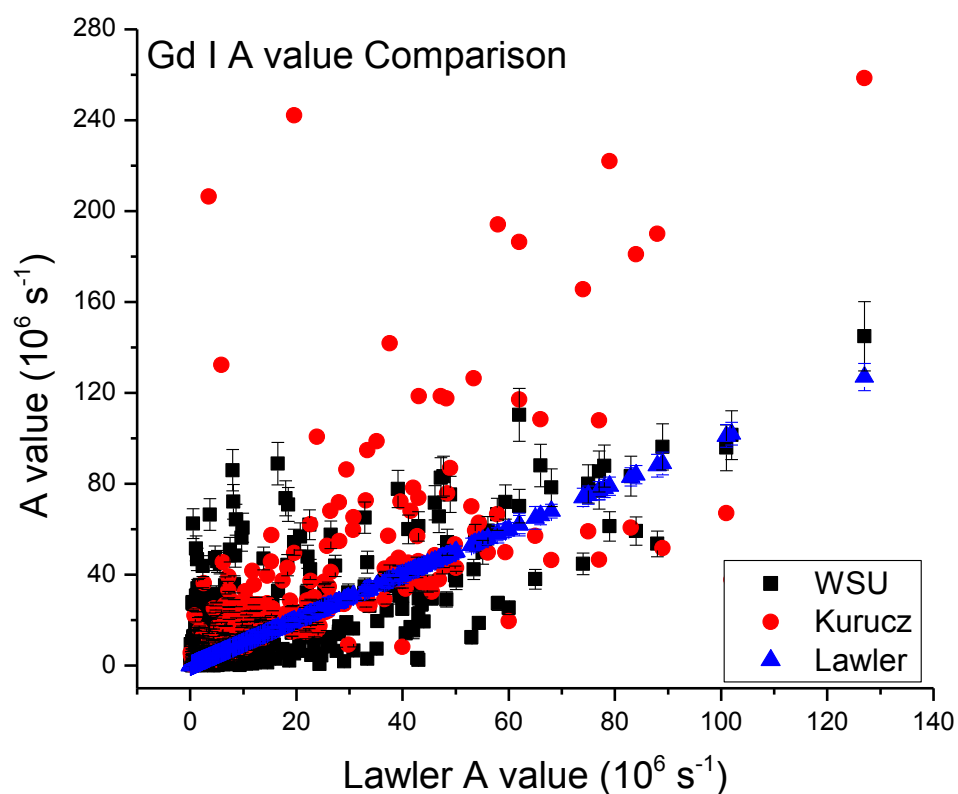


Figure 6.16 shows the transition probability (*A-value*) comparison of Gd I between this work and other previous works. The black squares signify this work, red circles represent *A-values* by Kurucz and Bell³³ and the upward blue triangles are the results of Lawler et al.⁶ The various works' *A-values* are plotted against the values of Lawler et al. so that points which lie on a slope of one represent perfect agreement with their results. The error bars shown in our work in the figure above incorporate the error in lifetimes as well as our uncertainty.

Figure 6.17 - 6.19 are histogram representations of the Gd I transition probability (*A*) percent differences between this work and the work of Lawler et al.⁶ The histograms show the number of times a given percent difference was reported relative to complete agreement (zero percent difference). The entire range of percent differences was partitioned according to

branching ratio strength to see if agreement between this work and other's work varies with branching ratio strength.

For those Gd I branches greater than 30% I found that 39.2% of the values agreed with Lawler within $\pm 10\%$, 60.0% agreed within $\pm 30\%$, 64.8% agreed within $\pm 50\%$, 71.2% agreed within $\pm 70\%$, 76% agreed within $\pm 90\%$, 79.2% agreed within $\pm 110\%$, 89% agreed within $\pm 210\%$ and all 100% of the values agreed within $\pm 590\%$. The average percent difference for branches greater than 30% was found to be 74.1%. Given that our stated uncertainty for this strength of branching ratio is 9.3% and 5% uncertainty in the lifetime from Lawler et al. for all of these levels in Gd I, the results show that we generally agree with those transition probabilities, since almost 50% of the values agree within our error estimates. There are outliers in Gd I along the positive side of zero percent, which show that our g_A values were larger than Lawler et al.'s values. I believe these larger over-estimates to be caused by spectral blending of neighboring lines.

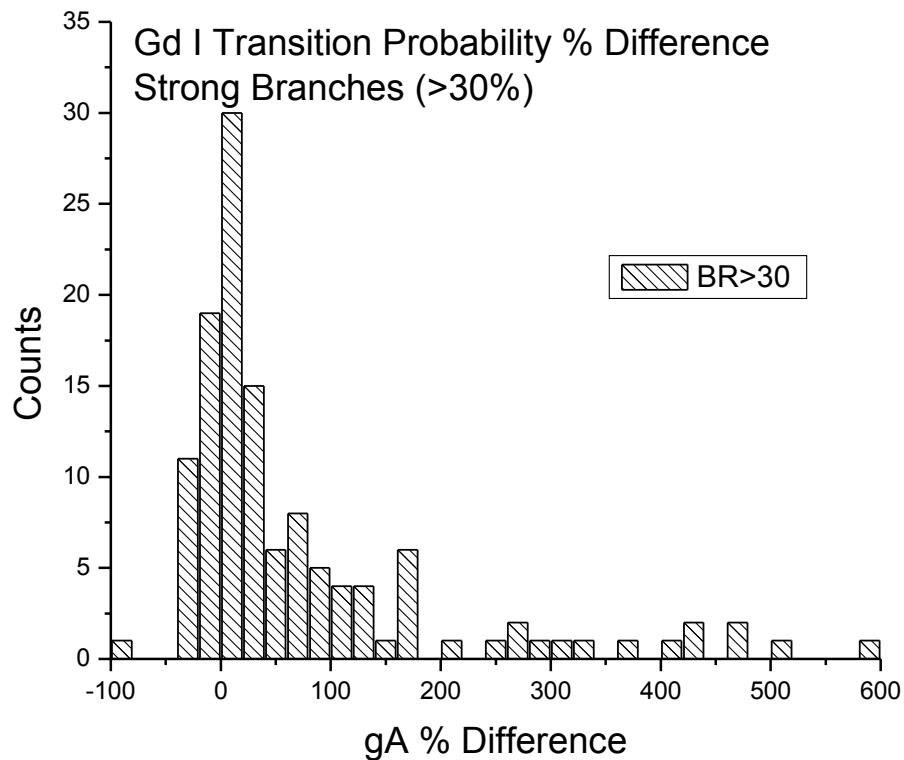


Figure 6.17 shows a histogram plot of the gA percent difference between this work and that of Lawler et al. for strong branches which are greater than 30 percent. The number of occurrences (counts) represents the number of percent difference values which lie within the given bin size (20%).

For Gd I branches which are between 30% and 10% I found that 61.3% of the values agreed within $\pm 50\%$ with Lawler (0% difference), 67% agreed within $\pm 150\%$, 71.0% agreed within $\pm 250\%$, 79.2% agreed within $\pm 350\%$, and all 100% of the values agreed within a percent difference of $\pm 2650\%$. The average percent difference for branches of medium strength was found to be 285%. Overall there is not very good agreement with the reported values from Lawler et al. The reason for the general discrepancy is not apparent although most of the values

in this branching ratio bracket lie on the positive side of zero and could suggest some systematic issues within our system. This could be related to overestimates in the LIBS profile fitting procedures when problematic issues occur for neighboring line, especially in the moderate strength branches.

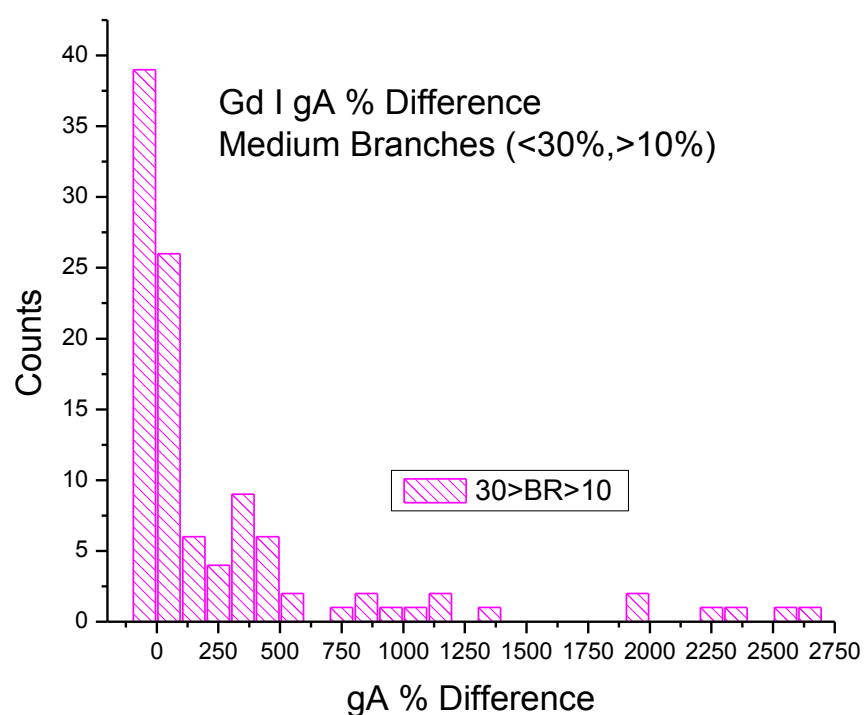


Figure 6.18 shows a histogram plot of the gA percent difference between this work and that of Lawler et al. for medium branches which are between 30 and 10 percent. The number of occurrences (counts) represents the number of percent difference values which lie within the given bin size (100%).

For the branches of Gd I which are less than 10% (figure 6.19) I found that 31.6% of the values agreed within $\pm 25\%$ with Lawler, 81.4% agreed within $\pm 75\%$, 86% agreed within $\pm 125\%$,

88.0% agreed within $\pm 175\%$, and all 100% of the values agreed within $\pm 925\%$. The average percent difference for branches weaker than 10% was found to be 37.2%. There is a general disagreement within the stated uncertainty of our branches (23.3%) and the lifetimes (5%) from Den Hartog et al. which gives us an overall leeway of $\sim 24\%$. It is again the case that outliers lie on the positive side of zero and could be systematically showing that our weak values are sometimes overestimated, which we do believe to be the case more often than not since many of the weak emission lines are shoulders to the moderate and strong branches. Also in the particular case of neutral emission lines, the integrated intensities tended to be rather weak in comparison to the singly-ionized or doubly-ionized intensities. Taking these into consideration we expect the neutral species as a whole to be less accurate than the singly-ionized, which is what our data show in Gd I.

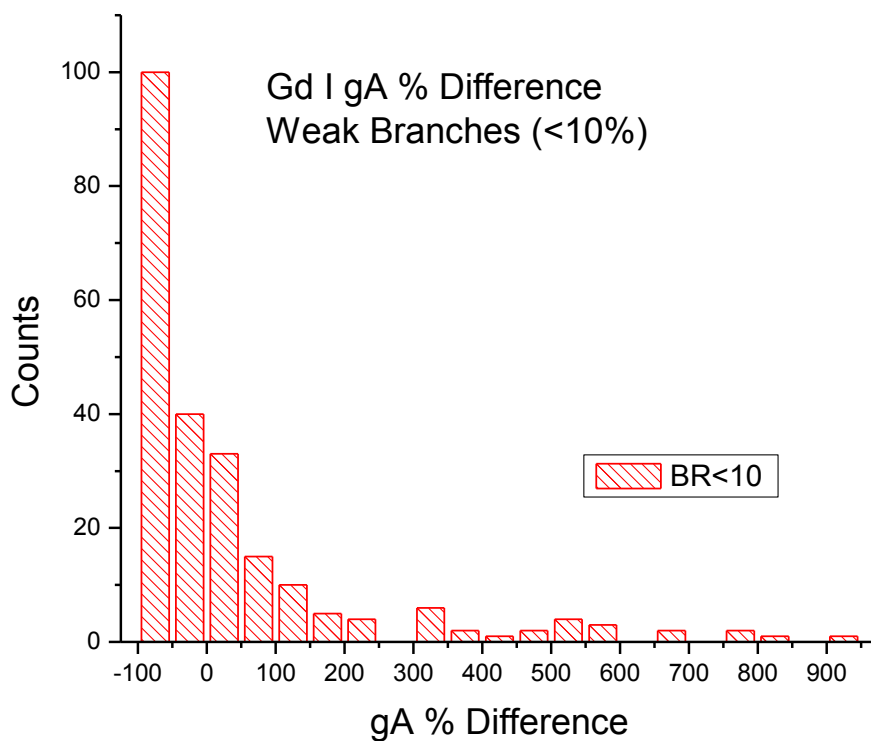


Figure 6.19 shows a histogram plot of the gA percent difference between this work and that of Lawler et al. for weak branches which are less than 10 percent. The number of occurrences (counts) represents the number of percent difference values which lie within the given bin size (50%).

6.5.5 - Singly-Ionized Gadolinium

In singly-ionized gadolinium (Gd II) our results show some agreement with the reported works of Den Hartog et al.¹⁰ A total of 480 radiative parameters were observed with 43 lines showing weak relative intensities, 11 blended lines, and 17 shouldered lines. In total, relative intensities for 946 emission lines of Gd II originating from a total of 164 upper energy states are listed in appendix 1

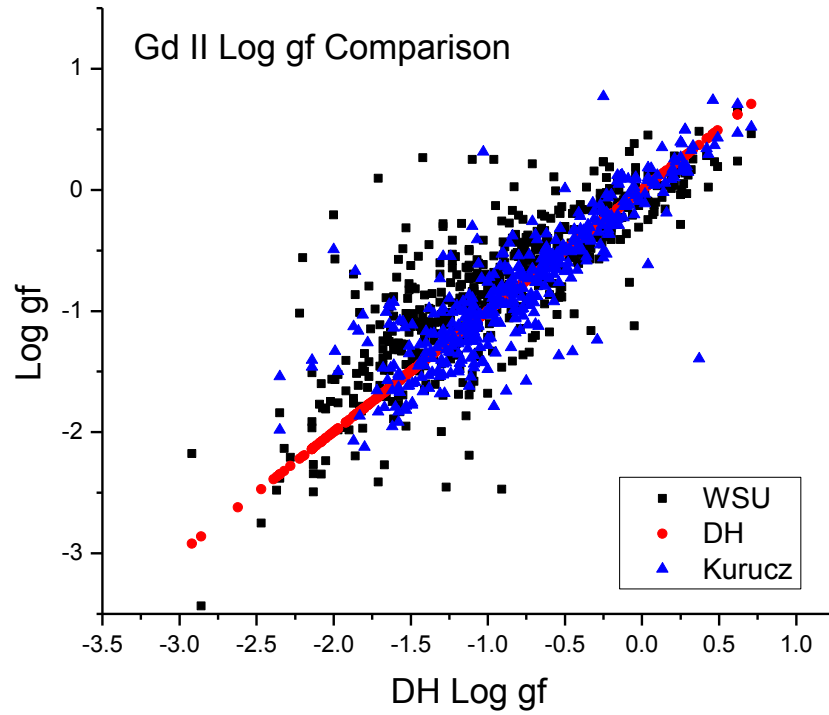


Figure 6.20 shows the Gd II $\log(gf)$ comparison between this work and other previous works. The black squares signify this work, red circles represent $\log(gf)$ values from Den Hartog et al.,¹⁰ and the blue triangles are the results tabulated by Kurucz and Bel.³³ The various works' $\log(gf)$ values are plotted against the values of Den Hartog et al. so that points which lie on a slope of one represent perfect agreement with Den Hartog et al. data.

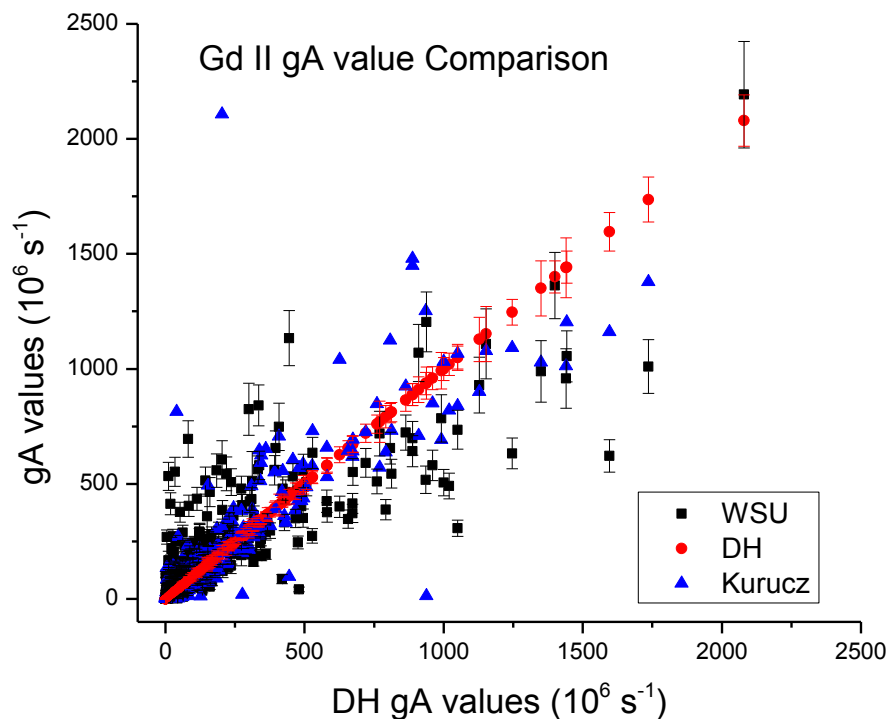


Figure 6.21 shows the transition probability (gA) comparison between this work (black squares), the work by Den Hartog et al.¹⁰ (red circles) and the listed values of Kurucz and Bell.³³ The various works' gA values are plotted against the values of Den Hartog et al. so that points which lie on a slope of one represent perfect agreement with Den Hartog's data. The error bars shown in this work incorporate error from lifetimes as well as uncertainties of this work.

Figure 6.22 – 6.24 show histogram representations of the Gd II transition probability (gA) percent differences $(WSU - DH)/DH (x100)$ between this work and that of Den Hartog et al. The histograms show the number of times a given percent difference was reported relative to complete agreement (zero percent difference). The entire range of percent differences was partitioned according to branching ratio strength to see if agreement between this work and other's work varies with branching ratio strength.

For those Gd II branches greater than 30% I found that 48.2% of the values agreed with Den Hartog within $\pm 12.5\%$, 62.0% agreed within $\pm 27.5\%$, 69.0% agreed within $\pm 42.5\%$, 89.7% agreed within $\pm 87.5\%$, and all 100% of the values agreed within $\pm 147.5\%$. The average percent difference for branches greater than 30% was found to be 12.1%. Given that our stated uncertainty for this strength of branching ratio is 9.3% and that the uncertainty in the lifetime from Den Hartog et al. for all of these levels in Gd II was 5%, the results show that we generally agree with those transition probabilities from Den Hartog et al.

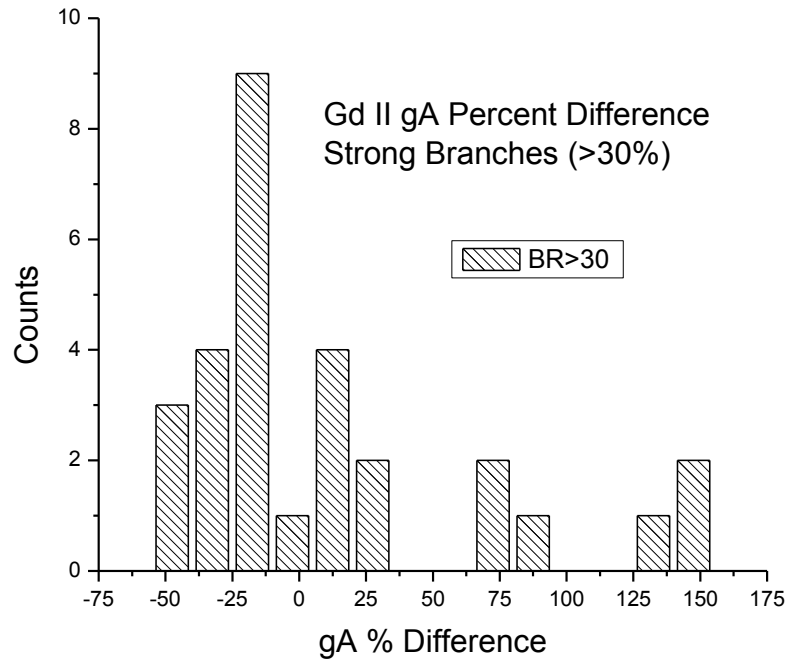


Figure 6.22 shows a histogram plot of the Gd II gA percent difference between this work and that of Den Hartog for strong branches which are greater than 30 percent. The number of occurrences (counts) represents the number of percent difference values which lie within the given bin size (15%).

For Gd II branches which are between 30% and 10% I found that 37.4% of the values agreed within $\pm 25\%$ with Den Hartog, 68.4% agreed within $\pm 55\%$, 75.5% agreed within $\pm 85\%$, 88.1% agreed within $\pm 205\%$ and all 100% of the values agreed within a percent difference of $\pm 745\%$. The average percent difference for branches between 30% and 10% was found to be 55%. Overall there is not very good agreement with the reported values from Den Hartog et al. The reason for the general discrepancy is not apparent although most of the values in this branching ratio bracket lie on the positive side of zero and could suggest some systematic issues

within our system. This could be related to overestimates in the LIBS profile fitting procedures when problematic issues occur for neighboring lines.

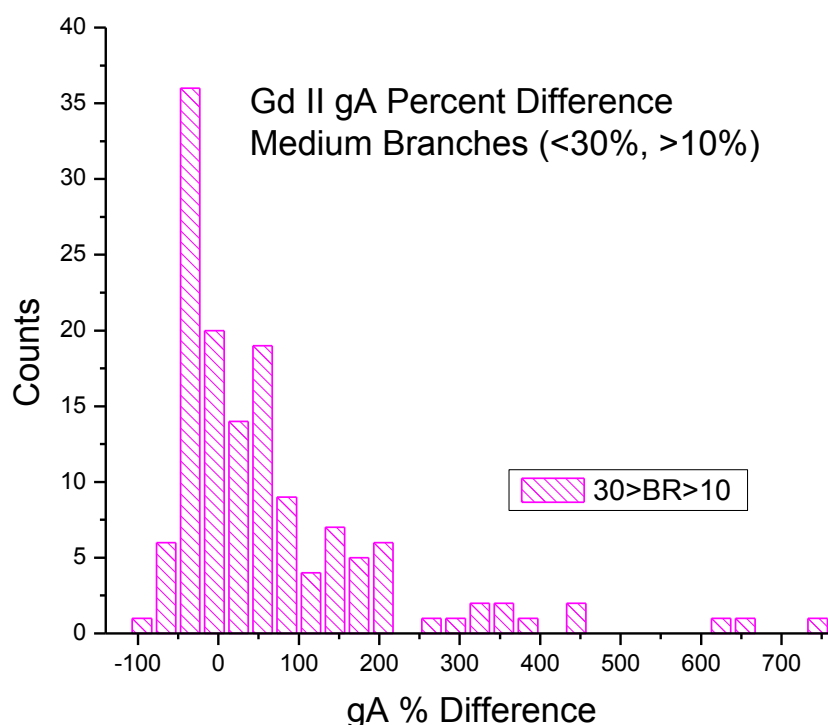


Figure 6.23 shows a histogram plot of the Gd II *gA* percent difference between this work and that of Den Hartog et al. for branches which are between 10 and 30 percent. The number of occurrences (counts) represents the number of percent difference values which lie within the given bin size (30%).

For the branches of Gd II which are less than 10% (figure 6.24) I found that 37.0% of the values agreed within $\pm 25\%$, 68.7% agreed within $\pm 75\%$, 78.6% agreed within $\pm 125\%$, 85.5% agreed within $\pm 175\%$, and all 100% of the values agreed within $\pm 4725\%$. The average percent difference for branches weaker than 10% was found to be 140.4%. There is a general

disagreement within the stated uncertainty of our branches (23.3%) and the lifetimes (5%) from Den Hartog et al. which gives us an overall leeway of ~24%. It is again the case that outliers lie on the positive side of zero and could be systematically showing that our weak values are sometimes overestimated, which we do believe to be the case more often than not since many of the weak emission lines are shoulders to the moderate and strong branches. Thus an overestimate is more likely than a weaker estimate by the ESAWIN 3000 software.

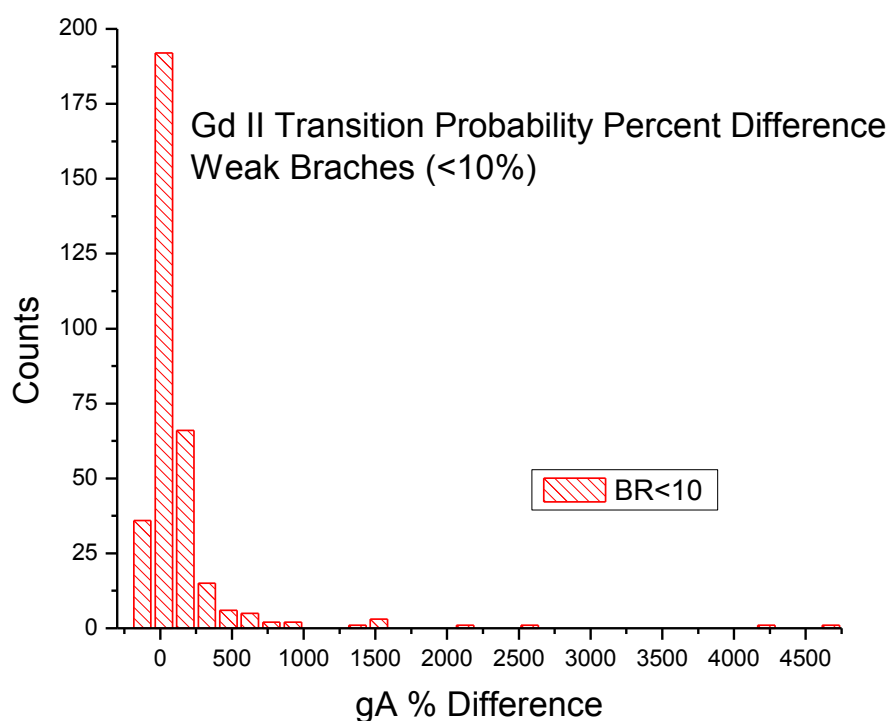


Figure 6.24 shows a histogram plot of the branching ratio percent difference between this work and that of Den Hartog et al. for Gd II branches which are less than 10 percent. The number of occurrences (counts) represents the number of percent difference values which lie within the given bin size (150%).

6.5.6 - Doubly-Ionized Gadolinium

The radiative parameters of doubly-ionized gadolinium are in relatively good agreement with the only other reported values in literature: those by Biémont et al.¹² who are associated with the DREAM Project.³⁵ Table 6.6 lists 40 transition probabilities belonging to Gd III with 3 lines noted as weak, 3 lines blended, and 5 lines noted as shouldered. In total we observed relative intensities for 44 emission lines in 6 energy levels of Gd III which are listed in appendix 1.

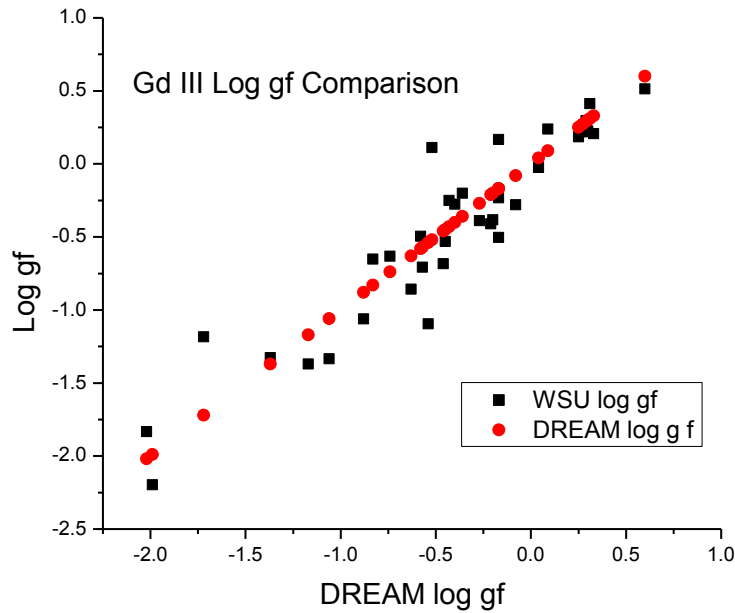


Figure 6.25 shows the $\log(gf)$ comparison between this work (black squares) and those of Biémont et al.¹² (red circles) who are associated with the DREAM Project. The various works' $\log(gf)$ values are plotted against the values of Biémont et al. so that data which lie on a slope of one represent perfect agreement with Biémont et al. data.

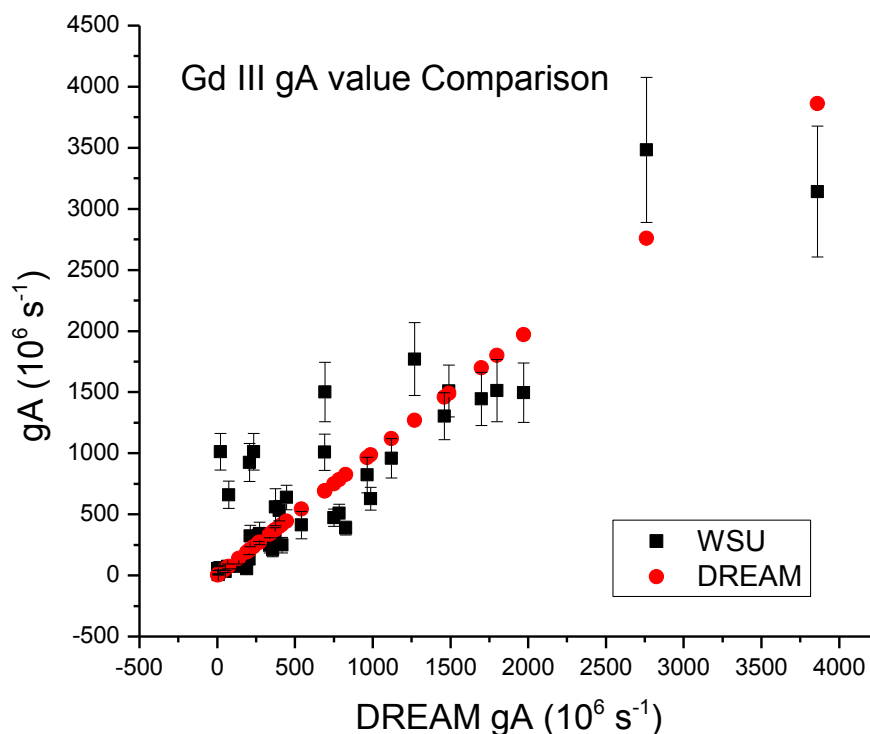


Figure 6.26 shows the transition probability (gA) comparison between this work and the work by Biémont et al. The black squares signify this work, red circles represent Biémont et al.'s work which is associated with the DREAM Project. The various works' gA values are plotted against the values of Biémont et al. so that data which lie on a slope of one represent perfect agreement with their data. The error bars shown in this work incorporate error from lifetimes as well as uncertainties of this work.

Figure 6.27 – 6.29 are histogram representations of the Gd III transition probability (gA) percent differences between this work and that of Biémont et al. The histograms show the number of times a given percent difference was reported relative to complete agreement (zero percent difference). The range of transition probability's percent differences was partitioned according to branching ratio strength to see if agreement between this work and Biémont et al.'s work does varies with branching ratio strength.

For those Gd III branches greater than 30% I found that 16.7% of the values agreed within $\pm 5\%$ with Biémont, 50% agreed within $\pm 15\%$, 83.3% agreed within $\pm 25\%$, and all 100% of the values agreed within $\pm 115\%$. The average percent difference for branches greater than 30% was found to be 14.4%. Given that our stated uncertainty for this strength of branching ratio is 9.3% and that the uncertainty in the lifetime we used for all of these levels in Gd III was 20%, the results show that we generally agree with those transition probabilities published by Biémont et al. There does exist a single outlier on the positive side of zero and this is from the 255 nm line in $48,860\text{ cm}^{-1}$, which is noted as a shouldered line and was likely misdiagnosed in the fitting as a single peak.

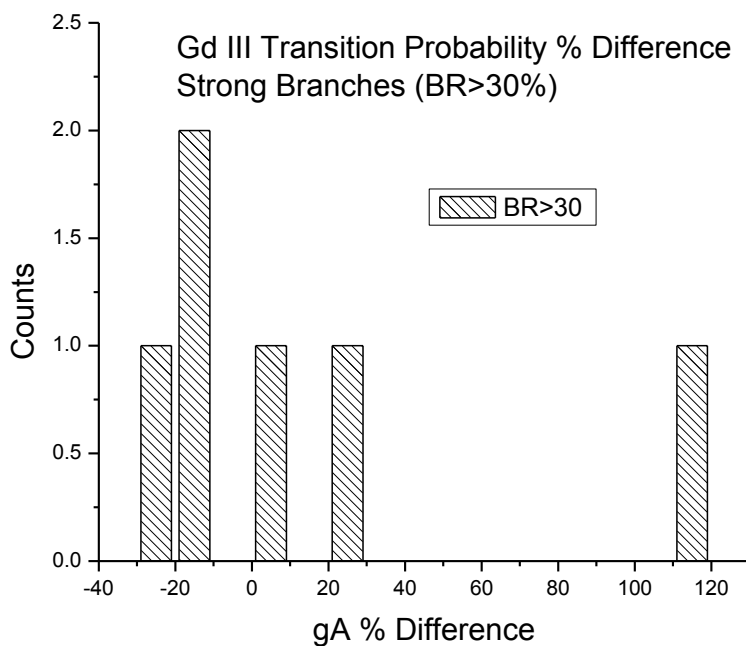


Figure 6.27 shows a Gd III histogram plot of the gA percent differences between this work and that of Biémont et al at DREAM for strong branches which are greater than 30 percent. The number of occurrences (counts) represents the number of percent difference values which lie within the given bin size (20%).

For Gd III branches which are between 30% and 10% I found that 62.5% of the values agreed with Biemont within $\pm 20\%$, 81.3% agreed within $\pm 60\%$, 93.8% agreed within $\pm 340\%$, and all 100% of the values agreed within $\pm 820\%$. The average percent difference for branches between 30% and 10% was found to be 90.1%. Overall there is good agreement with the reported values, however some outliers do exist. The reason for these is not apparent although they do lie on the positive side of zero and could suggest some systematic issues. As stated throughout this thesis, the likely explanation of these outliers is due the poor accuracy in our ability to measure the weak branches.

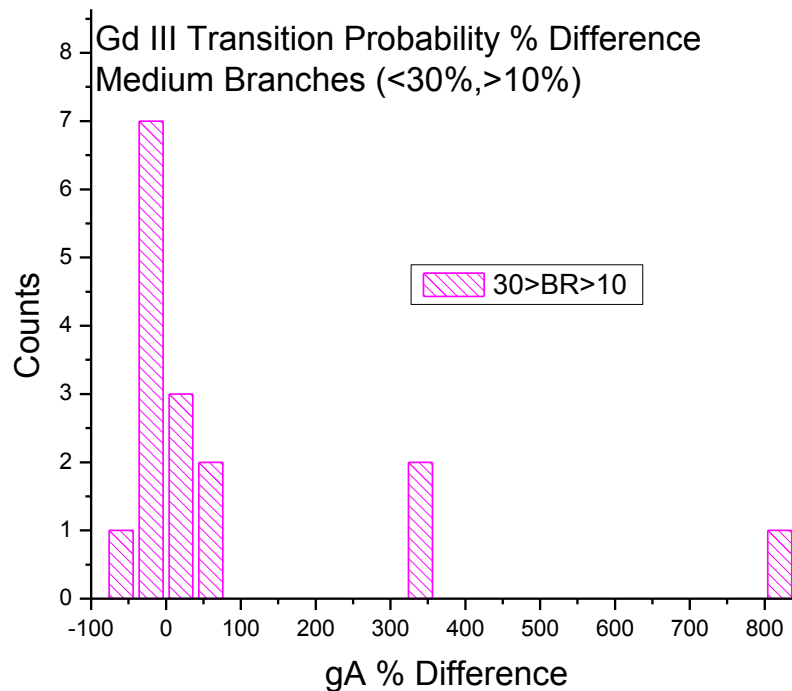


Figure 6.28 shows a histogram plot of the gA percent difference between this work and that of Biemont et al at DREAM for medium branches which are between 30 and 10 percent. The number of occurrences (counts) represents the number of percent difference values which lie within the given bin size (40%).

For those 18 branches in Gd III which are less than 10% (figure 6.29) I found that 44.5% of the values agreed within $\pm 25\%$, 74.0% agreed within $\pm 55\%$, 83.3% agreed within $\pm 85\%$, 88.8% agreed within $\pm 245\%$, and all 100% of the values agreed within $\pm 4875\%$. The average percent difference for branches weaker than 10% was found to be 356%. Despite the outliers in the weak branches there is a general agreement within the stated uncertainty of our branches (23.3%) and the lifetimes (20%) from Biémont et al. which gives us an overall leeway of 31%.

Again it appears that the outliers lie on the positive side of zero and could be systematically showing that our weak values are sometimes overestimated.

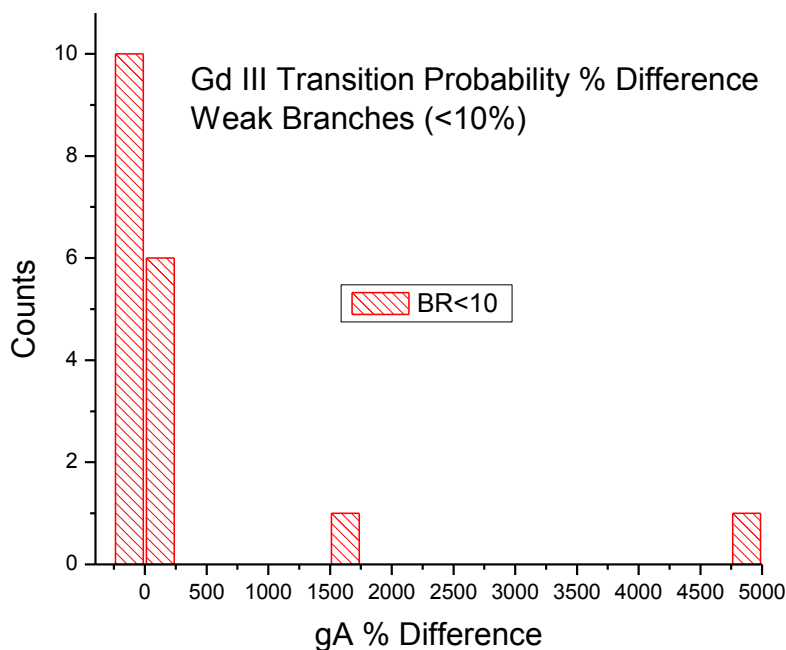


Figure 6.29 shows a histogram plot of the gA percent differences between this work and that of Biemont et al at DREAM for weak branches which are less than 10 percent. The number of occurrences (counts) represents the number of percent difference values which lie within the given bin range (250%).

6.6 - Summary

The agreement for the Sm I branches stronger than 30% is overall fairly good. The average percent differences for these strong Sm I branches lies at 74.1% and our stated uncertainty was around 9% with 45.5% of the values agreeing within a percent difference of $\pm 25\%$. It is worth noting however that when calculating transition probabilities and $\log(gf)$ values for branches which contain only a single transition (within the range of 200-800nm), the

strength of the branching ratio is obviously one, being the only allowed transition. In this case it would be reasonable to assume there would be good agreement between radiative parameters in this work and those values reported from other previous works for single branches from an upper state. However, it was observed that of the 25 upper energy levels in Sm I which had a single branch (between 200 and 800 nm), we calculated an average percent difference of 303% between our transition probabilities and those values from Kurucz, with a median percent difference of 79%. The total average uncertainty in our A-values, including a maximum lifetime uncertainty of 4%, for these individual branches was around 10%. It is possible but not likely that for these branches the stronger lines could be out of our spectral range; but in the case of rare earth metals it is known that the strong majority of emission lines in neutral samarium are found between 300-600 nm. It is therefore peculiar and unexplained as to why there is such strong disagreement between our results for those levels with single emission lines and those radiative parameters for the same lines reported by Kurucz. I believe that the major contributing factor to the disagreement between these transition probabilities lies with problematic lines in our fitting scheme. There appears to be a systematic trend of over estimating some of the stronger branches in Sm I and again it is believed that these result from blended and shouldered lines.

For the Sm I branches with moderate strength (between 10 and 30 %) we are again not very pleased with the agreement of the results; the average percent difference being -47% and only 16.7% of the values agreed within our stated uncertainty. However there were only 6 branches of Sm I in this category which makes generalizations on the whole difficult. For those branching ratios weaker than 10 we were not surprised by the range of scatter and are overall

pleased with the results, knowing that the weak branches do not contribute much to astrophysical abundance calculations since these weaker transitions are not seen.

The agreement for those Sm II branches stronger than 30% of the total is quite reasonable with almost half of the measurements agreeing within $\pm 10\%$. There are also some outliers in the strong branches of Sm II along the positive side of zero percent, which shows that these gA values were larger than Rehse et al.'s values. I believe these larger overestimates in our values to be caused by spectral blending of neighboring lines. For the Sm II branches with moderate strength (between 10 and 30 %) the agreement with Rehse et al.'s values is not very good having less than half of the measurements agreeing within our stated uncertainty of 10%. The general trend of the data show a systematic overestimate in our gA values compared to those from Rehse et al which I believe to be caused by the problematic blends and shouldering of emission lines. For those 3 Sm II branching ratios weaker than 10% we are not surprised by the range of scatter and are overall pleased with the results, knowing that the weak branches do not contribute much to astrophysical abundance calculations since these weaker transitions are not seen.

In the large branches ($>30\%$) of Sm III we observed overall good agreement with those of Biemont et al., since more than 58% lie within $\pm 15\%$ of perfect agreement, with an average percent difference of 32.6%. Again there is a trending overestimate of our strong branch ratio's transition probabilities. The exact reason for this is undetermined, but I believe it is related to problematic blending and shouldering of emission lines within the spectra. For the moderate strength branches in Sm III we generally disagree with Biemont et al.'s values, since we have only 25% of the values within our stated uncertainty budget. Peculiarly the majority of values lie on the negative side of perfect agreement; although with only 12 emission lines to speak of it is

difficult to make any concrete generalizations about this. The 5 weak branches in Sm III show poor agreement. All of the values lie on the negative side of perfect agreement which again could be signaling some systematic error, but since most of our other measurements tend to be overestimating the outliers, it is undetermined as to why this is.

The agreement for transition probabilities of the Gd I branches stronger than 30% of the total is reasonable, since nearly 40% of the values lie within our error budget alone (not including the lifetime uncertainty), and by 30% we agree with the majority of values by Lawler et al. For the Gd I branches with moderate strength (between 10 and 30%) there is a general disagreement with approximately little over half of the data agreeing to within $\pm 50\%$ of the values reported by Lawler et al. Again it is the case that the outliers tend to lie on the positive side of zero showing our moderate values to be overestimated. For those branching ratios weaker than 10 we are not surprised by the range of scatter and are overall pleased with the results, knowing that the weak branches do not contribute much to astrophysical abundance calculations since these weaker transitions are not seen. We found that in the weak branching ratio case 31.6% of the values were in agreement with an average percent difference of 37.2%. The general disagreement of the moderate and weak radiative parameters (transition probabilities and $\log(gf)$ values) in neutral gadolinium (Gd I) can be attributed to the numerous problematic emission lines. It was often seen to be the case that emission lines were blended causing the ESAWIN program to either not fit the peak at all, or to fit the overly-broad emission profile and attribute that integrated intensity to the emission line.

The agreement for those Gd II branches stronger than 30% of the total emissions is overall good, as 48.2% of the values lie within a percent difference of $\pm 12.5\%$ (and our stated

uncertainty is 9% not including the lifetime uncertainty). Again the outlier reside on the far positive side of perfect agreement with Den Hartog et al. Additionally, for these large Fe II branches we seem to have a systematic negative disagreement with Kurucz and Bell (i.e. our values are systematically less than theirs). For the branches with moderate strength (between 10 and 30 %) we do not have very good agreement, as only 37.4% of the values from the percent difference lie within $\pm 25\%$ of zero and our stated uncertainty is 10%. Also, another systematic shift seems to be in evidence with the majority of outlier on the positive side of zero and the average percent difference being 55%. The weak branches of Gd II show a general disagreement between this work and Den Hartog et al's values, since only 37.0% of our values are in agreement within our stated uncertainty and the average percent difference being 140%. It seems as if for singly-ionized gadolinium, due to its huge number of lines per level, we are systematically overestimating the strength of branches less than 30%. For those branching ratios weaker than 10% (which are numerous) we are not surprised by the range of scatter and are overall pleased with the results, knowing that the weak branches do not contribute much to astronomer's abundance calculations since they do not see the weak transitions. My conclusion is that the measurements of Gd II are in general good agreement with other works and can be useful for contributing to astronomer's needs.

In doubly-ionized gadolinium, the strong branches ($>30\%$) show a general agreement between our work and those of Biémont et al. - 50% of the percent difference values lie within 15% difference which is nearly within our error budget for this bracket when including the uncertainty in the lifetimes used. However as has been the case the outliers are on the positive side of zero implying that there have been overestimates in our values which I believe to be

caused by spectral blending. For the moderate strength branches of Gd III, between 30 and 10%, we found that 62.5% of the values lie within a percent difference of $\pm 20\%$, which shows good agreement between our reported transition probabilities. For the weak branches in Gd III we found 44.5% of the values agree within a percent difference of $\pm 25\%$ which is within our uncertainty estimates, thus showing a general agreement between values. However there are some outliers which do reside on the far positive side of zero. The likely explanation of the outliers on the positive side of zero is due to the ESAWIN 3000's fitting scheme which at times has been unable to properly resolve blended and shouldered lines.

Overall the results show good agreement with previous works for the singly ionized and doubly ionized states of gadolinium and samarium and therefore give the general conclusion that LIBS is a viable technique for measuring radiative parameters. The reason for poor agreement in the neutral species is likely due to the experimental conditions and spectral blending. In conclusion, it is good to keep in mind that it is not uncommon for research groups to publish papers reporting data for only a single upper energy level from a given ionization state of an atom. Therefore, the fact that we are able to measure many energy levels, from multiple ionization states simultaneously and from this provide radiative data with relatively good agreement to previous works speaks very positively towards using LIBS in future studies of atomic radiative parameters.

¹ A. Nishimura, H. Ohba, K. Ogura, and T. Shibata, "Measurement of the absolute oscillator strengths of gadolinium using an atomic vapor produced by electron beam heating," Opt. Comm. **110**, 561–564 (1994).

-
- ² S.E. Bisson, B. Comaskey, E.F. Worden, "Method to measure excited-level-to-excited-level branching ratios and atomic transition probabilities by time-resolved photoionization spectroscopy," *J. Opt. Soc. Am. B* **12**, 193-202 (1995).
- ³ M. Miyabe, I. Wakaida, and T. Arisawa, "Measurement of radiative lifetimes and branching ratio of Gd I using three-step resonance ionization spectroscopy," *Z. Phys. D* **39**, 181-187 (1997).
- ⁴ H.L. Xu, Z.K. Jiang, S. Svanberg, "Radiative lifetimes of Gd I and Gd II," *J. Phys. B.* **36**, 411-417 (2003).
- ⁵ E.A. Den Hartog, K.A. Bilty, J.E. Lawler, "Radiative lifetimes of neutral gadolinium," *J. Phys. B* **44**, 055001 (2011).
- ⁶ J.E. Lawler, K.A. Bilty, E.A. Den Hartog, "Atomic transition probabilities of Gd I," *J. Phys. B* **44**, 095001 (2011).
- ⁷ V.N. Gorshkov and V.A. Komarovskii, "Content of lanthanides in the solar photosphere," *Sov. Astron.* **30**, 333-336 (1986).
- ⁸ H. Bergstrom, E. Biemont, H. Lundberg, A. Persson, "Transition probabilities for Gd II and a new determination of the solar abundance of gadolinium," *Astron. Astrophys.* **192**, 335 (1988).
- ⁹ Z.G. Zhang, A. Persson, Z.S. Li, S. Svanberg, Z.K. Jiang, "Lifetime measurements in Gd II and Gd III using time-resolved laser spectroscopy," *Eur. Phys. J. D.* **13**, 301 (2001).
- ¹⁰ E.A. Den Hartog, J.E. Lawler, C. Sneden J.J. Cowan, "Improved laboratory transition probabilities for Gd II and application to the gadolinium abundance of the sun and three r-process rich metal-poor stars," *Astrophys. J. Suppl. Ser.* **167**, 292-314 (2006).

-
- ¹¹ D.C. Morton, “Atomic data for resonance absorption lines II. Wavelengths longward of the Lyman limit for heavy elements,” *Astrophys. J. Suppl. Ser.* **130**, 403-435 (2000).
- ¹² E. Biemont, G. Kohnen, P. Quinet, “Transition probabilities in Gd III,” *Astron. Astrophys.* **393**, 717-720 (2002).
- ¹³ P. Hannaford and R. M. Lowe, “Radiative lifetimes of low-lying levels in Sm I,” *J. Phys. B* **18**, 2365 – 2370 (1985).
- ¹⁴ D.M. Lucas, D.N. Stacey, C.D. Thompson, and R.B. Warrington, “High-precision relative oscillator strength measurements in Sm I by absorption spectroscopy,” *Phys. Scr.* **T70**, 145-150 (1997).
- ¹⁵ S.G. Porsev, “Calculation of lifetimes of low-lying odd-parity levels of Sm,” *Phys. Rev. A* **56**, 3535-3538 (1997).
- ¹⁶ S. Rochester, C.J. Bowers, D. Budker, D. DeMille, M. Zolotarev, “Measurement of lifetimes and tensor polarizabilities of odd-parity states of atomic samarium,” *Phys. Rev. A.* **59**, 3480-3495 (1999).
- ¹⁷ M.L. Shah, A.K. Pulhani, G.P. Gupta, B.M. Suri, “Measurements of radiative lifetimes, branching fractions, and absolute transition probabilities in atomic samarium using laser-induced fluorescence,” *J. Opt. Soc. Am. B.* **27**, 423-431 (2010).
- ¹⁸ D.R. Beck and S.M. O’Malley, “Improved RCI techniques for atomic $4f^n$ excitation energies: application to Sm I $4f^6\text{ }^6\text{ }^5D_J$ levels,” *J. Phys. B.* **43**, 215003 (2010).
- ¹⁹ W. Zhang, Y.Y. Feng, Z.W. Dai, “Radiative lifetime measurements of odd-parity moderately excited levels belonging to $J = 0,1,2,3$ series in Sm I,” *J. Opt. Soc. Am. B* **27**, 2255-2261 (2010).

-
- ²⁰ W. Zhang, Y.Y. Feng, G.J. Sun, Z.W. Dai, “Radiative lifetime measurements of odd-parity moderately excited levels belonging to $J=4,5,6,7$ series in Sm I,” *J. Phys. B.* **43**, 235005 (2010).
- ²¹ R.E. Luck, and H.E. Bond, “Extremely metal-deficient giants. II. Chemical abundances in 21 halo giants,” *Astrophys. J.* **244**, 919-925 (1981).
- ²² V.N. Gorshkov and V.A. Komarovskii, “Content of lanthanides in the solar photosphere,” *Sov. Astron.* **30**, 333-336 (1986).
- ²³ O. Vogel, B. Edvardsson, A. Wannstrom, A. Arnesen, R. Hallin, “Radiative lifetimes in Sm II and the solar samarium abundance,” *Phys. Scr.* **38**, 567-570 (1988).
- ²⁴ E. Biémont, N. Grevesse, P. Hannaford, R.M. Lowe, “Lifetimes in Sm II and the solar abundance of samarium,” *Astron. Astrophys.* **222**, 307–310 (1989).
- ²⁵ T.J. Scholl, R.A. Holt, D. Masterman, R.C. Rivest, S.D. Rosner, A. Sharikova, “Measurement of radiative lifetimes in Sm II,” *Can. J. Phys.* **80**, 1621–1629 (2002).
- ²⁶ H.L. Xu, S. Svanberg, P. Quinet, H.P. Garnir, E. Biémont, “Time-resolved laser-induced fluorescence lifetime measurements and relativistic Hartree-Fock calculations of transition probabilities in Sm II,” *J. Phys. B* **36**, 4773–4787 (2003).
- ²⁷ S.J. Rehse, R. Li, T.J. Scholl, A. Sharikova, R. Chatelain, R.A. Holt, S.D. Rosner, “Fast-ion-beam laser-induced-fluorescence measurements of spontaneous-emission branching ratios and oscillator strengths in Sm II,” *Can. J. Phys.* **84**, 723–771 (2006).
- ²⁸ J.E. Lawler, E.A. Den Hartog, C. Sneden, J.J. Cowan, “Improved laboratory transition probabilities for Sm II and application to the samarium abundances of the sun and three r-process-rich, metal-poor stars,” *Astrophys. J., Suppl. Ser.* **162**, 227–260 (2006).

-
- ²⁹ J.E. Lawler, E.A. Den Hartog, C. Sneden, J.J. Cowan, “Comparison of Sm II transition probabilities,” *Can. J. Phys.* **86**, 1033-1038 (2008).
- ³⁰ V.A. Dzuba, U.I. Safronova, W. R. Johnson, “Energy levels and lifetimes of Nd IV, Pm IV, Sm IV, and Eu IV,” *Phys. Rev. A* **68**, 032503 (2003).
- ³¹ E. Biémont, H.P. Garnir, U. Litzén, K. Nielsen, P. Quinet, S. Svanberg, G.M. Wahlgren, Z.G. Zhang, “Radiative lifetime and oscillator strength determinations in Sm III,” *Astron. Astrophys.* **399**, 343–349 (2003).
- ³² C.H. Corliss and W.R. Bozmann, Monograph 53. U.S. National Bureau of Standards, Washington, DC.
- ³³ R. L. Kurucz, B. Bell, *Atomic Line Data, Kurucz CD-ROM No. 23*, Cambridge, MA. Smithsonian Astrophysical Observatory (1995).
- ³⁴ V.A. Komarovskii and Y.M. Smirnov, “Experimental study of the absolute values of electronic transition probabilities in a samarium atom,” *Opt. Spectrosc.* **80**, 357-361 (1966).
- ³⁵ <http://w3.umons.ac.be/~astro/dream.shtml>

Chapter 7 – Copper & Iron

7.1 - Introduction

The spectrum of singly-ionized copper is of interest for several reasons. Accurate radiative parameters like branching ratios, transition probabilities (A_{ul}) and oscillator strengths ($\log(gf)$) are needed in areas in controlled thermonuclear fusion, astrophysics, and plasma physics.¹ In plasma physics, high temperature plasmas require reliable transition probabilities and lifetimes for impurity concentration estimates. Furthermore, oscillator strengths are used in comparison with theoretical models of core polarization² in atomic physics and in relativistic³ and non-relativistic⁴ quantum defect orbital calculations as well as techniques like the weakest bound electron potential model theory (WBEPM theory).^{5,6} It is known that the complex structure of the copper atom has caused theoreticians difficulty in accurately modeling transitions within the atom due to copper's 3d configuration and strong configuration interactions.⁶

In astrophysics, singly ionized copper is observed in interstellar H I clouds and various types of chemically peculiar (CP) stars like the Hg-Mn subgroup of Bp stars⁷ and Ap stars.⁸ A better understanding of zinc and copper abundances within some metal-poor stars could help unravel mysteries behind certain nucleosynthesis processes.⁹ By determining copper and zinc abundances within some 90 stars of the galactic halo it was shown that the s-process is one of the processes responsible for the observed chemical evolution.^{9,10} In order to more accurately model abundances in stars and thus gain better insight into stellar nucleosynthesis processes, radiative

parameters like experimentally determined copper transition probabilities and oscillator strengths are necessary.

Work in the spectrum of neutral iron has been ongoing since about 1925. The interest in the spectrum of iron and the corresponding radiative parameters is evident in the fact that work in this area is still being pursued in both theoretical and experimental physics. In fact, an international collaboration has begun with the sole purpose of determining accurate radiative parameters in singly ionized iron called the FERRUM project.^{11,12,13,14,15,16} Iron is of specific interest because of its complex $3d^6 4s^2$ configuration which gives rise to thousands of transitions which can be observed in the sun in order to make abundance estimates. The complexity of the half-filled 3d sub shell of Fe II makes theoretical modeling of the ion very difficult. Theoretical calculations of this type involve a large number of angular momentum couplings making the calculation quite complex.¹⁷ Therefore accurate experimental atomic data are needed in order to refine theoretical models.

One application of the transition probabilities in Fe II arises in the determination of relative intensities from forbidden lines. The ratio of these intensities is used to measure fluxes from starburst galaxies and properties of active galactic nuclei.¹⁸ The request and need for more accurate $\log(gf)$ values has been evident through recent iron abundance calculations in the sun which show $\log(gf)$ determinations in the past have been inadequate for comparing the sun with other stars. The current uncertainty in the sun's iron abundance (0.1 dex) is problematic in that the sun's elemental abundance is used as a standard against other astronomical objects like asteroids and other stars.¹⁹ Abundance calculations are derived mainly from oscillator strengths f which are commonly reported as the $\log(gf)$ value, where g is the degeneracy of the level.

Comparison between astrophysically determined $\log(gf)$ values and their experimental / theoretical counterparts can help to refine abundance models.

The aim of the work reported in this chapter is to provide accurate radiative parameters in copper and iron for use in resolving abundance issues, as well as expanding the list of relevant atomic data.

7.2 - Previous works

7.2.1 - Previous Work in Copper

The spectrum of Cu I and its radiative parameters have been studied for a while, dating back to 1936. For published oscillator strengths prior to 1970, Corliss²⁰ has tabulated lists as did Bielski²¹ for transition probabilities prior to 1975. In 1984, Cederquist et al.²² determined lifetimes in Cu I by the beam-foil method. In 1988 lifetimes of 17 levels in neutral copper were measured using the beam-laser technique incorporating LIF by Baier et al.²³ In 1989, Carlsson et al.²⁴ performed a delayed-coincidence photon-counting technique with a tunable dye laser in order to measure lifetimes from five levels in Cu I. Most of the recent work in the Cu I spectrum involves theoretical models and approximations matched against older experimental data. Some of the most recent experimental work is from van der Veer et al.²⁵ in 1993 using a hollow-cathode discharge tube to measure lifetimes by LIF. Zerne et al.²⁶ in 1994 used a copper vapor source and two tunable dye lasers to measure 8 lifetimes in neutral copper.

Biémont et al.²⁷ in 1996 used the relativistic Hartree-Fock method to calculate lifetimes in 43 states of Cu I and in their paper they noted that due to discrepancies between theoretical

and experimentally determined values there was a need for more accurate experimental values in Cu I. In 2002, Migdalek²⁸ used a theoretical combination of core-polarization with the relativistic Hartree-Fock model in order to calculate oscillator strengths in multiple atoms, two of which belonged to neutral copper. These proved to be in good agreement with previously reported experimental values. Quite recently, in 2011, Civis et al.²⁹ used infrared time-resolved Fourier transform spectroscopy (FTIR) on a copper vapor and determined transitions and oscillator strengths for 17 lines not previously reported in the infrared region of the spectrum.

Kono and Hattori³⁰ measured lifetimes and transition probabilities of Cu II belonging to 5 levels using a delayed-coincidence method in 1982. Prior³¹ determined transition rates of two metastable levels in singly ionized copper in 1984. Cederquist et al.²² in 1984 determined lifetimes for 8 levels in Cu II using a beam-foil method. Using a Hartree-Slater approximation, Theodosiou,³² in 1986, determined lifetimes of more than 150 Cu II levels. A few transition probabilities followed and the results were shown to be in agreement with prior experimental work. In 1994, Crespo Lopez-Urrutia et al.³³ determined transition probabilities for 47 lines in Cu II from a hollow discharge tube and the measured agreement between prior work and theirs was within 10%. Pinnington et al.³⁴ in 1997 reported lifetimes belonging to 12 states from 66,419 to 73,596 cm⁻¹ in Cu II and some resulting transition probabilities using HFR calculations were listed. Donnelly et al.³⁵ in 1999 calculated over 200 $\log(gf)$ values and transition probabilities using an LS-coupling scheme and relativistic approach and in concluding they called for more experimental work in order to refine theories and compare results.

In 2000, Biémont et al.³⁶ calculated transition rates using improved relativistic Hartree-Fock calculations which included core-polarization effects in Cu II. As a result 64 oscillator

strengths and transition probabilities were listed. Dong and Fritzsche³⁷ in 2005 provided 35 transition probabilities and improved energy levels using an improved Dirac-Fock wave functions for low-lying energy levels in Cu II. Ortiz et al.³⁸ in 2007 reported 41 transition probabilities in Cu II using laser-induced breakdown spectroscopy (LIBS) which were in good agreement with prior results. In 2008, Federman et al.³⁹ measured oscillator strengths in the ultraviolet region of the spectrum in Cu II using a beam-foil technique. Lastly, in 2009, Brown et al.⁴⁰ measured lifetimes and oscillator strengths for ultraviolet transitions in singly-ionized copper using ions from a beam-foil apparatus. The results proved to be in agreement with previously reported data.

7.2.2 – Previous Works in Iron

Beginning in 1989 Milford et al.⁴¹ measured relative intensities of neutral iron (Fe I) lines in order to further the effort of determining accurate radiative parameters of astrophysical relevance. Their work reported accuracies on the order of 7% and the relative intensities were used for oscillator strength calculations. In 1989, Thevenin⁴² theoretically determined 4597 oscillator strengths using data from the solar spectrum and compared these to older compilations which showed agreement between the two. In 1990, Peterson et al.⁴³ determined $\log(gf)$ values and used these for abundance determinations of nine metal-poor stars. In 1991, O'Brian et al.⁴⁴ determined 186 lifetimes and 640 transition probabilities in Fe I using time-resolved LIF. Also in 1991, Bard et al.⁴⁵ determined 114 oscillator strengths for lines in Fe I using a high-current hollow cathode discharge tube with FTS. Using 20 of these 114 experimentally determined oscillator strengths, a solar abundance of iron was determined and showed a discrepancy of 50 percent which calls for further research and better accuracy of atomic data.

In 1993 the same group published time-resolved LIF measurements of 43 lifetimes between 25,900 and 52,000 cm^{-1} in Fe I using a beam-laser technique.⁴⁶ Again in 1994 Bard et al.⁴⁷ determined oscillator strengths for 116 lines in Fe I using a combination of lifetimes from LIF and branching ratios from FTS. Uncertainties ranged from 7% for large f -values to 29% for small values. Fe I and Fe II oscillator strengths in the ultraviolet region were reported for the first time by Bergeson et al.⁴⁸ in 1996 using a hollow cathode discharge tube. In 1997 Bautista calculated energy levels and oscillator strengths for 32,316 oscillator strengths in Fe I which were incorporated into the IRON project.⁴⁹ In 2003, Borrero et al.⁵⁰ calculated atomic parameters in the infrared region using an improved model which fits the intensity profiles of lines emerging from the sun. In 2006 Gu et al.⁵¹ provided improved calculations of atomic parameters using a second-order many-body perturbation theory; the calculated $\log(gf)$ results agreed well with previous reports. Centeno and Socas-Navarro,⁵² in 2008, in an attempt to provide a new solar oxygen abundance determined $\log(gf)$ values for a few elements, neutral iron being one of them. This new data was compared to other values showing improved agreement.

Starting with work on Fe II initiated after 1988: oscillator strengths were determined by Kross and Kock⁵³ in 1987 using a hollow-cathode discharge with uncertainties between 10-25%. Fawcett,⁵⁴ in 1988 determined oscillator strengths for lines in singly ionized iron between 136.1 and 648.3 nm and used these to calculate abundances in a slow nova star. Also in 1988, Schade et al.⁵⁵ measured radiative lifetimes for 14 levels in Fe II using LIF on a vapor sputter from hollow cathode. In 1991 Biémont et al.⁵⁶ determined lifetimes by LIF on 12 for levels in Fe II and the results were applied to abundance determination of the sun in order to support the then recent theories of low values of iron. In 1997, Biémont et al.⁵⁷ determined 74 new transitions in

Fe II using FTS on iron emission from a hollow-cathode discharge. Li et al.⁵⁸ in collaboration with the FERRUM project, determined lifetimes for two levels in Fe II using LIF on a laser-produced plasma in 1999. Also in 1999, in collaboration with the FERRUM project, Sikstrom et al.⁵⁹ measured lifetimes for 6 levels between 61,512 and 64,041 cm^{-1} using LIF and 18 oscillator strengths which had uncertainties between 9 and 19%. Schnabel et al.⁶⁰ measured lifetimes with accuracies near 1% using time-resolved LIF for Fe II levels in 1999. These results were applied to a new solar abundance calculation.

In 2000 Schnabel et al.⁶¹ used time-resolved nonlinear LIF measurements to determine lifetimes of 5 branches in Fe II and their corresponding branching ratios and transition probabilities. Six highly excited levels near 10 eV in Fe II were measured using LIF in cooperation with the FERRUM project by Nilsson et al.⁶² in 2000. Also in 2000, Howk et al.⁶³ presented oscillator strengths for 11 ground-state transition in Fe II using ultraviolet observations of interstellar matter. A few of these $\log(gf)$ values were incompatible with previously reported data and the suggestion for more accurate experimental values was made. Two metastable lifetimes were determined using a beam-laser method by Rostohar et al.⁶⁴ in 2001. In cooperation with the FERRUM project, Pickering et al.⁶⁵ determined branching ratios and transition probabilities in the visible to ultraviolet region of singly ionized iron. In 2003, a beam-laser technique was applied by Hartman et al.⁶⁶ in order to measure transition probabilities in 13 forbidden lines of Fe II. In 2004 Schnabel et al.⁶⁷ measured lifetimes and transition probabilities in Fe II for 21 levels extending up to 47,000 cm^{-1} via LIF.

In 2005, Beck⁶⁸ calculated 264 f -values for transitions between ground and 45,412 cm^{-1} in Fe II. Also in 2005, Hibbert et al.⁶⁹ calculated improved oscillator strengths in order to

compare with certain B and D blobs of η Carinae. In 2006, the same group calculated oscillator strengths for lines near the infrared region of Fe II for the purpose of comparing observations in stellar media.⁷⁰ In 2009 Melendez et al.¹⁹ provided accurate oscillator strengths for 142 transitions between 400 and 800 nm. Also in 2009, Gurell et al.⁷¹, using a beam-laser technique, reported accurate transition probabilities as well as lifetimes of states belonging to Fe II. In 2010, Castelli and Kurucz⁷² calculated new energy levels for 109 branches of the 4f shell in Fe II ranging from 122,324 to 128,110 cm^{-1} . Also in 2010, Deb et al.¹⁸ calculated intensity ratios for emission lines originating in the infrared region of Fe II by interaction calculations for the purpose of measuring iron fluxes originating in active galactic nuclei.

This work is aimed at furthering the work on radiative parameters relevant to astrophysics and other areas by using laser-induced breakdown spectroscopy on copper and iron samples. Radiative parameters (e.g. relative intensities, branching ratios, $\log(gf)$ values, and gA values) in Fe I, II and Cu I, II are presented in the tables below and compared to previous works.

7.3 - Experimental Setup / Data Analysis / Uncertainties

The experimental setup, analysis of data, and determination of uncertainties were all thoroughly described in Chapter 5. The measurements on copper and iron described in this chapter were all performed utilizing exactly the same apparatus, procedures and uncertainties. Therefore the information is not repeated here. Representative spectra from both copper and iron are shown in Figure 7.1.

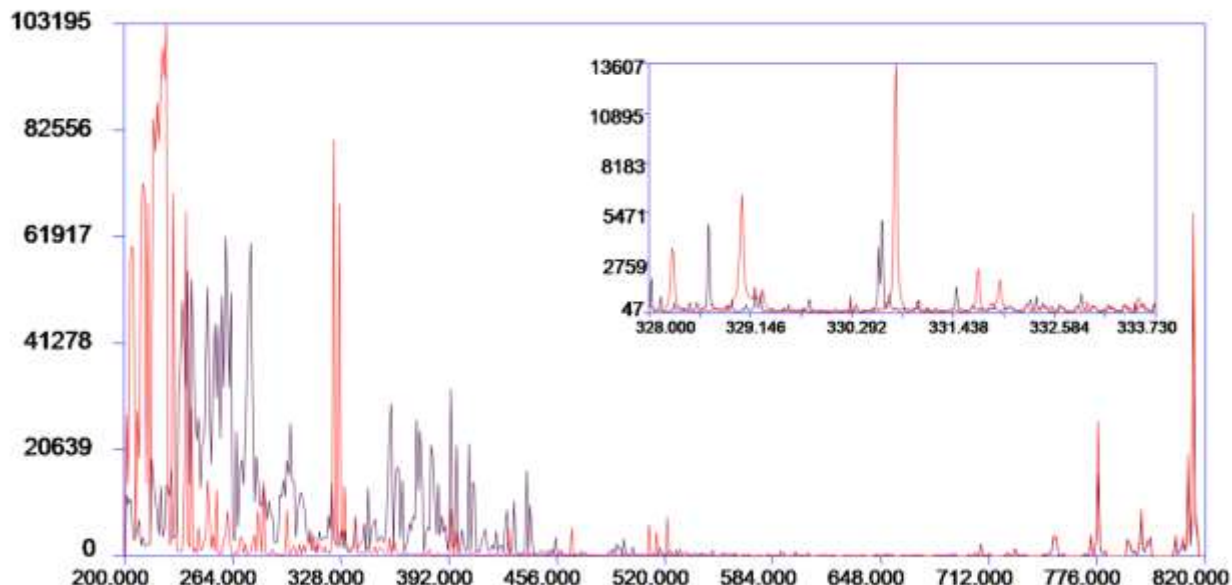


Figure 7.1 Shown above is an overlay of iron spectrum (purple) and copper spectrum (red) both are transition elements and their resulting spectra are similar in the shown region. Note the large number of lines in the UV/deep-UV end of the spectrum, where our ability to obtain accurate measurements decreases. The inset shows a few emission lines from both elements' spectra near 330 nm.

7.4 - Results

In LIBS spectra it sometimes occurs that line profiles are unresolved due to blending of emission lines with neighboring lines or weak signal to noise. Because of these issues some of the branching ratios are inaccurate, and therefore we list the branching ratios of all of our measured lines with annotations for the strong, blended, shouldered, or weak lines.

Branching ratios (BR) of measured branches in copper are listed in tables 7.1 and table 7.2 according to ionization state and energy level and are compared to previous works. Branching ratios (BR) of measured branches in iron are listed in tables 7.3 and table 7.4 according to ionization state and energy level and are compared to previous works. In this work

only transitions in the spectral range of 200-800 nm were observed and the corresponding radiative parameters presented.

Cu I Data

Table 7.1 Cu I radiative properties

s emission line has shoulder

w weak emission line

b blended emission line

o means the line is lower than our 225 nm efficiency calibration

Kurucz refers to work by Kurucz et al.⁷⁴

Upper Energy (cm ⁻¹)	Wavelength (nm)	WSU BR	BR Error	Kurucz BR		Upper Energy (cm ⁻¹)	Wavelength (nm)	WSU BR	BR Error	Kurucz BR	
30535	327.395	1.000	0.093	0.986		70998	312.610	0.883	0.084	0.815	
30535	578.213	-	-	0.014		70998	339.632	-	-	0.020	
						70998	366.573	0.035	0.008	0.057	w
30784	324.754	0.912	0.085	0.984		70998	375.948	0.073	0.017	0.053	s
30784	510.554	0.081	0.019	0.014		70998	397.996	-	-	0.008	
30784	570.024	0.006	0.002	0.002	b	70998	402.701	0.010	0.002	0.042	w
						70998	696.835	-	-	0.005	
40114	249.214	1.000	0.093	0.978							
40114	345.785	-	-	0.019		71098	338.481	0.396	0.039	0.071	
40114	372.076	-	-	0.003		71098	362.423	0.235	0.026	0.138	s
						71098	365.233	0.047	0.012	0.472	s
40944	244.164	1.000	0.093	0.981		71098	374.539	0.138	0.015	0.132	w
40944	360.930	-	-	0.019		71098	376.484	-	-	0.029	
						71098	396.417	-	-	0.030	
41153	333.784	1.000	0.093	1.000		71098	401.085	0.021	0.005	0.017	w
						71098	408.051	0.162	0.018	0.109	w
41563	329.282	0.570	0.053	0.187							
41563	353.038	0.430	0.040	0.813		71128	311.347	0.054	0.013	0.045	s
						71128	333.522	0.182	0.020	0.137	s
43514	309.399	1.000	0.093	1.000		71128	338.142	0.333	0.033	0.260	b
						71128	362.034	0.117	0.013	0.099	s
43726	307.380	0.201	0.021	0.176		71128	364.838	0.047	0.012	0.055	s
43726	327.981	0.799	0.074	0.824		71128	374.124	0.131	0.014	0.147	
						71128	382.088	0.036	0.009	0.060	w
44406	301.084	0.642	0.042	0.726		71128	407.558	0.081	0.020	0.103	w
44406	320.823	0.358	0.024	0.274		71128	662.163	0.018	0.004	0.037	w

					71128	690.592	-	-	0.057	
44544	224.427	0.723	0.067	0.593						
44544	299.838	-	-	0.008	71131	330.795	1.000	0.093	1.000	
44544	319.409	0.277	0.028	0.399						
					71178	332.963	0.180	0.019	0.194	s
44916	222.571	1.000	0.093	0.996	71178	337.566	0.082	0.020	0.070	s
44916	315.663	-	-	0.004	71178	361.374	0.445	0.042	0.434	
					71178	364.168	0.127	0.013	0.098	
44963	296.116	1.000	0.093	1.000	71178	373.420	0.086	0.020	0.128	
					71178	381.353	-	-	0.036	
45821	218.172	0.983	0.091	1.000	71178	395.163	0.016	0.004	0.008	w
45821	306.889	0.017	0.004	0.000	71178	399.801	0.065	0.015	0.011	w
					71178	659.960	-	-	0.006	
45879	217.895	0.929	0.086	0.966	71178	688.197	-	-	0.015	
45879	288.293	0.027	0.006	0.018						
45879	306.341	0.044	0.010	0.016	71268	309.992	0.279	0.029	0.122	
					71268	331.967	0.229	0.024	0.079	
46173	216.510	0.908	0.060	0.959	71268	360.202	0.437	0.041	0.772	
46173	285.873	0.012	0.002	0.001	71268	362.978	0.008	0.002	0.005	s
46173	303.610	0.079	0.015	0.040	71268	372.168	-	-	0.005	
					71268	380.048	0.037	0.009	0.012	w
46598	282.437	0.929	0.061	0.871	71268	405.238	0.009	0.002	0.004	w
46598	299.736	0.071	0.014	0.129						
					71291	329.054	0.563	0.052	0.210	
49383	202.434	0.269	0.028	0.688	71291	331.721	0.137	0.014	0.103	
49383	261.836	0.541	0.050	0.237	71291	359.913	0.300	0.031	0.682	
49383	276.639	0.189	0.020	0.074	71291	379.726	-	-	0.004	
					71291	655.102	-	-	0.001	
49383	202.433	1.000	0.093	1.000						
					71883	314.681	0.815	0.082	0.719	
49935	515.323	0.809	0.081	0.826	71883	365.676	0.185	0.021	0.238	w
49935	522.007	0.191	0.021	0.174	71883	388.842	-	-	0.043	
49942	521.820	1.000	0.093	1.000	71927	314.244	0.556	0.059	0.561	
					71927	329.239	0.292	0.031	0.107	w
55388	402.263	0.196	0.022	0.749	71927	354.496	0.096	0.011	0.124	w
55388	406.324	0.804	0.083	0.251	71927	363.256	0.056	0.015	0.092	s
					71927	365.085	-	-	0.034	
55391	406.264	1.000	0.093	1.000	71927	383.799	-	-	0.016	
					71927	388.174	-	-	0.024	
56030	223.009	1.000	0.093	1.000	71927	394.695	-	-	0.019	

						71927	654.452	-	-	0.009	
56651	219.959	1.000	0.093	1.000		71927	689.089	-	-	0.015	
57949	213.854	1.000	0.093	0.838	w	71979	324.316	0.675	0.063	0.654	
57949	674.965	-	-	0.162		71979	351.211	0.236	0.024	0.261	
						71979	370.053	0.090	0.021	0.085	w
58119	222.778	1.000	0.093	1.000							
						72017	328.271	0.770	0.072	0.672	
58569	356.613	0.934	0.092	0.382	w	72017	350.742	0.006	0.001	0.023	w
58569	359.801	0.066	0.016	0.618	w	72017	353.374	0.225	0.023	0.259	
						72017	369.532	-	-	0.022	
58691	219.975	1.000	0.093	1.000		72017	393.304	-	-	0.020	
						72017	650.638	-	-	0.004	
59249	348.161	-	-	0.639							
59249	351.199	1.000	0.093	0.361		72067	312.869	0.492	0.047	0.351	
						72067	323.390	0.072	0.017	0.131	w
59648	343.396	-	-	0.183		72067	352.748	0.394	0.038	0.296	
59648	346.351	-	-	0.817		72067	361.421	-	-	0.135	
						72067	381.751	-	-	0.014	
60066	338.539	-	-	0.836	w	72067	392.529	0.042	0.010	0.054	w
60066	341.411	-	-	0.164	w	72067	648.519	-	-	0.019	
60595	335.346	1.000	0.093	1.000	s	72093	302.260	0.080	0.019	0.087	
						72093	323.117	0.244	0.026	0.258	
62403	427.510	0.401	0.038	0.342		72093	349.806	0.046	0.011	0.054	w
62403	465.112	0.370	0.035	0.451		72093	352.423	0.552	0.052	0.454	
62403	470.459	0.089	0.021	0.067		72093	361.080	0.055	0.013	0.080	s
62403	479.703	0.004	0.001	0.003	w	72093	392.127	0.022	0.005	0.028	w
62403	529.251	0.112	0.012	0.117		72093	622.372	-	-	0.014	
62403	535.265	0.008	0.002	0.007	w	72093	647.422	-	-	0.019	
62403	555.492	0.011	0.003	0.007	w	72093	715.428	-	-	0.005	
62403	573.232	0.005	0.001	0.004	w						
62403	632.537	-	-	0.001		72105	335.448	0.267	0.031	0.343	w
						72105	362.733	0.733	0.076	0.559	
62948	417.774	0.033	0.008	0.023	s	72105	381.200	-	-	0.099	
62948	437.815	0.284	0.030	0.192							
62948	458.695	0.405	0.039	0.374		72151	326.828	0.203	0.021	0.316	
62948	467.478	0.115	0.012	0.113	s	72151	334.927	0.405	0.038	0.337	w
62948	484.224	-	-	0.009		72151	351.703	0.076	0.018	0.058	w
62948	514.410	0.063	0.015	0.101	w	72151	362.123	0.316	0.029	0.289	
62948	520.090	0.066	0.016	0.070	w						

62948	539.166	0.010	0.002	0.076	w	73103	293.306	0.022	0.005	0.019	w
62948	543.205	0.025	0.006	0.043	w	73103	316.968	0.323	0.031	0.269	
						73103	348.375	0.589	0.056	0.586	
63585	406.953	0.026	0.007	0.003	w	73103	377.189	0.067	0.016	0.089	w
63585	425.945	0.163	0.018	0.154		73103	667.218	-	-	0.037	
63585	441.556	0.085	0.021	0.089	w						
63585	453.971	0.459	0.046	0.367		73105	303.026	0.133	0.017	0.120	w
63585	469.747	0.138	0.015	0.077	w	73105	350.031	0.189	0.024	0.231	w
63585	503.425	0.064	0.016	0.087	w	73105	354.644	0.221	0.028	0.127	w
63585	521.277	0.013	0.003	0.041	w	73105	367.197	0.320	0.037	0.297	w
63585	525.052	0.038	0.010	0.122	w	73105	371.199	0.136	0.017	0.225	w
63585	535.500	0.013	0.003	0.059	w						
						73199	316.006	0.052	0.013	0.040	w
64472	410.422	0.038	0.009	0.036	s	73199	323.571	0.593	0.057	0.617	
64472	424.896	0.143	0.015	0.236		73199	339.202	-	-	0.018	
64472	450.937	0.489	0.047	0.352		73199	347.214	0.157	0.017	0.115	
64472	501.663	0.203	0.022	0.193		73199	348.885	0.084	0.020	0.075	w
64472	511.192	0.105	0.011	0.125		73199	365.936	0.113	0.012	0.099	w
64472	536.007	0.022	0.005	0.030		73199	369.911	-	-	0.026	
64472	537.688	-	-	0.008		73199	662.972	-	-	0.011	
64472	546.312	-	-	0.020							
						73305	301.202	0.139	0.014	0.124	w
64658	407.320	0.228	0.027	0.108	w	73305	314.951	0.047	0.011	0.036	s
64658	432.874	-	-	0.060		73305	322.465	0.172	0.018	0.220	b
64658	477.613	-	-	0.077		73305	345.941	0.031	0.007	0.042	b
64658	507.613	0.772	0.084	0.755	w	73305	347.599	0.461	0.043	0.455	
						73305	364.522	0.151	0.016	0.117	
67143	423.094	0.076	0.011	0.034	w	73305	658.346	-	-	0.007	
67143	450.741	0.559	0.071	0.506	w						
67143	476.742	0.135	0.019	0.153	w	73316	308.812	0.142	0.015	0.134	w
67143	486.616	0.230	0.029	0.307	w	73316	314.834	-	-	0.018	
						73316	322.342	0.140	0.014	0.213	
67972	412.327	0.295	0.041	0.334	w	73316	347.457	-	-	0.020	
67972	424.227	0.166	0.026	0.234	w	73316	352.002	0.422	0.039	0.400	
67972	433.598	0.226	0.031	0.107	w	73316	363.593	0.296	0.030	0.216	w
67972	452.513	0.313	0.043	0.326	w						
						73995	285.822	0.492	0.046	0.365	w
70853	314.031	0.557	0.071	0.543	s	73995	302.155	0.398	0.037	0.530	w
70853	378.006	0.068	0.022	0.046	w	73995	304.402	0.110	0.011	0.104	w
70853	379.987	0.157	0.022	0.095	w						
70853	399.370	-	-	0.011		75109	341.334	1.000	0.093	0.785	b

70853	400.302	0.106	0.015	0.119	w	75109	342.014	-	-	0.215	
70853	405.063	0.113	0.016	0.096	w						
70853	412.169	-	-	0.089		76959	263.493	1.000	0.093	1.000	w
70860	336.535	0.599	0.056	0.427		77031	262.997	1.000	0.093	1.000	w
70860	365.586	0.190	0.020	0.181	s						
70860	386.046	0.211	0.022	0.264	s	77906	264.531	1.000	0.093	1.000	
70860	674.142	-	-	0.128							
						78988	289.083	1.000	0.093	1.000	w
						79117	289.164	1.000	0.093	1.000	w

Table 7.1 Cu I radiative properties

s emission line has shoulder*w* weak emission line*b* blended emission line*o* means the line is lower than our 225 nm efficiency calibration*Kurucz* refers to work by Kurucz et al.⁷⁴**Cu II Data**

Table 7.2 Cu II radiative properties

s emission line has shoulder*w* weak emission line*b* blended emission line*o* means the line is lower than our 225 nm efficiency calibration*Kurucz* refers to work by Kurucz et al.⁷⁴

Upper Energy (cm-1)	Wavelength (nm)	WSU BR	BR Error	Kurucz BR		Upper Energy (cm-1)	Wavelength (nm)	WSU BR	BR Error	Kurucz BR	
66419	224.700	0.671	0.062	0.929	o	110084	228.942	0.034	0.008	0.003	w
66419	229.437	0.256	0.026	0.063	b	110084	237.075	0.055	0.013	0.063	
66419	235.664	0.041	0.010	0.004		110084	242.444	0.113	0.012	0.126	
66419	248.965	0.032	0.007	0.004		110084	248.579	0.277	0.028	0.373	
						110084	259.053	0.124	0.013	0.105	
67917	221.811	0.660	0.061	0.832	o	110084	270.319	0.309	0.029	0.254	
67917	227.626	0.203	0.021	0.147		110084	272.168	0.089	0.021	0.068	
67917	240.012	0.137	0.014	0.022	b	110084	273.977	-	-	0.008	
68448	214.898	0.276	0.028	0.178	o	110366	227.474	-	-	0.017	
68448	219.227	0.578	0.054	0.760	o	110366	235.501	0.066	0.015	0.079	

68448	236.989	0.145	0.015	0.063	b	110366	238.486	0.017	0.004	0.007	b
						110366	246.850	0.021	0.005	0.034	
68731	213.598	1.000	0.093	1.000	o	110366	252.930	0.246	0.025	0.299	
						110366	257.176	0.020	0.005	0.033	b
68850	222.887	1.000	0.093	1.000	o	110366	260.027	0.182	0.019	0.224	
						110366	268.275	-	-	0.001	
69868	208.531	0.065	0.015	0.012	o	110366	270.096	0.291	0.030	0.168	b
69868	212.604	0.400	0.037	0.365	o	110366	271.878	0.156	0.016	0.137	
69868	217.941	0.529	0.049	0.621	o						
69868	229.269	0.006	0.001	0.002		110632	244.264	1.000	0.093	1.000	
70841	204.380	0.188	0.019	0.401	o	111125	260.334	1.000	0.093	1.000	
70841	208.292	-	-	0.000	o						
70841	224.262	0.812	0.075	0.599	o	111219	251.895	1.000	0.093	1.000	
71494	201.690	0.041	0.010	0.026	o	114511	207.866	0.677	0.063	0.812	o
71494	205.498	0.233	0.024	0.438	o	114511	214.549	0.247	0.025	0.148	o
71494	210.480	0.238	0.024	0.207	o	114511	218.937	-	-	0.015	o
71494	221.027	0.489	0.045	0.329	o	114511	223.929	0.063	0.015	0.000	o
						114511	232.393	-	-	0.002	
71920	203.713	0.285	0.029	0.541	o	114511	241.419	-	-	0.004	
71920	218.963	0.715	0.066	0.459	o	114511	242.893	-	-	0.007	
						114511	244.333	0.013	0.003	0.011	w
73102	203.585	0.647	0.060	0.986	o						
73102	213.437	0.353	0.033	0.014	o	114756	237.841	1.000	0.093	1.000	
73353	202.549	0.230	0.024	0.223	o	115360	228.094	1.000	0.093	0.992	
73353	212.298	0.770	0.072	0.777	o	115360	505.066	-	-	0.008	
73596	201.558	-	-	0.035	o	115546	218.075	1.000	0.093	1.000	o
73596	211.210	1.000	0.093	0.965	o						
						115569	213.434	1.000	0.093	1.000	o
108015	240.334	0.238	0.025	0.329							
108015	252.659	0.056	0.013	0.071		115639	203.104	0.052	0.005	0.714	o
108015	254.481	0.360	0.033	0.301		115639	209.479	0.005	0.001	0.021	o
108015	262.067	-	-	0.003		115639	211.838	-	-	0.027	o
108015	268.930	0.141	0.014	0.112		115639	218.412	-	-	0.000	o
108015	273.734	0.006	0.001	0.005	w	115639	223.158	0.024	0.003	0.092	o
108015	276.967	0.188	0.019	0.168		115639	226.457	0.011	-0.011	0.001	b
108015	288.420	0.012	0.003	0.009	w	115639	228.665	0.026	0.003	0.136	b
						115639	235.019	-	-	0.001	

108336	238.495	0.014	0.003	0.018	b	115639	236.415	-	-	0.007
108336	247.333	0.119	0.012	0.138		115639	237.779	-	-	0.001
108336	250.627	0.427	0.040	0.444						
108336	259.881	0.078	0.018	0.093		115663	211.731	0.886	0.082	0.920 o
108336	266.629	0.060	0.014	0.053		115663	213.009	0.114	0.012	0.054 o
108336	271.351	0.165	0.017	0.163		115663	223.040	-	-	0.026 o
108336	274.527	0.027	0.006	0.024		115663	228.540	-	-	0.000
108336	283.737	0.044	0.010	0.029						
108336	285.775	0.017	0.004	0.001	b					
108336	287.770	0.049	0.011	0.037						

Table 7.2 Cu II radiative properties

s emission line has shoulder

w weak emission line

b blended emission line

o means the line is lower than our 225 nm efficiency calibration

Kurucz refers to work by Kurucz et al.⁷⁴

Fe I Data

Table 7.3 Fe I Branching ratios and radiative parameters

s emission line has shoulder

w weak emission line

b blended emission line

d emission lie within our spectral gaps

o means the line is lower than our 225 nm efficiency calibration

Kurucz refers to work by Kurucz et al.⁷³

Upper Energy (cm ⁻¹)	Wavelength (nm)	WSU BR	BR Error	Kurucz BR		Upper Energy (cm ⁻¹)	Wavelength (nm)	WSU BR	BR Error	Kurucz BR	
19562	511.041	1.000	0.066	0.958	s	43108.9	231.899	-	-	0.002	
19562	522.143	-	-	0.009		43108.9	234.159	-	-	0.010	
19562	791.286	-	-	0.033		43108.9	276.309	0.087	0.018	0.016	w
						43108.9	279.778	0.272	0.021	0.361	
19757	506.008	-	-	0.030		43108.9	282.556	0.426	0.030	0.606	
19757	516.890	1.000	0.066	0.880		43108.9	321.113	-	-	0.000	
19757	524.705	-	-	0.090		43108.9	327.260	0.008	0.002	0.000	w
						43108.9	391.145	0.004	0.001	0.000	w
22846	437.593	1.000	0.066	0.979	w	43108.9	425.631	0.049	0.010	0.003	w
22846	628.062	-	-	0.021		43108.9	428.684	0.026	0.005	0.000	w
22846	646.271	-	-	0.001		43108.9	444.957	0.053	0.011	0.000	b

						43108.9	449.627	0.033	0.007	0.001	w
22997	434.723	-	-	0.003		43108.9	467.308	0.020	0.004	0.000	w
22997	442.731	1.000	0.066	0.922	s	43108.9	473.582	0.014	0.003	0.000	w
22997	622.167	-	-	0.007		43108.9	479.265	-	-	0.000	
22997	640.031	-	-	0.062		43108.9	517.313	-	-	0.000	
22997	654.757	-	-	0.005		43108.9	526.444	0.010	0.002	0.000	w
						43108.9	532.613	-	-	0.000	
23111	432.574	0.968	0.064	0.025	b	43108.9	539.392	-	-	0.000	
23111	440.502	-	-	0.008		43108.9	592.115	-	-	0.000	
23111	446.165	0.032	0.006	0.935	b	43108.9	596.570	-	-	0.000	
23111	635.384	-	-	0.011		43108.9	606.581	-	-	0.000	
23111	649.894	-	-	0.014		43108.9	699.648	-	-	0.000	
23111	660.968	-	-	0.008		43108.9	727.756	-	-	0.000	
						43108.9	751.110	-	-	0.000	
23192	438.925	0.220	0.016	0.076	w						
23192	444.547	-	-	0.010		43137.48	231.746	0.015	0.003	0.000	b
23192	448.217	0.780	0.052	0.886	w	43137.48	234.002	0.009	0.002	0.001	w
23192	646.466	-	-	0.008		43137.48	235.591	-	-	0.005	
23192	657.423	-	-	0.012		43137.48	279.554	0.565	0.039	0.035	s
23192	664.808	-	-	0.007		43137.48	282.328	0.169	0.013	0.344	
						43137.48	284.398	0.174	0.013	0.613	
23270	446.657	1.000	0.066	0.998		43137.48	320.819	0.006	0.001	0.000	b
23270	661.383	-	-	0.002		43137.48	326.954	0.003	0.001	0.000	w
						43137.48	331.372	-	-	0.000	
24181	413.434	-	-	0.081		43137.48	390.708	0.016	0.003	0.000	w
24181	420.670	1.000	0.066	0.671	w	43137.48	393.427	-	-	0.000	
24181	425.832	-	-	0.240		43137.48	403.775	0.009	0.002	0.000	w
24181	594.928	-	-	0.004		43137.48	428.159	-	-	0.001	
24181	607.631	-	-	0.003		43137.48	444.391	-	-	0.000	
24181	617.301	-	-	0.001		43137.48	449.050	0.007	0.001	0.000	w
						43137.48	452.393	0.010	0.002	0.000	w
25900	385.991	0.773	0.051	0.786		43137.48	472.942	0.011	0.002	0.000	b
25900	392.291	0.161	0.012	0.087		43137.48	478.609	-	-	0.000	
25900	526.954	0.066	0.013	0.103		43137.48	492.494	0.006	0.001	0.000	w
25900	539.713	-	-	0.021		43137.48	525.653	-	-	0.000	
25900	550.146	-	-	0.002		43137.48	531.718	-	-	0.000	
25900	717.999	-	-	0.000		43137.48	531.803	-	-	0.000	
25900	749.472	-	-	0.000		43137.48	538.561	-	-	0.000	
						43137.48	591.114	-	-	0.000	
26140	382.444	0.342	0.023	0.250		43137.48	605.388	-	-	0.000	
26140	388.628	0.368	0.024	0.467		43137.48	605.530	-	-	0.000	

26140	393.030	0.176	0.013	0.140		43137.48	687.905	-	-	0.000	
26140	532.804	0.076	0.014	0.101		43137.48	725.451	-	-	0.000	
26140	542.970	0.038	0.007	0.038		43137.48	726.245	-	-	0.000	
26140	550.678	-	-	0.004		43137.48	749.501	-	-	0.000	
26140	705.824	-	-	0.000							
26140	736.215	-	-	0.000		43163.33	419.830	0.142	0.010	0.072	
26140	758.999	-	-	0.000		43163.33	423.594	0.140	0.010	0.169	
						43163.33	427.115	0.342	0.023	0.164	
26340	385.637	0.392	0.026	0.419		43163.33	492.050	0.239	0.017	0.316	
26340	389.971	0.186	0.014	0.233		43163.33	495.730	-	-	0.123	
26340	392.792	0.305	0.020	0.200		43163.33	498.555	0.025	0.005	0.008	
26340	537.149	0.057	0.011	0.094		43163.33	513.946	0.064	0.012	0.068	
26340	544.692	0.056	0.011	0.048		43163.33	526.656	0.038	0.007	0.078	
26340	549.752	-	-	0.006		43163.33	579.102	-	-	0.001	
26340	725.555	0.004	0.001	0.000	w	43163.33	587.273	-	-	0.000	
26340	747.673	-	-	0.000		43163.33	613.750	0.010	0.002	0.000	b
						43163.33	624.964	-	-	0.000	
26479	387.857	0.640	0.042	0.531		43163.33	633.995	-	-	0.000	
26479	390.648	0.057	0.011	0.067		43163.33	708.672	-	-	0.000	
26479	392.026	0.184	0.013	0.209							
26479	540.577	0.057	0.011	0.088	w	43321.08	274.698	0.994	0.066	0.956	
26479	545.561	0.062	0.012	0.106	w	43321.08	417.752	0.005	0.001	0.012	w
26479	739.943	-	-	0.000		43321.08	421.821	0.001	0.000	0.025	w
						43321.08	462.719	-	-	0.002	
26550	389.566	0.820	0.054	0.846		43321.08	511.695	-	-	0.000	
26550	543.452	0.180	0.013	0.154	w	43321.08	580.722	-	-	0.001	
						43321.08	589.111	-	-	0.004	
26875	371.994	0.987	0.065	0.996		43321.08	689.411	-	-	0.000	
26875	501.207	0.013	0.002	0.003	w	43321.08	713.677	-	-	0.000	
26875	512.736	-	-	0.001							
26875	671.032	-	-	0.000		43434.63	418.780	0.166	0.012	0.143	
						43434.63	422.221	0.067	0.013	0.054	
27167	367.991	0.152	0.011	0.088		43434.63	425.012	0.214	0.016	0.196	
27167	373.713	0.824	0.055	0.900		43434.63	489.149	0.262	0.019	0.272	
27167	493.969	0.010	0.002	0.001	w	43434.63	491.899	0.142	0.010	0.158	
27167	505.163	0.006	0.001	0.003	w	43434.63	493.881	0.026	0.005	0.025	w
27167	514.293	0.008	0.001	0.009	w	43434.63	506.877	0.019	0.004	0.021	w
27167	658.121	-	-	0.000		43434.63	519.234	0.076	0.015	0.100	
27167	684.467	-	-	0.000		43434.63	528.179	0.022	0.004	0.031	w
						43434.63	570.142	0.006	0.001	0.000	w
27395	364.930	0.152	0.011	0.002		43434.63	578.060	-	-	0.001	

27395	370.557	0.205	0.015	0.216		43434.63	584.806	-	-	0.000
27395	374.556	0.637	0.042	0.774		43434.63	614.541	-	-	0.000
27395	499.413	-	-	0.002		43434.63	623.271	-	-	0.000
27395	508.334	0.005	0.001	0.003	w	43434.63	629.745	-	-	0.000
27395	515.084	-	-	0.002		43434.63	695.300	-	-	0.000
27395	648.394	-	-	0.000		43434.63	715.847	-	-	0.000
27395	673.952	-	-	0.000						
27395	692.995	-	-	0.000		43633.53	418.704	0.215	0.017	0.202
						43633.53	421.448	-	-	0.000
27560	368.306	0.015	0.003	0.019	w	43633.53	423.360	0.172	0.014	0.174
27560	372.256	0.269	0.020	0.335		43633.53	487.132	0.199	0.016	0.205
27560	374.826	0.685	0.046	0.617		43633.53	489.075	0.227	0.018	0.195
27560	504.107	0.014	0.003	0.025	w	43633.53	490.331	0.061	0.013	0.043
27560	510.745	0.011	0.002	0.003	b	43633.53	513.925	0.127	0.010	0.081
27560	515.191	-	-	0.002		43633.53	522.686	-	-	0.099
27560	666.543	-	-	0.000		43633.53	571.487	-	-	0.000
27560	685.163	0.006	0.001	0.000	w	43633.53	578.080	-	-	0.000
						43633.53	582.788	-	-	0.000
27666	370.782	0.250	0.018	0.050		43633.53	615.637	-	-	0.000
27666	373.332	0.260	0.019	0.432		43633.53	621.952	-	-	0.000
27666	374.590	0.481	0.032	0.509		43633.53	626.111	-	-	0.000
27666	507.974	0.010	0.002	0.004	b	43633.53	685.813	-	-	0.000
27666	512.372	-	-	0.005		43633.53	705.795	-	-	0.000
27666	680.186	-	-	0.000		43633.53	719.185	-	-	0.000
29056	344.061	0.440	0.029	0.687		43763.98	419.143	0.303	0.020	0.221
29056	349.057	0.218	0.016	0.261		43763.98	421.034	0.181	0.013	0.162
29056	352.604	0.302	0.020	0.051		43763.98	485.974	0.102	0.007	0.128
29056	461.135	0.020	0.004	0.000	w	43763.98	487.214	0.197	0.014	0.226
29056	468.730	0.011	0.002	0.000	w	43763.98	487.821	0.087	0.017	0.088
29056	474.464	-	-	0.000		43763.98	519.146	0.130	0.009	0.175
29056	585.315	0.006	0.001	0.000	w	43763.98	573.752	-	-	0.000
29056	606.062	0.003	0.001	0.000	w	43763.98	578.389	-	-	0.000
29056	621.418	-	-	0.000		43763.98	580.778	-	-	0.000
						43763.98	616.946	-	-	0.000
29469	344.099	0.460	0.030	0.464		43763.98	621.038	-	-	0.000
29469	347.545	0.389	0.026	0.390		43763.98	699.354	-	-	0.000
29469	349.784	0.130	0.010	0.145		43763.98	712.499	-	-	0.000
29469	459.832	0.011	0.002	0.000	w					
29469	465.349	-	-	0.000		43922.66	227.603	0.080	0.016	0.120
29469	469.037	0.006	0.001	0.000	w	43922.66	229.779	0.074	0.015	0.165

29469	591.269	-	-	0.000		43922.66	231.310	0.106	0.008	0.099	
29469	605.876	0.004	0.001	0.000	w	43922.66	273.548	0.445	0.030	0.446	
						43922.66	276.203	-	-	0.114	
29733	344.388	0.291	0.022	0.309		43922.66	278.184	0.031	0.006	0.011	
29733	346.586	0.404	0.027	0.421		43922.66	312.933	0.006	0.001	0.008	w
29733	347.670	0.276	0.021	0.270		43922.66	318.768	0.005	0.001	0.001	w
29733	459.706	0.012	0.002	0.000	w	43922.66	322.966	-	-	0.000	
29733	463.305	0.017	0.003	0.000	w	43922.66	379.075	0.008	0.002	0.007	w
29733	596.345	-	-	0.000		43922.66	381.634	-	-	0.016	
						43922.66	391.363	0.028	0.005	0.010	w
31307	319.323	0.416	0.045	0.399	b	43922.66	414.229	0.022	0.004	0.000	b
31307	323.622	0.051	0.016	0.189	s	43922.66	429.404	0.178	0.013	0.002	
31307	410.074	0.289	0.031	0.022	s	43922.66	433.752	-	-	0.000	
31307	417.759	0.040	0.012	0.028	w	43922.66	436.870	-	-	0.000	
31307	423.984	0.110	0.013	0.001	w	43922.66	456.003	-	-	0.000	
31307	517.160	0.076	0.009	0.338	w	43922.66	461.269	-	-	0.000	
31307	533.290	0.020	0.006	0.023	w	43922.66	474.153	0.006	0.001	0.003	w
31307	726.699	-	-	0.000		43922.66	504.812	-	-	0.000	
						43922.66	510.403	-	-	0.000	
31323	319.166	0.044	0.009	0.064	w	43922.66	510.481	0.007	0.001	0.000	w
31323	323.461	0.108	0.008	0.032	b	43922.66	516.705	-	-	0.000	
31323	326.505	0.289	0.020	0.030	b	43922.66	564.889	-	-	0.000	
31323	417.491	-	-	0.018		43922.66	577.910	0.004	0.001	0.000	d
31323	423.707	0.027	0.005	0.001	b	43922.66	578.040	-	-	0.000	
31323	428.387	-	-	0.000		43922.66	652.644	-	-	0.000	
31323	516.749	0.331	0.023	0.612		43922.66	686.345	-	-	0.000	
31323	532.853	-	-	0.233		43922.66	687.055	-	-	0.000	
31323	544.687	0.202	0.015	0.009		43922.66	707.833	-	-	0.000	
31323	725.888	-	-	0.000							
31323	735.328	-	-	0.000		44243.67	225.951	0.219	0.019	0.190	
31323	772.321	-	-	0.001		44243.67	267.906	0.514	0.040	0.526	
						44243.67	271.166	-	-	0.283	
31686	319.699	0.593	0.041	0.028		44243.67	309.820	0.029	0.007	0.000	w
31686	322.671	0.018	0.004	0.001	w	44243.67	402.244	-	-	0.000	
31686	324.601	0.009	0.002	0.024	w	44243.67	406.015	-	-	0.000	
31686	417.274	0.022	0.004	0.011	w	44243.67	408.792	0.005	0.001	0.000	w
31686	421.812	-	-	0.000		44243.67	423.564	-	-	0.000	
31686	424.840	0.027	0.005	0.000	b	44243.67	443.769	-	-	0.000	
31686	522.719	0.286	0.022	0.869		44243.67	449.422	-	-	0.000	
31686	534.102	0.045	0.009	0.067	w	44243.67	488.621	-	-	0.000	
31686	707.210	-	-	0.000		44243.67	496.759	0.011	0.002	0.000	w

31686	716.168	-	-	0.000		44243.67	508.272	-	-	0.000	
31686	726.598	-	-	0.000		44243.67	551.183	-	-	0.000	
31686	751.212	-	-	0.000		44243.67	558.734	0.203	0.018	0.000	b
						44243.67	567.506	-	-	0.000	
31805	314.324	-	-	0.021		44243.67	648.173	-	-	0.000	
31805	318.490	0.155	0.015	0.226	w	44243.67	669.577	0.009	0.002	0.000	w
31805	321.440	-	-	0.187		44243.67	692.103	0.011	0.002	0.000	w
31805	409.246	0.111	0.011	0.002	w						
31805	415.217	0.134	0.013	0.028	w	44415.07	225.079	0.095	0.019	0.043	
31805	419.710	0.177	0.017	0.001	w	44415.07	227.207	0.017	0.003	0.086	
31805	504.176	0.110	0.010	0.262	w	44415.07	266.681	0.408	0.028	0.345	
31805	519.494	0.313	0.027	0.244	s	44415.07	269.911	0.037	0.007	0.246	
31805	530.736	-	-	0.030		44415.07	272.495	0.314	0.022	0.244	
31805	701.320	-	-	0.000		44415.07	308.183	0.071	0.014	0.000	w
31805	710.128	-	-	0.000		44415.07	313.840	-	-	0.000	
31805	744.569	-	-	0.000		44415.07	372.127	0.021	0.004	0.035	w
						44415.07	403.208	0.006	0.001	0.000	w
33096	302.064	0.351	0.023	0.314		44415.07	405.947	0.005	0.001	0.000	w
33096	305.909	0.114	0.008	0.135		44415.07	420.510	0.002	0.000	0.000	w
33096	382.043	0.472	0.031	0.521		44415.07	424.679	0.011	0.002	0.000	w
33096	388.705	0.061	0.012	0.027		44415.07	440.418	-	-	0.000	
33096	394.088	0.003	0.001	0.001	w	44415.07	445.986	-	-	0.000	
33096	473.359	-	-	0.001		44415.07	451.022	0.009	0.002	0.000	w
33096	486.837	-	-	0.000		44415.07	484.561	-	-	0.000	
33096	643.084	-	-	0.001		44415.07	492.564	-	-	0.000	
33096	741.914	-	-	0.000		44415.07	497.961	-	-	0.000	
33096	751.238	-	-	0.000		44415.07	503.881	-	-	0.000	
						44415.07	549.597	0.002	0.000	0.000	w
33507	298.357	0.134	0.010	0.164		44415.07	553.433	0.002	0.000	0.000	w
33507	302.107	0.184	0.013	0.268		44415.07	562.038	-	-	0.000	
33507	304.760	0.199	0.015	0.167		44415.07	641.049	-	-	0.000	
33507	382.588	0.364	0.024	0.351		44415.07	664.566	-	-	0.000	
33507	387.802	0.108	0.008	0.045		44415.07	683.987	-	-	0.000	
33507	391.718	0.008	0.001	0.003	s						
33507	464.319	-	-	0.000		44458.92	229.441	0.631	0.046	0.749	
33507	477.280	0.003	0.001	0.000	w	44458.92	275.369	-	-	0.147	
33507	486.753	-	-	0.000		44458.92	376.803	0.077	0.016	0.103	w
33507	626.513	-	-	0.000		44458.92	401.389	0.074	0.016	0.000	w
33507	633.533	-	-	0.001		44458.92	464.724	0.154	0.012	0.000	w
33507	660.802	-	-	0.000		44458.92	507.810	0.065	0.013	0.000	w
33507	728.722	-	-	0.000		44458.92	553.788	-	-	0.000	

33507	777.028	-	-	0.000		44458.92	590.996	-	-	0.000	
33507	791.383	-	-	0.000		44458.92	660.368	-	-	0.000	
33695	296.690	0.289	0.021	0.225		44677	394.738	0.093	0.008	0.003	b
33695	373.486	0.631	0.042	0.746		44677	398.063	0.016	0.004	0.001	w
33695	379.851	0.074	0.014	0.027		44677	401.171	0.012	0.003	0.002	w
33695	460.294	0.004	0.001	0.003	w	44677	457.933	0.010	0.002	0.000	w
33695	698.852	0.001	0.000	0.000	d	44677	461.119	0.078	0.018	0.001	b
33695	710.315	-	-	0.000		44677	463.562	0.016	0.004	0.000	w
33695	718.857	-	-	0.000		44677	476.840	0.019	0.004	0.003	b
33695	765.821	-	-	0.000		44677	487.761	0.062	0.014	0.001	w
						44677	532.418	0.313	0.025	0.354	
33802	299.443	0.292	0.021	0.287		44677	539.317	-	-	0.074	
33802	302.049	-	-	0.129		44677	561.564	0.314	0.025	0.401	
33802	303.739	0.247	0.018	0.212		44677	570.938	0.040	0.009	0.031	w
33802	383.422	0.297	0.022	0.296		44677	578.466	0.014	0.003	0.001	d
33802	387.250	0.137	0.010	0.069		44677	640.000	-	-	0.129	
33802	389.801	0.027	0.005	0.005		44677	747.751	0.012	0.003	0.000	b
33802	470.664	-	-	0.000		44677	748.611	-	-	0.000	
33802	479.873	-	-	0.000		44677	776.670	-	-	0.000	
33802	615.162	-	-	0.000							
33802	621.928	-	-	0.001		44760.75	226.910	-	-	0.091	
33802	629.779	-	-	0.000		44760.75	227.862	-	-	0.004	
33802	648.187	-	-	0.000		44760.75	228.330	0.046	0.010	0.111	w
33802	701.606	-	-	0.000		44760.75	271.844	0.600	0.045	0.643	
33802	773.357	-	-	0.000		44760.75	273.098	-	-	0.137	
33802	783.325	-	-	0.000		44760.75	314.452	-	-	0.003	
						44760.75	369.803	0.055	0.012	0.002	b
33947	298.145	0.176	0.013	0.269		44760.75	372.564	0.016	0.004	0.002	b
33947	300.728	0.193	0.014	0.113		44760.75	378.931	0.023	0.005	0.000	b
33947	302.403	0.127	0.009	0.201		44760.75	396.583	0.032	0.007	0.002	w
33947	381.296	0.371	0.025	0.326		44760.75	404.368	0.024	0.005	0.002	b
33947	385.082	0.079	0.015	0.068	s	44760.75	421.435	-	-	0.001	
33947	387.604	0.021	0.004	0.006	w	44760.75	456.026	0.028	0.006	0.000	w
33947	467.465	0.022	0.004	0.000	w	44760.75	458.294	-	-	0.001	
33947	476.548	0.010	0.002	0.000	w	44760.75	460.509	-	-	0.001	
33947	609.708	-	-	0.000		44760.75	489.460	-	-	0.000	
33947	616.354	-	-	0.000		44760.75	500.142	-	-	0.000	
33947	624.065	-	-	0.001		44760.75	508.269	-	-	0.000	
33947	642.135	-	-	0.013		44760.75	544.681	0.157	0.013	0.000	
33947	694.520	-	-	0.004		44760.75	551.205	0.019	0.004	0.000	w

33947	764.757	-	-	0.000		44760.75	580.635	-	-	0.000	
33947	774.504	-	-	0.000		44760.75	618.788	-	-	0.000	
						44760.75	647.459	-	-	0.000	
34017	300.095	0.339	0.022	0.381		44760.75	649.002	-	-	0.000	
34017	301.763	0.051	0.010	0.040							
34017	302.584	0.239	0.017	0.206		45061.33	392.063	-	-	0.001	
34017	384.044	0.211	0.015	0.279		45061.33	395.078	-	-	0.000	
34017	386.552	0.152	0.011	0.092		45061.33	397.520	-	-	0.002	
34017	474.959	-	-	0.000		45061.33	453.087	-	-	0.000	
34017	613.699	0.008	0.001	0.000	b	45061.33	455.445	-	-	0.001	
34017	621.343	-	-	0.001		45061.33	457.144	0.017	0.004	0.001	w
34017	639.254	-	-	0.000		45061.33	468.256	0.039	0.008	0.001	w
34017	691.151	-	-	0.000		45061.33	478.783	-	-	0.002	
34017	715.147	-	-	0.000		45061.33	486.378	-	-	0.000	
34017	770.316	-	-	0.000		45061.33	521.739	0.087	0.017	0.060	b
						45061.33	528.362	0.193	0.015	0.170	
34040	293.690	0.123	0.009	0.105		45061.33	533.993	0.140	0.011	0.148	b
34040	297.324	0.256	0.019	0.149		45061.33	558.676	0.420	0.029	0.400	
34040	368.746	0.100	0.019	0.065		45061.33	565.882	0.075	0.015	0.076	b
34040	374.949	0.429	0.028	0.619		45061.33	571.213	-	-	0.005	
34040	379.955	0.084	0.016	0.059		45061.33	624.632	-	-	0.057	
34040	453.115	0.004	0.001	0.002	w	45061.33	641.165	0.028	0.006	0.075	d
34040	465.450	0.004	0.001	0.000	w	45061.33	726.857	-	-	0.001	
34040	606.285	-	-	0.000		45061.33	727.670	-	-	0.000	
34040	693.362	-	-	0.000		45061.33	747.459	-	-	0.000	
34040	701.499	-	-	0.000		45061.33	754.153	-	-	0.000	
34040	746.152	-	-	0.000		45061.33	773.342	-	-	0.000	
34040	759.379	-	-	0.000							
						45509.15	390.565	-	-	0.000	
34122	300.814	0.606	0.040	0.638		45509.15	392.207	-	-	0.001	
34122	384.997	0.394	0.026	0.360		45509.15	447.970	-	-	0.001	
34122	617.334	-	-	0.001		45509.15	449.023	0.067	0.015	0.000	w
34122	686.195	-	-	0.000		45509.15	449.539	-	-	0.001	
						45509.15	476.007	-	-	0.000	
34329	291.216	0.022	0.004	0.026		45509.15	521.518	0.246	0.021	0.170	b
34329	294.788	0.213	0.016	0.160		45509.15	525.346	-	-	0.031	
34329	297.313	0.250	0.018	0.106		45509.15	527.316	0.116	0.010	0.128	w
34329	370.925	0.108	0.008	0.122		45509.15	556.962	0.377	0.029	0.368	w
34329	375.823	0.310	0.020	0.495		45509.15	560.295	0.193	0.016	0.156	w
34329	379.500	0.090	0.017	0.090		45509.15	623.264	-	-	0.055	
34329	447.251	0.004	0.001	0.000	b	45509.15	633.682	-	-	0.088	

34329	459.265	0.002	0.000	0.001	w	45509.15	723.243	-	-	0.000	
34329	468.029	-	-	0.000		45509.15	736.617	-	-	0.000	
34329	595.833	-	-	0.000		45509.15	747.449	-	-	0.000	
34329	602.179	-	-	0.000							
34329	626.764	-	-	0.000		45562.97	219.408	-	-	0.000	
34329	687.544	-	-	0.000		45562.97	221.430	-	-	0.000	
34329	730.385	-	-	0.000		45562.97	222.852	-	-	0.000	
34329	743.054	-	-	0.000		45562.97	261.797	0.188	0.017	0.003	b
34329	752.252	-	-	0.000		45562.97	264.227	-	-	0.068	
						45562.97	266.040	0.025	0.006	0.233	w
34363	297.012	0.364	0.025	0.332		45562.97	297.650	0.008	0.002	0.000	s
34363	298.646	0.015	0.003	0.027	b	45562.97	302.923	0.007	0.002	0.044	w
34363	299.450	0.557	0.038	0.181		45562.97	306.712	0.248	0.020	0.202	
34363	379.009	0.041	0.008	0.326		45562.97	356.878	0.030	0.007	0.001	
34363	381.452	0.012	0.002	0.076	b	45562.97	359.145	0.006	0.001	0.001	w
34363	467.283	0.010	0.002	0.001	w	45562.97	367.748	0.136	0.012	0.000	
34363	600.944	-	-	0.000		45562.97	387.867	0.274	0.022	0.300	
34363	608.271	-	-	0.002		45562.97	401.141	0.009	0.002	0.012	w
34363	625.426	-	-	0.023		45562.97	404.933	-	-	0.012	
34363	675.015	-	-	0.014		45562.97	407.649	0.040	0.009	0.031	w
34363	697.885	-	-	0.018		45562.97	424.260	0.003	0.001	0.002	w
						45562.97	428.815	0.004	0.001	0.031	w
34547	292.901	0.084	0.016	0.057		45562.97	439.927	0.004	0.001	0.000	w
34547	295.394	0.271	0.020	0.149		45562.97	466.197	-	-	0.008	
34547	297.010	0.139	0.010	0.085		45562.97	470.962	-	-	0.000	
34547	372.762	0.142	0.010	0.177		45562.97	471.028	0.007	0.002	0.050	w
34547	376.379	0.281	0.021	0.429		45562.97	476.322	-	-	0.000	
34547	378.788	0.081	0.015	0.101		45562.97	516.973	0.005	0.001	0.000	b
34547	454.702	-	-	0.000		45562.97	527.857	0.004	0.001	0.000	b
34547	463.291	0.003	0.001	0.001	w	45562.97	527.965	0.002	0.001	0.001	w
34547	588.175	-	-	0.000		45562.97	589.516	-	-	0.000	
34547	594.358	-	-	0.000		45562.97	616.876	-	-	0.000	
34547	601.524	-	-	0.000		45562.97	617.450	-	-	0.000	
34547	618.295	-	-	0.000		45562.97	634.180	-	-	0.000	
34547	666.717	-	-	0.000		45562.97	787.846	-	-	0.000	
34547	731.182	-	-	0.000							
34547	740.086	-	-	0.000		45978	376.005	0.942	0.066	0.995	
						45978	503.078	0.058	0.012	0.004	w
34556	296.936	0.809	0.053	0.528		45978	599.894	-	-	0.000	
34556	378.668	0.191	0.014	0.399	w						
34556	601.221	-	-	0.002		46313.57	217.808	0.252	0.020	0.350	

34556	666.344	-	-	0.072		46313.57	219.184	0.234	0.019	0.364	
						46313.57	220.072	0.080	0.017	0.089	
34692	294.134	0.041	0.009	0.045		46313.57	259.087	0.002	0.000	0.011	w
34692	295.736	0.125	0.010	0.142		46313.57	260.829	-	-	0.003	
34692	296.526	0.211	0.017	0.093	s	46313.57	261.984	-	-	0.000	
34692	374.336	0.285	0.021	0.208		46313.57	296.187	-	-	0.000	
34692	376.719	0.338	0.025	0.512		46313.57	299.807	-	-	0.000	
34692	460.200	-	-	0.001		46313.57	347.565	0.182	0.015	0.082	w
34692	589.280	-	-	0.000		46313.57	349.714	0.032	0.007	0.063	
34692	596.324	-	-	0.000		46313.57	352.183	0.027	0.006	0.030	w
34692	612.802	-	-	0.000		46313.57	357.867	0.008	0.002	0.005	w
34692	660.334	-	-	0.000		46313.57	373.571	-	-	0.000	
34692	682.204	-	-	0.000		46313.57	392.985	-	-	0.000	
34692	732.230	-	-	0.000		46313.57	395.542	0.005	0.001	0.000	w
						46313.57	415.439	0.076	0.016	0.000	
34782	287.417	0.012	0.002	0.016		46313.57	425.861	-	-	0.002	
34782	358.911	0.024	0.005	0.004	w	46313.57	427.838	0.008	0.002	0.000	w
34782	364.784	0.359	0.024	0.357		46313.57	454.877	0.007	0.001	0.000	w
34782	438.354	0.596	0.039	0.612		46313.57	454.939	0.027	0.006	0.000	
34782	649.498	0.006	0.001	0.009	w	46313.57	464.089	-	-	0.000	
34782	659.387	-	-	0.001		46313.57	497.656	-	-	0.000	
34782	666.742	0.001	0.000	0.000	w	46313.57	502.193	0.016	0.003	0.001	w
34782	706.953	0.001	0.000	0.000	w	46313.57	507.735	-	-	0.000	
34782	765.094	-	-	0.000		46313.57	532.601	-	-	0.000	
34782	782.056	-	-	0.000		46313.57	564.529	-	-	0.000	
						46313.57	588.296	-	-	0.000	
34844	358.120	1.000	0.066	1.000		46313.57	589.570	0.044	0.009	0.000	w
34844	646.912	-	-	0.000		46313.57	590.094	-	-	0.000	
34844	656.722	-	-	0.000							
34844	761.509	-	-	0.000		46982.34	249.587	0.240	0.018	0.216	
						46982.34	362.318	0.145	0.011	0.310	
35257	283.546	-	-	0.010		46982.34	365.375	0.022	0.004	0.019	w
35257	286.931	0.045	0.009	0.016		46982.34	395.667	0.502	0.034	0.363	
35257	352.894	0.009	0.002	0.000	w	46982.34	430.937	0.070	0.014	0.076	s
35257	358.571	0.082	0.016	0.042		46982.34	478.875	0.022	0.004	0.014	w
35257	363.146	0.525	0.035	0.581		46982.34	484.565	-	-	0.001	
35257	429.412	0.073	0.014	0.035		46982.34	550.435	-	-	0.000	
35257	440.475	0.260	0.019	0.310		46982.34	565.795	-	-	0.000	
35257	564.587	-	-	0.000							
35257	639.360	0.008	0.001	0.005	d	47005.51	361.500	0.155	0.016	0.000	w
35257	646.273	-	-	0.001		47005.51	364.287	0.031	0.008	0.000	w

35257	683.983	-	-	0.000		47005.51	410.476	0.059	0.015	0.000	w
35257	695.082	-	-	0.000		47005.51	413.797	0.061	0.016	0.000	w
35257	738.262	-	-	0.000		47005.51	416.396	0.206	0.021	0.000	b
35257	754.043	-	-	0.000		47005.51	429.173	0.054	0.014	0.000	w
35257	768.553	-	-	0.000		47005.51	473.677	0.268	0.024	0.153	
						47005.51	496.609	0.167	0.017	0.098	
35379	282.569	0.065	0.012	0.001		47005.51	503.925	-	-	0.017	
35379	351.382	0.041	0.008	0.036		47005.51	636.837	-	-	0.000	
35379	357.010	0.569	0.038	0.717		47005.51	718.731	-	-	0.276	
35379	427.176	0.325	0.021	0.241		47005.51	751.102	-	-	0.427	
35379	625.255	-	-	0.003		47005.51	771.036	-	-	0.028	
35379	634.415	-	-	0.000							
35379	641.220	-	-	0.000		47171.48	215.993	0.261	0.020	0.171	w
35379	678.326	0.001	0.000	0.000	d	47171.48	256.223	-	-	0.141	
35379	731.677	-	-	0.000		47171.48	341.851	0.521	0.040	0.676	
35379	747.174	-	-	0.000		47171.48	361.966	0.033	0.007	0.005	w
						47171.48	412.686	0.148	0.013	0.006	w
35612	280.725	-	-	0.000		47171.48	446.314	-	-	0.001	
35612	284.042	-	-	0.004		47171.48	481.445	-	-	0.000	
35612	286.386	0.016	0.003	0.004	s	47171.48	509.322	-	-	0.000	
35612	354.071	-	-	0.001		47171.48	560.023	0.037	0.008	0.000	w
35612	358.532	0.199	0.015	0.129							
35612	361.877	0.548	0.037	0.730		47812.12	209.086	-	-	0.006	
35612	422.975	0.009	0.002	0.000	w	47812.12	210.921	0.075	0.015	0.002	b
35612	433.705	0.018	0.003	0.010		47812.12	244.521	0.151	0.012	0.017	
35612	441.512	0.194	0.014	0.119		47812.12	247.234	0.386	0.027	0.402	
35612	553.512	0.008	0.002	0.000	w	47812.12	249.401	0.094	0.007	0.057	
35612	558.984	-	-	0.000		47812.12	278.968	0.040	0.008	0.010	w
35612	580.106	-	-	0.000		47812.12	283.595	-	-	0.065	
35612	631.802	-	-	0.001		47812.12	330.353	0.013	0.003	0.007	s
35612	667.796	0.006	0.001	0.000	s	47812.12	354.620	0.014	0.003	0.009	w
35612	678.371	-	-	0.000		47812.12	356.737	0.016	0.003	0.019	w
35612	686.029	-	-	0.000		47812.12	367.935	-	-	0.003	
35612	734.417	-	-	0.000		47812.12	371.122	0.034	0.007	0.177	w
35612	748.174	-	-	0.000		47812.12	383.086	0.019	0.004	0.026	w
35612	782.668	0.002	0.000	0.000	d	47812.12	387.292	-	-	0.047	
						47812.12	391.084	0.006	0.001	0.067	w
35768	279.501	0.090	0.017	0.000		47812.12	416.055	0.007	0.001	0.003	w
35768	282.789	0.018	0.003	0.000		47812.12	421.941	0.133	0.010	0.004	
35768	346.650	0.003	0.000	0.000	w	47812.12	425.895	-	-	0.021	
35768	352.126	0.072	0.014	0.034		47812.12	430.219	0.013	0.003	0.039	w

35768	356.538	0.294	0.022	0.451		47812.12	463.109	-	-	0.000	
35768	420.203	0.112	0.008	0.099		47812.12	465.829	-	-	0.002	
35768	430.790	0.403	0.027	0.408		47812.12	471.911	-	-	0.003	
35768	548.774	-	-	0.000		47812.12	526.386	-	-	0.011	
35768	619.156	0.005	0.001	0.006	w	47812.12	542.140	-	-	0.000	
35768	625.636	0.001	0.000	0.001	w	47812.12	554.995	-	-	0.002	
35768	660.911	-	-	0.000		47812.12	669.227	-	-	0.001	
35768	671.268	0.002	0.000	0.000	w	47812.12	694.282	-	-	0.001	
35768	711.455	-	-	0.000							
35768	726.099	-	-	0.000		48231.27	207.268	-	-	0.008	
35768	739.543	-	-	0.000		48231.27	242.040	0.024	0.005	0.127	w
						48231.27	244.697	-	-	0.029	
35856	282.080	0.017	0.004	0.000	b	48231.27	275.742	0.223	0.019	0.209	
35856	284.392	0.144	0.012	0.002		48231.27	346.628	-	-	0.023	
35856	285.890	0.015	0.003	0.002	s	48231.27	349.425	0.012	0.003	0.005	w
35856	355.412	0.196	0.016	0.004	w	48231.27	351.480	-	-	0.010	
35856	358.698	0.160	0.013	0.160		48231.27	362.345	0.147	0.013	0.226	
35856	360.886	0.438	0.032	0.830		48231.27	377.030	0.063	0.014	0.116	w
35856	429.147	0.007	0.001	0.000	w	48231.27	381.104	0.057	0.013	0.075	b
35856	436.790	0.011	0.002	0.002	b	48231.27	408.922	0.014	0.003	0.027	w
35856	546.111	-	-	0.000		48231.27	414.607	-	-	0.034	
35856	551.437	-	-	0.000		48231.27	422.596	0.146	0.013	0.092	w
35856	557.600	0.013	0.003	0.000	b	48231.27	451.843	-	-	0.001	
35856	571.982	-	-	0.000		48231.27	456.906	-	-	0.000	
35856	613.179	-	-	0.000		48231.27	462.755	-	-	0.002	
35856	667.287	-	-	0.000		48231.27	515.020	-	-	0.009	
35856	674.695	-	-	0.000		48231.27	528.443	-	-	0.004	
35856	734.715	-	-	0.000		48231.27	542.374	0.314	0.025	0.002	w
35856	767.951	-	-	0.000		48231.27	650.961	-	-	0.001	
35856	774.405	-	-	0.000							
						48382.6	206.620	0.048	0.010	0.000	w
36079	277.085	0.048	0.010	0.000	b	48382.6	241.156	-	-	0.007	
36079	280.317	0.048	0.010	0.000	w	48382.6	243.794	-	-	0.000	
36079	282.600	0.024	0.005	0.000		48382.6	274.596	-	-	0.004	
36079	348.301	0.021	0.004	0.001	w	48382.6	344.819	0.023	0.005	0.000	w
36079	352.617	0.197	0.015	0.021		48382.6	347.586	-	-	0.006	
36079	355.852	0.133	0.010	0.084		48382.6	349.619	-	-	0.000	
36079	414.767	0.010	0.002	0.006	w	48382.6	360.368	0.026	0.005	0.003	w
36079	425.079	0.135	0.010	0.149		48382.6	374.891	-	-	0.005	
36079	432.576	0.374	0.026	0.723		48382.6	378.918	0.013	0.003	0.031	w
36079	539.539	-	-	0.000		48382.6	406.406	-	-	0.000	

36079	544.737	-	-	0.000		48382.6	412.021	0.043	0.009	0.033	w
36079	564.777	-	-	0.000		48382.6	419.910	0.693	0.049	0.833	
36079	613.662	0.007	0.001	0.015	w	48382.6	448.774	0.015	0.003	0.001	w
36079	647.563	0.003	0.001	0.000	w	48382.6	453.767	0.026	0.005	0.001	w
36079	657.502	-	-	0.000		48382.6	459.536	0.026	0.005	0.007	w
36079	664.693	-	-	0.000		48382.6	511.036	0.054	0.011	0.016	w
36079	710.020	-	-	0.000		48382.6	524.249	0.033	0.007	0.043	w
36079	722.870	-	-	0.000		48382.6	537.957	-	-	0.009	
36079	755.019	-	-	0.000		48382.6	644.610	-	-	0.000	
36686	272.502	0.218	0.016	0.002		49434.16	235.190	0.083	0.017	0.002	w
36686	275.627	0.194	0.014	0.004		49434.16	332.750	-	-	0.000	
36686	335.949	0.008	0.001	0.000	w	49434.16	335.326	0.017	0.004	0.000	w
36686	341.090	0.002	0.000	0.001	w	49434.16	360.668	0.782	0.057	0.953	
36686	345.228	0.004	0.001	0.006	w	49434.16	389.745	0.036	0.008	0.022	w
36686	404.581	0.439	0.029	0.824		49434.16	428.544	0.062	0.013	0.021	w
36686	414.387	0.131	0.010	0.146		49434.16	433.095	-	-	0.002	
36686	522.430	-	-	0.000		49434.16	484.967	-	-	0.001	
36686	585.827	-	-	0.000		49434.16	496.851	0.019	0.004	0.000	w
36686	591.625	-	-	0.000							
36686	623.073	-	-	0.010		49477.1	437.449	0.183	0.020	0.053	w
36686	632.269	-	-	0.001		49477.1	478.966	0.606	0.060	0.824	w
36686	667.799	0.003	0.001	0.005	w	49477.1	496.870	0.211	0.021	0.088	w
36686	680.685	-	-	0.000		49477.1	636.289	-	-	0.035	
36686	692.486	-	-	0.000							
36686	774.827	-	-	0.002		49726.98	201.033	-	-	0.000	
36686.16	795.494	0.002	0.000	0.000	d	49726.98	202.729	-	-	0.000	
						49726.98	233.580	-	-	0.000	
36766.96	271.903	0.549	0.037	0.757		49726.98	236.054	-	-	0.002	
36766.96	275.014	0.293	0.022	0.213		49726.98	238.029	-	-	0.000	
36766.96	277.211	0.076	0.015	0.019		49726.98	264.817	0.014	0.003	0.005	w
36766.96	340.152	0.004	0.001	0.004	w	49726.98	268.983	0.100	0.008	0.083	w
36766.96	344.267	0.002	0.000	0.001	w	49726.98	310.693	-	-	0.000	
36766.96	347.350	-	-	0.000		49726.98	332.065	0.031	0.006	0.004	w
36766.96	403.263	0.006	0.001	0.001	b	49726.98	333.920	0.029	0.006	0.002	s
36766.96	413.004	-	-	0.000		49726.98	343.711	0.019	0.004	0.000	s
36766.96	420.078	0.056	0.011	0.000		49726.98	346.491	-	-	0.014	
36766.96	520.234	0.007	0.001	0.003	w	49726.98	356.898	0.109	0.008	0.024	
36766.96	525.065	0.006	0.001	0.002	w	49726.98	360.545	0.372	0.026	0.521	
36766.96	543.659	-	-	0.000		49726.98	363.830	0.187	0.014	0.213	
36766.96	588.810	-	-	0.000		49726.98	385.346	0.009	0.002	0.004	w

36766.96	619.951	-	-	0.000		49726.98	390.390	0.062	0.012	0.079
36766.96	629.055	-	-	0.000		49726.98	393.772	-	-	0.006
36766.96	635.634	-	-	0.000		49726.98	397.465	0.013	0.003	0.002 w
36766.96	676.961	-	-	0.000		49726.98	425.376	-	-	0.000
36766.96	688.632	-	-	0.000		49726.98	427.670	0.046	0.009	0.003
36766.96	717.747	-	-	0.000		49726.98	432.791	-	-	0.006
36766.96	790.412	-	-	0.000		49726.98	478.174	-	-	0.000
						49726.98	491.139	0.008	0.002	0.000 w
37157.56	272.090	0.279	0.021	0.557		49726.98	501.666	-	-	0.000
37157.56	274.241	0.294	0.022	0.331		49726.98	612.791	-	-	0.031
37157.56	275.633	0.268	0.020	0.106		49726.98	784.013	-	-	0.000
37157.56	339.698	0.002	0.000	0.001	w	49726.98	788.363	-	-	0.000
37157.56	342.699	0.111	0.008	0.001						
37157.56	344.695	-	-	0.000		50342.14	322.579	0.655	0.044	0.575
37157.56	406.445	0.012	0.002	0.000	b	50342.14	361.016	0.307	0.021	0.318
37157.56	413.294	0.022	0.004	0.000		50342.14	363.582	0.030	0.006	0.008 w
37157.56	509.870	0.007	0.001	0.001	w	50342.14	426.000	-	-	0.100
37157.56	514.509	-	-	0.000		50342.14	600.552	-	-	0.000
37157.56	519.871	0.002	0.000	0.002	w	50342.14	642.507	0.008	0.002	0.000 b
37157.56	532.351	-	-	0.000		50342.14	645.058	-	-	0.000
37157.56	567.860	-	-	0.000						
37157.56	613.965	-	-	0.000		50377.91	322.207	0.434	0.029	0.255
37157.56	620.231	-	-	0.000		50377.91	324.419	0.208	0.016	0.291
37157.56	670.590	-	-	0.000		50377.91	360.550	0.334	0.023	0.156
37157.56	698.169	-	-	0.000		50377.91	363.110	-	-	0.165
37157.56	703.499	0.003	0.001	0.000	w	50377.91	365.110	-	-	0.006
37157.56	779.707	-	-	0.000		50377.91	374.896	-	-	0.127
37157.56	779.890	-	-	0.000		50377.91	408.416	0.007	0.001	0.000 w
						50377.91	425.351	-	-	0.000
37162.74	269.007	0.014	0.003	0.002	w	50377.91	430.707	0.017	0.003	0.000 w
37162.74	272.052	0.009	0.002	0.000	w	50377.91	578.477	-	-	0.000
37162.74	274.202	-	-	0.002						
37162.74	335.632	0.003	0.001	0.000	w	50423.14	321.738	0.082	0.007	0.178
37162.74	339.638	-	-	0.000		50423.14	323.943	0.284	0.023	0.403
37162.74	342.638	0.014	0.003	0.004	s	50423.14	325.999	0.026	0.006	0.010 w
37162.74	396.926	0.166	0.013	0.217		50423.14	362.514	0.074	0.017	0.025 w
37162.74	406.359	0.627	0.043	0.639		50423.14	364.508	0.084	0.008	0.009 w
37162.74	413.206	0.152	0.012	0.118		50423.14	366.033	0.023	0.005	0.001 w
37162.74	509.735	0.008	0.002	0.000	w	50423.14	374.262	0.045	0.010	0.085 w
37162.74	514.372	0.001	0.000	0.000	w	50423.14	380.956	0.039	0.009	0.012 w
37162.74	532.204	-	-	0.000		50423.14	407.663	0.123	0.011	0.157

37162.74	575.397	-	-	0.000		50423.14	411.695	-	-	0.001	
37162.74	605.100	-	-	0.000		50423.14	424.534	0.033	0.008	0.036	w
37162.74	613.769	0.007	0.001	0.009	w	50423.14	429.870	-	-	0.001	
37162.74	620.031	-	-	0.001		50423.14	434.124	-	-	0.001	
37162.74	659.291	-	-	0.005		50423.14	467.885	0.050	0.012	0.060	
37162.74	670.357	-	-	0.000		50423.14	522.979	0.021	0.005	0.000	w
37162.74	697.916	-	-	0.000		50423.14	523.400	0.110	0.010	0.000	w
37162.74	766.429	-	-	0.003		50423.14	576.967	-	-	0.002	
37162.74	779.392	-	-	0.000		50423.14	590.992	-	-	0.000	
37162.74	779.575	-	-	0.000		50423.14	597.644	-	-	0.000	
37162.74	794.183	-	-	0.000		50423.14	610.197	-	-	0.000	
						50423.14	639.180	-	-	0.000	
37409.54	272.358	0.368	0.025	0.347		50423.14	659.196	0.007	0.002	0.000	d
37409.54	273.731	0.485	0.032	0.453		50423.14	664.536	-	-	0.000	
37409.54	274.407	0.121	0.009	0.192		50423.14	682.146	-	-	0.000	
37409.54	339.764	0.003	0.001	0.001	w	50423.14	727.762	-	-	0.000	
37409.54	341.726	0.005	0.001	0.000	w	50423.14	732.068	-	-	0.018	
37409.54	409.033	-	-	0.000		50423.14	753.918	-	-	0.000	
37409.54	507.922	0.013	0.002	0.004	w						
37409.54	513.147	-	-	0.001		50522.95	320.708	0.027	0.005	0.016	w
37409.54	525.302	-	-	0.000		50522.95	358.674	-	-	0.246	
37409.54	559.847	0.006	0.001	0.000	w	50522.95	361.207	0.097	0.019	0.098	w
37409.54	575.488	-	-	0.000		50522.95	422.743	0.876	0.059	0.638	
37409.54	610.684	-	-	0.000		50522.95	594.099	-	-	0.001	
37409.54	686.095	-	-	0.000		50522.95	635.127	-	-	0.000	
37409.54	691.242	-	-	0.000		50522.95	637.619	-	-	0.000	
37409.54	696.294	-	-	0.000		50522.95	660.157	-	-	0.000	
37409.54	764.679	-	-	0.000							
37409.54	791.077	-	-	0.000		50651.72	357.024	1.000	0.066	1.000	
						50651.72	632.425	-	-	0.000	
37521.16	269.424	0.004	0.001	0.000	w						
37521.16	271.532	0.513	0.036	0.000	w	50833.43	317.545	0.079	0.015	0.077	
37521.16	272.897	0.046	0.009	0.000		50833.43	319.693	0.398	0.027	0.536	
37521.16	335.552	0.001	0.000	0.000	w	50833.43	354.722	0.035	0.007	0.003	w
37521.16	338.480	0.002	0.000	0.000	w	50833.43	357.200	0.132	0.010	0.146	
37521.16	340.427	0.016	0.003	0.002		50833.43	359.135	0.011	0.002	0.004	w
37521.16	400.524	0.096	0.007	0.206		50833.43	368.600	0.213	0.016	0.153	
37521.16	407.174	0.286	0.020	0.770		50833.43	400.954	0.055	0.011	0.002	
37521.16	500.587	0.030	0.006	0.000	b	50833.43	417.264	0.016	0.003	0.001	w
37521.16	505.058	-	-	0.000		50833.43	422.417	0.061	0.012	0.079	b
37521.16	510.224	-	-	0.000		50833.43	511.990	-	-	0.000	

37521.16	522.239	-	-	0.000		50833.43	595.289	-	-	0.000	
37521.16	556.369	0.003	0.001	0.000	w	50833.43	622.841	-	-	0.000	
37521.16	600.554	-	-	0.000		50833.43	641.832	-	-	0.000	
37521.16	606.548	-	-	0.011		50833.43	646.894	-	-	0.000	
37521.16	654.624	-	-	0.007							
37521.16	680.879	-	-	0.000		50861.32	321.406	0.502	0.037	0.566	
37521.16	685.948	-	-	0.000		50861.32	323.021	0.102	0.008	0.100	
37521.16	758.206	0.001	0.000	0.000	d	50861.32	324.143	0.004	0.001	0.001	w
37521.16	758.379	0.001	0.000	0.002	d	50861.32	360.253	0.051	0.011	0.074	b
37521.16	784.151	-	-	0.000		50861.32	361.315	0.007	0.001	0.010	w
						50861.32	361.999	-	-	0.005	
38175.35	261.871	0.013	0.002	0.002	w	50861.32	374.700	0.073	0.015	0.158	w
38175.35	264.756	0.006	0.001	0.002	w	50861.32	379.336	0.040	0.009	0.007	w
38175.35	266.791	-	-	0.002		50861.32	404.398	0.012	0.003	0.026	w
38175.35	324.597	0.002	0.000	0.000	w	50861.32	407.688	0.101	0.008	0.015	b
38175.35	328.342	0.004	0.001	0.000	w	50861.32	410.024	0.011	0.002	0.008	w
38175.35	331.145	0.001	0.000	0.000	w	50861.32	426.017	-	-	0.004	
38175.35	381.584	0.788	0.053	0.835		50861.32	429.032	0.026	0.006	0.001	w
38175.35	390.295	0.158	0.012	0.137		50861.32	431.007	-	-	0.000	
38175.35	396.606	0.006	0.001	0.009	w	50861.32	458.482	0.026	0.006	0.000	w
38175.35	484.709	-	-	0.000		50861.32	467.327	0.015	0.003	0.018	w
38175.35	488.900	0.007	0.001	0.001	w	50861.32	473.160	0.015	0.003	0.003	w
38175.35	504.982	0.009	0.002	0.009	w	50861.32	511.662	-	-	0.000	
38175.35	543.708	-	-	0.000		50861.32	521.368	-	-	0.000	
38175.35	570.155	0.003	0.001	0.001	w	50861.32	524.616	-	-	0.000	
38175.35	577.846	-	-	0.000		50861.32	576.070	-	-	0.000	
38175.35	583.393	0.002	0.000	0.000	w	50861.32	586.013	0.014	0.003	0.000	w
38175.35	618.020	-	-	0.000		50861.32	591.049	-	-	0.000	
38175.35	627.734	-	-	0.000		50861.32	593.511	-	-	0.000	
38175.35	651.837	-	-	0.000		50861.32	612.797	-	-	0.000	
38175.35	711.217	-	-	0.000		50861.32	709.308	-	-	0.001	
38175.35	722.366	0.002	0.000	0.001	w	50861.32	729.526	-	-	0.003	
38175.35	722.522	-	-	0.000		50861.32	743.191	-	-	0.000	
38175.35	735.054	-	-	0.000							
						50967.83	316.195	0.085	0.016	0.062	
38678.03	261.277	-	-	0.003		50967.83	353.039	0.072	0.014	0.017	w
38678.03	263.259	-	-	0.011		50967.83	355.493	0.805	0.053	0.902	
38678.03	264.542	0.025	0.005	0.005	b	50967.83	414.937	0.037	0.007	0.019	w
38678.03	323.009	0.045	0.009	0.000		50967.83	620.026	-	-	0.000	
38678.03	325.721	0.010	0.002	0.000	s						
38678.03	327.524	-	-	0.000		51604.1	312.003	-	-	0.001	

38678.03	382.782	0.622	0.042	0.767		51604.1	313.910	-	-	0.006	
38678.03	388.851	0.201	0.015	0.190		51604.1	315.450	-	-	0.083	
38678.03	473.176	0.005	0.001	0.000	w	51604.1	349.460	0.012	0.003	0.000	w
38678.03	477.170	-	-	0.000		51604.1	350.861	0.047	0.010	0.005	w
38678.03	481.778	-	-	0.000		51604.1	351.868	0.037	0.008	0.021	w
38678.03	492.477	0.008	0.002	0.002	w	51604.1	358.415	0.025	0.005	0.011	w
38678.03	522.715	0.084	0.016	0.014		51604.1	364.550	-	-	0.033	
38678.03	561.530	-	-	0.006		51604.1	368.937	0.235	0.020	0.261	
38678.03	566.767	-	-	0.000		51604.1	388.933	0.029	0.006	0.001	w
38678.03	608.526	-	-	0.000		51604.1	392.601	0.117	0.010	0.090	
38678.03	631.150	-	-	0.000		51604.1	395.702	-	-	0.212	
38678.03	635.503	-	-	0.001		51604.1	409.095	0.010	0.002	0.013	w
38678.03	697.047	-	-	0.000		51604.1	412.946	0.030	0.007	0.008	w
38678.03	697.193	-	-	0.000		51604.1	415.778	0.066	0.014	0.205	w
38678.03	718.915	-	-	0.000		51604.1	443.378	0.092	0.008	0.035	b
						51604.1	451.645	-	-	0.001	
38995.73	261.075	-	-	0.003		51604.1	492.550	-	-	0.000	
38995.73	262.337	0.167	0.012	0.010		51604.1	501.925	-	-	0.000	
38995.73	262.957	0.382	0.026	0.007		51604.1	504.934	-	-	0.000	
38995.73	322.384	-	-	0.000		51604.1	513.465	0.021	0.005	0.000	w
38995.73	324.150	0.003	0.000	0.000	w	51604.1	540.152	-	-	0.000	
38995.73	384.105	0.422	0.028	0.969		51604.1	552.425	-	-	0.001	
38995.73	470.042	0.006	0.001	0.000	w	51604.1	561.562	0.238	0.020	0.004	
38995.73	474.513	0.011	0.002	0.000	w	51604.1	566.185	-	-	0.000	
38995.73	484.888	-	-	0.000		51604.1	569.169	0.011	0.002	0.000	w
38995.73	514.174	-	-	0.004		51604.1	578.699	-	-	0.000	
38995.73	527.337	0.009	0.002	0.004	w	51604.1	586.111	0.011	0.002	0.001	w
38995.73	556.739	-	-	0.001		51604.1	625.121	-	-	0.000	
38995.73	618.740	-	-	0.000		51604.1	631.277	-	-	0.000	
38995.73	622.923	-	-	0.000		51604.1	643.955	-	-	0.000	
38995.73	627.022	-	-	0.001		51604.1	670.149	-	-	0.000	
38995.73	681.941	-	-	0.000		51604.1	673.798	-	-	0.005	
38995.73	702.858	-	-	0.000		51604.1	692.016	0.008	0.002	0.000	w
38995.73	719.012	-	-	0.000		51604.1	692.265	-	-	0.000	
38995.73	794.109	-	-	0.001		51604.1	744.466	0.011	0.002	0.000	w
						51604.1	773.418	-	-	0.000	
39625.8	252.285	0.503	0.033	0.751							
39625.8	254.961	-	-	0.093							
39625.8	305.745	0.217	0.016	0.112		52431.42	219.696	-	-	0.002	
39625.8	309.997	0.107	0.008	0.027		52431.42	302.564	0.442	0.040	0.498	s
39625.8	313.411	0.007	0.001	0.003	w	52431.42	304.693	0.068	0.018	0.004	w

39625.8	361.566	-	-	0.000		52431.42	325.473	-	-	0.024	
39625.8	369.378	0.098	0.019	0.000		52431.42	348.967	0.053	0.014	0.058	w
39625.8	452.861	0.066	0.013	0.014		52431.42	379.752	0.363	0.033	0.409	
39625.8	499.741	-	-	0.000		52431.42	383.321	0.066	0.017	0.004	
39625.8	503.954	-	-	0.000		52431.42	423.404	-	-	0.000	
39625.8	526.594	-	-	0.000		52431.42	432.434	0.007	0.002	0.000	w
39625.8	533.148	-	-	0.000							
39625.8	558.190	-	-	0.000		52512.45	224.515	0.016	0.003	0.001	w
39625.8	567.165	-	-	0.000		52512.45	225.370	0.015	0.003	0.006	w
39625.8	575.335	-	-	0.000		52512.45	252.808	-	-	0.013	
39625.8	631.052	-	-	0.000		52512.45	287.392	0.057	0.012	0.001	w
39625.8	644.693	0.002	0.000	0.000	w	52512.45	289.057	0.006	0.001	0.000	w
39625.8	653.968	-	-	0.000		52512.45	292.875	-	-	0.026	
39625.8	664.218	-	-	0.000		52512.45	303.310	0.010	0.002	0.028	w
39625.8	746.017	-	-	0.000		52512.45	307.843	0.265	0.020	0.114	
39625.8	753.102	-	-	0.000		52512.45	317.636	0.014	0.003	0.062	w
39625.8	769.126	-	-	0.000		52512.45	336.897	-	-	0.005	
						52512.45	338.133	-	-	0.013	
39969.84	250.113	0.203	0.015	0.179		52512.45	339.338	0.040	0.009	0.012	w
39969.84	252.744	0.321	0.021	0.495		52512.45	354.802	0.053	0.011	0.065	w
39969.84	254.598	0.173	0.013	0.177		52512.45	360.382	0.023	0.005	0.112	w
39969.84	306.724	0.152	0.011	0.090		52512.45	364.582	0.147	0.012	0.380	w
39969.84	310.067	0.062	0.012	0.036		52512.45	382.945	0.030	0.006	0.017	w
39969.84	312.565	0.025	0.005	0.005		52512.45	386.159	-	-	0.053	
39969.84	357.122	0.013	0.003	0.000	b	52512.45	400.376	0.033	0.007	0.048	w
39969.84	364.741	-	-	0.000		52512.45	418.155	0.291	0.022	0.033	
39969.84	370.247	-	-	0.000		52512.45	431.054	-	-	0.002	
39969.84	445.912	0.022	0.004	0.007		52512.45	431.738	-	-	0.001	
39969.84	449.456	0.021	0.004	0.009		52512.45	533.266	-	-	0.004	
39969.84	463.012	0.004	0.001	0.000	w	52512.45	559.265	-	-	0.003	
39969.84	495.363	-	-	0.000		52512.45	642.006	-	-	0.001	
39969.84	517.220	-	-	0.000							
39969.84	523.542	0.003	0.000	0.000	w	52513.55	219.301	0.021	0.005	0.000	w
39969.84	528.091	-	-	0.000		52513.55	301.814	0.009	0.002	0.010	w
39969.84	556.306	-	-	0.000		52513.55	303.932	0.010	0.002	0.014	w
39969.84	564.164	-	-	0.000		52513.55	324.605	0.008	0.002	0.001	w
39969.84	583.557	-	-	0.000		52513.55	347.969	-	-	0.004	
39969.84	630.699	-	-	0.000		52513.55	378.571	0.098	0.008	0.012	w
39969.84	639.451	-	-	0.000		52513.55	382.118	0.482	0.036	0.609	
39969.84	639.574	-	-	0.000		52513.55	421.936	0.289	0.021	0.330	
39969.84	649.374	-	-	0.000		52513.55	430.903	0.082	0.017	0.019	w

39969.84	727.343	-	-	0.000						
39969.84	749.076	-	-	0.000		52613.08	218.823	-	-	0.000
39969.84	749.293	-	-	0.000		52613.08	220.992	-	-	0.000
						52613.08	246.008	-	-	0.006
40052.03	252.219	0.093	0.019	0.726		52613.08	300.909	0.024	0.005	0.056
40052.03	254.066	0.519	0.036	0.024		52613.08	303.015	0.121	0.009	0.400
40052.03	255.261	0.012	0.002	0.077	w	52613.08	304.559	0.007	0.001	0.006 w
40052.03	309.278	0.097	0.007	0.081	s	52613.08	312.683	0.007	0.001	0.001 w
40052.03	311.764	0.031	0.006	0.044	b	52613.08	323.559	-	-	0.006
40052.03	313.415	0.023	0.005	0.005	w	52613.08	326.554	0.050	0.010	0.018
40052.03	363.650	0.049	0.010	0.000	w	52613.08	346.768	0.004	0.001	0.001 w
40052.03	369.124	-	-	0.000		52613.08	350.847	0.016	0.003	0.047
40052.03	444.283	-	-	0.036		52613.08	356.552	0.610	0.041	0.000
40052.03	447.802	-	-	0.004		52613.08	377.149	-	-	0.005
40052.03	451.858	-	-	0.002		52613.08	380.670	0.132	0.010	0.450
40052.03	461.256	-	-	0.000		52613.08	384.721	-	-	0.002
40052.03	487.679	-	-	0.000		52613.08	420.171	-	-	0.000
40052.03	521.298	-	-	0.000		52613.08	429.062	0.009	0.002	0.000 w
40052.03	525.808	-	-	0.000		52613.08	438.201	-	-	0.000
40052.03	561.560	0.168	0.013	0.000		52613.08	506.458	0.020	0.004	0.002 w
40052.03	580.771	-	-	0.000		52613.08	642.202	-	-	0.000
40052.03	584.455	-	-	0.000						
40052.03	636.107	-	-	0.000		52655	300.530	0.030	0.006	0.024 w
40052.03	636.229	-	-	0.000		52655	376.554	0.928	0.063	0.976
40052.03	654.269	-	-	0.000		52655	428.292	0.042	0.008	0.000 w
40052.03	723.020	-	-	0.000						
40052.03	732.637	-	-	0.000		53093.52	216.545	0.021	0.004	0.000 w
40052.03	744.491	0.007	0.001	0.000	w	53093.52	296.620	0.126	0.009	0.004 w
						53093.52	298.665	0.022	0.004	0.008 w
40207.09	248.637	0.433	0.029	0.373		53093.52	318.605	-	-	0.001
40207.09	251.237	0.110	0.008	0.536		53093.52	341.084	0.007	0.001	0.000 w
40207.09	253.069	0.086	0.017	0.015	w	53093.52	370.435	0.117	0.009	0.001
40207.09	304.508	0.016	0.003	0.032	b	53093.52	373.831	0.201	0.015	0.343
40207.09	307.802	0.004	0.001	0.014	w	53093.52	411.854	0.433	0.029	0.526
40207.09	310.264	-	-	0.002		53093.52	420.394	0.072	0.014	0.118
40207.09	354.121	0.268	0.020	0.000						
40207.09	361.611	-	-	0.000		53169.17	295.612	-	-	0.000
40207.09	367.022	0.034	0.007	0.000		53169.17	327.573	0.042	0.009	0.000 w
40207.09	441.243	0.006	0.001	0.004	w	53169.17	329.684	0.026	0.005	0.000 w
40207.09	444.713	0.020	0.004	0.025	w	53169.17	380.198	-	-	0.053
40207.09	457.980	-	-	0.000		53169.17	513.368	0.423	0.031	0.411 w

40207.09	489.607	-	-	0.000		53169.17	543.719	-	-	0.001	
40207.09	510.949	-	-	0.000		53169.17	545.544	0.509	0.037	0.515	w
40207.09	517.117	-	-	0.000		53169.17	561.959	-	-	0.005	
40207.09	521.555	0.021	0.004	0.000		53169.17	774.269	-	-	0.016	
40207.09	549.058	-	-	0.000							
40207.09	556.711	-	-	0.000		53229.94	220.954	-	-	0.000	
40207.09	575.586	-	-	0.000		53229.94	221.782	-	-	0.000	
40207.09	629.893	0.002	0.000	0.000	w	53229.94	248.302	-	-	0.018	
40207.09	630.012	-	-	0.000		53229.94	281.584	-	-	0.000	
40207.09	715.002	-	-	0.000		53229.94	283.182	-	-	0.004	
40207.09	735.992	-	-	0.000		53229.94	286.845	0.056	0.012	0.237	
						53229.94	296.848	0.010	0.002	0.022	w
40231.33	251.084	0.156	0.012	0.343		53229.94	301.189	0.013	0.003	0.000	w
40231.33	252.914	0.417	0.028	0.256		53229.94	310.556	0.040	0.008	0.000	w
40231.33	254.097	0.216	0.016	0.243		53229.94	328.943	0.037	0.008	0.003	w
40231.33	307.572	0.103	0.008	0.077		53229.94	330.122	0.011	0.002	0.045	w
40231.33	310.030	0.047	0.009	0.057		53229.94	331.270	0.017	0.004	0.023	w
40231.33	311.663	0.019	0.004	0.007		53229.94	345.991	0.070	0.015	0.118	w
40231.33	361.294	0.001	0.000	0.000	w	53229.94	351.296	0.052	0.011	0.020	w
40231.33	366.696	-	-	0.000		53229.94	355.285	0.037	0.008	0.084	w
40231.33	440.771	0.004	0.001	0.002	w	53229.94	372.702	0.232	0.019	0.000	
40231.33	444.234	0.018	0.003	0.010		53229.94	375.745	0.059	0.012	0.079	w
40231.33	448.225	0.006	0.001	0.004	w	53229.94	389.193	0.073	0.015	0.266	
40231.33	457.472	-	-	0.000		53229.94	405.971	0.016	0.003	0.055	w
40231.33	483.451	-	-	0.000		53229.94	418.119	-	-	0.006	
40231.33	516.469	0.005	0.001	0.000	w	53229.94	418.762	0.254	0.020	0.010	b
40231.33	520.896	0.007	0.001	0.000	w	53229.94	513.609	0.006	0.001	0.004	w
40231.33	555.960	-	-	0.000		53229.94	537.683	-	-	0.003	
40231.33	574.784	-	-	0.000		53229.94	613.727	0.016	0.003	0.005	w
40231.33	578.392	-	-	0.000							
40231.33	628.932	-	-	0.000		53275.16	326.439	0.098	0.019	0.000	w
40231.33	629.051	-	-	0.000		53275.16	542.407	0.902	0.061	1.000	w
40231.33	646.681	-	-	0.000							
40231.33	713.764	-	-	0.000		60172.06	207.421	0.005	0.001	0.000	w
40231.33	723.135	-	-	0.000		60172.06	209.968	-	-	0.000	
40231.33	734.681	-	-	0.000		60172.06	234.549	0.054	0.011	0.000	
40231.33	787.909	-	-	0.000		60172.06	246.528	0.074	0.015	0.000	
						60172.06	247.549	0.022	0.004	0.058	
40491.27	252.429	0.691	0.046	0.846		60172.06	252.890	-	-	0.000	
40491.27	309.158	0.253	0.018	0.135		60172.06	254.392	0.062	0.012	0.727	
40491.27	443.061	0.057	0.011	0.019		60172.06	259.958	0.682	0.047	0.032	

40491.27	477.449	-	-	0.000		60172.06	261.888	-	-	0.097	
40491.27	569.822	-	-	0.000		60172.06	263.616	0.002	0.000	0.015	w
40491.27	635.987	-	-	0.000		60172.06	274.731	-	-	0.011	
40491.27	709.789	-	-	0.000		60172.06	277.286	0.002	0.000	0.011	w
40491.27	772.092	-	-	0.000		60172.06	278.988	0.008	0.002	0.000	
						60172.06	280.837	0.001	0.000	0.001	w
41018.05	246.218	0.047	0.009	0.029	w	60172.06	294.490	0.065	0.013	0.001	w
41018.05	247.978	0.361	0.024	0.350		60172.06	295.588	-	-	0.006	
41018.05	249.116	0.388	0.026	0.576		60172.06	298.025	-	-	0.031	
41018.05	300.303	0.068	0.013	0.013		60172.06	318.866	0.008	0.002	0.000	w
41018.05	302.646	0.048	0.009	0.021		60172.06	324.579	-	-	0.001	
41018.05	304.202	0.042	0.008	0.009		60172.06	329.144	0.003	0.001	0.000	w
41018.05	351.305	0.016	0.003	0.001	w	60172.06	366.217	-	-	0.000	
41018.05	356.411	0.013	0.003	0.000	w	60172.06	373.595	0.013	0.003	0.006	w
41018.05	425.995	-	-	0.000		60172.06	430.979	-	-	0.001	
41018.05	429.228	0.006	0.001	0.000	w	60172.06	432.290	-	-	0.002	
41018.05	432.954	0.003	0.001	0.000	w	60172.06	661.599	-	-	0.000	
41018.05	441.575	-	-	0.000							
41018.05	465.732	-	-	0.000		60365.7	243.974	0.359	0.026	0.586	
41018.05	496.298	0.004	0.001	0.000	w	60365.7	245.356	0.106	0.008	0.028	w
41018.05	500.384	0.002	0.000	0.000	w	60365.7	258.655	-	-	0.005	
41018.05	532.656	-	-	0.000		60365.7	273.277	0.020	0.004	0.001	w
41018.05	549.910	0.002	0.000	0.000	w	60365.7	291.802	0.251	0.020	0.367	
41018.05	553.212	-	-	0.000		60365.7	293.905	-	-	0.012	
41018.05	599.272	-	-	0.000		60365.7	316.908	0.009	0.002	0.000	w
41018.05	599.380	-	-	0.000		60365.7	321.940	0.255	0.020	0.000	
41018.05	615.365	-	-	0.000							
41018.05	675.805	-	-	0.000		60754.71	204.943	-	-	0.081	
41018.05	684.200	-	-	0.000		60754.71	207.430	0.010	0.002	0.001	w
41018.05	694.527	-	-	0.000		60754.71	231.386	0.015	0.003	0.000	
41018.05	741.908	-	-	0.000		60754.71	243.036	-	-	0.001	
						60754.71	244.028	0.104	0.008	0.151	w
42784.35	278.811	0.990	0.066	1.000		60754.71	249.217	-	-	0.000	
42784.35	427.336	0.010	0.002	0.000	w	60754.71	250.675	0.054	0.012	0.073	w
42784.35	431.595	-	-	0.000		60754.71	256.078	-	-	0.072	
42784.35	474.507	-	-	0.000		60754.71	257.950	0.038	0.008	0.003	
42784.35	526.149	-	-	0.000		60754.71	259.627	0.007	0.001	0.004	w
42784.35	599.410	-	-	0.000		60754.71	270.401	0.504	0.037	0.332	
42784.35	608.352	-	-	0.000		60754.71	272.876	0.104	0.009	0.067	
42784.35	715.909	-	-	0.000		60754.71	274.524	0.002	0.000	0.001	w
42784.35	742.112	-	-	0.000		60754.71	276.314	0.026	0.005	0.017	w

					60754.71	289.521	0.089	0.019	0.004	
42815.86	426.047	0.392	0.026	0.333	60754.71	290.582	-	-	0.000	
42815.86	429.923	0.159	0.012	0.127	60754.71	292.937	-	-	0.081	
42815.86	495.760	0.290	0.021	0.345	60754.71	313.048	0.003	0.001	0.001	w
42815.86	500.612	0.064	0.012	0.043	60754.71	318.553	0.006	0.001	0.005	w
42815.86	504.421	-	-	0.002	60754.71	322.948	-	-	0.000	
42815.86	523.294	0.096	0.018	0.149	60754.71	358.564	-	-	0.001	
42815.86	590.997	-	-	0.000	60754.71	365.634	0.012	0.003	0.000	w
42815.86	627.128	-	-	0.000	60754.71	420.419	0.027	0.006	0.075	w
42815.86	638.840	-	-	0.000	60754.71	421.666	-	-	0.030	
					60754.71	568.302	-	-	0.000	
42911.91	232.964	-	-	0.005	60754.71	621.807	-	-	0.000	
42911.91	277.822	0.173	0.013	0.223	60754.71	637.035	-	-	0.000	
42911.91	281.329	0.499	0.034	0.772	60754.71	727.115	-	-	0.000	
42911.91	323.158	0.010	0.002	0.001	w	60754.71	747.360	-	-	0.000
42911.91	425.019	0.272	0.020	0.000						
42911.91	429.231	0.014	0.003	0.000	w					
42911.91	432.336	0.022	0.004	0.000	w					
42911.91	448.893	0.009	0.002	0.000	w					
42911.91	471.651	-	-	0.000						
42911.91	478.043	-	-	0.000						
42911.91	522.640	-	-	0.000						
42911.91	531.962	-	-	0.000						
42911.91	545.186	-	-	0.000						
42911.91	594.861	-	-	0.000						
42911.91	603.666	-	-	0.000						
42911.91	613.918	-	-	0.000						
42911.91	709.429	-	-	0.000						
42911.91	735.151	-	-	0.000						
42911.91	762.394	-	-	0.000						

Table 7.3 Fe I Branching ratios and radiative parameters

s emission line has shoulder

w weak emission line

b blended emission line

d emission lie within our spectral gaps

o means the line is lower than our 225 nm efficiency calibration

Kurucz refers to work by Kurucz et al.⁷⁴

Fe II Data

Table 7.4 Fe II radiative properties
s emission line has shoulder
w weak emission line
b blended emission line
o means the line is lower than our 225 nm efficiency calibration
Kurucz refers to work by Kurucz et al.⁷⁴

Upper Energy (cm ⁻¹)	Wavelength (nm)	WSU BR	BR Error	Kurucz BR		Upper Energy (cm ⁻¹)	Wavelength (nm)	WSU BR	BR Error	Kurucz BR	
38660.04	258.588	0.267	0.028	0.322		63465	200.771	-	-	0.077	<i>o</i>
38660.04	261.187	0.335	0.031	0.435		63465	201.709	0.012	0.003	0.070	<i>o</i>
38660.04	263.132	0.350	0.033	0.241		63465	221.639	0.007	0.002	0.001	<i>o</i>
38660.04	271.751	-	-	0.000		63465	224.255	0.021	0.005	0.001	<i>o</i>
38660.04	275.933	0.002	0.000	0.000	<i>w</i>	63465	232.768	-	-	0.000	
38660.04	279.075	0.003	0.001	0.000	<i>w</i>	63465	234.480	-	-	0.001	
38660.04	325.589	0.004	0.001	0.001		63465	237.136	0.007	0.002	0.000	<i>w</i>
38660.04	330.286	0.001	0.000	0.000	<i>w</i>	63465	240.005	-	-	0.003	
38660.04	396.940	0.034	0.008	0.000		63465	243.500	0.274	0.030	0.000	
38660.04	438.178	-	-	0.000		63465	246.682	0.303	0.030	0.546	
38660.04	448.492	-	-	0.000		63465	247.243	0.173	0.019	0.251	
38660.04	551.021	-	-	0.000		63465	249.007	-	-	0.000	
38660.04	559.935	0.001	0.000	0.000	<i>w</i>	63465	265.331	-	-	0.000	
38660.04	560.714	0.001	0.000	0.000	<i>w</i>	63465	267.231	0.063	0.016	0.001	<i>w</i>
38660.04	585.373	0.001	0.000	0.000	<i>w</i>	63465	273.649	-	-	0.003	
38660.04	589.872	-	-	0.000		63465	278.899	-	-	0.000	
38660.04	623.937	-	-	0.000		63465	311.430	0.010	0.002	0.018	
38660.04	630.753	-	-	0.000		63465	311.469	0.008	0.002	0.008	<i>w</i>
38660.04	635.929	-	-	0.000		63465	311.658	0.023	0.006	0.020	
38660.04	651.608	-	-	0.000		63465	315.832	-	-	0.000	
38660.04	777.711	-	-	0.000		63465	365.677	0.008	0.002	0.000	<i>w</i>
38660.04	788.525	-	-	0.000		63465	367.378	0.007	0.002	0.000	<i>w</i>
38660.04	793.142	0.000	0.000	0.000	<i>w</i>	63465	381.022	-	-	0.000	
						63465	395.131	0.024	0.006	0.000	
38858.96	259.837	0.265	0.027	0.520		63465	395.918	0.003	0.001	0.000	<i>w</i>
38858.96	261.762	0.235	0.024	0.174		63465	539.354	-	-	0.000	
38858.96	263.105	0.433	0.040	0.305		63465	695.987	-	-	0.000	
38858.96	274.427	0.018	0.004	0.000		63465	716.229	-	-	0.000	
38858.96	277.534	0.001	0.000	0.000	<i>w</i>	63465	746.665	-	-	0.000	
38858.96	279.704	-	-	0.000		63465	750.413	0.058	0.014	0.000	
38858.96	323.493	-	-	0.000		63465	754.379	-	-	0.000	
38858.96	328.129	0.004	0.001	0.001							
38858.96	331.266	0.002	0.000	0.000	<i>w</i>	63949	207.816	0.018	0.004	0.020	<i>o</i>

38858.96	393.829	0.001	0.000	0.000	w	63949	210.108	-	-	0.000	o
38858.96	396.937	0.043	0.010	0.000		63949	229.243	0.028	0.007	0.004	
38858.96	444.525	-	-	0.000		63949	231.716	-	-	0.000	
38858.96	487.709	-	-	0.000		63949	235.120	0.216	0.023	0.258	
38858.96	545.045	-	-	0.000		63949	235.960	0.161	0.017	0.096	
38858.96	554.527	-	-	0.000		63949	236.688	-	-	0.010	
38858.96	569.613	-	-	0.000		63949	241.989	0.036	0.009	0.004	w
38858.96	583.029	-	-	0.000		63949	243.008	0.386	0.037	0.564	
38858.96	586.454	-	-	0.000		63949	259.528	0.010	0.002	0.008	w
38858.96	622.935	-	-	0.000		63949	262.090	-	-	0.001	
38858.96	627.983	-	-	0.000		63949	263.307	-	-	0.000	
38858.96	631.631	-	-	0.000		63949	264.621	0.010	0.003	0.004	w
38858.96	643.268	-	-	0.000		63949	265.907	0.003	0.001	0.001	w
38858.96	764.821	-	-	0.000		63949	272.891	0.098	0.011	0.027	
38858.96	776.345	-	-	0.000		63949	297.885	0.017	0.004	0.001	w
38858.96	780.820	-	-	0.000		63949	301.260	0.003	0.001	0.000	w
						63949	307.929	0.001	0.000	0.000	w
39013.21	260.709	0.554	0.052	0.649		63949	312.901	0.004	0.001	0.000	w
39013.21	262.041	0.080	0.019	0.014		63949	322.084	-	-	0.000	
39013.21	262.829	0.331	0.031	0.335		63949	327.964	0.005	0.001	0.001	w
39013.21	276.350	-	-	0.000		63949	328.339	0.004	0.001	0.000	w
39013.21	278.502	-	-	0.000		63949	724.893	-	-	0.000	
39013.21	326.476	0.004	0.001	0.000	w	63949	726.492	-	-	0.000	
39013.21	329.582	0.004	0.001	0.001	w						
39013.21	331.399	-	-	0.000		64041	207.419	0.009	0.003	0.043	o
39013.21	391.450	-	-	0.000		64041	209.702	-	-	0.012	o
39013.21	394.521	0.004	0.001	0.000	w	64041	229.688	0.015	0.005	0.023	s
39013.21	398.161	0.009	0.002	0.000	w	64041	231.222	-	-	0.005	
39013.21	484.066	-	-	0.000		64041	231.355	0.005	0.001	0.001	w
39013.21	496.721	-	-	0.000		64041	235.448	0.148	0.020	0.280	
39013.21	540.500	0.014	0.003	0.000	w	64041	236.173	0.075	0.023	0.078	
39013.21	549.823	-	-	0.000		64041	241.451	-	-	0.005	
39013.21	564.650	-	-	0.000		64041	242.465	0.089	0.012	0.010	
39013.21	581.195	-	-	0.000		64041	243.226	0.196	0.027	0.446	
39013.21	602.121	-	-	0.000		64041	245.486	-	-	0.000	
39013.21	621.957	-	-	0.000		64041	261.459	0.182	0.025	0.010	w
39013.21	625.535	-	-	0.000		64041	262.670	0.053	0.016	0.007	w
39013.21	636.946	-	-	0.000		64041	263.180	-	-	0.001	
39013.21	771.525	-	-	0.000		64041	265.257	0.013	0.004	0.016	w
						64041	272.206	0.036	0.011	0.037	
39109.31	261.383	0.581	0.054	0.802		64041	274.490	-	-	0.007	

39109.31	262.167	0.281	0.029	0.196		64041	297.069	0.109	0.015	0.008	w
39109.31	277.759	-	-	0.000		64041	300.426	0.005	0.002	0.007	w
39109.31	328.541	0.004	0.001	0.000	w	64041	306.162	-	-	0.000	
39109.31	330.346	0.004	0.001	0.002	w	64041	307.058	0.013	0.004	0.001	
39109.31	393.030	0.060	0.014	0.000		64041	310.189	-	-	0.003	
39109.31	396.643	0.005	0.001	0.000	w	64041	312.002	-	-	0.001	
39109.31	481.824	-	-	0.000		64041	326.977	0.003	0.001	0.001	w
39109.31	494.360	-	-	0.000		64041	327.349	0.004	0.001	0.001	w
39109.31	561.602	0.027	0.006	0.000		64041	359.765	-	-	0.001	
39109.31	577.966	-	-	0.000		64041	386.339	0.002	0.000	0.000	w
39109.31	598.656	-	-	0.000		64041	522.707	0.042	0.013	0.000	
39109.31	621.796	-	-	0.000		64041	624.757	-	-	0.000	
39109.31	750.448	0.038	0.009	0.000		64041	719.325	-	-	0.000	
						64041	720.084	-	-	0.000	
41968.05	238.204	0.666	0.062	1.000		64041	721.663	-	-	0.000	
41968.05	249.330	0.323	0.030	0.000		64041	722.968	-	-	0.000	
41968.05	382.690	0.003	0.001	0.000	w						
41968.05	462.240	-	-	0.000		64087	209.498	0.005	0.001	0.058	o
41968.05	472.407	-	-	0.000		64087	218.622	-	-	0.008	o
41968.05	482.574	-	-	0.000		64087	229.443	0.017	0.004	0.004	s
41968.05	486.774	-	-	0.000		64087	231.106	-	-	0.000	
41968.05	490.386	0.005	0.001	0.000	w	64087	233.686	0.004	0.001	0.027	w
41968.05	517.164	0.003	0.001	0.000	w	64087	235.913	0.242	0.027	0.387	
41968.05	604.455	-	-	0.000		64087	236.472	0.226	0.025	0.000	
41968.05	618.537	-	-	0.000		64087	242.192	0.002	0.001	0.008	w
41968.05	632.822	-	-	0.000		64087	242.951	0.055	0.014	0.011	
41968.05	640.221	-	-	0.000		64087	243.495	0.138	0.015	0.375	
						64087	245.205	-	-	0.000	
42114.82	237.374	0.172	0.018	0.116		64087	261.020	0.020	0.005	0.000	w
42114.82	239.563	0.503	0.047	0.864		64087	262.349	0.040	0.010	0.000	
42114.82	248.420	0.117	0.012	0.004		64087	262.858	-	-	0.024	
42114.82	251.910	0.060	0.014	0.000		64087	271.862	0.035	0.009	0.007	
42114.82	292.659	0.092	0.022	0.016		64087	274.139	0.023	0.006	0.068	
42114.82	380.552	0.043	0.010	0.000		64087	300.006	0.007	0.002	0.011	w
42114.82	388.308	0.005	0.001	0.000		64087	305.507	0.007	0.002	0.001	
42114.82	459.124	-	-	0.000		64087	305.727	0.084	0.021	0.000	w
42114.82	469.153	0.002	0.000	0.000	w	64087	306.619	0.001	0.000	0.000	w
42114.82	483.320	-	-	0.000		64087	309.742	-	-	0.004	
42114.82	486.881	-	-	0.000		64087	311.549	-	-	0.001	
42114.82	489.990	0.001	0.000	0.000	w	64087	326.851	0.001	0.000	0.002	w
42114.82	513.267	0.004	0.001	0.000	w	64087	357.539	0.025	0.006	0.000	

42114.82	517.871	-	-	0.000		64087	359.164	-	-	0.000	
42114.82	599.138	-	-	0.000		64087	385.645	0.064	0.016	0.000	
42114.82	612.970	-	-	0.000		64087	386.395	0.002	0.001	0.001	w
42114.82	619.669	-	-	0.000		64087	521.439	-	-	0.000	
42114.82	626.997	-	-	0.000		64087	521.834	-	-	0.000	
42114.82	634.260	-	-	0.000		64087	609.116	-	-	0.000	
42114.82	675.494	-	-	0.000		64087	622.946	-	-	0.000	
						64087	685.659	-	-	0.000	
42237.03	236.687	-	-	0.000		64087	713.502	-	-	0.000	
42237.03	238.863	0.277	0.029	0.371		64087	716.924	-	-	0.000	
42237.03	240.489	0.466	0.043	0.607							
42237.03	247.668	0.020	0.005	0.003		64286	206.368	0.011	0.003	0.076	o
42237.03	251.137	0.020	0.005	0.001		64286	208.628	0.001	0.000	0.000	o
42237.03	253.737	-	-	0.000		64286	228.400	0.029	0.007	0.047	
42237.03	291.615	0.002	0.000	0.000	w	64286	229.917	0.004	0.001	0.001	
42237.03	295.378	0.156	0.016	0.017		64286	230.048	0.002	0.000	0.001	w
42237.03	347.574	-	-	0.000		64286	234.095	0.006	0.001	0.077	
42237.03	378.790	0.046	0.011	0.000		64286	234.811	0.377	0.035	0.019	
42237.03	386.473	0.001	0.000	0.000	w	64286	240.028	0.055	0.013	0.068	
42237.03	460.275	0.003	0.001	0.000	w	64286	241.030	-	-	0.016	
42237.03	466.478	-	-	0.000		64286	241.782	0.056	0.013	0.125	
42237.03	467.018	-	-	0.000		64286	244.015	0.028	0.007	0.000	
42237.03	484.000	-	-	0.000		64286	259.791	-	-	0.001	
42237.03	487.072	0.003	0.001	0.000	w	64286	260.987	0.013	0.003	0.055	
42237.03	510.066	-	-	0.000		64286	261.490	0.002	0.000	0.000	w
42237.03	514.613	-	-	0.000		64286	263.540	0.007	0.002	0.019	
42237.03	518.053	-	-	0.000		64286	270.399	0.125	0.013	0.381	
42237.03	528.411	0.009	0.002	0.000	w	64286	272.652	0.008	0.002	0.014	w
42237.03	608.411	-	-	0.000		64286	294.918	0.092	0.022	0.063	
42237.03	615.010	-	-	0.000		64286	298.226	-	-	0.007	
42237.03	617.815	-	-	0.000		64286	303.878	0.001	0.000	0.002	w
42237.03	629.380	-	-	0.000		64286	304.760	0.091	0.021	0.002	
42237.03	669.962	-	-	0.000		64286	307.844	0.020	0.005	0.002	
42237.03	683.964	-	-	0.000		64286	309.630	0.013	0.003	0.008	
						64286	324.372	0.013	0.003	0.012	
42334.82	238.306	0.243	0.028	0.030	s	64286	324.739	0.035	0.008	0.002	b
42334.82	239.924	0.269	0.031	0.458		64286	356.615	0.006	0.001	0.001	w
42334.82	241.052	0.273	0.028	0.498		64286	382.708	0.002	0.000	0.000	w
42334.82	250.521	0.008	0.002	0.004		64286	516.084	-	-	0.000	
42334.82	253.109	0.001	0.000	0.000	w	64286	615.318	-	-	0.000	
42334.82	254.913	0.092	0.011	0.000		64286	706.841	0.003	0.001	0.000	w

42334.82	290.786	0.002	0.001	0.000	w	64286	707.574	-	-	0.000	
42334.82	294.527	0.003	0.001	0.000	w	64286	710.359	-	-	0.000	
42334.82	297.052	0.049	0.013	0.009							
42334.82	346.396	0.001	0.000	0.000	w	64425	208.024	0.020	0.005	0.061	o
42334.82	348.799	-	-	0.000		64425	217.018	0.003	0.001	0.005	o
42334.82	385.018	0.038	0.010	0.000		64425	227.676	-	-	0.001	
42334.82	416.998	-	-	0.000		64425	229.314	0.003	0.001	0.000	w
42334.82	458.212	0.002	0.000	0.000	w	64425	231.854	0.019	0.005	0.025	
42334.82	464.894	0.001	0.000	0.000	w	64425	234.046	0.033	0.009	0.173	
42334.82	475.451	-	-	0.000		64425	234.596	-	-	0.000	
42334.82	484.762	-	-	0.000		64425	240.225	0.171	0.020	0.030	
42334.82	487.128	0.019	0.005	0.000		64425	240.972	0.005	0.001	0.018	w
42334.82	512.035	-	-	0.000		64425	241.507	0.024	0.006	0.179	
42334.82	515.441	-	-	0.000		64425	243.189	-	-	0.000	
42334.82	517.896	-	-	0.000		64425	258.736	0.001	0.000	0.000	w
42334.82	525.694	-	-	0.000		64425	260.042	-	-	0.005	
42334.82	604.164	-	-	0.000		64425	260.543	0.185	0.021	0.078	b
42334.82	611.332	-	-	0.000		64425	269.386	0.006	0.002	0.016	w
42334.82	614.103	-	-	0.000		64425	271.622	0.148	0.017	0.327	
42334.82	665.600	-	-	0.000		64425	296.994	0.145	0.017	0.053	
42334.82	679.418	-	-	0.000		64425	302.383	-	-	0.001	
						64425	302.599	0.149	0.017	0.000	
42401.3	239.542	-	-	0.107		64425	303.473	0.002	0.001	0.000	w
42401.3	240.666	0.538	0.052	0.532		64425	306.532	0.005	0.001	0.011	w
42401.3	241.331	0.292	0.028	0.350		64425	308.302	-	-	0.002	
42401.3	252.683	0.021	0.005	0.003	w	64425	323.279	-	-	0.012	
42401.3	254.481	-	-	0.000		64425	353.268	-	-	0.000	
42401.3	293.951	-	-	0.001		64425	354.855	0.003	0.001	0.000	w
42401.3	296.466	0.066	0.016	0.001		64425	380.682	0.060	0.016	0.000	
42401.3	297.935	0.038	0.009	0.006		64425	381.412	0.006	0.002	0.001	w
42401.3	345.600	0.003	0.001	0.000	w	64425	512.405	-	-	0.000	
42401.3	347.991	-	-	0.000		64425	512.787	-	-	0.000	
42401.3	350.820	-	-	0.000		64425	596.825	0.009	0.002	0.000	
42401.3	415.845	0.039	0.009	0.000	w	64425	670.125	-	-	0.000	
42401.3	425.149	0.003	0.001	0.000	w	64425	696.696	-	-	0.000	
42401.3	456.820	-	-	0.000		64425	699.959	-	-	0.000	
42401.3	463.462	-	-	0.000		64425	703.408	-	-	0.000	
42401.3	473.953	-	-	0.000							
42401.3	485.555	-	-	0.000		64806	215.237	0.063	0.016	0.115	o
42401.3	500.074	-	-	0.000		64806	217.703	0.041	0.010	0.098	o
42401.3	513.680	-	-	0.000		64806	229.823	0.256	0.028	0.136	

42401.3	516.118	-	-	0.000		64806	232.517	0.061	0.015	0.000	w
42401.3	523.862	-	-	0.000		64806	235.796	-	-	0.005	
42401.3	601.746	-	-	0.000		64806	239.304	-	-	0.005	
42401.3	611.606	-	-	0.000		64806	256.209	0.330	0.033	0.364	
42401.3	646.294	-	-	0.000		64806	263.957	0.180	0.020	0.266	
42401.3	676.363	-	-	0.000		64806	298.938	0.005	0.001	0.000	w
						64806	298.973	-	-	0.001	
42439.82	240.443	0.309	0.031	0.227		64806	348.574	-	-	0.001	
42439.82	241.107	0.435	0.044	0.765		64806	362.489	0.056	0.014	0.004	w
42439.82	254.232	0.117	0.013	0.002		64806	375.946	0.007	0.002	0.004	w
42439.82	296.128	0.012	0.003	0.002		64806	583.549	-	-	0.001	
42439.82	297.594	0.018	0.005	0.003		64806	653.433	-	-	0.000	
42439.82	347.525	0.095	0.011	0.000	w						
42439.82	350.347	0.002	0.000	0.000	w	64832	204.069	0.036	0.008	0.238	o
42439.82	415.180	0.004	0.001	0.000	w	64832	206.279	-	-	0.001	o
42439.82	424.454	0.002	0.001	0.000	w	64832	224.692	0.045	0.011	0.042	o
42439.82	473.089	-	-	0.000		64832	227.067	0.001	0.000	0.000	w
42439.82	484.648	0.001	0.000	0.000	w	64832	230.335	0.016	0.004	0.030	
42439.82	499.113	0.003	0.001	0.000	w	64832	231.141	0.015	0.003	0.000	w
42439.82	515.094	-	-	0.000		64832	231.840	0.011	0.003	0.000	
42439.82	600.354	-	-	0.000		64832	236.924	0.004	0.001	0.014	w
42439.82	644.689	0.001	0.000	0.000	w	64832	237.900	-	-	0.038	
						64832	253.711	0.111	0.012	0.000	
42658.22	234.350	0.324	0.030	0.624		64832	256.159	-	-	0.004	
42658.22	236.483	0.270	0.028	0.228		64832	257.321	0.019	0.005	0.049	
42658.22	238.076	0.232	0.024	0.118		64832	258.576	0.525	0.050	0.022	
42658.22	245.110	0.032	0.008	0.004		64832	259.803	-	-	0.002	
42658.22	248.507	0.001	0.000	0.001	w	64832	266.466	0.188	0.020	0.529	
42658.22	251.053	-	-	0.000		64832	290.246	0.009	0.002	0.008	
42658.22	288.076	0.079	0.019	0.008		64832	293.449	0.002	0.000	0.002	w
42658.22	291.747	0.007	0.002	0.001		64832	299.774	-	-	0.000	
42658.22	342.558	0.002	0.001	0.000	w	64832	304.484	0.005	0.001	0.005	w
42658.22	372.839	0.007	0.002	0.000	w	64832	313.172	0.001	0.000	0.003	w
42658.22	380.281	0.002	0.000	0.000	w	64832	318.730	0.007	0.002	0.012	w
42658.22	451.519	0.005	0.001	0.000	w	64832	319.084	0.003	0.001	0.002	w
42658.22	457.486	-	-	0.000		64832	501.946	-	-	0.000	
42658.22	458.006	-	-	0.000		64832	681.267	-	-	0.000	
42658.22	474.328	-	-	0.000		64832	682.679	0.001	0.000	0.000	w
42658.22	477.278	0.002	0.001	0.000	w						
42658.22	499.336	-	-	0.000		65110	202.918	0.004	0.001	0.024	o
42658.22	503.692	-	-	0.000		65110	205.103	0.031	0.009	0.184	o

42658.22	506.987	-	-	0.000		65110	224.182	0.006	0.002	0.005	o
42658.22	516.903	0.036	0.008	0.016		65110	225.644	0.008	0.002	0.030	w
42658.22	593.206	-	-	0.000		65110	225.770	0.013	0.004	0.000	
42658.22	599.477	-	-	0.000		65110	229.666	0.012	0.003	0.018	s
42658.22	602.141	-	-	0.000		65110	230.356	0.022	0.006	0.004	s
42658.22	613.122	-	-	0.000		65110	235.375	0.014	0.004	0.001	w
42658.22	651.570	-	-	0.000		65110	236.338	0.024	0.007	0.004	w
42658.22	664.807	-	-	0.000		65110	237.061	0.092	0.011	0.011	
						65110	239.207	0.002	0.001	0.000	w
43238.59	233.280	0.272	0.028	0.443		65110	254.348	0.138	0.017	0.002	
43238.59	234.830	0.447	0.042	0.372		65110	255.495	0.045	0.013	0.007	
43238.59	235.911	0.215	0.022	0.172		65110	255.977	0.066	0.018	0.079	
43238.59	244.973	-	-	0.001		65110	257.941	0.015	0.004	0.014	
43238.59	247.446	-	-	0.000		65110	264.508	0.014	0.004	0.008	
43238.59	249.170	-	-	0.000		65110	266.664	0.235	0.029	0.577	
43238.59	283.337	-	-	0.000		65110	287.925	0.005	0.002	0.008	w
43238.59	286.887	0.014	0.003	0.002		65110	291.076	0.002	0.001	0.003	w
43238.59	289.283	0.005	0.001	0.001		65110	296.458	0.045	0.012	0.000	
43238.59	335.878	0.002	0.001	0.000	w	65110	297.298	0.193	0.024	0.000	w
43238.59	338.136	-	-	0.000		65110	300.232	-	-	0.008	
43238.59	372.067	0.002	0.000	0.000	w	65110	301.930	0.006	0.002	0.000	w
43238.59	401.849	0.003	0.001	0.000	w	65110	315.932	-	-	0.000	
43238.59	439.986	0.002	0.000	0.000	w	65110	316.280	0.006	0.002	0.013	w
43238.59	446.144	0.004	0.001	0.000	w	65110	346.440	0.001	0.000	0.000	w
43238.59	455.857	-	-	0.000		65110	371.014	-	-	0.000	
43238.59	464.410	-	-	0.000		65110	495.043	0.001	0.000	0.000	w
43238.59	466.581	-	-	0.000		65110	495.399	-	-	0.000	
43238.59	489.382	-	-	0.000		65110	667.957	-	-	0.000	
43238.59	492.492	0.002	0.000	0.000	w	65110	669.973	-	-	0.000	
43238.59	494.733	-	-	0.000							
43238.59	501.844	0.032	0.008	0.008		65364	201.878	0.023	0.005	0.039	o
43238.59	572.875	-	-	0.000		65364	222.038	0.084	0.020	0.073	o
43238.59	579.316	-	-	0.000		65364	224.358	-	-	0.001	o
43238.59	581.804	-	-	0.000		65364	226.626	0.008	0.002	0.012	w
43238.59	627.823	-	-	0.000		65364	227.548	0.003	0.001	0.000	w
43238.59	640.103	-	-	0.000		65364	228.334	0.003	0.001	0.001	w
						65364	233.976	0.003	0.001	0.029	w
43620.96	232.740	0.237	0.025	0.235		65364	250.333	0.115	0.012	0.552	
43620.96	233.801	0.350	0.033	0.423		65364	252.716	0.093	0.022	0.037	
43620.96	234.428	0.241	0.025	0.327		65364	255.068	0.103	0.011	0.208	
43620.96	245.126	0.039	0.009	0.000		65364	256.262	0.412	0.038	0.001	

43620.96	246.818	0.034	0.008	0.000	w	65364	285.834	0.109	0.011	0.022	
43620.96	283.773	-	-	0.000		65364	307.717	0.031	0.007	0.026	
43620.96	286.117	0.007	0.002	0.001		65364	308.042	0.010	0.002	0.000	w
43620.96	287.485	0.003	0.001	0.000	w	65364	313.417	0.003	0.001	0.000	w
43620.96	331.618	-	-	0.000		65364	657.447	-	-	0.000	
43620.96	333.819	0.001	0.000	0.000	w						
43620.96	336.421	0.009	0.002	0.000	w	65556	201.095	-	-	0.023	o
43620.96	395.766	0.003	0.001	0.000	w	65556	203.241	0.034	0.008	0.131	o
43620.96	404.185	-	-	0.000		65556	221.092	0.016	0.004	0.000	o
43620.96	432.704	0.013	0.003	0.000	w	65556	223.392	0.066	0.016	0.239	o
43620.96	438.659	-	-	0.000		65556	226.554	-	-	0.002	
43620.96	448.045	-	-	0.000		65556	227.334	0.002	0.000	0.000	w
43620.96	458.400	0.016	0.004	0.000		65556	228.009	0.127	0.013	0.003	
43620.96	471.319	0.004	0.001	0.000	w	65556	232.925	0.008	0.002	0.000	
43620.96	483.387	-	-	0.000		65556	233.869	0.002	0.000	0.001	w
43620.96	485.545	-	-	0.000		65556	249.131	0.256	0.027	0.001	
43620.96	492.393	0.039	0.009	0.013		65556	251.491	0.035	0.008	0.031	
43620.96	560.591	0.001	0.000	0.000	w	65556	252.611	-	-	0.007	
43620.96	569.139	0.001	0.000	0.000	w	65556	253.820	0.121	0.013	0.018	
43620.96	599.060	-	-	0.000		65556	255.003	0.203	0.021	0.378	
43620.96	624.806	-	-	0.000		65556	261.419	-	-	0.019	
						65556	284.268	-	-	0.002	
44232.51	226.008	0.051	0.012	0.020		65556	287.340	0.100	0.010	0.106	
44232.51	227.992	0.053	0.012	0.016		65556	293.401	0.003	0.001	0.000	w
44232.51	236.000	0.211	0.022	0.097		65556	297.911	-	-	0.002	
44232.51	239.148	0.036	0.008	0.011		65556	306.224	0.026	0.006	0.036	
44232.51	275.574	0.632	0.059	0.855		65556	311.535	-	-	0.001	
44232.51	352.163	-	-	0.000		65556	311.873	-	-	0.001	
44232.51	358.795	0.005	0.001	0.000	w	65556	484.332	-	-	0.000	
44232.51	418.429	-	-	0.000		65556	650.503	-	-	0.000	
44232.51	426.743	-	-	0.000							
44232.51	438.432	-	-	0.000		65580	200.999	-	-	0.138	o
44232.51	441.360	-	-	0.000		65580	220.976	0.005	0.001	0.303	o
44232.51	443.913	-	-	0.000		65580	223.273	-	-	0.003	o
44232.51	462.934	0.003	0.001	0.001	w	65580	225.519	0.012	0.003	0.001	
44232.51	466.676	0.001	0.000	0.000	w	65580	226.432	0.051	0.012	0.011	s
44232.51	531.662	0.005	0.001	0.001		65580	227.211	0.012	0.003	0.003	
44232.51	542.526	0.002	0.000	0.000	w	65580	232.796	0.027	0.006	0.021	
44232.51	547.767	0.001	0.000	0.000	w	65580	248.983	0.245	0.026	0.200	
44232.51	553.485	0.001	0.000	0.000	w	65580	251.340	0.004	0.001	0.008	w
44232.51	559.137	-	-	0.000		65580	253.667	0.501	0.049	0.227	

44232.51	590.937	-	-	0.000		65580	254.848	-	-	0.011	
44232.51	722.137	-	-	0.000		65580	284.076	0.133	0.014	0.064	
44232.51	742.295	-	-	0.000		65580	305.680	0.005	0.001	0.010	w
44232.51	784.139	-	-	0.000		65580	306.001	0.003	0.001	0.001	w
						65580	311.305	0.003	0.001	0.001	w
44446.88	224.918	0.063	0.015	0.015	o	65580	648.220	-	-	0.000	
44446.88	226.882	0.005	0.001	0.003							
44446.88	228.349	0.001	0.000	0.000	w	65931	201.703	0.029	0.007	0.003	o
44446.88	234.812	0.276	0.029	0.188		65931	220.126	0.008	0.002	0.001	o
44446.88	237.928	0.114	0.012	0.054		65931	221.535	-	-	0.000	o
44446.88	240.260	0.034	0.008	0.007		65931	221.657	0.016	0.004	0.000	o
44446.88	273.955	0.422	0.039	0.707		65931	225.411	0.020	0.005	0.001	w
44446.88	277.273	0.001	0.000	0.000	w	65931	226.075	-	-	0.000	
44446.88	322.774	0.056	0.013	0.022		65931	230.907	0.072	0.017	0.000	
44446.88	349.523	0.003	0.001	0.000		65931	231.835	0.072	0.018	0.023	w
44446.88	356.055	0.003	0.001	0.000	w	65931	232.530	0.049	0.012	0.044	
44446.88	417.769	0.001	0.000	0.000	w	65931	234.595	-	-	0.000	
44446.88	422.873	-	-	0.000		65931	249.140	-	-	0.372	
44446.88	423.317	0.007	0.002	0.002		65931	250.239	0.470	0.046	0.444	
44446.88	437.222	-	-	0.000		65931	250.702	0.058	0.014	0.036	w
44446.88	439.728	-	-	0.000		65931	252.586	-	-	0.018	
44446.88	458.384	0.006	0.001	0.001		65931	258.880	0.052	0.013	0.025	
44446.88	462.052	-	-	0.000		65931	260.944	0.041	0.010	0.025	
44446.88	464.824	0.000	0.000	0.000	w	65931	281.268	0.024	0.006	0.000	w
44446.88	473.145	0.001	0.000	0.000	w	65931	284.275	0.002	0.000	0.000	w
44446.88	536.287	0.001	0.000	0.000	w	65931	289.406	0.015	0.004	0.004	w
44446.88	541.407	0.007	0.002	0.000	w	65931	290.206	0.057	0.014	0.001	w
44446.88	543.580	-	-	0.000		65931	293.002	-	-	0.000	
44446.88	552.513	-	-	0.000		65931	294.619	-	-	0.000	
44446.88	583.543	-	-	0.000		65931	307.936	0.002	0.000	0.000	w
44446.88	594.137	-	-	0.000		65931	308.266	-	-	0.000	
44446.88	711.126	-	-	0.000		65931	336.848	0.008	0.002	0.000	w
44446.88	730.665	-	-	0.000		65931	360.035	-	-	0.000	
44446.88	765.549	-	-	0.000		65931	475.688	0.004	0.001	0.000	w
44446.88	771.172	-	-	0.000		65931	476.017	-	-	0.000	
44446.88	791.231	-	-	0.000		65931	633.195	-	-	0.001	
						65931	633.784	-	-	0.000	
44753.8	223.375	-	-	0.000	o	65931	635.006	-	-	0.000	
44753.8	225.313	0.034	0.008	0.019							
44753.8	226.759	0.037	0.009	0.012		66013	201.372	-	-	0.000	o
44753.8	233.131	0.114	0.012	0.110		66013	218.882	-	-	0.000	o

44753.8	236.202	0.070	0.016	0.048		66013	221.136	-	-	0.000	o
44753.8	238.501	0.028	0.007	0.013		66013	224.234	0.026	0.006	0.005	o
44753.8	271.670	0.008	0.002	0.000	w	66013	224.998	-	-	0.002	o
44753.8	274.932	0.666	0.063	0.789		66013	225.660	0.018	0.004	0.000	w
44753.8	319.607	0.016	0.004	0.007		66013	230.474	0.034	0.008	0.024	
44753.8	345.812	0.001	0.000	0.000	w	66013	231.398	0.014	0.003	0.023	
44753.8	352.205	0.005	0.001	0.000	w	66013	246.328	0.099	0.010	0.207	
44753.8	412.479	-	-	0.000		66013	248.635	0.284	0.030	0.608	
44753.8	417.453	-	-	0.000		66013	249.730	0.007	0.002	0.031	w
44753.8	417.886	0.003	0.001	0.001	w	66013	250.912	0.058	0.014	0.033	
44753.8	431.431	0.001	0.000	0.000	w	66013	252.068	0.011	0.003	0.029	w
44753.8	433.870	0.001	0.000	0.000	w	66013	258.335	0.008	0.002	0.002	w
44753.8	452.022	0.001	0.000	0.000	w	66013	280.625	0.002	0.000	0.000	w
44753.8	455.589	0.004	0.001	0.001		66013	283.619	0.071	0.017	0.005	w
44753.8	458.284	-	-	0.000		66013	289.522	0.079	0.019	0.027	
44753.8	466.371	-	-	0.000		66013	293.913	0.267	0.028	0.000	w
44753.8	527.600	-	-	0.001		66013	302.001	0.018	0.004	0.001	w
44753.8	532.555	-	-	0.000		66013	307.166	0.005	0.001	0.001	w
44753.8	534.657	-	-	0.000		66013	307.494	-	-	0.000	
44753.8	543.297	-	-	0.000		66013	473.853	-	-	0.000	
44753.8	573.272	-	-	0.000		66013	630.530	-	-	0.001	
44753.8	583.494	-	-	0.000		66013	631.739	-	-	0.000	
44753.8	695.932	-	-	0.000							
44753.8	714.634	-	-	0.000		66078	201.106	-	-	0.006	o
44753.8	747.969	-	-	0.000		66078	209.500	0.002	0.001	0.003	o
44753.8	753.337	-	-	0.000		66078	219.416	-	-	0.002	o
44753.8	772.467	0.012	0.003	0.000	w	66078	220.937	-	-	0.000	o
44753.8	783.806	-	-	0.000		66078	223.293	-	-	0.002	o
						66078	225.326	-	-	0.001	
44784.76	225.156	0.012	0.003	0.004	s	66078	225.836	0.001	0.000	0.000	w
44784.76	226.600	0.008	0.002	0.007		66078	231.047	0.000	0.000	0.000	w
44784.76	227.605	0.008	0.002	0.002		66078	231.738	0.002	0.000	0.013	w
44784.76	236.029	0.134	0.014	0.180		66078	232.233	0.002	0.000	0.047	w
44784.76	238.325	0.112	0.012	0.104		66078	233.788	0.118	0.012	0.000	
44784.76	239.923	0.190	0.020	0.010		66078	248.122	-	-	0.001	
44784.76	271.441	0.139	0.014	0.168		66078	249.322	0.178	0.018	0.253	
44784.76	274.698	0.276	0.029	0.483		66078	249.782	0.047	0.011	0.566	
44784.76	276.894	0.045	0.011	0.014		66078	257.898	-	-	0.002	
44784.76	319.291	0.018	0.004	0.004		66078	259.947	0.400	0.037	0.097	
44784.76	321.331	0.035	0.008	0.019		66078	283.092	0.005	0.001	0.003	w
44784.76	351.821	0.001	0.000	0.000	w	66078	287.985	0.004	0.001	0.001	w

44784.76	378.335	0.001	0.000	0.000	w	66078	288.180	0.004	0.001	0.001	w
44784.76	411.952	0.001	0.000	0.000	w	66078	288.974	0.008	0.002	0.000	w
44784.76	417.346	0.001	0.000	0.001	w	66078	291.745	0.003	0.001	0.001	
44784.76	425.834	-	-	0.000		66078	293.348	-	-	0.000	
44784.76	433.288	0.001	0.000	0.000	w	66078	306.876	0.002	0.001	0.002	
44784.76	435.177	0.007	0.002	0.001	w	66078	333.773	0.003	0.001	0.000	w
44784.76	454.947	0.005	0.001	0.003		66078	335.189	0.001	0.000	0.000	w
44784.76	457.634	0.001	0.000	0.000	w	66078	358.140	0.214	0.022	0.000	
44784.76	459.568	0.001	0.000	0.000	w	66078	358.787	0.005	0.001	0.000	w
44784.76	465.698	-	-	0.000		66078	472.386	-	-	0.000	
44784.76	526.248	-	-	0.000		66078	472.710	0.001	0.000	0.000	w
44784.76	531.678	0.003	0.001	0.000		66078	554.195	-	-	0.000	
44784.76	533.773	-	-	0.000		66078	624.735	-	-	0.001	
44784.76	572.256	-	-	0.000		66078	627.357	-	-	0.000	
44784.76	582.442	-	-	0.000		66078	629.135	-	-	0.000	
44784.76	713.056	-	-	0.000							
44784.76	744.934	-	-	0.000		66249	208.754	0.134	0.014	0.338	o
44784.76	746.241	-	-	0.000		66249	211.073	0.095	0.023	0.146	o
44784.76	751.583	-	-	0.000		66249	222.447	0.044	0.011	0.086	o
44784.76	770.623	-	-	0.000		66249	224.970	-	-	0.002	o
44784.76	781.908	-	-	0.000		66249	228.038	0.006	0.001	0.001	w
						66249	231.317	0.086	0.021	0.000	
45044.17	225.275	-	-	0.000		66249	247.077	0.473	0.046	0.132	
45044.17	226.269	0.010	0.003	0.006		66249	254.274	0.087	0.021	0.292	
45044.17	226.856	0.003	0.001	0.002		66249	286.578	-	-	0.000	
45044.17	236.860	0.076	0.011	0.201		66249	286.611	0.005	0.001	0.000	w
45044.17	238.439	0.084	0.012	0.079		66249	331.885	0.006	0.001	0.000	w
45044.17	272.754	0.282	0.036	0.289		66249	344.475	-	-	0.001	
45044.17	274.918	0.388	0.050	0.358	w	66249	356.606	0.031	0.008	0.001	w
45044.17	276.181	0.096	0.014	0.039		66249	538.239	0.032	0.008	0.000	w
45044.17	316.667	-	-	0.000		66249	597.145	-	-	0.000	
45044.17	318.674	0.014	0.005	0.011							
45044.17	321.044	0.023	0.007	0.009		66377	217.985	-	-	0.001	o
45044.17	374.657	0.003	0.001	0.000	w	66377	219.367	-	-	0.000	o
45044.17	382.193	0.003	0.001	0.000		66377	219.486	-	-	0.001	o
45044.17	407.595	0.003	0.001	0.000	w	66377	223.167	-	-	0.003	o
45044.17	412.875	-	-	0.000		66377	223.818	0.006	0.001	0.000	o
45044.17	421.180	0.001	0.000	0.000	w	66377	228.553	-	-	0.002	
45044.17	430.318	0.002	0.001	0.001	w	66377	229.461	0.043	0.011	0.038	
45044.17	441.683	0.001	0.000	0.001	w	66377	230.143	0.008	0.002	0.014	w
45044.17	452.263	0.004	0.001	0.003		66377	232.165	0.024	0.006	0.000	

45044.17	454.152	-	-	0.000		66377	246.401	0.150	0.017	0.462	
45044.17	460.138	-	-	0.000		66377	247.477	0.239	0.027	0.356	
45044.17	519.159	0.007	0.002	0.000		66377	247.930	-	-	0.021	
45044.17	526.481	0.001	0.000	0.000	w	66377	249.772	0.228	0.026	0.021	
45044.17	551.985	-	-	0.000		66377	255.924	0.015	0.004	0.023	
45044.17	573.770	-	-	0.000		66377	257.942	0.031	0.008	0.006	
45044.17	730.807	-	-	0.000		66377	277.783	0.036	0.009	0.005	
45044.17	731.022	-	-	0.000		66377	280.715	0.070	0.018	0.000	w
45044.17	732.065	-	-	0.000		66377	285.717	0.089	0.023	0.032	b
45044.17	755.516	-	-	0.000		66377	286.497	0.023	0.006	0.012	w
						66377	289.221	0.013	0.003	0.000	w
45079.88	223.669	0.002	0.000	0.001	o	66377	290.797	0.009	0.002	0.000	w
45079.88	225.094	0.040	0.010	0.012		66377	303.763	-	-	0.000	
45079.88	226.086	0.022	0.006	0.008		66377	304.085	-	-	0.001	
45079.88	234.396	0.120	0.013	0.112		66377	331.862	0.006	0.001	0.000	w
45079.88	236.659	0.054	0.014	0.039		66377	354.344	0.009	0.002	0.000	w
45079.88	238.236	-	-	0.016		66377	465.804	-	-	0.000	
45079.88	269.283	0.120	0.013	0.005	b	66377	615.802	-	-	0.000	
45079.88	272.488	0.132	0.015	0.038		66377	616.359	-	-	0.000	
45079.88	274.648	0.471	0.048	0.762		66377	617.515	-	-	0.001	
45079.88	316.309	0.003	0.001	0.001	w	66377	618.470	-	-	0.000	
45079.88	318.311	0.010	0.002	0.004							
45079.88	348.205	0.005	0.001	0.000	w	66412	216.986	0.003	0.001	0.001	o
45079.88	374.156	-	-	0.000		66412	221.366	0.128	0.013	0.119	o
45079.88	407.003	0.002	0.000	0.000	w	66412	222.245	0.017	0.004	0.008	o
45079.88	412.267	0.003	0.001	0.000	w	66412	243.930	0.336	0.031	0.745	
45079.88	420.547	0.001	0.000	0.000	w	66412	248.425	0.508	0.047	0.127	
45079.88	427.816	0.001	0.000	0.000	w	66412	298.100	0.007	0.002	0.000	w
45079.88	429.657	0.002	0.000	0.000	w	66412	298.405	-	-	0.000	
45079.88	448.918	0.001	0.000	0.000	w						
45079.88	451.534	0.003	0.001	0.001	w	66464	216.743	0.020	0.005	0.019	o
45079.88	453.417	0.004	0.001	0.000	w	66464	218.952	0.022	0.005	0.000	o
45079.88	459.383	0.002	0.000	0.000	w	66464	221.112	0.026	0.006	0.007	o
45079.88	518.198	-	-	0.000		66464	221.989	0.112	0.012	0.081	o
45079.88	523.463	0.003	0.001	0.001	w	66464	222.738	0.067	0.016	0.008	o
45079.88	525.493	-	-	0.000		66464	228.103	-	-	0.001	
45079.88	562.750	0.001	0.000	0.000	w	66464	243.622	0.034	0.008	0.033	
45079.88	572.596	-	-	0.000		66464	245.878	0.505	0.048	0.742	
45079.88	698.356	-	-	0.000		66464	248.105	0.055	0.013	0.053	
45079.88	728.905	-	-	0.000		66464	249.235	0.055	0.013	0.046	
45079.88	730.156	-	-	0.000		66464	277.119	0.027	0.006	0.010	

45079.88	735.270	-	-	0.000		66464	297.640	0.007	0.002	0.000	w
45079.88	753.482	-	-	0.000		66464	297.944	0.068	0.016	0.000	
45079.88	764.267	-	-	0.000		66464	302.969	0.003	0.001	0.001	w
						66464	613.099	-	-	0.000	
45206.45	225.441	0.001	0.000	0.002	w						
45206.45	226.024	0.037	0.009	0.012	b	66522	207.568	0.010	0.004	0.023	o
45206.45	237.519	0.088	0.021	0.283		66522	217.298	0.013	0.005	0.030	o
45206.45	273.697	0.159	0.017	0.366		66522	218.790	0.011	0.005	0.000	o
45206.45	274.949	0.665	0.064	0.312		66522	221.100	0.022	0.009	0.006	o
45206.45	317.034	0.002	0.000	0.003	w	66522	223.093	-	-	0.001	o
45206.45	319.380	0.019	0.005	0.018		66522	223.593	-	-	0.000	o
45206.45	372.392	-	-	0.000		66522	228.700	-	-	0.001	
45206.45	379.836	0.024	0.006	0.000		66522	229.377	0.045	0.018	0.029	
45206.45	418.320	0.000	0.000	0.000	w	66522	229.862	0.007	0.003	0.008	w
45206.45	427.333	0.001	0.000	0.000	w	66522	231.385	0.013	0.005	0.000	
45206.45	438.539	0.001	0.000	0.001	w	66522	245.417	0.143	0.025	0.020	b
45206.45	450.829	0.002	0.000	0.003	w	66522	246.591	0.148	0.026	0.535	
45206.45	514.820	-	-	0.000		66522	247.041	0.124	0.022	0.211	
45206.45	547.083	-	-	0.000		66522	254.978	0.348	0.055	0.076	b
45206.45	722.239	-	-	0.000		66522	256.980	0.027	0.011	0.005	
45206.45	722.449	-	-	0.000		66522	279.577	-	-	0.004	
						66522	284.348	0.059	0.023	0.022	w
45289.8	224.035	0.003	0.001	0.001	o	66522	284.538	-	-	0.023	
45289.8	225.018	0.018	0.004	0.006		66522	285.311	0.004	0.002	0.002	w
45289.8	225.599	-	-	0.003		66522	288.013	0.006	0.002	0.001	w
45289.8	235.489	0.154	0.016	0.097		66522	289.575	-	-	0.000	
45289.8	237.050	0.085	0.020	0.056		66522	302.749	-	-	0.000	
45289.8	270.938	0.012	0.003	0.001	w	66522	328.897	0.004	0.001	0.000	w
45289.8	273.073	0.228	0.024	0.102		66522	330.272	0.005	0.002	0.000	w
45289.8	274.320	0.452	0.043	0.730		66522	352.532	0.003	0.001	0.000	w
45289.8	314.222	-	-	0.000		66522	353.159	0.009	0.003	0.000	w
45289.8	316.198	0.009	0.002	0.001		66522	462.678	-	-	0.000	
45289.8	318.532	0.002	0.000	0.001	w	66522	530.424	-	-	0.000	
45289.8	371.239	-	-	0.000		66522	540.881	-	-	0.000	
45289.8	378.637	0.011	0.003	0.000	w	66522	587.541	-	-	0.000	
45289.8	403.554	0.007	0.002	0.000	w	66522	607.868	-	-	0.000	
45289.8	408.728	0.003	0.001	0.000	w	66522	610.350	-	-	0.001	
45289.8	416.866	-	-	0.000		66522	612.032	-	-	0.000	
45289.8	425.815	-	-	0.000		66522	612.971	-	-	0.000	
45289.8	436.941	-	-	0.000							
45289.8	447.293	0.004	0.001	0.000	w	66589	216.154	0.015	0.004	0.000	o

45289.8	449.141	0.002	0.000	0.001	w	66589	218.352	0.009	0.002	0.004	o
45289.8	454.994	-	-	0.000		66589	221.373	0.096	0.011	0.013	o
45289.8	512.620	0.006	0.001	0.000	w	66589	222.117	0.070	0.018	0.085	o
45289.8	519.758	0.002	0.001	0.002	w	66589	222.762	0.068	0.018	0.008	o
45289.8	544.598	0.002	0.001	0.000	w	66589	227.452	-	-	0.002	
45289.8	565.794	-	-	0.000		66589	228.351	0.006	0.001	0.001	w
45289.8	717.916	-	-	0.000		66589	242.879	0.081	0.021	0.004	
45289.8	718.123	-	-	0.000		66589	245.122	0.062	0.016	0.065	
45289.8	719.130	-	-	0.000		66589	246.186	0.267	0.028	0.758	
45289.8	741.747	-	-	0.000		66589	247.335	0.199	0.023	0.002	
						66589	248.457	0.094	0.011	0.012	w
46967.44	214.605	0.005	0.001	0.002	o	66589	254.544	-	-	0.040	
46967.44	215.916	-	-	0.000	o	66589	276.158	-	-	0.000	
46967.44	216.829	0.001	0.000	0.000	o	66589	279.056	0.012	0.003	0.005	w
46967.44	224.461	0.004	0.001	0.002	o	66589	284.769	-	-	0.000	
46967.44	226.536	-	-	0.000		66589	289.017	0.013	0.003	0.000	w
46967.44	227.980	-	-	0.000		66589	296.833	0.003	0.001	0.000	w
46967.44	256.254	0.348	0.033	0.580		66589	301.821	0.002	0.001	0.000	w
46967.44	259.154	0.206	0.021	0.197		66589	302.139	-	-	0.000	
46967.44	261.107	0.078	0.018	0.023		66589	461.254	0.004	0.001	0.000	w
46967.44	298.483	0.190	0.020	0.138		66589	609.543	-	-	0.000	
46967.44	300.265	0.135	0.014	0.056							
46967.44	326.724	-	-	0.000		66613	207.179	0.018	0.006	0.019	o
46967.44	349.467	0.001	0.000	0.000	w	66613	209.463	0.010	0.003	0.025	o
46967.44	377.958	0.002	0.000	0.000	w	66613	216.872	0.009	0.003	0.007	o
46967.44	382.493	0.004	0.001	0.000	w	66613	218.358	0.011	0.004	0.000	o
46967.44	389.610	-	-	0.000		66613	220.659	0.029	0.010	0.025	o
46967.44	395.841	0.001	0.000	0.000	w	66613	223.142	0.042	0.015	0.000	o
46967.44	397.417	0.002	0.000	0.000	w	66613	226.160	-	-	0.000	
46967.44	413.841	-	-	0.000		66613	228.902	0.012	0.004	0.001	w
46967.44	416.062	0.001	0.000	0.000	w	66613	229.385	0.059	0.020	0.028	
46967.44	417.661	0.008	0.002	0.000	w	66613	230.902	0.051	0.018	0.000	
46967.44	422.717	-	-	0.000		66613	244.873	0.006	0.002	0.004	w
46967.44	472.015	-	-	0.000		66613	246.491	0.191	0.029	0.752	
46967.44	476.379	-	-	0.000		66613	251.941	0.162	0.025	0.039	w
46967.44	478.060	-	-	0.000		66613	256.384	0.153	0.024	0.052	w
46967.44	508.699	-	-	0.000		66613	283.619	0.082	0.013	0.018	w
46967.44	516.731	0.014	0.003	0.000		66613	283.651	0.019	0.006	0.024	w
46967.44	617.001	-	-	0.000		66613	283.808	0.067	0.010	0.003	
46967.44	640.725	-	-	0.000		66613	287.265	-	-	0.002	
46967.44	641.692	-	-	0.000		66613	327.922	0.001	0.000	0.000	w

46967.44	645.638	-	-	0.001		66613	329.289	-	-	0.000	
46967.44	659.639	-	-	0.000		66613	340.208	0.026	0.009	0.000	
46967.44	667.890	-	-	0.000		66613	351.412	-	-	0.000	
46967.44	742.396	-	-	0.000		66613	352.035	-	-	0.000	
						66613	461.059	-	-	0.000	
47389.78	213.964	0.009	0.002	0.002	o	66613	527.894	0.004	0.001	0.001	w
47389.78	214.861	-	-	0.000	o	66613	538.250	0.048	0.017	0.000	w
47389.78	215.390	-	-	0.000	o	66613	584.438	-	-	0.000	
47389.78	224.388	0.001	0.000	0.001	o	66613	604.547	-	-	0.001	
47389.78	225.805	-	-	0.000		66613	607.001	-	-	0.000	
47389.78	256.348	0.204	0.024	0.490		66613	796.645	-	-	0.000	
47389.78	258.258	0.193	0.022	0.291							
47389.78	259.373	0.149	0.017	0.048		66672	216.592	0.019	0.005	0.000	o
47389.78	294.765	0.129	0.015	0.076		66672	217.956	0.025	0.006	0.001	o
47389.78	296.503	0.068	0.018	0.023		66672	218.074	-	-	0.000	o
47389.78	298.555	0.078	0.020	0.067		66672	221.706	0.010	0.002	0.012	o
47389.78	344.383	0.022	0.006	0.000		66672	222.349	0.098	0.010	0.100	o
47389.78	350.740	0.001	0.000	0.000	w	66672	227.021	0.008	0.002	0.000	w
47389.78	372.017	0.134	0.016	0.000	w	66672	227.918	-	-	0.002	
47389.78	376.411	-	-	0.000		66672	228.590	-	-	0.000	
47389.78	383.301	-	-	0.000		66672	230.585	-	-	0.000	
47389.78	390.855	0.010	0.003	0.000	b	66672	244.622	0.105	0.011	0.003	
47389.78	400.208	-	-	0.000		66672	245.682	0.048	0.012	0.072	
47389.78	408.876	0.002	0.000	0.000	w	66672	246.128	0.303	0.029	0.731	
47389.78	410.419	0.001	0.000	0.000	w	66672	247.944	0.160	0.017	0.004	w
47389.78	415.301	0.001	0.000	0.000	w	66672	254.006	0.000	0.000	0.004	w
47389.78	462.787	-	-	0.000		66672	255.993	0.168	0.018	0.068	
47389.78	468.596	-	-	0.000		66672	275.524	-	-	0.000	
47389.78	488.693	-	-	0.000		66672	278.409	-	-	0.000	
47389.78	505.692	-	-	0.000		66672	283.328	0.023	0.006	0.000	w
47389.78	623.839	-	-	0.000		66672	284.095	-	-	0.000	
47389.78	623.995	-	-	0.000		66672	286.773	0.007	0.002	0.000	w
47389.78	624.756	-	-	0.001		66672	288.322	-	-	0.000	
47389.78	641.755	-	-	0.000		66672	301.064	-	-	0.000	
						66672	301.380	-	-	0.000	
47626.08	213.775	0.004	0.001	0.002	o	66672	328.643	-	-	0.000	
47626.08	214.299	-	-	0.001	o	66672	350.677	0.020	0.005	0.000	w
47626.08	224.606	-	-	0.000	o	66672	459.794	0.007	0.002	0.000	w
47626.08	256.691	0.256	0.028	0.382							
47626.08	257.792	0.306	0.030	0.425		67001	205.527	0.062	0.015	0.140	o
47626.08	294.440	0.184	0.020	0.156		67001	215.062	0.113	0.012	0.143	o

47626.08	296.462	0.063	0.016	0.031		67001	216.523	0.009	0.002	0.000	o
47626.08	341.602	0.003	0.001	0.001	w	67001	218.786	0.014	0.004	0.017	o
47626.08	347.856	0.003	0.001	0.000	w	67001	220.737	-	-	0.000	o
47626.08	379.860	0.074	0.018	0.000		67001	221.227	0.011	0.003	0.000	o
47626.08	387.277	0.096	0.011	0.000	w	67001	226.225	0.008	0.002	0.004	w
47626.08	396.458	0.004	0.001	0.000	w	67001	226.887	0.031	0.008	0.006	w
47626.08	406.476	0.003	0.001	0.000	w	67001	227.362	-	-	0.001	
47626.08	457.779	0.004	0.001	0.000	w	67001	228.852	-	-	0.000	
47626.08	483.113	-	-	0.000		67001	242.569	0.096	0.010	0.081	
47626.08	614.774	-	-	0.001		67001	243.716	0.172	0.019	0.029	
47626.08	614.926	-	-	0.001		67001	244.156	0.009	0.002	0.007	b
						67001	251.905	0.311	0.031	0.531	
59663.46	216.434	0.059	0.015	0.080	o	67001	253.859	-	-	0.027	
59663.46	217.369	-	-	0.005	o	67001	275.887	0.006	0.002	0.000	w
59663.46	218.470	0.005	0.001	0.000	o	67001	280.532	0.014	0.004	0.005	w
59663.46	242.041	0.005	0.001	0.000	w	67001	280.717	-	-	0.002	
59663.46	245.164	0.002	0.000	0.000	w	67001	281.470	0.004	0.001	0.000	w
59663.46	255.374	0.016	0.004	0.006	w	67001	284.099	-	-	0.003	
59663.46	257.437	0.342	0.034	0.873		67001	285.618	0.066	0.016	0.002	
59663.46	260.642	0.195	0.022	0.000		67001	298.427	0.009	0.002	0.000	w
59663.46	264.112	0.016	0.004	0.030		67001	323.802	0.020	0.005	0.000	w
59663.46	268.351	-	-	0.000		67001	325.135	0.029	0.007	0.000	w
59663.46	272.220	0.054	0.014	0.000		67001	346.686	0.005	0.001	0.000	w
59663.46	272.903	0.078	0.019	0.000	w	67001	347.292	-	-	0.000	
59663.46	275.054	-	-	0.000		67001	452.659	-	-	0.000	
59663.46	295.109	0.008	0.002	0.004	w	67001	452.957	0.006	0.001	0.000	w
59663.46	297.461	-	-	0.000		67001	517.299	0.004	0.001	0.000	w
59663.46	305.435	0.001	0.000	0.000	w	67001	527.240	-	-	0.001	
59663.46	311.990	-	-	0.000		67001	590.692	0.003	0.001	0.000	w
59663.46	353.268	-	-	0.000		67001	593.035	-	-	0.000	
59663.46	353.318	0.136	0.015	0.000		67001	594.624	-	-	0.000	
59663.46	353.562	0.020	0.005	0.001		67001	595.510	-	-	0.000	
59663.46	358.943	0.020	0.005	0.000		67001	786.114	-	-	0.000	
59663.46	424.742	0.031	0.008	0.000							
59663.46	427.038	0.007	0.002	0.000	w	67274	204.378	0.033	0.008	0.078	o
59663.46	445.585	0.003	0.001	0.000	w	67274	206.601	0.032	0.008	0.112	o
59663.46	465.002	-	-	0.000		67274	213.805	-	-	0.017	o
59663.46	466.093	-	-	0.000		67274	215.249	0.062	0.016	0.000	o
						67274	217.485	0.052	0.013	0.073	o
60402.34	213.026	0.038	0.009	0.015	o	67274	219.896	-	-	0.000	o
60402.34	213.932	-	-	0.001	o	67274	222.827	0.014	0.004	0.000	o

60402.34	227.032	0.008	0.002	0.000	w	67274	225.488	0.010	0.003	0.006	w
60402.34	237.787	-	-	0.003		67274	225.957	0.103	0.012	0.012	
60402.34	250.643	0.072	0.018	0.002	w	67274	227.429	0.005	0.001	0.000	w
60402.34	252.630	0.625	0.062	0.930		67274	240.971	0.017	0.004	0.014	w
60402.34	255.715	0.028	0.007	0.000	w	67274	242.536	0.072	0.018	0.046	
60402.34	258.385	0.002	0.000	0.000	w	67274	247.811	0.118	0.013	0.087	
60402.34	259.055	0.046	0.011	0.032		67274	252.109	0.362	0.037	0.536	
60402.34	265.935	-	-	0.000		67274	278.397	-	-	0.004	
60402.34	266.851	-	-	0.000		67274	278.428	0.056	0.014	0.007	w
60402.34	267.507	0.006	0.002	0.000	w	67274	278.579	0.009	0.002	0.001	w
60402.34	269.573	0.014	0.003	0.000	w	67274	281.909	-	-	0.001	
60402.34	288.810	0.034	0.008	0.013		67274	320.961	0.020	0.005	0.001	w
60402.34	290.438	0.009	0.002	0.000	w	67274	322.270	0.022	0.006	0.000	w
60402.34	291.062	0.006	0.001	0.000	w	67274	332.722	-	-	0.000	
60402.34	302.142	-	-	0.001		67274	343.431	-	-	0.000	
60402.34	304.957	-	-	0.000		67274	344.025	-	-	0.000	
60402.34	337.309	-	-	0.000		67274	447.416	-	-	0.000	
60402.34	344.279	0.003	0.001	0.000	w	67274	510.085	-	-	0.002	
60402.34	344.558	0.014	0.004	0.000	w	67274	519.748	0.013	0.003	0.000	w
60402.34	345.692	0.009	0.002	0.002	w	67274	581.305	-	-	0.000	
60402.34	349.666	0.038	0.009	0.000	w	67274	583.574	-	-	0.000	
60402.34	351.971	-	-	0.000		67274	756.773	-	-	0.000	
60402.34	371.626	0.048	0.012	0.000							
60402.34	411.814	-	-	0.000		67516	211.905	0.016	0.004	0.034	o
60402.34	413.972	-	-	0.000		67516	214.017	-	-	0.003	o
60402.34	449.552	-	-	0.000		67516	216.080	-	-	0.003	o
60402.34	450.571	-	-	0.000		67516	216.918	0.008	0.002	0.007	o
60402.34	645.512	-	-	0.000		67516	217.632	0.002	0.001	0.004	o
						67516	222.752	0.049	0.012	0.002	o
60625.45	223.241	-	-	0.000	o	67516	237.528	0.371	0.035	0.001	
60625.45	248.156	0.001	0.000	0.000	w	67516	239.672	0.030	0.007	0.080	
60625.45	251.057	-	-	0.000		67516	241.787	0.167	0.017	0.385	
60625.45	253.900	0.707	0.067	0.656		67516	242.860	-	-	0.001	
60625.45	255.058	0.122	0.013	0.011	w	67516	269.260	0.338	0.032	0.462	
60625.45	256.046	-	-	0.012		67516	288.593	0.014	0.003	0.013	
60625.45	263.161	-	-	0.279		67516	288.879	0.001	0.000	0.000	w
60625.45	284.034	0.050	0.012	0.029		67516	293.601	0.003	0.001	0.005	w
60625.45	287.106	0.023	0.006	0.011		67516	575.914	-	-	0.000	
60625.45	290.146	0.006	0.002	0.000							
60625.45	291.692	0.003	0.001	0.000	w	69102	205.757	0.016	0.005	0.005	o
60625.45	330.627	0.061	0.015	0.000		69102	207.094	-	-	0.000	o

60625.45	360.260	0.009	0.002	0.000	w	69102	209.163	-	-	0.000	o
60625.45	360.706	-	-	0.000		69102	210.946	-	-	0.000	o
60625.45	368.098	0.017	0.004	0.000	w	69102	211.393	-	-	0.007	o
						69102	215.952	0.041	0.013	0.004	o
60807.23	222.338	0.020	0.005	0.001	o	69102	216.556	0.043	0.013	0.001	o
60807.23	224.964	-	-	0.000	o	69102	216.988	0.013	0.004	0.000	o
60807.23	247.041	0.029	0.007	0.000		69102	218.345	0.052	0.016	0.269	o
60807.23	249.916	-	-	0.000		69102	230.797	0.012	0.004	0.004	w
60807.23	253.880	0.328	0.031	0.396		69102	231.836	0.211	0.029	0.000	w
60807.23	254.859	-	-	0.090		69102	232.233	0.047	0.015	0.000	w
60807.23	255.708	0.005	0.001	0.010	w	69102	239.233	0.015	0.005	0.039	w
60807.23	261.908	0.037	0.009	0.132		69102	240.995	-	-	0.001	
60807.23	263.101	0.430	0.040	0.328		69102	260.761	-	-	0.001	
60807.23	282.575	-	-	0.014		69102	264.906	0.018	0.006	0.011	w
60807.23	285.615	0.011	0.003	0.018		69102	265.072	-	-	0.111	
60807.23	287.061	0.001	0.000	0.003	w	69102	265.743	0.033	0.010	0.544	w
60807.23	288.624	0.002	0.001	0.003	w	69102	268.085	0.073	0.023	0.000	w
60807.23	290.153	0.003	0.001	0.000		69102	269.438	0.031	0.009	0.000	w
60807.23	298.489	0.126	0.013	0.003		69102	280.807	0.012	0.004	0.000	w
60807.23	328.651	-	-	0.000		69102	303.163	0.269	0.033	0.001	
60807.23	332.763	-	-	0.000		69102	304.330	0.016	0.005	0.001	w
60807.23	340.919	-	-	0.000		69102	323.132	-	-	0.000	
60807.23	347.024	0.001	0.000	0.000	w	69102	323.658	0.064	0.020	0.000	w
60807.23	358.355	0.001	0.000	0.000	w	69102	510.181	-	-	0.001	
60807.23	365.650	0.003	0.001	0.000	w	69102	529.246	0.035	0.011	0.001	w
60807.23	366.116	0.002	0.001	0.000	w						
60807.23	629.066	-	-	0.000		69427	207.752	-	-	0.000	o
						69427	209.952	-	-	0.009	o
60837.57	246.856	-	-	0.003		69427	212.621	-	-	0.006	o
60837.57	252.539	0.299	0.031	0.627		69427	215.470	-	-	0.001	o
60837.57	253.684	0.513	0.048	0.324		69427	229.080	0.019	0.005	0.038	w
60837.57	282.333	0.068	0.016	0.011		69427	235.254	-	-	0.025	
60837.57	288.371	0.081	0.019	0.034		69427	262.647	0.353	0.038	0.476	
60837.57	357.527	0.037	0.009	0.000		69427	262.675	0.281	0.030	0.441	w
60837.57	357.966	0.002	0.001	0.000	w	69427	300.207	-	-	0.000	
						69427	310.472	0.007	0.002	0.000	w
60887.6	221.941	-	-	0.000	o	69427	320.292	-	-	0.000	
60887.6	246.551	-	-	0.000		69427	501.867	0.339	0.036	0.003	
60887.6	249.414	0.048	0.011	0.002	b						
60887.6	252.220	0.025	0.006	0.099		69607	203.644	0.032	0.008	0.168	o
60887.6	253.363	0.477	0.045	0.628		69607	204.849	0.006	0.002	0.038	o

60887.6	254.338	0.255	0.027	0.211		69607	204.953	-	-	0.000	o
60887.6	261.357	-	-	0.015		69607	208.159	-	-	0.000	o
60887.6	281.934	0.022	0.005	0.005		69607	208.725	-	-	0.000	o
60887.6	284.961	0.038	0.009	0.020		69607	212.838	0.002	0.001	0.000	o
60887.6	287.955	0.013	0.003	0.001	b	69607	213.625	0.039	0.009	0.000	o
60887.6	289.478	0.057	0.013	0.019		69607	214.216	-	-	0.001	o
60887.6	327.785	-	-	0.000		69607	215.967	0.014	0.003	0.000	o
60887.6	356.889	0.024	0.006	0.000		69607	228.234	-	-	0.000	
60887.6	357.326	0.010	0.002	0.000	w	69607	229.156	-	-	0.003	
60887.6	364.578	0.032	0.008	0.000	w	69607	229.544	0.003	0.001	0.000	w
						69607	231.123	0.035	0.008	0.047	
60956.78	210.538	-	-	0.000	o	69607	236.381	0.167	0.018	0.087	
60956.78	221.601	-	-	0.000	o	69607	238.101	-	-	0.005	
60956.78	224.209	-	-	0.005	o	69607	254.908	0.300	0.029	0.438	
60956.78	247.206	0.011	0.003	0.000		69607	257.376	0.004	0.001	0.006	w
60956.78	248.985	0.154	0.016	0.001		69607	261.575	-	-	0.003	
60956.78	249.139	-	-	0.000		69607	262.228	-	-	0.000	
60956.78	253.891	0.479	0.045	0.370		69607	264.508	0.029	0.007	0.046	
60956.78	254.734	0.027	0.007	0.095		69607	265.825	0.038	0.009	0.092	
60956.78	260.885	0.010	0.002	0.021		69607	276.619	-	-	0.008	
60956.78	262.070	0.063	0.015	0.159		69607	276.886	0.208	0.022	0.000	
60956.78	262.959	0.084	0.020	0.294		69607	299.730	0.021	0.005	0.023	
60956.78	265.602	0.008	0.002	0.000	w	69607	317.950	0.081	0.019	0.028	w
60956.78	284.400	0.043	0.010	0.018		69607	404.883	0.007	0.002	0.001	w
60956.78	285.833	0.092	0.022	0.031		69607	405.121	0.007	0.002	0.000	w
60956.78	286.438	0.004	0.001	0.000	w	69607	463.532	0.004	0.001	0.002	w
60956.78	288.899	0.001	0.000	0.002	w	69607	513.632	-	-	0.000	
60956.78	297.162	-	-	0.000		69607	514.019	0.003	0.001	0.000	w
60956.78	299.885	0.001	0.000	0.002	w	69607	514.823	-	-	0.000	
60956.78	327.043	-	-	0.000		69607	652.012	-	-	0.000	
60956.78	331.115	-	-	0.001		69607	652.419	-	-	0.000	
60956.78	338.097	0.001	0.000	0.000	w	69607	678.422	0.001	0.000	0.000	w
60956.78	339.189	0.011	0.003	0.000	w	69607	679.977	-	-	0.000	
60956.78	343.014	0.001	0.000	0.000	w						
60956.78	345.232	0.002	0.001	0.000	w	69650	203.462	-	-	0.007	o
60956.78	363.661	0.002	0.001	0.000	w	69650	204.769	-	-	0.000	o
60956.78	364.122	-	-	0.000		69650	206.792	0.056	0.014	0.222	o
60956.78	404.681	0.007	0.002	0.000	w	69650	208.534	-	-	0.000	o
60956.78	438.616	-	-	0.000		69650	208.971	-	-	0.000	o
60956.78	623.202	-	-	0.000		69650	213.425	-	-	0.000	o
60956.78	623.766	-	-	0.000		69650	214.014	-	-	0.000	o

						69650	214.436	0.016	0.004	0.001	o
60989.44	221.441	0.005	0.001	0.006	o	69650	215.762	-	-	0.000	o
60989.44	224.045	0.003	0.001	0.000	o	69650	227.913	-	-	0.001	
60989.44	245.933	0.004	0.001	0.001	w	69650	228.926	-	-	0.001	
60989.44	248.782	-	-	0.000		69650	229.313	0.006	0.001	0.005	w
60989.44	252.710	0.103	0.012	0.303		69650	236.136	0.010	0.003	0.004	w
60989.44	253.681	0.425	0.045	0.466		69650	237.852	0.050	0.013	0.065	
60989.44	254.522	0.088	0.010	0.128		69650	257.085	0.240	0.026	0.486	
60989.44	260.663	0.087	0.023	0.008		69650	261.114	0.308	0.031	0.004	
60989.44	261.845	0.157	0.018	0.027	w	69650	261.274	-	-	0.001	
60989.44	281.127	0.006	0.002	0.004		69650	261.926	-	-	0.000	
60989.44	284.136	0.001	0.000	0.001	w	69650	264.201	0.060	0.015	0.101	
60989.44	285.567	0.053	0.014	0.040		69650	265.515	0.015	0.004	0.002	w
60989.44	287.113	0.021	0.006	0.010		69650.48	276.5494	0.006223	0.001549	0.012818	w
60989.44	288.627	0.005	0.001	0.000	w	69650.48	298.2059	0.064692	0.016101	0.058514	
60989.44	296.874	-	-	0.001		69650.48	299.3357	0.00403	0.001003	0.001973	w
60989.44	326.694	0.002	0.000	0.002	w	69650.48	317.5067	0.017331	0.004313	0.002564	w
60989.44	330.757	0.001	0.000	0.000	w	69650.48	318.0149	0.06626	0.016492	0.020021	
60989.44	338.814	-	-	0.000		69650.48	404.1641	0.020477	0.005097	0.000143	w
60989.44	344.843	0.001	0.000	0.000	w	69650.48	404.4012	0.005525	0.001375	0.000739	w
60989.44	356.030	0.003	0.001	0.000	w	69650.48	454.9192	0.032469	0.008081	0.002044	
60989.44	363.229	0.033	0.009	0.000	w	69650.48	462.5893	0.006911	0.00172	0.00092	w
60989.44	363.689	0.002	0.000	0.000	w	69650.48	510.7245	-	-	1.33E-05	
						69650.48	512.4754	0.015511	0.00386	2.62E-06	w
61035.29	211.072	0.067	0.016	0.042	o	69650.48	513.661	-	-	3.36E-06	
61035.29	212.110	-	-	0.005	o	69650.48	650.2333	-	-	3.57E-06	
61035.29	234.259	-	-	0.001		69650.48	650.5542	-	-	3.88E-06	
61035.29	237.184	0.003	0.001	0.002	w	69650.48	676.4053	-	-	0.000112	
61035.29	251.641	-	-	0.003							
61035.29	254.874	0.570	0.053	0.856	b	71432.68	259.2785	1	0.093	1	
61035.29	258.819	-	-	0.081							
61035.29	263.052	-	-	0.001		72261.73	201.4482	-	-	0.000527	o
61035.29	283.623	0.072	0.017	0.001	w	72261.73	213.4576	-	-	0.000708	o
61035.29	293.148	0.006	0.001	0.004	w	72261.73	215.1879	0.02766	0.006515	7.5E-05	o
61035.29	336.934	-	-	0.003		72261.73	216.8915	0.02729	0.006428	0.00089	o
61035.29	336.980	0.063	0.015	0.002		72261.73	217.7542	0.007521	0.001772	0.002327	o
61035.29	401.350	0.007	0.002	0.000	w	72261.73	238.7435	0.111436	0.011603	0.049865	
61035.29	419.909	0.209	0.022	0.000		72261.73	253.8205	0.379427	0.035671	0.490408	
61035.29	438.074	-	-	0.000		72261.73	254.0415	-	-	0.000528	
61035.29	748.265	0.003	0.001	0.000	w	72261.73	257.6862	0.446665	0.041992	0.454555	
						72261.73	554.4915	-	-	8.32E-06	

61041.75	210.162	-	-	0.000	o	72261.73	733.463	-	-	0.000109	
61041.75	211.044	0.012	0.003	0.002	o						
61041.75	223.782	0.008	0.002	0.000	o	72352.02	201.0823	-	-	0.000336	o
61041.75	234.224	0.015	0.004	0.023		72352.02	201.7852	-	-	0.021094	o
61041.75	246.688	0.229	0.025	0.002		72352.02	202.312	0.002945	0.000728	0.003449	o
61041.75	248.612	-	-	0.000		72352.02	203.873	-	-	2.55E-06	o
61041.75	251.600	0.014	0.003	0.001	w	72352.02	214.7704	0.028774	0.007109	0.074303	o
61041.75	254.184	0.112	0.012	0.334		72352.02	215.5871	0.003919	0.000968	0.013699	o
61041.75	254.833	0.007	0.002	0.085	w	72352.02	215.9307	-	-	0.000285	o
61041.75	261.487	0.004	0.001	0.016	w	72352.02	217.3267	0.007945	0.001963	0.006392	o
61041.75	262.373	0.059	0.014	0.097		72352.02	221.9701	-	-	0.017839	o
61041.75	263.007	0.095	0.023	0.248		72352.02	223.4861	-	-	0.003903	o
61041.75	265.004	0.002	0.000	0.000	w	72352.02	238.2298	-	-	0.013865	
61041.75	283.571	0.122	0.013	0.135		72352.02	240.3835	0.005368	0.001326	0.012194	w
61041.75	285.141	0.020	0.005	0.013	w	72352.02	244.0423	0.086188	0.021294	0.376708	
61041.75	285.742	0.014	0.003	0.012	w	72352.02	244.611	0.089124	0.022202	0.325117	
61041.75	296.413	0.020	0.005	0.021		72352.02	246.5942	0.144737	0.015808	1.87E-07	
61041.75	299.123	0.002	0.001	0.006	w	72352.02	247.7384	0.080439	0.019874	0.018449	
61041.75	330.186	0.002	0.001	0.000	w	72352.02	257.0878	0.16446	0.017962	0.048962	
61041.75	336.861	0.002	0.001	0.000	w	72352.02	257.3181	0.049287	0.012177	0.026606	
61041.75	337.128	0.238	0.026	0.000		72352.02	276.9334	0.243077	0.026549	0.032609	
61041.75	338.214	-	-	0.000		72352.02	292.4162	-	-	0.001037	
61041.75	342.017	-	-	0.000		72352.02	364.3678	0.021708	0.005363	9.39E-05	
61041.75	344.222	-	-	0.001		72352.02	364.5605	0.043562	0.010763	9.17E-05	w
61041.75	362.998	-	-	0.000		72352.02	411.1877	0.001955	0.000483	0.001106	w
61041.75	401.245	-	-	0.000		72352.02	450.1368	0.002622	0.000648	1.82E-05	w
61041.75	403.294	0.010	0.002	0.001	w	72352.02	450.4343	0.003414	0.000843	7.22E-05	w
61041.75	436.987	0.013	0.003	0.000		72352.02	451.0513	0.011955	0.002954	0.000158	w
61041.75	437.950	-	-	0.000		72352.02	451.5609	0.008519	0.002105	0.000244	w
61041.75	619.918	-	-	0.000		72352.02	552.9932	-	-	0.001179	
61041.75	768.862	-	-	0.000		72352.02	553.0543	-	-	3.69E-06	
						72352.02	553.2864	-	-	0.000147	
61093.41	209.934	0.004	0.001	0.000	o	72352.02	572.9792	-	-	2.41E-05	
61093.41	210.814	0.009	0.002	0.008	o	72352.02	669.1163	-	-	6.44E-06	
61093.41	223.524	-	-	0.000	o	72352.02	728.636	-	-	2.93E-06	
61093.41	233.941	0.048	0.012	0.114		72352.02	730.4849	-	-	2.38E-06	
61093.41	246.374	0.041	0.010	0.007	s						
61093.41	248.293	-	-	0.003		72650.66	200.5759	-	-	0.001892	o
61093.41	251.273	-	-	0.002		72650.66	211.6993	0.043046	0.01051	0.054203	o
61093.41	253.850	0.257	0.027	0.148		72650.66	213.4011	0.022249	0.005432	0.010868	o
61093.41	254.497	0.122	0.013	0.182		72650.66	214.2074	-	-	0.000462	o

61093.41	261.134	-	-	0.016		72650.66	215.0764	-	-	0.027436	o
61093.41	262.017	-	-	0.061		72650.66	215.9247	-	-	0.001364	o
61093.41	262.650	0.079	0.019	0.152		72650.66	220.5078	-	-	0.003139	o
61093.41	264.641	0.011	0.003	0.000	w	72650.66	236.5463	-	-	0.000151	
61093.41	283.156	0.280	0.030	0.261		72650.66	238.6695	0.0099	0.002417	3.66E-06	w
61093.41	284.721	0.007	0.002	0.009	w	72650.66	242.8365	0.72115	0.070277	0.823983	
61093.41	285.321	0.003	0.001	0.003	w	72650.66	245.9183	-	-	0.002805	
61093.41	295.960	0.042	0.010	0.029		72650.66	251.5551	-	-	0.000302	
61093.41	298.661	0.006	0.001	0.001	w	72650.66	255.1284	0.151923	0.016397	0.063531	
61093.41	329.623	0.003	0.001	0.000	w	72650.66	255.3551	-	-	0.00793	
61093.41	336.276	0.014	0.003	0.000	w	72650.66	360.4445	0.016409	0.004006	1.4E-05	w
61093.41	336.542	0.013	0.003	0.000	w	72650.66	444.4539	0.01329	0.003245	0.000299	w
61093.41	337.624	0.003	0.001	0.000	w	72650.66	445.0547	0.022032	0.005379	7.41E-06	w
61093.41	341.414	-	-	0.000		72650.66	542.7826	-	-	0.00149	
61093.41	343.611	0.004	0.001	0.002	w	72650.66	544.0068	-	-	0.000104	
61093.41	362.319	0.026	0.006	0.000		72650.66	544.2905	-	-	2.19E-06	
61093.41	400.415	0.003	0.001	0.000	w	72650.66	563.3371	-	-	1.58E-06	
61093.41	402.455	0.003	0.001	0.001	w	72650.66	713.1146	-	-	1.1E-05	
61093.41	436.002	0.004	0.001	0.000	w	72650.66	714.8855	-	-	8.07E-07	
61093.41	436.961	0.020	0.005	0.000							
61093.41	617.938	-	-	0.000		73091.59	209.7406	-	-	0.020995	o
61093.41	618.493	-	-	0.000		73091.59	211.411	-	-	0.00225	o
61093.41	765.819	-	-	0.000		73091.59	212.2022	0.006492	0.001608	0.000458	o
						73091.59	213.0551	0.024591	0.006089	0.049022	o
61332.76	208.884	-	-	0.001	o	73091.59	213.8875	-	-	0.004921	o
61332.76	209.755	0.008	0.002	0.021	o	73091.59	218.3835	0.018352	0.004544	0.032057	o
61332.76	210.779	0.004	0.001	0.007	o	73091.59	234.1036	0.016482	0.004081	0.000112	
61332.76	232.638	0.005	0.001	0.001	w	73091.59	236.183	-	-	5.82E-05	
61332.76	235.522	0.093	0.022	0.009		73091.59	240.2629	0.128432	0.014057	0.079819	
61332.76	244.929	0.003	0.001	0.005	w	73091.59	243.2794	0.212632	0.023273	0.055753	
61332.76	246.826	0.032	0.007	0.018		73091.59	248.7945	-	-	0.004918	
61332.76	249.770	0.125	0.013	0.000		73091.59	252.2892	0.432231	0.042716	0.661726	
61332.76	252.956	0.353	0.033	0.749		73091.59	252.5109	0.144215	0.015785	0.086888	s
61332.76	256.841	0.044	0.010	0.160		73091.59	354.8038	0.010242	0.002536	0.000725	w
61332.76	260.384	0.003	0.001	0.001	w	73091.59	435.9087	0.00633	0.001567	4.18E-06	w
61332.76	261.009	0.028	0.007	0.001	w	73091.59	436.4865	-	-	5.87E-06	
61332.76	262.975	0.126	0.013	0.000		73091.59	530.0922	-	-	0.000193	
61332.76	281.249	0.007	0.002	0.009	w	73091.59	531.2597	-	-	1.06E-05	
61332.76	283.385	0.004	0.001	0.001	w	73091.59	531.5303	-	-	1.19E-06	
61332.76	290.612	0.007	0.002	0.011		73091.59	691.3694	-	-	6.4E-05	
61332.76	296.541	0.110	0.011	0.003		73091.59	693.0338	-	-	1.55E-05	

61332.76	333.590	0.006	0.001	0.000		73091.59	779.7405	-	-	4.01E-06	
61332.76	333.634	0.003	0.001	0.000	w						
61332.76	333.852	0.007	0.002	0.003	w	73751.28	206.8769	-	-	0.000316	o
61332.76	338.645	-	-	0.000		73751.28	208.5018	-	-	0.002601	o
61332.76	396.613	0.003	0.001	0.000	w	73751.28	209.2714	-	-	6.26E-07	o
61332.76	398.614	0.007	0.002	0.000		73751.28	210.1008	-	-	0.002988	o
61332.76	414.727	-	-	0.000		73751.28	210.9102	0.143427	0.015009	0.076053	o
61332.76	431.498	0.023	0.005	0.000		73751.28	215.2808	-	-	0.00035	o
61332.76	432.437	0.001	0.000	0.000	w	73751.28	230.5418	0.013815	0.00327	8.62E-05	w
61332.76	609.468	-	-	0.000		73751.28	232.5582	0.090934	0.021527	0.063267	
61332.76	731.968	-	-	0.000		73751.28	236.5127	-	-	3.41E-05	
61332.76	752.030	-	-	0.000		73751.28	239.4352	0.005983	0.001416	0.001486	w
						73751.28	244.7756	0.536436	0.050687	0.733933	
61347.61	249.326	0.997	0.093	1.000		73751.28	248.1575	0.005194	0.00123	0.036455	w
61347.61	351.122	0.003	0.001	0.000	w	73751.28	248.372	0.195346	0.020443	0.081283	
						73751.28	346.6866	0.008865	0.002099	3.46E-06	w
61527.62	242.720	0.027	0.006	0.006		73751.28	530.4392	-	-	3.08E-06	
61527.62	248.212	0.161	0.017	0.289		73751.28	661.2039	-	-	1.27E-05	
61527.62	249.318	0.581	0.055	0.644		73751.28	662.7261	-	-	0.001129	
61527.62	276.936	0.158	0.017	0.053							
61527.62	282.743	0.021	0.005	0.008		73966.83	205.9581	-	-	0.00051	o
61527.62	348.916	0.043	0.010	0.000	w	73966.83	209.1532	-	-	0.002378	o
61527.62	349.334	0.010	0.002	0.000		73966.83	243.2874	0.42257	0.039629	0.963917	
						73966.83	243.4904	0.56817	0.053284	0.033194	
61587.21	218.546	-	-	0.000	o	73966.83	506.5821	0.00926	0.002176	1.06E-06	w
61587.21	242.369	0.325	0.044	0.000	w						
61587.21	245.135	0.029	0.010	0.003	w	73969.77	205.9456	-	-	0.000444	o
61587.21	247.845	0.138	0.021	0.023		73969.77	207.5559	0.014918	0.004231	0.00013	o
61587.21	248.948	0.083	0.012	0.215		73969.77	209.1403	-	-	0.003868	o
61587.21	249.890	0.237	0.032	0.695		73969.77	209.9424	-	-	0.002169	o
61587.21	256.662	-	-	0.021		73969.77	229.3859	0.066989	0.018998	0.006073	
61587.21	276.479	0.006	0.002	0.003	w	73969.77	243.27	0.291456	0.032992	0.015354	w
61587.21	279.389	0.057	0.019	0.032		73969.77	243.473	0.561266	0.063533	0.969384	
61587.21	282.267	0.003	0.001	0.001	w	73969.77	246.8188	0.065371	0.018539	0.002481	w
61587.21	283.730	0.008	0.003	0.006		73969.77	651.7854	-	-	9.71E-05	
61587.21	320.434	0.006	0.002	0.000	w						
61587.21	348.192	0.008	0.003	0.000	w	77861.63	253.7138	0.353896	0.032936	0.417506	
61587.21	348.608	0.001	0.000	0.000	w	77861.63	255.0152	0.342775	0.031901	0.119185	
61587.21	355.508	0.100	0.015	0.000		77861.63	278.5192	0.16112	0.016607	0.301848	
						77861.63	279.6628	0.010254	0.002391	0.030633	w
61726.08	207.181	0.013	0.003	0.000	o	77861.63	280.6223	0.001803	0.00042	3.06E-05	w

61726.08	217.885	-	-	0.000	o	77861.63	283.98	0.113078	0.011655	0.123817	
61726.08	220.406	-	-	0.000	o	77861.63	297.2746	-	-	0.002405	
61726.08	242.591	0.031	0.008	0.001	s	77861.63	299.1818	0.017073	0.003981	0.003885	
61726.08	244.303	0.013	0.003	0.000	w	77861.63	301.9554	-	-	7.02E-06	
61726.08	244.452	0.330	0.032	0.911		77861.63	395.4716	-	-	1.02E-05	
61726.08	249.025	-	-	0.002		77861.63	580.0143	-	-	1.23E-06	
61726.08	249.836	0.081	0.019	0.015	w	77861.63	632.8925	-	-	2.24E-06	
61726.08	255.751	0.064	0.015	0.045		77861.63	637.1721	-	-	0.000668	
61726.08	256.889	0.014	0.003	0.013		77861.63	670.2096	-	-	9.46E-07	
61726.08	257.743	0.004	0.001	0.003	w						
61726.08	260.282	0.010	0.002	0.000		78690.85	208.5871	-	-	0.007526	o
61726.08	278.309	0.004	0.001	0.002	w	78690.85	211.2316	-	-	1.4E-05	o
61726.08	279.681	0.008	0.002	0.001	w	78690.85	211.3366	-	-	2.28E-07	o
61726.08	280.260	0.201	0.021	0.001	b	78690.85	211.763	-	-	0.000216	o
61726.08	282.616	0.022	0.005	0.000		78690.85	213.2477	0.005938	0.001443	0.003313	o
61726.08	290.518	0.002	0.000	0.002	w	78690.85	214.1029	-	-	0.050665	o
61726.08	293.121	-	-	0.000		78690.85	221.2209	0.013115	0.003187	0.004554	o
61726.08	319.014	-	-	0.000		78690.85	234.8659	-	-	1.49E-07	
61726.08	322.888	-	-	0.000		78690.85	235.5662	-	-	0.002779	
61726.08	329.523	0.003	0.001	0.001	w	78690.85	246.6766	0.680765	0.066032	0.632077	
61726.08	330.561	-	-	0.000		78690.85	246.9833	0.055623	0.013517	0.243046	
61726.08	334.193	0.019	0.005	0.000	w	78690.85	295.9835	0.145485	0.015629	0.052438	
61726.08	336.298	0.014	0.003	0.000	w	78690.85	296.1107	-	-	0.000716	
61726.08	353.761	0.025	0.006	0.000		78690.85	322.3199	-	-	0.000233	
61726.08	354.197	0.140	0.015	0.000		78690.85	326.1515	0.012748	0.003098	0.000646	w
61726.08	392.459	-	-	0.000		78690.85	342.5563	0.009827	0.002388	0.000136	w
61726.08	424.295	0.003	0.001	0.000	w	78690.85	350.1863	-	-	7.3E-06	
61726.08	594.683	-	-	0.000		78690.85	350.7395	0.003993	0.00097	2.89E-05	w
						78690.85	351.0476	0.008135	0.001977	2.79E-05	w
62065.52	205.733	0.014	0.003	0.026	o	78690.85	419.6914	0.033195	0.008067	3.05E-05	w
62065.52	216.285	-	-	0.001	o	78690.85	420.2522	-	-	0.000959	
62065.52	218.768	0.014	0.003	0.014	o	78690.85	420.2859	0.016655	0.004047	0.000503	w
62065.52	240.609	0.008	0.002	0.006	w	78690.85	469.7982	0.00434	0.001055	3.19E-06	w
62065.52	242.293	-	-	0.005		78690.85	471.6212	-	-	7.26E-06	
62065.52	242.439	-	-	0.188		78690.85	499.2468	0.005734	0.001393	6.39E-05	w
62065.52	246.937	0.096	0.023	0.010	w	78690.85	547.7986	0.004449	0.001081	3.44E-06	w
62065.52	247.735	0.056	0.013	0.093		78690.85	547.926	-	-	6.32E-06	
62065.52	253.549	0.320	0.030	0.213							
62065.52	254.667	0.174	0.018	0.242		80346.02	242.4288	0.466316	0.061289	0.001177	w
62065.52	255.507	0.068	0.016	0.073		80346.02	263.4628	0.004826	0.001589	0.006375	w
62065.52	258.001	0.004	0.001	0.000	w	80346.02	263.7305	-	-	0.00435	

62065.52	275.703	0.012	0.003	0.021	w	80346.02	272.213	0.130567	0.019006	0.001035	
62065.52	277.050	0.023	0.005	0.002		80346.02	283.188	-	-	0.088271	
62065.52	277.618	0.005	0.001	0.008	w	80346.02	284.4959	0.028541	0.009398	0.130243	w
62065.52	279.930	0.056	0.013	0.042		80346.02	285.1723	0.311212	0.040903	0.567128	
62065.52	287.680	0.022	0.005	0.023		80346.02	303.3444	0.007164	0.002359	0.037068	w
62065.52	290.232	0.016	0.004	0.002		80346.02	305.5352	0.044275	0.014579	0.157705	
62065.52	315.595	0.005	0.001	0.002	w	80346.02	483.3641	-	-	1.32E-05	
62065.52	319.386	0.063	0.015	0.006		80346.02	517.7027	-	-	2.45E-05	
62065.52	325.877	0.023	0.006	0.020		80346.02	525.8026	-	-	0.000178	
62065.52	326.892	-	-	0.000		80346.02	548.6824	-	-	0.000166	
62065.52	330.443	-	-	0.001		80346.02	552.2871	-	-	0.000112	
62065.52	332.501	0.002	0.000	0.001	w	80346.02	570.7176	0.007099	0.002338	0.00076	w
62065.52	349.562	0.005	0.001	0.001	w	80346.02	575.0883	-	-	0.000734	
62065.52	349.988	-	-	0.001		80346.02	592.2211	-	-	0.001901	
62065.52	387.298	-	-	0.000		80346.02	595.5508	-	-	0.001726	
62065.52	418.269	0.010	0.002	0.000	w	80346.02	709.1574	-	-	5.22E-06	
62065.52	582.913	-	-	0.000		80346.02	727.9533	-	-	0.000885	
62065.52	583.406	0.001	0.000	0.000	w	80346.02	764.7722	-	-	0.000143	
62083.11	216.202	0.029	0.007	0.197	o	82853.66	225.1824	0.540883	0.050302	0.687238	
62083.11	218.684	0.009	0.002	0.009	o	82853.66	244.5107	0.223211	0.022991	0.292767	
62083.11	239.489	0.015	0.004	0.055		82853.66	245.3917	0.235906	0.024298	0.01943	
62083.11	242.190	0.001	0.000	0.004	w	82853.66	258.8481	-	-	0.000562	
62083.11	245.911	-	-	0.033		82853.66	449.7526	-	-	1.18E-06	
62083.11	246.830	0.011	0.003	0.053		82853.66	582.6699	-	-	8.62E-07	
62083.11	247.627	0.010	0.002	0.049		82853.66	593.6277	-	-	6.46E-07	
62083.11	253.436	0.077	0.019	0.002							
62083.11	254.553	0.025	0.006	0.011	s	83459.67	224.1421	0.011145	0.002601	0.267643	o
62083.11	272.738	0.233	0.025	0.134		83459.67	224.92	0.097015	0.022643	0.379038	o
62083.11	275.569	0.404	0.039	0.001		83459.67	225.4075	0.003585	0.000837	0.095667	w
62083.11	276.915	0.044	0.011	0.022	w	83459.67	243.0882	0.014413	0.003364	0.134338	
62083.11	278.369	0.081	0.019	0.295		83459.67	243.4819	0.120078	0.012389	0.051979	
62083.11	279.792	0.013	0.003	0.012		83459.67	243.7105	0.037726	0.008805	0.046447	
62083.11	287.535	0.012	0.003	0.040		83459.67	248.5508	-	-	0.01358	
62083.11	315.420	0.019	0.005	0.062		83459.67	250.9365	-	-	0.005378	
62083.11	319.207	-	-	0.002		83459.67	258.4882	0.000505	0.000118	0.00068	w
62083.11	326.704	0.001	0.000	0.001	w	83459.67	260.2338	0.001097	0.000256	0.001127	w
62083.11	332.306	0.003	0.001	0.006	w	83459.67	260.476	-	-	0.000949	
62083.11	342.682	-	-	0.000		83459.67	261.3379	-	-	0.000742	
62083.11	349.347	0.003	0.001	0.010		83459.67	261.9086	0.049711	0.011603	0.000341	
62083.11	349.772	0.010	0.002	0.000		83459.67	273.9499	0.648236	0.060389	0.000357	

62083.11	582.316	-	-	0.000		83459.67	277.1577	0.002509	0.000586	0.000998	w
						83459.67	278.9855	0.007515	0.001754	0.000596	
62125.6	205.479	0.002	0.001	0.000	o	83459.67	465.3164	-	-	7.35E-05	
62125.6	206.322	-	-	0.000	o	83459.67	466.9267	0.003495	0.000816	5.29E-05	w
62125.6	207.313	0.004	0.001	0.006	o	83459.67	469.1736	0.002105	0.000491	3.25E-06	w
62125.6	228.423	0.055	0.013	0.007	w	83459.67	495.2376	0.000863	0.000201	3.39E-06	w
62125.6	231.203	0.025	0.006	0.075		83459.67	499.9965	-	-	7.24E-06	
62125.6	240.262	0.087	0.021	0.001							
62125.6	242.086	-	-	0.000		83558.54	224.4208	0.017411	0.004444	0.274847	o
62125.6	244.918	0.003	0.001	0.011	w	83558.54	224.906	0.303826	0.03095	0.457292	o
62125.6	247.981	0.191	0.020	0.011		83558.54	242.8969	0.177463	0.020022	0.158276	w
62125.6	251.714	0.076	0.018	0.293		83558.54	243.1245	0.043603	0.011128	0.098989	w
62125.6	255.115	0.034	0.008	0.059		83558.54	250.3153	0.246528	0.027814	0.00423	w
62125.6	255.715	0.012	0.003	0.141	w	83558.54	259.5657	0.004283	0.001093	0.001976	w
62125.6	257.602	0.277	0.029	0.000		83558.54	260.6641	0.184191	0.020781	0.002056	
62125.6	275.113	0.035	0.008	0.106	w	83558.54	261.2319	-	-	0.000444	
62125.6	277.156	0.004	0.001	0.007	w	83558.54	276.4	0.01538	0.003925	0.000465	w
62125.6	284.065	0.128	0.013	0.207		83558.54	278.2178	0.004585	0.00117	0.001385	w
62125.6	289.727	0.029	0.007	0.056		83558.54	463.1849	0.002729	0.000696	3.56E-05	w
62125.6	324.992	-	-	0.004		83558.54	499.8843	-	-	5.1E-06	
62125.6	325.034	0.001	0.000	0.003	w						
62125.6	325.240	0.001	0.000	0.000	w	83713.54	220.9034	0.065599	0.015716	0.232271	o
62125.6	329.788	0.009	0.002	0.005	w	83713.54	221.8893	-	-	0.002749	o
62125.6	384.518	0.004	0.001	0.002	w	83713.54	222.8734	0.095337	0.022841	0.263209	o
62125.6	386.399	0.003	0.001	0.000	w	83713.54	240.3189	0.006323	0.001515	0.001276	w
62125.6	401.521	0.004	0.001	0.000	w	83713.54	241.0271	-	-	0.112529	
62125.6	417.220	0.011	0.003	0.000	w	83713.54	241.5967	0.006923	0.001659	0.014166	w
62125.6	418.098	0.003	0.001	0.005	w	83713.54	243.5	0.460118	0.043999	0.356025	
62125.6	581.368	-	-	0.000		83713.54	246.9917	0.042696	0.010229	0.001771	
62125.6	709.703	-	-	0.000		83713.54	253.2101	0.021144	0.005066	0.000522	w
62125.6	767.565	-	-	0.000		83713.54	254.5926	0.30186	0.028865	0.011343	
						83713.54	256.5983	-	-	0.002534	
62151.56	205.369	-	-	0.003	o	83713.54	256.8024	-	-	8.15E-05	
62151.56	206.212	0.003	0.001	0.008	o	83713.54	258.7642	-	-	4.53E-05	
62151.56	218.357	0.002	0.001	0.001	o	83713.54	272.0572	-	-	0.000489	
62151.56	228.287	0.002	0.001	0.001	w	83713.54	321.1302	-	-	8.89E-06	
62151.56	240.112	-	-	0.000		83713.54	436.4384	-	-	2.47E-06	
62151.56	241.934	0.001	0.000	0.001	w	83713.54	454.6772	-	-	2.03E-06	
62151.56	244.763	0.029	0.010	0.000	w	83713.54	461.4551	-	-	0.000164	
62151.56	247.207	0.007	0.002	0.058		83713.54	461.8068	-	-	1.31E-06	
62151.56	247.821	0.013	0.004	0.007		83713.54	463.6496	-	-	1.63E-05	

62151.56	254.110	0.082	0.012	0.351		83713.54	464.0812	-	-	0.000793	
62151.56	254.946	0.155	0.023	0.383		83713.54	505.8103	-	-	1.57E-06	
62151.56	255.545	0.022	0.008	0.118		83713.54	684.2197	-	-	7.4E-07	
62151.56	257.430	0.083	0.013	0.001							
62151.56	274.916	0.391	0.053	0.002	w	83726.36	220.8407	0.132739	0.016066	0.284348	o
62151.56	276.391	0.004	0.001	0.015	w	83726.36	221.8261	0.124951	0.015124	0.288358	o
62151.56	276.956	-	-	0.002		83726.36	239.4003	0.015423	0.004223	0.014987	w
62151.56	286.970	0.002	0.001	0.003	w	83726.36	240.2448	0.235696	0.028528	0.104379	w
62151.56	289.509	0.018	0.006	0.010		83726.36	240.9525	-	-	0.000452	
62151.56	318.510	0.002	0.001	0.001	w	83726.36	243.4239	0.132498	0.016037	0.301465	
62151.56	324.718	0.022	0.008	0.030	s	83726.36	253.1279	-	-	0.000145	
62151.56	324.966	0.001	0.000	0.004	w	83726.36	254.5094	0.31914	0.034877	0.004136	
62151.56	325.975	-	-	0.000		83726.36	256.5139	0.007373	0.002019	0.00026	
62151.56	329.506	0.001	0.000	0.000	w	83726.36	320.9979	-	-	9.68E-06	
62151.56	331.552	-	-	0.000		83726.36	432.7616	0.003525	0.000965	3.64E-06	w
62151.56	348.937	0.035	0.012	0.000	w	83726.36	461.5333	0.013599	0.003723	4.95E-06	w
62151.56	384.134	-	-	0.000		83726.36	463.805	0.015057	0.004123	0.00145	w
62151.56	386.011	0.120	0.018	0.000		83726.36	503.6367	-	-	2.08E-06	
62151.56	416.769	-	-	0.000							
62151.56	417.645	0.005	0.002	0.000	w	84035.14	237.643	0.949148	0.092504	0.999997	
62151.56	580.003	-	-	0.000		84035.14	427.0533	0.050852	0.012417	2.75E-06	w
62151.56	580.491	-	-	0.000							
62151.56	790.632	-	-	0.000		84296.83	218.092	-	-	3.14E-05	o
						84296.83	236.1737	0.409642	0.04007	0.068368	
62158.11	215.852	0.009	0.002	0.000	o	84296.83	236.9955	0.508087	0.049699	0.920039	
62158.11	218.326	-	-	0.000	o	84296.83	249.5234	0.010037	0.00246	0.011404	w
62158.11	239.060	0.002	0.000	0.000	w	84296.83	425.6005	0.026061	0.006387	1.15E-05	w
62158.11	241.751	0.001	0.000	0.000	w	84296.83	428.9279	0.014767	0.003619	1.51E-06	w
62158.11	245.459	0.100	0.010	0.031		84296.83	450.046	-	-	1.97E-06	
62158.11	246.374	0.030	0.007	0.025	s	84296.83	451.5707	0.031406	0.007696	1.32E-05	w
62158.11	247.167	-	-	0.009		84296.83	489.567	-	-	2.03E-06	
62158.11	252.955	0.413	0.039	0.794		84296.83	491.3107	-	-	8.08E-06	
62158.11	254.068	0.105	0.011	0.093		84296.83	528.0248	-	-	1.1E-06	
62158.11	272.181	0.020	0.005	0.012		84296.83	537.4621	-	-	6.29E-05	
62158.11	275.001	0.180	0.019	0.004		84296.83	546.7719	-	-	5.52E-05	
62158.11	276.341	-	-	0.001							
62158.11	277.789	0.023	0.005	0.002		84326.91	218.9087	0.009643	0.002302	0.000251	o
62158.11	279.206	-	-	0.000		84326.91	219.8665	0.006529	0.001559	0.122773	o
62158.11	286.916	0.034	0.008	0.006	w	84326.91	220.615	0.024514	0.005852	0.278755	o
62158.11	314.676	0.003	0.001	0.000	w	84326.91	237.5143	0.150671	0.015899	0.009163	
62158.11	318.444	0.002	0.000	0.000	w	84326.91	238.0675	0.175562	0.018526	0.04529	

62158.11	325.905	0.025	0.006	0.020		84326.91	238.445	0.135221	0.014269	0.00571	
62158.11	331.480	0.018	0.004	0.000		84326.91	239.9153	0.326624	0.03112	0.17192	
62158.11	341.803	0.023	0.005	0.000		84326.91	243.3043	-	-	0.051306	
62158.11	348.434	-	-	0.000		84326.91	245.59	0.014051	0.003354	0.295106	
62158.11	348.857	0.011	0.003	0.000	w	84326.91	250.6765	0.016448	0.003926	0.010004	w
						84326.91	252.8187	-	-	0.001052	
62293.16	238.290	-	-	0.077		84326.91	254.4883	0.051498	0.012293	0.001637	w
62293.16	243.582	0.002	0.000	0.001	w	84326.91	254.7199	-	-	5.68E-05	
62293.16	244.647	0.120	0.012	0.103		84326.91	256.0897	-	-	3.31E-05	
62293.16	271.184	0.222	0.023	0.136		84326.91	267.5902	0.000813	0.000194	0.002326	w
62293.16	276.750	0.641	0.060	0.683		84326.91	270.65	0.060654	0.014479	0.003226	
62293.16	339.836	-	-	0.000		84326.91	312.141	0.001031	0.000246	2.9E-06	w
62293.16	340.232	0.015	0.004	0.000		84326.91	314.925	-	-	4.09E-06	
						84326.91	417.8626	0.002622	0.000626	5.14E-06	w
62322.43	204.651	-	-	0.000	o	84326.91	430.292	0.002828	0.000675	2.77E-06	w
62322.43	215.089	-	-	0.000	o	84326.91	442.3373	0.002287	0.000546	1.41E-05	w
62322.43	217.545	0.042	0.011	0.145	o	84326.91	447.2622	0.003149	0.000752	0.000403	w
62322.43	239.130	-	-	0.006		84326.91	448.7497	-	-	0.000633	
62322.43	240.794	0.018	0.005	0.039		84326.91	450.2975	-	-	7.9E-06	
62322.43	240.938	0.001	0.000	0.005	w	84326.91	450.8247	0.00345	0.000823	4.03E-05	w
62322.43	245.380	0.042	0.011	0.077		84326.91	451.2328	0.00345	0.000824	0.000199	w
62322.43	246.167	-	-	0.059		84326.91	462.0412	-	-	1.5E-05	
62322.43	251.907	0.103	0.012	0.002		84326.91	467.555	-	-	2.88E-06	
62322.43	253.011	0.101	0.012	0.164		84326.91	467.9307	0.002232	0.000533	6.35E-06	w
62322.43	253.840	0.150	0.018	0.011		84326.91	474.8378	-	-	3.49E-05	
62322.43	256.302	-	-	0.000		84326.91	479.211	-	-	1.09E-05	
62322.43	273.763	0.034	0.009	0.007	w	84326.91	556.9599	0.006725	0.001605	4.48E-06	w
62322.43	275.092	-	-	0.006		84326.91	656.6533	-	-	2.43E-06	
62322.43	275.651	0.141	0.017	0.024	w	84326.91	665.3816	-	-	2.71E-06	
62322.43	277.930	0.169	0.020	0.299							
62322.43	285.569	0.055	0.015	0.062		84527.78	216.9986	-	-	0.000202	o
62322.43	288.083	0.085	0.023	0.025		84527.78	217.9499	0.042295	0.012346	0.001014	o
62322.43	313.056	0.001	0.000	0.000	w	84527.78	234.892	0.087485	0.011289	0.003205	w
62322.43	316.786	0.036	0.010	0.049		84527.78	235.7049	0.1611	0.020788	0.145514	
62322.43	323.171	0.002	0.000	0.005	w	84527.78	236.3861	0.351839	0.040993	0.822986	
62322.43	324.169	0.001	0.000	0.001	w	84527.78	238.7642	0.009101	0.002657	0.017126	w
62322.43	327.660	0.005	0.001	0.004	w	84527.78	248.0932	0.090448	0.011671	0.000183	
62322.43	329.684	0.001	0.000	0.001	w	84527.78	249.4202	0.0856	0.011046	0.00622	w
62322.43	346.450	0.001	0.000	0.001	w	84527.78	251.345	0.014353	0.00419	0.003437	w
62322.43	346.868	0.010	0.003	0.006	b	84527.78	424.1308	0.021822	0.00637	6.6E-06	w
62322.43	383.481	-	-	0.000		84527.78	438.4406	0.044856	0.013094	1.25E-06	w

62322.43	413.821	0.002	0.001	0.000	w	84527.78	445.0663	0.011663	0.003404	3.05E-06	w
62322.43	574.788	-	-	0.000		84527.78	446.9085	0.063928	0.018661	1.2E-06	w
						84527.78	447.1785	-	-	4.16E-06	
		-	-			84527.78	450.2157	-	-	1.56E-06	
62689.88	203.123	0.005	0.001	0.000	o	84527.78	463.2035	0.005117	0.001494	1.09E-06	w
62689.88	203.947	-	-	0.002	o	84527.78	487.9807	-	-	5.98E-06	
62689.88	215.819	0.020	0.005	0.000	o	84527.78	530.8707	-	-	2E-06	
62689.88	225.515	0.190	0.020	0.025		84527.78	537.5877	-	-	1.68E-05	
62689.88	237.047	-	-	0.001		84527.78	539.9517	0.010394	0.003034	5.66E-06	w
62689.88	238.823	0.004	0.001	0.079		84527.78	550.7961	-	-	6.41E-05	
62689.88	241.579	-	-	0.002	w						
62689.88	243.960	0.269	0.029	0.000		84863.35	215.4292	-	-	0.005175	o
62689.88	244.557	0.043	0.010	0.737		84863.35	233.0542	-	-	0.003807	
62689.88	250.680	0.047	0.011	0.001	w	84863.35	233.8545	0.091696	0.012064	0.010014	w
62689.88	251.493	0.010	0.002	0.016		84863.35	246.044	0.672789	0.079921	0.978268	
62689.88	252.076	-	-	0.002	w	84863.35	412.4606	-	-	3.17E-05	
62689.88	253.910	0.132	0.014	0.000		84863.35	415.5774	-	-	0.000103	
62689.88	270.906	-	-	0.120		84863.35	416.9705	0.013534	0.004028	1.69E-06	w
62689.88	272.338	0.084	0.020	0.001		84863.35	418.7493	-	-	1.3E-05	
62689.88	272.886	0.023	0.006	0.000		84863.35	428.4068	-	-	1.3E-06	
62689.88	282.603	-	-	0.013		84863.35	438.8536	0.041235	0.012272	3.68E-05	w
62689.88	285.065	0.003	0.001	0.000		84863.35	440.3033	0.029137	0.008672	0.000308	w
62689.88	313.140	0.002	0.000	0.000	w	84863.35	476.3515	-	-	3.43E-05	
62689.88	319.137	0.086	0.021	0.000	w	84863.35	478.0021	-	-	0.000145	
62689.88	319.377	-	-	0.000		84863.35	499.0768	0.015356	0.00457	5.77E-06	w
62689.88	320.351	-	-	0.000		84863.35	512.6841	0.028267	0.008413	1.31E-05	w
62689.88	323.761	0.012	0.003	0.000		84863.35	518.4388	-	-	2.28E-06	
62689.88	325.736	0.015	0.004	0.001		84863.35	521.5763	0.05636	0.016773	0.001137	w
62689.88	342.501	-	-	0.000	w	84863.35	530.3395	0.010521	0.003131	0.000894	w
62689.88	376.350	0.004	0.001	0.000		84863.35	541.8059	-	-	7.29E-06	
62689.88	378.151	0.011	0.003	0.000	w	84863.35	687.1548	0.041107	0.012234	9.85E-07	w
62689.88	407.621	0.032	0.008	0.000	w						
62689.88	408.459	0.009	0.002	0.000	w	84938.18	217.6782	0.113519	0.014086	5.77E-05	o
62689.88	562.437	-	-	0.000	w	84938.18	218.1348	-	-	0.000235	o
62689.88	562.896	-	-	0.000		84938.18	234.6514	0.093725	0.01163	0.027605	w
62689.88	665.810	-	-	0.000		84938.18	235.0182	0.177844	0.022067	0.302359	
62689.88	682.369	-	-	0.000		84938.18	235.2312	0.310876	0.034829	0.658756	
62689.88	758.347	-	-	0.000		84938.18	239.7375	0.018987	0.005329	6.27E-05	w
62689.88	796.778	-	-	0.000		84938.18	241.9563	0.03583	0.010057	0.000374	w
62689.88	799.648			0.000		84938.18	250.5887	-	-	0.001306	
		-	-			84938.18	250.8132	-	-	0.000396	

62829.08	203.369	0.012	0.003	0.000	o	84938.18	251.6123	0.154121	0.019124	0.007435	w
62829.08	204.332	0.007	0.002	0.015	o	84938.18	252.1413	-	-	0.001243	
62829.08	224.809	-	-	0.000	o	84938.18	263.2822	0.005525	0.001551	1.46E-05	w
62829.08	227.501	0.065	0.018	0.000		84938.18	266.2437	0.089573	0.011114	8.25E-05	w
62829.08	240.769	0.211	0.025	0.000	w	84938.18	267.9299	-	-	7.32E-05	
62829.08	243.727	0.396	0.043	0.068							
62829.08	247.332	-	-	0.898		85172.81	216.5717	0.025274	0.006683	0.001559	o
62829.08	251.195	-	-	0.011		85172.81	217.0235	0.007423	0.001963	0.001937	o
62829.08	269.888	-	-	0.001		85172.81	233.7289	0.006632	0.001754	0.004567	w
62829.08	278.498	-	-	0.002		85172.81	233.9396	0.098722	0.011539	0.00582	
62829.08	317.725	0.071	0.019	0.001		85172.81	249.1234	0.64803	0.068393	0.402028	
62829.08	317.766	0.096	0.011	0.003		85172.81	250.135	-	-	0.277128	
62829.08	374.388	0.002	0.001	0.000	w	85172.81	250.6578	0.072199	0.019091	0.037227	w
62829.08	390.488	-	-	0.000	w	85172.81	264.5903	0.00824	0.002179	0.06577	w
62829.08	406.149	-	-	0.000		85172.81	266.2556	0.017906	0.004735	0.194314	w
62829.08	728.232	0.140	0.017	0.000		85172.81	391.9021	0.035394	0.009359	6.63E-05	w
62829.08	750.424	-	-	0.000		85172.81	414.1759	0.023548	0.006226	9.39E-05	w
62829.08	783.903			0.000		85172.81	419.3441	-	-	0.000153	
		0.018	0.004			85172.81	433.7701	0.02896	0.007658	0.000375	w
62945.04	202.075	-	-	0.133	o	85172.81	436.0199	0.003757	0.000993	7.71E-05	w
62945.04	212.245	0.003	0.001	0.004	o	85172.81	447.4272	-	-	0.000916	
62945.04	214.637	0.001	0.000	0.011	o	85172.81	450.1091	0.004322	0.001143	0.001134	w
62945.04	235.621	0.005	0.001	0.002	w	85172.81	460.537	-	-	0.001899	
62945.04	237.236	0.191	0.020	0.004	w	85172.81	462.5481	0.011137	0.002945	0.002684	w
62945.04	237.376	0.007	0.002	0.002		85172.81	490.8696	-	-	1.01E-05	
62945.04	241.686	0.042	0.010	0.001	w	85172.81	491.5354	-	-	7.08E-06	
62945.04	242.450	0.110	0.012	0.001		85172.81	538.6389	0.00576	0.001523	0.000392	w
62945.04	248.016	0.212	0.023	0.491		85172.81	558.5359	-	-	0.000115	
62945.04	249.086	0.165	0.017	0.239		85172.81	629.917	0.002696	0.000713	0.000175	w
62945.04	249.889	-	-	0.035		85172.81	634.9133	-	-	0.00076	
62945.04	252.275	0.005	0.001	0.000		85172.81	761.4176	-	-	7.23E-05	
62945.04	269.174	0.003	0.001	0.014		85172.81	768.7937	-	-	1.3E-05	
62945.04	270.458	0.002	0.001	0.004	w	85172.81	771.4027	-	-	0.000209	
62945.04	270.999	0.008	0.002	0.001	w	85172.81	784.5227	-	-	0.000413	
62945.04	273.201	0.003	0.001	0.017		85172.81	790.4062	-	-	8.64E-05	
62945.04	280.579	0.000	0.000	0.007	w						
62945.04	283.005	0.002	0.000	0.000	w	86124.3	209.7295	-	-	0.000312	o
62945.04	307.069	0.004	0.001	0.002	w	86124.3	210.6181	-	-	0.000143	o
62945.04	310.657	0.024	0.006	0.004	w	86124.3	226.3984	-	-	2.89E-05	
62945.04	316.794	0.012	0.003	0.001		86124.3	227.1535	-	-	0.00392	
62945.04	317.753	-	-	0.025		86124.3	227.7862	0.023281	0.005908	0.00687	w

62945.04	321.108	0.029	0.007	0.001		86124.3	229.9936	-	-	0.012462	
62945.04	323.050	-	-	0.000	w	86124.3	238.6375	0.090647	0.023003	0.246373	
62945.04	339.132	-	-	0.000		86124.3	239.865	0.266449	0.02989	0.444656	w
62945.04	339.533	0.144	0.015	0.000		86124.3	241.6447	0.137849	0.015464	0.274599	
62945.04	374.536	0.009	0.002	0.000		86124.3	392.0635	-	-	0.004767	
62945.04	403.424	-	-	0.000	w	86124.3	394.8786	0.168915	0.018949	0.000339	
62945.04	554.477	-	-	0.000		86124.3	396.1362	0.114517	0.012847	4.99E-05	w
62945.04	554.924	-	-	0.000		86124.3	397.2251	0.007203	0.001828	6.44E-06	w
62945.04	670.688	-	-	0.000		86124.3	397.7414	-	-	4.57E-05	
62945.04	781.793	-	-	0.000		86124.3	400.408	0.026628	0.006757	1.39E-05	w
62945.04	783.654	-	-	0.000		86124.3	406.1966	-	-	1.74E-06	
62945.04	785.194			0.000		86124.3	409.7503	0.008226	0.002087	0.000849	w
	-	-				86124.3	415.5315	0.076614	0.019442	1.23E-05	w
63272.98	200.744	-	-	0.036	o	86124.3	417.1369	0.023402	0.005939	0.000114	w
63272.98	201.549	-	-	0.111	o	86124.3	420.0167	-	-	1.9E-05	
63272.98	213.136	0.002	0.001	0.002	o	86124.3	426.1002	-	-	4.66E-05	
63272.98	222.587	0.229	0.027	0.001	o	86124.3	431.2988	-	-	0.001212	
63272.98	233.814	0.070	0.019	0.000		86124.3	449.3529	-	-	0.002152	
63272.98	235.541	-	-	0.000	b	86124.3	450.8214	0.03565	0.009047	0.000269	w
63272.98	238.222	-	-	0.002		86124.3	452.7016	-	-	5.89E-06	
63272.98	240.537	0.242	0.029	0.000		86124.3	457.79	0.02062	0.005233	7.53E-05	w
63272.98	241.118	0.111	0.013	0.004	w	86124.3	469.5207	-	-	2.06E-06	
63272.98	247.067	0.116	0.014	0.486		86124.3	481.5446	-	-	0.000244	
63272.98	247.857	0.156	0.018	0.278		86124.3	486.618	-	-	0.000205	
63272.98	248.424	-	-	0.028		86124.3	489.3812	-	-	2.35E-05	
63272.98	250.204	-	-	0.000		86124.3	495.0838	-	-	2.43E-06	
63272.98	266.691	0.005	0.001	0.003		86124.3	497.088	-	-	0.000158	
63272.98	268.079	0.002	0.001	0.002	w	86124.3	537.2548	-	-	1.85E-05	
63272.98	268.611	-	-	0.003	w	86124.3	721.1681	-	-	1.82E-06	
63272.98	278.020	0.001	0.000	0.000		86124.3	725.8963	-	-	6.28E-07	
63272.98	280.402	0.007	0.002	0.004	w	86124.3	741.9854	-	-	1.64E-06	
63272.98	307.523	0.002	0.000	0.002	w	86124.3	742.0525	-	-	7.52E-07	
63272.98	313.305	0.012	0.003	0.005	w						
63272.98	313.536	0.004	0.001	0.025							
63272.98	314.475	0.015	0.004	0.006							
63272.98	317.760	-	-	0.000							
63272.98	319.663	0.005	0.001	0.000							
63272.98	335.793	-	-	0.001	w						
63272.98	368.266	0.002	0.000	0.000							
63272.98	369.990	0.009	0.002	0.000	w						
63272.98	398.154	0.007	0.002	0.000	w						

63272.98	398.954	0.003	0.001	0.000	w
63272.98	544.572	-	-	0.000	w
63272.98	545.003	-	-	0.000	
63272.98	726.225	-	-	0.000	
63272.98	764.014	-	-	0.000	
63272.98	765.477	-		0.000	

Table 7.4 Fe II radiative properties

s emission line has shoulder

w weak emission line

b blended emission line

o means the line is lower than our 225 nm efficiency calibration

Kurucz refers to work by Kurucz et al.⁷⁴

7.5 - Conclusions

Branching ratios for neutral and singly ionized copper and iron are presented in the tables above and compared to the tabulated work of Kurucz and Bell.⁷⁴ For each of these elements and their respective ionizations we show a graphical representation of the data above in order to see how the two works agree. For each element and ionization I present a branching ratio comparison where the BR's of Kurucz and this work are plotted against Kurucz's BR in order to show any systematic trends. However this type of plot gives a biased perspective to the BRs presented in contrast to this work's BRs because they lie along a straight line giving the illusion of optimum accuracy. In order to give a better representation of the level of agreement, 3 histogram plots were made showing the representative percent differences between this work's BRs and those of Kurucz and Bell and each is discussed in further detail below. The percent difference are partitioned according to branching ratio strength (greater than 30%, between 30 and 10%, and less than 10%) in order to reveal any systematic deviations which might depend upon branching ratio strength.

7.5.1 - Neutral Copper

Figure 7.2 shows the relatively good agreement between this work's BRs presented in table 7.1 and that of Kurucz and Bell. A good majority of lines agree within the given uncertainty (error bars) as shown in figure 7.2 below. As is common with LIBS analysis when measuring branching ratios or radiative parameters which depend on branching ratio strength, sometimes branches deviate from reported values due to problematic emission lines within the same upper level. Despite these erroneous lines, the level of agreement between this work's BRs and those listed by Kurucz and Bell is rather good. Of the 192 total emission lines derived from 68 upper energy levels reported in table 7.2 above, 80 were noted as weak, 5 were blended and 21 had shouldering emission lines. The relative intensities for these lines are listed in appendix 1.

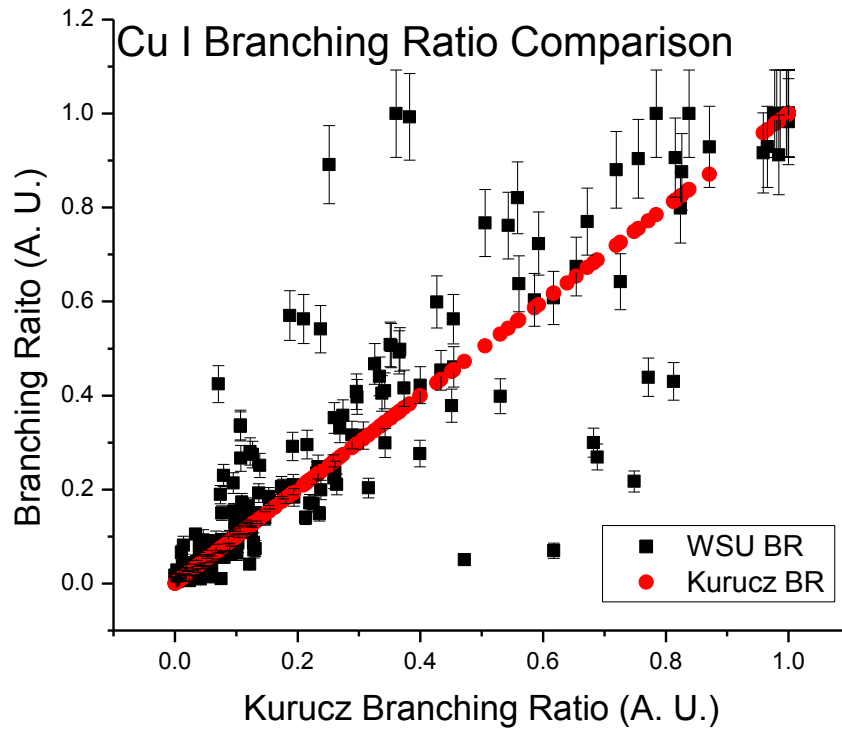


Figure 7.2 shows the branching ratio (BR) comparison between this work and the work by Kurucz and Bell74. The black squares signify this work and red diamonds represent Kurucz and Bell's work plotted against the values of Kurucz et al.; so that data which lie on a slope of one represent perfect agreement with Kurucz data. The error bars shown are the uncertainties from this work listed in the table 5.1.

Figures 7.3, 7.4 and 7.5 show Cu I histogram representations of the percent differences $(WSU - Kurucz)/Kurucz \times 100\%$ between this work and that of Kurucz and Bell74 for various branching ratio strengths. The histograms show the number of times a given percent difference was reported relative to complete agreement (zero percent difference). The percent differences were partitioned according to branching ratio strength to see if agreement between this work and

Kurucz depended on the strength of the branch; the idea being that weaker branches should have typically worse agreement since we have difficulty measuring them.

For those Cu I branches greater than 30% (figure 7.3) we found that 58.9% of the reported values agreed within a percent difference of $\pm 15\%$, 72.6% of the values agreed within a percent difference of $\pm 30\%$, 85.0% agreed within $\pm 45\%$, 89.0% of the values agreed within a percent difference of $\pm 60\%$, 91.7% agreed within $\pm 75\%$, 93.2% agreed within a percent difference of $\pm 90\%$, and by $\pm 177\%$ all 100% of the percent difference values are accounted for.

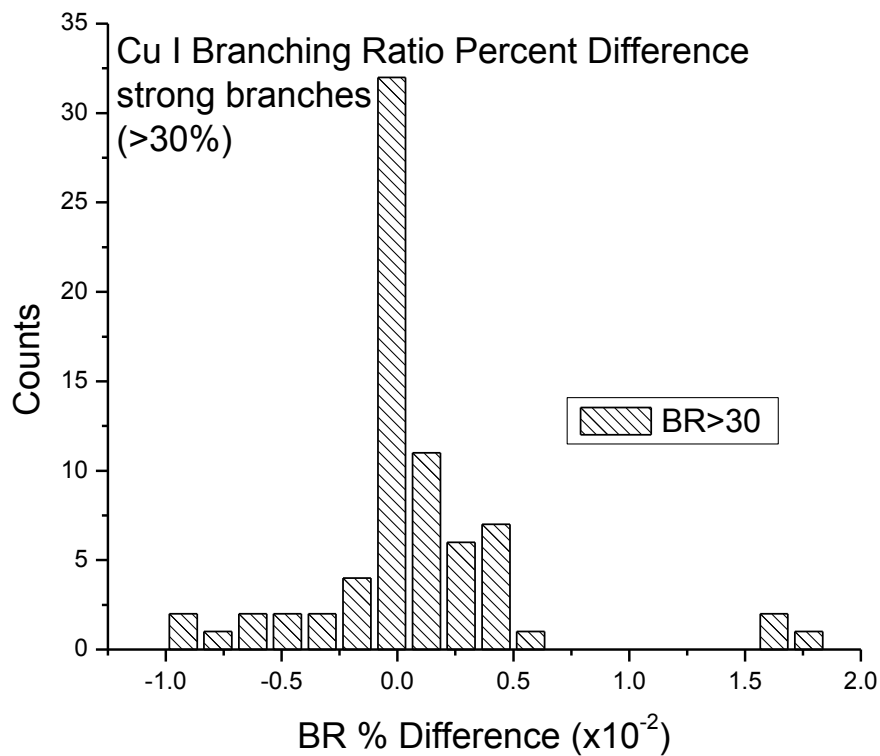


Figure 7.3 shows a histogram plot of the branching ratio percent difference between this work and that of Kurucz and Bell74 for branches which are greater than 30 percent of the all transitions out of their respective upper states. The number of occurrences (counts) represents the number of branching ratio percent difference values which lie within the given bin range (15%).

For those branches which are between 30% and 10% (figure 7.4) we found that 50.0% of the reported values agreed within $\pm 12.5\%$ with Kurucz, 77.6% percent of the values agreed within $\pm 37.5\%$, 82.8% agreed within $\pm 62.5\%$, 84.5% of the values agreed within $\pm 87.5\%$, 86.2% of the values agreed within $\pm 112.5\%$, 93.1% of the values agreed within a percent difference of $\pm 137.5\%$, and all values lie within a percent difference of $\pm 262.5\%$. Although there is excellent agreement with most of these values (less than 12.5% difference for most with an uncertainty of

10% on the reported value) there does seem to be a “tail” on the positive end the distribution. Since positive values indicate that our values are too large ($(WSU - Kurucz)/Kurucz \times 100\%$), this indicates we may be systematically overestimating the strengths of several branches. Since our lowest accuracy is in measuring smaller branches, this is the likely explanation.

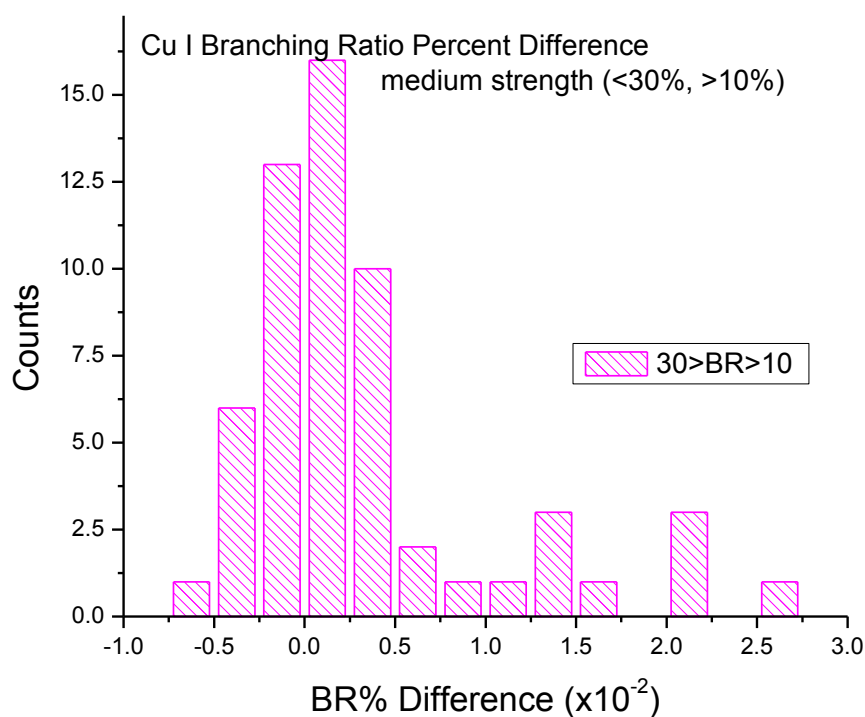


Figure 7.4 shows a histogram plot of the branching ratio percent difference between this work and that of Kurucz and Bell74 for branches which are between 30 and 10 percent of the all transitions out of their respective upper states. The number of occurrences (counts) represents the number of branching ratio percent difference values which lie within the given bin range (25%).

Lastly, for those branches of Cu I which are less than 10% (figure 7.5) the bins had a percent difference width of 50%. We found that 60.32% of these values agreed within $\pm 25\%$ with Kurucz, 74.6% of the values agreed within $\pm 75\%$, 82.6% agreed within $\pm 125\%$, 87.3% agreed within $\pm 175\%$, 90.5% agreed within $\pm 225\%$, 92.1% agreed within $\pm 275\%$, 95.2% agreed within $\pm 475\%$ and 100% of the values agreed within a percent difference $\pm 975\%$. Again, this shows good agreement since over 60% of the values agreed within 25% and the uncertainty on the measurement of these weak branches is actually 23.3%. The distribution also shows several outliers that are not in any kind of agreement with accepted values. There are not many occurrences of this discrepancy. These specific values will need to be revisited to determine what was wrong with the measurement, although as stated, there are so many difficulties in measuring small lines that it may be impossible to determine. However, when such a deviation does occur, it does tell us that the branches for the entire level may not be accurate.

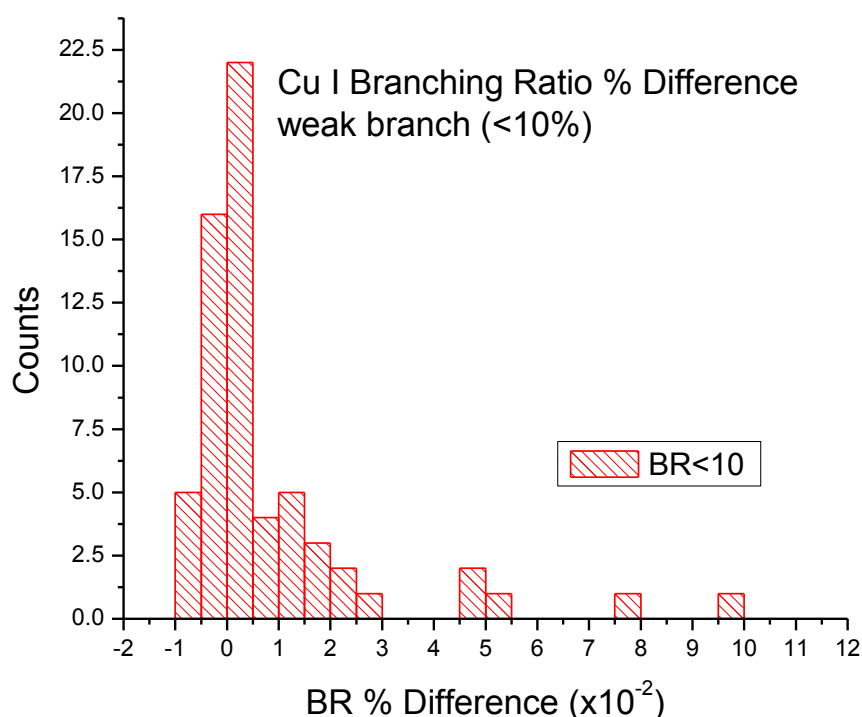


Figure 7.5 shows a histogram plot of the branching ratio percent difference between this work and that of Kurucz and Bell74 for branches which are less than 10 percent of the all transitions out of their respective upper states. The number of occurrences (counts) represents the number of branching ratio percent difference values which lie within the given bin range (50%).

7.5.2 - Singly-Ionized Copper

In total we attempted to observe 2,088 emission lines from 211 upper energy levels in Cu II. We had difficulty in observing the emission lines from energy levels larger than $115,663 \text{ cm}^{-1}$ since it was often the case that there was on average more than 20 emission lines from each upper energy level beyond this limit, and of these we were rarely able to detect even half of the expected emissions. For the vast majority of these lines the strongest branch was near 50% in

strength and the rest were usually very weak ($<5\%$). This caused issues since the LIBS technique has difficulty measuring relative intensities of branches which are weak. Furthermore, in order to sufficiently populate levels higher than $115,663\text{ cm}^{-1}$ requires a plasma temperature greater than 200,000 Kelvin which we do not claim to be able to do with confidence especially at the set experimental conditions (delay time and pressure). Because of these two facts I will limit the presented data to those lines which we were able to detect consistently with decent accuracies, which was found to be from energy levels below $115,663\text{ cm}^{-1}$. For this reason I will list only 79 of the 2,088 emission lines which are derived from 27 upper energy levels. The data for these are listed in table 7.2. All other relative intensities for any of the other 2000 observed emission lines will be listed in appendix 1 if they are considered accurate and reliable data.

Overall, the data we list and compare in Cu II are in good agreement with that of Kurucz and Bell. Figure 7.6 shows this agreement in a graphical representation where we plot our branching ratios and Kurucz's BR against Kurucz's BR in order to reveal any systematic discrepancies, of which we find none. Because this is not the best way to compare the data (since Kurucz and Bell's listed BR are themselves not perfect,) I then use histograms to present the percent difference between my work and their work.

Of the 79 emission lines listed in table 7.2 for Cu II, 6 were observed and noted as weak, 16 has shouldering emission lines, and 37 were outside of our zone of confidence for our spectral efficiency factor. Yet despite all of these setbacks and problematic lines, the results for the lines listed above show good agreement in Cu II.

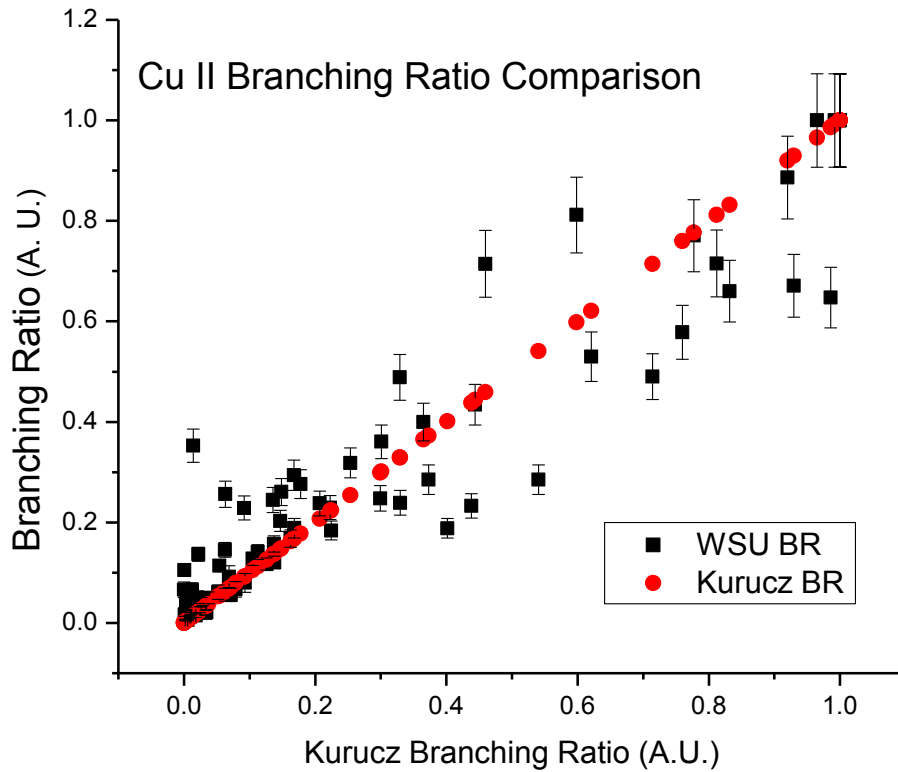


Figure 7.6 shows the Cu II branching ratio (BR) comparison between this work and the work by Kurucz and Bell.⁷⁴ The black squares signify this work, red circles represent Kurucz and Bell's work. The various work's BR's are plotted against the values of Kurucz so that data which lie on a slope of one represent perfect agreement with Kurucz data. The error bars shown are the uncertainties from this work listed in the table 5.1.

For those Cu II branches greater than 30% (figure 7.7) we found that 46.7% of the values agreed within a percent difference of $\pm 5\%$ with Kurucz, 56.7% of the values agreed within a percent difference of $\pm 15\%$, 73.3% agreed within $\pm 25\%$, 83.3% of the values agreed within a percent difference of $\pm 35\%$, 93.3% agreed within $\pm 45\%$ and all values agreed within a percent difference of $\pm 55\%$.

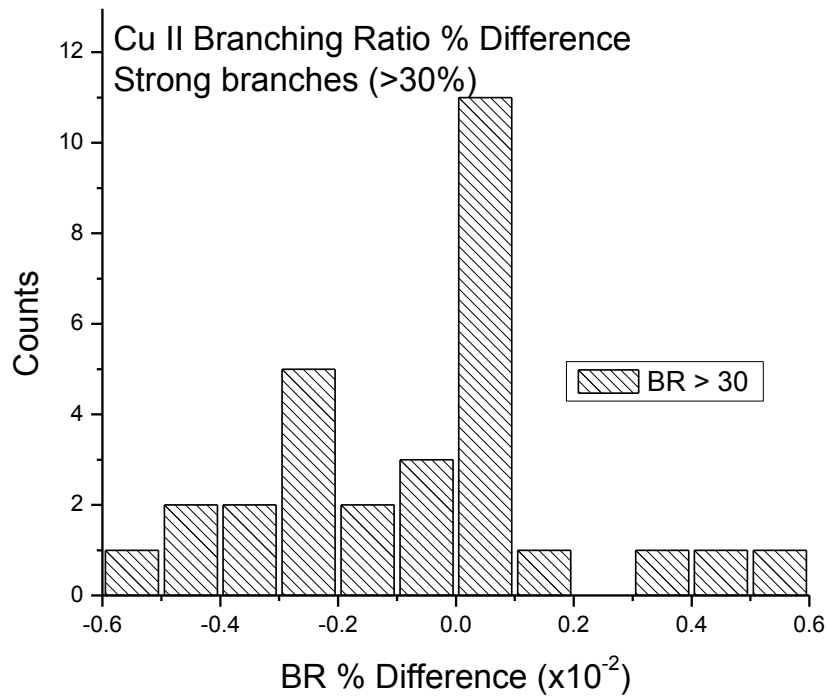


Figure 7.7 shows a histogram plot of the Cu II branching ratio percent difference between this work and that of Kurucz and Bell74 for branches which are greater than 30 percent of the all transitions out of their respective upper states. The number of occurrences (counts) represents the number of branching ratio percent difference values which lie within the given bin range (10%).

For those branches which are between 30% and 10% (figure 7.8) we found that 53.0% of the reported values agreed within $\pm 10\%$ with Kurucz, 76.47% percent of the values agreed within $\pm 30\%$, 82.35% agreed within $\pm 50\%$, 94.1% of the values agreed within $\pm 70\%$, and 100% of the values agreed within a percent difference of $\pm 90\%$. As with the medium strength branches in Cu I, there seems to be a systematic over-determination of the medium strength branches, as

indicated by a number of measurements on the positive tail of the distribution. However, since there are only four occurrences, it is very difficult to draw statistical significance from this.

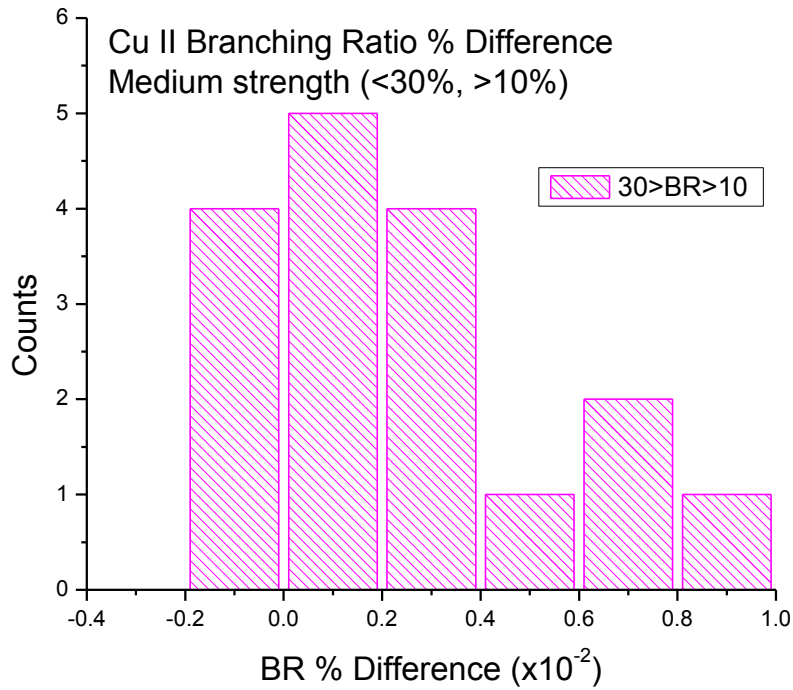


Figure 7.8 shows a histogram plot of the branching ratio percent difference between this work and that of Kurucz and Bell74 for branches of Cu II which are between 30 and 10 percent of the all transitions out of their respective upper states. The number of occurrences (counts) represents the number of branching ratio percent difference values which lie within the given bin range (20%).

Lastly, for those branches of Cu II which are less than 10% (figure 7.9) the bins had a percent difference width of 125%. We found that 90.6% of these reported values agreed within $\pm 112.5\%$ with Kurucz. Two occurrences of clear outliers in the data on the positive tail of the distribution are in very poor agreement. To put these types of “weak” branch deviations into

perspective, however, bear in mind that if we report a sub-one percent branch of 0.6% and Kurucz reports a branch of 0.2% (as in the $69,868\text{ cm}^{-1}$ level, for example), this results in a 200% deviation in the histogram! However the impact on the overall determination of the branching ratios is negligible since the size of the branch is insignificant. Many authors do not even attempt to measure or report these values. .

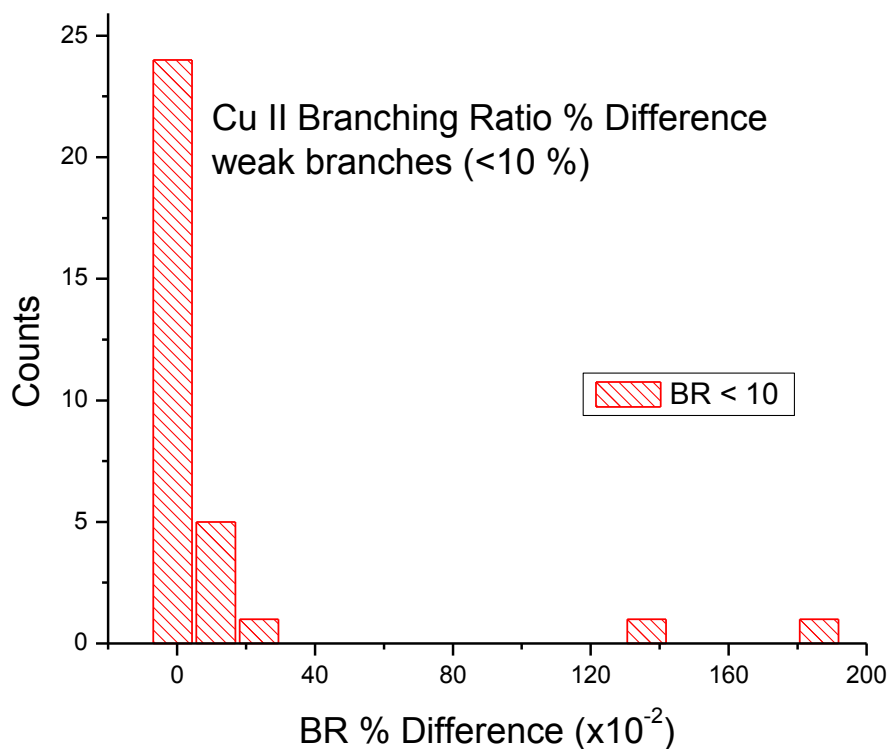


Figure 7.9 shows a histogram plot of the branching ratio percent difference between this work and that of Kurucz and Bell74 for branches which are less than 10 percent of the all transitions out of their respective upper states. The number of occurrences (counts) represents the number of branching ratio percent difference values which lie within the given bin size (125%).

In the case of singly-ionized copper there was one other group (Ortiz et al.⁸) who reported transition probabilities which were produced by laser-induced breakdown spectroscopy combined with previously determined lifetimes, and it is worth comparing our results to the few values they reported which we were also able to detect. The 18 lines compared between this work and Ortiz et al.'s work stem from 6 upper energy levels which are 114,511, 115,639, 115,663, 116,371, 117,231 and 117,883 (all in cm^{-1}) in Cu II. In the case of the larger branches they report 6% uncertainty, for the medium branches 13%, and for weak lines their uncertainty is larger (unreported).

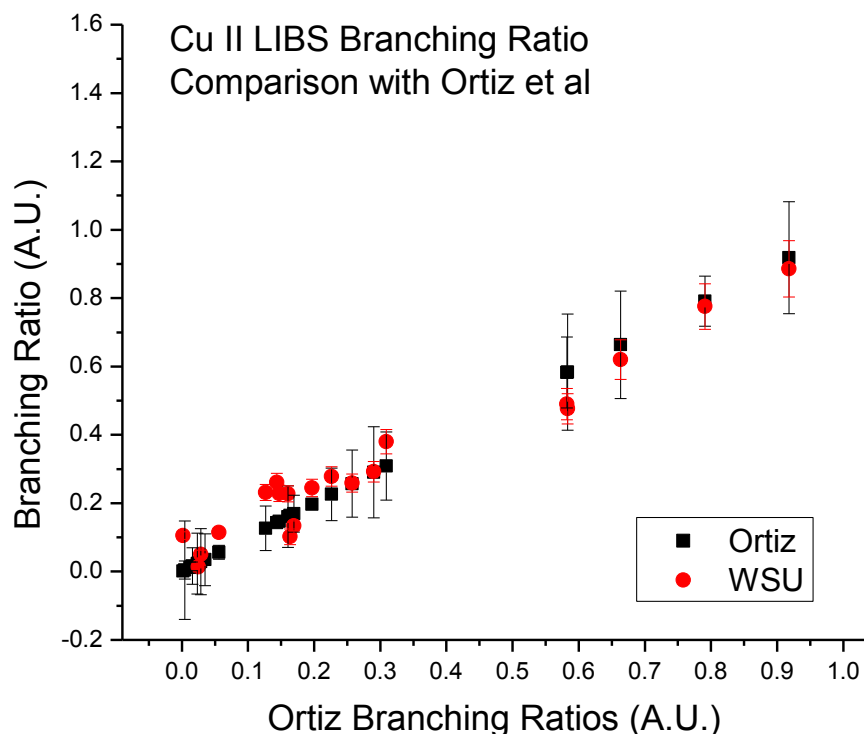


Figure 7.10 shows a LIBS branching ratio comparison between this work and that of Ortiz et al in some low-lying levels in Cu II. The black squares represent the work of Ortiz et al. and the red circles are this work at WSU. All branching ratios were plotted against the values of Ortiz et al. in order to show any systematic trend in the data, so that perfect agreement between the values would lie on a slope of one.

Upon comparing the branching ratios between this work and that of Ortiz et al. the graph above in figure 7.10 shows that our results are generally in good agreement with Ortiz et al. within both groups' stated uncertainties. For our large branches ($>30\%$) we show that 60% of our values agreed within $\pm 7\%$ from perfect agreement (0% difference), and all 100% of the large branches are found within $\pm 23\%$. The reason for the 2 points (residing near a branching ratio of 60%) which disagree within our stated uncertainty is due to an overestimate of a weak/blended branches from the $116,371\text{cm}^{-1}$ level and in the case of the $117,883\text{ cm}^{-1}$ level we were unable to

observe two of the four branches which they were able to detect which obviously overestimates our reported branching ratios for that level. Overall, for the large branches in Cu II we show very acceptable agreement with the works of Ortiz et al.

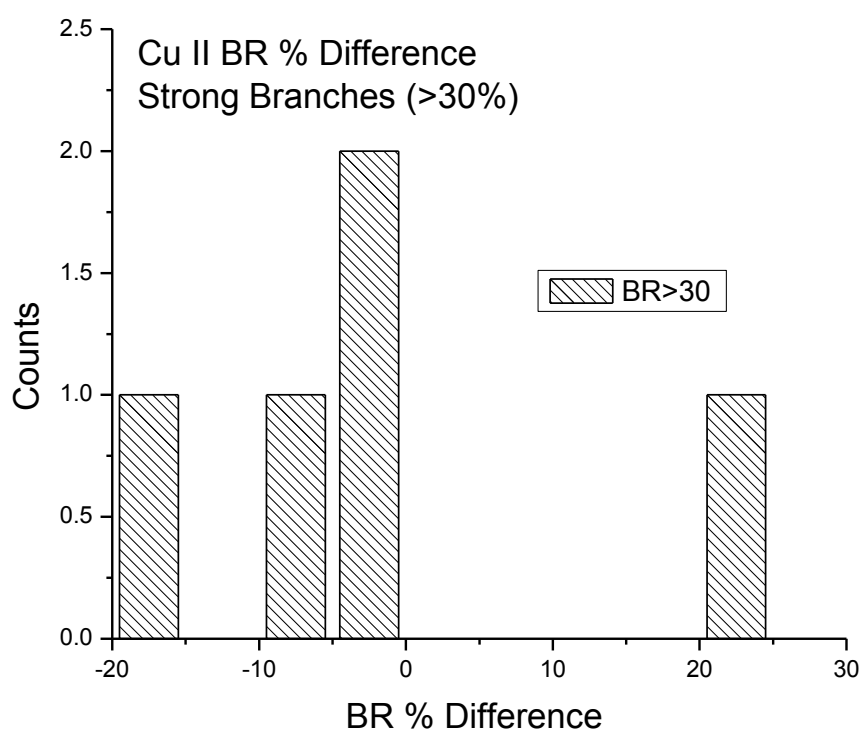


Figure 7.11 shows a histogram plot of the Cu II LIBS branching ratio percent difference between this work and that of Ortiz et al. for branches which are greater than 30 percent of the all transitions out of their respective upper states. The number of occurrences (counts) represents the number of branching ratio percent difference values which lie within the given bin range (5%).

For the moderate strength branching ratios of Cu II compared between the two LIBS experiments (between 10 and 30%) we show that only 20% of values agree within $\pm 2.5\%$, 50% agree within $\pm 22.5\%$, 70% agree by $\pm 40\%$, and all points lie in agreement by ± 82.5 . Overall this is not good agreement. The discrepancy is shown to be caused by blended and missing branches. For example, in the same levels described above ($116,371\text{cm}^{-1}$ and $117,883\text{ cm}^{-1}$) for the large branches, the moderate strength branches are also affected by the same problematic emission lines except on a larger scale since their relative strengths are smaller compared to the strong branches. However despite this disagreement between absolute values, the branches show overall good agreement within the stated uncertainties of both parties, showing that 8 of the 11 medium strength branches agree, and those that don't are due to problematic emission within their respective upper states.

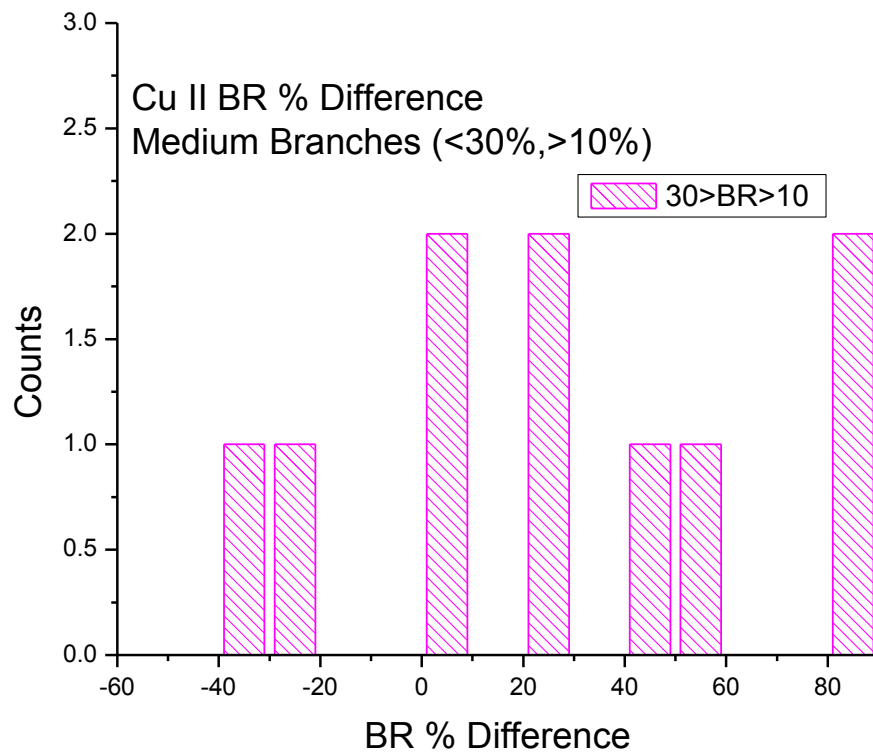


Figure 7.12 shows a histogram plot of the LIBS branching ratio percent difference between this work and that of Ortiz et al. for branches of Cu II which are between 30 and 10 percent of the all transitions out of their respective upper states. The number of occurrences (counts) represents the number of branching ratio percent difference values which lie within the given bin range (20%).

In the weak branching ratio case (<10%) we show that 25% of our values agree within $\pm 10.5\%$ with Ortiz, 50% of the values agree within $\pm 25.5\%$, 75% of the 4 points agree within $\pm 97.5\%$ and all of them are within agreement by 5705.5%. Despite the disagreement within absolute branching ratios, the agreement within stated uncertainty shows that we agree for 2 of the 4 weak transitions and the reason for the discrepancy is due to the difficulty in measuring

weak branches when they are shouldered, blended, and generally difficult to measure due to insufficient S/N as also noted by Ortiz et al.

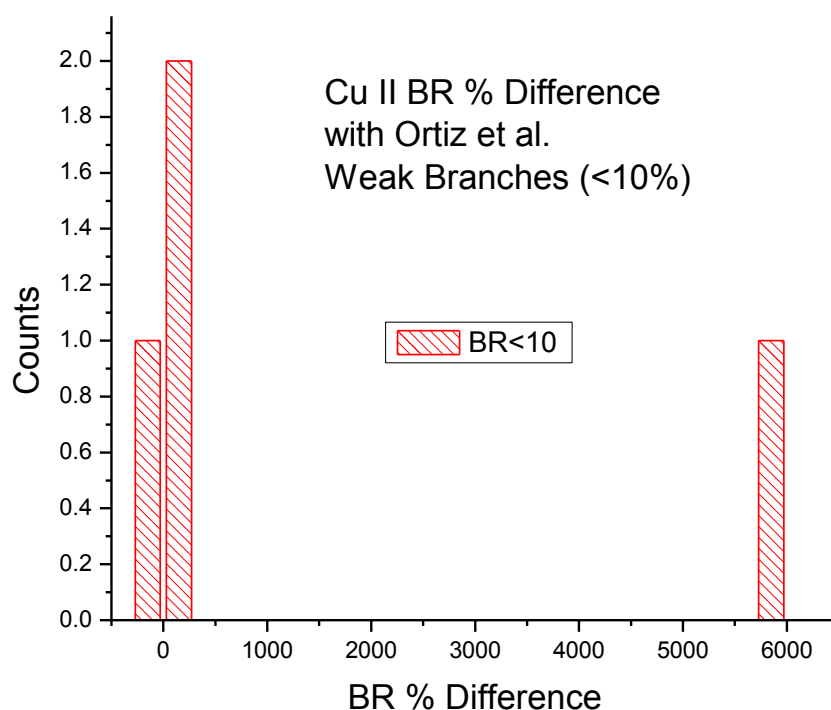


Figure 7.13 shows a histogram plot of the LIBS branching ratio percent difference between this work and that of Ortiz et al. for branches which are less than 10 percent of all transitions out of their respective upper states. The number of occurrences (counts) represents the number of branching ratio percent difference values which lie within the given bin size (300%).

7.5.3 - Neutral Iron

The deviation of this work's branching ratios (BR) from those listed by Kurucz and Bell⁷⁴ for neutral iron (Fe I) is very reasonable. There are some larger deviations and these occur mainly because “problematic” emission lines (blended, weak, shouldered) stemming mostly from

weak transitions. When branches from an upper level are erroneous or problematic the resulting branching strength of other “good” lines are affected since each branch’s strength is dependent upon the measured relative intensity of the other branches from the level. Table 7.3 lists BRs for 776 emission lines stemming from 108 upper energy levels in Fe I. Of these 776 lines, 363 were noted as weak, 53 were noted as blended, 21 were shouldered and 11 resided in our spectral gaps. A list of all Fe I relative intensities which were measured with confidence are presented in appendix 1.

As in the case of singly-ionized copper, here too we are faced with the issue of many unobserved emission lines from an upper energy state. Since iron is a transition metal it has many spontaneous transitions from many upper levels. Because I was unable to observe more than half of the branches from some higher lying levels and because within these unobserved lines were the reported stronger branches, I will not list and analyze some of the transitions in Fe I because I could not report these branching ratios with any confidence in their accuracies. In total I attempted to observe 10,000 emission lines from 444 upper energy levels in Fe I. I had difficulty in observing the emission lines from energy levels larger than $60,755\text{ cm}^{-1}$ since it was often the case that there was on average more than 20 emission lines from each upper energy level beyond this limit, and of these, many emission lines were undetectable. All other relative intensities for any of the other emission lines not listed above will be listed in appendix 1 if they are considered accurate and reliable data.

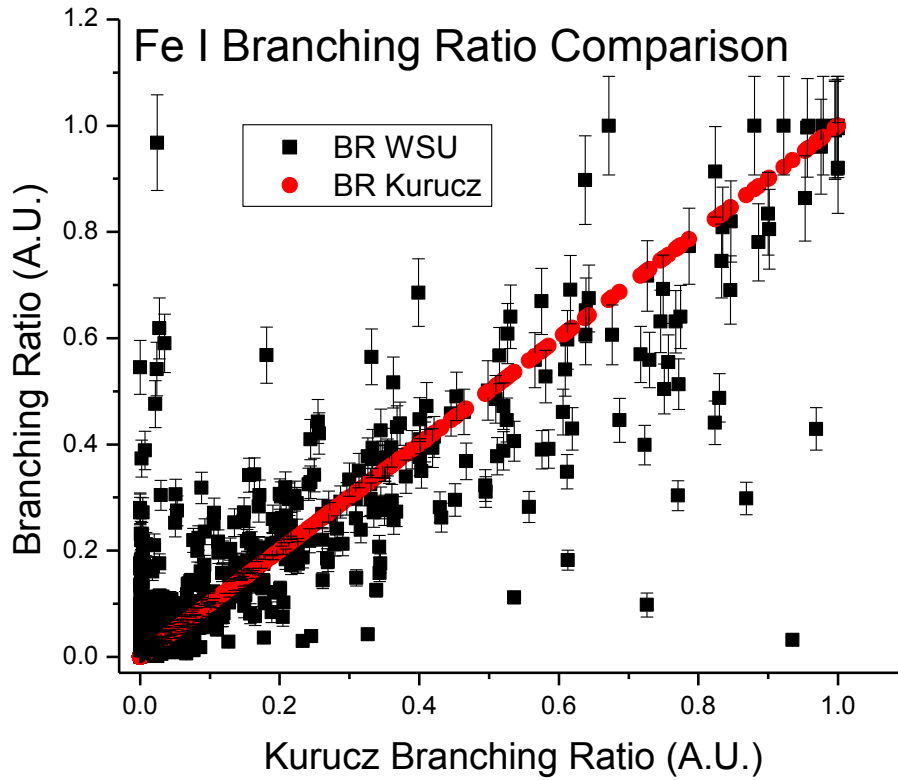


Figure 7.14 shows the branching ratio (BR) comparison between this work and the work by Kurucz and Bell.⁷⁴ The black squares signify this work, red circles represent Kurucz and Bell's work. The various work's BR's are plotted against the values of Kurucz so that data which lie on a slope of one represent perfect agreement with Kurucz data. The error bars shown are the uncertainties from this work listed in the table 5.1.

Figure 7.14 shows the relatively good agreement between this works BRs presented in table 7.3 and that of Kurucz and Bell. The majority of lines lie within the stated uncertainty (error bars) of our measurements. The purpose of plotting BR versus BR is to show any systematic trends or deviations between measured branching ratios. However this form of plot

gives a biased perspective to the BRs of Kurucz and Bell in contrast to this work's BRs by lying along a straight line. In order to give a better representation of the level of agreement, 3 histogram plots were made showing the calculated percent difference between this work's measured Fe BRs and those of Kurucz and Bell and are discussed in further detail below.

Figures 7.15, 7.16 and 7.17 are Fe I histogram representations of the percent difference $(WSU - Kurucz)/Kurucz (x100)$ between this work and that of Kurucz and Bell⁷⁴ for various branching ratio strengths. The histograms are comprised of the number of occurrences found at various percent differences from Kurucz and Bell's values. The percent differences were compared for three branching ratio strengths to see if agreement between this work and other's depends on the strength of the branch; the idea being that weaker branches should have typically worse agreement since we have difficulty measuring them.

For those Fe I branches greater than 30% (figure 7.15) we found that 52.8% of our reported values agreed within a percent difference of $\pm 15\%$ with Kurucz, 81.3% of the values agree within a percent difference of $\pm 30\%$, 89.4% agreed within $\pm 45\%$, 95% of all values agreed within a percent difference of $\pm 60\%$, 96.3 agreed within $\pm 75\%$, and 100% are found to agree within a percent difference of $\pm 90\%$.

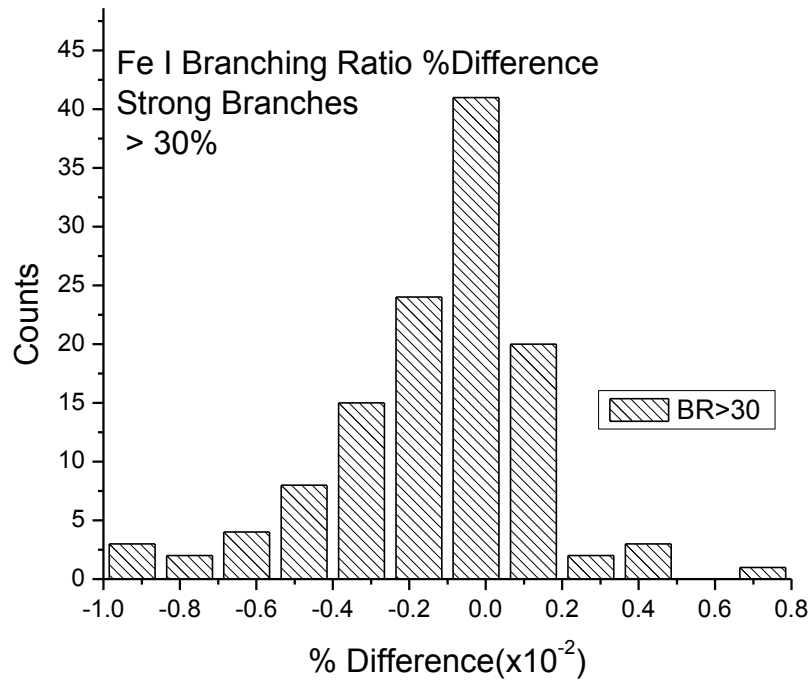


Figure 7.15 shows a histogram plot of the branching ratio percent difference between this work and that of Kurucz and Bell74 for branches which are greater than 30 percent of all transitions out of their respective upper states. The number of occurrences (counts) represents the number of branching ratio percent difference values which lie within the given bin range (15%).

For those branches which are between 30% and 10% (figure 7.16) we found that 42.9% of our reported values agreed within $\pm 20\%$ with Kurucz, 70.6% percent of the values agreed within $\pm 40\%$, 82.4% agreed within $\pm 60\%$, 91.6% of the values agreed within $\pm 80\%$, 95.8% of the values agreed within a percent difference of $\pm 100\%$, and 100% of the values agreed within a percent difference of $\pm 200\%$.

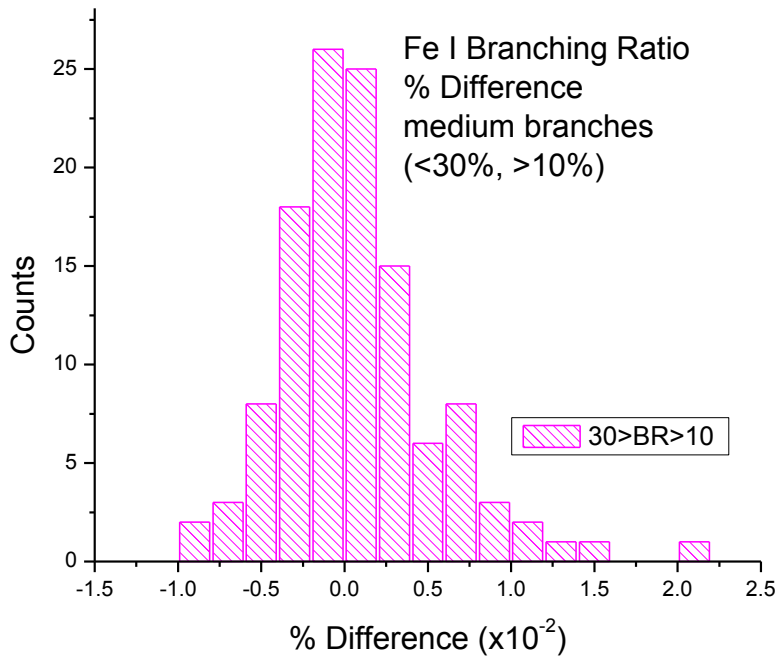


Figure 7.16 shows a histogram plot of the branching ratio percent difference between this work and that of Kurucz and Bell⁷⁴ for branches which are between 30 and 10 percent of the transitions out of their respective upper states. The number of occurrences (counts) represents the number of branching ratio percent difference values which lie within the given bin size (20%).

For those branches of Fe I which are less than 10% (figure 7.17) we used bins with percent difference width of 50%. We found that 80.92% of these values agreed within $\pm 50\%$ with Kurucz, 86.79% of the values agreed within $\pm 100\%$, 90.9% agreed within $\pm 150\%$, and 92.3% agreed within $\pm 200\%$. Again several large outliers exist for these very weak branches, but discrepancies for branches below 1% are expected to be large.

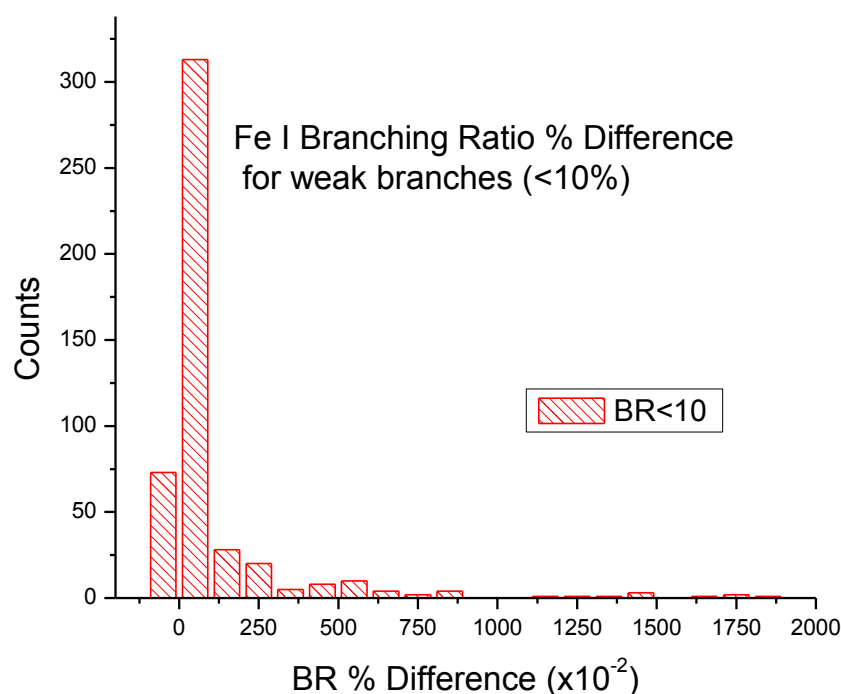


Figure 7.17 shows a histogram plot of the branching ratio percent difference between this work and that of Kurucz and Bell74 for branches which are less than 10 percent of all transitions out of their respective upper states. The number of occurrences (counts) represents the number of branching ratio percent difference values which lie within the given bin size (50%).

7.5.4 - Singly Ionized Iron

The deviation of this work's branching ratios (BR) from those listed by Kurucz and Bell74 for singly-ionized iron (Fe II) is overall not good. There are some larger deviations and these occur mainly because "problematic" emission lines (blended, weak, shouldered) stemming from weak transitions as explained above. Table 7.4 lists BRs for 1,453 emission lines stemming from 108 upper energy levels. Of these 1,453 lines 688 were noted as weak, 15 were noted as

blended, 14 were shouldered and 153 resided beyond our spectral efficiency confidence range ($<225\text{nm}$). A list of all of these Fe II relative intensities are presented in appendix 1.

As is the case in Cu I and Fe I, here too I was faced with the issue of many unobserved emission lines from numerous upper energy states. Because I was unable to observe more than half of the branches from some higher lying energy levels and because within these unobserved lines were the reported stronger branches, I have neglected to list and analyze some of the transition in Fe II because I cannot report these branching ratios with any confidence. In total, I attempted to observe 20,400 emission lines from 708 upper energy levels in Fe II. I had difficulty in observing the emission lines from energy levels larger than $86,142\text{ cm}^{-1}$ since it was often the case that there were on average more than 25 emission lines from each upper energy level beyond this limit, and of these we were rarely able to detect even half of them. All other relative intensities for any of the other emission lines not listed above will be listed in appendix 1 if they are considered accurate and reliable data.

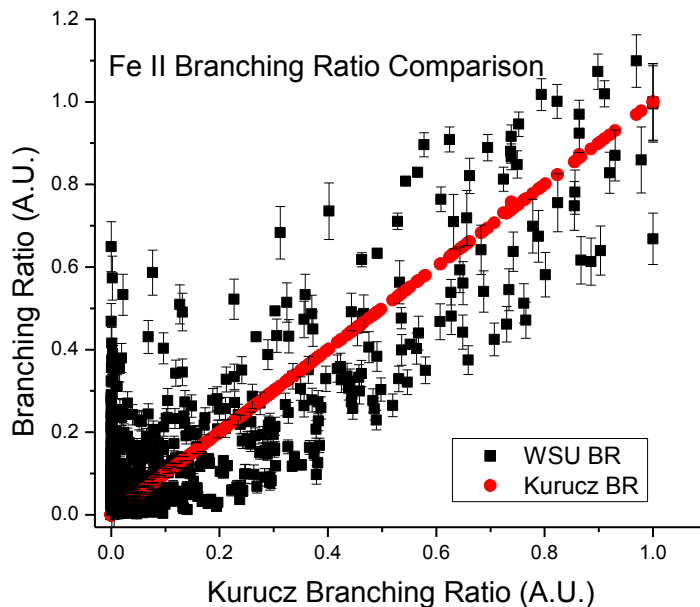


Figure 7.18 shows the branching ratio (BR) comparison between this work and the work by Kurucz and Bell.⁷⁴ The black squares signify this work, red circles represent Kurucz and Bell's work. The various work's BR's are plotted against the values of Kurucz so that data which lie on a slope of one represent perfect agreement with Kurucz data. The error bars shown are the uncertainties from this work listed in the table 5.1.

Figures 7.19, 7.20 and 7.21 are histogram representations of the percent difference $(WSU - Kurucz)/Kurucz (x100)$ between this work and that of Kurucz and Bell for branching ratios of Fe II. The histograms show the number of times a given percent difference was reported relative to complete agreement (zero percent difference). The percent differences were partitioned according to branching ratio strength to see if agreement between this work and that of Kurucz and Bell depends on branching ratio strength; the idea being that weaker branches should have typically worse agreement since we have difficulty measuring them.

For those Fe II branches with branching ratio strength greater than 30% (figure 7.19) we found that 11.5% of our reported values agreed within a percent difference of $\pm 12.5\%$ with Kurucz, 29.5% of the values agreed within a percent difference of $\pm 27.5\%$, 59.0% agreed within $\pm 42.5\%$, 80.3% of all values agreed within a percent difference of $\pm 57.5\%$, 93.4% agreed within $\pm 72.5\%$, and 100% agreed within a percent difference of $\pm 92.5\%$. For the larger branches we used bins of width 15%.

Interestingly, for these large Fe II branches we seem to have a systematic negative disagreement with Kurucz and Bell (i.e. our values are systematically less than theirs). No explanation exists for this discrepancy, however it is noted that in Fe II typically several strong branches (one to three per energy level) exist in the region of the spectrum where our spectral efficiency calibration curve begins to become strongly wavelength dependent. This is perhaps an indicator that with the current optical system, atomic systems with levels with many branches in the 200-300 nm range (e.g. Cu and Fe) are not attractive candidates for measurement.

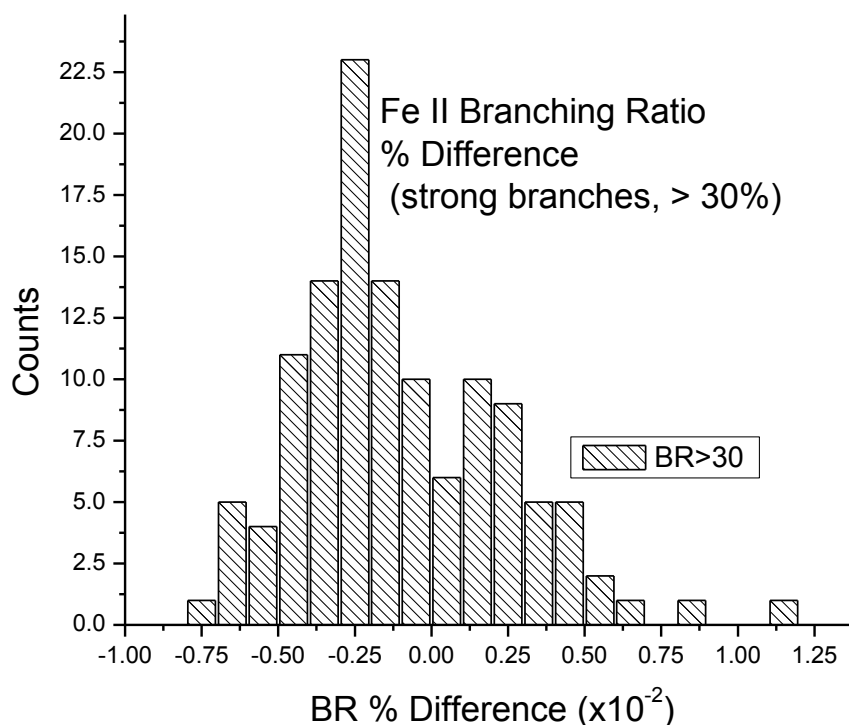


Figure 7.19 shows a Fe II histogram plot of the branching ratio percent difference between this work and that of Kurucz and Bell74 for branches which are greater than 30 percent of all transitions out of their respective upper states. The number of occurrences (counts) represents the number of branching ratio percent difference values which lie within the given bin range (15%).

For those branches which are between 30% and 10% (figure 7.20) we found that 22.0% of the values agreed within $\pm 12.5\%$ with Kurucz, 53.2% percent of the values agreed within $\pm 37.5\%$, 87.9% agreed within $\pm 62.5\%$, 90.7% of the values agreed within $\pm 87.5\%$, 91.6% of the values agreed within a percent difference of $\pm 112.5\%$, and 100% of the values agreed within a percent difference of $\pm 312.5\%$. For the moderate strength branches bins of size 25% were used.

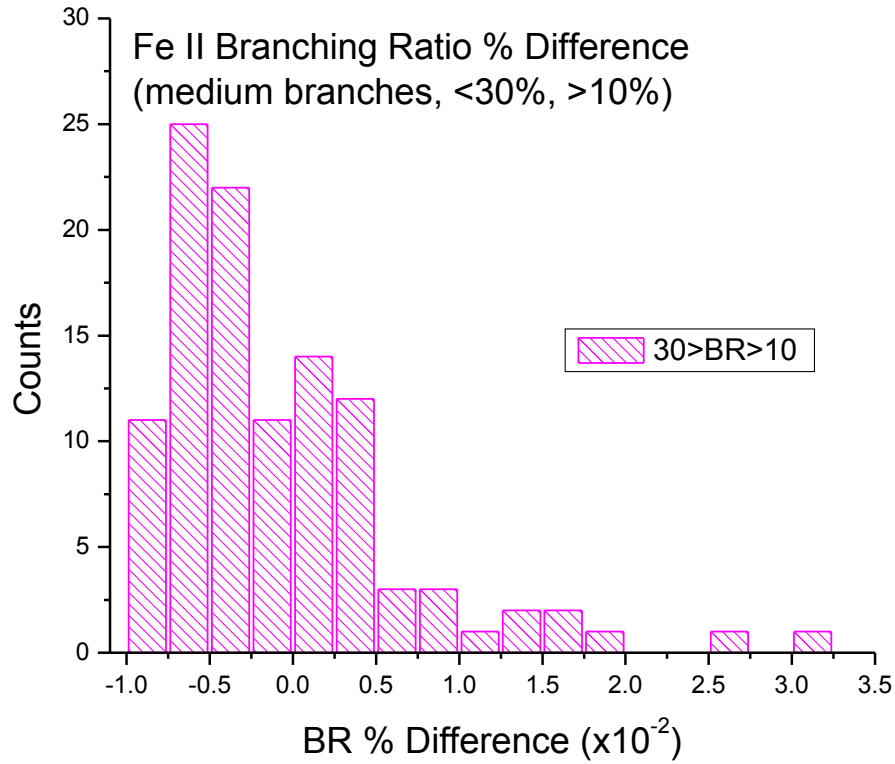


Figure 7.20 shows a Fe II histogram plot of the branching ratio percent difference between this work and that of Kurucz and Bell74 for branches which are between 30 and 10 percent of the transitions out of their respective upper states. The number of occurrences (counts) represents the number of branching ratio percent difference values which lie within the given bin range (25%).

For those branches of Fe II which are less than 10% (figure 7.21) we used bins with percent difference widths of 100%. We found that 79.05% of our reported values agreed within $\pm 50\%$ with Kurucz, 84.2% of the values agreed within $\pm 150\%$. The remaining outliers disagree by more than this amount.

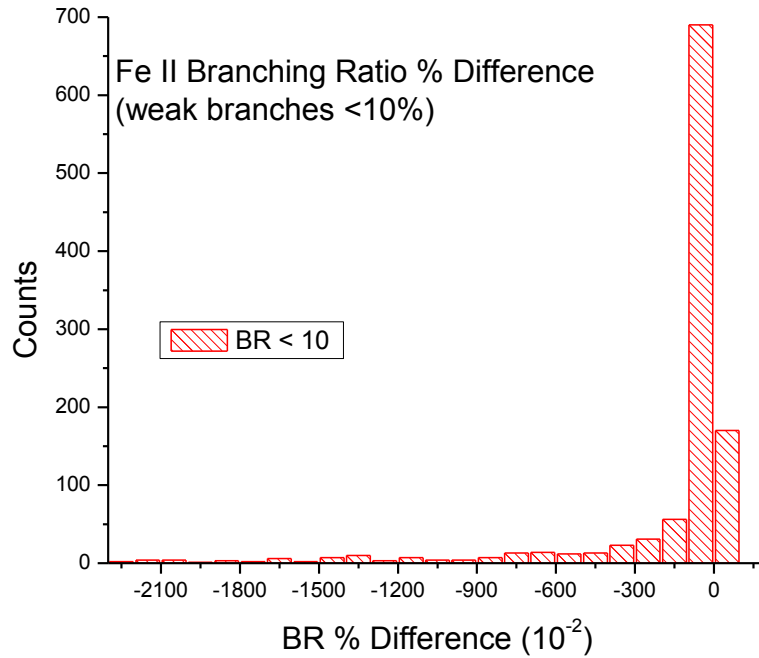


Figure 7.21 shows a histogram plot of the branching ratio percent difference between this work and that of Kurucz and Bell74 for Fe II branches which are less than 10 percent of all transitions out of their respective upper states. The number of occurrences (counts) represents the number of branching ratio percent difference values which lie within the given bin range (100%).

7.6 - Summary

The agreement for those Cu I branches stronger than 30% of the total emissions out of the upper state is quite reasonable. The central peak of a Gaussian fit to the histogram of percent differences lies at 7.7% and our stated uncertainty was around 9%. For the branches with moderate strength (between 10 and 30 %) we are again pleased with the results although the center of a Gaussian fit to the percent difference histogram was 32%. For those branching ratios weaker than 10% we were not surprised by the range of scatter and are overall pleased with the

results, knowing that the weak branches do not contribute much to astrophysical abundance calculations since these weaker transitions are not seen.

The agreement for those Cu II branches stronger than 30% of the total is quite reasonable with almost half of the measurements agreeing within 5%. For the branches with moderate strength (between 10 and 30%) we are again pleased with the results, with over half of the measurements agreeing within our stated uncertainty of 10%. For those branching ratios weaker than 10% we are not surprised by the range of scatter and are overall pleased with the results, knowing that the weak branches do not contribute much to astrophysical abundance calculations since these weaker transitions are not seen.

Overall the comparison shows good agreement between the LIBS measured branching ratios reported in this work and those by Ortiz et al. In the case of the transitions from the level at $114,511 \text{ cm}^{-1}$ we were missing two of the five transitions which caused our three values to be overestimated in comparison to their five branches by about 5.2% for the large branch, 15.6% for the medium strength branch, and 290% for the weak transition. It is due to these setbacks that I believe we show disagreement within our LIBS measurement comparisons. For those branches which Ortiz et al. were unable to observe which contributed significantly to a given level's branching ratios, they incorporated theoretical branching fractions and rescaled all of their branching ratios for that level accordingly. This is a reasonable solution for small scale measurements, but in my case, where I was tasked with observing thousands of emission lines from multiple ionization states this was not reasonable. Perhaps a future adjustment to the method of observing branching ratios in LIBS could incorporate this technique for small scale

interests. It was noted above that the large majority of our values agree within both groups' stated uncertainties and I am pleased with the overall results.

The agreement for those Fe I branches stronger than 30% of the total is quite reasonable. 52.8% of the values lie within a percent difference of $\pm 15\%$. A Gaussian fit to the percent difference distribution had a center at -12%, indicating a slightly negative systematic bias. For the branches with moderate strength (between 10 and 30%) we are again pleased with the results with approximately half of the data agreeing to within 20% of the values reported by Kurucz. For those branching ratios weaker than 10% we are not surprised by the range of scatter and are overall pleased with the results, knowing that the weak branches do not contribute much to astrophysical abundance calculations since these weaker transitions are not seen.

The agreement for those Fe II branches stronger than 30% of the total emissions is overall not very good, as only 11.5% of the values lie within a percent difference of $\pm 12.5\%$ (and our stated uncertainty is 9%). Additionally, for these large Fe II branches we seem to have a systematic negative disagreement with Kurucz and Bell (i.e. our values are systematically less than theirs). For the branches with moderate strength (between 10 and 30%) we again see not very good agreement, as only 22.0% of the values lie within $\pm 12.5\%$ of agreement and our stated uncertainty is 10%. Also, another systematic shift seems to be in evidence. It seems as if for iron, due to its huge number of lines per level, we are systematically underestimating the strength of branches $>10\%$. For those branching ratios weaker than 10% (which are numerous) we are not surprised by the range of scatter and are overall pleased with the results, knowing that the weak branches do not contribute much to astronomer's abundance calculations since they themselves do not see the weaker transitions. Our conclusion is that the measurements of Fe II require

further investigation, but that the spectral location of the majority of the strong lines in Fe II (<250 nm) is very problematic for our way of making measurements.

In conclusion, it is good to keep in mind that it is not uncommon for research groups to publish papers reporting data for only a single upper energy level from a given ionization state of an atom. Therefore the fact that we are able to measure many energy levels from multiple ionization states simultaneously, and from this provide radiative data with relatively good agreement to previous works, speaks very positively towards using LIBS in future studies of atomic radiative parameters.

¹ B. Bascheck, "The role of oscillator strengths in modeling and analyzing stellar spectra," Phys. Scr. **T8**, 21-25 (1984).

² K.T. Cheng and Y. Kim, "Energy Levels, Wavelengths, and Transition Probabilities of Cu-like Ions," At. Data Nucl. Data Tables **22**, 547-563 (1978).

³ J. Karwowski and I. Martin, "Quasirelativistic formulation of the quantum-defect-orbital method," Phys. Rev. A **43**, 4832-4836 (1991).

⁴ I. Martin and G. Simons, "New procedure for generating valence and Rydberg orbitals. II. Atomic photoionization cross sections," J. Chem. Phys. **62**, 4799-4804 (1975).

⁵ N. Zheng, *A New Outline of Atomic Theory*, Jiang Su Education Press, Nanjing, P. R. China, (1988).

⁶ N. Zheng, T. Wang, R. Yang, "Transition probability of Cu I, Ag I and Au I from weakest bound electron potential model theory," J. Chem. Phys. **113**, 6169-6173 (2000).

-
- ⁷ B.N.G. Guthrie, “New line identification in the blue spectra of Hg-Mn stars,” *Mon. Not. R. Astron. Soc.* **216**, 1-17 (1985).
- ⁸ M. Ortiz, R. Mayo, E. Biemont, P. Quinet, G. Malcheva, K. Blagoev, “Radiative parameters for some transitions arising from the $3d^94d$ and $3d^84s^2$ electronic configurations in Cu II spectrum,” *J. Phys. B* **40**, 167–176 (2007).
- ⁹ T.V. Mishenina, V.V. Kotyukh, C. Soubiran, C. Travaglio, M Busso, “Abundances of Cu and Zn in metal-poor stars: clues for Galaxy evolution,” *Astron. Astrophys.* **396**, 189-202 (2002).
- ¹⁰ C. Sneden, R.G. Gratton, D.A. Crocker, “Trends in copper and zinc abundances for disk and halo stars,” *Astron. Astrophys.* **246**, 354-367 (1991).
- ¹¹ J. Gurell, H. Hartman, R. Blackwell-Whitehead, H. Nilsson, E. Bäckström, L.O. Norlin, P. Royen, S. Mannervik, “The FERRUM project: Transition probabilities for forbidden lines in [Fe II] and experimental metastable lifetimes,” *Astron. Astrophys.* **508**, 525–529 (2009).
- ¹² C.M. Sikström, M. Schultz-Johanning, M. Kock, Z.-S. Li, H. Nilsson, S. Johansson, H. Lundberg, A.J.J. Raassen, “The FERRUM project: Experimental lifetimes of highly excited Fe II $3d^64p$ levels and transition probabilities,” *J. Phys. B* **32**, 5687 (1999).
- ¹³ Z.S. Li, H. Lundberg, C.M. Sikström, S. Johansson, “The FERRUM project: radiative lifetimes of intermediate-excitation states of Fe II measured in a fluorescence signal induced by laser pumping from a metastable state,” *Eur. Phys. J. D* **6**, 9 (1999).
- ¹⁴ Z.S. Li, H. Lundberg, U. Berzinsh, S. Johansson, S. Svanberg, “The FERRUM project: radiative lifetimes of the $3d5(6S)4s4p(3P) \gamma 6P^\circ$ states of Fe II measured with time-resolved vacuum ultraviolet laser spectroscopy,” *J. Phys. B* **33**, 5593 (2000).

-
- ¹⁵ H. Nilsson, C.M. Sikström, Z.S. Li, H. Lundberg, A.J.J. Raassen, S. Johansson, D.S. Leckrone, S. Svanberg, “The FERRUM project: new experimental and theoretical f-values for 4p-4d transitions in Fe II applied to HST spectra of χ Lupi,” *Astrophys. J.* **362**, 410 (2000).
- ¹⁶ S. Johansson, A. Derkatch, M.P. Donnelly, H. Hartman, A. Hibbert, H. Karlsson, M. Kock, Z.S. Li, D.S. Leckrone, U. Litzén, H. Lundberg, S. Mannervik, L.-O. Norlin, H. Nilsson, J. Pickering, T. Raassen, D. Rostohar, P. Royen, A. Schmitt, M. Johanning, C.M. Sikström, P.L. Smith, S. Svanberg, G.M. Wahlgren, “The FERRUM Project: New f-value data for Fe II and astrophysical applications,” *Phys. Scr.* **T100**, 71 (2002).
- ¹⁷ A. Hibbert and G. Corrége, “Transitions in Fe II,” *Phys. Scr.* **T119**, 61–66 (2005).
- ¹⁸ N.C. Deb and A. Hibbert, “Calculation of intensity ratios of observed infrared [Fe II] lines,” *Astrophys. J.* **711**, L104–L107 (2010).
- ¹⁹ J. Meléndez and B. Barbuy, “Both accurate and precise gf-values for Fe II lines,” *Astron. Astrophys.* **497**, 611–617 (2009).
- ²⁰ C.H. Corliss, “A review of oscillator strengths for lines of Cu I,” *J. Res. Nat. Bur. Stand.* **74A**, 781 (1970).
- ²¹ A. Bielski, “A critical survey of atomic transition probabilities for Cu I,” *J. Quant. Spectrosc. Radiat. Transfer* **15**, 463–472 (1975).
- ²² H. Cederquist, S. Mannervik, M. Kisielinski, P. Forsberg, I. Martinson, L.J. Curtis, P.S. Ramanujam, “Lifetimes of some excited levels in Cu I and Cu II,” *Phys. Scr.* **T8**, 104–106 (1984).
- ²³ S. Baier, M. Martins, B.R. Müller, P. Zimmermann, “Lifetime measurements and Stark mixing of autoionizing Cu I-states,” *Z. Phys. D* **10**, 445–449 (1988).

-
- ²⁴ J. Carlsson, L. Sturesson, S. Svanberg, "Accurate time-resolved laser spectroscopy on sputtered metal atoms," *Z. Phys. D* **11**, 287 (1989).
- ²⁵ W.E. van der Veer, R.J.J. van Diest, A. Dönszelmann, "Lifetime measurements of the $3d^9 4s$ (1D) $4p$ configuration of Cu I," *Z. Phys. D* **25**, 201 (1993).
- ²⁶ R. Zerne, J. Larsson, S. Svanberg, "Determination of radiative lifetimes in the $3d^{10} np\ ^2P$ sequence of neutral copper by time-resolved VUV laser spectroscopy," *Phys. Rev. A* **49**, 128-133 (1994).
- ²⁷ E. Biémont, F. Fryczynski, P. Palmeri, P. Quinet, C.J. Zeippen, "Radiative lifetimes for states in Cu I," *J. Quant. Spectrosc. Radiat. Transfer* **55**, 215–224 (1996).
- ²⁸ J. Migdalek, "Model potential approach to core polarization in SCF calculations," *Phys. Scr.* **T100**, 47-54 (2002).
- ²⁹ S. Civis, I. Matulkova, J. Cihelka, P. Kubelik, K. Kawaguchi, V.E. Chernov, "Time-resolved FTIR emission spectroscopy of Cu in the $1800\text{--}3800\text{ cm}^{-1}$ region: transitions involving f and g states and oscillator strengths," *J. Phys. B* **44**, 025002 (2011).
- ³⁰ A. Kono and S. Hattori, "Lifetimes and transition probabilities in Cu II," *J. Opt. Soc. Am.* **72**, 601-605 (1982).
- ³¹ M.H. Prior, "Radiative decay rates of metastable Ar III and Cu II ions," *Phys. Rev. A* **30**, 3051-3055 (1984).
- ³² C.E. Theodosiou, "Lifetimes of singly excited states in Cu^+ and Ag^+ ," *J. Opt. Soc. Am. B* **3**, 1107–1112 (1986).
- ³³ J.R. Crespo López-Urrutia, B. Kenner, T. Neger, H. Jäger, "Absolute transition probabilities of Cu II lines," *J. Quant. Spectrosc. Radiat. Transfer* **52**, 111–114 (1994).

-
- ³⁴ E.H. Pinnington, G. Rieger, J.A. Kernahan, E. Biémont, “Beam-laser measurements and relativistic Hartree-Fock calculations of the lifetimes of the $3d^9 4p$ levels in Cu II,” *Can. J. Phys.* **75**, 1–9 (1997).
- ³⁵ D. Donnelly, A. Hibbert, K.L. Bell, “Oscillator strengths for transitions in singly ionized copper,” *Phys. Scr.* **59**, 32–48 (1999).
- ³⁶ E. Biémont, E.H. Pinnington, P. Quinet, C.J. Zeippen, “Core-polarization effects in Cu II,” *Phys. Scr.* **61**, 567–580 (2000).
- ³⁷ C.Z. Dong and S. Fritzsche, “Relativistic, relaxation, and correlation effects in spectra of Cu II,” *Phys. Rev. A* **72**, 012507 (2005).
- ³⁸ M. Orrtiz, R. Mayo, E. Biémont, P. Quinet, G. Malcheva, K. Blagoev, “Radiative parameters for some transitions arising from the $3d^9 4d$ and $3d^8 4s^2$ electronic configurations in Cu II spectrum,” *J. Phys. B* **40**, 167–176 (2007).
- ³⁹ S.R. Federman, L.J. Curtis, M. Brown, S. Cheng, R.E. Irving, S. Torok, R.M. Schectman, “Oscillator strengths for ultraviolet transitions in P II and Cu II,” *J. Phys.: Conf. Ser.* **130**, 012007 (2008).
- ⁴⁰ M.S. Brown, S.R. Federman, R.E. Irving, S. Cheng, L.J. Curtis, “Lifetimes and oscillator strengths for ultraviolet transitions in singly ionized copper,” *Astrophys. J.* **702**, 880–883 (2009).
- ⁴¹ P.N. Milford, B.J. O'Mara, J.E. Ross, “Measurement of relative intensities of Fe I lines of astrophysical interest,” *J. Quant. Spectrosc. Radiat. Transfer* **41**, 433–438 (1989).
- ⁴² F. Thevenin, “Oscillator strengths from the solar spectrum,” *Astron. Astrophys., Suppl. Ser.* **77**, 137–154 (1989).

-
- ⁴³ R.C. Peterson, R.L. Kurucz, B.W. Carney, “Relative abundance determinations in extremely metal poor giants. II. Transition probabilities and the abundance determinations,” *Astrophys. J.* **350**, 173 (1990).
- ⁴⁴ T.R. O'Brian, M.E. Wickliffe, J.E. Lawler, W. Whaling, J.W. Brault, “Lifetimes, transition probabilities, and level energies in Fe I,” *J. Opt. Soc. Am. B* **8**, 1185 (1991).
- ⁴⁵ A. Bard, A. Kock, M. Kock, “Fe I oscillator strengths of lines of astrophysical interest,” *Astron. Astrophys.* **248**, 315 (1991).
- ⁴⁶ D. Engelke, A. Bard, M. Kock, “Radiative lifetimes of Fe I levels of astrophysical interest,” *Z. Phys. D* **27**, 325-328 (1993).
- ⁴⁷ A. Bard and M. Kock, “Fe I oscillator strengths for lines with excitation energies between 3 and 7 eV,” *Astron. Astrophys.* **282**, 1014-1020 (1994).
- ⁴⁸ S.D. Bergeson, K.L. Mullman, J.E. Lawler, “High-sensitivity absorption spectroscopy in Fe II,” *Astrophys. J.* **464**, 1050-1056 (1996).
- ⁴⁹ M.A. Bautista, “Atomic data from the IRON Project. XX. Photoionization cross sections and oscillator strengths for Fe I,” *Astron. Astrophys., Suppl. Ser.* **122**, 167-176 (1997).
- ⁵⁰ J.M. Borrero, L.R. Bellot Rubio, P.S. Barklem, J.C. del Toro Iniesta, “Accurate atomic parameters for near-infrared spectral lines,” *Astron. Astrophys.* **404**, 749–762 (2003)r
- ⁵¹ M.F. Gu, T. Holczer, E. Behar, S.M. Kahn, “Inner-shell absorption lines of Fe VI - Fe XVI: A many-body perturbation theory approach,” *Astrophys. J.* **641**, 1227–1232 (2006).
- ⁵² R. Centeno and H. Socas-Navarro, “A new approach to the solar oxygen abundance problem,” *Astrophys. J.* **682**, L61–L64 (2008).

-
- ⁵³ S. Kroll and M. Kock, "Fe II oscillator strengths," *Astron. Astrophys., Suppl. Ser.* **67**, 225-230 (1987).
- ⁵⁴ B.C. Fawcett, "Fe II oscillator strengths for identified lines in spectra of the Sun and of the slow nova RR Tel," *At. Data Nucl. Data Tables* **40**, 1–8 (1988).
- ⁵⁵ W. Schade, B. Mundt, V. Helbig, "Radiative lifetimes of Fe II levels," *J. Phys. B* **21**, 2691-2696 (1988).
- ⁵⁶ E. Biémont, M. Baudoux, R.L. Kurucz, W. Ansbacher, E.H. Pinnington, "The solar abundance of iron: a "final" word!" *Astron. Astrophys.* **249**, 539-543 (1991).
- ⁵⁷ E. Biémont, S. Johansson, P. Palmeri, "The lowest 5g-6h supermultiplet of Fe II," *Phys. Scr.* **55**, 559-565 (1997).
- ⁵⁸ Z.S. Li, H. Lundberg, C. M. Sikström, S. Johansson, "The FERRUM project: radiative lifetimes of intermediate excitation states of Fe II measured in a fluorescence signal induced by laser pumping from a metastable state," *Eur. Phys. J. D* **6**, 9-14 (1999).
- ⁵⁹ C.M. Sikström, M. Schultz-Johanning, M. Kock, Z.-S. Li, H. Nilsson, S. Johansson, H. Lundberg, A.J.J. Raassen, "The FERRUM project: Experimental lifetimes of highly excited Fe II 3d⁶4p levels and transition probabilities," *J. Phys. B* **32**, 5687-5697 (1999).
- ⁶⁰ R. Schnabel, M. Kock, H. Holweger, "Selected Fe II lifetimes and f-values suitable for a solar abundance study," *Astron. Astrophys.* **342**, 610-615 (1999).
- ⁶¹ R. Schnabel, M. Schultz-Johanning, M. Kock, "Fe II lifetimes and transition probabilities," *Astron. Astrophys.* **414**, 1169–1176 (2004).
- ⁶² H. Nilsson, C.M. Sikström, Z.S. Li, H. Lundberg, A.J.J. Raassen, S. Johansson, D.S. Leckrone, S. Svanberg, "The FERRUM project: new experimental and theoretical f-values for

4p-4d transitions in Fe II applied to HST spectra of χ Lupi,” *Astron. Astrophys.* **362**, 410-414 (2000).

⁶³ J.C. Howk, K.R. Sembach, K.C. Roth, J.W. Kruk, “Empirical verification of the Fe II oscillator strengths in the FUSE bandpass,” *Astrophys. J.* **544**, 867-872 (2000).

⁶⁴ D. Rostohar, A. Derkach, H. Hartman, S. Johansson, H. Lundberg, S. Mannervik, L.-O. Norlin, P. Royen, A. Schmitt, “Lifetime measurements of metastable states in Fe^+ ,” *Phys. Rev. Lett.* **86**, 1466-1470 (2001).

⁶⁵ J.C. Pickering, S. Johansson, P.L. Smith, “The FERRUM project: Branching ratios and atomic transition probabilities of Fe II transitions from the $3d^6(a^3F)4p$ subconfiguration in the visible to VUV spectral region,” *Astron. Astrophys.* **377**, 361-367 (2001).

⁶⁶ H. Hartman, A. Derkach, M.P. Donnelly, T. Gull, A. Hibbert, S. Johansson, H. Lundberg, S. Mannervik, L.-O. Norlin, D. Rostohar, P. Royen, P. Schef, “The FERRUM Project: Experimental transition probabilities of [Fe II] and astrophysical applications,” *Astron. Astrophys.* **397**, 1143–1149 (2003).

⁶⁷ R. Schnabel, M. Schultz-Johanning, M. Kock, “Fe II lifetimes and transition probabilities,” *Astron. Astrophys.* **414**, 1169–1176 (2004).

⁶⁸ D.R. Beck, “Ab initio electric dipole f values for Fe II ($3d^64s + 3d^7$) $J=9/2 \rightarrow 3d^64p$ $J=9/2$ transitions,” *Phys. Scr.* **71**, 447–452 (2005).

⁶⁹ A. Hibbert and G. Corrége, “Transitions in Fe II,” *Phys. Scr.* **T119**, 61–66 (2005).

⁷⁰ G. Corrége and A. Hibbert, “Oscillator strengths of near-infrared lines of Fe II,” *Astrophys. J.* **636**, 1166–1171 (2006).

⁷¹ J. Gurell, H. Hartman, R. Blackwell-Whitehead, H. Nilsson, E. Bäckström, L.O. Norlin, P.

Royen, S. Mannervik, “The FERRUM project: Transition probabilities for forbidden lines in [Fe II] and experimental metastable lifetimes,” *Astron. Astrophys.* **508**, 525–529 (2009).

⁷² F. Castelli and R.L. Kurucz, “New Fe II energy levels from stellar spectra,” *Astron. Astrophys.* **520**, A57-A62 (2010).

⁷³ R.L. Kurucz and B. Bell, *Atomic Line Data, Kurucz CD-ROM No. 23*, Cambridge, MA. Smithsonian Astrophysical Observatory (1995).

⁷⁴ R.L. Kurucz and B. Bell, *Atomic Line Data, Kurucz CD-ROM No. 23*, Cambridge, MA. Smithsonian Astrophysical Observatory (1995).

Chapter 8 – Conclusions and Future Work

The results presented in this work reveal that LIBS is a viable technique for determining branching ratios, relative intensities, oscillator strengths, and transition probabilities. The rapidity with which the measurements can be made, the ability to excite high-lying energy levels, and the ability to ionize multiple states makes LIBS a useful contributor for determining atomic properties in laboratory astrophysics.

I was able to report transition probabilities, oscillator strengths, branching ratios (BR), and relative intensities (RI) for 405 energy levels in gadolinium, 158 energy levels in neodymium, 559 levels in praseodymium, and 323 levels in samarium; as well as determining BR and RI's for two transition metals (279 levels in copper and 216 levels in iron). Altogether approximately 13,100 identified emission lines were observed with their corresponding relative intensities. Other unidentified radiative parameters for emission lines were not presented due to the lack of published literature in identified atomic states and their corresponding transitions.

The largest contribution to discrepancies with other works' values was due to problematic emission lines which were blended or weak emission lines which were sometimes undetected causing a larger uncertainty. Both of these issues result in effects to all the branching ratios originating from their respective parent energy level. Two possible solutions to the issue would be better resolution in the spectrometer which would separate the blended lines and hopefully be sufficient for resolving the weak emissions, and the use of a tunable probing laser on our laser-induced plasma to excite single upper state levels which would eliminate the blended lines altogether (except for multiplet cases when the lines are neighboring one another). With the tunable-dye laser, the weak lines would still arise but the hope would be that there would be so

few of them that they would not be blended so that the échelle spectrometer used in this work would be able to resolve them easily. As noted in chapter 3, the échelle spectrometer used in my research is good throughout the spectral range of 200-800 nm, providing up to 0.005 nm resolution in the UV which is top notch. In order to better observe weak lines, a more sensitive detector is required. Since already the ICCD used in the échelle spectrometer is very good, improvements in this area are limited. Collecting more light may be the best approach and is described below.

Another option to handle problematic lines was mentioned in chapter 7 where I reported that Ortiz et al.'s group, who also used LIBS to measure radiative parameters in Cu II, incorporated theoretical transition probabilities when emission lines were problematic and erroneously measured. As I've already mentioned this solution for problematic lines works fine when dealing with only 7 energy levels, as Ortiz's group did, but on a larger scale with hundreds of levels as I presented in this work this idea is not very plausible, since it would be very time consuming.

Despite the contributions made to the field of astrophysically relevant atomic data, improvements to the apparatus and method can still be made.

8.1 – Improvements to the Branching Ratio Apparatus

In chapter 3 it was mentioned that less than 1% of the light radiated from the plasma is actually observed with the apparatus used in this work due to the small numerical aperture of the fiber-optic cable. One improvement which allows for greater collection of the radiated light is to use a high-quality condenser lens, perhaps a bi-convex lens, near the ablation site like our

original plan mentioned earlier in this dissertation. The problem with the lens and microscope objective we used was the large amount of absorbed light in the UV region and the extreme sensitivity to minute adjustments in calibration. The proposed lens should be composed of high performance UV fused silica able to transmit radiation in the UV and through the visible spectrum, where most of the astrophysically relevant transitions occur for neutrals and singly-ionized states.

A second method of improving the collected light is through the use of large diameter parabolic mirrors positioned near the target inside the ablation chamber in order to increase the amount of collected light. This method would eliminate the use of lenses altogether from the experiment. Such high-quality parabolic reflectors have already been acquired for this experiment, but not implemented. Reflective optics have much better chromatic performance than any comparable transmission optics and have excellent reflectance in the UV. This would reduce uncertainties due to transmission and absorption in the optics while greatly increasing the amount of collected light.

Thirdly, the use of a low pressure vacuum-tight chamber is unnecessary. The steel chamber used in this work could potentially be replaced with a simpler fiberglass-enclosure. The main improvement being to increase the enclosed volume so that the entire apparatus including mirrors (or lenses) and fiber can all be rigidly fashioned within the chamber and mechanically calibrated and aligned. Upon researching the optimum parameters for LIBS detection of atomic data, we determined that it is preferable to not use ultra-low pressure (mTorr range) but rather low pressures on the order of 10's to 100's of Torr (10's to 100's of mbar). Because of this we

believe that the fiberglass-enclosure would suffice. This would eliminate the need for windows since the entire optical collection apparatus would be inside the vacuum chamber.

8.2 – Lifetime Experiment

In preliminary work for this thesis, the idea was proposed to alter the apparatus from branching ratio studies to atomic lifetime studies. The focus was on measuring a problematic lifetime in gallium coined the “Gallium Problem”¹ by Dworetsky et al. which other experimental techniques were unable to measure due to the energy necessary to excite the atom up to the high-lying $4s5p^3P_2$ level ($118,727.89 \text{ cm}^{-1}$) in singly-ionized gallium. As discussed in chapter 1, the method of such a lifetime measurement would incorporate the use of photon-detection via single-photon sensitive avalanche photodiodes (APD) which should be filtered by two narrow band-pass filters for the transitions of interest – the photon at 541.631 nm signifying that the level has been populated and the photon at 633.407 nm indicating that the level was depopulated (figure 8.1).

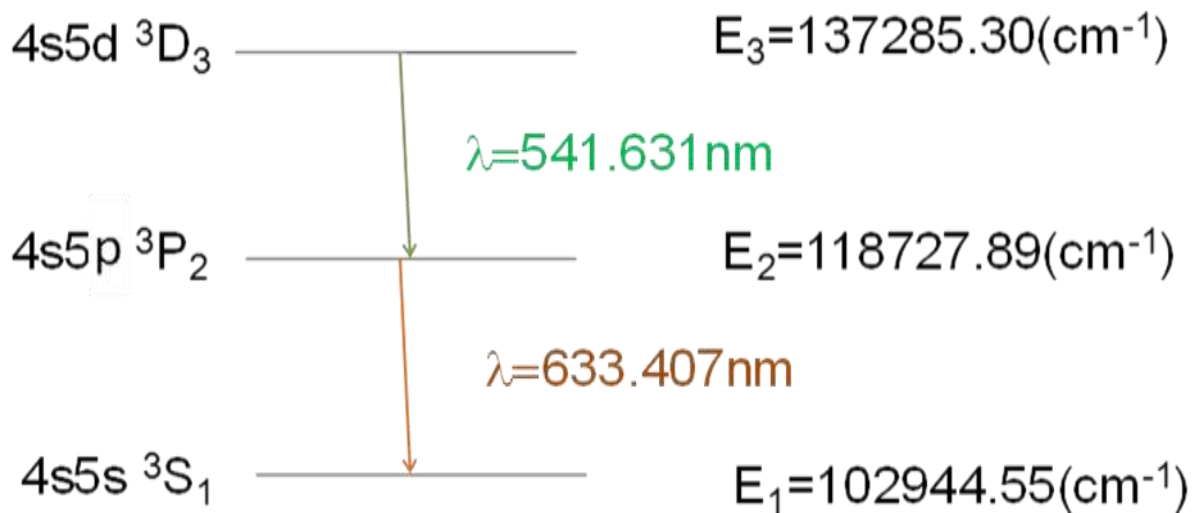


Figure 8.1 A diagram displaying the cascade transitions for the $4s5p\ ^3P_2$ level in Ga II. The 541.631 nm line signifies the start photon, the 633.407 nm line signifies the stop photon.

The APD's would be situated on either side of a 50:50 Pellicle beamsplitter. The APD's will output discrete pulses upon detection of individual photons. These pulses will be input to constant fraction discriminators whose outputs will serve as start and stop pulses for a time-to-pulse-height converter. This device outputs TTL pulses whose amplitudes are proportional to the time delay between arriving start and stop pulses. The pulses are then input to a pulse-height-analyzer (PHA) which records a histogram of the number of coincidences detected versus the delay time. The use of a histogram plot from the triggered delay time between detection of the photons would allow an exponential fit of the slope thus identifying the lifetime of the energy level. A schematic of the apparatus is shown in figure 8.2

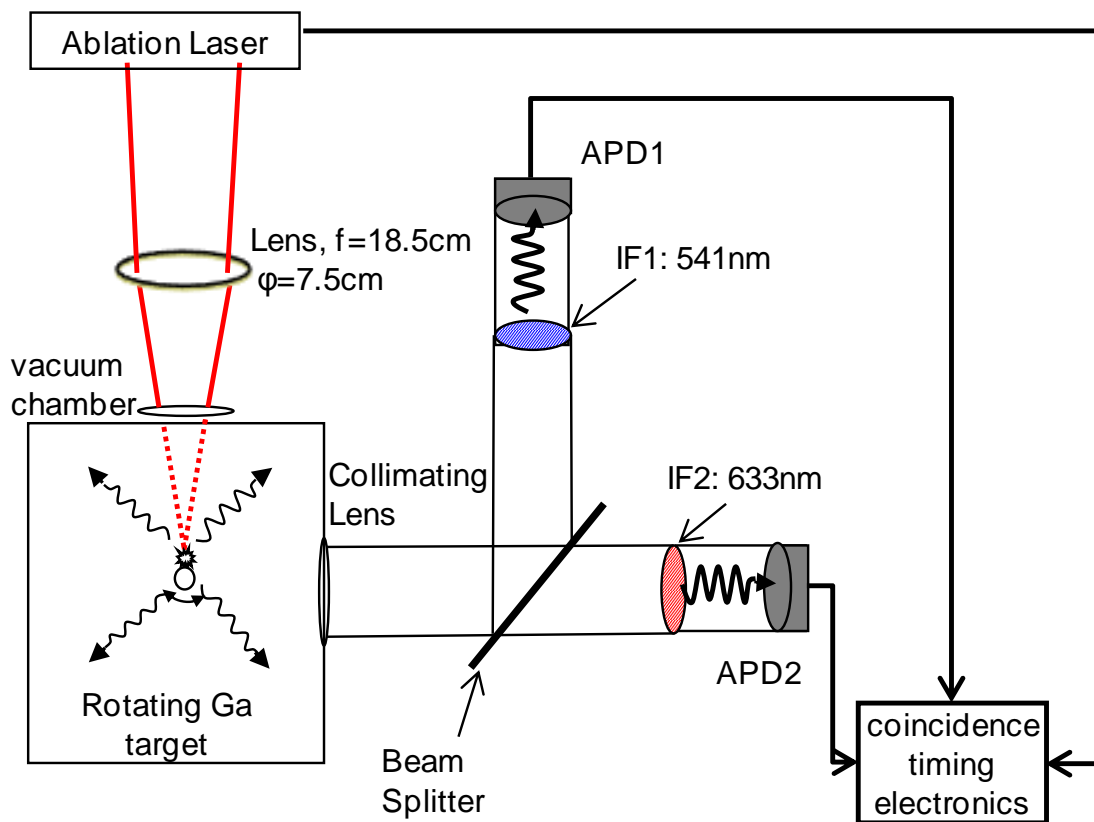


Figure 8.2 A schematic of the laser-induced plasma apparatus used to perform atomic lifetime measurements via the cascade-photon-coincidence technique. Single-photon sensitive avalanche photodiodes with narrow bandpass interference filters will observe the same region of the plasma via a single set of collection optics and subsequent splitting by a Pellicle beamsplitter. Measurement of the delay between the arrival of coincident photons into and out of the energy level will allow a measurement of the level lifetime.

Using a laser-induced plasma and our Échelle spectrometer for detection, our preliminary results already reveal an obvious detection of both the “start” and “stop” photons, signifying population of the desired energy level in the plasma and the occurrence of photon-cascading.

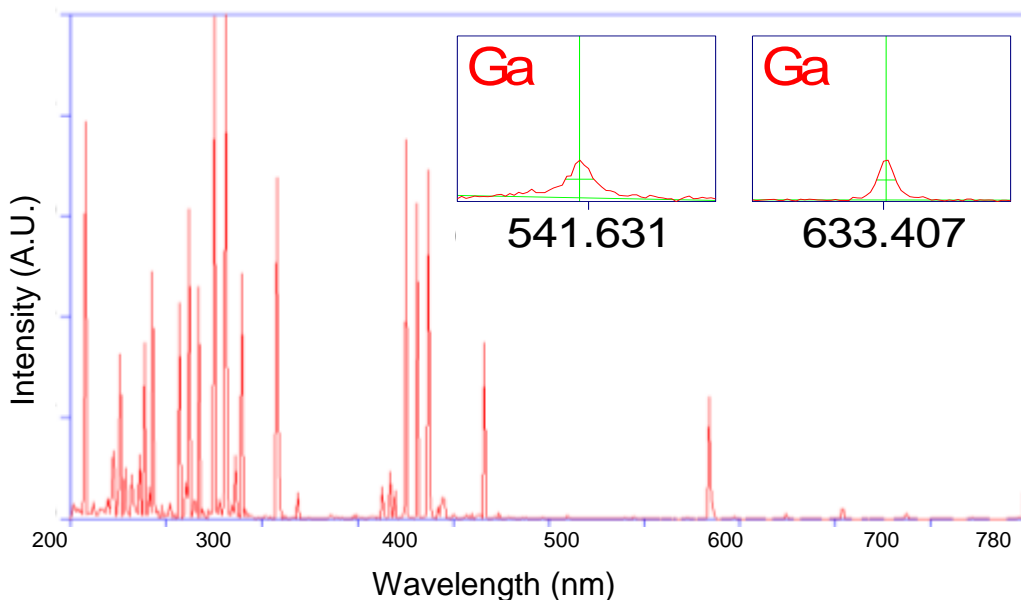


Figure 8.3 LIBS spectrum from solid Ga target, 200 – 780 nm. Strong Ga I and Ga II lines are visible. The inset shows that the start transition at 541 nm and the stop transition at 633 nm are both visible and unblended in the spectrum from laser-ablated Ga.

Of course, the lifetime work presented here is not limited to gallium studies. Any metallic sample may be input into the chamber as the target and the corresponding lifetime could be measured in an identical fashion, assuming the requisite narrow bandpass interference filters could be obtained.

8.3 – LIBS-LIF

The use of laser-induced breakdown spectroscopy (LIBS) - as an ion source - in conjunction with laser-induced fluorescence (LIF) - used to excite a specific level – for atomic lifetime measurements has already been incorporated by Shen et al.² in 2008 for the detection of uranium in metals. Hilbk-Kortenbruck et al.³ in 2001 also used LIBS-LIF in analysis of some heavy metals in soils because of its sensitive and selective abilities. Telle et al.⁴ in 2001 analyzed

metallic samples using LIBS-LIF. Lastly Zhang et al.⁵ used LIBS-LIF for atomic data in Gd II and Gd III in 2001.

The advantage to this method is that it incorporates some of the best parts of both techniques, while minimizing the weaknesses. While LIBS is fantastic at exciting highly-energized levels in neutral and multiply ionized states, the blending or overlapping of emission lines from all the simultaneous decays can create problems when measuring integrated intensities. Laser-induced fluorescence on the other hand is fantastic in its ability to single out transitions from a specific upper state but lacks the ability through tunable-dye lasers to sufficiently populate many of the highly energetic levels. By subsequently focusing a tunable-dye laser into the plasma plume created by LIBS, the plasma becomes the ion source and LIF is able to excite a transition within multiply-ionized species which it independently would not be able to. As described above, the cascading-photon coincidence technique could be incorporated and the atomic lifetime could also be determined through the coupled use of LIBS-LIF (sometimes called LIP-LIF).

¹ M.M. Dworetsky, C.M. Jomaron, C.A. Smith, “The gallium problem in HgMn stars,” *Astron. Astrophys.* **333**, 665–672 (1998).

² X.K. Shen and Y.F. Lu, “Detection of uranium in solids by using laser-induced breakdown spectroscopy combined with laser-induced fluorescence,” *Appl. Opt.* **47**, 1810-1815 (2008).

³ F. Hilbk-Kortenbruck, R. Noll, P. Wintjens, H. Falk, C. Becker, “Analysis of heavy metals in soils using laser-induced breakdown spectrometry combined with laser-induced fluorescence,” *Spectrochim. Acta B* **56**, 933–945 (2001).

-
- ⁴ H.H. Telle, D.C.S Beddows, G.W. Morris, O. Samek, "Sensitive and selective spectrochemical analysis of metallic samples: the combination of laser-induced breakdown spectroscopy and laser-induced fluorescence spectroscopy," *Spectrochim. Acta B* **56**, 947–960 (2001).
- ⁵ Z.G. Zhang, A. Persson, Z.S. Li, S. Svanberg, J. Zhankui, "Lifetime measurements in Gd II and Gd III using time-resolved laser spectroscopy," *Eur. Phys. J. D* **13**, 301-304 (2001).

Appendix 1

Introduction

Appendix 1 is a tabulation of all measured relative intensities and branching ratios for each of the elements and their respective ionization states which were studied in this research. The tables are categorized according to upper state energy level (in cm^{-1}) and within each energy state the observed relative intensities, the calculated branching ratios, and some transition probabilities as well as some oscillator strengths are listed according to increasing wavelength.

The main reason for tabulating the relative intensities from my work is because of the fact that unresolved blended or shouldered emission lines led to inaccurate determinations of the integrated peak intensity which correspondingly affected all branches belonging to the same parent upper state energy level. Because of this issue, it is useful to list just the observed relative intensities of the individual emission lines for anyone who would be interested in viewing the emission lines scaled only by the strongest peak within that parent level, rather than being scaled by the summation of all integrated intensities, as in the case of branching ratios.

Due to the fact that the lists in appendix 1 are quite extensive, requiring more than 250 pages of tables, this description of the content in appendix 1 is standing as a proxy for appendix 1. However for those interested in the tabulated data within appendix 1, downloads are available upon request via email to myself (Caleb Ryder) at ba4830@wayne.edu or Dr. Steven Rehse at rehse@uwindsor.ca.

Appendix 2 - Programming Codes

Given the massive amount of data (>60,000 emission lines) requiring analysis, I needed a partially-automated method in which to:

- 1) Create hundreds of regions of interest (ROI) text files “.roi” for the numerous upper energy states, which partition the ESAWIN spectrum into branches corresponding to their respective upper states.
- 2) Extract the emission intensity from the spectral information file “.spe” (output from ESAWIN).
- 3) Store the selected emission intensity data file “.dat” in separate folders according to upper state energy and species.
- 4) Multiply each emission line’s integrated area $I(\lambda)$ by its corresponding spectral correction factor $\varepsilon(\lambda)$.
- 5) Statistically analyze the spectrally-corrected integrated-intensities $I'(\lambda)$, relative intensities (RI), and branching ratios (BR) for each upper energy state from the 6 elements and their respective ionization states. I wanted to know the wavelength of the transition, each measured value (I' , RI, BR), the mean value, standard deviation, and the standard deviation on the mean (SDOM) for every emission line derived from every branch.
- 6) Collect the data from each upper energy state according to its element and ionization and compile the data into one excel spreadsheet according to species and output it for user readability.

In order to accomplish these goals I created multiple programs. One program creates hundreds of the “.roi” files quickly using Microsoft visual basic which is a stand-alone program (the installation of Microsoft visual basic isn’t necessary to run the program), and three other programs to address collection, storage, and analysis of the data through matlab.

Appendix 2.1 - Roi Maker

The Roi-Maker program does exactly as the title says, it creates *region of interest* (ROI) text files “.roi” to input into the ESAWIN program. The ESAWIN program uses these “.roi” files

in order to look at specific emission lines and calculate the integrated intensities, as well as other analytical calculations like FWHM, and relative intensities of the lines listed in the “.roi” file.

An example of the ESAWIN software incorporating the ROI is shown in figure A2.1.

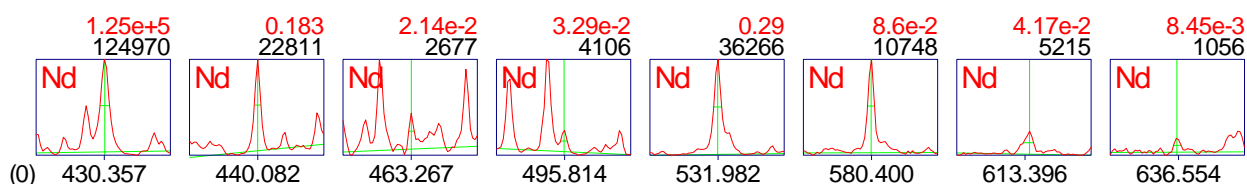


Figure Appendix 2.1 shows the typical ROI output from ESAWIN, which contains information about the emission lines listed in the “.roi” text file.

The format of a typical “.roi” text file looks like the insert shown below. The only variation is in the middle region and a few values towards to top column, therefore manipulation and duplication of the files was possible for a program.

```

18      Version
2500    Amplification
10000   Gate Width
3000    Gate Delay
5       On-Chip Accus
0       Fl Voltage
5       Clean Pulses
-1      1          input_conc
0       flags
-1      ref_conc
8       no_rois
-1.000000      conc_00
      ktb-file
Nd      430.357 1      b      0.000000 1.000000 0.000000 1000.00      x
Nd      440.082 1      b      0      0.000000 1.000000 0.000000 1000.00      x
Nd      463.267 1      b      0      0.000000 1.000000 0.000000 1000.00      x
Nd      495.814 1      b      0      0.000000 1.000000 0.000000 1000.00      x
Nd      531.982 1      b      0      0.000000 1.000000 0.000000 1000.00      x
Nd      580.400 1      b      0      0.000000 1.000000 0.000000 1000.00      x
Nd      613.396 1      b      0      0.000000 1.000000 0.000000 1000.00      x
Nd      636.554 1      b      0      0.000000 1.000000 0.000000 1000.00      x
[EVAL]
0
0      0      0
-1     0      0
-1     0.000000 0.000000

```

```

0      0      0
[ROT]
0      0      0      0      1      0
9
Nd      0
Nd      1
Ar      0
Ar      1
Na      0
Na      1
Ca      0
Ca      1
H       0
[CALC]
3
0      110      30
0      0
[CLASSI]
0      0      0      0
[SUBST]
0

```

The Roi Maker program is a graphical user-interface (GUI) which looks like figure A2.2. The user is asked to input the element symbol (according to the period table's abbreviation), the location of an excel file listing all upper states and their corresponding spontaneous transitions (usually found in NIST tables or from Kurucz database), and the output folder location where the forthcoming “.roi” files will be saved according to the upper energy states listed in the excel file.

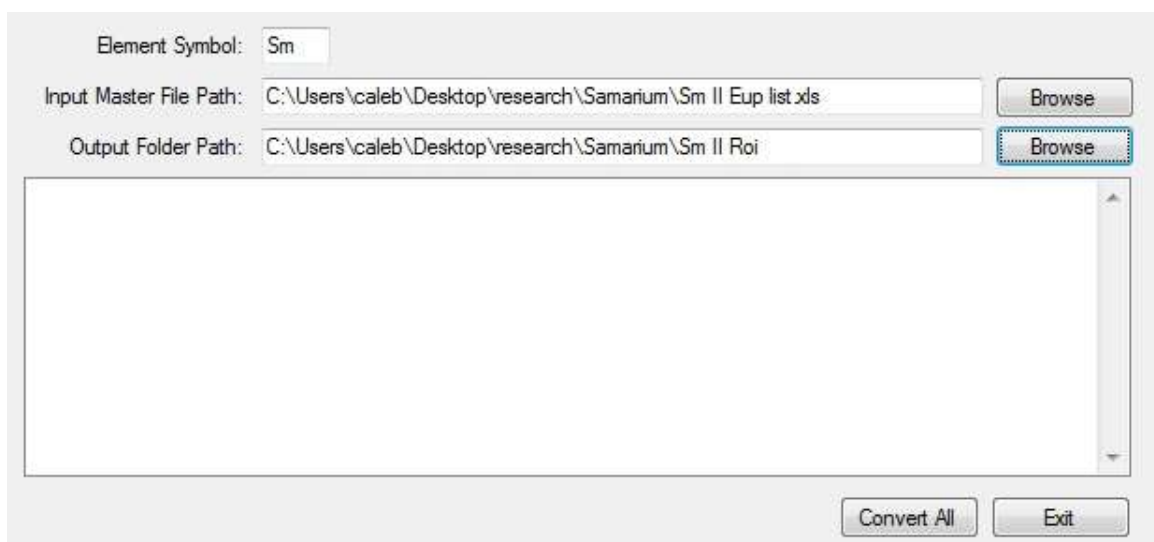


Figure Appendix 2.2 shows the GUI appearance for the Roi-Maker program.

The Excel file “.xls” containing all of the upper energies for a given species and the wavelengths of the emission lines belonging to those energies should be in the exact format shown in table A2.1 below: wavelength in column 1 and upper energy (cm^{-1}) in column 2. The excel file’s location is then typed manually into the Roi-Maker program. In this way the Roi-Maker program is used once for every individual species (element and ionization state) of interest in order to create hundreds (sometimes thousands) of “.roi” files for a given species. This method is extremely time efficient compared to entering every upper level’s transitions into the ESAWIN program one-by-one, which would take a long time to create the “.roi” files for all of the upper levels with their corresponding numerous emission lines.

Wl / nm	E_upper_lev.
695.773	23697.401
701.773	23697.401
692.499	24528.042
450.694	25609.049
586.073	25609.049
389.469	25668.692
393.483	25668.692
399.321	25668.692
442.615	25668.692
449.829	25668.692
480.257	25668.692
595.645	25668.692
663.433	25668.692

Table Appendix 2.1 shows an example of the chart format to input into the Roi Maker program.

The source code for the Roi-Maker program using Microsoft Visual Basic language is shown below.

```
Option Explicit On
Imports System
Imports System.IO
Imports System.Data.OleDb

Public Class Form1

    Public inputFile As String
    Public outputFolderPath As String
    Public FileNames As String

    Private Sub Form1_Load(ByVal sender As System.Object, ByVal e As
System.EventArgs) Handles MyBase.Load
        Me.btnConvert.Enabled = False
        Me.txtElementSymbol.Focus()
    End Sub

    Private Sub btnBrowseInputFolder_Click(ByVal sender As System.Object, ByVal e
As System.EventArgs) Handles btnBrowseInputFolder.Click
        Dim fdlg As OpenFileDialog = New OpenFileDialog()
        fdlg.Title = "Select Master Excel File"
        fdlg.InitialDirectory = ""
        fdlg.Filter = "ExcelFile (*.xls)|*.xls"
        fdlg.FilterIndex = 2
        fdlg.RestoreDirectory = True
        If fdlg.ShowDialog() = DialogResult.OK Then
            inputFile = fdlg.FileName
            txtInputFilePath.Text = (fdlg.FileName)
        End If
    End Sub

    Private Sub btnBrowseOutputFolder_Click(ByVal sender As System.Object, ByVal e
As System.EventArgs) Handles btnBrowseOutputFolder.Click
        ' First create a FolderBrowserDialog object
        Dim FolderBrowserDialog1 As New FolderBrowserDialog

        ' Then use the following code to create the Dialog window
        ' Change the .SelectedPath property to the default location
        With FolderBrowserDialog1
            ' Desktop is the root folder in the dialog.
            .RootFolder = Environment.SpecialFolder.Desktop
            ' Select the C:\Windows directory on entry.
            .SelectedPath = ""
            ' Prompt the user with a custom message.
            .Description = "Select the source directory"
            If .ShowDialog = DialogResult.OK Then
                ' Display the selected folder if the user clicked on the OK
button.
                outputFolderPath = .SelectedPath
            End If
        End With
    End Sub
End Class
```

```

    If outputFolderPath <> "" Then
        Me.txtOutputFolderPath.Text = outputFolderPath.ToString
        Call UpdateConvertButton()
    End If
End Sub

Public Sub UpdateConvertButton()
    If inputFile <> "" And outputFolderPath <> "" And txtElementSymbol.Text <>
"" Then
        Me.btnConvert.Enabled = True
    Else
        Exit Sub
    End If
End Sub

Private Sub btnExit_Click(ByVal sender As System.Object, ByVal e As
System.EventArgs) Handles btnExit.Click
    Me.Dispose()
    Application.Exit()
End Sub

Private Sub btnConvert_Click(ByVal sender As System.Object, ByVal e As
System.EventArgs) Handles btnConvert.Click
    ' make a reference to a directory
    Me.btnConvert.Enabled = False
    Dim di As New IO.FileInfo(inputFile)
    ' Dim dra As IO.FileInfo

    'list the names of all files in the specified directory
    Call ExceltoTab(di)
    Me.btnConvert.Enabled = True

End Sub

Sub ExceltoTab(ByRef file)
    Dim DA As New OleDbDataAdapter
    Dim DS As New DataSet
    Dim ColumnCount As Integer
    Dim RowCount As Integer
    Dim readfile As String = (file.ToString)
    Dim StrConn As String
    StrConn = ("Provider=Microsoft.Jet.OLEDB.4.0;Data Source=" & readfile &
";Extended Properties=""Excel 8.0;HDR=Yes;IMEX=1""")
    Dim objConn As New OleDbConnection(StrConn)
    Try
        If ConnectionState.Open.Equals(False) Then
            objConn.Open()
        End If

    Catch ex As Exception
        Console.WriteLine(ex.ToString)
        Exit Sub
    End Try

    Dim objCmd As New OleDbCommand("Select * from [Sheet1$]", objConn)
    objCmd.CommandType = CommandType.Text

```

```

Try
    DA.SelectCommand = objCmd
    DA.Fill(DS, "XLData")
Catch ex As Exception
    Console.WriteLine(ex.ToString)
End Try

Entry:
    RowCount = DS.Tables(0).Rows.Count
    ColumnCount = DS.Tables(0).Columns.Count
    Dim FirstRow2ndCol As String = (DS.Tables(0).Rows(0).Item(1))

    Dim firstRow1ndCol As String = (DS.Tables(0).Rows(0).Item(0))
    Dim FileName As String = (DS.Tables(0).Rows(0).Item(1))

    If FirstRow2ndCol <> "" Then

        Dim ObjStreamWriter As IO.StreamWriter = New
        IO.StreamWriter(txtOutputFolderPath.Text & "\" & txtElementSymbol.Text & "_" &
        FirstRow2ndCol & ".roi")
        Dim originalPath As String = (txtOutputFolderPath.Text & "\" &
        txtElementSymbol.Text & "_" & FirstRow2ndCol & ".roi")
        LbProgress.Items.Insert(0, "Created File: " & FirstRow2ndCol)
        Me.Refresh()

        Dim dr As DataRow
        Dim dt As DataTable
        dt = DS.Tables(0)
        Dim i As Integer = 0
        For Each dr In dt.Rows
            Dim check As String = (dr(1).ToString)
            If check = FirstRow2ndCol Then
                Dim currentvalue As String = (dr(0).ToString)
                ObjStreamWriter.WriteLine(txtElementSymbol.Text & vbTab &
                currentvalue & vbTab & Ks_Program.My.Resources._Static)
                i = i + 1
                dr.Delete()
            ElseIf check <> FirstRow2ndCol Then
                DS.AcceptChanges()
                DS.Dispose()
                ObjStreamWriter.WriteLine(Ks_Program.My.Resources.Ending)
                ObjStreamWriter.Close()
                Dim WriteBack As IO.StreamReader = New
                IO.StreamReader(originalPath)
                Dim Fulltext As String = (WriteBack.ReadToEnd)
                WriteBack.Close()
                Dim ObjStreamWriter2 As New IO.StreamWriter(originalPath)

                ObjStreamWriter2.WriteLine(Ks_Program.My.Resources.Begining.Replace("$",
                i.ToString) & vbCr)
                ObjStreamWriter2.WriteLine(Fulltext & vbCrLf)
                ObjStreamWriter2.Close()
                i = 0
                GoTo Entry
            End If
        Next
    ElseIf FirstRow2ndCol = "" Then
        Exit Sub
    End If

```



```

End If
objCmd.Dispose()
objCmd = Nothing
objConn.Close()
objConn.Dispose()
objConn = Nothing
LbProgress.Items.Insert(0, "Finsihed Processing: " & readfile)
Me.Refresh()

End Sub

End Class

```

Appendix 2.2 - CreateFoldersForEachRoiInEUpsList

The next code I wrote involved the use of matlab, a more robust matrix-computational program compared to Microsoft Visual Basic, the name of the code is *CreateFoldersForEachRoiInEUpsList*. The purpose of this code is to create folders appropriately titled according to the upper energy state numerical value in wavenumbers (cm^{-1}) (i.e. 18171.819 cm^{-1}). The purpose for needing multiple folders labeled according to upper state energy is because the .dat spectral information (output from ESAWIN's ROI values) are by default stored in a given folder location and given a common default name. This causes issues if I am interested in multiple upper energy levels' ROI information because the default name and location of the .dat files will overwrite the previous upper energy state's .dat files. Therefore storing the .dat output in separate folders which are titled according to upper energy state seems practical. The numerous folders (labeled according to upper energy) are located within a single root folder according to species and ionization. For example, the folder pertaining to the 18171.819 cm^{-1} level of Nd I contains data files (".dat") output from ESAWIN which have the *ROI* information sorted according to file number. The folder corresponding to this energy level which is located within the Nd I root folder ("...\neodymium\2011_04_23\042311\Nd_I) is

“...\neodymium\2011_04_23\042311\Nd_I\Nd_Up18171.819”. Again, the reason for writing this code was due to the vast amount of folders that would otherwise need to be created by hand individually which is a rather time consuming process (~1000 between all ionizations, species and upper energy levels).

CreateFoldersForEachRoiInEupsList code:

```
% This program will create a .roi files with appropriate wavelengths
% according to the various EUP for the given element. It requires a list of
% wavelengths in column 1 and the Corresponding EUPs in Column 2 stored in
% an excel (.xls) file which are located on "sheet1" of that excel file.
% The output(s) will be in .roi format and will be separated according to
% the number of EUPs which are listed in the .xls file called "FeII", for
% example. It requires that you take a ".roi" EUp file
% (Ex: Neo_EUp23229.991) and convert it to a ".xls" file and then input it
% into the program.

%trial 1 took about 171 seconds for Iron II with all its 707 EUPs

tic
format long g;

%get the element symbol from the user
ElementSym = input('What element is it? input element symbol "C" for carbon:
','s');
ElementSym = char(ElementSym);
IonizLevel = input('What ionization level are these Energies for? input ionization
as "II" for singly ionized: ','s');

%% Get the list of wavelengths and Upper energy levels (cm^-1) from a list in
%an excel file (.xls)...should be stored on the sheet labeled "Sheet1"
[filenameExcl,pathnameExcl]= uigetfile({'*.xls','Excel files (*.xls)'; '*.xlsx',
'Excel_07 files (*.xlsx)'; '*.*','All Files (*.*)'},'select the excel file to
input "GdII Wavelength vs EUps"');
FileLocationExcl = strcat(pathnameExcl,filenameExcl);
FileLocationExcl = char(FileLocationExcl);
[ExcelInWaveEUp,ExcelInWaveEUpHeaders,ExcelInWaveEUpRaw] =
xlsread(FileLocationExcl , 'Sheet1');

SizeExcelInWaveEUp = size(ExcelInWaveEUp);

%%%%%%%%%%%%%%%%%%%%%%%%%%%%%%%%%%%%%%%%%%%%%%%%%%%%%%%%%%%%%%%%%%%%%%%%
%where do you want to output these roi EUP folders to
Pathout = input('Where do you want to output these roi EUP folders, what path,
just copy/paste it here: ','s');
Pathout = char(Pathout);
%%
% in this section I'm going to pick out the Eups and put them in a column
% vector called EUpList2. Also the corresponding wavelengths for these EUPs
```

```

% are listed as separate columns in a matrix called Array2.
count = 0; count1 = 0; ExcelEUp = []; ExcelEUp2 = []; EUpList = [];
Array = []; %Array2 = [];
LEExcelEUp = 0;

for RR = 1:SizeExcelInWaveEUp(1)
    LEExcelEUp = 0;
    count1 = count1 + 1;
    ExcelEUp = ExcelInWaveEUp(ExcelInWaveEUp(:,2)==ExcelInWaveEUp(RR,2)); %stores
# of identical emissions lines for a given EUp, # of identical EUps in list
    LEExcelEUp=length(ExcelEUp);

    %takes only the wavelengths with identical EUps
    %for each iteration of RR I need to "store" the cells of ExcelEUp
    %somewhere so they aren't overwritten for the next iteration of RR.
    if RR<SizeExcelInWaveEUp(1)
        if ExcelInWaveEUp(RR,2)~=ExcelInWaveEUp(RR+1,2)
            count = count+1;%keeps count of diff 0
            EUpList(RR) = ExcelInWaveEUp(RR,2);%store the different EUps
            EUpList2 = EUpList(EUpList~=0);%only store diff EUps, no zeros
            Array((1:LEExcelEUp),RR) = ExcelEUp;
            Array2 = Array; %this is a list of wavelengths from all EUps
        end

        elseif RR==SizeExcelInWaveEUp(1)
            EUpList(RR) = ExcelInWaveEUp(RR,2);%store the different EUps
            EUpList2 = EUpList(EUpList~=0);%only store diff EUps, no zeros
            Array((1:LEExcelEUp),RR) = ExcelEUp;
            Array2 = Array; %this is a list of wavelengths from all EUps
        end
    end
end
Array2(:, find(sum(abs(Array2)) == 0)) = []; %Deletes columns of zeros
SizeArray2 = size(Array2);

if isequal(length(EUpList2),SizeArray2(2))~=1
    disp(' there is a problem b/c the # of Eups doesnt match the col in Array2:
line 82');
end
%%
% Now that we have the number of emission lines which come from a given EUP
% I can create the same number of rows for the ".roi" file accordingly.
Array3 = Array2;
Indxx = (Array2 ~=0); %makes a logical array for numbers no = to 1 same size as
Array2
SIndxx = sum(Indxx); %sum up the columns from Indxx == a count of nonzeros in each
colm of Array2

%trying to create an array with the important info in the "middle" of a roi
%file by making the program look to see how many emission lines (rows) are in each
%Eup (Columns) and then create a generic array accordingly by "sandwiching"
%the data onto the sides of the wavelengths like a roi does
Cnt = 0; Cnt2 = 0; OutputRow = 0; OutputRowB = 0;
for CCC=1:SizeArray2(2)
    IonizLevel = char(IonizLevel); ElementSym = char(ElementSym);
    pathnameExcl = char(pathnameExcl);
    StrEUpList2 = num2str(EUpList2(CCC), '%.3f');
    ElemAndUp = strcat(ElementSym, '_Up');

```

```

ElemAndUp=char(ElemAndUp);
StrEUpList3 = strcat(ElemAndUp, StrEUpList2);
StrEUpList3 = char(StrEUpList3);
OutputEUpRoiFolder = strcat(Pathout,'\ ',StrEUpList3);
    if (exist(OutputEUpRoiFolder) == 0)
        mkdir(OutputEUpRoiFolder);
    end
clear StrEUpList2
end
toc

```

Appendix 2.3 - AutomaticFinalDataCreatorV1

The purpose of the matlab script called *AutomaticFinalDataCreatorV1* is to mimic the *DataFilterWorkBook.xls* program which Narmatha Jeyasingham wrote. Her program takes the .dat files that are the output of ESAWIN which contain ROI information (integrated area of peaks) as well as many other parameters of the emission lines, and it sorts through these .dat files and picks out the information which is pertinent to our studies: the integrated area of the peaks listed in the ROI file. When the pertinent data is extracted from the .dat file it is stored in a .xls file titled *FinalData.xls*. The *AutomaticFinalDataCreatorV1* differs from Narmatha's program because my program will duplicate the same process which *DataFilterWorkBook.xls* does, but on top of this my program will automatically create these *FinalData.xls* files for every upper energy level which you input into the program in a text file, whereas Narmatha's program works for only a single level at a time. Each upper energy level should already have its .dat files stored in separate upper energy folders named according to the wavenumber of the upper energy level. Therefore my program requires a list of the upper energy levels you desire to have *FinalData.xls* files generated for, and it will ask you to select the root folder where all of these upper energy folders are located within. From here the program automatically generates all of the

FinalData.xls files for every upper energy level which was listed in the text file (usually called UpperEnergyNdI.txt) and it outputs them to the appropriate upper energy folder.

```
AutomaticFinalDataCreatorV1 ()

tic
format long g;

%get the number of .dat files per EUp (stored in each EUp folder)
NumDatFiles = input('how many .dat files are stored in each EUp to be analyzed
into final_data?: ');

%get the Element symbol which is used to look for as a string in the .dat
%files
ElementSymbl = input('what element is it? input answer as the element symbol (Iron
= Fe): ','s');

%get the list of Upper Energy Levels for the element in (cm^-1) from a 1
%column text file.
[filenameEUps,pathnameEUps]= uigetfile({'*.txt','Text files (*.txt)'; '*.dat',
'Data files (*.dat)'; '*.*','All Files (*.*)'},'select the file with the list of
Upper Energies to input.. Ex: Nd II EUps.txt');
fileLocationEUps = strcat(pathnameEUps,filenameEUps);
fidEUps = fopen(fileLocationEUps);
EUpsList = textscan(fidEUps,'%s'); %returns a 1 column cell array of strings
fclose(fidEUps);
EUpsList = EUpsList{:}; %get rid of matlab's cell in a cell format==> 1 coulumn
with multi rows
EUpsListNum = str2double(EUpsList);
%convet the strings in EUpsList to numbers(double format)

disp('got to 34')

count = 0;
filenameHeaders = [];
filenameExcl = [];

clear ii
for ii = 1:(length(EUpsList))
    count = count + 1
    %string together the folder location where the .dat files are
    %located....
    %use some sort of iteration to get matlab to sequentially pass
    %through them.

    %pathnameDat = C:\Users\caleb\Desktop\research\Copper\2011_04_29\042911\dat
junk\Cu_Up115662.550\

    if ii==1 %for the first entry only let the user show where the files are
located and pick the first dat file

        [filenameDat,pathnameDat]= uigetfile({'*.dat','Data files (*.dat)';
'*..*','All Files (*.*)'},'select the 1st .dat file from the 1st EUp Ex:
042711_001.dat');
```

```

        fileLocationDat = strcat(pathnameDat,filenameDat);
        pathnameDat2 = pathnameDat;
    else
        AA=length(EUpsList{ii});    %now let program get the rest of the .dat
files stored in teh EUps list entered earlier
        pathnameDatBegin = pathnameDat2(1:(end-10));
        EUpIndx = char(EUpsList{ii});
        pathnameDat = strcat(pathnameDatBegin, EUpIndx, '\')
    end

%%%%%%%%%%%%%%%%%%%%%%%%%%%%%%%%%%%%%%%%%%%%%%%%%%%%%%%%%%%%%%%%%%%%%%%%
    clear jj;
    for jj = 1:NumDatFiles

        %042711_001.dat ... 042711_024.dat
        %eval(['A_' num2str(i) '=i'])
        %have user input the 1st .dat file from the 1st EUp to be sorted.

%%%%%%%%%%%%%%%%%%%%%%%%%%%%%%%%%%%%%%%%%%%%%%%%%%%%%%%%%%%%%%%%%%%%%%%%5
%below I have to let the program iterate through the Eups in teh list in
%order to automatically "grab" the .dat files which need to be sorted... jj
%is the index of the .dat files which are located in the "iith" Eup folder.

%in order to iterate throught the .dat files I have to allow the counter to
%range from 1-999 any longer than this and ESA wouldnt be able to
%accomidate the files.

        if ((jj>0) && (jj <= 9))
            filenameDatStart = filenameDat(1:end-5);
            filenameDatStart = char(filenameDatStart);
            Ending = int2str(jj);
            Ending2 = char(Ending);
            filenameDatStartIter = [filenameDatStart, Ending2];
            FileNameEnd = strcat(filenameDatStartIter, '.dat');
            fileLocationDat = strcat(pathnameDat,FileNameEnd);
        elseif ((jj>9) && (jj <=99))
            filenameDatStart = filenameDat(1:end-6);
            filenameDatStart = char(filenameDatStart);
            Ending = int2str(jj);
            Ending2 = char(Ending);
            filenameDatStartIter = [filenameDatStart, Ending2];
            FileNameEnd = strcat(filenameDatStartIter, '.dat');
            fileLocationDat = strcat(pathnameDat,FileNameEnd);
        elseif ((jj>99) && (jj<=999))
            filenameDatStart = filenameDat(1:end-7);
            filenameDatStart = char(filenameDatStart);
            Ending = int2str(jj);
            Ending2 = char(Ending);
            filenameDatStartIter = [filenameDatStart, Ending2];
            FileNameEnd = strcat(filenameDatStartIter, '.dat');
            fileLocationDat = strcat(pathnameDat,FileNameEnd);
        else
            disp('counter of jj is too large')
            error('counter of jj is too large');
        end
    end

```

```

disp('got to 119')
    fidDat = fopen(fileLocationDat); %opens the .dat file stored in the
location
    EUpsListDat1 = textscan(fidDat,'%s'); %returns a 1 column cell array of
strings
    fclose(fidDat);
    EUpsListDat2 = EUpsListDat1{:}; %get rid of matlab's cell in a cell
%format==> 1 coulumn with multi rows
    EUpsListDatNum = str2double(EUpsListDat2);
    disp('got to 125')
    ElementSymb1 = char(ElementSymb1);
    EUpsListDat2(strcmpi(EUpsListDat2,ElementSymb1));% tells how many 'Cu''s
%there are in the list how many emission lines
    ElemSymb1CellLocatnRow = find(strcmpi(EUpsListDat2,ElementSymb1));
%returns cell location of the 'Cu' entries in the .dat file
    EUpsListDatCells = EUpsListDatNum(ElemSymb1CellLocatnRow + 2);
%returns, in a single column, the integrated area's which Esa calculates for the
%emission lines
    EUpsListDatCells(isnan(EUpsListDatCells)) = 0;
    disp('got to 131')
    if jj==1
        finalDataMatrix = zeros(length(EUpsListDatCells),NumDatFiles);
    end

        finalDataMatrix(:,jj) = EUpsListDatCells; %stores each column of .datas
(multiple emission lines/ column)

    end
disp('got to 139')

    finalDataMatrixT = finalDataMatrix'; %transposes array above so that each
column corresponds to a single emiission line's integrated areas

%%%%%%%%%%%%%%%%%%%%%%%%%%%%%%%%%%%%%%%%%%%%%%%%%%%%%%%%%%%%%%%%%%%%%%%%
    % if the transposed array has any columns which are all zeros (noise,
    % np, invalids) then replace the 1st row of that column with the value
    % 1 so that in the next matlab script it won't be eliminated
    disp('got to 148')
    SizefinalDataMatrixT= size(finalDataMatrixT);
    SumfinalDataMatrixT = sum(finalDataMatrixT);
    for uu=1:SizefinalDataMatrixT(2)
        if SumfinalDataMatrixT(1,uu) == 0

            finalDataMatrixT(1,uu) = 1;
            disp('Appended column of zeros in finalDataMatrixT to a single cell
with a 1 in the empty column ')
        end
    end

    %store/outputs the finalDataMatrix to an excel file called "Final_Data.xls"
    pathnameExcl = char(pathnameDat);
    OutPutFileExclName = strcat(pathnameExcl, 'Final_Data.xls')
    xlswrite(OutPutFileExclName, finalDataMatrixT, 'Sorted Data' , 'A1'); % store
it in a sheet called "Sorted Data", starting with cell A1
disp('got to 165')
    disp('1 round completed')

```

```

clear finalDataMatrix
clear finalDataMatrixT
clear EUpsListDat1
clear SumfinalDataMatrixT
end
toc

```

Appendix 2.4 - AutomaticImportHeaders2ExcelAndFValueCorrectV7

The purpose of the *AutomaticImportHeaders2ExcelAndFValueCorrectV7* program is to analyze the integrated intensities output from ESAWIN as *.dat* files which are located in their separate folders according to upper energy state and stored in Excel files called *FinalData.xls*. This program computes the statistical *mean*, *standard deviation*, and *standard deviation on the mean* for integrated intensities (I), relative intensities (R.I.), and branching ratios (B.R.) and outputs this information to separate sheets in an excel file (“*.xls*”) titled according to the appropriate upper state energy and stores it in the appropriate folder. The data from each of the 5 different pressures are analyzed and stored in separate sheets within the output excel file. For example the Nd I upper state 18171.819 cm^{-1} will have an excel file named *Nd_Up18171.819.xls* as an output from this program which contains all the statistical information for the integrated intensities, relative intensities, and branching ratios pertaining to that upper state and its allowed transitions and the pressure.

AutomaticImportHeaders2ExcelAndFValueCorrectV7 code:

```

%this function automatically will iterate through the Eup folders which
%contain 'Final Data' excel files (.xls) and will shift the top two rows
%down and replace them with headers which contain the element of the roi
%and their corresponding wavelengths. It will also save the updated excel
%file as a new excel file and replace any strings in the file with zeros. The
program will do this for all of the Eups which are listed in the text file which
%needs to be 1st input by the user. It requires the numerous 'final data.xls'
files to be stored in separate folders which are titled according to their Eup Ex:

```



```

"C:/.../Neo_EUp23229.991/" the folder title should be 15 characters long
%or at least the same length and you could alter the code in this program.

% this program takes 35 minutes for Nd II which has 46 Upper energies.

%%
tic
format long g;

%%%%%%%%%%%%%%%%%%%%%%%%%%%%%%%%%%%%%%%%%%%%%%%%%%%%%%%%%%%%%%%%%%%%%%%%
%get the list of Fvalue-Wavelengths and their corresponding Fvlaues in the
%format Wavelength(nm)|FValues stored in an excel (.xls) format
%~(30,000'=Row' x 2'=Col')
[filenameFValues,pathnameFValues]= uigetfile('*.xls','get excel file containing
the 2 columns of Wavelengths|Fvalues called FValueList:')
infile = strcat(pathnameFValues,filenameFValues);
[FValuesDataIn,FValuesTextIn] = xlsread(infile);
% FValuesDataIn;
% FValuesTextIn;
FValuesDataIn(isnan(FValuesDataIn)) = 0; % if the Data has any NaN's make them 0
RowsByColsFValue = size(FValuesDataIn);

%get the list of Upper Energy Levels for the element in (cm^-1) from a 1
%column text file.
[filenameEUps,pathnameEUps]= uigetfile({'*.txt','Text files (*.txt)'; '*.dat',
'Data files (*.dat)'; '*.*','All Files (*.*)'},'select the file with the list of
Upper Energies to input.. Ex: Nd II EUps.txt');
fileLocationEUps = strcat(pathnameEUps,filenameEUps);
fidEUps = fopen(fileLocationEUps);
EUpsList = textscan(fidEUps,'%s'); %returns a 1 column cell array of strings
fclose(fidEUps);
EUpsList = EUpsList{:}; %get rid of matlab's cell in a cell format==> 1 coulumn
with multi rows
EUpsListNum = str2double(EUpsList);
%convet the strings in EUpsList to numbers(double format)

ElementAbbrv = input('what element is it? (abbreviate it with symbol like Sm for
Samarium): ', 's');

count = 0;
filenameHeaders = [];
filenameExcl = [];

%%
for i = 1:(length(EUpsList))
    count = count + 1

    %% Need to see if "filename" is empty, b/c you only want user input ONCE
    %% this can only work for roi b/c they have right filename format
    %%

    filenameHeaders = char(filenameHeaders);
    if isempty(filenameHeaders)

        [filenameHeaders,pathnameHeaders]= uigetfile({'*.roi','Roi files (*.roi)';
        '*.txt','Text files (*.txt)'; '*.dat', 'Data files (*.dat)'; '*.*','All Files
        (*.*)'},'select the header file to input preferably a .roi but .dat works too!');
    end
end

```

```

        fileLocationHeaders = strcat(pathnameHeaders,filenameHeaders);

elseif isequal(filenameHeaders(end-3:end),'.roi')

    filenameHeaders = strcat(EUpsList(i), '.roi');
    ElementAbbrv = char(ElementAbbrv);
    ElementAbbrv2 = strcat(ElementAbbrv,'_');
    filelocationh = strcat(pathnameHeaders, ElementAbbrv2);
    fileLocationHeaders = strcat(filelocationh,filenameHeaders);

else

    [filenameHeaders,pathnameHeaders]= uigetfile({'*.roi','Roi files (*.roi)';
    '*.txt','Text files (*.txt)'; '*.dat', 'Data files (*.dat)'; '*.*','All Files
    (*.*)'}, 'select the header file to input preferably a .roi but .dat works too2');
    fileLocationHeaders = strcat(pathnameHeaders,filenameHeaders);
end
fileLocationHeaders = char(fileLocationHeaders);
fid = fopen(fileLocationHeaders);
allstrings = textscan(fid,'%s'); %returns a 1 column cell array of strings
fclose(fid);
allstrings = allstrings{:}; %converts the cell array into a 1 column matrix
%note: this last line is needed to undo
%the strange cell-within-a-cell output that textscan uses.
%%

%import the excel file "final data" and get its data
if isempty(filenameExcl)

    [filenameExcl,pathnameExcl]= uigetfile({'*.xls','Excel files (*.xls)';
    '*.xlsx', 'Excel_07 files (*.xlsx)'; '*.*','All Files (*.*)'}, 'select the excel
    file to input "finaldata"');
    FileLocationExcl = strcat(pathnameExcl,filenameExcl);

else

    filenameExcl = char(EUpsList(i));
    pathnameExclFirstPart = pathnameExcl(1:(end-16));
    pathnameExclFirstPart=char(pathnameExclFirstPart);
    pathnameExcl =
    strcat(pathnameExclFirstPart,ElementAbbrv2,'Up',EUpsList(i),'\');
    FileLocationExcl = strcat(pathnameExcl,'Final_Data.xls');
    FileLocationExcl = char(FileLocationExcl);

end

FileLocationExcl = char(FileLocationExcl);
ExcelInFile = xlsread(FileLocationExcl , 'Sorted Data');
%initialsize = size(ExcelInFile)
%line below takes all the strings "NaN" and turns them into zeros
ExcelInFile(isnan(ExcelInFile)) = 0;

%make sure that youre dealing with the same Eup level in Excel and ".roi or
.dat" file
% if ~isequal(pathname(end-15:end-1),pathnameExcl(end-15:end-1))
%     disp('error1"Excel file" and ".roi or .dat" file are not from same Eup')
% elseif ~isequal(pathname(end-15:end-1),pathnameExcl(end-15:end-1))

```

```

%      disp('error2"Excel file" and ".roi or .dat" file are not from same Eup')
% else
%      disp('error3"Excel file" and ".roi or .dat" file are not from same Eup')
%      error
% end

%%
%%%%% here I'm getting the wavelengths from the .dat or .roi files

filenameHeaders = char(filenameHeaders);
if isequal((filenameHeaders((end-3):end)),'.dat')

    % make another array (1 column) of all the cells but convert them
    %from strings to numbers(double format)
    allNum = str2double(allstrings);
    wavelengths1 = find((0<allNum) & (allNum < 1));
    %if the numbers are btwn 0 & 1 then they're wavelengths cells, FIND
    %and record their cell index in a column
    Wavelengths = allNum((0<allNum)&(allNum<1));
    Wavelengths = 1000*Wavelengths';
    %taking only the cells with wavelengths and make a single column of
    %them
    % % wavelengths1(isnan(wavelengths1))= 0;
    % % WavelengthsB=wavelengths1(:,any(wavelengths1,1));

elseif isequal(filenameHeaders(end-3:end),'.roi')

    % make another array (1 column) of all the cells but convert them
    %from strings to numbers(double format)
    allNum = str2double(allstrings);
    wavelengths1 = find((100.000<allNum) & (allNum < 999.999));
    %if the numbers are btwn 100.000 & 999.999 then they're hopefully
    %wavelengths cells

    %here I need to make sure that the numbers we found above
    %correspond to wavelengths even though they're within the necessary
    %range.... to do this, I will make sure they're paired-up with the
    %necessary Element symbol (Ex: Pr) stored in the Roi file... bc the
    %element symbol should be 1 cell in front of the wavelength it
    %corresponds to in the roi file.
    for aa=length(wavelengths1):-1:1
        if ~isequal(ElementAbbrev,char(allstrings(wavelengths1(aa,:)-1)))

            wavelengths1(aa,:)= '';
        end
    end

    %FIND and record their cell index in a column
    Wavelengths = allNum(wavelengths1);
    Wavelengths = Wavelengths';
    %taking only the cells with wavelengths and make a single column of
    %them

else
    disp('first file type isnt consistent with program requirements')

```

```

        error('first file type isnt consistent with program requirements')
    end

    %%

    % Make another array (1 column) of all the cells which are 1-step above
    %the wavelength cells b/c these equal the Element Symbols.
    ElemIndex = wavelengths1 - 1;
    for j = 1:(length(ElemIndex))
        ElementSymbols(j) = allstrings(ElemIndex(j));
    end
    ElementSymbols;

    %%

    %*****I think we have a problem if there is more than just 1 column
    %missing b/c xlsread which cuts off the initial columns if they have
    %all NonZero numbers in them to make matlab fill in more than 1 column
    %if needs be use subtraction to get the number of missing columns
    %required to fill in.

    %see if column lengths of all 3 matricies are equal if not do something
    %about it
    RowByCol = size(ExcelInFile);
    if (RowByCol(2)>length(ElementSymbols)) && (RowByCol(2)>length(Wavelengths))
        disp('the excel file "Final Data" matrix has more columns than the
headers')
        for jj = 1:(RowByCol(2) - length(ElementSymbols))
            ElementSymbols = [NaN(1,jj) ElementSymbols];
            Wavelengths = [zeros(1,jj), Wavelengths];
        end
    elseif (RowByCol(2)<length(ElementSymbols)) &&
(RowByCol(2)<length(Wavelengths))
        disp('the excel file "Final Data" matrix has less columns than the
headers')
        for kk = 1:(length(ElementSymbols) - RowByCol(2))
            ExcelInFile = [zeros(RowByCol(1),kk) , ExcelInFile];
        end
    else
        disp('"Final Data" file matches up with headers file')
    end

    %% %%%%%%%%%%%%%%%%%%%%%%%%%%%%%%%%%%%%%%%%%%%%%%%%%%%%%%%%%%%%%%%%%%%%%%%%%%%%%%%
    %here I am going to sort through the f-value list and find the f-values
    %which is closest to the emission line wavelength and retain it for
    %further use
    RowsByColsData = size(ExcelInFile);
    RowsByColsWavelengths = size(Wavelengths);
    Diff(RowsByColsFValue(1),RowsByColsWavelengths(2)) = 0;

    for mm = 1:RowsByColsWavelengths(2)

        for nn=1:RowsByColsFValue(1)
            % subtract the difference between wavelengths from ExcelData
            % and FValues to find the minimum which will be the closest

```

```

        % wavelength. Next we will take the fValue corresponding to
        % that closest wavelength in FValues list
        Diff(nn,mm) = abs(FValuesDataIn(nn,1) - Wavelengths(1,mm));

    end

end

[C,Indices] = min(Diff);
%% Here I am going to use the f-value which I just found above and apply
%it to the data
MultiplyFactor = FValuesDataIn(Indices,2)';
SizeMultiplyFactor = size(MultiplyFactor);
EUpDataInFValue(RowsByColsData(1),RowsByColsData(2)) = 0;

if SizeMultiplyFactor(2) == RowsByColsWavelengths(2)
    for rr = 1:RowsByColsData(1)
        for cc = 1:RowsByColsData(2)
            EUpDataInFValue(rr,cc) = ExcelInFile(rr,cc)*MultiplyFactor(1,cc);
        end
    end
else
    disp('size of MultiplyFactor line 229 and size of Wavelengths arent
equal')
    error('size of MultiplyFactor line 229 and size of Wavelengths arent
equal');
end

clear rr
clear cc
%EUpDataInFValue(1,:) = Wavelengths(1,:);
%EUpDataInFValue(1,:) = ExcelInFile(1,:); %takes the 1st row of ExcelInFile
%which is the wavelength's and it retains them by putting them into
%EUpDataInFValue's 1st row

%%
%%since the data from roi pertains to 5 different pressures (50 total
%files for 1 roi = 10 files / pressure) I will seperate these pressure
%from the mass of 50 into 5 columns of 10 and average them and get
%the standard deviation and fractional standard deviation (std/avg)

SizeEUpDataInFValue = size(EUpDataInFValue);
EUpDataInFValueAvg((SizeEUpDataInFValue(1)/10),(SizeEUpDataInFValue(2)))=0;
EUpDataInFValueStdV((SizeEUpDataInFValue(1)/10),(SizeEUpDataInFValue(2)))=0;

for rr=1:(SizeEUpDataInFValue(1)/10) %10 is the number of rows per Pressure in
12142010 data
    for cc=1:SizeEUpDataInFValue(2)
        RR = (rr-1)*10; %starts at zero for rr=1
        EUpDataInFValueAvg(rr,cc) =
mean(EUpDataInFValue((RR+1):(RR+10)),cc);
        EUpDataInFValueStdV(rr,cc) =
std(EUpDataInFValue((RR+1):(RR+10)),cc,0,1);

    end
end
EUpDataInFValueP8_83=EUpDataInFValue(1:10,:);

```

```

EUpDataInFValueP8_3=EUpDataInFValue(11:20,:);
EUpDataInFValueP7_85=EUpDataInFValue(21:30,:);
EUpDataInFValueP6=EUpDataInFValue(31:40,:);
EUpDataInFValueP4=EUpDataInFValue(41:50,:);
EUpDataInFValueAvg;
EUpDataInFValueStdV;

EUpDataInFValueFracStdV = EUpDataInFValueStdV./EUpDataInFValueAvg;

EUpDataInFValueFracStdV(isnan(EUpDataInFValueFracStdV))=0; %sets all NaN
values to zero

%Using the location of the excel file's "path name" save all the info
(ElementSymbols, Wavelengths, ExcelInFile) in 1
% in a new file which takes its name from the last 15 characters in "path
name"
pathnameExcl = char(pathnameExcl);
OutPutFileExclName = strcat(pathnameExcl, pathnameExcl((end - 15):(end - 1)),
'.xls')
xlswrite(OutPutFileExclName, ElementSymbols, 'sheet1' , 'A1');
xlswrite(OutPutFileExclName, Wavelengths, 'sheet1' , 'A2');
xlswrite(OutPutFileExclName, ExcelInFile, 'sheet1' , 'A3');

xlswrite(OutPutFileExclName, MultiplyFactor, 'WithFValue' , 'A1');
xlswrite(OutPutFileExclName, ElementSymbols, 'WithFValue' , 'A2');
xlswrite(OutPutFileExclName, Wavelengths, 'WithFValue' , 'A3');
xlswrite(OutPutFileExclName, EUpDataInFValue, 'WithFValue' , 'A4');

xlswrite(OutPutFileExclName, ElementSymbols, 'Press8.83Analysis' , 'A1');
xlswrite(OutPutFileExclName, Wavelengths, 'Press8.83Analysis' , 'A2');
xlswrite(OutPutFileExclName, EUpDataInFValueP8_83, 'Press8.83Analysis' ,
'A3');
xlswrite(OutPutFileExclName, EUpDataInFValueAvg(1,:), 'Press8.83Analysis' ,
'A14');
xlswrite(OutPutFileExclName, EUpDataInFValueStdV(1,:), 'Press8.83Analysis' ,
'A16');
xlswrite(OutPutFileExclName, EUpDataInFValueFracStdV(1,:), 'Press8.83Analysis'
, 'A18');

xlswrite(OutPutFileExclName, ElementSymbols, 'Press8.3Analysis' , 'A1');
xlswrite(OutPutFileExclName, Wavelengths, 'Press8.3Analysis' , 'A2');
xlswrite(OutPutFileExclName, EUpDataInFValueP8_3, 'Press8.3Analysis' , 'A3');
xlswrite(OutPutFileExclName, EUpDataInFValueAvg(2,:), 'Press8.3Analysis' ,
'A14');
xlswrite(OutPutFileExclName, EUpDataInFValueStdV(2,:), 'Press8.3Analysis' ,
'A16');
xlswrite(OutPutFileExclName, EUpDataInFValueFracStdV(2,:), 'Press8.3Analysis'
, 'A18');

xlswrite(OutPutFileExclName, ElementSymbols, 'Press7.85Analysis' , 'A1');
xlswrite(OutPutFileExclName, Wavelengths, 'Press7.85Analysis' , 'A2');
xlswrite(OutPutFileExclName, EUpDataInFValueP7_85, 'Press7.85Analysis' ,
'A3');
xlswrite(OutPutFileExclName, EUpDataInFValueAvg(3,:), 'Press7.85Analysis' ,
'A14');

```

```

        xlswrite(OutPutFileExclName, EUpDataInFValueStdV(3,:), 'Press7.85Analysis' ,
'A16');
        xlswrite(OutPutFileExclName, EUpDataInFValueFracStdV(3,:), 'Press7.85Analysis'
, 'A18');

        xlswrite(OutPutFileExclName, ElementSymbols, 'Press6Analysis' , 'A1');
        xlswrite(OutPutFileExclName, Wavelengths, 'Press6Analysis' , 'A2');
        xlswrite(OutPutFileExclName, EUpDataInFValueP6, 'Press6Analysis' , 'A3');
        xlswrite(OutPutFileExclName, EUpDataInFValueAvg(4,:), 'Press6Analysis' ,
'A14');
        xlswrite(OutPutFileExclName, EUpDataInFValueStdV(4,:), 'Press6Analysis' ,
'A16');
        xlswrite(OutPutFileExclName, EUpDataInFValueFracStdV(4,:), 'Press6Analysis' ,
'A18');

        xlswrite(OutPutFileExclName, ElementSymbols, 'Press4Analysis' , 'A1');
        xlswrite(OutPutFileExclName, Wavelengths, 'Press4Analysis' , 'A2');
        xlswrite(OutPutFileExclName, EUpDataInFValueP4, 'Press4Analysis' , 'A3');
        xlswrite(OutPutFileExclName, EUpDataInFValueAvg(5,:), 'Press4Analysis' ,
'A14');
        xlswrite(OutPutFileExclName, EUpDataInFValueStdV(5,:), 'Press4Analysis' ,
'A16');
        xlswrite(OutPutFileExclName, EUpDataInFValueFracStdV(5,:), 'Press4Analysis' ,
'A18');

        clear wavelengths1
        clear Wavelengths
        clear ElementSymbols
        clear MultiplyFactor
        clear EUpTextIn
        clear EUpDataInFValue
        clear Diff
        clear EUpDataInFValueAvg
        clear EUpDataInFValueStdV
        clear EUpDataInFValueFracStdV
        clear EUpDataInFValueP4
        clear EUpDataInFValueP6
        clear EUpDataInFValueP7_85
        clear EUpDataInFValueP8_3
        clear EUpDataInFValueP8_83

end
toc

```

Appendix 2.5 - AutomaticAllPressureOutput2ExcelAllEUpWithRelIntV5

After running *AutomaticImportHeaders2ExcelAndFValueCorrectV7* all of the integrated intensity, RI, and BR information are stored in separate sheets under their respective upper state energies folders according to species and ionizations. The program

AutomaticAllPressureOutput2ExcelAllEUpWithRelIntV5 gathers the data from these folders and outputs them all to a single excel sheet within an “.xls” file under the species and ionization root folder for the user’s advantage. In more detail, this program takes all relevant parameters (integrated intensity, relative intensity, branching ratio) for a given element/ionization which are located in excel files stored in folders, each excel file located within its respective upper state energy, and it will collect all of the information pertaining to an given element and its ionization state and merge all of the upper state energies into one single excel file which is partitioned into separate sheets according to pressure, relative intensity, integrated intensity and branching ratio.

AutomaticAllPressureOutput2ExcelAllEUpWithRelIntV5 code:

```
%this program takes in the EUp excel files which have been processed by
%AutomaticImportHeaders2ExcelAndFValueCorrectV4() and it further sorts and
%analyzes the data according to pressure and according to upper energy level...
%furthermore Branching ratios are calculated as well as the corresponding
%uncertainty and the entire mix is output to an excel file appropriately labeled
%for each corresponding pressure (in a separate sheet)

%this program takes approximately 3 minutes for Nd II with 46 EUPs to run through
tic
format long g;

%get the list of Upper Energy Levels for the element in (cm^-1) from a 1 column
text file.
[filenameEUp,pathnameEUp]= uigetfile({'*.txt','Text files (*.txt)'; '*.dat',
'Data files (*.dat)'; '*.*','All Files (*.*)'},'select the file with the list of
Upper Energies to input.. Ex: Nd II EUp');
fileLocationEUp = strcat(pathnameEUp,filenameEUp);
fidEUp = fopen(fileLocationEUp);
EUpList = textscan(fidEUp,'%s');%returns a 1 column cell array of strings
fclose(fidEUp);
EUpList = EUpList{:}; %get rid of matlab's cell in a cell format==>
%1 column with multi rows
EUpListNum = str2double(EUpList);
count = 0;
filenameExcel = [];

ElementAbbrev = input('what element is it? (abbreviate it with symbol like Sm for
Samarium): ', 's');

PressSheetList =
{'Press8.83Analysis'},['Press8.3Analysis'],['Press7.85Analysis'],['Press6Analysis
'],['Press4Analysis'];
```



```

%%
for pr = 1:length(PressSheetList)

    for i = 1:(length(EUpsList))

        count = count + 1
        %%
        if isempty(filenameExcl)
            %for first round have user input
            [filenameExcl,pathnameExcl]= uigetfile({'*.xls','Excel files (*.xls)';
            '*.xlsx','Excel_07 files (*.xlsx)'; '*.','All Files (*.*)'},'select the 1st
            excel file corresponding to the lowest Upper Energy to input "Neo_Up22696.885.xls"
            this is output from the prior matlab script');
            FileLocationExcl = strcat(pathnameExcl,filenameExcl);
        else
            ElementAbbrv=char(ElementAbbrv);
            pathnameExclFirstPart = pathnameExcl(1:(end-15));
            pathnameExcl2 =
            strcat(pathnameExclFirstPart,ElementAbbrv,'_Up',EUpsList(i),'\\');
            filenameExcl = char(EUpsList(i));
            filenameExcl = strcat(ElementAbbrv,'_Up',filenameExcl,'.xls');
            filenameExcl = char(filenameExcl);
            FileLocationExcl = strcat(pathnameExcl2,filenameExcl);
        end
        %%
        FileLocationExcl = char(FileLocationExcl);
        PressSheetIndx = PressSheetList(pr);
        PressSheetIndx = char(PressSheetIndx);

        if ~exist(FileLocationExcl)
            FileLocationExcl(end-18)='';
        end

        [ExcelNum,ExcelStrng,ExcelRaw] = xlsread(FileLocationExcl ,
        PressSheetIndx);
        %line below takes all the strings "NaN" and turns them into zeros
        ExcelRawT = ExcelRaw'; %transpose the matrix
        ExcelRawT(:,17) = []; % getting rid of empty columns of "NaN"s
        ExcelRawT(:,15) = [];
        ExcelRawT(:,13) = [];
        RByC = size(ExcelRawT);
        %%

        %here I want to take the rows which only have 'Nd' in col 1 and not the other
        %elements like 'Be' 'C' and the rest of those which I dont need for the analysis
        %from the .roi output

        ExcelStrng2 = char(ExcelStrng);
        RByCC = size(ExcelStrng2);
        Ndrows = [];
        Ndrows1=[];

        ElementAbbrv1=ElementAbbrv(1);
        ElementAbbrv2=ElementAbbrv(2);
        ElementAbbrv1=char(ElementAbbrv1);
        ElementAbbrv2=char(ElementAbbrv2);
        for RR=1:RByCC(1)

```

```

        if (ExcelStrng2(RR,1) == ElementAbbrv1)
            for CC = 1:RRByCC(2)
                if (ExcelStrng2(RR,CC) == ElementAbbrv1) &&
(ExcelStrng2(RR,CC+1) == ElementAbbrv2)

                    Ndrows1 = [ExcelStrng2(RR,CC),ExcelStrng2(RR,CC+1)];
                    Ndrows(RR,1) = [RR];

                end
            end
        end
    end
    Ndrows = Ndrows(find(Ndrows~=0)); %keeps index of only non-zero rows
    ExcelRawT2 = ExcelRawT(Ndrows,:); %drops rows with zeros in them

    clear Ndrows %clear the matrix for next EUp to follow from EUpList
    clear Ndrows1
    clear RR
    clear CC

    %calculating BR avg below

    ExcelRawT2Group = ExcelRawT2(:,3:12); % column 3-12 has Intensities which
I'll use for BR
    ExcelRawT2GroupMat=cell2mat(ExcelRawT2Group); %convert cell to matrix
double format

%here I'm going to work with the Intensities in order to make relative intensity
%calculations too.

    ExcelRawT2B=ExcelRawT2; %copy ExcelRawT2 as ExcelRawT2B
    ExcelRawT2BDouble=cell2mat(ExcelRawT2B(:,3:12)); %convert the cell format
into a workable format (double)
    MaxExcelRawT2BDouble=max(ExcelRawT2BDouble,[],1); %calculate the max of
the maxs so that you can divide by it
    % divide each of the intensities from each separate emission line by the
max

    [yyy,zzz]=size(ExcelRawT2BDouble);
    BadRICol = zeros(yyy,1);
    ColCountRI = zeros(yyy,1);
    for yy=1:yyy
        for zz=1:zzz

RelIntExcelRawT2B(:,zz)=ExcelRawT2BDouble(:,zz)./MaxExcelRawT2BDouble(:,zz);
%above creates a matrix of Relative Intensities from the ROI intensities
        if RelIntExcelRawT2B(yy,zz) ==0
            BadRICol(yy,1) = BadRICol(yy,1) + 1;
        end

    end
    ColCountRI(yy,1) = 10 - BadRICol(yy,1);
    if ColCountRI(yy,1)==0
        ColCountRI(yy,1) = 1; %incase of 0 make it 1 b/c you can't divide
by 0 in stdev
    end
end
end

```

```

clear zz
clear yy
clear BadRICol

RelIntAvgExcelRawT2B = sum(RelIntExcelRawT2B,2)./ColCountRI;

%calculating the Relative Intensity Standard Deviation
RISize = size(RelIntExcelRawT2B);

for hhh=1:RISize(1)
    for iii=1:RISize(2)
        RIDiff(hhh,iii)= RelIntExcelRawT2B(hhh,iii) -
RelIntAvgExcelRawT2B(hhh,1);
        if RIDiff(hhh,iii)==(RelIntAvgExcelRawT2B(hhh,1).*-1)
            RIDiff(hhh,iii)=0;
        end
    end
end
RIDiffSqr = RIDiff.*RIDiff;
SizeRIDiffSqr = size(RIDiffSqr);
RIDiffSqrSum =sum(RIDiffSqr,2);
SizeColCountRI = size(ColCountRI);
ColCountRISqrt = zeros(SizeColCountRI(1),SizeColCountRI(2));
ColCountRISqrt = sqrt(ColCountRI-1);
SizeRIDiffSqrSum = size(RIDiffSqrSum);
for HHH=1:SizeRIDiffSqrSum(1)

    if ColCountRISqrt(HHH,1) ==0
        ColCountRISqrt(HHH,1)=1;
    end
end
clear SizeRIDiffSqrSum
clear RIDiff
clear RIDiffSqr

%creating standard deviation not including the zeroes
LengthRIDiffSqrSum = length(RIDiffSqrSum);
LengthColCountRISqrt=length(ColCountRISqrt);
if LengthRIDiffSqrSum==LengthColCountRISqrt
    AlmostRIStdl = RIDiffSqrSum./(ColCountRI-1);
    RIStdv = sqrt(AlmostRIStdl); %creates 1 Col of BRSTDV from the 10 BR
columns

else
    error('length of BRDiffSqrSum and ColCountSqrt arent equal')
end
RIStdv(isnan(RIStdv)) = 0;

%creating Standard deviation on the mean for Relative Intensities
SIZEExcelRawT2RI = size(RelIntExcelRawT2B);
RIStdvM=RIStdv./sqrt(SIZEExcelRawT2RI(2));%creates stdev on mean of line
above
RIStdvM(isnan(RIStdvM)) = 0; % eliminates NaN's from matrix and makes them
zeros
%%%%% working on Branching Ratios here on out
ExcelRawT2GroupColSum = sum(ExcelRawT2GroupMat,1); %calculate sum of
columns in a 1 row vector

```

```

SizeGroup=size(ExcelRawT2Group);
BadBRGroup = 0;
BadBRCol = zeros(SizeGroup(1),1);
ColCount = zeros(SizeGroup(1),1);%make a 1 col vector to keep track of bad
BR to subtract from total count in BR-AVG...
ExcelRawT2BR=zeros(SizeGroup(1),SizeGroup(2));

%below here, in the 2 for loops, I am going to omit from the BR calculations any
intensities which are zeros
for RRR=1:(SizeGroup(1))
    for CCC=1:(SizeGroup(2))
        if double(ExcelRawT2Group{RRR,CCC})<=0.740472273634510 %less than
this # is garbage which I put in as '1'
            BadBRGroup = BadBRGroup + 1; %keep track of Number of bad BRs,
so u dont count them
            ExcelRawT2GroupMat(RRR,CCC)= 0;
        end

ExcelRawT2BR(RRR,CCC)=ExcelRawT2GroupMat(RRR,CCC)./ExcelRawT2GroupColSum(CCC);
%above creates a 13x10 matrix of BRs from the ROI intensities
if ExcelRawT2BR(RRR,CCC) ==0
    BadBRCol(RRR,1) = BadBRCol(RRR,1) + 1;
end
end
ColCount(RRR,1) = 10 - BadBRCol(RRR,1);
if ColCount(RRR,1)==0
    ColCount(RRR,1) = 1; %in case of 0 make it 1 b/c you can't
%divide by 0 in stdev
end
end
clear CCC
clear RRR

%creating the BR avg and trying to NOT include the zeros
ExcelRawT2BRSum=sum(ExcelRawT2BR,2); %make 1 col of BR summed up
ExcelRawT2BRAvg = ExcelRawT2BRSum./ColCount; %make 1 col of BRAVGs

ExcelRawT2BRAvg(isnan(ExcelRawT2BRAvg)) = 0;
%calculating the BR Standard Deviation
BRSize = size(ExcelRawT2BR);

for RRR = 1:BRSize(1)
    for CCC=1:BRSize(2)
        BRDiff(RRR,CCC)= ExcelRawT2BR(RRR,CCC) - ExcelRawT2BRAvg(RRR,1);
        if BRDiff(RRR,CCC)==(ExcelRawT2BRAvg(RRR,1).*-1)
            BRDiff(RRR,CCC)=0;
        end
    end
end
end
BRDiffSqr = BRDiff.*BRDiff;
SizeBRDiffSqr = size(BRDiffSqr);
BRDiffSqrSum =sum(BRDiffSqr,2);
SizeColCount = size(ColCount);
ColCountSqrt = zeros(SizeColCount(1),SizeColCount(2));
ColCountSqrt = sqrt(ColCount-1);
SizeBRDiffSqrSum = size(BRDiffSqrSum);
for rrr=1:SizeBRDiffSqrSum(1)

```



```

RIExcelDataOut=horzcat(ExcelWavelengths2,ExcelIntensityStat2,RelIntExcelRawT2B2,RelIntAvgExcelRawT2B2,RIStdv2,RIStdvM2);
    IntensityExcelDataOut =
horzcat(ExcelWavelengths2,ExcelIntensityStat2,ExcelRawT2BDouble,ExcelIntensityStat2);

ExcelDat=[ExcelElems3,ExcelWavelengths2,ExcelIntensityStat,ExcelRawT2BR,ExcelRawT2BRAvg,BRStdv,BRStdvM];
    ExcelDataOut(isnan(ExcelDataOut))=0;
    RIExcelDataOut(isnan(RIExcelDataOut))=0;
    IntensityExcelDataOut(isnan(IntensityExcelDataOut))=0;
    ExcelDataOut2 = num2cell(ExcelDataOut);
    RIExcelDataOut2=num2cell(RIExcelDataOut);
    IntensityExcelDataOut2=num2cell(IntensityExcelDataOut);
    if i==1
        Headers17 = {'Wavelength', ['Intensity Avg'], ['Stdv'],
['FracStdv'], ['BR1'], ['BR2'], ['BR3'], ['BR4'], ['BR5'], ['BR6'], ['BR7'],
['BR8'], ['BR9'], ['BR10'], ['BranchRatioAvg'], ['BRStdv'], ['BRStdvMean']};
        RIHeaders17 = {'Wavelength', ['Intensity Avg'], ['Stdv'],
['FracStdv'], ['RI1'], ['RI2'], ['RI3'], ['RI4'], ['RI5'], ['RI6'], ['RI7'],
['RI8'], ['RI9'], ['RI10'], ['RelIntAvg'], ['RIStdv'], ['RIStdvMean']};
        IntensityHeaders17 = {'Wavelength', ['Intensity Avg'], ['Stdv'],
['FracStdv'], ['Int1'], ['Int2'], ['Int3'], ['Int4'], ['Int5'], ['Int6'],
['Int7'], ['Int8'], ['Int9'], ['Int10'], ['IntAvg'], ['Stdv'], ['FracStdv']};
        %ExcelAllEUps = vertcat(Headers, EUpsListII, ExcelRawT2);
        ExcelAllEUps = vertcat(Headers17, EUpsListIII17, ExcelDataOut2);
        RIExcelAllEUps = vertcat(RIHeaders17, EUpsListIII17, RIExcelDataOut2);
        IntensityExcelAllEUps = vertcat(IntensityHeaders17, EUpsListIII17,
IntensityExcelDataOut2);
%vertcat will let you concatenate (join) arrays with the same number of columns
%even if the number of rows are different, unlike the "[ ]" function
        HeadersElemSymb = {'Element Symbol'};
        ExcelElemSymb =
vertcat(HeadersElemSymb,EUpsListIIElemSymb,ExcelElems(:,1));
    else
        ExcelAllEUps = vertcat(ExcelAllEUps,Blank17, EUpsListIII17, Blank17,
ExcelDataOut2);
        RIExcelAllEUps = vertcat(RIExcelAllEUps,Blank17, EUpsListIII17,
Blank17, RIExcelDataOut2);
        IntensityExcelAllEUps = vertcat(IntensityExcelAllEUps,Blank17,
EUpsListIII17, Blank17, IntensityExcelDataOut2);
        ExcelElemSymb =
vertcat(ExcelElemSymb,BlankElemSymb,EUpsListIIElemSymb,BlankElemSymb,ExcelElems(:,
1));
        RIExcelElemSymb =
vertcat(ExcelElemSymb,BlankElemSymb,EUpsListIIElemSymb,BlankElemSymb,ExcelElems(:,
1));
        IntensityExcelElemSymb =
vertcat(ExcelElemSymb,BlankElemSymb,EUpsListIIElemSymb,BlankElemSymb,ExcelElems(:,
1));
    end
    clear BRDiffSqrSum
    clear RIDiffSqrSum
    clear RelIntExcelRawT2B
    clear ExcelRawT2BDouble
end

```

```

%Need to "step back" 1 folder in order to deposit the excel file in a folder 1
%folder back... must do this using the string for the pathname dont forget to
%account for the 5 different pressure sheets to be output to different excel files
%(or sheets) completely
%FileLocationExcl='C:\Users\caleb\Documents\MATLAB\ForPracticeEups\Neo_Up22696.885
\Neo_Up22696.885.xls'
FileLocationExclOut1 = char(FileLocationExcl);
FileLocationExclOutFirst = FileLocationExclOut1(1:(end - 34));
FileLocationExclOutFirst = char(FileLocationExclOutFirst);
FileLocationExclOutLast = '\Iro_AllEUpsAnalyzed';
FileLocationExclOutLast = char(FileLocationExclOutLast);
FileLocationExclOut =
strcat(FileLocationExclOutFirst,FileLocationExclOutLast, '.xls')
if pr<6
    xlswrite(FileLocationExclOut , ExcelElemSymb , PressSheetIndx,'A1' );
    xlswrite(FileLocationExclOut , ExcelAllEUps , PressSheetIndx,'B1' );

    PressSheetIndx1 = strcat('RelInt',PressSheetIndx);
    PressSheetIndx1=char(PressSheetIndx1);
    xlswrite(FileLocationExclOut , RIExcelElemSymb , PressSheetIndx1,'A1' );
    xlswrite(FileLocationExclOut , RIExcelAllEUps , PressSheetIndx1,'B1' );

    PressSheetIndx2 = strcat('Inten',PressSheetIndx);
    PressSheetIndx2=char(PressSheetIndx2);
    xlswrite(FileLocationExclOut , IntensityExcelElemSymb ,
PressSheetIndx2,'A1' );
    xlswrite(FileLocationExclOut , IntensityExcelAllEUps ,
PressSheetIndx2,'B1' )
end
end
clear ExcelRaw
clear ExcelRawT
clear ExcelElems
toc

```

ABSTRACT**OSCILLATOR STRENGTH MEASUREMENTS IN SINGLY-IONIZED,
DOUBLY-IONIZED AND NEUTRAL LANTHANIDES AND TRANSITION
ELEMENTS (SM, ND, PR, GD, CU, AND FE) USING LASER-INDUCED
BREAKDOWN.**

by

CALEB A. RYDER**May 2012****Advisor:** Dr. Steven J. Rehse**Major:** Physics**Degree:** Doctor of Philosophy

Models for stellar nucleosynthesis, age determinations for stars in the Milky Way's galactic halo, and stellar chemical abundance determinations are dependent upon accurate atomic spectroscopic data to allow the correct interpretation of stellar absorption and emission spectra. It is well known that calculations of many astrophysically important atomic parameters are limited due to line blending, insufficient spectral resolution of some key spectral lines, and also the complicated electronic structure of the important heavy elements. Astrophysicists have therefore looked to laboratory astrophysics experiments to provide accurate atomic data to help resolve these limiting issues. In this dissertation, laser-induced breakdown spectroscopy (LIBS) has been employed for the first time on a large scale as a spectroscopic technique for the rapid and convenient production of atomic and ionic plasmas as sources of atomic emission in order to determine radiative properties in astrophysically relevant lanthanides (Gd, Nd, Pr and Sm) and transition metals (Cu and Fe).

Nanosecond laser pulses incident on pure elemental targets in a rarified argon environment were used to create high-temperature plasmas. The resulting spontaneous emission from the high-temperature micro-plasmas was dispersed in a spectrally-corrected high-resolution broadband Échelle spectrometer and detected with a high-sensitivity intensified CCD camera which allowed the simultaneous determination of the relative intensities of thousands of decay branches from hundreds of excited energy levels and multiple ionization states. These experimentally measured relative emission intensities were used to calculate branching ratios (branching fractions) which were then combined with previously obtained atomic lifetimes to calculate transition probabilities and oscillator strengths.

In two transition metals, emission intensities have been measured for 192 transitions from 68 excited states in neutral copper and 79 emission lines from 27 excited states in singly-ionized copper as well as 776 emission lines from 108 excited states in neutral iron and 1453 emission lines from 108 excited states in singly-ionized iron.

In four important lanthanide elements, emission intensities have been measured for 587 lines of 113 excited states in neutral gadolinium, 480 lines from 43 excited states of singly-ionized gadolinium, and 40 lines in 6 states of doubly-ionized gadolinium; 121 emission lines from 93 excited states in neutral neodymium, 368 lines from 46 excited states in singly-ionized neodymium, and two lines from a single excited level of doubly-ionized neodymium; 19 lines from 19 excited levels of neutral praseodymium, 367 lines from 41 excited states in singly-ionized praseodymium, and 359 lines from 7 excited levels of doubly-ionized praseodymium; 137 lines from 70 excited states in neutral samarium, 713 lines from 115 excited states in singly-ionized samarium, and 49 lines from 17 excited levels of doubly-ionized samarium. The degree of uncertainty for strong emission lines is 6.6%, for moderate lines 7.3%, and 19% for weak transitions. This degree of uncertainty is typical for such laboratory astrophysics work and is usually an improvement upon available calculations.

The transition probabilities in Nd I, Nd III, Pr I, Sm II, Sm III, Gd I, Gd II, Gd III, Cu II and Fe I show overall good agreement with other published works. For the branches in Nd II, Pr II, Sm I, and Cu I the results show overall fair agreement with other works. The parameters in Pr III and Fe II show relatively poor agreement with previous works and is believed to be the result of attempts to measure numerous problematic lines within the parent energy levels.

AUTOBIOGRAPHICAL STATEMENT

Education

- Wayne State University, Detroit, MI: Doctor of Philosophy (Expected Graduate: December 2011).

Thesis: Oscillator Strength Measurements in Singly-Ionized, Doubly-Ionized and Neutral Lanthanides and Transition Elements (Sm, Nd, Pr, Gd, Cu, and Fe) Using Laser-Induced Breakdown Spectroscopy.

- Wayne State University, Detroit, MI: M.S. Physics (Graduation: August 2009)
- Western Michigan University, Kalamazoo, MI: B.S. Physics (December 2005)

Work Experience

- Graduate Teaching and Research Assistant: Wayne State University, MI, 2006 – 2011
- Lecturer in Physics: Wayne State University, Michigan, 2010.

Awards

- American Association of Physics Teachers Outstanding Teaching award, Wayne State University (Department of Physics and Astronomy) 2007.
- First Place Award, Graduate Research Day: Wayne State University (Department of Physics and Astronomy), 2010

Selected Presentations

- “Laser-induced breakdown spectroscopy for branching ratio and atomic lifetime measurements in singly-ionized neodymium and gallium,” WSU (Department of Physics and Astronomy) Graduate Research Day, 2010

Selected Publication

- S.J. Rehse and C.A. Ryder, “Laser-induced breakdown spectroscopy for branching ratio and atomic lifetime measurements in singly-ionized neodymium and gallium,” *Spectrochimica Acta B* **64**, Pages: 974-980 (2009).